

ANP-10332NP
Revision 0

**AURORA-B: An Evaluation Model for
Boiling Water Reactors; Application to
Loss of Coolant Accident Scenarios**

February 2014

**AURORA-B: An Evaluation Model for Boiling
Water Reactors; Application to Loss of
Coolant Accident Scenarios**

AREVA Inc.

ANP-10332NP
Revision 0

**AURORA-B: An Evaluation Model for Boiling
Water Reactors; Application to Loss of
Coolant Accident Scenarios**

Copyright © 2014

AREVA Inc.
All Rights Reserved

Nature of Changes

Item	Page	Description and Justification
1.	All	This is a new document.

Contents

	<u>Page</u>
Abstract.....	xxxviii
1.0 Introduction	1-1
2.0 Summary.....	2-1
2.1 General Summary.....	2-1
2.2 Application of the EMDAP	2-1
2.3 Compliance with the Standard Review Plan.....	2-2
2.4 Compliance with 10 CFR 50.46.....	2-2
2.4.1 Figures of Merit	2-3
2.4.2 10 CFR 50.46 Appendix K Documentation	2-3
2.5 Emerging Issues	2-3
2.5.1 Proposed 10 CFR 50.46c.....	2-3
2.5.2 Conductivity Degradation	2-3
2.5.3 Fuel Relocation	2-4
2.5.4 Generic Safety Issue 191	2-4
3.0 Regulatory Requirements Summary.....	3-1
3.1 Regulatory Requirements	3-1
3.1.1 Application of the Evaluation Model Development and Assessment Process (EMDAP), Regulatory Guide 1.203.....	3-1
3.2 Compliance with Appendix K to 10 CFR Part 50 Documentation	3-2
3.3 Compliance with Standard Review Plan 15.6.5.....	3-2
4.0 Establish Requirements for Evaluation Model Capability (EMDAP Element 1).....	4-1
4.1 Documentation.....	4-1
4.1.1 Regulatory Basis, Chapter 15, Section 15.0.2; Item 1	4-1
4.2 Accident Scenario Identification Process (SIP) as per (SRP, Chapter 15, Section 15.0.2, Item 2)	4-2
4.2.1 Regulatory Basis.....	4-2
4.3 Analysis Purpose, Transient Class, and Power Plant Class (EMDAP Step 1)	4-2
4.3.1 Analysis Purpose	4-2
4.3.2 Transient Class.....	4-2
4.3.3 Power Plant Class.....	4-3
4.4 Figures of Merit (EMDAP Step 2).....	4-3
4.4.1 Application Specific Considerations	4-4
4.5 Identify Systems, Components, Phases, Geometries, Fields, and Processes that Must Be Modeled (EMDAP Step 3).....	4-6
4.6 Identify and Rank Key Phenomena and Processes (EMDAP Step 4)	4-7
5.0 Develop Assessment Base (EMDAP Element 2); Chapter 15 Section 15.0.2, Item 4	5-1
5.1 Regulatory Basis.....	5-1

5.2	Specify Objectives for Assessment Base (EMDAP Step 5)	5-1
5.3	Perform Scaling Analysis and Identify Similarity Criteria (EMDAP Step 6)	5-1
5.4	Identify Existing Data and/or Perform Integral Effects Tests and Separate Effects Tests to Complete the Database (EMDAP Step 7)	5-1
5.4.1	Appendix K Requirements	5-2
5.4.2	Core Simulator Qualification	5-3
5.4.3	RODEX4 Qualification	5-3
5.4.4	Rod Bundle Pressure Drop Tests	5-4
5.4.5	Jet-Pump Performance Tests	5-4
5.4.6	Steam Separator Tests	5-4
5.4.7	Critical Power Tests	5-5
5.4.8	CCFL Mini-Loop Tests	5-5
5.4.9	Rod Bundle Void Tests	5-5
5.4.10	Christensen Void Tests	5-6
5.4.11	Allis-Chalmers Void Tests	5-6
5.4.12	GE Level Swell Tests	5-6
5.4.13	THTF Mixture Level Tests	5-7
5.4.14	TLTA Boiloff Tests	5-7
5.4.15	Bennett Tube Tests	5-8
5.4.16	THTF Steady State Tests	5-8
5.4.17	FCTF Spray and Steam Cooling Tests	5-9
5.4.18	THTF Reflood Tests	5-9
5.4.19	FLECHT SEASET Reflood Tests	5-10
5.4.20	CCTF Reflood Tests	5-10
5.4.21	Marviken Critical Flow Tests	5-11
5.4.22	UPTF CCFL and Entrainment Tests	5-11
5.4.23	SSTF Integral Tests	5-12
5.4.24	TLTA Integral Tests	5-13
5.4.25	FIST Integral Tests	5-14
5.5	Evaluate Effects of IET Distortions and SET Scaleup Capability (EMDAP Step 8)	5-20
5.6	Determine Experimental Uncertainties as Appropriate (EMDAP Step 9)	5-20
6.0	Develop Evaluation Model (EMDAP Element 3); Chapter 15, Section 15.0.2, Item 2	6-1
6.1	Establish an Evaluation Model Development Plan (EMDAP Step 10)	6-1
6.2	Appendix K Compliance Models	6-1
6.2.1	I.A. Sources of heat during the LOCA	6-1
6.2.2	I.A.1. The Initial Stored Energy in the Fuel	6-4
6.2.3	I.A.2. Fission Heat	6-4
6.2.4	I.A.3. Decay of Actinides	6-5
6.2.5	I.A.4. Fission Product Decay	6-5
6.2.6	I.A.5. Metal-Water Reaction Rate	6-6
6.2.7	I.A.6. Reactor Internals Heat Transfer	6-6

6.2.8	I.A.7. Pressurized Water Primary-to-Secondary Heat Transfer	6-7
6.2.9	I.B. Swelling and Rupture of the Cladding and Fuel Rod Thermal Parameters	6-7
6.2.10	I.C.1.a Break Characteristics and Flow	6-7
6.2.11	I.C.1.b. Discharge Model.....	6-8
6.2.12	I.C.1.c. End of Blowdown	6-8
6.2.13	I.C.1.d. Noding Near the Break and the ECCS Injection Points.....	6-9
6.2.14	I.C.2. Frictional Pressure Drops	6-10
6.2.15	I.C.3. Momentum Equation.....	6-11
6.2.16	I.C.4. Critical Heat Flux	6-11
6.2.17	I.C.5. Post-CHF Heat Transfer Correlations	6-12
6.2.18	I.C.6. Pump Modeling.....	6-14
6.2.19	I.C.7. Core Flow Distribution During Blowdown (<i>Applies only to pressurized water reactors</i>)	6-14
6.2.20	I.D.1. Single Failure Criterion	6-15
6.2.21	I.D.2. Containment Pressure	6-15
6.2.22	I.D.3. Calculation of Reflood Rate for Pressurized Water Reactors	6-16
6.2.23	I.D.4. Steam Interaction with Emergency Core Cooling Water in Pressurized Water Reactors	6-16
6.2.24	I.D.5. Refill and Reflood Heat Transfer for Pressurized Water Reactors	6-16
6.2.25	I.D.6. Convective Heat Transfer Coefficients for Boiling Water Reactor Fuel Rods Under Spray Cooling	6-17
6.2.26	I.D.7. The Boiling Water Reactor Channel Box Under Spray Cooling	6-18
6.2.27	II. Required Documentation.....	6-18
6.3	Establish Evaluation Model Structure (EMDAP Step 11).....	6-20
6.3.1	Code Structure.....	6-21
6.3.2	Field Equations	6-22
6.3.3	Closure Relations.....	6-23
6.3.4	Code Numerics	6-24
6.3.5	Additional Features	6-24
6.3.6	External Data Transfer	6-25
6.3.7	Plant Model Nodalization.....	6-27
	6.3.7.1 Pressure Vessel Region.....	6-28
	6.3.7.2 Upper Plenum.....	6-36
	6.3.7.3 Core Region.....	6-36
	6.3.7.4 Lower Plenum	6-41
	6.3.7.5 Steam Lines.....	6-41
	6.3.7.6 Recirculation System	6-42
	6.3.7.7 Plant Parameters Data.....	6-44
6.3.8	Hot Channel Model	6-45
6.4	Develop or Incorporate Closure Models (EMDAP Step 12)	6-49
6.4.1	Appendix K Requirements.....	6-49
6.4.2	Stored Energy	6-49
	6.4.2.1 Limiting Power History	6-49

6.4.2.2	Bounding Centerline Temperature	6-50
6.4.3	Decay Heat	6-52
6.4.3.1	Fission Product Decay	6-52
6.4.3.2	Actinide Decay Heat	6-52
6.4.4	Metal-Water Reaction	6-52
6.4.5	Fuel Swell, Rupture, and Relocation	6-53
6.4.6	Discharge Model	6-58
6.4.7	Upper Plenum Mixing Model	6-59
6.4.7.1	Condensation Model	6-59
6.4.7.2	Simplified Empirical Model	6-60
6.4.8	Heat Transfer Correlation Selection Logic	6-61
6.4.9	Appendix K Prevention of Return to Nucleate Boiling and Transition Boiling	6-64
6.4.10	Critical Heat Flux	6-67
6.4.11	Transition Boiling Heat Transfer	6-69
6.4.12	Minimum Film Boiling Temperature	6-70
6.4.13	Film Boiling Heat Transfer	6-76
6.4.13.1	Boiling Heat Transfer to Liquid	6-76
6.4.13.2	Convection Heat Transfer to Vapor	6-78
6.4.14	Radiation Heat Transfer From Wall to Fluid	6-84
6.4.15	Surface to Surface Radiation Heat Transfer	6-84
6.4.16	Vapor Convection Heat Transfer	6-85
6.4.17	Appendix K BWR Core Spray Heat Transfer	6-85
6.4.18	3-D Heat Transfer within Fuel Bundle	6-87
7.0	Assess Evaluation Model Adequacy (EMDAP Element 4)	7-1
7.1	Regulatory Basis	7-2
7.2	Determine Model Pedigree and Applicability to Simulate Physical Processes (EMDAP Step 13)	7-2
7.3	Prepare Input and Perform Calculations to Assess Model Fidelity or Accuracy (EMDAP Step 14)	7-2
7.3.1	Appendix K Requirements	7-3
7.3.2	Summary of Core Simulator Qualification	7-3
7.3.3	Summary of RODEX4 Qualification	7-4
7.3.4	Rod Bundle Void Tests	7-5
7.3.4.1	FRIGG2 Void Tests	7-7
7.3.4.2	FRIGG3 Void Tests	7-7
7.3.4.3	ATRIUM-10A Void Tests	7-8
7.3.5	Christensen Void Tests	7-13
7.3.6	Allis-Chalmers Large Diameter Void Tests	7-18
7.3.6.1	2.9 Inch Void Tests	7-19
7.3.6.2	18 Inch Void Tests	7-20
7.3.6.3	36 Inch Void Tests	7-20
7.3.7	GE Level Swell Test	7-25
7.3.8	THTF Mixture Level Test	7-30
7.3.8.1	Level Swell Results	7-33
7.3.8.2	Rod Temperature Results	7-33
7.3.9	TLTA Boiloff Test	7-49
7.3.9.1	TLTA Test 6441-6 Results	7-52

7.3.9.2	TLTA Test 6441-7 Results	7-52
7.3.10	Bennett Tube	7-72
7.3.11	THTF Steady State Film Boiling Tests.....	7-79
7.3.11.1	Comparison of THTF and CE/Columbia Dispersed Film Boiling Data	7-80
7.3.12	FCTF Spray and Steam Cooling Tests.....	7-82
7.3.12.1	FCTF Test 64: No Steam Updraft	7-84
7.3.12.2	FCTF Test 63: [.....].....	7-85
7.3.12.3	FCTF Test 66: [.....].....	7-85
7.3.12.4	FCTF Test 79: [.....].....	7-86
7.3.12.5	FCTF Test 29: [.....].....	7-86
7.3.13	THTF Reflood	7-98
7.3.14	FLECHT Reflood and Steam Cooling Tests	7-108
7.3.14.1	Rod Surface Temperatures at 78 in (SEASET) and 60 in (Skew).....	7-109
7.3.14.2	Rod Surface Temperatures at 90 in (SEASET) and 84 in (Skew).....	7-110
7.3.14.3	Rod Surface Temperatures at 111 in (SEASET) and 108 in (Skew).....	7-110
7.3.14.4	Maximum Cladding Temperature	7-110
7.3.14.5	Steam Cooling Results.....	7-110
7.3.15	CCTF Test	7-134
7.3.16	Marviken	7-143
7.3.17	UPTF	7-154
7.3.17.1	UPTF Tests 6 and 7	7-155
7.3.17.2	Tests 10 and 12	7-157
7.3.17.3	Tests 10 and 29	7-158
7.4	Assess Scalability of Models (EMDAP Step 15).....	7-168
7.5	Determine Capability of Field Equations to Represent Processes and Phenomena and the Ability of Numeric Solutions to Approximate Equation Set (EMDAP Step 16)	7-168
7.6	Determine Applicability of Evaluation Model to Simulate System Components (EMDAP Step 17)	7-169
7.6.1	Rod Bundle Pressure Drop	7-169
7.6.2	Jet-pump Performance Tests	7-173
7.6.2.1	EGG-LTSF 1/6 Scale Tests	7-174
7.6.2.2	Other Jet-pump Tests	7-175
7.6.2.3	Two-Phase Tests	7-176
7.6.3	Steam Separator Tests	7-184
7.6.3.1	Two Stage Steam Separator	7-184
7.6.3.2	Three Stage Steam Separator	7-185
7.6.4	Critical Power Tests	7-191
7.6.5	CCFL Mini Loop Test	7-191
7.7	Prepare Input and Perform Calculations to Assess System Interactions and Global Capability (EMDAP Step 18).....	7-195
7.7.1	SSTF Integral Tests	7-195

7.7.1.1	Assessment of the SSTF System Test EA3.1 Run 111, BWR/4 LOCA	7-198
7.7.1.2	Assessment of the SSTF System Test SRT-3 Run 26, BWR/6 LOCA	7-202
7.7.2	TLTA Integral Tests.....	7-231
7.7.2.1	TLTA Large Break Test 6425-2 Simulation	7-233
7.7.2.2	TLTA Small Break Test 6432-1 Simulation.....	7-254
7.7.3	FIST Integral Tests.....	7-268
7.7.3.1	BWR/6 Large Break Test 6DBA1-B	7-275
7.7.3.2	BWR/6 Small Break Test 6SB2C	7-294
7.7.3.3	BWR/6 LPCI Line Break Test 6LB1.....	7-316
7.7.3.4	BWR/4 Large Break Test 4DBA1	7-339
7.7.4	BWR/4 Baseline Analyses.....	7-360
7.7.5	BWR/4 Reduced ECCS Analyses	7-398
7.7.6	BWR/6 Baseline Analyses.....	7-409
7.8	Assess Scalability of Integrated Calculations and Data for Distortions (EMDAP Step 19).....	7-445
	The scalability.....	7-445
7.9	Determine Evaluation Model Biases and Uncertainties (EMDAP Step 20).....	7-445
7.9.1	Regulatory Basis: Appendix K Conservatism in AURORA-B LOCA EM	7-446
7.9.2	Examples of Appendix K Conservatism for Select Assessments.....	7-446
7.9.2.1	TLTA Case 6432-1.....	7-446
7.9.2.2	FIST Small Break Case.....	7-453
7.9.3	Time Step Sensitivity Analyses	7-457
7.9.4	Hot Channel Axial Nodalization Sensitivity Analyses	7-461
7.9.5	Core Axial Power Shape Sensitivity Analyses	7-463
7.9.6	Core Radial Sensitivity Analyses.....	7-466
7.9.6.1	BWR/4 Bundle Radial Power Sensitivity Analysis	7-466
7.9.6.2	SSTF Bundle Radial Power Sensitivity Analysis	7-468
7.9.6.2.1	T026_y52 Base Case (13 Bundle Groups) Results	7-472
7.9.6.2.2	T026_y53 Case (9 Bundle Groups) Results	7-488
7.9.6.2.3	T026_y54 Case (9 Bundle Groups) Results	7-502
7.9.6.2.4	T026_y55 Case (9 Bundle Groups) Results	7-514
7.9.6.2.5	T026_y48 Case (3 Bundle Groups) Results	7-523
8.0	Adequacy Decision.....	8-1
8.1	Code Versions Used in the Adequacy Decision	8-1
8.2	Summary of Updates to S-RELAP5 since AURORA-B AOO Submittal.....	8-2

9.0 Application Methodology Description9-1

9.1 Application for LOCA Analysis9-2

9.1.1 EM Applicability for Event Analysis9-2

9.1.2 Use of Analysis Results9-2

9.1.3 Plant Operating Conditions Envelope9-2

9.1.4 Plant Parameters9-2

10.0 Quality Assurance Program (QAP)10-1

11.0 Documentation11-1

12.0 Uses, Updates, and Modifications12-1

12.1 Updates and Changes to Components of the EM12-1

12.2 Plant Modifications and Applications12-2

12.3 Definitions of Significance12-3

12.4 Code Modifications12-3

13.0 References13-1

Appendix A BWR ECCSA-1

Tables

	<u>Page</u>
Table 4-1 BWR LOCA PIRT.....	4-9
Table 5-1 AURORA-B LOCA Evaluation Model Assessment Matrix	5-16
Table 6-1 Code Structure.....	6-21
Table 6-2 Field & Transport Equations.....	6-23
Table 6-3 Processes and Closure Relations	6-23
Table 6-4 Additional Features	6-24
Table 6-5 Description of Reactor Vessel Components.....	6-30
Table 6-6 Example Bundle Distribution	6-39
Table 6-7 Relocation Packing Fractions for Limited Strains	6-55
Table 7-1 Rod Bundle Void Fraction Test Characteristics	7-9
Table 7-2 Christensen Test Characteristics	7-15
Table 7-3 Allis-Chalmers Large Diameter Void Test Characteristics	7-21
Table 7-4 Summary of THTF and BWR ATRIUM-10 Rod Bundles.....	7-35
Table 7-5 Summary of TLTA Tests under the BD/ECC 1A Program	7-53
Table 7-6 Summary of TLTA Boil-off Tests under the BD/ECC 1A Program	7-54
Table 7-7 Conditions for Bennet Tube Tests 5358 and 5379	7-74
Table 7-8 FCTF Analyzed Test Matrix	7-87
Table 7-9 High-Pressure Reflood THTF Test Matrix	7-100
Table 7-10 FLECHT SEASET, FLECHT Skewed Test Conditions	7-111
Table 7-11 Summary of PCT Results for CCTF Tests.....	7-136
Table 7-12 Marviken Critical Flow Test Nozzle Dimensions for the Nine Tests Selected.....	7-145
Table 7-13 Summary of Marviken Tests Statistical Results.....	7-146
Table 7-14 Summary of Marviken Tests Statistical Results with Moody Option.....	7-146
Table 7-15 UPTF Test 6 and 7 Calculated S-RELAP5 Downcomer Penetration Rates and Evaluation Periods.....	7-158
Table 7-16 Pressure Drop Benchmark Statistics by Exit Flow Quality (Calculated - Measured) / Measured	7-170
Table 7-17 Jet-Pump Characteristic Information	7-177
Table 7-18 Summary of SSTF Bundle Grouping	7-206
Table 7-19 SSTF Bundles with DP Measurements	7-206

Table 7-20	Measured and Predicted Major Event Timing for TLTA Test 6425-2	7-236
Table 7-21	FIST Test 6DBA1 Initial Conditions	7-278
Table 7-22	Measured and Predicted Major Event Timing for FIST 6DBA1	7-279
Table 7-23	FIST Test 6SB2C Initial Conditions	7-298
Table 7-24	Predicted Major Event Timing for FIST 6SB2C with L1 Calculated from ΔP	7-299
Table 7-25	FIST Test 6LB1 Initial Conditions	7-320
Table 7-26	Measured and Predicted Major Event Timing for FIST 6LB1	7-321
Table 7-27	FIST Test 4DBA1 Initial Conditions	7-343
Table 7-28	Measured and Predicted Major Event Timing for FIST 4DBA1	7-344
Table 7-29	BWR/4 Initial Conditions	7-362
Table 7-30	BWR/4 Reactor System Parameters	7-362
Table 7-31	ATRIUM-10 Fuel Assembly Parameters	7-363
Table 7-32	BWR/4 High-Pressure Coolant Injection Parameters	7-364
Table 7-33	BWR/4 Low-Pressure Coolant Core Spray Parameters	7-365
Table 7-34	BWR/4 Low-Pressure Coolant Injection Parameters	7-366
Table 7-35	BWR/4 Automatic Depressurization System Parameters	7-367
Table 7-36	BWR/4 ECCS Single Failure	7-368
Table 7-37	BWR/4 Recirculation Line Break Results for SF-BATT	7-369
Table 7-38	BWR/4 Recirculation Line Break Results for SF-LPCI	7-370
Table 7-39	BWR/4 Recirculation Line Break Results for SF-LOCA	7-371
Table 7-40	Results for Highest PCT for Example BWR/4 Recirculation Line Break 0.10 ft ² Split Pump Discharge SF-BATT Top-Peaked Axial	7-372
Table 7-41	Event Times for Example BWR/4 Small Recirculation Line Break 0.1 ft ² Split Pump Discharge SF-BATT Mid-Peaked Axial	7-373
Table 7-42	Results for Example BWR/4 Large Recirculation Line Break 1.0 DEG Pump Suction SF-LOCA Mid-Peaked Axial	7-374
Table 7-43	Event Times for Example BWR/4 Large Recirculation Line Break 1.0 DEG Pump Suction SF-LOCA Mid-Peaked Axial	7-375
Table 7-44	Results for Highest PCT Recirculation Line Break 0.40 ft ² Split Pump Discharge Reduced ECCS Top-Peaked Axial	7-399
Table 7-45	Events Times for BWR/4 Recirculation Line Break 0.4 ft ² Split Pump Discharge Reduced ECCS Top-Peaked Axial	7-400
Table 7-46	BWR/6 Example Problem Initial Conditions	7-411
Table 7-47	BWR/6 Example Reactor System Parameters	7-411

Table 7-48	BWR/6 High-Pressure Coolant Core Spray Parameters.....	7-412
Table 7-49	BWR/6 Low-Pressure Coolant Core Spray Parameters	7-413
Table 7-50	BWR/6 Low-Pressure Coolant Injection Parameters	7-414
Table 7-51	BWR/6 Automatic Depressurization System Parameters	7-415
Table 7-52	BWR/6 ECCS Single Failure	7-415
Table 7-53	BWR/6 Recirculation Line Break Results for SF-LPCI.....	7-416
Table 7-54	BWR/6 Recirculation Line Break Results for SF-LPCS	7-417
Table 7-55	BWR/6 Recirculation Line Break Results for SF-HPCS.....	7-418
Table 7-56	Results for Highest PCT for Example BWR/6 Recirculation Line Break 1.0 DEG Pump Suction SF-LPCS Mid-Peaked Axial	7-419
Table 7-57	Event Times for Highest PCT for Example BWR/6 Large Recirculation Line Break 1.0 DEG Pump Suction SF-LPCS Mid- Peaked Axial.....	7-420
Table 7-58	Results for Example BWR/6 Small Recirculation Line Break 0.05 DEG Pump Discharge SF-HPCS Mid-Peaked Axial.....	7-421
Table 7-59	Event Times for Example BWR/6 Small Recirculation Line Break 0.05 ft ² Split Pump Discharge SF-HPCS Mid-Peaked Axial 102% Licensing Power 105% Flow	7-422
Table 7-60	LOCA Time Step Study Variables	7-458
Table 7-61	Summary of Bundle Groups in SSTF Parametric Cases	7-471
Table 7-62	SSTF Central Bundle Grouping (Base Case, 13 Groups, T026_y52) and Bundles in Counter-Current Flow	7-474
Table 7-63	SSTF Central Bundle Grouping for Case T026_y53 and Bundles in Counter-Current Flow.....	7-491
Table 7-64	SSTF Central Bundle Grouping for Case T026_y54 and Bundles in Counter-Current Flow.....	7-504
Table 7-65	SSTF Central Bundle Grouping for Case T026_y55 and Bundles in Counter-Current Flow.....	7-516
Table 7-66	SSTF Central Bundle Grouping for Case T026_y48 and Bundles in Counter-Current Flow.....	7-525

This document contains a total of 730 pages.

Figures

	<u>Page</u>
Figure 6-1	Example Axial Power Distributions.....6-3
Figure 6-2	External Data Transfer to AURORA-B LOCA EM.....6-26
Figure 6-3	Overview of Reactor Vessel Nodalization (Jet-Pump Plant)6-31
Figure 6-4	Typical Nodalization of Downcomer and Mid-Vessel Region (Jet-Pump Plant)6-32
Figure 6-5	Azimuthal Nodalization of Lower Downcomer Region (Jet-Pump Plant)6-33
Figure 6-6	Nodalization of Lower Vessel Region (Jet-Pump Plant)6-34
Figure 6-7	Nodalization of Upper Vessel Region (Jet-Pump Plant)6-35
Figure 6-8	Nodalization of Core and Bypass Region6-40
Figure 6-9	Nodalization of Recirculation Lines6-43
Figure 6-10	Hot Channel Model6-48
Figure 6-11	Halden Centerline Temperature Upper Bound6-51
Figure 6-12	Relocation Packing Factor Data and Bounds6-56
Figure 6-13	Limiting Strain Cases6-56
Figure 6-14	ORNL MRBT 8x8 Assembly Rupture6-57
Figure 6-15	Sketch of Boiling Curve.....6-62
Figure 6-16	Schematic of Heat Transfer Regime Selection Logic6-63
Figure 6-17	Appendix K Heat Transfer Lockout Logic During Blowdown.....6-66
Figure 6-18	Functional Behavior of Groeneveld-Stewart T _{min} Correlation.....6-73
Figure 6-19	Functional Behavior of Groeneveld-Stewart T _{min} Correlation at P < 2 MPa6-73
Figure 6-20	Calculated and Measured T _{min}6-74
Figure 6-21	T _{min} versus Steam Quality at 2 MPa6-74
Figure 6-22	Calculated versus Measured T _{min}6-75
Figure 6-23	Bromley Correlation Attenuation versus Void Fraction in S-RELAP5.....6-79
Figure 6-24	Bromley HTC with Helmholtz and Taylor Characteristic Length, 14.7 and 292 psia6-80
Figure 6-25	Comparison of Saturated Film Boiling Data with Modified Bromley Correlation6-81
Figure 6-26	Heat Transfer Coefficient for Transition and Film Boiling at 60 psi6-82
Figure 6-27	KWU Reflood Data Compared to Modified Bromley Correlation.....6-82

Figure 6-28	Comparison of Measured Heat Transfer Coefficients with Various Correlations for TLTA Test 4914, Run 8.....	6-83
Figure 6-29	Dispersed Film Boiling Calculated versus Measured HTC for Steady State THTF Tests.....	6-83
Figure 7-1	Calculated vs. Measured Results for all FRIGG2 Void Fraction Tests.....	7-10
Figure 7-2	Calculated vs. Measured Results for all FRIGG3 Void Fraction Tests.....	7-11
Figure 7-3	Calculated vs. Measured Results for all ATRIUM-10A Void Fraction Tests.....	7-12
Figure 7-4	Calculated vs. Measured Results for all Christensen Tests.....	7-16
Figure 7-5	Christensen Tests at 600 psia with varying Subcooling.....	7-17
Figure 7-6	Calculated vs. Measured Results for all 2.9 Inch Diameter Void Fraction Allis-Chalmers Tests.....	7-22
Figure 7-7	Calculated vs. Measured Results for all 18 Inch Diameter Void Fraction Allis-Chalmers Tests.....	7-23
Figure 7-8	Calculated vs. Measured Results for all 36 Inch Diameter Void Fraction Allis-Chalmers Tests.....	7-24
Figure 7-9	GE Small Blowdown Vessel.....	7-27
Figure 7-10	Nodalization for 1 ft GE Test 1004-3.....	7-28
Figure 7-11	Predicted Void Fraction for GE 1ft 1004-3 at 40 Seconds.....	7-29
Figure 7-12	Predicted Void Fraction for GE 1ft 1004-3 Test at 100 Seconds.....	7-29
Figure 7-13	Schematic of THTF.....	7-36
Figure 7-14	Diagram of THTF Test Section.....	7-37
Figure 7-15	Cross-Section View of THTF Test Section.....	7-38
Figure 7-16	Axial Locations of Thermocouples in THTF Test Section.....	7-39
Figure 7-17	Map of Rods in THTF Simulated Fuel Bundle.....	7-40
Figure 7-18	Cross-Sectional View of THTF Simulated Fuel Rod.....	7-41
Figure 7-19	S-RELAP5 Nodalization of ORNL THTF for Level Swell Test.....	7-42
Figure 7-20	Calculated and Reported Void Fraction for THTF Test DD.....	7-43
Figure 7-21	Calculated and Reported Void Fraction for THTF Test I.....	7-43
Figure 7-22	Calculated and Reported Void Fraction for THTF Test J.....	7-44
Figure 7-23	Calculated and Reported Void Fraction for THTF Test K.....	7-44
Figure 7-24	Calculated and Reported Void Fraction for THTF Test M.....	7-45
Figure 7-25	Calculated and Reported Void Fraction for THTF Test N.....	7-45
Figure 7-26	Calculated and Reported Temperature THTF Test I.....	7-46

Figure 7-27	Calculated and Reported Temperature THTF Test J.....	7-46
Figure 7-28	Calculated and Reported Temperature THTF Test K.....	7-47
Figure 7-29	Calculated and Reported Temperature THTF Test M.....	7-47
Figure 7-30	Calculated and Reported Temperature THTF Test N.....	7-48
Figure 7-31	TLTA System Configuration 5.....	7-55
Figure 7-32	Elevation Scaling Comparison BWR/6 vs. TLTA.....	7-56
Figure 7-33	TLTA System Configuration 5A.....	7-57
Figure 7-34	Nodalization of TLTA-5A.....	7-58
Figure 7-35	Comparison of the Measured and Predicted Downcomer Void Fractions for TLTA Boil-Off Test 6441-6.....	7-59
Figure 7-36	Comparison of the Measured and Predicted Bypass Void Fractions for TLTA Boil-Off Test 6441-6.....	7-59
Figure 7-37	Comparison of the Measured and Predicted Bundle Void Fractions at DP Cell Location 27 for TLTA Boil-Off Test 6441-6.....	7-60
Figure 7-38	Comparison of the Measured and Predicted Bundle Void Fractions at DP Cell Location 28 for TLTA Boil-Off Test 6441-6.....	7-60
Figure 7-39	Comparison of the Measured and Predicted Bundle Void Fractions at DP Cell Location 29 for TLTA Boil-Off Test 6441-6.....	7-61
Figure 7-40	Comparison of the Measured and Predicted Bundle Void Fractions at DP Cell Location 30 for TLTA Boil-Off Test 6441-6.....	7-61
Figure 7-41	Comparison of the Measured and Predicted Bundle Void Fractions at DP Cell Location 31 for TLTA Boil-Off Test 6441-6.....	7-62
Figure 7-42	Comparison of the Measured and Predicted Cladding Temperatures at 107" Elevation for TLTA Boil-Off Test 6441-6.....	7-62
Figure 7-43	Comparison of the Measured and Predicted Cladding Temperatures at 115" Elevation for TLTA Boil-Off Test 6441-6.....	7-63
Figure 7-44	Comparison of the Measured and Predicted Cladding Temperatures at 120" Elevation for TLTA Boil-Off Test 6441-6.....	7-63
Figure 7-45	Comparison of the Measured and Predicted Cladding Temperatures at 130" Elevation for TLTA Boil-Off Test 6441-6.....	7-64
Figure 7-46	Comparison of the Measured and Predicted Cladding Temperatures at 135" Elevation for TLTA Boil-Off Test 6441-6.....	7-64
Figure 7-47	Comparison of the Measured and Predicted Cladding Temperatures at 140" and 143" Elevation for TLTA Boil-Off Test 6441-6.....	7-65
Figure 7-48	Comparison of the Measured and Predicted Downcomer Void Fractions for TLTA Boil-Off Test 6441-7.....	7-65
Figure 7-49	Comparison of the Measured and Predicted Bypass Void Fractions for TLTA Boil-Off Test 6441-7.....	7-66

Figure 7-50	Comparison of the Measured and Predicted Bundle Void Fractions at DP Cell Location 27 for TLTA Boil-Off Test 6441-7	7-66
Figure 7-51	Comparison of the Measured and Predicted Bundle Void Fractions at DP Cell Location 28 for TLTA Boil-Off Test 6441-7	7-67
Figure 7-52	Comparison of the Measured and Predicted Bundle Void Fractions at DP Cell Location 29 for TLTA Boil-Off Test 6441-7	7-67
Figure 7-53	Comparison of the Measured and Predicted Bundle Void Fractions at DP Cell Location 30 for TLTA Boil-Off Test 6441-7	7-68
Figure 7-54	Comparison of the Measured and Predicted Bundle Void Fractions at DP Cell Location 31 for TLTA Boil-Off Test 6441-7	7-68
Figure 7-55	Comparison of the Measured and Predicted Cladding Temperatures at 107" Elevation for TLTA Boil-Off Test 6441-7	7-69
Figure 7-56	Comparison of the Measured and Predicted Cladding Temperatures at 115" Elevation for TLTA Boil-Off Test 6441-7	7-69
Figure 7-57	Comparison of the Measured and Predicted Cladding Temperatures at 120" Elevation for TLTA Boil-Off Test 6441-7	7-70
Figure 7-58	Comparison of the Measured and Predicted Cladding Temperatures at 130" Elevation for TLTA Boil-Off Test 6441-7	7-70
Figure 7-59	Comparison of the Measured and Predicted Cladding Temperatures at 135" Elevation for TLTA Boil-Off Test 6441-7	7-71
Figure 7-60	Comparison of the Measured and Predicted Cladding Temperatures at 140" Elevation for TLTA Boil-Off Test 6441-7	7-71
Figure 7-61	Diagram of Test Section and Flange Arrangement for the Bennett Heated Tube Tests	7-75
Figure 7-62	Arrangement of Thermocouples for the Bennett Heated Tube Tests	7-76
Figure 7-63	Nodalization for the Bennett Heated Tube Tests	7-77
Figure 7-64	Wall Temperature Profiles - Bennett Test 5358	7-78
Figure 7-65	Wall Temperature Profiles - Bennett Test 5379	7-78
Figure 7-66	THTF Calculated versus Measured HTC	7-81
Figure 7-67	THTF Calculated versus Measured HTC for All Data	7-81
Figure 7-68	Diagram of FCTF Test Section	7-88
Figure 7-69	FCTF Test 64 Average Rod Model Surface Temperatures at 65-in	7-89
Figure 7-70	FCTF Test 64 Average Rod Model Surface Temperatures at 75-in	7-89
Figure 7-71	FCTF Test 64 Average Rod Model Surface Temperatures at 85-in	7-90
Figure 7-72	FCTF Test 64 Average Power Rod Surface Temperatures for the All Rod Model	7-90

Figure 7-73	FCTF Test 64 Peak Power Rod Surface Temperatures at Mid-plane with Radiation.....	7-91
Figure 7-74	FCTF Test 63 Average Rod Surface Temperatures at 65-in	7-91
Figure 7-75	FCTF Test 63 Average Rod Surface Temperatures at 75-in	7-92
Figure 7-76	FCTF Test 63 Average Rod Surface Temperatures at 85-in	7-92
Figure 7-77	FCTF Test 66 Average Rod Surface Temperatures at 65-in	7-93
Figure 7-78	FCTF Test 66 Average Rod Surface Temperatures at 75-in	7-93
Figure 7-79	FCTF Test 66 Average Rod Surface Temperatures at 85-in	7-94
Figure 7-80	FCTF Test 66 Average Rod Surface Temperatures for Insulated Channels at 75-in.....	7-94
Figure 7-81	FCTF Test 79 Average Rod Surface Temperatures at 65-in	7-95
Figure 7-82	FCTF Test 79 Average Rod Surface Temperatures at 75-in	7-95
Figure 7-83	FCTF Test 79 Average Rod Surface Temperatures at 85-in	7-96
Figure 7-84	FCTF Test 29 Average Rod Surface Temperatures at 65-in	7-96
Figure 7-85	FCTF Test 29 Average Rod Surface Temperatures at 75-in	7-97
Figure 7-86	FCTF Test 29 Average Rod Surface Temperatures at 85-in	7-97
Figure 7-87	S-RELAP5 Nodalization of ORNL THTF for Reflood Tests	7-101
Figure 7-88	Temperatures at Level G, THTF Test 3.02.10C, 400 psia, 6.5 in/sec	7-102
Figure 7-89	Temperatures at Level G, THTF Test 3.02.10D, 600 psia, 5.6 in/sec	7-102
Figure 7-90	Temperatures at Level G, THTF Test 3.02.10E, 605 psia, 5.4 in/sec	7-103
Figure 7-91	Temperatures at Level G, THTF Test 3.02.10F, 1006 psia, 1.1 in/sec	7-103
Figure 7-92	Temperatures at Level G, THTF Test 3.02.10G, 989 psia, 2.8 in/sec	7-104
Figure 7-93	Temperatures at Level G, THTF Test 3.02.10H, 303 psia, 2.2 in/sec	7-104
Figure 7-94	Temperatures at Level G, THTF Test 3.09.10O, 563 psia, 4.8 in/sec	7-105
Figure 7-95	Temperatures at Level G, THTF Test 3.09.10P, 621 psia, 3.6 in/sec	7-105
Figure 7-96	Temperatures at Level G, THTF Test 3.09.10Q, 573 psia, 2.3 in/sec	7-106
Figure 7-97	Temperatures at Level G, THTF Test 3.09.10R, 1065 psia, 4.6 in/sec	7-106

Figure 7-98	Temperatures at Level G, THTF Test 3.09.10S, 1092 psia, 4.0 in/sec	7-107
Figure 7-99	FLECHT-SEASET Bundle Cross Section.....	7-112
Figure 7-100	FLECHT Skewed Bundle Cross Section	7-113
Figure 7-101	FLECHT-SEASET Axial Power Profile*	7-114
Figure 7-102	FLECHT Skewed Axial Power Profile*	7-114
Figure 7-103	FLECHT-SEASET / Flecht Skewed Bundle Axial Nodalization.....	7-115
Figure 7-104	Heater - Rod Surface Temperatures at 78 in, FLECHT-SEASET Test 31302.....	7-116
Figure 7-105	Heater - Rod Surface Temperatures at 78 in, FLECHT-SEASET Test 31504.....	7-116
Figure 7-106	Heater - Rod Surface Temperatures at 78 in, FLECHT-SEASET Test 31701.....	7-117
Figure 7-107	Heater - Rod Surface Temperatures at 78 in, FLECHT-SEASET Test 31805.....	7-117
Figure 7-108	Heater - Rod Surface Temperatures at 78 in, FLECHT-SEASET Test 32013.....	7-118
Figure 7-109	Heater - Rod Surface Temperatures at 78 in, FLECHT-SEASET Test 34209.....	7-118
Figure 7-110	Heater - Rod Surface Temperatures at 60 in, FLECHT Skewed Test 13609.....	7-119
Figure 7-111	Heater - Rod Surface Temperatures at 60 in, FLECHT Skewed Test 13914.....	7-119
Figure 7-112	Heater - Rod Surface Temperatures at 90 in, FLECHT-SEASET Test 31203.....	7-120
Figure 7-113	Heater - Rod Surface Temperatures at 90 in, FLECHT-SEASET Test 31302.....	7-120
Figure 7-114	Heater - Rod Surface Temperatures at 90 in, FLECHT-SEASET Test 31504.....	7-121
Figure 7-115	Heater - Rod Surface Temperatures at 90 in, FLECHT-SEASET Test 31701.....	7-121
Figure 7-116	Heater - Rod Surface Temperatures at 90 in, FLECHT-SEASET Test 31805.....	7-122
Figure 7-117	Heater - Rod Surface Temperatures at 90 in, FLECHT-SEASET Test 32013.....	7-122
Figure 7-118	Heater - Rod Surface Temperatures at 90 in, FLECHT-SEASET Test 34209.....	7-123
Figure 7-119	Heater - Rod Surface Temperatures at 84 in, FLECHT Skewed Test 13609.....	7-123

Figure 7-120	Heater - Rod Surface Temperatures at 84 in, FLECHT Skewed Test 13914.....	7-124
Figure 7-121	Heater - Rod Surface Temperatures at 111 in, FLECHT-SEASET Test 31203.....	7-124
Figure 7-122	Heater - Rod Surface Temperatures at 111 in, FLECHT-SEASET Test 31302.....	7-125
Figure 7-123	Heater - Rod Surface Temperatures at 111 in, FLECHT-SEASET Test 31504.....	7-125
Figure 7-124	Heater - Rod Surface Temperatures at 111 in, FLECHT-SEASET Test 31701.....	7-126
Figure 7-125	Heater - Rod Surface Temperatures at 111 in, FLECHT-SEASET Test 31805.....	7-126
Figure 7-126	Heater - Rod Surface Temperatures at 111 in, FLECHT-SEASET Test 32013.....	7-127
Figure 7-127	Heater - Rod Surface Temperatures at 111 in, FLECHT-SEASET Test 34209.....	7-127
Figure 7-128	Heater - Rod Surface Temperatures at 108 in, FLECHT Skewed Test 13609.....	7-128
Figure 7-129	Heater - Rod Surface Temperatures at 108 in, FLECHT Skewed Test 13914.....	7-128
Figure 7-130	Maximum Cladding Temperature at All Measured Elevations, FLECHT-SEASET Test 31203.....	7-129
Figure 7-131	Maximum Cladding Temperature at All Measured Elevations, FLECHT-SEASET Test 31302.....	7-129
Figure 7-132	Maximum Cladding Temperature at All Measured Elevations, FLECHT-SEASET Test 31504.....	7-130
Figure 7-133	Maximum Cladding Temperature at All Measured Elevations, FLECHT-SEASET Test 31701.....	7-130
Figure 7-134	Maximum Cladding Temperature at All Measured Elevations, FLECHT-SEASET Test 31805.....	7-131
Figure 7-135	Maximum Cladding Temperature at All Measured Elevations, FLECHT-SEASET Test 32013.....	7-131
Figure 7-136	Maximum Cladding Temperature at All Measured Elevations, FLECHT-SEASET Test 34209.....	7-132
Figure 7-137	Maximum Cladding Temperature at All Measured Elevations, FLECHT Skewed Test 13609.....	7-132
Figure 7-138	Maximum Cladding Temperature at All Measured Elevations, FLECHT Skewed Test 13914.....	7-133
Figure 7-139	Heater-Rod Surface Temperatures Steam Cooling FLECHT-SEASET Test 33056.....	7-133

Figure 7-140	Comparison of Rod Surface Temperature for High Power Bundle at 1.830 m Elevation, CCTF Test Run 54.....	7-137
Figure 7-141	Comparison of Rod Surface Temperature for High Power Bundle at 2.035 m Elevation, CCTF Test Run 54.....	7-137
Figure 7-142	Comparison of Peak Surface Temperature vs. Elevation for High Power Bundle, CCTF Test Run 54.....	7-138
Figure 7-143	Comparison of Rod Surface Temperature for High Power Bundle at 1.830 m Elevation, CCTF Test Run 62.....	7-138
Figure 7-144	Comparison of Rod Surface Temperature for High Power Bundle at 2.035 m Elevation, CCTF Test Run 62.....	7-139
Figure 7-145	Comparison of Peak Surface Temperature vs. Elevation for High Power Bundle, CCTF Test Run 62.....	7-139
Figure 7-146	Comparison of Rod Surface Temperature for High Power Bundle at 1.830 m Elevation, CCTF Test Run 67.....	7-140
Figure 7-147	Comparison of Rod Surface Temperature for High Power Bundle at 2.035 m Elevation, CCTF Test Run 67.....	7-140
Figure 7-148	Comparison of Peak Surface Temperature vs. Elevation for High Power Bundle, CCTF Test Run 67.....	7-141
Figure 7-149	Comparison of Rod Surface Temperature for High Power Bundle at 1.830 m Elevation, CCTF Test Run 68.....	7-141
Figure 7-150	Comparison of Rod Surface Temperature for High Power Bundle at 2.035 m Elevation, CCTF Test Run 68.....	7-142
Figure 7-151	Comparison of Peak Surface Temperature vs. Elevation for High Power Bundle, CCTF Test Run 68.....	7-142
Figure 7-152	Marviken Test Facility Diagram	7-147
Figure 7-153	Marviken Test Nozzles Dimensions	7-148
Figure 7-154	Typical Temperature Profile Specification for Marviken Tests	7-149
Figure 7-155	Nodalization for Marviken Tests	7-150
Figure 7-156	Break Mass Flow at the Nozzle Entrance, Marviken Test 2 – []	7-151
Figure 7-157	Break Mass Flow at the Nozzle Entrance, Marviken Test 6 – []	7-151
Figure 7-158	Comparison of Measured and Predicted Mass Fluxes [] for all Nine Marviken Tests	7-152
Figure 7-159	Break Mass Flow at the Nozzle Entrance, Marviken Test 2 – []	7-152
Figure 7-160	Break Mass Flow at the Nozzle Entrance, Marviken Test 6 – []	7-153

Figure 7-161	Comparison of Measured and Predicted Mass Fluxes [] for all Nine Marviken Tests.....	7-153
Figure 7-162	Lower Plenum Liquid Mass Inventory for UPTF Test 6 Run 135	7-159
Figure 7-163	Lower Plenum Liquid Mass Inventory for UPTF Test 6 Run 131	7-159
Figure 7-164	Lower Plenum Liquid Mass Inventory for UPTF Test 6 Run 132	7-160
Figure 7-165	Lower Plenum Liquid Mass Inventory for UPTF Test 6 Run 133	7-160
Figure 7-166	Lower Plenum Liquid Mass Inventory for UPTF Test 6 Run 136	7-161
Figure 7-167	Lower Plenum Liquid Mass Inventory for UPTF Test 7 Run 203	7-161
Figure 7-168	ECC Penetration Rate to Downcomer for All UPTF Tests 6 and 7	7-162
Figure 7-169	Calculated Kutateladze Parameters UPTF Test 10 Run 080.....	7-162
Figure 7-170	Calculated Downflow Comparison UPTF Test 10 Run 080 ($m=1.0$, $c=1.8$, $\beta=1.0$)	7-163
Figure 7-171	Calculated Kutateladze Parameters UPTF Test 12 Run 014.....	7-163
Figure 7-172	Calculated Downflow Comparison UPTF Test 12 Run 014 ($m=1.0$, $c=1.8$, $\beta=1.0$)	7-164
Figure 7-173	Countercurrent Flow of Steam and Water UPTF Test 10B.....	7-164
Figure 7-174	Water Carryover to Steam Generators UPTF Test 10B.....	7-165
Figure 7-175	Countercurrent Flow of Steam and Water UPTF Test 29B.....	7-165
Figure 7-176	Cumulative Water Carryover to Steam Generators UPTF Test 29B.....	7-166
Figure 7-177	Cumulative Water Fallback to Lower Core UPTF Test 29B.....	7-166
Figure 7-178	Upper Plenum Water Mass UPTF Test 29B.....	7-167
Figure 7-179	Histogram of Relative Error for Pressure Drop Benchmark	7-171
Figure 7-180	Two-Phase Pressure Drop Benchmark	7-171
Figure 7-181	Relative Error vs. Exit Void Fraction for Pressure Drop Benchmark	7-172
Figure 7-182	N-M Plot of 1/6 Scale Jet-Pump Results	7-179
Figure 7-183	Alternate Plot of 1/6 Scale Jet-Pump Results.....	7-179
Figure 7-184	N-M Plot of Browns Ferry Jet-Pump Results.....	7-180
Figure 7-185	N-M Plot of Columbia Generating Station & LaSalle Jet-Pump Results.....	7-180
Figure 7-186	INL Test 1, Drive Pressure.....	7-181
Figure 7-187	INL Test 1, Drive Pressure Drop	7-181
Figure 7-188	INL Test 1, Suction Pressure Drop.....	7-182
Figure 7-189	INL Test 2, Discharge Pressure	7-182
Figure 7-190	INL Test2, Drive Pressure Drop	7-183
Figure 7-191	INL Test 2, Suction Pressure Drop.....	7-183

Figure 7-192	Carryover Comparison for 2-Stage Separator with Mass Flow Rate of 372,000 lb/hr	7-186
Figure 7-193	Carryover Comparison for 2-Stage Separator with Mass Flow Rate of 550,000 lb/hr	7-186
Figure 7-194	Carryunder Comparison for 2-Stage Separator with Mass Flow Rate of 372,000 lb/hr	7-187
Figure 7-195	Carryunder Comparison for 2-Stage Separator with Mass Flow Rate of 550,000 lb/hr	7-187
Figure 7-196	Differential Pressure Comparison for 2-Stage Separator.....	7-188
Figure 7-197	Carryover Comparison for 3-Stage Separator with Mass Flow Rate of 355,000 lb/hr	7-188
Figure 7-198	Carryover Comparison for 3-Stage Separator with Mass Flow Rate of 500,000 lb/hr	7-189
Figure 7-199	Carryunder Comparison for 3-Stage Separator with Mass Flow Rate of 355,000 lb/hr	7-189
Figure 7-200	Carryunder Comparison for 3-Stage Separator with Mass Flow Rate of 500,000 lb/hr	7-190
Figure 7-201	Differential Pressure Comparison for 3-Stage Separator.....	7-190
Figure 7-202	ATRIUM-10 Upper Tie Plate CCFL	7-194
Figure 7-203	ATRIUM-10 Grid Spacer CCFL.....	7-194
Figure 7-204	Thirty-degree Steam Section Test Facility.....	7-207
Figure 7-205	SSTF Test Section Schematic	7-208
Figure 7-206	SSTF Nodalization	7-209
Figure 7-207	SSTF Bundle Nodalization	7-210
Figure 7-208	SSTF Bundle Grouping	7-211
Figure 7-209	SSTF Bundle DP Measurements	7-212
Figure 7-210	SSTF Core Spray injection into the UP Volumes (2-Phase Level below the Sparger Elevation)	7-213
Figure 7-211	SSTF BWR/4: Ring 1 Collapsed Levels	7-214
Figure 7-212	SSTF BWR/4: Ring 2 Collapsed Levels	7-214
Figure 7-213	SSTF BWR/4: Ring 3 Collapsed Levels	7-215
Figure 7-214	SSTF BWR/4: Calculated and Measured Ring 3 DPs (F031 vs. B5).....	7-215
Figure 7-215	SSTF BWR/4: Calculated and Measured Ring 2 DPs (F025 vs. B26).....	7-216
Figure 7-216	SSTF BWR/4: Calculated and Measured Ring 2 DPs (F026 vs. B40).....	7-216

Figure 7-217	SSTF BWR/4: Calculated and Measured LP Liquid Temperature in Ring 1	7-217
Figure 7-218	SSTF BWR/4: Calculated and Measured LP Liquid Temperature in Ring 2	7-217
Figure 7-219	SSTF BWR/4: Calculated and Measured LP Liquid Temperature in Ring 3	7-218
Figure 7-220	SSTF BWR/4: Calculated and Measured UP Collapsed Levels in Ring 1	7-218
Figure 7-221	SSTF BWR/4: Calculated and Measured UP Collapsed Levels in Ring 2	7-219
Figure 7-222	SSTF BWR/4: Calculated and Measured UP Collapsed Levels in Ring 3	7-219
Figure 7-223	SSTF BWR/4: Calculated and Measured Liquid Temperature at UP Bottom in Ring 1	7-220
Figure 7-224	SSTF BWR/4: Calculated and Measured Liquid Temperature at UP Bottom in Ring 2	7-220
Figure 7-225	SSTF BWR/4: Calculated and Measured Liquid Temperature at UP Bottom in Ring 3	7-221
Figure 7-226	SSTF BWR/4: Calculated and Measured Liquid Temperature in Apex Bundle (Below UTP)	7-221
Figure 7-227	SSTF BWR/4: Calculated and Measured Liquid Temperature in Peripheral Bundle (Below UTP)	7-222
Figure 7-228	SSTF BWR/6: Ring 1 Collapsed Levels	7-222
Figure 7-229	SSTF BWR/6: Ring 2 Collapsed Levels	7-223
Figure 7-230	SSTF BWR/6: Ring 3 Collapsed Levels	7-223
Figure 7-231	SSTF BWR/6: Calculated and Measured Ring 3 DPs (F031 vs. B5).....	7-224
Figure 7-232	SSTF BWR/6: Calculated and Measured Ring 3 DPs (F031 vs. B4).....	7-224
Figure 7-233	SSTF BWR/6: Calculated and Measured Ring 2 DPs (F025 vs. B26).....	7-225
Figure 7-234	SSTF BWR/6: Calculated and Measured Ring 2 DPs (F022 vs. B12).....	7-225
Figure 7-235	SSTF BWR/6: Calculated and Measured Ring 2 DPs (F026 vs. B40).....	7-226
Figure 7-236	SSTF BWR/6: Calculated and Measured Ring 1 DPs (F013 vs. B54).....	7-226
Figure 7-237	SSTF BWR/6: Calculated and Measured UP Collapsed Levels in Ring 1	7-227

Figure 7-238	SSTF BWR/6: Calculated and Measured UP Collapsed Levels in Ring 2	7-227
Figure 7-239	SSTF BWR/6: Calculated and Measured UP Collapsed Levels in Ring 3	7-228
Figure 7-240	SSTF BWR/6: Calculated and Measured Liquid Temperature at UP Bottom in Ring 1	7-228
Figure 7-241	SSTF BWR/6: Calculated and Measured Liquid Temperature at UP Bottom in Ring 2	7-229
Figure 7-242	SSTF BWR/6: Calculated and Measured Liquid Temperature at UP Bottom in Ring 3	7-229
Figure 7-243	SSTF BWR/6: Calculated and Measured Liquid Temperatures in Apex Bundle (Below UTP)	7-230
Figure 7-244	SSTF BWR/6: Calculated and Measured Liquid Temperatures in Peripheral Bundle (Below UTP)	7-230
Figure 7-245	Broken Loop Jet Pump Exit Flow Rate – TLTA Test 6425-2	7-237
Figure 7-246	Broken Loop Jet Pump Exit Flow Rate (Expanded) – TLTA Test 6425-2	7-237
Figure 7-247	Suction Side Break Flow Rate – TLTA Test 6425-2	7-238
Figure 7-248	Discharge Side Break Flow Rate – TLTA Test 6425-2	7-238
Figure 7-249	Steam Dome Pressure History – TLTA Test 6425-2	7-239
Figure 7-250	HPCS Flow Rate – TLTA Test 6425-2	7-239
Figure 7-251	LPCI Flow Rate – TLTA Test 6425-2	7-240
Figure 7-252	LPCS Flow Rate – TLTA Test 6425-2	7-240
Figure 7-253	Total ECC Flow Rate – TLTA Test 6425-2	7-241
Figure 7-254	Bundle SEO Flow Rate –TLTA Test 6425-2	7-241
Figure 7-255	Bundle SEO Flow Rate (Expanded) –TLTA Test 6425-2	7-242
Figure 7-256	Intact Loop Jet Pump Exit Flow rate – TLTA Test 6425-2	7-242
Figure 7-257	Steam Line Flow Rate – TLTA Test 6425-2	7-243
Figure 7-258	Annulus Fluid Mass History – TLTA Test 6425-2	7-243
Figure 7-259	Bypass Fluid Mass History – TLTA Test 6425-2	7-244
Figure 7-260	Upper Plenum Fluid Mass History – TLTA Test 6425-2	7-244
Figure 7-261	Bundle Fluid Mass History – TLTA Test 6425-2	7-245
Figure 7-262	Lower Plenum Fluid Mass History – TLTA Test 6425-2	7-245
Figure 7-263	Guide Tube Fluid Mass History – TLTA Test 6425-2	7-246
Figure 7-264	Total Fluid Mass History – TLTA Test 6425-2	7-246
Figure 7-265	Bundle Exit Flow Rate – TLTA Test 6425-2	7-247

Figure 7-266	Bypass Exit Flow Rate – TLTA Test 6425-2.....	7-247
Figure 7-267	Comparison of Measured and Predicted Heater Wall Temperatures, 10 inch Elevation – TLTA Test 6425-2	7-248
Figure 7-268	Comparison of Measured and Predicted Heater Wall Temperatures, 35 inch Elevation – TLTA Test 6425-2	7-248
Figure 7-269	Comparison of Measured and Predicted Heater Wall Temperatures, 50 inch Elevation – TLTA Test 6425-2	7-249
Figure 7-270	Comparison of Measured and Predicted Heater Wall Temperatures, 71 inch Elevation – TLTA Test 6425-2	7-249
Figure 7-271	Comparison of Measured and Predicted Heater Wall Temperatures, 90 inch Elevation – TLTA Test 6425-2	7-250
Figure 7-272	Comparison of Measured and Predicted Heater Wall Temperatures, 100 inch Elevation – TLTA Test 6425-2	7-250
Figure 7-273	Comparison of Measured and Predicted Heater Wall Temperatures, 107 inch Elevation – TLTA Test 6425-2	7-251
Figure 7-274	Comparison of Measured and Predicted Heater Wall Temperatures, 120 inch Elevation – TLTA Test 6425-2	7-251
Figure 7-275	Comparison of Measured and Predicted Heater Wall Temperatures, 130 inch Elevation – TLTA Test 6425-2	7-252
Figure 7-276	Comparison of Measured and Predicted Heater Wall Temperatures, 140 inch Elevation – TLTA Test 6425-2	7-252
Figure 7-277	Comparison of Measured and Predicted Peak Cladding Temperature (PCT) – TLTA Test 6425-2	7-253
Figure 7-278	Predicted Heater Wall Temperature Histories at Different Elevations – TLTA Test 6425-2.....	7-253
Figure 7-279	Schematic of TLTA Configuration 5C	7-257
Figure 7-280	S-RELAP5 Nodalization of TLTA Configuration 5C	7-258
Figure 7-281	Predicted Total Break Flow Rate – TLTA Test 6432-1	7-259
Figure 7-282	Comparison of Predicted and Measured ADS Flow Rate – TLTA Test 6432-1.....	7-259
Figure 7-283	Comparison of Predicted and Measured Steam Dome Pressure- TLTA Test 6432-1	7-260
Figure 7-284	Comparison of Predicted and Measured LPCI Flow Rate – TLTA Test 6432-1.....	7-260
Figure 7-285	Comparison of Predicted and Measured LPCS Flow Rate – TLTA Test 6432-1.....	7-261
Figure 7-286	Comparison of Predicted and Measured Bundle Mass – TLTA Test 6432-1.....	7-261

Figure 7-287	Comparison of Predicted and Measured Bypass Mass – TLTA Test 6432-1.....	7-262
Figure 7-288	Comparison of Predicted and Measured Lower Plenum Mass – TLTA Test 6432-1	7-262
Figure 7-289	Comparison of Predicted and Measured Upper Plenum Mass – TLTA Test 6432-1	7-263
Figure 7-290	Comparison of Predicted and Measured Annulus Mass – TLTA Test 6432-1.....	7-263
Figure 7-291	Comparison of Predicted and Measured Guide Tube Mass – TLTA Test 6432-1.....	7-264
Figure 7-292	Comparison of Predicted and Measured Total Vessel Mass – TLTA Test 6432-1	7-264
Figure 7-293	Comparison of Measured and Predicted Heater Wall Temperatures, 10 inch Elevation – TLTA Test 6432-1	7-265
Figure 7-294	Comparison of Measured and Predicted Heater Wall Temperatures, 63 inch Elevation – TLTA Test 6432-1	7-265
Figure 7-295	Comparison of Measured and Predicted Heater Wall Temperatures, 103 inch Elevation – TLTA Test 6432-1	7-266
Figure 7-296	Comparison of Measured and Predicted Heater Wall Temperatures, 120 inch Elevation – TLTA Test 6432-1	7-266
Figure 7-297	Comparison of Measured and Predicted Heater Wall Temperatures, 143 inch Elevation – TLTA Test 6432-1	7-267
Figure 7-298	FIST Vessel Nodalization.....	7-273
Figure 7-299	FIST Broken Recirculation Loop Nodalization	7-274
Figure 7-300	Steam Dome Pressure – FIST Test 6DBA1	7-280
Figure 7-301	Steam Dome Pressure (to 50 sec) – FIST Test 6DBA1.....	7-280
Figure 7-302	Predicted Lower Plenum Void Fractions – FIST Test 6DBA1	7-281
Figure 7-303	Lower Downcomer Void Fraction – FIST Test 6DBA1	7-281
Figure 7-304	Predicted Suction Side Break Flow Rate – FIST Test 6DBA1	7-282
Figure 7-305	Predicted Discharge Side Break Flow Rate – FIST Test 6DBA1	7-282
Figure 7-306	ADS Flow – FIST Test 6DBA1	7-283
Figure 7-307	Core Inlet Flow Rate – FIST Test 6DBA1.....	7-283
Figure 7-308	Core Inlet Flow Rate (Expanded) – FIST Test 6DBA1	7-284
Figure 7-309	Jet Pump 1 Exit Flow Rate – FIST Test 6DBA1	7-284
Figure 7-310	Jet Pump 1 Exit Flow Rate (Expanded) – FIST Test 6DBA1	7-285
Figure 7-311	Jet Pump 2 Exit Flow Rate (Expanded) – FIST Test 6DBA1	7-285
Figure 7-312	Mass of Fluid in Upper Plenum – FIST Test 6DBA1.....	7-286

Figure 7-313	Mass of Fluid in Bypass – FIST Test 6DBA1	7-286
Figure 7-314	Mass of Fluid in Bundle – FIST Test 6DBA1	7-287
Figure 7-315	Mass of Fluid in Intact Loop Jet Pump – FIST Test 6DBA1	7-287
Figure 7-316	Mass of Fluid in Broken Loop Jet Pump – FIST Test 6DBA1	7-288
Figure 7-317	Total Mass of Fluid in the Vessel – FIST Test 6DBA1	7-288
Figure 7-318	Void Fraction in Bundle Near 37 in. Elevation – FIST Test 6DBA1	7-289
Figure 7-319	Void Fraction in Bundle Near 57 in. Elevation – FIST Test 6DBA1	7-289
Figure 7-320	Void Fraction in Bundle Near 117 in. Elevation – FIST Test 6DBA1	7-290
Figure 7-321	Heater Midpoint Elevation Surface Temperature – FIST Test 6DBA1	7-290
Figure 7-322	Peak Temperature Node History – FIST Test 6DBA1	7-291
Figure 7-323	Void Fraction in Bypass Near 37 in. Elevation – FIST Test 6DBA1	7-291
Figure 7-324	Void Fraction in Bypass Near 71 in. Elevation – FIST Test 6DBA1	7-292
Figure 7-325	Void Fraction in Bypass Near 117 in. Elevation – FIST Test 6DBA1	7-292
Figure 7-326	Void Fraction in Lower Plenum Upper – FIST Test 6DBA1	7-293
Figure 7-327	Upper Plenum Pressure – FIST Test 6SB2C	7-300
Figure 7-328	Lower Plenum Pressure – FIST Test 6SB2C	7-300
Figure 7-329	Bundle Pressure – FIST Test 6SB2C	7-301
Figure 7-330	Steam Line Pressure – FIST Test 6SB2C	7-301
Figure 7-331	Measured and Predicted ADS Flow Rates – FIST Test 6SB2C	7-302
Figure 7-332	Bundle Pressure Drop – FIST Test 6SB2C	7-302
Figure 7-333	Bypass Pressure Drop – FIST Test 6SB2C	7-303
Figure 7-334	Total Downcomer Pressure Drop – FIST Test 6SB2C	7-303
Figure 7-335	Mass of Fluid in Bundle – FIST Test 6SB2C	7-304
Figure 7-336	Mass of Fluid in Bypass – FIST Test 6SB2C	7-304
Figure 7-337	Mass of Fluid in Intact Loop Jet Pump – FIST Test 6SB2C	7-305
Figure 7-338	Mass of Fluid in Broken Loop Jet Pump – FIST Test 6SB2C	7-305
Figure 7-339	Mass of Fluid in Lower Plenum above Jet Pump Exit – FIST Test 6SB2C	7-306
Figure 7-340	Mass of Fluid in Lower Plenum below Jet Pump Exit – FIST Test 6SB2C	7-306
Figure 7-341	Total Fluid Mass in Vessel – FIST Test 6SB2C	7-307
Figure 7-342	Mass of Fluid in Upper Plenum – FIST Test 6SB2C	7-307

Figure 7-343	Predicted Bundle and Bypass to Upper Plenum Flow Rate – FIST Test 6SB2C	7-308
Figure 7-344	Void Fraction in Bundle near 37" Elevation – FIST Test 6SB2C	7-308
Figure 7-345	Void Fraction in Bundle near 57" Elevation – FIST Test 6SB2C	7-309
Figure 7-346	Void Fraction in Bundle near 117" Elevation – FIST Test 6SB2C	7-309
Figure 7-347	Predicted Bundle to Bypass Leakage Flow Rate – FIST Test 6SB2C	7-310
Figure 7-348	Bundle Inlet Flow Rate – FIST Test 6SB2C	7-310
Figure 7-349	Bundle Inlet Flow Rate (Expanded) – FIST Test 6SB2C	7-311
Figure 7-350	Lower Plenum (Upper Section) Void Fraction – FIST Test 6SB2C	7-311
Figure 7-351	Heater Midpoint Temperature – FIST Test 6SB2C	7-312
Figure 7-352	Heater Midpoint Average Temperature – FIST Test 6SB2C	7-312
Figure 7-353	Peak Temperature Node History – FIST Test 6SB2C	7-313
Figure 7-354	Void Fraction in Bypass near 37" Elevation – FIST Test 6SB2C	7-313
Figure 7-355	Void Fraction in Bypass near 71" Elevation – FIST Test 6SB2C	7-314
Figure 7-356	Void Fraction in Bypass near 117" Elevation – FIST Test 6SB2C	7-314
Figure 7-357	Upper Plenum Liquid and Saturation Temperature – FIST Test 6SB2C	7-315
Figure 7-358	Steam Dome Pressure History – FIST Test 6LB1	7-322
Figure 7-359	Steam Dome Pressure History (Expanded) – FIST Test 6LB1	7-322
Figure 7-360	Bypass Void Fraction at LPCI Line Elevation – FIST Test 6LB1	7-323
Figure 7-361	Lower Plenum Void Fraction near Jet Pump Exit – FIST Test 6LB1	7-323
Figure 7-362	Predicted Void Fractions in all Lower Plenum Nodes – FIST Test 6LB1	7-324
Figure 7-363	LPCS and LPCI Flow Rates – FIST Test 6LB1	7-324
Figure 7-364	Void Fraction at Jet Pump Exit – FIST Test 6LB1	7-325
Figure 7-365	Upper Plenum Pressure History – FIST Test 6LB1	7-325
Figure 7-366	Lower Plenum Pressure History – FIST Test 6LB1	7-326
Figure 7-367	Bundle Pressure History – FIST Test 6LB1	7-326
Figure 7-368	Steam Line Pressure History – FIST Test 6LB1	7-327
Figure 7-369	Steam Line Flow Rate – FIST Test 6LB1	7-327
Figure 7-370	ADS Flow Rate – FIST Test 6LB1	7-328
Figure 7-371	Void in Bundle at 37" Elevation – FIST Test 6LB1	7-328
Figure 7-372	Void in Bundle at 57" Elevation – FIST Test 6LB1	7-329
Figure 7-373	Void in Bundle at 117" Elevation – FIST Test 6LB1	7-329

Figure 7-374	Bundle Pressure Drop – FIST Test 6LB1	7-330
Figure 7-375	Mass of Fluid in Bundle – FIST Test 6LB1	7-330
Figure 7-376	Void in Bypass at 37" Elevation – FIST Test 6LB1	7-331
Figure 7-377	Void in Bypass at 71" Elevation – FIST Test 6LB1	7-331
Figure 7-378	Void in Bypass at 117" Elevation – FIST Test 6LB1	7-332
Figure 7-379	Bypass Pressure Drop – FIST Test 6LB1	7-332
Figure 7-380	Mass of Fluid in Bypass – FIST Test 6LB1	7-333
Figure 7-381	Broken Loop Jet Pump Mass – FIST Test 6LB1	7-333
Figure 7-382	Intact Loop Jet Pump Mass – FIST Test 6LB1	7-334
Figure 7-383	Mass of Lower Plenum Above Jet Pump Exit – FIST Test 6LB1	7-334
Figure 7-384	Mass of Lower Plenum Below Jet Pump Exit – FIST Test 6LB1	7-335
Figure 7-385	Upper Plenum Mass – FIST Test 6LB1	7-335
Figure 7-386	Total Mass in Vessel – FIST Test 6LB1	7-336
Figure 7-387	Heater Midpoint Surface Temperature – FIST Test 6LB1	7-336
Figure 7-388	Peak Temperature Node History – FIST Test 6LB1	7-337
Figure 7-389	Bundle to Bypass Leakage Rate – FIST Test 6LB1	7-337
Figure 7-390	Bundle Inlet Flow Rate – FIST Test 6LB1	7-338
Figure 7-391	Liquid Temperature in Upper Plenum Node 1 – FIST Test 6LB1	7-338
Figure 7-392	Steam Dome Pressure History – FIST Test 4DBA1	7-345
Figure 7-393	Steam Dome Pressure (Expanded) – FIST Test 4DBA1	7-345
Figure 7-394	Lower Downcomer Void Fraction – FIST Test 4DBA1	7-346
Figure 7-395	Lower Downcomer Void Fraction (Expanded) – FIST Test 4DBA1	7-346
Figure 7-396	Void Fraction in Lower Plenum in Vicinity of Jet Pump Exit – FIST Test 4DBA1	7-347
Figure 7-397	Predicted Lower Plenum Void Fractions – FIST Test 4DBA1	7-347
Figure 7-398	Void Fractions in Lower Plenum Above Jet Pump Exit – FIST Test 4DBA1	7-348
Figure 7-399	Predicted Void Fractions in Fuel Support and Bundle Node 1– FIST Test 4DBA1	7-348
Figure 7-400	ECC Flow Rates – FIST Test 4DBA1	7-349
Figure 7-401	Upper Plenum Pressure – FIST Test 4DBA1	7-349
Figure 7-402	Lower Plenum Pressure – FIST Test 4DBA1	7-350
Figure 7-403	Bundle Exit Pressure – FIST Test 4DBA1	7-350
Figure 7-404	Steam Line Pressure – FIST Test 4DBA1	7-351
Figure 7-405	Mass of Lower Plenum below Jet Pump Exit – FIST Test 4DBA1	7-351

Figure 7-406	Mass of Lower Plenum above Jet Pump Exit – FIST Test 4DBA1.....	7-352
Figure 7-407	Broken Loop Jet Pump Mass – FIST Test 4DBA1.....	7-352
Figure 7-408	Intact Loop Jet Pump Mass – FIST Test 4DBA1	7-353
Figure 7-409	Void in Bundle near 37 inch Elevation – FIST Test 4DBA1	7-353
Figure 7-410	Void in Bundle near 57 inch Elevation – FIST Test 4DBA1	7-354
Figure 7-411	Void in Bundle near 77 inch Elevation – FIST Test 4DBA1	7-354
Figure 7-412	Void in Bundle near 117 inch Elevation – FIST Test 4DBA1	7-355
Figure 7-413	Mass of Fluid in Bundle – FIST Test 4DBA1	7-355
Figure 7-414	Heater Surface Temperature near 36 inch Elevation – FIST Test 4DBA1	7-356
Figure 7-415	Heater Surface Midpoint Temperature – FIST Test 4DBA1.....	7-356
Figure 7-416	Peak Temperature Node History – FIST Test 4DBA1	7-357
Figure 7-417	Mass of Fluid in Bypass – FIST Test 4DBA1.....	7-357
Figure 7-418	Mass of Fluid in Upper Plenum – FIST Test 4DBA1.....	7-358
Figure 7-419	Total Mass in Vessel – FIST Test 4DBA1	7-358
Figure 7-420	Steam Line Flow Rate – FIST Test 4DBA1	7-359
Figure 7-421	ADS Flow Rate – FIST Test 4DBA1.....	7-359
Figure 7-422	BWR/4 Axial Power Distributions	7-376
Figure 7-423	BWR/4 SBA Upper Plenum Pressure.....	7-377
Figure 7-424	BWR/4 SBA Break Flow Rate	7-377
Figure 7-425	BWR/4 SBA Total Jet Pump Flow	7-378
Figure 7-426	BWR/4 SBA Core Outlet Flow.....	7-378
Figure 7-427	BWR/4 SBA Intact Loop Jet Pump Drive Flow	7-379
Figure 7-428	BWR/4 SBA Intact Loop Jet Pump Suction Flow.....	7-379
Figure 7-429	BWR/4 SBA Intact Loop Jet Pump Exit Flow.....	7-380
Figure 7-430	BWR/4 SBA Broken Loop Jet Pump Drive Flow.....	7-380
Figure 7-431	BWR/4 SBA Broken Loop Jet Pump Suction Flow	7-381
Figure 7-432	BWR/4 SBA Broken Loop Jet Pump Exit Flow	7-381
Figure 7-433	BWR/4 SBA ADS/SRV Flows.....	7-382
Figure 7-434	BWR/4 SBA LPCS Flow.....	7-382
Figure 7-435	BWR/4 SBA HPCI Flow	7-383
Figure 7-436	BWR/4 SBA LPCI Flow.....	7-383
Figure 7-437	BWR/4 SBA Lower Plenum Liquid Mass	7-384
Figure 7-438	BWR/4 SBA Core Channels Liquid Mass.....	7-384

Figure 7-439	BWR/4 SBA Guide Tube Liquid Mass	7-385
Figure 7-440	BWR/4 SBA Bypass Liquid Mass	7-385
Figure 7-441	BWR/4 SBA Upper Plenum Liquid Mass	7-386
Figure 7-442	BWR/4 SBA Jet Pump Exit Liquid Mass	7-386
Figure 7-443	BWR/4 SBA Central Region Peak Node Temperature	7-387
Figure 7-444	BWR/4 LBA Upper Plenum Pressure	7-387
Figure 7-445	BWR/4 LBA Break Flow Rate	7-388
Figure 7-446	BWR/4 LBA Total Jet Pump Flow	7-388
Figure 7-447	BWR/4 LBA Core Outlet Flow	7-389
Figure 7-448	BWR/4 LBA Intact Loop Jet Pump Drive Flow	7-389
Figure 7-449	BWR/4 LBA Intact Loop Jet Pump Suction Flow	7-390
Figure 7-450	BWR/4 LBA Intact Loop Jet Pump Exit Flow	7-390
Figure 7-451	BWR/4 LBA Broken Loop Jet Pump Drive Flow	7-391
Figure 7-452	BWR/4 LBA Broken Loop Jet Pump Suction Flow	7-391
Figure 7-453	BWR/4 LBA Broken Loop Jet Pump Exit Flow	7-392
Figure 7-454	BWR/4 LBA ADS/SRV Flows	7-392
Figure 7-455	BWR/4 LBA LPCS Flow	7-393
Figure 7-456	BWR/4 LBA HPCI Flow	7-393
Figure 7-457	BWR/4 LBA LPCI Flow	7-394
Figure 7-458	BWR/4 LBA Lower Plenum Liquid Mass	7-394
Figure 7-459	BWR/4 LBA Core Channels Liquid Mass	7-395
Figure 7-460	BWR/4 LBA Guide Tube Liquid Mass	7-395
Figure 7-461	BWR/4 LBA Bypass Liquid Mass	7-396
Figure 7-462	BWR/4 LBA Upper Plenum Liquid Mass	7-396
Figure 7-463	BWR/4 LBA Jet Pump Exit Liquid Mass	7-397
Figure 7-464	BWR/4 LBA Central Region Peak Node Temperature	7-397
Figure 7-465	BWR/4 Reduced ECCS Upper Plenum Pressure	7-401
Figure 7-466	BWR/4 Reduced ECCS Break Flow Rate	7-401
Figure 7-467	BWR/4 Reduced ECCS Total Jet Pump Flow	7-402
Figure 7-468	BWR/4 Reduced ECCS Core Outlet Flow	7-402
Figure 7-469	BWR/4 Reduced ECCS ADS/SRV Flows	7-403
Figure 7-470	BWR/4 Reduced ECCS LPCS Flow	7-403
Figure 7-471	BWR/4 Reduced ECCS HPCI Flow	7-404
Figure 7-472	BWR/4 Reduced ECCS LPCI Flow	7-404

Figure 7-473	BWR/4 Reduced ECCS Lower Plenum Liquid Mass	7-405
Figure 7-474	BWR/4 Reduced ECCS Core Channels Liquid Mass	7-405
Figure 7-475	BWR/4 Reduced ECCS Guide Tube Liquid Mass	7-406
Figure 7-476	BWR/4 Reduced ECCS Bypass Liquid Mass	7-406
Figure 7-477	BWR/4 Reduced ECCS Upper Plenum Liquid Mass	7-407
Figure 7-478	BWR/4 Reduced ECCS Jet Pump Exit Liquid Mass	7-407
Figure 7-479	BWR/4 Reduced ECCS Central Region Peak Node Temperature	7-408
Figure 7-480	BWR/6 Mid-Peaked Axial Power Distribution	7-423
Figure 7-481	BWR/6 LBA Upper Plenum Pressure	7-424
Figure 7-482	BWR/6 LBA Break Flow Rate	7-424
Figure 7-483	BWR/6 LBA Total Jet Pump Flow	7-425
Figure 7-484	BWR/6 LBA Core Outlet Flow	7-425
Figure 7-485	BWR/6 LBA Intact Loop Jet Pump Drive Flow	7-426
Figure 7-486	BWR/6 LBA Intact Loop Jet Pump Suction Flow	7-426
Figure 7-487	BWR/6 LBA Intact Loop Jet Pump Exit Flow	7-427
Figure 7-488	BWR/6 LBA Broken Loop Jet Pump Drive Flow	7-427
Figure 7-489	BWR/6 LBA Broken Loop Jet Pump Suction Flow	7-428
Figure 7-490	BWR/6 LBA Broken Loop Jet Pump Exit Flow	7-428
Figure 7-491	BWR/6 LBA ADS/SRV Flows	7-429
Figure 7-492	BWR/6 LBA LPCS Flow	7-429
Figure 7-493	BWR/6 LBA HPCS Flow	7-430
Figure 7-494	BWR/6 LBA LPCI Flow	7-430
Figure 7-495	BWR/6 LBA Lower Plenum Liquid Mass	7-431
Figure 7-496	BWR/6 LBA Core Channels Liquid Mass	7-431
Figure 7-497	BWR/6 LBA Guide Tube Liquid Mass	7-432
Figure 7-498	BWR/6 LBA Bypass Liquid Mass	7-432
Figure 7-499	BWR/6 LBA Upper Plenum Liquid Mass	7-433
Figure 7-500	BWR/6 LBA Jet Pump Exit Liquid Mass	7-433
Figure 7-501	BWR/6 LBA Central Region Peak Node Temperature	7-434
Figure 7-502	BWR/6 SBA Upper Plenum Pressure	7-434
Figure 7-503	BWR/6 SBA Break Flow Rate	7-435
Figure 7-504	BWR/6 SBA Total Jet Pump Flow	7-435
Figure 7-505	BWR/6 SBA Core Outlet Flow	7-436
Figure 7-506	BWR/6 SBA Intact Loop Jet Pump Drive Flow	7-436

Figure 7-507	BWR/6 SBA Intact Loop Jet Pump Suction Flow.....	7-437
Figure 7-508	BWR/6 SBA Intact Loop Jet Pump Exit Flow.....	7-437
Figure 7-509	BWR/6 SBA Broken Loop Jet Pump Drive Flow.....	7-438
Figure 7-510	BWR/6 SBA Broken Loop Jet Pump Suction Flow	7-438
Figure 7-511	BWR/6 SBA Broken Loop Jet Pump Exit Flow	7-439
Figure 7-512	BWR/6 SBA ADS/SRV Flows.....	7-439
Figure 7-513	BWR/6 SBA LPCS Flow.....	7-440
Figure 7-514	BWR/6 SBA HPCS Flow	7-440
Figure 7-515	BWR/6 SBA LPCI Flow	7-441
Figure 7-516	BWR/6 SBA Lower Plenum Liquid Mass	7-441
Figure 7-517	BWR/6 SBA Core Channels Liquid Mass.....	7-442
Figure 7-518	BWR/6 SBA Guide Tube Liquid Mass	7-442
Figure 7-519	BWR/6 SBA Bypass Liquid Mass.....	7-443
Figure 7-520	BWR/6 SBA Upper Plenum Liquid Mass.....	7-443
Figure 7-521	BWR/6 SBA Jet Pump Exit Liquid Mass.....	7-444
Figure 7-522	BWR/6 SBA Central Region Peak Node Temperature	7-444
Figure 7-523	Comparison of Measured and Predicted Heater Wall Temperatures, 19 inch Elevation – TLTA Test 6432-1 with Appendix-K Assumptions	7-448
Figure 7-524	Comparison of Measured and Predicted Heater Wall Temperatures, 63 inch Elevation – TLTA Test 6432-1 with Appendix-K Assumptions	7-448
Figure 7-525	Comparison of Measured and Predicted Heater Wall Temperatures, 83 inch Elevation – TLTA Test 6432-1 with Appendix-K Assumptions	7-449
Figure 7-526	Comparison of Measured and Predicted Heater Wall Temperatures, 100 inch Elevation – TLTA Test 6432-1 with Appendix-K Assumptions	7-449
Figure 7-527	Comparison of Measured and Predicted Heater Wall Temperatures, 120 inch Elevation – TLTA Test 6432-1 with Appendix-K Assumptions	7-450
Figure 7-528	Comparison of Measured and Predicted Heater Wall Temperatures, 143 inch Elevation – TLTA Test 6432-1 with Appendix-K Assumptions	7-450
Figure 7-529	Comparison of Measured and Predicted Peak Cladding Temperature – TLTA Test 6432-1 with Appendix-K Assumptions	7-451
Figure 7-530	Comparison of Measured and Predicted Bundle Mass – TLTA Test 6432-1 with Appendix-K Assumptions	7-451

Figure 7-531	Comparison of Measured and Predicted Upper Plenum Mass – TLTA Test 6432-1 with Appendix-K Assumptions	7-452
Figure 7-532	Comparison of the Measured and Predicted Mid-Point Heater Rod Temperatures – FIST Test 6SB2C with App-K Assumptions.....	7-454
Figure 7-533	Comparison of the Measured and Predicted PCT – FIST Test 6SB2C with App-K Assumptions	7-454
Figure 7-534	Comparison of the Measured and Predicted Bundle Mass – FIST Test 6SB2C with App-K Assumptions	7-455
Figure 7-535	Comparison of the Measured and Predicted Bundle Void Fraction at 37”– FIST Test 6SB2C with App-K Assumptions.....	7-455
Figure 7-536	Comparison of the Measured and Predicted Bundle Void Fraction at 57”– FIST Test 6SB2C with App-K Assumptions.....	7-456
Figure 7-537	Comparison of the Measured and Predicted Bundle Void Fraction at 117”– FIST Test 6SB2C with App-K Assumptions.....	7-456
Figure 7-538	Time Step Study, LBA, MID Result for 1.0 DEG PS SF-LOCA.....	7-459
Figure 7-539	Time Step Study, LBA, TOP Result for 1.0 DEG PD SF-BATT	7-459
Figure 7-540	Time Step Study, SBA, MID Result for 0.10 ft2 DES PD SF-BATT	7-460
Figure 7-541	Time Step Study, SBA, TOP Result for 0.10 ft2 DES PD SF-BATT	7-460
Figure 7-542	Core Node Sensitivity – Large and Small Break Result.....	7-462
Figure 7-543	Mid-peaked Hot Channel Vs. Top-peaked Hot Channel Cases	7-465
Figure 7-544	Top-peaked Hot Channel Vs. Entire Core Top-peaked Cases	7-465
Figure 7-545	Uniform vs. Non-uniform Channels and Radial Power	7-467
Figure 7-546	SSTF Base Case (T026_y52) – Liquid and Vapor Mass Flows at F011 SEO	7-475
Figure 7-547	SSTF Base Case (T026_y52) – Liquid and Vapor Mass Flows at F012 SEO	7-475
Figure 7-548	SSTF Base Case (T026_y52) – Liquid and Vapor Mass Flows at F013 SEO	7-476
Figure 7-549	SSTF Base Case (T026_y52) – Liquid and Vapor Mass Flows at F014 SEO	7-476
Figure 7-550	SSTF Base Case (T026_y52) – Liquid and Vapor Mass Flows at F021 SEO	7-477
Figure 7-551	SSTF Base Case (T026_y52) – Liquid and Vapor Mass Flows at F022 SEO	7-477
Figure 7-552	SSTF Base Case (T026_y52) – Liquid and Vapor Mass Flows at F023 SEO	7-478
Figure 7-553	SSTF Base Case (T026_y52) – Liquid and Vapor Mass Flows at F024 SEO	7-478

Figure 7-554	SSTF Base Case (T026_y52) – Liquid and Vapor Mass Flows at F025 SEO	7-479
Figure 7-555	SSTF Base Case (T026_y52) – Liquid and Vapor Mass Flows at F026 SEO	7-479
Figure 7-556	SSTF Base Case (T026_y52) – Liquid and Vapor Mass Flows at F027 SEO	7-480
Figure 7-557	SSTF Base Case (T026_y52) – Liquid and Vapor Mass Flows at F028 SEO	7-480
Figure 7-558	SSTF Base Case (T026_y52) – Liquid and Vapor Mass Flows at F031 SEO	7-481
Figure 7-559	SSTF Base Case (T026_y52) – Collapsed Level in F011	7-481
Figure 7-560	SSTF Base Case (T026_y52) – Collapsed Level in F022	7-482
Figure 7-561	SSTF Base Case (T026_y52) – Collapsed Level in F025	7-482
Figure 7-562	SSTF Base Case (T026_y52) – Collapsed Level in F026	7-483
Figure 7-563	SSTF Base Case (T026_y52) – Collapsed Level in F028	7-483
Figure 7-564	SSTF Base Case (T026_y52) – Collapsed Level in F031	7-484
Figure 7-565	SSTF Base Case (T026_y52) – Liquid and Vapor Mass Flows at F012 UTP	7-484
Figure 7-566	SSTF Base Case (T026_y52) – Liquid and Vapor Mass Flows at F013 UTP	7-485
Figure 7-567	SSTF Base Case (T026_y52) – Liquid and Vapor Mass Flows at F023 UTP	7-485
Figure 7-568	SSTF Base Case (T026_y52) – Liquid and Vapor Mass Flows at F025 UTP	7-486
Figure 7-569	SSTF Base Case (T026_y52) – Liquid and Vapor Mass Flows at F026 UTP	7-486
Figure 7-570	SSTF Base Case (T026_y52) – Liquid and Vapor Mass Flows at F028 UTP	7-487
Figure 7-571	SSTF Base Case (T026_y52) – Liquid and Vapor Mass Flows at F031 UTP	7-487
Figure 7-572	SSTF Case T026_y53 – Liquid and Vapor Mass Flows at F011 SEO	7-492
Figure 7-573	SSFT Case T026_y53 – Liquid and Vapor Mass Flows at F013 SEO	7-492
Figure 7-574	SSTF Case T026_y53 – Liquid and Vapor Mass Flows at F021 SEO	7-493
Figure 7-575	SSTF Case T026_y53 – Liquid and Vapor Mass Flows at F022 SEO	7-493

Figure 7-576	SSTF Case T026_y53 – Liquid and Vapor Mass Flows at F023 SEO	7-494
Figure 7-577	SSTF Case T026_y53 – Liquid and Vapor Mass Flows at F025 SEO	7-494
Figure 7-578	SSTF Case T026_y53 – Liquid and Vapor Mass Flows at F026 SEO	7-495
Figure 7-579	SSTF Case T026_y53 – Liquid and Vapor Mass Flows at F028 SEO	7-495
Figure 7-580	SSTF Case T026_y53 – Liquid and Vapor Mass Flows at F031 SEO	7-496
Figure 7-581	SSTF Case T026_y53 – Collapsed Level in F011	7-496
Figure 7-582	SSTF Case T026_y53 – Collapsed Level in F023	7-497
Figure 7-583	SSTF Case T026_y53 – Collapsed Level in F025	7-497
Figure 7-584	SSTF Case T026_y53 – Collapsed Level in F026	7-498
Figure 7-585	SSTF Case T026_y53 – Collapsed Level in F028	7-498
Figure 7-586	SSTF Case T026_y53 – Collapsed Level in F031	7-499
Figure 7-587	SSTF Case T026_y53 – Liquid and Vapor Mass Flows at F025 UTP	7-499
Figure 7-588	SSTF Case T026_y53 – Liquid and Vapor Mass Flows at F026 UTP	7-500
Figure 7-589	SSTF Case T026_y53 – Liquid and Vapor Mass Flows at F028 UTP	7-500
Figure 7-590	SSTF Case T026_y53 – Liquid and Vapor Mass Flows at F031 UTP	7-501
Figure 7-591	SSTF Case T026_y54 – Liquid and Vapor Mass Flows at F011 SEO	7-505
Figure 7-592	SSTF Case T026_y54 – Liquid and Vapor Mass Flows at F013 SEO	7-505
Figure 7-593	SSTF Case T026_y54 – Liquid and Vapor Mass Flows at F021 SEO	7-506
Figure 7-594	SSTF Case T026_y54 – Liquid and Vapor Mass Flows at F022 SEO	7-506
Figure 7-595	SSTF Case T026_y54 – Liquid and Vapor Mass Flows at F023 SEO	7-507
Figure 7-596	SSTF Case T026_y54 – Liquid and Vapor Mass Flows at F025 SEO	7-507
Figure 7-597	SSTF Case T026_y54 – Liquid and Vapor Mass Flows at F026 SEO	7-508

Figure 7-598	SSTF Case T026_y54 – Liquid and Vapor Mass Flows at F028 SEO	7-508
Figure 7-599	SSTF Case T026_y54 – Liquid and Vapor Mass Flows at F031 SEO	7-509
Figure 7-600	SSTF Case T026_y54 – Collapsed Level in F022	7-509
Figure 7-601	SSTF Case T026_y54 – Collapsed Level in F023	7-510
Figure 7-602	SSTF Case T026_y54 – Collapsed Level in F025	7-510
Figure 7-603	SSTF Case T026_y54 – Collapsed Level in F026	7-511
Figure 7-604	SSTF Case T026_y54 – Collapsed Level in F028	7-511
Figure 7-605	SSTF Case T026_y54 – Collapsed Level in F031	7-512
Figure 7-606	SSTF Case T026_y54 – Liquid and Vapor Mass Flows at F028 UTP	7-512
Figure 7-607	SSTF Case T026_y54 – Liquid and Vapor Mass Flows at F031 UTP	7-513
Figure 7-608	SSTF Case T026_y55 – Liquid and Vapor Mass Flows at F011 SEO	7-517
Figure 7-609	SSTF Case T026_y55 – Liquid and Vapor Mass Flows at F022 SEO	7-517
Figure 7-610	SSTF Case T026_y55 – Liquid and Vapor Mass Flows at F025 SEO	7-518
Figure 7-611	SSTF Case T026_y55 – Liquid and Vapor Mass Flows at F026 SEO	7-518
Figure 7-612	SSTF Case T026_y55 – Liquid and Vapor Mass Flows at F028 SEO	7-519
Figure 7-613	SSTF Case T026_y55 – Liquid and Vapor Mass Flows at F031 SEO	7-519
Figure 7-614	SSTF Case T026_y55 – Collapsed Level in F026	7-520
Figure 7-615	SSTF Case T026_y55 – Collapsed Level in F028	7-520
Figure 7-616	SSTF Case T026_y55 – Collapsed Level in F031	7-521
Figure 7-617	SSTF Case T026_y55 – Liquid and Vapor Mass Flows at F028 UTP	7-521
Figure 7-618	SSTF Case T026_y55 – Liquid and Vapor Mass Flows at F031 UTP	7-522
Figure 7-619	SSTF Case T026_y48 – Liquid and Vapor Mass Flows at F013 SEO	7-526
Figure 7-620	SSTF Case T026_y48 – Liquid and Vapor Mass Flows at F025 SEO	7-526

Figure 7-621 SSTF Case T026_y48 – Liquid and Vapor Mass Flows at F031
SEO7-527

Figure 7-622 SSTF Case T026_y48 – Collapsed Level in F013.....7-527

Figure 7-623 SSTF Case T026_y48 – Collapsed Level in F025.....7-528

Figure 7-624 SSTF Case T026_y48 – Collapsed Level in F0317-528

Figure 7-625 SSTF Case T026_y48 – Liquid and Vapor Mass Flows at F031
UTP7-529

Abstract

AURORA-B is an evaluation model for predicting the dynamic response of boiling water reactors (BWRs) during transient, postulated accident, and beyond design-basis accident scenarios. AURORA-B consists of a multi-physics code system based on three extensively validated computer codes, the S-RELAP5 thermal-hydraulic system code, a kinetics version of the MICROBURN-B2 core simulator, and the RODEX4 fuel thermal-mechanical code. This report specifically addresses the modification and utilization of AURORA-B for BWR LOCA scenarios (referred to as AURORA-B LOCA). The LOCA methodology uses S-RELAP5 and RODEX4; however, the 3-D kinetics module is not utilized, instead the native S-RELAP5 point kinetics methods are used.

The content of this report is created in accordance with Regulatory Guide 1.203, "Transient and Accident Analysis Methods" as well as the Standard Review Plan (SRP) for Chapter 15. The method is meant to meet the requirements of 10 CFR Part 50 Appendix K, "ECCS Evaluation Models", otherwise known as an Appendix K method.

This report presents the framework of the AURORA-B LOCA evaluation model and its qualification for BWR LOCA analyses. In addition, an application methodology is presented that is specifically focused on analysis of LOCA scenarios. Appendix K analysis principles are used in the application methodology to demonstrate 10 CFR Part 50.46 criteria are met.

Nomenclature

<u>Acronym</u>	<u>Definition</u>
ABWR	Advanced Boiling Water Reactor
APF	Axial Peaking Factor
ADS	Automatic Depressurization System
AOO	Anticipated Operational Occurrence
ASME	American Society of Mechanical Engineers
BDHT	Blowdown Heat Transfer
BWR	Boiling Water Reactor
CB	Core Bypass
CCD	Component Calculational Device
CCFL	Counter Current Flow Limitation
CCTF	Cylindrical Core Test Facility
CET	Component Effects Test
CFD	Computational Fluid Dynamics
CFR	Code of Federal Regulations
CHF	Critical Heat Flux
CPR	Critical Power Ratio
CSAU	Code Scaling Applicability and Uncertainty
DC	Downcomer
ECCS	Emergency Core Cooling System
EFW	Extended Flow Window
EM	Evaluation Model
EMDAP	Evaluation Model Development and Assessment Process
EPRI	Electric Power Research Institute
EPU	Extended Power Uprate
FCTF	Fuel Cooling Test Facility
FIST	Full Integral Simulation Test
FMA	Foundation Methodology Assessment
FoM	Figure of Merit
FLECHT	Full Length Emergency Cooling Heat Transfer
FLECHT-SEASET	Full Length Emergency Cooling Heat Transfer Separate Effects and Systems Effects Test
FTR	Feedwater Temperature Reduction
FWHOOS	Feedwater Heater Out of Service
GDC	General Design Criteria
GE	General Electric
GT	Guide Tube

HPCI	High Pressure Coolant Injection
HPCS	High Pressure Core Spray
HTC	Heat Transfer Coefficient
HTFS	Heat Transfer and Fluid Flow Service
IET	Integral Effects Test
IN	Information Notice
ISP	International Standard Problem
JP	Jet Pump
K-I	Katuoka-Ishii Correlation
KWU	Kraftwerk Union AG
LHGR	Linear Heat Generation Rate
LOCA	Loss of Coolant Accident
LOFT	Loss of Fluid Test
LP	Lower Plenum
LPCI	Low Pressure Coolant Injection
LPCS	Low Pressure Core Spray
LTR	Licensing Topical Report
LTSF	LOFT Test Support Facility
LUT	Look Up Table
LWR	Light Water Reactor
MAPLHGR	Maximum Average Planer LHGR
MCPR	Minimum Critical Power Ratio
MSIV	Main Steam Isolation Valve
PCT	Peak Clad Temperature
PIRT	Phenomena Identification and Ranking Table
PWR	Pressurized Water Reactor
RIP	Reactor Internal Pump
RLBLOCA	Realistic Large Break Loss of Coolant Accident
RP	Recirculation Pump
RPF	Radial Peaking Factor
SE	Safety Evaluation
SEO	Side Entry Orifice
SET	Separate Effects Test
SIP	Scenario Identification Process
SL	Steam Line
SLO	Single Loop Operation
SSTF	Steam Sector Test Facility
SRP	Standard Review Plan
SRV	Safety/Relief Valve

TBV	Turbine Bypass Valve
TCV	Turbine Control Valve
THTF	Thermal Hydraulic Test Facility
TLTA	Two Loop Test Apparatus
TSV	Turbine Stop Valve
UP	Upper Plenum
UPTF	Upper Plenum Test Facility
USNRC	US Nuclear Regulatory Commission
UTP	Upper Tie Plate

1.0 Introduction

AURORA-B is a comprehensive evaluation model developed by AREVA Inc. for predicting the dynamic response of boiling water reactors (BWRs) during transient, postulated accident, and beyond design-basis accident scenarios. The evaluation model (EM) contains a multi-physics code system with flexibility to incorporate all the necessary elements for analysis of the full spectrum of BWR events that are postulated to affect the nuclear steam supply system of the BWR plant.

The AURORA-B EM is designed to be broadly applicable to many BWR events and calculational procedures (e.g. deterministic or statistical procedures). However, the relevant event characteristics differ depending on the event scenario and the criteria that are being evaluated. The differences in events, criteria, and calculational procedures are addressed by defining specific application methodologies. Compliance with all applicable regulations will be assured for the defined events and criteria when the AURORA-B EM is applied within the framework of a specific application methodology.

This Licensing Topical Report (LTR) presents the AURORA-B EM and qualification of the EM for analysis of BWR loss of coolant accidents (LOCA). To differentiate the LOCA application to the transient application of Reference 1, the EM of this LTR is referred to as AURORA-B LOCA. The EM of Reference 1 is referred to as AURORA-B AOO.

10 CFR 50.46 Appendix K deterministic analysis principles are applied to obtain the peak cladding temperature (PCT), local cladding oxidation, and core-wide cladding oxidation (Reference 2). These parameters are used to demonstrate compliance with the acceptance criteria for a postulated LOCA as stated in 10 CFR 50.46. The application methodology is applied to demonstrate compliance of plant operations with the relevant General Design Criteria (GDC) stipulated in Appendix A of 10 CFR 50 (Reference 3). GDC 35 requires an emergency core cooling system (ECCS) that satisfies the requirements of 10 CFR 50.46.

The AURORA-B LOCA Appendix K application is intended for the entire spectrum of break sizes and locations. Breaks are assumed to occur anywhere within the operating domain for a BWR. The operating domain consists of the plant specific power and flow map, which may include extensions, i.e., Extended Power Uprate (EPU), Extended Flow Window (EFW), etc.

AREVA Inc.

- MB2-K – This CCD uses advanced nodal expansion methods to solve the three-dimensional, two-group, neutron kinetics equations. The MB2-K code is consistent with the MICROBURN-B2 steady state core simulator (Reference 7). Unlike the AURORA-B AOO application, the AURORA-B LOCA application presented in this LTR does not use MB2-K. A 3-D kinetics solution is not necessary; therefore, a point kinetics model is used with input or modeling parameters based on an appropriate Core Simulator code; for example MICROBURN-B2. The point kinetics model is the native model in S-RELAP5 that has been used in PWR applications of S-RELAP5. A point kinetics model has been historically used in Appendix K applications as well as being acceptable for realistic LOCA methods (Section 3.2.2 of Reference 10).

This LTR defines the AURORA-B LOCA EM and the Appendix K application methodology by establishing the requirements, developing the assessment base, developing the capabilities of the EM, and assessing the adequacy of the EM. Additional details for the application methodology are then presented, including the means by which operational constraints are confirmed or established that assure compliance with applicable regulations and how conservative initial conditions, boundary conditions (and appropriate technical bases), and assumed equipment operational characteristics are selected. Finally, the uses and application requirements for AURORA-B LOCA are established.

2.0 Summary

2.1 General Summary

AURORA-B LOCA analyses evaluate the system response following the start of a LOCA and specifically evaluate peak cladding temperature (PCT), local cladding oxidation, and core-wide cladding oxidation. This LTR demonstrates compliance with the acceptance criteria as stated in 10 CFR 50.46 for a postulated LOCA under 10 CFR 50 Appendix K rules.

The purpose of this document is to demonstrate the AURORA-B LOCA analysis methodology and analysis results for application to BWR power plants. Specifically, the method is intended for BWR designs with refloodable internal volume; for example, GE BWR/3 - BWR/6 designs with internal jet pumps - these designs incorporate a refloodable volume to the top of the jet pumps. The method is not intended for BWR power plants with external recirculation pumps where vessel refill may not be achieved following large breaks and the mitigation of the heatup of the bundles for some scenarios depend solely on top down cooling from core spray directly into the bundles. The GE BWR/2 design fits this classification.

The AURORA-B LOCA methodology is intended to be applicable for all LOCA events which include breaks in all piping connected to the reactor vessel and/or inventory loss from actuation of safety/relief valves. Containment analysis is not included in the AURORA-B LOCA methodology; however, mass and energy output from the methodology can be used in other downstream analyses based on other methodologies.

2.2 Application of the EMDAP

The EMDAP has been defined by the US Nuclear Regulatory Commission (USNRC) as an acceptable process for developing and accessing evaluation methodologies that may be used to analyze the behavior of a nuclear power plant. Methodology developers are encouraged to follow the EMDAP process as it streamlines the review cycle and regulatory interactions. Additional emphasis is placed on the EMDAP since Regulatory Guide 1.203 is designed to be complementary to the guidance provided to USNRC reviewers that is found in Chapter 15.0.2 of NUREG-0800, the Standard Review Plan (SRP) for the Review of Safety Analysis Reports for Nuclear Power Plants (Reference 11).

The S-RELAP5 computer code has been selected as the foundation on which to build AURORA-B because of AREVA's extensive history and experience with the code, including a number of USNRC approved methodologies. The S-RELAP5 computer code is USNRC approved for pressurized water reactor (PWR) large and small break LOCA analysis, and PWR non-LOCA transient analysis (References 5, 16, and 17). Particularly, the realistic large break LOCA (RLBLOCA) methodology is based on the Code Scaling Applicability and Uncertainty (CSAU) process (Reference 18) that is defined for best estimate LOCA applications, and is a predecessor to the EMDAP. Since the S-RELAP5 code and documentation have undergone extensive review and revision to ensure accuracy and clarity for the RLBLOCA methodology, application of the EMDAP in AURORA-B development is reduced in scope compared to development of an entirely new code system using EMDAP. Instead, the EMDAP is utilized to guide the refinement and extension of the existing tools for use in the new evaluation model and assure they are adequate for addressing the systems, components, phenomena, etc. associated with BWR events. Since AURORA-B LOCA is based on Appendix K requirements where the method is conservative and precludes the need for uncertainty analyses, a graded approach with EMDAP is used.

A summary of the changes made to S-RELAP5 relative to the code and documentation supporting the RLBLOCA methodology is provided in Section 8.2. In addition, changes made to both the code and BWR model supporting the AURORA-B AOO methodology is provided in Section 8.2.

The following sections define the process for completing the EMDAP by outlining how each step of the EMDAP is addressed.

2.3 Compliance with the Standard Review Plan

The EMDAP process complements the standard review plan. Specifically for the AURORA-B LOCA EM, the applicable SRP Section is 15.6.5, *Loss-of-Coolant Accidents Resulting from Spectrum of Postulated Piping Breaks Within the Reactor Coolant Pressure Boundary*.

2.4 Compliance with 10 CFR 50.46

This document describes AREVA's LOCA analysis methodology for the evaluation of emergency core cooling system performance for BWRs. Analyses and evaluations are

performed in accordance with the requirements of 10 CFR Part 50. This document is based on Appendix K requirements of 10 CFR Part 50.

2.4.1 Figures of Merit

The figures of merit are described and detailed in Section 4.4.

2.4.2 10 CFR 50.46 Appendix K Documentation

Required documentation for Appendix K is presented in Section 6.2.27.

2.5 *Emerging Issues*

2.5.1 Proposed 10 CFR 50.46c

This document was completed before a final USNRC ruling for 10 CFR 50.46c was completed. The new ruling is anticipated to change figures of merit (criteria limits), i.e., peak cladding temperature and cladding oxidation criteria to address cladding embrittlement via hydrogen uptake in the cladding, etc. It is anticipated that the AURORA-B LOCA methodology will remain unchanged, only the criteria will change; for example, at a given fuel rod exposure the new criteria could set lower peak cladding temperature and local cladding oxidization limits, AURORA-B LOCA would then be used to calculate and assess those parameters against the new limits.

2.5.2 Conductivity Degradation

The U.S. Nuclear Regulatory Commission (USNRC) issued Information Notice (IN) 2009-23 (No. ML091550527), dated October 8, 2009 for concerns regarding the use of historical fuel thermal conductivity models in the safety analysis of operating reactor plants. IN 2009-23 discusses how historical fuel thermal mechanical codes may over predict fuel rod thermal conductivity at higher burn-ups based on new experimental data. This new experimental data showed significant degradation of fuel pellet thermal conductivity with exposure. The USNRC staff concluded that the use of the older legacy fuel models will result in predicted fuel pellet conductivities that are higher than the expected values. AURORA-B LOCA incorporated RODEX4 as the fuel model. RODEX4 is a state-of-the-art fuel code that fully accounts for burnup degradation of fuel thermal conductivity; therefore, the concerns of IN 2009-23 were addressed by the use of RODEX4.

2.5.3 Fuel Relocation

Under a condition of fuel relocation, wherein the fuel above the ballooned region drops into the ballooned region, it has been postulated that increased decay heat generation due to the increased fuel mass in the ballooned region will lead to an increase in cladding heat flux resulting in higher cladding temperatures. Fuel relocation is discussed in Section 6.4.5.

2.5.4 Generic Safety Issue 191

The effect of debris accumulation on fuel bundles during a LOCA event have recently been revisited by the industry. At the time this document was created, no new criteria or conditions were defined; however, in the event that a new scenario is determined it is anticipated that the AURORA-B LOCA model could be adjusted to address the issue. For example, if new criteria determined that the BWR fuel inlet orifice became blocked by debris after a certain period of time, the model could be adjusted to model the blockage.

3.0 Regulatory Requirements Summary

3.1 Regulatory Requirements

Licensees and vendors use a variety of methods to evaluate the transients and accidents that could occur at a given nuclear power plant. The USNRC staff reviews these methods to ensure that they provide a realistic or conservative result and that they adhere to the requirements of the Code of Federal Regulations (CFR). Regulations, which are applicable to transient and accident analysis methods, are found in 10 CFR 50.34, 10 CFR 50.46, and 10 CFR 50 Appendix K. Additionally, because the results of the transient and accident analysis methods are important to the safety of nuclear power plants, these methods must be maintained under a quality assurance program (Reference 12) which meets the criteria set forth in 10 CFR 50 Appendix B.

3.1.1 Application of the Evaluation Model Development and Assessment Process (EMDAP), Regulatory Guide 1.203

To assure uniformity for documentation, the USNRC created Regulatory Guide 1.203 to complement the Standard Review Plan (SRP), NUREG-0800; specifically Chapter 15, Section 15.0.2.

Regulatory Guide 1.203 provides guidance in developing and assessment of evaluation models for accident and transient analyses. In addition, Appendix A of Regulatory Guide 1.203 also provides information regarding emergency core cooling system (ECCS) analysis, and Appendix B provides an example of the EMDAP Process (EMDAP) for different analysis modification scenarios. Both Regulatory Guide 1.203 and SRP Chapter 15, Section 15.0.2 provide guidance to the licensee and the vendor to verify that the evaluation model is adequate to simulate the accident under consideration. This includes methods to estimate the uncertainty in the calculation, as in the case for best estimate LOCA methods; or to ensure that the results of the analysis are demonstrably conservative, as in the case of a LOCA in Appendix K to 10 CFR Part 50, which is the basis of AURORA-B LOCA.

3.2 *Compliance with the Standard Review Plan, Chapter 15, Section 15.0.2.*

NUREG-0800 Chapter 15, Section 15.0.2 provides guidance to the Nuclear Regulatory Commission (USNRC) reviewer with respect to reviewing the technical contents of a submittal,

typically a Topical Report (TR) document pertinent to transient and accident analysis methodology. To accomplish this task, the USNRC provided the reviewer a list of criteria in Chapter 15.0.2 of the SRP as a means of arriving at a sound technical conclusion. The areas of considerations listed in Chapter 15.0.2 are provided below and meant to complement the EMDAP document:

- Item 1. Documentation. Refer to Section 4.1.
- Item 2. Evaluation Model. Refer to Section 6.0.
- Item 3. Accident Scenario Identification Process. Refer to Section 4.2.
- Item 4. Code Assessment Database. Refer to Sections 5.0 and 7.0.
- Item 5. Uncertainty Analysis. Refer to Section 7.9.
- Item 6. Quality Assurance (QA) Plan. Refer to Reference 12. Reference 12 is the basis for quality assurance in both the development and application of AURORA-B LOCA.

3.2 Compliance with Appendix K to 10 CFR Part 50 Documentation

The Appendix K criteria is provided in Section 6.2. Appendix K documentation requirements are discussed in Section 6.2.27.

3.3 Compliance with Standard Review Plan 15.6.5

SRP 15.6.5 details items for review specific to LOCA break spectrum analyses. The items relevant to BWRs and the AURORA-B LOCA methodology are summarized below along with AREVA's approach to each item. AURORA-B LOCA methodology is not used directly to assess radiological items. Dose assessments are not part of AURORA-B LOCA.

- *10 CFR 50.46 criteria met which includes GDC 35 ECCS criteria to prevent fuel and clad damage that would interfere with core cooling and metal-water reaction would be limited to negligible amounts.*

The AURORA-B LOCA methodology is applied to access these criteria as outlined in Section 4.4.

- *Parameters and assumptions conservatively chosen.*
 - *2% power uncertainty unless lower is justified.*

- *Maximum linear heat generation rate (LHGR) used based on technical specifications.*
- *All permitted axial power shapes addressed.*
- *Initial stored energy conservatively calculated.*
- *Appropriate analyses support credit taken for control rod insertion*
- *Analysis conservatively address the operation of the reactor coolant pump*
- *A conservatively low minimum containment pressure is used.*

These parameters and assumptions are consistent with an Appendix K model and AURORA-B LOCA.

- *Reactor protection system actions, safety injection actuation and delivery are consistent with set points and associated uncertainties and delay times listed on the SAR.*

These items are plant specific and are addressed with the application of the methodology. Data defining these parameters are obtained from the specific plant parameters document, refer to Section 9.1.4.

- *Analytical techniques and computer programs used.*

This LTR describes the tools used.

- *Available ECCS from failure modes, scope of break spectrum (initial conditions, break size and location) and sufficient resolutions.*

These items are plant specific and are addressed with the application of the methodology.

- *LOCA analysis is carried out until the top of active fuel has been covered with two-phase mixture and cladding temperature has been reduced to near saturation temperature.*

The analyses are intended to be carried out until the hot rod has quenched and returned to near saturation temperature. [

]

- *Address fuel LOCA sequence of events to the point where the plant is in the long-term cooling mode and removal of decay heat has been well established for both large and small breaks.*

As noted earlier, the run is carried out until the hot rod is quenched. At this point in time long term cooling starts.

- *Long term cooling analysis.*

Long-term coolability addresses the issue of reflooding the core and maintaining a water level adequate to cool the core and remove decay heat for an extended time period following a LOCA. For non-recirculation line breaks, the core can be reflooded to the top of the active fuel and be adequately cooled indefinitely. For BWR jet pump plants with recirculation line breaks, the top of jet pumps are at approximately two-thirds core height. Because of this geometry, the core is refloodable to at least two-thirds core height with the largest breaks. When the liquid refloods to this level, coolant is lost out the break via liquid spilling into the downcomer region from the top of the jet pumps. Initially, the heat flux in the core will maintain a two-phase water level over the entire length of the core. Eventually, the heat flux will not be adequate to maintain a two-phase water level over the entire length of the core. Beyond this time, the upper third of the core will remain wetted and adequately cooled by core spray. Maintaining water level at two-thirds core height with one core spray system operating is sufficient to maintain long-term coolability as demonstrated by the NSSS vendor. Since fuel temperatures during long-term cooling are low relative to the PCT and are not significantly affected by fuel design, this conclusion is generic for any fuel design.

4.0 Establish Requirements for Evaluation Model Capability (EMDAP Element 1)

The following subsections establish the application envelope (analysis purpose, plant types, and transient types) of the EM addressed within the context of this LTR. The constituent phenomena, processes, and key parameters are then identified within the application envelope and their importance is determined. As stated in SRP 15.0.2, an EM is the calculation framework for evaluating the behavior of the reactor coolant system during a postulated accident or transient. It includes one or more computer programs and other information necessary for application of the calculation framework to a specific accident, such as mathematical models used, assumptions (with associated bases) included in the programs, a procedure for treating the program input and output information, specification of those portions of the analysis not included in the computer programs, values of parameters, and other information necessary to specify the calculation procedure.

4.1 Documentation

4.1.1 Regulatory Basis, Chapter 15, Section 15.0.2; Item 1

The development of an evaluation model for use in reactor safety licensing calculations requires a substantial amount of documentation. This documentation includes:

- *The evaluation model (Section 6.0).*
- *The accident scenario identification process (Section 4.2).*
- *The code assessment (Section 7.0)*
- *The uncertainty analysis (Section 7.9).*
- *A theory manual (Reference 6).*
- *A user manual (Reference 13).*
- *A QA plan (Reference 12).*

4.2 Accident Scenario Identification Process (SIP) as per (SRP, Chapter 15, Section 15.0.2, Item 2)

4.2.1 Regulatory Basis

The accident scenario identification process is a structured process used to identify and rank the reactor component and physical phenomena modeling requirements based on (a) their importance to acceptable modeling of the scenario and (b) their impact on the figures of merit for the calculation (e.g., peak cladding temperature and maximum and average cladding oxidation thicknesses). It is also used to identify the key figures of merit or acceptance criteria for the accident.

4.3 Analysis Purpose, Transient Class, and Power Plant Class (EMDAP Step 1)

The analysis purpose, transient class, and plant class are defined below in order to define the application envelope (i.e. the target applications). The sections address the major points of each topic. Where necessary, reference is made to more comprehensive descriptions of the plant-class-specific and/or plant-specific details.

4.3.1 Analysis Purpose

The analysis purpose is to demonstrate compliance of plant operations with relevant GDC stipulated in Appendix A of 10 CFR 50 (Reference 3). This is done by confirming or establishing operational constraints that ensure all relevant acceptance criteria delineated in the plant licensing basis are satisfied during plant operations for the plants and scenarios analyzed with this EM. Specifically, GDC 35 requires that an emergency core cooling system (ECCS) is available that provides abundant cooling. The ECCS must be able to provide effective cooling such that clad metal-water reaction is limited to negligible amounts and fuel and clad damage would not interfere with continued effective core cooling. The system must have suitable redundancy to be able to function assuming a single failure. The requirements for ECCS performance are given in 10 CFR 50.46 and Appendix K to 10 CFR 50. Section 6.3 of the SRP (Reference 11) addresses the ECCS.

4.3.2 Transient Class

The transient class is defined in SRP Chapter 15 as Section 15.6.5, *Loss-of-Coolant Accidents Resulting from Spectrum of Postulated Piping Breaks Within the Reactor Coolant Pressure*

Boundary. The SRP is consistent with the EMDAP process and provides review guidance for the EM. Relevant items of the SRP for this LTR are noted in Section 3.3.

In some instances the licensing basis for a plant may differ from the SRP. Provided that the licensing basis of the plant does not significantly depart from the SRP bases, the AURORA-B LOCA EM supports the licensing basis of each plant to which it is applied by analyzing the plant-specific scenarios, consistent with the criteria defined in the licensing basis documents for the plant.

The operating domain (allowable combinations of core thermal power and total core flow rate) from which events may be initiated is delineated in the plant licensing basis documentation for each plant; this may include operation at EPU conditions with expanded power and flow windows, including EFW.

4.3.3 Power Plant Class

The range of power plant classes includes BWR plant types with refloodable internal volume; for example, GE BWR/3 – BWR/6 designs with internal jet pumps - these designs incorporate a refloodable volume to the top of the jet pumps. The method is not intended for BWR plants types with external recirculation pumps where vessel refill may not be achieved following large breaks and the mitigation of the heatup of the bundles for some scenarios depend solely on top down cooling from core spray directly into the bundles. The GE BWR/2 design fits this classification. A detailed description of the BWR plant types is provided in Section 6.0 of Reference 19. The description not only includes discussion of plant-class hardware such as recirculation system design, but also includes a summary of plant-specific differences that have been observed in operating plants as a result of equipment modernization efforts and evolution of plant operational parameters. Reference 19 does not address LOCA events and is not detailed for ECCS. ECCS equipment specific for LOCA is presented in Appendix A.

4.4 ***Figures of Merit (EMDAP Step 2)***

The figures of merit (FoM) evaluated with the EM are parameters that demonstrate compliance with applicable acceptance criteria defined in 10 CFR 50.46. Specifically, the FoM (also known as acceptance criteria measures) considered are those necessary to demonstrate compliance with the 10 CFR 50.46 acceptance criteria. The precise role of the AURORA-B LOCA EM in

calculating FoM for comparison to the applicable acceptance criteria is described in Section 4.4.1. The FoM include the evaluation of maximum cladding temperature and maximum local and core wide oxidation. These FoM are used to provide assurance that fuel integrity is maintained for selected events.

The specific acceptance criteria used for demonstrating compliance of plant operations is defined in 10 CFR 50.46 and is the licensing basis of each plant. The following list of acceptance criteria is taken from the SRP 15.6.5, and is affected by the fuel mechanical, nuclear, and/or thermal hydraulic design.

- The calculated maximum fuel element cladding temperature shall not exceed 2,200 F.
- The calculated local oxidation of the cladding shall nowhere exceed 17% of the total cladding thickness before oxidation.
- The calculated amount of hydrogen generated from the chemical reaction of the cladding with water or steam shall not exceed 1% of the hypothetical amount that would be generated if all the metal in the cladding cylinders surrounding the fuel, excluding the cladding surrounding the plenum volume, were to react.
- Calculated changes in core geometry shall be such that the core remains coolable.
- After any calculated successful initial operation of the ECCS, the calculated core temperature shall be maintained at an acceptably low value, and decay heat shall be removed for the extended period of time required by the long-lived radioactivity.

The acceptance criteria described above may be revised by USNRC rulemaking activities subsequent to approval of this LTR. As a result, the licensing basis of plants may be modified to reflect the revised criteria through USNRC approved License Amendment Requests that are submitted by the plant licensee. In such cases, AURORA-B LOCA EM analysis conclusions will address the acceptance criteria found in the licensing basis of plants to which it is applied. Section 2.5 of this LTR addresses emerging issues that may result in criteria changes.

4.4.1 Application Specific Considerations

This LTR describes an EM for confirming or establishing operational constraints that assure compliance of plant operations with specific acceptance criteria. This section defines the context by which this LTR fits into the confirmation or establishment of the operational constraints. In particular, the role of the AURORA-B LOCA EM in demonstrating the applicable acceptance criteria are satisfied during plant operations for the target scenarios is identified.

Figure of Merit 1

The peak cladding temperature is the primary parameter for LOCA analyses based on the criteria of 10 CFR 50.46. The calculated PCT will not shall not exceed 2,200 F.

The EM described in this LTR will be applied to evaluate applicable cladding temperature based on the criteria of 10 CFR 50.46.

Figure of Merit 2

Based on the criteria of 10 CFR 50.46, the local oxidation of the calculated local oxidation of the cladding shall nowhere exceed 17% of the total cladding thickness before oxidation.

The EM described in this LTR will be applied to evaluate applicable local oxidation criteria based on the criteria of 10 CFR 50.46.

Figure of Merit 3

Based on the criteria of 10 CFR 50.46, the core wide hydrogen generated shall not exceed 1% of hypothetical amount if all fuel metal cladding (excluding cladding in the plenum volume) were to react.

The EM described in this LTR will be applied to evaluate applicable core-wide hydrogen criteria based on the criteria of 10 CFR 50.46.

The two remaining criteria of 10 CFR 50.46 are not directly evaluated by the AURORA-B LOCA methodology.

Figure of Merit 4

Calculated changes in core geometry shall be such that the core remains coolable.

Conformance with FoM 1 and 2 will achieve coolable geometry.

Figure of Merit 5

Long term coolability shall be achieved by maintaining an acceptably low core temperature and decay heat shall be removed for an extended period of time.

Long term coolability is achieved following the time of peak clad temperature once the core refloods above the top of active fuel, or for the largest breaks in jet pump plants, the core is reflooded to two-thirds core height (the height of the jet pumps) the upper third of the core is cooled by steam cooling and/or core spray; the fuel has quenched and remains quenched. This criteria is met and demonstrated by the design of the ECCS and is not a function of fuel design. Demonstration is made by the NSSS; therefore, long term cooling analysis is not required as part of an AURORA-B LOCA assessment. AURORA-B LOCA could be used to determine such parameters as the time to core reflood and the ECCS required to maintain a water level, etc.

4.5 Identify Systems, Components, Phases, Geometries, Fields, and Processes that Must Be Modeled (EMDAP Step 3)

The capability of an EM to calculate the target applications rests on the characteristics of the EM. Knowing the target applications and FoM (e.g. \EMDAP Steps 1 and 2), the characteristics of the EM are now defined. These characteristics are used in later stages of the EMDAP to define the code development activities. Capabilities were added or refined through the methodology development process and directed code development. The first step in defining the capabilities is identifying the systems, components, phases, geometries, fields, and processes that must be modeled:

- **System, subsystems, and modules:** The BWR system, its subsystems, and modules are described in Section 4 of Reference 19. The information provided in the reference is extensive and is not repeated here. Systems specific to ECCS are discussed in Appendix A.
- **Constituents:** The thermal-hydraulic constituent in the BWR events of interest is water.
- **Phases:** The phases of water are limited to the liquid and vapor forms.

- **Geometrical Configurations (phase topology or flow regime):** The geometrical configuration of the water is generally defined by the “wet-wall” vertical flow regimes, from bubbly to annular mist flow (void fraction from 0.0 to 1.0). In addition the “wet-wall” horizontal flow regime is encountered within external recirculation, feedwater, and other piping. The “dry-wall” vertical flow regime is experienced as water level is lost during a LOCA in the core and surrounding regions of the reactor. In addition, stratification and annular mist flow (void fraction from ~0.99 to 1.0) are experienced in horizontal flow. The geometrical configurations of the heat structures are Cartesian, cylindrical, and/or spherical.
- **Fields:** The physical quantities that are being transported in the thermal-hydraulic transport equations include mass, momentum, and thermal energy of the liquid and vapor phases, and thermal energy in the heat structures.
- **Transport Processes:** An extensive number of mechanisms are needed to determine the transport of, and interactions between, constituent phases throughout the system. These include (but are not limited to):
 - Transport properties defining the inter- and intra-nodal mass transport between the liquid and vapor phases
 - Transport properties defining the inter- and intra-nodal momentum transport between phases and interaction with surfaces, structures, and restrictions
 - Transport properties defining the inter- and intra-nodal energy transport between the liquid and vapor phases plus addition/removal of energy from heat structures
 - Material properties defining intra-nodal energy transport within heat structures
 - Properties defining energy deposition within the fuel rods from fission
 - Properties defining the neutron kinetics models
 - Properties defining the production and decay of isotopes that emit ionizing or non-ionizing radiation (i.e. decay heat and delayed neutron precursors)

4.6 Identify and Rank Key Phenomena and Processes (EMDAP Step 4)

Plant behavior is not equally influenced by all processes and phenomena that occur during a LOCA. The candidate phenomena for the target scenarios have been reviewed to identify the most important phenomena in order to achieve a manageable set for a wide range of target scenarios. This has been performed by identifying and ranking the phenomena of the target scenarios with respect to their influence on the defined FoM. The information provided in this section summarizes the comprehensive phenomena identification and ranking process (PIRT).

The PIRT development was accomplished by assembling a panel of BWR LOCA experts. The panel reviewed the LOCA scenarios and used their collective expertise to identify phenomena and processes which may be important to analyze the scenarios. For LOCA analyses, a spectrum of both large and small break LOCAs is part of the scenario. The limiting break is

identified through sufficient analyses to determine the highest peak clad temperature (PCT), the highest local clad oxidation, and the highest core wide oxidation percentage. The analyses must also be carried out long enough that long term cooling conditions can be achieved. The analyses must also consider the case with a severed ECC injection line, along with the degraded ECC injection into the intact loops. The BWR LOCA PIRT development included the review of existing PIRTs containing phenomena related to a LOCA or to the analytical method proposed for BWR LOCA use. [

] Differences were discussed and changes made as appropriate to develop the final PIRT table for AURORA-B LOCA.

The LOCA scenario is broken into three phases: Blowdown (BD), Refill (RF), and Reflood (RRF). The following definitions were used in developing the PIRT. [

] The final PIRT is presented in Table 4-1. [

] The PIRT presents the phenomena in terms High (H), Medium (M), or Low (L).

- **H:** The phenomena are considered to have high importance. Modeling of these phenomena must be accurate or conservative under Appendix K. The models associated with these phenomena must be validated.
- **M:** The phenomena are considered to have medium importance. Modeling of these phenomena are not as crucial as H, but should nevertheless be appropriate for the scenario.
- **L:** The phenomena are considered to have low importance. Accurate modeling of these phenomena are not considered important.

This image shows a completely blank white page. It is surrounded by a thick black border that frames the entire area. There are no markings, text, or illustrations on the page itself.

5.0 Develop Assessment Base (EMDAP Element 2); Chapter 15 Section 15.0.2, Item 4

This section focuses on the experimental database that is relevant to the scenarios being considered. In addition, the suitability of the experimental scaling of the data is addressed and scaling issues are discussed.

5.1 *Regulatory Basis*

The code assessment base provides a complete assessment of all code models against applicable experimental data and/or exact solutions in order to demonstrate that the code is adequate for analyzing the chosen scenario.

5.2 *Specify Objectives for Assessment Base (EMDAP Step 5)*

The objectives of the assessment base are to provide experimental data to assess the requirements established in Element 1 (Section 4.0). In particular, BWR components, processes, and phenomena that were identified in Step 3 (Section 4.5) and ranked as important in Step 4 (Section 4.6) require assessment. The assessment base includes separate effects experiments needed to develop and assess empirical correlations and other closure models, integral systems tests to assess system interactions and global code capability, and plant transient data that demonstrate the system interactions for scenarios based on full scale plant data.

5.3 *Perform Scaling Analysis and Identify Similarity Criteria (EMDAP Step 6)*

In general, the scaling compromises of test data are minimal and assessments are well-characterized. This is because the assessment base includes full scale data. Discussion of scaling is provided in Section 7.6 (EMDAP Step 17) and Section 7.7 (EMDAP Step 18) as appropriate.

5.4 *Identify Existing Data and/or Perform Integral Effects Tests and Separate Effects Tests to Complete the Database (EMDAP Step 7)*

Several authoritative works are available in the public domain that survey existing test facilities and available experimental data. These works are more focused on pressurized water reactor loss of coolant accidents, but test facilities and experimental data are identified within these sources for generally applicable facilities and data as well as BWR specific facilities and data.

The sources include *The Compendium of ECCS Research for Realistic LOCA Analysis* (Reference 60), *Evaluation of the Separate Effects Tests (SET) Validation Matrix* (Reference 61), *CSNI Integral Test Facility Validation Matrix for the Assessment of Thermal-Hydraulic Codes for LWR LOCA and Transients* (Reference 62), and *TRAC-M Validation Test Matrix* (Reference 63). Applicable facilities are selected and included into the assessment database.

The USNRC approved LTRs and theory manuals associated with the CCDs mentioned in Section 1.0 have been inspected. The AURORA-B LOCA EM is intentionally built upon USNRC approved methodologies in order to take benefit from the prior assessment work.

A matrix of test facilities is provided in Table 5-1 that defines the experimental database supporting this LTR versus highly ranked PIRT phenomena listed in Section 4.6. This table defines the assessment matrix for the evaluation model. The use of data from test facilities in evaluating highly ranked PIRT phenomena are indicated in the table. The types of data are as follows;

- Foundation methodology assessments (FMA): Assessments inherent for the specific methodology; for example, assessments performed to validate RODEX4 centerline temperature are part of the base methodology.
- Component effects tests (CET): Assessments specific to a component; for example, jet pumps.
- Separate effects tests (SET): Assessments focused on specific phenomena.
- Integral effects tests (IET): Assessments that simulate conditions and events that the EM is intended to analyze. The test will involve a large portion of the highly ranked phenomena of the PIRT.

A brief description of each assessment is presented as follows.

5.4.1 Appendix K Requirements

This topic is not a specific test or assessment, but as the name implies, this topic refers to phenomena, correlations or modeling that are required of Appendix K (Reference 2); for example, the Moody critical model for the discharge of the break.

[]

5.4.2 Core Simulator Qualification

MICROBURN-B2 is the core simulator code currently used for BWR cores and consists of both neutronic and thermal-hydraulic models, Reference 7. XCOBRA is a steady-state thermal-hydraulic code used to predict steady-state thermal hydraulic performance of fuel bundles at various operating conditions and power distributions, Reference 23. XCOBRA does not contain neutronic models, power distributions are input to the code. MICROBURN-B2 and XCOBRA are presented as examples of the current codes; future qualified core simulators are anticipated to be equally applicable. Refer to Figure 6-2 for additional information on data transfer between codes.

5.4.3 RODEX4 Qualification

RODEX4 is a best estimate thermal mechanical fuel code used to predict fuel rod characteristics versus exposure, References 8 and 9.

5.4.4 Rod Bundle Pressure Drop Tests

Rod bundle pressure drop tests were based on the ATLAS (GE) and KATHY (AREVA) test facilities. The test facilities assess single bundles for various reactor operating conditions.

5.4.5 Jet-Pump Performance Tests

The primary jet pump performance tests were performed in Loss of Fluid Test (LOFT) Support Facility operated at Idaho National Laboratory and were based on 1/6 scale jet pump. In addition, other full scale jet pump tests are utilized to demonstrate the acceptable scalability of the LOFT test.

5.4.6 Steam Separator Tests

Full-scale test data was used to develop and validate the steady state performance (pressure drop, carryover and carryunder) of the two and three stage steam separators.

5.4.7 Critical Power Tests

Fuel specific rod bundle critical power tests were based on KATHY (AREVA) test facilities. The test facilities assess single bundles for various reactor operating conditions. Test assessments validate the application of fuel specific CPR correlation in setting initial conditions.

5.4.8 CCFL Mini-Loop Tests

The mini-loop is a [

]

5.4.9 Rod Bundle Void Tests

Rod bundle void tests were based on FRIGG loop facility and KATHY (AREVA) test facility. Specifically, FRIGG2 void distributions test performed in the FRIGG loop facility consisted of a test section with 36 heated rods of uniform axial and radial power distribution and was designed to provide a full-scale simulation of a boiling channel for the Marviken reactor. The FRIGG3 void distribution experiments were performed as a follow-on test after the FRIGG2 tests. The test section was essentially the same as the earlier test with a change to a milder radial power

peaking. [

]

5.4.10 Christensen Void Tests

The Christensen void fraction tests were performed in a test apparatus at the Argonne National Laboratory. The test section for these experiments was a stainless steel uniformly heated vertical rectangular tube. The primary purpose of these tests was to study void oscillations and stability in BWR systems, but the experiments also provided data on steady state axial void distributions, particularly for the subcooled boiling region.

5.4.11 Allis-Chalmers Void Tests

The Allis-Chalmers void fraction tests were large diameter adiabatic void fraction tests. The assessments considered a 2.9 in diameter pipe, an 18 inch diameter pipe and a 36 inch diameter pipe.

5.4.12 GE Level Swell Tests

The GE Level Swell Test is essentially a small break blowdown of a vertical vessel 14 ft high by 1 ft in diameter.

5.4.13 THTF Mixture Level Tests

The THTF facility, operated by ORNL, is a large high pressure thermal-hydraulic loop with non-nuclear (electrically heated) rods simulating a nuclear fuel bundle consisting of 64 rods. The test bundle is an electrically heated 8x8 rod bundle based on PWR rod designs. However, the test facility provides similar geometry to the smaller diameter rods of advanced BWR fuel designs. The facility was designed to simulate the thermal-hydraulic environments expected during LOCA events. The level swell test series investigates the steady-state thermal-hydraulic behavior of the rod-bundle when the operating conditions produce a two-phase mixture that only extends about 70 to 80% up the test section.

5.4.14 TLTA Boiloff Tests

The two-loop test apparatus (TLTA) was built to simulate LOCA scenarios in a BWR. The TLTA is a scaled version of a BWR/6, with one fuel bundle. The apparatus includes one full-length (150 inches long) fuel bundle simulator. The original TLTA configuration used a 7x7 rod bundle, and later TLTA configurations used an 8x8 rod bundle, and other sequential modifications to arrive at a better representation of the BWR LOCA event being simulated. Most of the tests simulated LOCA events (integral tests) with one series 5A test simulating boiloff.

5.4.15 Bennett Tube Tests

The Bennett heated tube experiments were conducted by the UKAEA Research Group to measure the dryout or critical heat flux (CHF) location and the surface temperature profiles in the region beyond the dryout point. The test tube was a simple heated tube 0.497-inch I.D. and 0.625-inch O.D. with a total length of 19 feet.

5.4.16 THTF Steady State Tests

Refer to the Section 5.4.13 discussion on the THTF apparatus. Specific to this test series is steady state film boiling heat transfer tests for various operating conditions.

5.4.17 FCTF Spray and Steam Cooling Tests

The AREVA Fuel Cooling Test Facility (FCTF) [

]

5.4.18 THTF Reflood Tests

Refer to the Section 5.4.13 discussion on the THTF apparatus. Specific to this test series are ORNL high pressure reflood tests with the pressures ranging from 303 to 1092 psia. Reflood is simulated by establishing a water level with 25-30 percent of the rod bundle uncovered at steady-state. The transient is initiated by increasing the inlet makeup flow rate to simulate reflood.

5.4.19 FLECHT SEASET Reflood Tests

The Full-Length Emergency Cooling Heat Transfer Separate Effects and Systems Effects Test (FLECHT SEASET) and Full-Length Emergency Cooling Heat Transfer (FLECHT) skewed series of tests were intended for PWR LOCA forced reflood phenomena; however, the test series provides good data for the SET phenomena assessments for BWR LOCA, particularly heat transfer phenomena for peak cladding temperature and rod quench predictions. The FLECHT-SEASET facility used the Westinghouse 17x17 geometry for the reference fuel design while the FLECHT facility used the Westinghouse 15x15 geometry for the reference fuel design; the tests consisted of a single 161-rod bundle for the FLECHT SEASET tests and a single 105-rod bundle for the FLECHT skewed tests.

5.4.20 CCTF Reflood Tests

The Cylindrical Core Test Facility (CCTF) Core-II Test Series were undertaken to provide a data base for large-break LOCA reflood behavior in PWRs. CCTF is a full-height, 1/21 scale model of the primary coolant system of 4-loop PWR plant. The facility was designed to reasonably simulate the flow conditions, including ECC flow behavior in the downcomer, and reactor core responses in the primary system of a PWR during the refill and reflood phases of a LOCA.

5.4.21 Marviken Critical Flow Tests

The Marviken Full Scale Critical Flow Tests have been conducted as a multi-national project at the Marviken Power Station in Sweden. The test facility consists of four major components: a full scale BWR vessel, a discharge pipe attaching to the bottom of the vessel, a test nozzle connecting to the downstream end of the discharge pipe, and a rupture disk bundle attaching to the downstream end of the nozzle. The Marviken test data has been widely used in assessing critical flow models of various system codes.

5.4.22 UPTF CCFL and Entrainment Tests

The Upper Plenum Test Facility (UPTF) was operated by Kraftwerk Union AG (KWU) where several separate effects and integral tests were run. The UPTF was designed to simulate a German four loop 3,900 MWt pressurized water reactor (PWR) primary system, similar in size and geometry as a Westinghouse four-loop PWR. The facility was intended to provide a full-scale simulation of thermal-hydraulic behavior in the primary system during the end-of-blowdown, refill, and reflood phases of a PWR large break loss-of-coolant accident (LBLOCA). Though this test facility was developed to study PWR LOCA phenomena, some of the specific

SET tests are equally applicable for BWR LOCA, specifically, [

]

5.4.23 SSTF Integral Tests

The full scale 30-degree steam sector test facility (SSTF) mocks up 58 individual fuel bundles, the surrounding peripheral and interstitial bypass region, upper plenum (UP) and lower plenum (LP), guide tubes, jet pump flow paths, downcomer, and ECCS injection systems. The integral tests involve BWR system refill/reflood during a LOCA event. The system transients were experimental simulations of the later phase of the LOCA blowdown from 150 psia with core heat simulated by steam injections.

5.4.24 TLTA Integral Tests

Refer to the previous discussion on the TLTA description (Section 5.4.14). The TLTA integral tests simulate large and small break BWR LOCA.

5.4.25 FIST Integral Tests

The Full Integral Simulation Test (FIST) facility was created as an upgrade to TLTA to eliminate most scaling issues. Like TLTA, FIST is a single bundle test facility. FIST represents a full height scaling of the vessel and internal components. The facility has accurately scaled components and ECC systems representing a GE BWR/6 plant scaled to 1/624 which represents the single bundle in FIST. The facility consists of two recirculation loops with two jet pumps.



Table 5-1 AURORA-B LOCA Evaluation Model Assessment Matrix

[illegible]

Where:

CB – Core bypass
DC – Downcomer
GT – Guide tubes
JP – Jet pump
LP – Lower plenum
RL – Recirculation line
RP – Recirculation pump
SL – Steam line
UP – Upper plenum

5.5 *Evaluate Effects of IET Distortions and SET Scaleup Capability (EMDAP Step 8)*

The experimental database includes full size prototypic SET or component data for all highly ranked PIRT phenomena and processes that are not treated as initial conditions or plant parameters. In some situations where reduced scale SETs or component tests were used to develop models (for example TLTA jet pump height and LTSF 1/6 scale jet pump), full height data is available to confirm the scale-up of the model (for example FIST).

5.6 *Determine Experimental Uncertainties as Appropriate (EMDAP Step 9)*

Considerations for experimental uncertainty were made during selection of the experimental database. In some instances, measurement errors, experimental biases, or other aspects of experimentation were identified in experimental data that impacted an assessment. Where applicable, issues with experimental data are discussed for the specific assessment.

6.0 Develop Evaluation Model (EMDAP Element 3); Chapter 15, Section 15.0.2, Item 2

As previously discussed, an EM is a collection of calculational devices (computer codes) and procedures developed and organized to meet the requirements established in Element 1. This EMDAP Element describes the integration of the devices into a cohesive package for assessment in EMDAP Element 4.

6.1 Establish an Evaluation Model Development Plan (EMDAP Step 10)

A development plan was established at the initiation of the model development and revised as the development progressed to guide the development process. The plan identified methodology requirements and specifies the procedures and work practices to which the development efforts are to adhere. The procedures and work practices define processes for ensuring compliance with applicable QA criteria (including Appendix B to 10 CFR 50).

Taken as a whole, the development plan plus adherence to procedures and work practices ensure that the EM has been developed to specific design requirements, meets expectations for documentation and programming standards, addresses transportability requirements, and is developed within the framework of applicable QA criteria and configuration control procedures.

6.2 Appendix K Compliance Models

The foundation of the AURORA-B LOCA methodology is based on the requirements of 10 CFR 50 Appendix K. The following subsections list the 10 CFR 50 Appendix K requirements (in italics) followed by the explanation of compliance with the AURORA-B LOCA EM.

6.2.1 I.A. Sources of heat during the LOCA

For the heat sources listed in paragraphs I.A.1 to 4 of this appendix it must be assumed that the reactor has been operating continuously at a power level at least 1.02 times the licensed power level (to allow for instrumentation error), with the maximum peaking factor allowed by the technical specifications. An assumed power level lower than the level specified in this paragraph (but not less than the licensed power level) may be used provided the proposed alternative value has been demonstrated to account for uncertainties due to power level instrumentation error. A range of power distribution shapes and peaking factors representing power distributions that may occur over the core lifetime must be studied. The selected

combination of power distribution shape and peaking factor should be the one that results in the most severe calculated consequences for the spectrum of postulated breaks and single failures that are analyzed.

Infinite operating time at 102% of licensed power is assumed. This LTR does not address the methodology to create lower alternative power uncertainties; however a lower alternative value may be applied if justified based on other USNRC approved methodology. It is assumed that values larger than 2% are acceptable as conservative relative to Appendix K requirements.

[

]

[
]



Figure 6-1 Example Axial Power Distributions

6.2.2 I.A.1. The Initial Stored Energy in the Fuel

The steady-state temperature distribution and stored energy in the fuel before the hypothetical accident shall be calculated for the burn-up that yields the highest calculated cladding temperature (or, optionally, the highest calculated stored energy). To accomplish this, the thermal conductivity of the UO_2 shall be evaluated as a function of burn-up and temperature, taking into consideration differences in initial density, and the thermal conductance of the gap between the UO_2 and the cladding shall be evaluated as a function of the burn-up, taking into consideration fuel densification and expansion, the composition and pressure of the gases within the fuel rod, the initial cold gap dimension with its tolerances, and cladding creep.

The RODEX4 thermal-mechanical code is used in the EM to determine stored energy. The conservative application of the code for storage energy is presented in Section 6.4.2. RODEX4 contains all of the above mentioned features.

6.2.3 I.A.2. Fission Heat

Fission heat shall be calculated using reactivity and reactor kinetics. Shutdown reactivities resulting from temperatures and voids shall be given their minimum plausible values, including allowance for uncertainties, for the range of power distribution shapes and peaking factors indicated to be studied above. Rod trip and insertion may be assumed if they are calculated to occur.

Fission heat is calculated using the point kinetics model in S-RELAP5. This point kinetics model is unchanged from the standard RELAP5 model. [

]

The point reactor kinetics model computes both the immediate fission power and the power from decay of fission products. The immediate power is that released at the time of fission and

includes power from kinetic energy of the fission products and neutron moderation. Decay power is generated as the fission products undergo radioactive decay based on draft ANS 1971 standard. Additional information is provided in Reference 6, Section 11.1.

6.2.4 I.A.3. Decay of Actinides

The heat from the radioactive decay of actinides, including neptunium and plutonium generated during operation, as well as isotopes of uranium, shall be calculated in accordance with fuel cycle calculations and known radioactive properties. The actinide decay heat chosen shall be that appropriate for the time in the fuel cycle that yields the highest calculated fuel temperature during the LOCA.

The actinide model describes the production of ^{239}U , ^{239}Np and ^{239}Pu from neutron capture by ^{238}U as detailed in Reference 6, Section 11.3 and is consistent with the 1979 ANS standard. [

]

6.2.5 I.A.4. Fission Product Decay

The heat generation rates from radioactive decay of fission products shall be assumed to be equal to 1.2 times the values for infinite operating time in the ANS Standard (Proposed American Nuclear Society Standards- "Decay Energy Release Rates Following Shutdown of Uranium-Fueled Thermal Reactors." Approved by Subcommittee ANS-5, ANS Standards Committee, October 1971). This standard has been approved for incorporation by reference by the Director of the Federal Register. A copy of the standard is available for inspection at the NRC Library, 11545 Rockville Pike, Rockville, Maryland 20852-2738. The fraction of the locally generated gamma energy that is deposited in the fuel (including the cladding) may be different from 1.0; the value used shall be justified by a suitable calculation.

Decay heat from fission products are based on the draft ANS 1971 standard and use 1.2 times the values for infinite operating time. The standard is in table form as detailed in Reference 6 Section 11.2.1.

The suitable calculation for gamma energy deposited in the fuel is AREVA's BWR fuel management reactor physics code used for reload licensing analyses.

6.2.6 I.A.5. Metal-Water Reaction Rate

The rate of energy release, hydrogen generation, and cladding oxidation from the metal/water reaction shall be calculated using the Baker-Just equation (Baker, L., Just, L.C., "Studies of Metal Water Reactions at High Temperatures, III. Experimental and Theoretical Studies of the Zirconium-Water Reaction," ANL-6548, page 7, May 1962). This publication has been approved for incorporation by reference by the Director of the Federal Register. A copy of the publication is available for inspection at the NRC Library, 11545 Rockville Pike, Two White Flint North, Rockville, Maryland 20852-2738. The reaction shall be assumed not to be steam limited. For rods whose cladding is calculated to rupture during the LOCA, the inside of the cladding shall be assumed to react after the rupture. The calculation of the reaction rate on the inside of the cladding shall also follow the Baker-Just equation, starting at the time when the cladding is calculated to rupture, and extending around the cladding inner circumference and axially no less than 1.5 inches each way from the location of the rupture, with the reaction assumed not to be steam limited.

The metal-water reaction rate is calculated using the Baker-Just equation as stated in Appendix K, which is applied to the outer cladding surface as required. Once cladding rupture has been predicted, the reaction is initiated on the interior cladding surface as well. [

] Per Appendix K, the reaction is conservatively assumed to not be steam limited. The effects of swelling and rupture also are included (Reference 25) and are based on NUREG 0630 (Reference 24).

6.2.7 I.A.6. Reactor Internals Heat Transfer

Heat transfer from piping, vessel walls, and non-fuel internal hardware shall be taken into account.

Heat transfer from significant nonnuclear sources is included in the calculations. These sources are discussed in Section 6.3 and include:

- Reactor vessel
- Recirculation loop piping
- Lower plenum internals

- Steam dryers
- Shroud
- Shroud dome and separators

6.2.8 I.A.7. Pressurized Water Primary-to-Secondary Heat Transfer

Heat transferred between primary and secondary systems through heat exchangers (steam generators) shall be taken into account. (Not applicable to Boiling Water Reactors).

This requirement does not apply for BWRs.

6.2.9 I.B. Swelling and Rupture of the Cladding and Fuel Rod Thermal Parameters

Each evaluation model shall include a provision for predicting cladding swelling and rupture from consideration of the axial temperature distribution of the cladding and from the difference in pressure between the inside and outside of the cladding, both as functions of time. To be acceptable the swelling and rupture calculations shall be based on applicable data in such a way that the degree of swelling and incidence of rupture are not underestimated. The degree of swelling and rupture shall be taken into account in calculations of gap conductance, cladding oxidation and embrittlement, and hydrogen generation.

The calculations of fuel and cladding temperatures as a function of time shall use values for gap conductance and other thermal parameters as functions of temperature and other applicable time-dependent variables. The gap conductance shall be varied in accordance with changes in gap dimensions and any other applicable variables.

The NUREG-0630 (Reference 24) model is used to calculate swelling and rupture as documented in Reference 25. The rupture and swelling model is discussed in Section 6.4.5

6.2.10 I.C.1.a Break Characteristics and Flow

In analyses of hypothetical loss-of-coolant accidents, a spectrum of possible pipe breaks shall be considered. This spectrum shall include instantaneous double-ended breaks ranging in cross-sectional area up to and including that of the largest pipe in the primary coolant system. The analysis shall also include the effects of longitudinal splits in the largest pipes, with the split area equal to the cross-sectional area of the pipe.

The method is intended to analyze a spectrum of both large and small breaks which includes double-ended breaks and longitudinal splits.

6.2.11 I.C.1.b. Discharge Model

For all times after the discharging fluid has been calculated to be two-phase in composition, the discharge rate shall be calculated by use of the Moody model (F. J. Moody, "Maximum Flow Rate of a Single Component. Two-Phase Mixture," Journal of Heat Transfer, Transactions of the American Society of Mechanical Engineers, 87, No. 1, February, 1965). This publication has been approved for incorporation by reference by the Director of the Federal Register. A copy of this publication is available for inspection at the NRC Library, 11545 Rockville Pike, Rockville, Maryland 20852-2738. The calculation shall be conducted with at least three values of a discharge coefficient applied to the postulated break area, these values spanning the range from 0.6 to 1.0. If the results indicate that the maximum clad temperature for the hypothetical accident is to be found at an even lower value of the discharge coefficient, the range of discharge coefficients shall be extended until the maximum clad temperatures calculated by this variation has been achieved.

S-RELAP5 includes the option for Moody critical flow. The Moody critical flow model is used at the break for two-phase conditions. Moody critical flow is also used at other locations that could influence the break discharging fluid; [

] The
guillotine breaks are limited to the pipe area times discharge coefficients from [

]

6.2.12 I.C.1.c. End of Blowdown

(Applies Only to Pressurized Water Reactors.) For postulated cold leg breaks, all emergency cooling water injected into the inlet lines or the reactor vessel during the bypass period shall in the calculations be subtracted from the reactor vessel calculated inventory. This may be executed in the calculation during the bypass period, or as an alternative the amount of emergency core cooling water calculated to be injected during the bypass period may be subtracted later in the calculation from the water remaining in the inlet lines, downcomer, and

reactor vessel lower plenum after the bypass period. This bypassing shall end in the calculation at a time designated as the "end of bypass," after which the expulsion or entrainment mechanisms responsible for the bypassing are calculated not to be effective. The end-of-bypass definition used in the calculation shall be justified by a suitable combination of analysis and experimental data. Acceptable methods for defining "end of bypass" include, but are not limited to, the following: (1) Prediction of the blowdown calculation of downward flow in the downcomer for the remainder of the blowdown period; (2) Prediction of a threshold for droplet entrainment in the upward velocity, using local fluid conditions and a conservative critical Weber number.

This requirement does not apply to BWRs; however, this point in time is important since requirements to avoid a return to nucleate boiling are lifted after the end of blowdown.

Appendix K does not provide criteria for end of blowdown for BWRs. [

]

6.2.13 I.C.1.d. Noding Near the Break and the ECCS Injection Points

The noding in the vicinity of and including the broken or split sections of pipe and the points of ECCS injection shall be chosen to permit a reliable analysis of the thermodynamic history in these regions during blowdown.

The geometry of the pipes are explicitly modeled. [

]

6.2.14 I.C.2. Frictional Pressure Drops

The frictional losses in pipes and other components including the reactor core shall be calculated using models that include realistic variation of friction factor with Reynolds number, and realistic two-phase friction multipliers that have been adequately verified by comparison with experimental data, or models that prove at least equally conservative with respect to maximum clad temperature calculated during the hypothetical accident. The modified Baroczy correlation (Baroczy, C. J., "A Systematic Correlation for Two-Phase Pressure Drop," Chem. Enging. Prog. Symp. Series, No. 64, Vol. 62, 1965) or, combination of the Thom correlation (Thom, J.R.S., Prediction of Pressure Drop During Forced Circulation Boiling of Water," Int. J. of Heat & Mass Transfer, 7, 709-724, 1964) for pressures equal to or greater than 250 psia and the Martinelli-Nelson correlation (Martinelli, R. C. Nelson, D.B., "Prediction of Pressure Drop During Forced Circulation Boiling of Water," Transactions of ASME, 695-702, 1948) for pressures lower than 250 psia is acceptable as a basis for calculating realistic two-phase friction multipliers.

The referenced correlations stated in Appendix K are commonly considered in the development of thermal-hydraulic computer codes. Other similar correlations have been developed and used extensively in the public domain. In S-RELAP5 wall friction is presented in Sections 3.5 - 3.6 of Reference 6 and summarized as follows. [

] Besides the history of these correlations in the public domain, the adequacy of these correlations are demonstrated in the pressure drop assessments as summarized in Section 7.6.1.

6.2.15 I.C.3. Momentum Equation

The following effects shall be taken into account in the conservation of momentum equation: (1) temporal change of momentum, (2) momentum convection, (3) area change momentum flux, (4) momentum change due to compressibility, (5) pressure loss resulting from wall friction, (6) pressure loss resulting from area change, and (7) gravitational acceleration. Any omission of one or more of these terms under stated circumstances shall be justified by comparative analyses or by experimental data.

S-RELAP5 contains all of the required terms as described in Section 2.1 of Reference 6.

6.2.16 I.C.4. Critical Heat Flux

- a) *Correlations developed from appropriate steady-state and transient-state experimental data are acceptable for use in predicting the critical heat flux (CHF) during LOCA transients. The computer programs in which these correlation's are used shall contain suitable checks to assure that the physical parameters are within the range of parameters specified for use of the correlations by their respective authors.*
- b) *Steady-state CHF correlations acceptable for use in LOCA transients include, but are not limited to, the following:*
 - (1) *W 3. L. S. Tong, "Prediction of Departure from Nucleate Boiling for an Axially Non-uniform Heat Flux Distribution," Journal of Nuclear Energy, Vol. 21, 241-248, 1967.*
 - (2) *B&W-2. J. S. Gellerstedt, R. A. Lee, W.J. Oberjohn, R. H. Wilson, L. J. Stanek, "Correlation of Critical Heat Flux in a Bundle Cooled by Pressurized Water," Two-Phase Flow and Heat Transfer in Rod Bundles, ASME, New York, 1969.*
 - (3) *Hench-Levy. J. M. Healzer, J. E. Hench, E. Janssen, S. Levy, "Design Basis for Critical Heat Flux Condition In Boiling Water Reactors," 186, GE Company Private report, July 1966.*
 - (4) *Macbeth. R. V. Macbeth, "An Appraisal of Forced Convection Burnout Data," Proceedings of the Institute of Mechanical Engineers, 1965-1966.*
 - (5) *Barnett. P. G. Barnett, "A Correlation of Burnout Data for Uniformly Heated Annuli and Its Uses for Predicting Burnout in Uniformly Heated Rod Bundles," AFEW-R463, 1966.*
 - (6) *Hughes. E. D. Hughes, "A Correlation of Rod Bundle Critical Heat Flux for Water in the Pressure Range 150 to 726 psia," IN-1412, Idaho Nuclear Corporation, July 1970.*

- c) *Correlations of appropriate transient CHF data may be accepted for use in LOCA transient analyses if comparisons between the data and the correlations are provided to demonstrate that the correlations predict values of CHF which allow for uncertainty in the experimental data throughout the range of parameters for which the correlations are to be used. Where appropriate, the comparisons shall use statistical uncertainty analysis of the data to demonstrate the conservatism of the transient correlation.*
- d) *Transient CHF correlations acceptable for use in LOCA transients include, but are not limited to, the following:*
 - (1) *GE transient CHF. B. C. Slifer, J. E. Hench, "Loss-of-Coolant Accident and Emergency Core Cooling Models for General Electric Boiling Water Reactors," NEDO-10329, General Electric Company, Equation C-32, April 1971.*
- e) *After CHF is first predicted at an axial fuel rod location during blowdown, the calculation shall not use nucleate boiling heat transfer correlations at that location subsequently during the blowdown even if the calculated local fluid and surface conditions would apparently justify the reestablishment of nucleate boiling. Heat transfer assumptions characteristic of return to nucleate boiling (rewetting) shall be permitted when justified by the calculated local fluid and surface conditions during the reflood portion of a LOCA.*

The CHF correlation used is based on the 2006 Groeneveld critical heat flux look up table (2006 CHF LUT) of Reference 41. Justification for the correlation is presented in Section 6.4.10.

Restriction to reestablishment of nucleate boiling is presented in Section 6.4.9.

6.2.17 I.C.5. Post-CHF Heat Transfer Correlations

- a) *Correlations of heat transfer from the fuel cladding to the surrounding fluid in the post-CHF regimes of transition and film boiling shall be compared to applicable steady-state and transient-state data using statistical correlation and uncertainty analyses. Such comparison shall demonstrate that the correlations predict values of heat transfer coefficient equal to or less than the mean value of the applicable experimental heat transfer data throughout the range of parameters for which the correlations are to be used. The comparisons shall quantify the relation of the correlations to the statistical uncertainty of the applicable data.*
- b) *The Groeneveld flow film boiling correlation (equation 5.7 of D.C. Groeneveld, "An Investigation of Heat Transfer in the Liquid Deficient Regime," AECL-3281, revised December 1969) and the Westinghouse correlation of steady-state transition boiling*

("Proprietary Redirect/Rebuttal Testimony of Westinghouse Electric Corporation," USNRC Docket RM-50-1, page 25-1, October 26, 1972) are acceptable for use in the post-CHF boiling regimes. In addition, the transition boiling correlation of McDonough, Milich, and King (J.B. McDonough, W. Milich, E.C. King, "An Experimental Study of Partial Film Boiling Region with Water at Elevated Pressures in a Round Vertical Tube," Chemical Engineering Progress Symposium Series, Vol. 57, No.32, pages 197-208, (1961) is suitable for use between nucleate and film boiling. Use of all these correlations is restricted as follows:

- (1) The Groeneveld correlation shall not be used in the region near its low-pressure singularity.*
 - (2) The first term (nucleate) of the Westinghouse correlation and the entire McDonough, Milich, and King correlation shall not be used during the blowdown after the temperature difference between the clad and the saturated fluid first exceeds 300 F.*
 - (3) Transition boiling heat transfer shall not be reapplied for the remainder of the LOCA blowdown, even if the clad superheat returns below 300 F, except for the reflood portion of the LOCA when justified by the calculated local fluid and surface conditions.*
- c) Evaluation models approved after October 17, 1988, which make use of the Dougall-Rohsenow flow film boiling correlation (R.S. Dougall and W.M. Rohsenow, "Film Boiling on the Inside of Vertical Tubes with Upward Flow of Fluid at Low Qualities," MIT Report Number 9079 26, Cambridge, Massachusetts, September 1963) may not use this correlation under conditions where non-conservative predictions of heat transfer result. Evaluation models that make use of the Dougall-Rohsenow correlation and were approved prior to October 17, 1988, continue to be acceptable until a change is made to, or an error is corrected in, the evaluation model that results in a significant reduction in the overall conservatism in the evaluation model. At that time continued use of the Dougall-Rohsenow correlation under conditions where non-conservative predictions of heat transfer result will no longer be acceptable. For this purpose, a significant reduction in the overall conservatism in the evaluation model would be a reduction in the calculated peak fuel cladding temperature of at least 50°F from that which would have been calculated on October 17, 1988, due either to individual changes or error corrections or the net effect of an accumulation of changes or error corrections.*

Transition boiling is based on the Appendix K "acceptable to use" McDonough, Milich and King correlation. The correlation and its justification and use are presented in Section 6.4.11.

[

] The correlations

and their justification and use are presented in Section 6.4.13. Restriction to reestablishment of transition boiling is presented in Section 6.4.9.

6.2.18 I.C.6. Pump Modeling

The characteristics of rotating primary system pumps (axial flow, turbine, or centrifugal) shall be derived from a dynamic model that includes momentum transfer between the fluid and the rotating member, with variable pump speed as a function of time. The pump model resistance used for analysis should be justified. The pump model for the two-phase region shall be verified by applicable two-phase pump performance data. For BWR's after saturation is calculated at the pump suction, the pump head may be assumed to vary linearly with quality, going to zero for one percent quality at the pump suction, so long as the analysis shows that core flow stops before the quality at pump suction reaches one percent.

Two-phase pump performance degradation data is based on an Electrical Power Research Institute (EPRI) model (Reference 14) which is incorporated into the S-RELAP5 PUMP component model (Reference 6, Section 6.2.3). With the exception of the two-phase degradation model, the S-RELAP5 PUMP component model is the same as that of RELAP5/MOD3 which is a model consisting of four-quadrant single-phase homologous curves used to characterize the pump head and torque based on functions of volumetric flow and pump speed. Input for the model is obtained for each individual reactor from the plant parameters document.

6.2.19 I.C.7. Core Flow Distribution During Blowdown (Applies only to pressurized water reactors)

- a) *The flow rate through the hot region of the core during blowdown shall be calculated as a function of time. For the purpose of these calculations the hot region chosen shall not be greater than the size of one fuel bundle. Calculations of average flow and flow in the hot region shall take into account cross flow between regions and any flow blockage calculated to occur during blowdown as a result of cladding swelling or rupture. The calculated flow*

shall be smoothed to eliminate any calculated rapid oscillations (period less than 0.1 seconds),

- b) *A method shall be specified for determining the enthalpy to be used as input data to the hot channel heatup analysis from quantities calculated in the blowdown analysis, consistent with the flow distribution calculations.*

This section of Appendix K does not apply to BWRs; [

]

6.2.20 I.D.1. Single Failure Criterion

An analysis of possible failure modes of ECCS equipment and of their effects on ECCS performance must be made. In carrying out the accident evaluation the combination of ECCS subsystems assumed to be operative shall be those available after the most damaging single failure of ECCS equipment has taken place.

The single failure scenarios are determined for each plant. The worst single failure scenario that produces the highest PCT is determined from the evaluation. Additional calculations with different possible single failures may be required unless the limiting single failure is evident.

6.2.21 I.D.2. Containment Pressure

The containment pressure used for evaluating cooling effectiveness during reflood and spray cooling shall not exceed a pressure calculated conservatively for this purpose. The calculation shall include the effects of operation of all installed pressure-reducing systems and processes.

For BWR LOCA scenarios, atmospheric back pressure has traditionally been assumed as adequate and conservative. [

]

6.2.22 I.D.3. Calculation of Reflood Rate for Pressurized Water Reactors

The refilling of the reactor vessel and the time and rate of reflooding of the core shall be calculated by an acceptable model that takes into consideration the thermal and hydraulic characteristics of the core and of the reactor system. The primary system coolant pumps shall be assumed to have locked impellers if this assumption leads to the maximum calculated cladding temperature; otherwise the pump rotor shall be assumed to be running free. The ratio of the total fluid flow at the core exit plane to the total liquid flow at the core inlet plane (carryover fraction) shall be used to determine the core exit flow and shall be determined in accordance with applicable experimental data (for example, "PWR FLECHT (Full Length Emergency Cooling Heat Transfer) Final Report," Westinghouse Report WCAP-7665, April 1971; "PWR Full Length Emergency Cooling Heat Transfer (FLECHT) Group I Test Report," Westinghouse Report WCAP-7435, January 1970; "PWR FLECHT (Full Length Emergency Cooling Heat Transfer) Group II Test Report," Westinghouse Report WCAP-7544, September 1970; "PWR FLECHT Final Report Supplement," Westinghouse Report WCAP-7931, October 1972). The effects on reflooding rate of the compressed gas in the accumulator which is discharged following accumulator water discharge shall also be taken into account.

This requirement does not apply for BWRs.

6.2.23 I.D.4. Steam Interaction with Emergency Core Cooling Water in Pressurized Water Reactors

The thermal-hydraulic interaction between steam and all emergency core cooling water shall be taken into account in calculating the core reflooding rate. During refill and reflood, the calculated steam flow in unbroken reactor coolant pipes shall be taken to be zero during the time that accumulators are discharging water into those pipes unless experimental evidence is available regarding the realistic thermal-hydraulic interaction between the steam and the liquid. In this case, the experimental data may be used to support an alternate assumption.

This requirement does not apply for BWRs.

6.2.24 I.D.5. Refill and Reflood Heat Transfer for Pressurized Water Reactors

- a) *For reflood rates of one inch per second or higher, reflood heat transfer coefficients shall be based on applicable experimental data for unblocked cores including FLECHT results ("PWR FLECHT (Full Length Emergency Cooling Heat Transfer) Final Report,"*

Westinghouse Report WCAP-7665, April 1971). The use of a correlation derived from FLECHT data shall be demonstrated to be conservative for the transient to which it is applied; presently available FLECHT heat transfer correlations ("PWR Full Length Emergency Cooling Heat Transfer (FLECHT) Group I Test Report," Westinghouse Report WCAP-7544, September 1970; "PWR FLECHT Final Report Supplement," Westinghouse Report WCAP-7931, October 1972) are not acceptable. Westinghouse Report WCAP-7665 has been approved for incorporation by reference by the Director of the Federal Register. A copy of this report is available for inspection at the NRC Library, 11545 Rockville Pike, Rockville, Maryland 20852-2738. Now correlations or modifications to the FLECHT heat transfer correlations are acceptable only after they are demonstrated to be conservative, by comparison with FLECHT data, for a range of parameters consistent with the transient to which they are applied.

- b) During refill and during reflood when reflood rates are less than one inch per second, heat transfer calculations shall be based on the assumption that cooling is only by steam, and shall take into account any flow blockage calculated to occur as a result of cladding swelling or rupture as such blockage might affect both local steam flow and heat transfer.*

These requirements do not apply for BWRs.

6.2.25 I.D.6. Convective Heat Transfer Coefficients for Boiling Water Reactor Fuel Rods Under Spray Cooling

Following the blowdown period convective heat transfer shall be calculated using coefficients based on appropriate experimental data. For reactors with jet pumps and having fuel rods in a 7 x 7 fuel bundle array, the following convective coefficients are acceptable:

- a) During the period following lower plenum flashing but prior to the core spray reaching rated flow, a convective heat transfer coefficient of zero shall be applied to all fuel rods*
- b) During the period after core spray reaches rated flow but prior to reflooding, convective heat transfer coefficients of 3.0, 3.5, 1.5, and 1.5 Btu/(hr-ft²-F) shall be applied to the fuel rods in the outer corners, outer row, next to outer row, and to those remaining in the interior, respectively, of the bundle.*
- c) After the two-phase reflooding fluid reaches the level under consideration, a convective heat transfer coefficient of 25 Btu/(hr-ft²-F) shall be applied to all fuel rods.*

Convective heat transfer coefficients during core spray are determined from the applicable heat transfer correlations and validated by the assessments; therefore they met the requirement of “coefficients based on appropriate experimental data”. The method is further described in Section 6.4.17.

6.2.26 I.D.7. The Boiling Water Reactor Channel Box Under Spray Cooling

Following the blowdown period, heat transfer from, and wetting of, the channel box shall be based on appropriate experimental data. For reactors with jet pumps and fuel rods in a 7 x 7 fuel bundle array, the following heat transfer coefficients and wetting time correlation are acceptable.

- a) *During the period after lower plenum flashing, but prior to core spray reaching rated flow, a convective coefficient of zero shall be applied to the fuel bundle channel box.*
- b) *During the period after core spray reaches rated flow, but prior to wetting of the channel, a convective heat transfer coefficient of 5 Btu/(hr-ft²-F) shall be applied to both sides of the channel box.*
- c) *Wetting of the channel box shall be assumed to occur 60,seconds after the time determined using the correlation based on the Yamanouchi analysis ("Loss-of-Coolant Accident and Emergency Core Cooling Models for General Electric Boiling Water Reactors," General Electric Company Report NEDO-10329, April 1971). This report was approved for Incorporation by reference by the Director of the Federal Register. A copy of the report is available for inspection at the NRC Library, 11545 Rockville Pike, Rockville, Maryland 2738.*

Convective heat transfer coefficients during core spray are determined from the applicable heat transfer correlations and validated by the assessments; therefore they met the requirement of “coefficients based on appropriate experimental data”. The acceptable approach described above is not used. The method is further described in Section 6.4.17.

6.2.27 II. Required Documentation

- 1a. *A description of each evaluation model shall be furnished. The description shall be sufficiently complete to permit technical review of the analytical approach including the equations used, their approximations in difference form, the assumptions made, and the*

values of all parameters or the procedure for their selection, as for example, in accordance with a specified physical law or empirical correlation.

This LTR is intended to meet this requirement.

- 1b. A complete listing of each computer program, in the same form as used in the evaluation model, must be furnished to the Nuclear Regulatory Commission upon request.*

The computer code will be furnished upon request.

- 2. For each computer program, solution convergence shall be demonstrated by studies of system modeling or nodding and calculation time steps.*

The AURORA-B LOCA EM is developed following the EMDAP process. The EMPDAP process details the applicable experimental information and data that is use to compare to the EM as presented in this report. Sensitivity studies are presented in Sections 7.9.3 and 7.9.4.

- 3. Appropriate sensitivity studies shall be performed for each evaluation model, to evaluate the effect on the calculated results of variations in nodding, phenomena assumed in the calculation to predominate, including pump operation or locking and values of parameters over their applicable ranges. For items to which results are shown to be sensitive, the choices made shall be justified.*

Same response as Item 2.

- 4. To the extent practicable, predictions of the evaluation model, or portions thereof, shall be compared with applicable experimental information.*

Comparisons of the EM with applicable experimental information is described in Section 5.4.

- 5. General Standards for Acceptability. Elements of evaluation models reviewed will include technical adequacy of the calculational methods, including: For models covered by 50.46(a)(1)(ii), compliance with required features of section I of this Appendix K; and, for models covered by 50.46(a)(1)(1), assurance of a high level of probability that the performance criteria of 50.46(b) would not be exceeded.*

No additional requirements are included in this item.

6.3 *Establish Evaluation Model Structure (EMDAP Step 11)*

The EM structure includes the structure of the CCDs, as well as the structure that combines the devices into the overall EM. This structure is based on the principles of Element 1 (especially Step 3), as well as the requirements established in Element 1 and Step 10 and significant experience with analyzing BWR events. The structure consists of the following six ingredients:

1. *Systems and components:* The EM structure is able to analyze the behavior of all systems and components that play a role in the target scenarios.
2. *Constituents and phases:* The EM structure is able to analyze the behavior of all constituents and phases relevant to the target scenarios.
3. *Field equations:* The field equations are solved to determine the transport of the quantities of interest.
4. *Closure relations:* Correlations and equations that help to evaluate the terms in the field equations by providing code capability to model and scale particular processes are available.
5. *Numerics:* The numerics provide the capability to perform efficient and reliable calculations.
6. *Additional features:* Additional features are available to provide the capability to model boundary conditions and control systems.

The structure defined in this section addresses the systems, components, phases, geometries, fields, and processes described in Section 4.5 (EMDAP Step 3). How each ingredient is addressed in the EM is summarized in the subsections 6.3.1 through 6.3.5. As described in Section 8.0, the EM development was an iterative process until the EM was determined to be adequate for the target applications. The status of the EM structure described in the subsections reflects the final product of the development process, as indicated by having models available for all the required code structures. References 6 and 9 provide more detail on the theoretical descriptions for each of the component calculational devices. Note, because of the importance of selecting proper closure relationships for the governing equations, the specific models are treated separately in EMDAP Step 12, but the basic processes are defined here because the code structure must be able to accommodate the closure relationships.

The way in which the component calculational devices are integrated to form the EM is discussed in Sections 6.3.6, including external data transfers and spatial and temporal coupling. A high level description of the nodalization of the plant model is provided in Section 6.3.7. Finally, a hot channel model designed to analyze local FoM based on results from a system scale calculation is addressed in Section 6.3.8.

6.3.1 Code Structure

To properly model a BWR plant, a code system must have a structure that adequately models the important systems and components of the plant with respect to the target scenarios. As indicated in Table 6-1, the code system has the ability to model all relevant features of the plant. The specific configuration of the structure (e.g. plant nodalization) is described in Section 6.3.7.

Table 6-1 Code Structure

--

6.3.2 Field Equations

The field and transport equations (conservation of mass, momentum, energy, neutron flux, etc.) possess the capability of addressing phenomena and processes occurring in the plant during the target scenarios for the specified set of constituents and phases. As indicated in Table 6-2, the code system has the ability to model all necessary field equations that have been identified.

The thermal-hydraulic and thermal conduction field equations used within S-RELAP5 are the same as used in the RLBLOCA methodology described in Reference 5 and AURORA-B AOO described in Reference 1 and other USNRC approved methodologies based on RELAP5. Extensive technical detail related to the field equations is provided in the S-RELAP5 theoretical description (Reference 6).

For LOCA analysis, the fission power is calculated from a simpler point kinetics model instead of the 3-D kinetics model used for AURORA-B AOO. [

]

For the point reactor kinetics model, the power is computed using the space-independent or point kinetic approximation which assumes that power can be separated into space and time functions. This approximation is adequate for cases in which the space distribution remains nearly constant. The point reactor kinetics model computes both the immediate fission power and the power from decay of fission products. The immediate power is that released at the time of fission and includes power from kinetic energy of the fission products and neutron moderation. Decay power is generated as the fission products undergo radioactive decay. The equations are presented in Reference 6, Section 11.

No field equations are used within the kernel of the RODEX4 fuel thermal-mechanical code that is implemented within S-RELAP5. Instead, the RODEX4 kernel calculates the fuel properties based on the temperature predictions of the S-RELAP5 thermal conduction equations.

Table 6-2 Field & Transport Equations

--

6.3.3 Closure Relations

Many processes and closure relations are required to support the basic field equations. The primary thermal-hydraulic, thermal conduction, and neutron kinetics processes and closure relations that model highly ranked PIRT phenomena are summarized in Table 6-3. This table summarizes the processes and closure relations at a high level. Additional closure relations are described separately in Section 6.4 (EMDAP Step 12).

Table 6-3 Processes and Closure Relations

--

Table 6-4 Additional Features

6.3.4 Code Numerics

Numerical solution techniques are available to solve the field equations. The numerical solution techniques contained in S-RELAP5 for the thermal-hydraulic and thermal conduction equations are described in Reference 6, and are the same as used in other RELAP5 based methodologies.

Numerical solution techniques for fuel rod material properties are derived from RODEX4 and are described in Reference 9.

6.3.5 Additional Features

Additional features are available to model control systems within the EM. The relevant BWR control systems (feedwater, pressure, recirculation, etc.) are modeled to modulate elements of the code structure, nodalization, and boundary conditions. The relevant trip systems are modeled using control variable and trip components to determine time of scram and turn on/off elements of the code structure such as recirculation pumps.

6.3.6 External Data Transfer

External data transfer is an important element of the procedures for treating the input information (particularly the code input arising from the assumed plant state at transient initiation). The amount and content of data that must be transferred to the EM from external data sources is important in assuring accurate modeling of the BWR plant at the target initial conditions. A summary schematic highlighting important elements of the external data transfer is shown in Figure 6-2.



Figure 6-2 External Data Transfer to AURORA-B LOCA EM

6.3.7 Plant Model Nodalization

Modeling of the plant hydraulic components and heat structures is a mathematical mapping from the physical system to the computational framework of the EM. It is recognized that different approaches to the nodalization may yield different results (the “user effect”). The EM relies on a consistent approach to defining the nodalization of the BWR plant to minimize the user effect. Because of the complexity of nuclear power plants and design variations between like plants; the concept of a “standard nuclear power plant nodalization” cannot apply without great simplification and requires clarification.

Nodalization has traditionally referred to the mathematical representation of the physical system (e.g. flow areas, lengths, and volumes), but this is just one element. A “standard nodalization” considers all computer code input necessary to represent the physical plant and any engineered features influencing plant performance. These include trips and control systems, component dynamics (e.g., pumps), and safety system performance. In addition, computer codes include model options and other plant-independent input for specific phenomenological code models that must be specified to ensure consistency with the assessment base of the EM.

In order to achieve the above, detailed technical guidance has been developed to define the framework under which standardized input models are prepared for the EM. Specifically, the purpose of the technical guidance is to establish a consistent approach for the following parameters;

- Nodalization of hydrodynamic components, heat structures, and their connections, plus flow and pressure boundary conditions
- Modeling practices for components and processes (including selection of phenomenological code models)
- Control variable and trip definition, and their use
- Material properties
- Initialization of the components and structures

The following sections summarize the key aspects of the technical guidance for nodalization of hydrodynamic components and heat structures, as well as the modeling practices for key components and processes. The AURORA-B LOCA EM nodalization is based on the AURORA-B AOO EM nodalization (Reference 1) which also included requirements for

establishing the control variables, trip definitions, and their use from Reference 20. The following sections repeat information provided in Reference 1. Modifications specifically for the AURORA-B LOCA EM are identified.

6.3.7.1 Pressure Vessel Region

The motivation for selecting the heat structure placement and nodalization is to provide adequate modeling of stored energy. The primary motivation in selecting the hydrodynamic nodalization is defining a physically accurate representation of volumes, flow areas, and lengths to ensure accurate modeling of liquid and steam inventory and modeling the fluid momentum or “inertia” in the system.


The hydrodynamic nodalization of the pressure vessel region is shown in Figure 6-3 through Figure 6-7, and the S-RELAP5 hydrodynamic component type is defined in Table 6-5. [

]

[] The scheme is similar to the 3-region TRAC model used in the USNRC sponsored SSTF assessment of Reference 64, where the core bypass and upper and lower plenums are modeled as three concentric rings.

Though not indicated in Figure 6-3 through Figure 6-7, [

] (Note that the drawings are not to scale.)



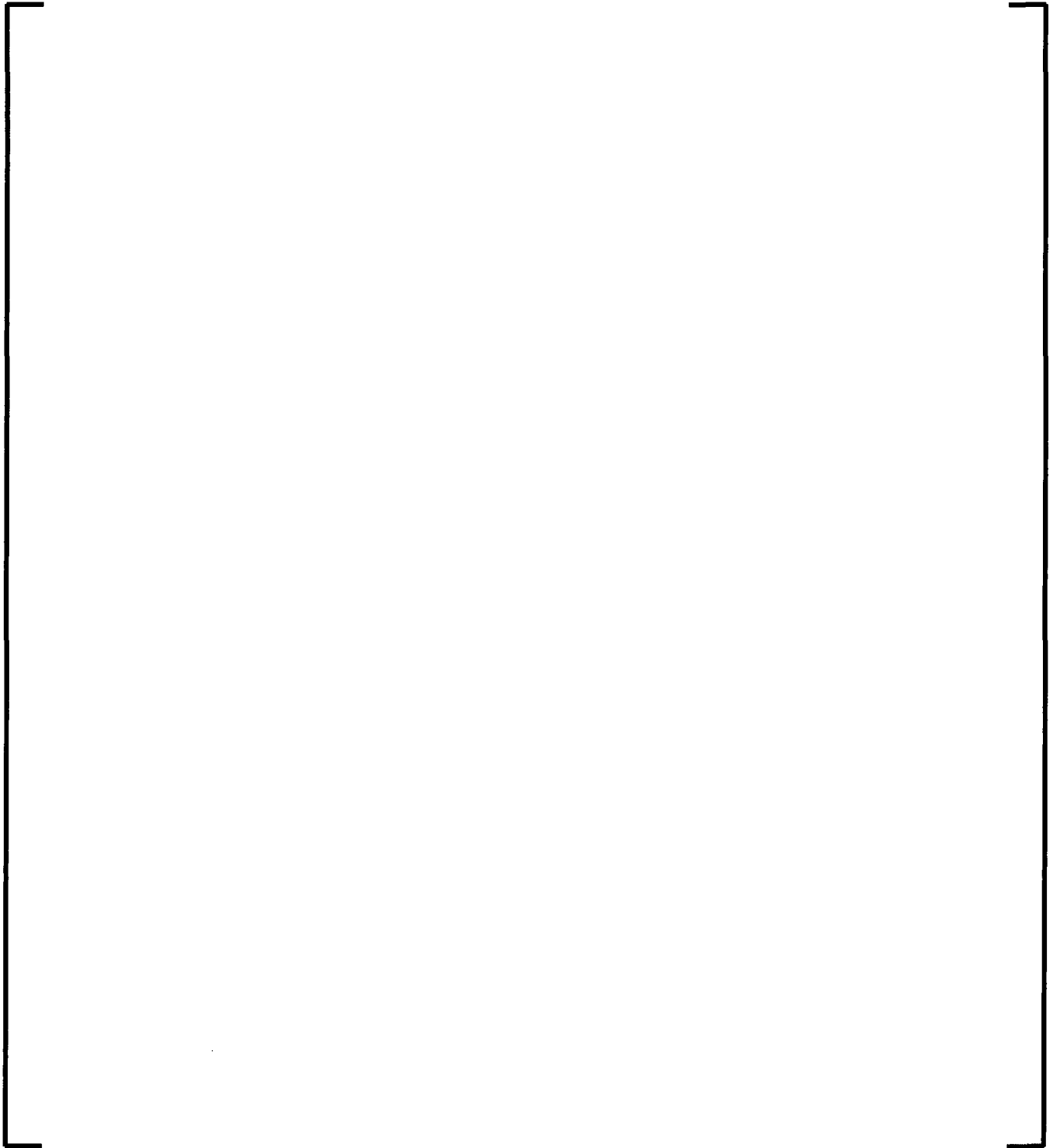


Figure 6-3 Overview of Reactor Vessel Nodalization (Jet-Pump Plant)

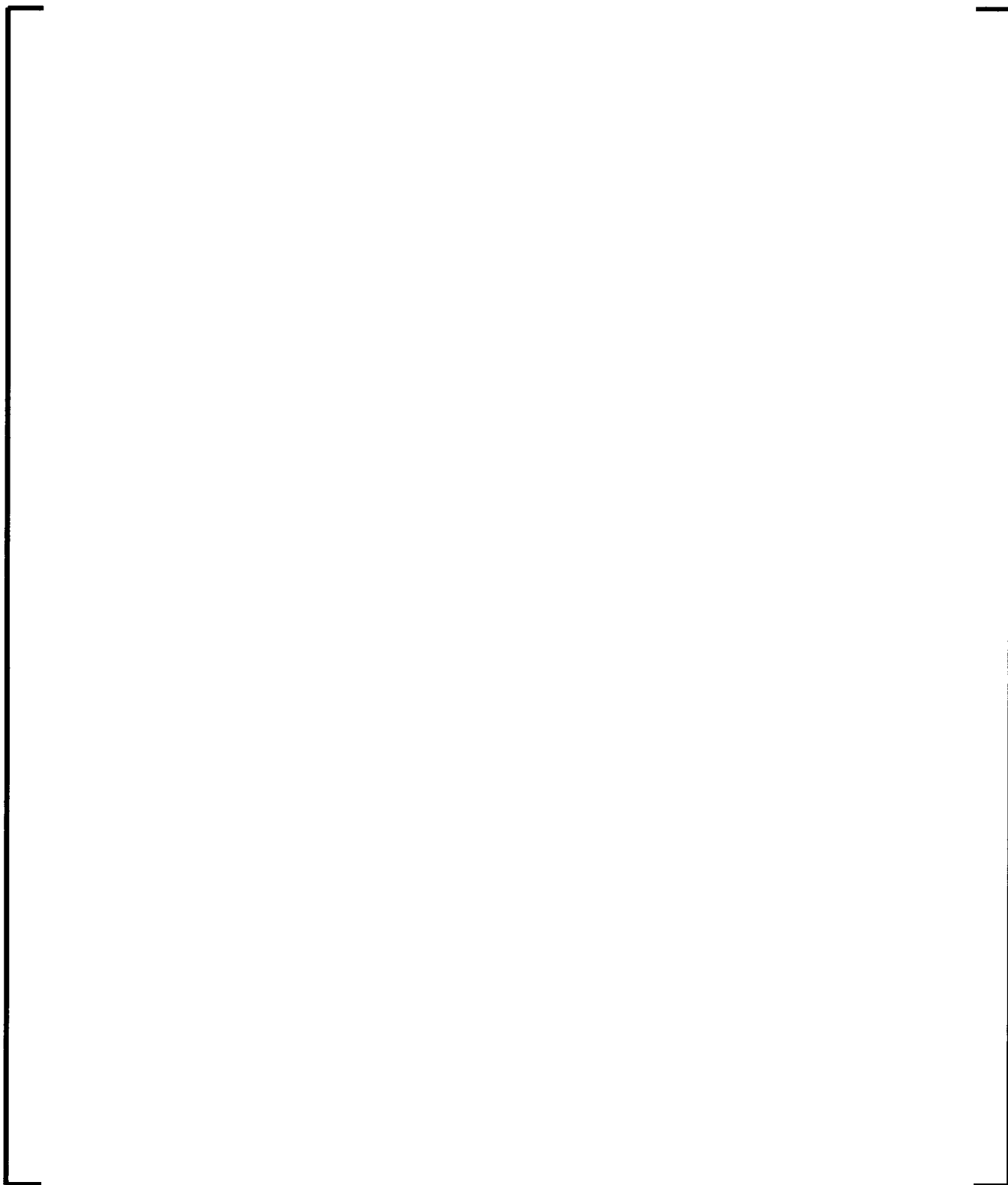


Figure 6-4 Typical Nodalization of Downcomer and Mid-Vessel Region (Jet-Pump Plant)



Figure 6-5 Azimuthal Nodalization of Lower Downcomer Region (Jet-Pump Plant)

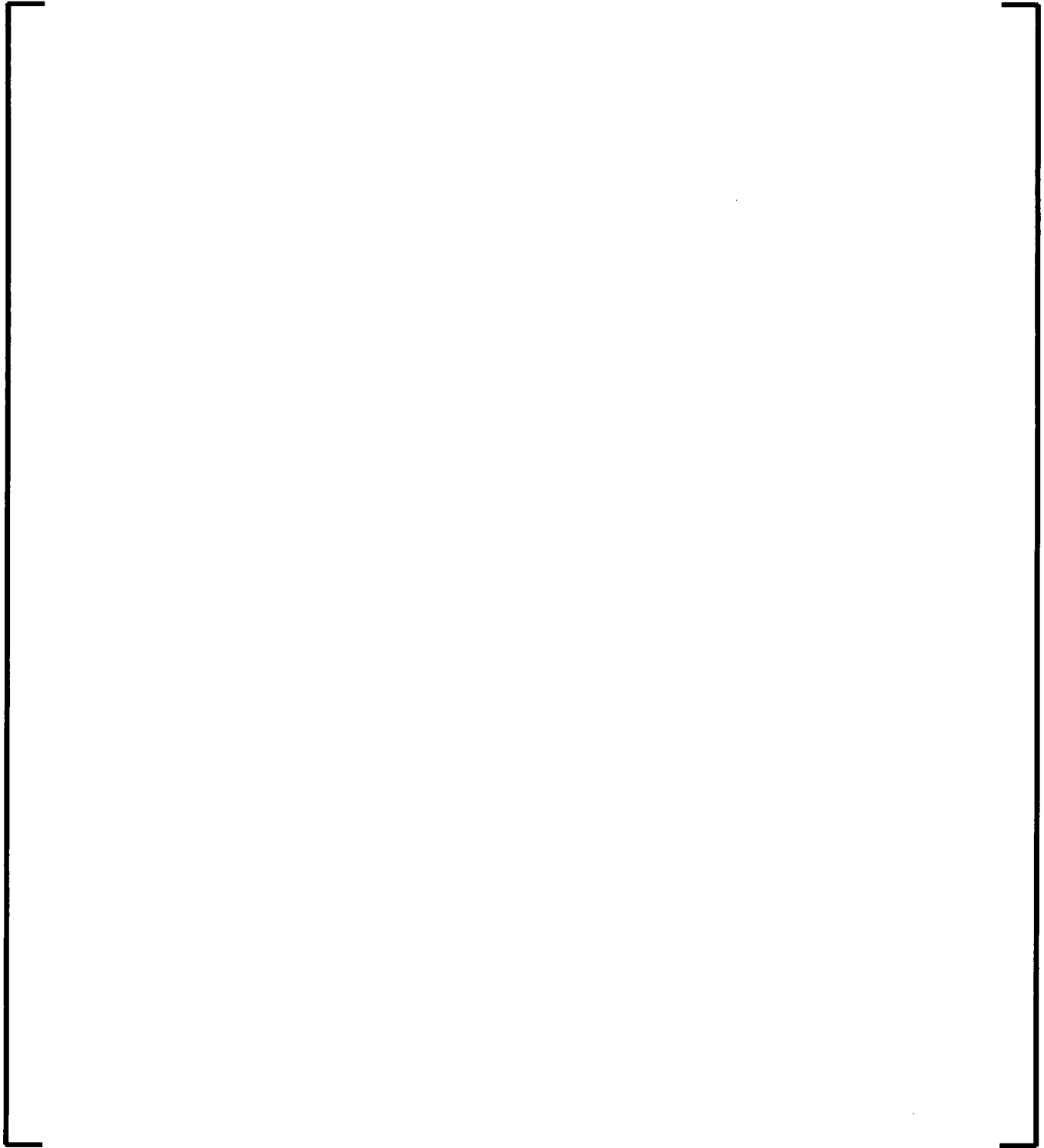


Figure 6-6 Nodalization of Lower Vessel Region (Jet-Pump Plant)

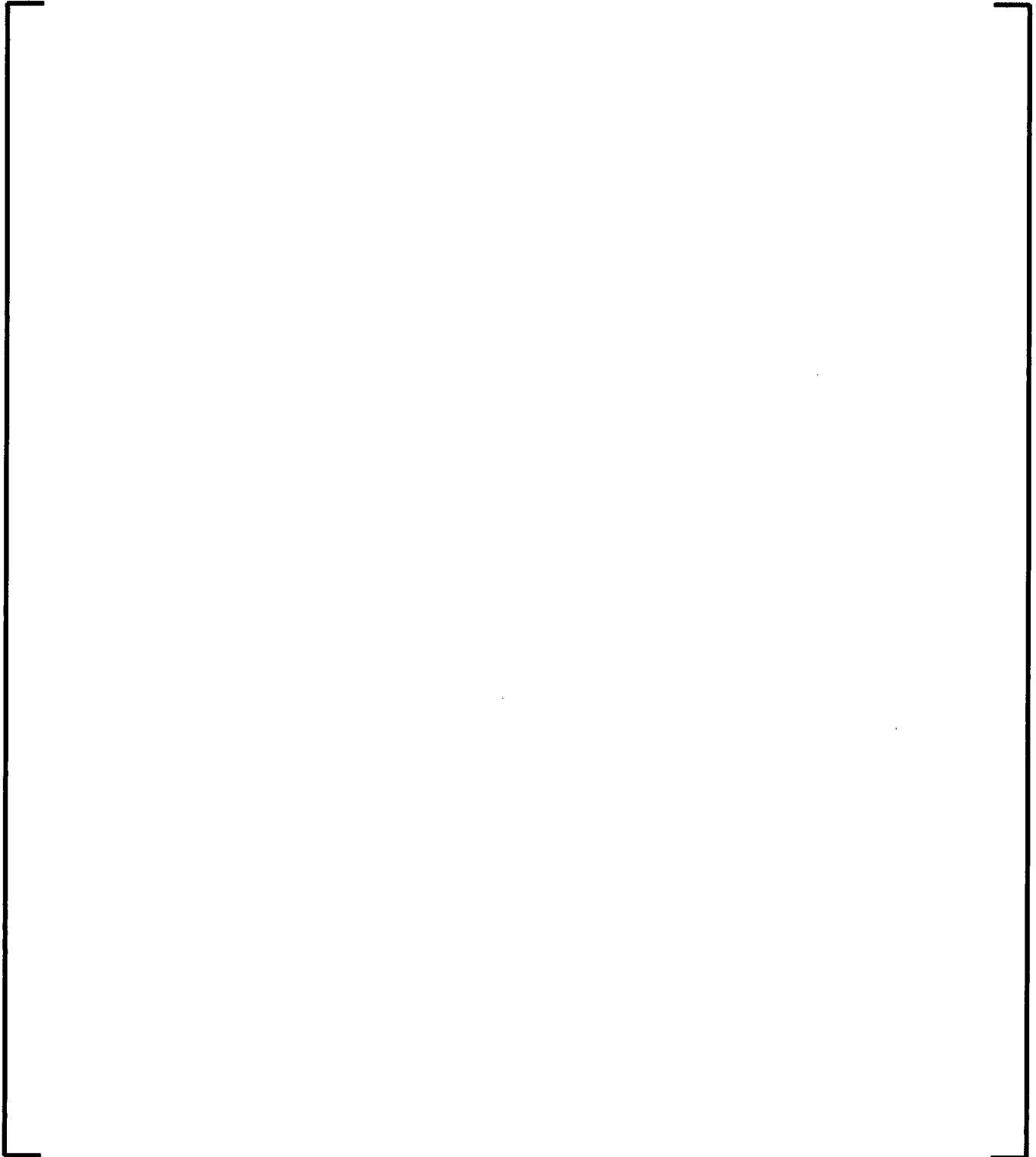


Figure 6-7 Nodalization of Upper Vessel Region (Jet-Pump Plant)

6.3.7.2 Upper Plenum

For low pressure and high pressure core sprays, the upper plenum is nodalized to model the interactions between core spray and steam exiting the bundles. [

]

6.3.7.3 Core Region

The nodalization of the fuel bundles, flow channels, water channels/rods, core bypass region, and associated heat structures are developed in a manner consistent with the steady state core simulator and fuel design data. Modeling of the vertical distance between hydrodynamic nodes is also consistent with the distances used in the steady state core simulator. The input for flow area, heated surface area, hydraulic diameter, etc. for each node is based on the best available data for the fuel designs and core layout. [

]

Modeling of spacer grid and tie plate pressure losses in the fuel bundles and pressure losses in the inlet orifices, core support plate, core bypass, and lower tie plate to core bypass leakage pathways are based on the best available data. [

]

There are four leakage paths for which reverse flow (also called backflow) is important in the LOCA evaluation. These leakage paths are included as junctions in the LOCA modeling of the reactor. These leakage paths are between the bypass and core regions, the bypass and lower plenum, and the CRGTs and lower plenum. The backflow leakage usually occurs during the refill period when makeup water flows into the bypass and CRGT regions and from there into the core and lower plenum. During the refill period, wall temperatures are generally above the saturation temperature; thus, water flowing through these flow paths may void and limit the flow beyond that caused by single-phase form losses. This is known as the hot wall effect. The hot wall effect is insignificant if the fluid supplying the leakage path is sufficiently subcooled. If there is little or no subcooling, the reverse flows are reduced to account for the hot wall effects.

Consistent with the upper plenum, [

] LOCA analysis are generally not cycle specific and are performed for a change in an operating domain, plant system or fuel type; therefore, the LOCA fuel grouping is intended to be generic.

[

] During the LOCA event, different directional channel flows can occur in the core (Reference 64). There can be some bundles in co-current upflow, some bundles in co-current downflow, and some bundles in counter current flow, occurring simultaneously and at various times. []

Table 6-6 Example Bundle Distribution

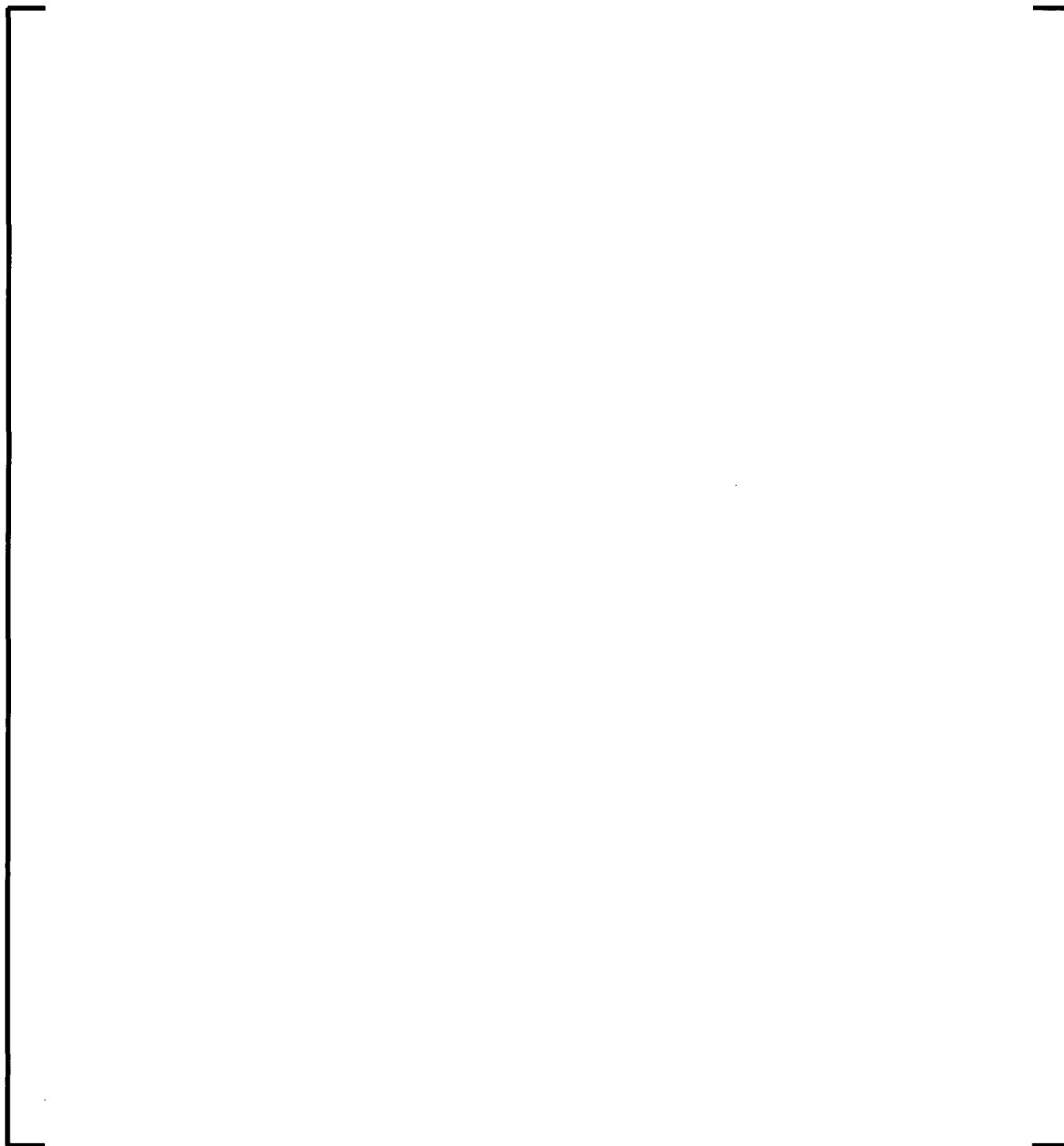


Figure 6-8 Nodalization of Core and Bypass Region

6.3.7.4 Lower Plenum

The lower plenum region was significantly changed from the AURORA-B AOO EM. [

]

6.3.7.5 Steam Lines

Unlike the reactor pressure vessel internals, which are fairly consistent from plant to plant, the configuration of steam lines in a BWR can vary widely. This is especially true outside of the containment. While varying widely in configuration, preservation of several key physical characteristics in the nodalization of the steam lines ensures good fidelity of numerical predictions. [

]

6.3.7.6 Recirculation System



Figure 6-9 Nodalization of Recirculation Lines

6.3.7.7 Plant Parameters Data

Plant parameters data are those parameters used in preparing input to the EM that describe the configuration of a given plant. [

]

The plant parameters data provides necessary information for the physical plant and any engineered features influencing plant performance as part of the “standard nodalization”. The data are obtained from plant drawings, plant design data and specifications, component/equipment design data and specifications, plant system manuals, Technical Specifications, startup test data, plant operation data, and other similar sources.

The following list summarizes key plant parameters data used in developing input to the EM;

The approach for selecting specific values for plant parameters data that assure plant operations are bounded is described in Section 9.0 for the application methodology.

6.3.8 Hot Channel Model

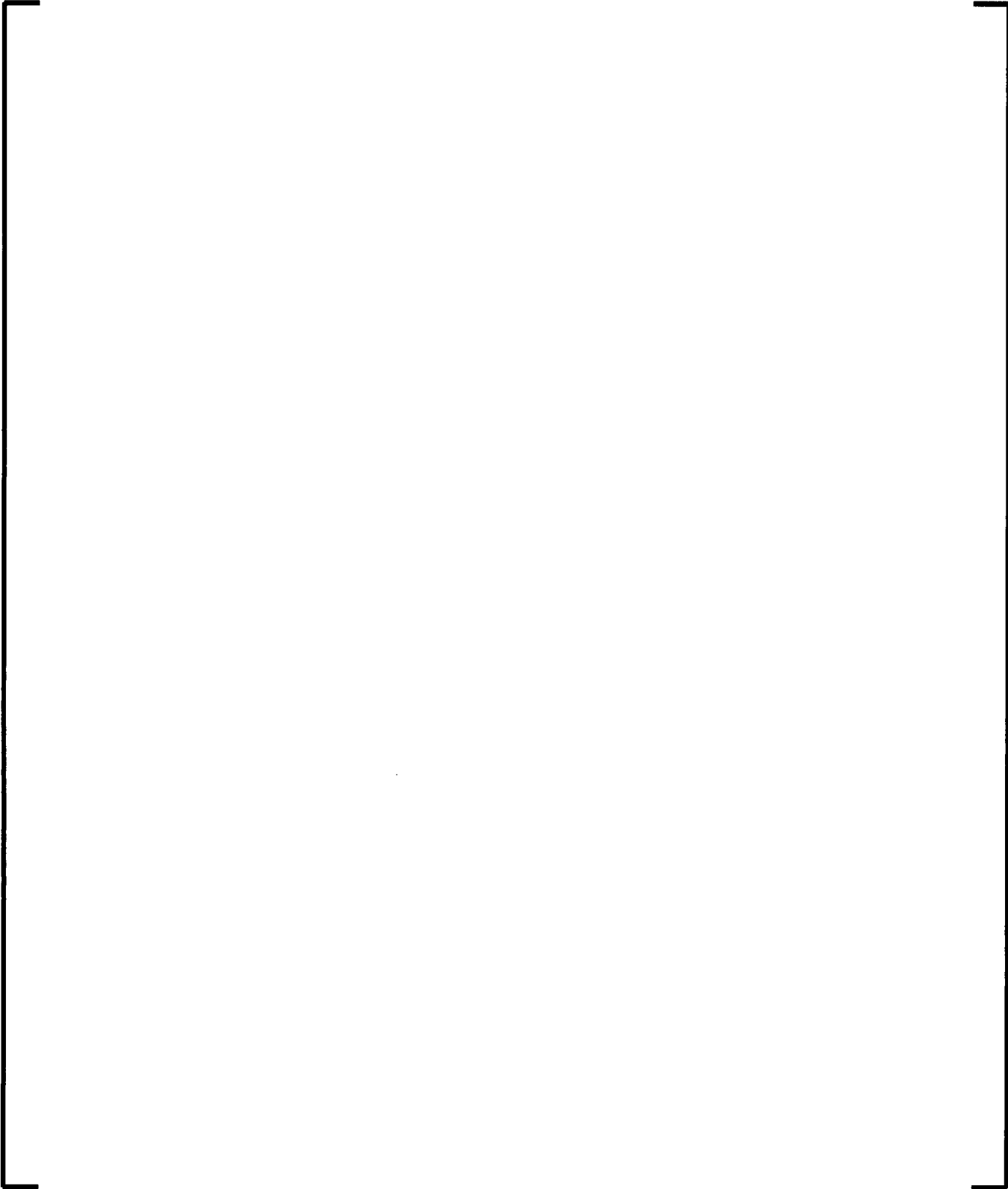




Figure 6-10 Hot Channel Model

6.4 *Develop or Incorporate Closure Models (EMDAP Step 12)*

Models and closure relations identified in EMDAP Step 3 that did not already exist within the component calculational devices were developed or incorporated in the EM. The needed closure relations and process models were created, refined and/or assessed based on test data depending on their origin and pedigree.

A large number of models and closure relations are necessary to analyze the target scenarios, many of which are not associated with predicting highly ranked phenomena and processes. The theory manuals for the CCDs provide in-depth descriptions of the models and closure relations. In addition, the validation and assessment of the CCDs address the basis, range of applicability, and accuracy of the models and closure relations. The following subsections provide a summary of the closure models developed for AURORA-B LOCA and for compliance with Appendix K requirements.

6.4.1 Appendix K Requirements

Appendix K requirements are addressed in Section 6.2. The Appendix K requirements were defined in the early 70s, since that time, evaluation models have become much more advanced and have inherently included many of the aspects defined in Appendix K; this is true for S-RELAP5 where many of the Appendix K requirements are achieved by model input. Some Appendix K requirements are achieved by a change to an existing S-RELAP5 model or by adding a new model. Most of the additions to S-RELAP5 needed to model a BWR were accomplished with the development of the AURORA-B AOO EM (Reference 1). The key closure models for the LOCA EM are presented in the following subsections.

6.4.2 Stored Energy

6.4.2.1 Limiting Power History

6.4.2.2 Bounding Centerline Temperature

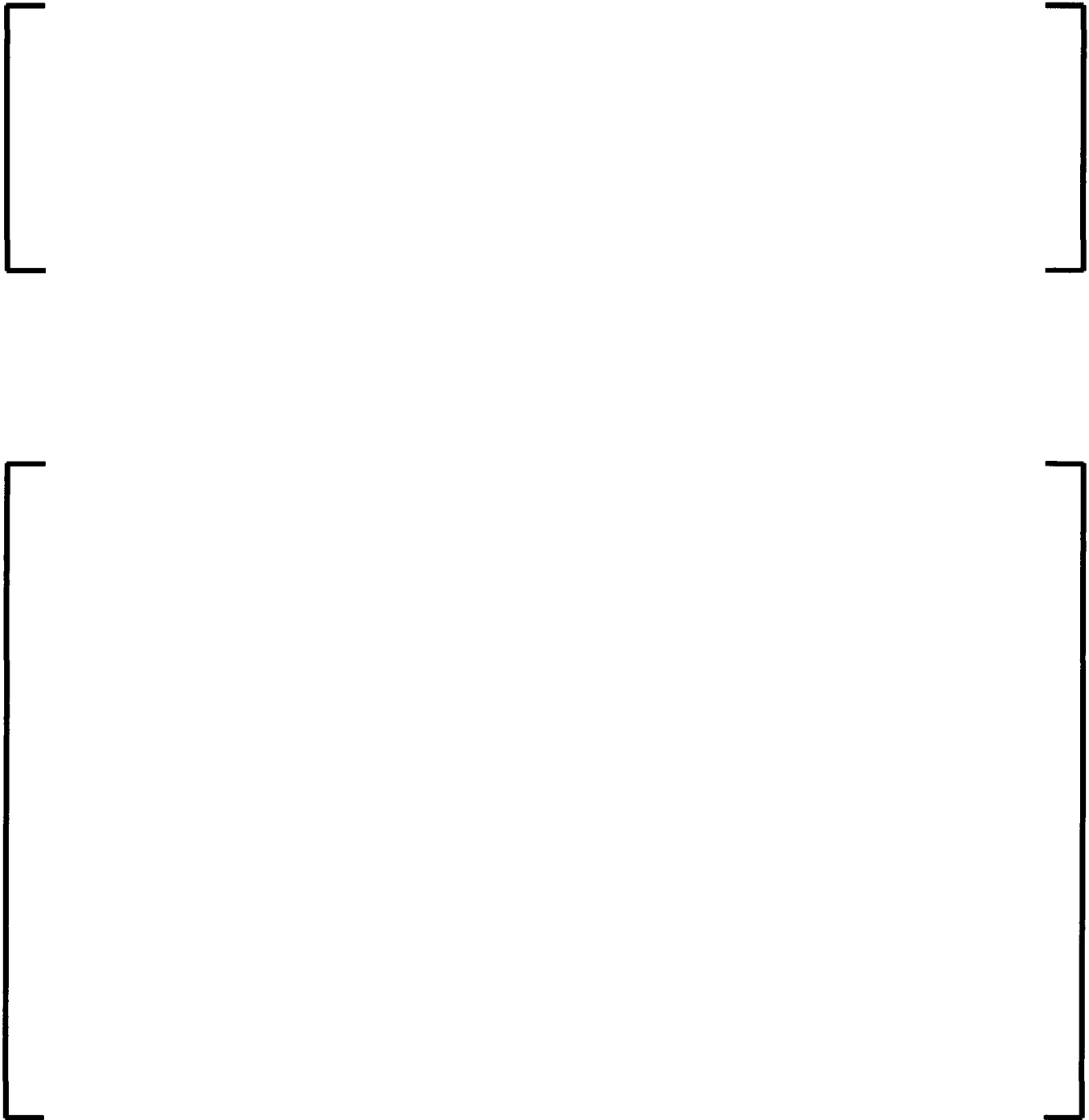


Figure 6-11 Halden Centerline Temperature Upper Bound

6.4.3 Decay Heat

6.4.3.1 Fission Product Decay

The ANS-71 Draft Standard decay heat table is installed in S-RELAP5 and is chosen as a code option (Reference 6 Section 11.2.1). As required by Appendix K, the option includes the multiplier of 1.2. This option is not new and has been used in the AREVA PWR Appendix K small break LOCA methodology.

6.4.3.2 Actinide Decay Heat

The actinide model describes the production of ^{239}U , ^{239}Np and ^{239}Pu from neutron capture by ^{238}U as detailed in Reference 6 Section 11.3. [

]

6.4.4 Metal-Water Reaction

The steam oxidation of the zirconium (Zr) cladding is an exothermic reaction. The reaction of zirconium and steam is treated using the rate-dependent correlation developed by Baker-Just, as required by Appendix K and is not steam limited.

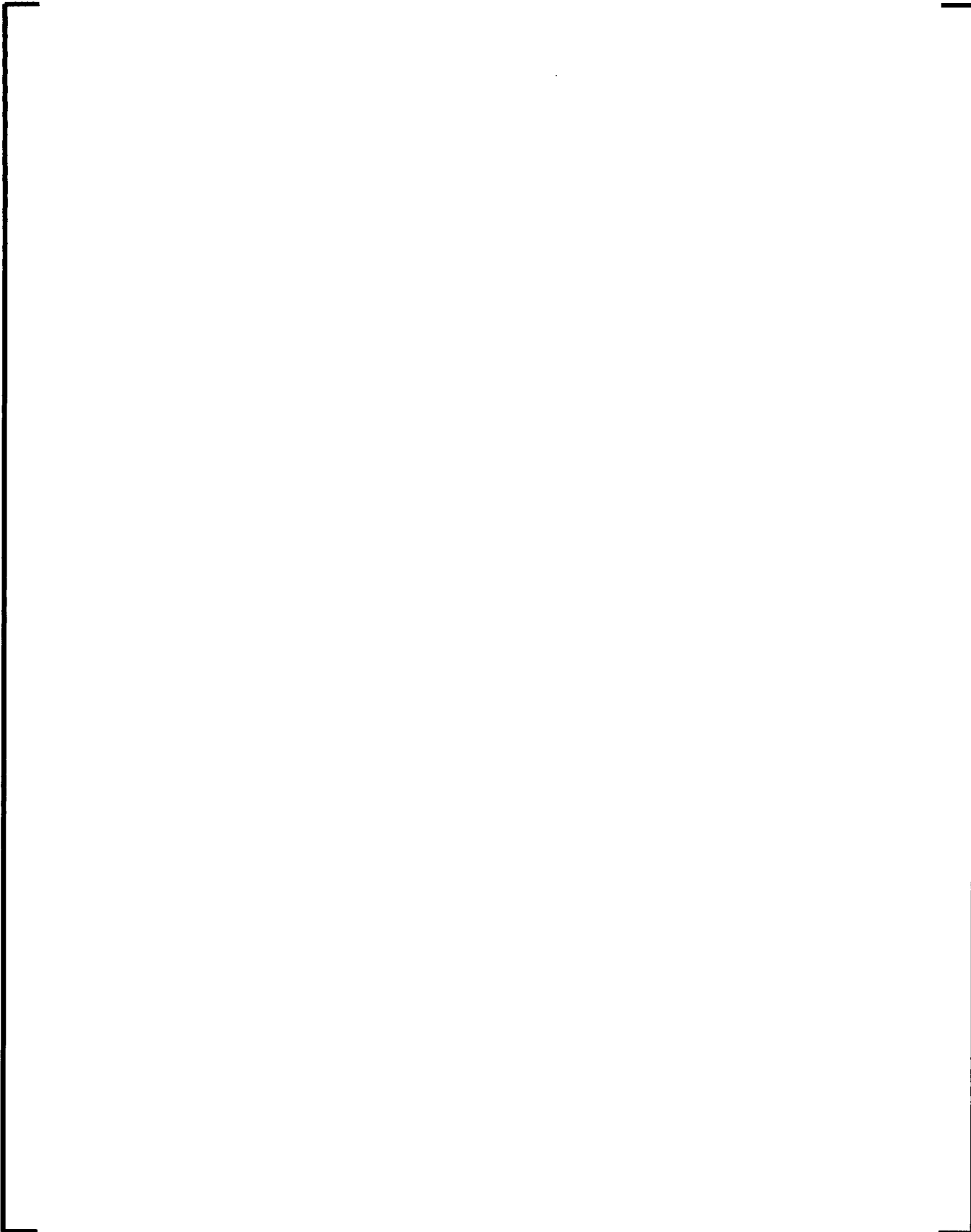
The metal-water reaction model is coupled with the cladding ballooning and rupture model to account for the thinning of the oxide layers with strain, and to account for the reaction of the inside cladding surface. Inside metal-water reaction is modeled only on the ruptured fuel rod axial node. Clad thinning increases the rate that steam (oxygen) can diffuse through the oxide layer, and hence increases the metal-water heat release. Additional theory is presented in Reference 6, Section 7.4.10.

6.4.5 Fuel Swell, Rupture, and Relocation

The AREVA clad ballooning and rupture model (Reference 25) has been implemented in the S-RELAP5/RODEX4 model. The model is based on NUREG 0630 (Reference 24) and has been used in previous AREVA LOCA methodologies. The clad ballooning and rupture model is used to compute the radial displacement due to clad ballooning and rupture at each axial elevation as a function of the hoop stress, the average cladding temperature and the dimensionless cladding heatup rate. Clad ballooning and/or rupture only occurs when the clad temperatures are high, and the inside rod pressure is greater than the pressure in the coolant channel.

Tests performed with irradiated fuel rods experiencing LOCA have shown an accumulation of fuel debris in the swollen region (called ballooning) of the burst cladding which resulted from fuel fragments slumping from upper locations. This process, generally called fuel relocation, is initiated at the time of the cladding burst and the driving forces are both gravity and the pressure difference between the rod upper plenum and the channel outside the fuel rod.

The model used in S-RELAP5 is []:



[

]

For BWRs, the impact of flow blockage from swelling and rupture has been shown experimentally not to be significant on heat transfer from core spray or bottom reflood (References 24, 30 and 31). [

]

Table 6-7 Relocation Packing Fractions for Limited Strains

[

]



Figure 6-12 Relocation Packing Factor Data and Bounds



Figure 6-13 Limiting Strain Cases

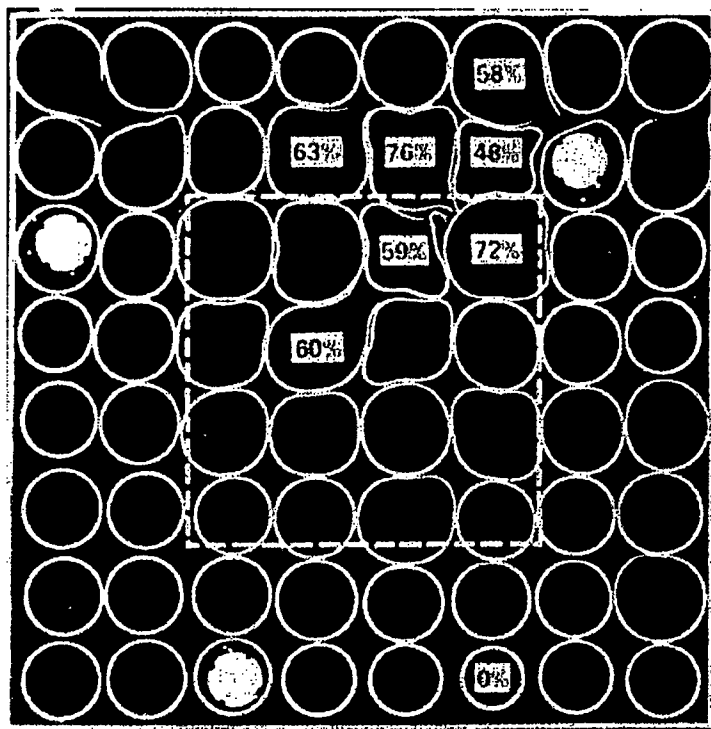


Figure 6-14 ORNL MRBT 8x8 Assembly Rupture

6.4.6 Discharge Model

Appendix K requires the Moody critical flow model be used for the evaluation of the break discharge when the conditions at the break are two-phase. The Moody critical flow model is defined in Reference 6 Section 5.2. [

As stated in Appendix K, the calculation is conducted with at least three values of a discharge coefficient applied to the postulated break area, these values spanning the range from [

]

A split break is a longitudinal opening or hole in the piping that results in a single break flow path to the containment. [

] Consistent with Appendix K, the maximum area considered for a split break is the maximum cross-sectional area of the piping containing the break. Smaller areas are considered as needed to establish a trend showing that these breaks are not limiting relative to fuel acceptance criteria such as PCT.

In addition to breaks in the recirculation line, consideration of breaks in other reactor coolant system piping is part of a LOCA break spectrum analysis. Although the recirculation line large break results in the largest coolant inventory loss, it may not necessarily result in the most severe challenge to event acceptance criteria such as PCT.

- The double-ended rupture of a main steam line is expected to result in the fastest depressurization of the reactor vessel, however, the high heat transfer during the blowdown period and the rapid initiation of the low-pressure ECCS may lead to PCTs significantly less than the limiting recirculation line break.
- Special consideration is required when the postulated break occurs in ECCS piping. Although ECCS piping breaks are small relative to a recirculation pipe DEG break, the potential to disable an ECCS system increases their severity.
- Non-recirculation line breaks outside of the containment are inherently less challenging to fuel limits than breaks inside the containment. For breaks outside containment, isolation or check valve closure will terminate break flow prior to the loss of significant liquid inventory and the core will remain covered.

6.4.7 Upper Plenum Mixing Model

During a LOCA event, the core spray injection into the upper plenum is in the form of spray when the sparger nozzles are not covered by a two-phase mixture or in the form of submerged jets when the sparger nozzles are covered. The heat transfer of the upper plenum vapor and liquid to the subcooled spray injection is a complex mixing phenomena. Detailed spray and submerged jet models were developed for TRAC (References 33 and 34). The predicted results from these detailed models were reported to be in limited agreement with the test results (Figure 4.3-8 of Reference 35); [

]

6.4.7.1 Condensation Model

A spray droplet condensation model is implemented to address core spray into the upper plenum. [

]

6.4.7.2 Simplified Empirical Model

6.4.8 Heat Transfer Correlation Selection Logic

The wall-to-fluid heat transfer coefficients depend on heat transfer regimes. A sketch of a typical boiling curve is shown in Figure 6-15 for the purpose of describing boiling heat transfer regimes. The boiling heat transfer regimes are separated by incipience of boiling temperature (T_{IB}), critical heat flux temperature (T_{CHF}) and minimum film boiling temperature (T_{min}). Below T_{IB} , the heat transfer regime is single-phase liquid convection, between T_{IB} and T_{CHF} is nucleate boiling, between T_{CHF} and T_{min} is transition boiling, and above T_{min} is film boiling.

The selection logic for the main heat transfer regimes is illustrated in Figure 6-16. The variables appearing in the figure are:

q''_{CHF}	=	critical heat flux (CHF)
q''_{FB}	=	total heat flux for film boiling
q''_{TB}	=	total heat flux for transition boiling
q''	=	total wall-to-fluid heat flux
T_{CHF}	=	wall temperature at the CHF
T_{IB}	=	wall temperature at the incipience of boiling
T_{min}	=	minimum film boiling temperature
$T_{sat}(P_s)$	=	saturation temperature at partial steam pressure
$T_{sat}(P)$	=	saturation temperature at total pressure

T_w = wall temperature
 X_e = equilibrium quality
 α_g = void fraction

Single-phase liquid and nucleate boiling correlations are unchanged from previous versions of S-RELAP5 and are presented in Sections 4.2 and 4.3 of Reference 6; heat transfer in those regimes are not highly ranked phenomenon for the BWR LOCA methodology. Later sections address post CHF heat transfer correlations.

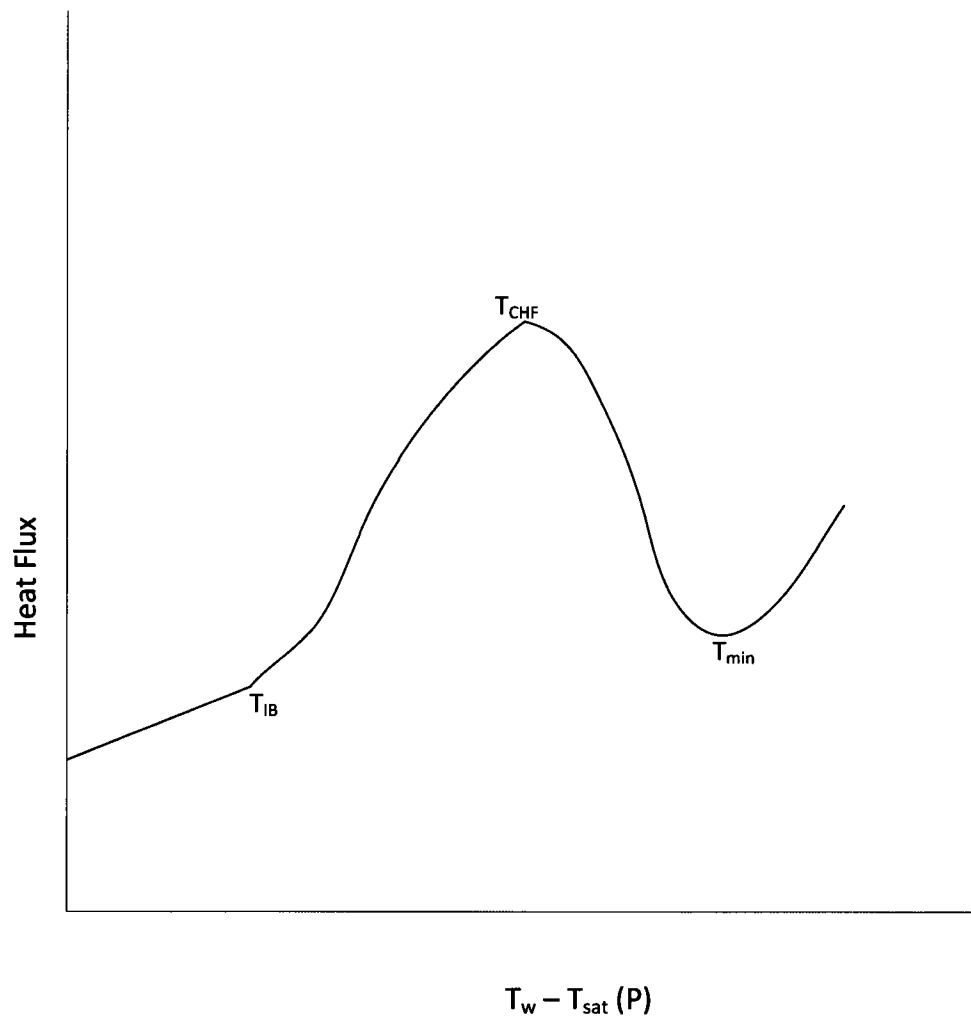


Figure 6-15 Sketch of Boiling Curve



Figure 6-16 Schematic of Heat Transfer Regime Selection Logic

6.4.9 Appendix K Prevention of Return to Nucleate Boiling and Transition Boiling

After CHF is determined to occur at a specific axial fuel location during blowdown, a return to nucleate boiling is not allowed. The node is locked out from nucleate boiling. [

]

If the temperature difference between the cladding and saturated fluid exceeds 300°F during blowdown, the node is not allowed to return to transition or nucleate boiling. The node is locked out from transition and nucleate boiling even if conditions predict a return to transition or nucleate boiling. The lockout is removed during the refill stage when a return to transition or nucleate boiling is allowed.

Figure 6-17 shows the Appendix K nucleate and transition boiling lockout logic. Lockouts to return to nucleate or transition boiling are only applied during the blowdown phase. Note that the figure assumes that T_{\min} and 300 °F superheat lockout are not the same value.

[

]

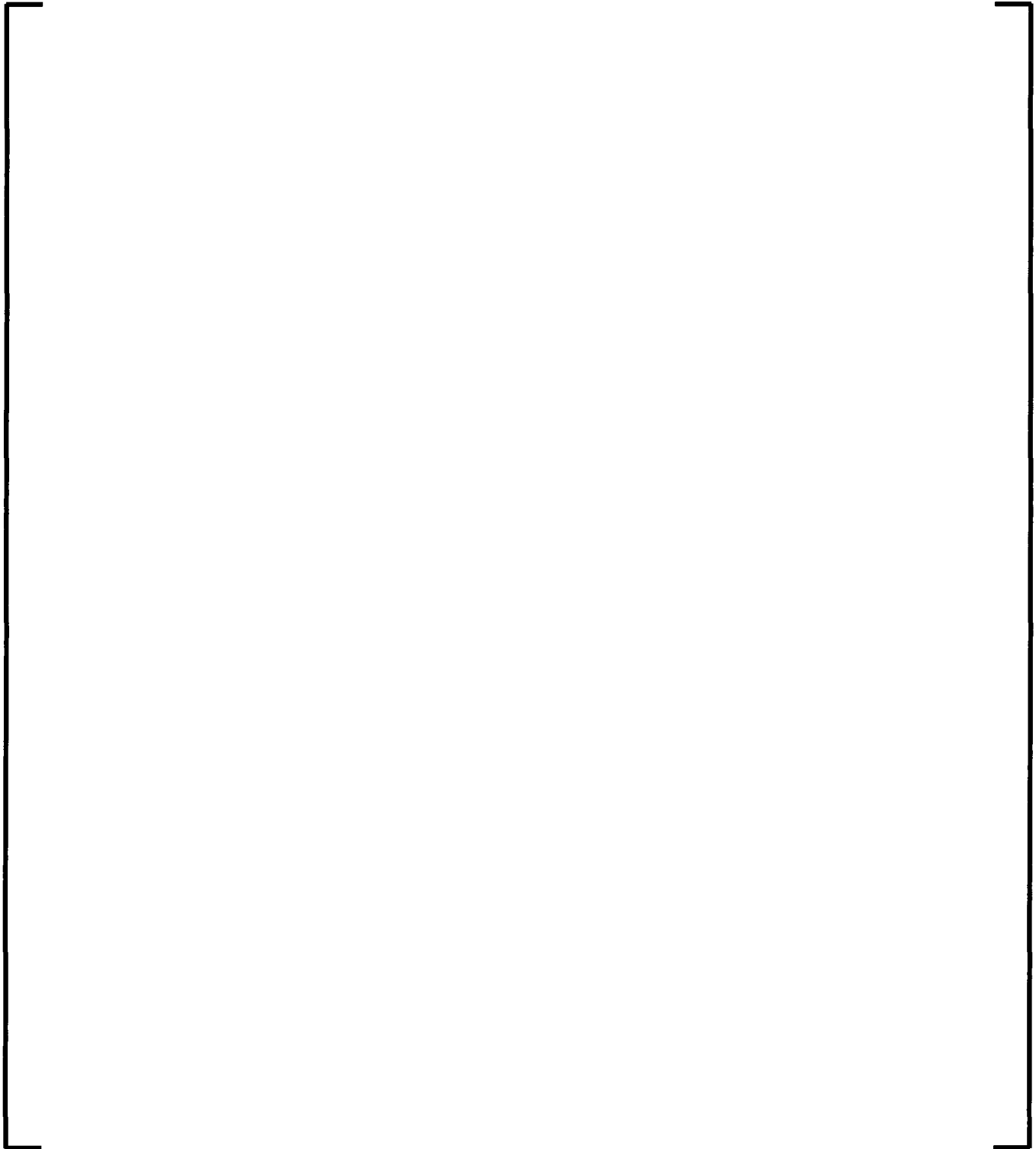


Figure 6-17 Appendix K Heat Transfer Lockout Logic During Blowdown

6.4.10 Critical Heat Flux

Preferably, the CHF would be calculated from fuel specific correlations. Fuel specific correlations generally are considered very accurate with small uncertainties because they are based on fuel specific CHF/CPR tests. Unfortunately, these correlations are limited in their range of applicability based on thermal hydraulic conditions. For example, AREVA BWR CHF/CPR correlations have strict boundary conditions (pressure, flow, etc.), once these boundary conditions are exceeded either conservative calculations are made (if allowed), or CHF/dryout has assumed to occur. These fuel specific correlations would exceed their boundaries within a few seconds following the start of the LOCA causing a need for an alternative. To overcome this restriction, a general steady state CHF correlation was chosen. The chosen general correlation was the Groeneveld 2006 CHF look up table (LUT). It is an alternate to the Biasi CHF correlation originally included in RELAP5. The Groeneveld 2006 CHF LUT was chosen over Biasi and Appendix K “acceptable” steady state CHF correlations (W-3, B&W-2, Hensch-Levy, Macbeth, Barnett and Hughes) due to its reputation as a modern CHF correlation with an extensive database. It is commonly accepted as the correlation of choice for general CHF correlations.

The LUT method is reported in a series of papers by Groeneveld et al., in 1986, 1995, 2005 and 2006 (References 38 - 41). The functional form of the LUT is critical heat flux as a function of pressure, mass flux and steam quality. The 2006 LUT is based on more than 25000 CHF data points referenced to heated tubes of 8 mm diameter. Table values range as follows:

Quality	-0.5 to 1.0 (X<0 implies subcooling)
Pressure	100 to 21000 kPa
Mass Flux	0 to 8000 kg/(s-m ²)
Critical Heat Flux	0 to 44 MW/m ²

The 2006 LUT provides values that are within the range of the physical parameters expected in a BWR LOCA analyses.

To improve the application of the LUT for bundled rods, correction factors are commonly applied to the method and are summarized in Reference 6, Section 4.4.5. The correction factors are utilized for AURORA-B LOCA. The correction factors consist of:

- Subchannel or Tube Cross Section
- Square Bundle
- Heated Length
- Axial Heat Flux
- Radial Heat Flux
- Grid Spacer
- Cold Wall
- Vertical Low Flow

Open literature demonstrated good results applying the LUT method to rod bundles as featured in References 42 and 43. Many of the rod bundle related correction factors are taken from Lee, Reference 42. Lee demonstrated improved predictive performance of the 1995 LUT when his rod-bundle factors were applied to data from the Columbia University Heat Transfer Research Facility (HTRF). Another example of the LUT applied for rod bundles is Reference 43 which considered the application of the 2005 LUT to the computation of critical power in two rod-bundle designs (8x8 NUPEC and AREVA BWR ATRIUM 10). Of special interest for that reference is the computation of critical power for an AREVA fuel design. Applying only the hydraulic diameter factor, the critical power for the AREVA fuel is under-predicted with a reported mean error of 4.6%.

Reference 41, presents a statistical summary of the 2006 LUT relative to its database. For a constant inlet enthalpy process, the LUT has an “rms” error of 7.1%. [

]

The LUT method has been demonstrated to be applicable to fuel rod bundles [

]

[

]

6.4.11 Transition Boiling Heat Transfer

The McDonough, Milich and King (MMK) transition film boiling correlation (Reference 44) is implemented in S-RELAP5 for the AURORA-B LOCA EM. Appendix K states that MMK is acceptable for use in the post-CHF boiling regimes with the following restrictions:

The first term (nucleate) of the Westinghouse correlation and the entire McDonough, Milich, and King correlation shall not be used during the blowdown after the temperature difference between the clad and the saturated fluid first exceeds 300 °F,

Transition boiling heat transfer shall not be reapplied for the remainder of the LOCA blowdown, even if the clad superheat returns below 300 °F, except for the reflood portion of the LOCA when justified by the calculated local fluid and surface conditions.

These restrictions are implemented and discussed in Section 6.4.9.

The MMK correlation defines the heat transfer to the liquid phase as:

$$q''_f = q'_{CHF} - h(T_w - T_{w,CHF})$$

The heat transfer to the vapor phase is zero. The heat transfer coefficient (h) is defined for three pressures (800 psia, 1200 psia and 2000 psia). These pressures were defined by the test conditions.

The S-RELAP5 computational process continuously provides the wall temperature T_w from the conduction solution and q''_{CHF} from the CHF LUT. $T_{w,CHF}$ is computed by equating q''_{CHF} to the nucleate boiling heat flux from Chen's nucleate boiling correlation and using a Newton iteration method to solve for T_w at the CHF.

The transition boiling heat flux is selected as the maximum of the transition boiling heat flux and the film boiling heat flux when T_w is below T_{min} . The transition boiling heat flux is set to zero when T_w is above T_{min} .

Linear interpolation is used to define the heat transfer coefficient at intermediate pressures. The heat transfer coefficient at 800 psia is applied at pressures less than 800 psia.

The conservative computations of heater rod wall temperature for the FLECHT-SEASET and THTF reflood experiment reported in Sections 7.3.13 and 7.3.14 demonstrate the acceptable application of the MMK correlation over a pressure range appropriate to BWR LOCA analysis.

6.4.12 Minimum Film Boiling Temperature

The minimum film boiling temperature (T_{min}) marks the division between transition boiling and film boiling regions. Between T_{CHF} and T_{min} is the transition boiling region and above T_{min} is the film boiling region. This is classically known as the “Leidenfrost point”.

Appendix K transition boiling lockout criterion depicts a relation for T_{min} in British units as:

$$T_{min} = T_{sat} + 300 \text{ }^{\circ}\text{F}$$

Reference 45 presents the Groeneveld-Stewart minimum film boiling temperature correlation, which is used after the blowdown period. It is an empirical correlation that defines T_{min} over three regions. It is presented here in units of pressure in MPa and temperature in K. For saturated water, the correlation defines:

$$T_{min} = 557.85 + 44.1P - 3.72P^2; \quad P < 9 \text{ MPa}, \quad X > 0$$

For subcooled water, expressed as a negative steam quality ($X < 0$), the correlation includes an additional term that increases T_{min} for the subcooled region:

$$T_{min} = 557.85 + 44.1P - 3.72P^2 - \frac{10^4 X}{2.82 + 1.22P}; \quad P < 9 \text{ MPa}, \quad X < 0$$

The effects of mass flux were experimentally found to be negligible (Reference 45).

For pressure greater than 9 MPa, interpolation is used to extend T_{min} to the critical point as:

$$T_{min} = [T_{min} - T_{sat}]_{9 \text{ MPa}} \frac{P_{crit} - P}{P_{crit} - 9} + T_{sat}; \quad P \geq 9 \text{ MPa}$$

S-RELAP5 uses a more conservative form:

$$T_{\min} = \left[T_{\min,9\text{MPa}} - T_{\text{sat}} \right] \frac{P_{\text{crit}} - P}{P_{\text{crit}} - 9} + T_{\text{sat}}$$

This interpolation ramps T_{\min} from the value calculated at 9 MPa to the critical temperature as the pressure approaches the critical pressure. BWR LOCA analysis is not concerned with pressures greater than 9 MPa (1305 psia).

The functional behavior is shown in Figure 6-18 for saturated water. The S-RELAP5 interpolation follows below the reference interpolation above 9 MPa. The curves for both interpolations are bounded by T_{sat} and the current Appendix K criterion of $T_{\min} = T_{\text{sat}} + 300^\circ\text{F}$ for pressures above approximately 0.26 MPa. The lower pressure functional behavior is shown in Figure 6-19. The Groeneveld-Stewart correlation is a bit less conservative than the current Appendix K criterion below 0.26 MPa and it is conservative above 0.26 MPa.

Figure 6-20 shows a comparison of the Groeneveld-Stewart correlation to the data from their own experiments and data from Winfrith, Reference 46. The data are for saturated water. The data tends to follow the above correlation.

The Groeneveld-Stewart correlation includes the effect of subcooled water and that produces an increase in T_{\min} with subcooling. Figure 6-21 presents a plot of the calculated and measured T_{\min} for both subcooled and saturated water at 2 MPa.

Figure 6-22 presents a plot of the calculated versus measured T_{\min} using the Groeneveld-Stewart correlation using their data and also the Winfrith data (Reference 46). Data from both subcooled and saturated water are included. The comparisons between the calculated and measured values are respectable. The overall mean ratio is 0.996 and the standard deviation is 0.052.

It is known that T_{\min} is affected by the test section material properties and oxidized surfaces. Higher values of T_{\min} have been measured by others with zircaloy and oxidized zircaloy. Dhir, Catton and Duffy, Reference 47, explored the quenching of zircaloy and stainless steel rods in the same rod bundle geometry. They conclude "*Under identical flow conditions zircaloy is observed to quench faster than stainless steel.*" Peterson and Bajorek, Reference 48, present

an extensive test series that measured T_{min} using test sections of Zircaloy-4, 316 Stainless Steel, and 1018 Carbon Steel. These were well controlled quench tests for a vertical heated cylinder in a pool of water with pressure ranging from 0.101 to 3.0 MPa and subcooling from 0 to 34 °C. The primary conclusion is stated as:

The results show that T_{min} increases with pressure, liquid subcooling, surface roughness, and surface oxidation. T_{min} is a strong function of pressure at low pressure, but asymptotically approaches a constant value as pressure increases. T_{min} is also a function of surface material properties, with Zircaloy-4 being found to have the highest minimum film boiling temperature compared to carbon steel and stainless steel. For Zircaloy-4, an oxide layer was found to significantly increase T_{min} .

Figure 7 reported in Reference 48 shows the impact of material properties on T_{min} . Of significance is the higher T_{min} of Zircaloy 4, and especially zirconium oxide, as compared to stainless steel. The Groeneveld-Stewart correlation is based on stainless steel type test sections; thus, it conservatively predicts a T_{min} that is less than the more realistic values expected for nuclear bundles with zirconium alloy fuel rod cladding.

The Groeneveld-Stewart correlation for minimum film boiling temperature is an appropriate choice for use in BWR LOCA analysis using an Appendix K approach. It is applicable to the wide range of pressure conditions expected in BWR LOCA analysis. The correlation produces conservative (lower) T_{min} based on separate investigators having experimentally shown that T_{min} is higher for zircaloy and especially zirconium oxide as compared to stainless steel type materials.



Figure 6-18 Functional Behavior of Groeneveld-Stewart T_{\min} Correlation



Figure 6-19 Functional Behavior of Groeneveld-Stewart T_{\min} Correlation at $P < 2$ MPa

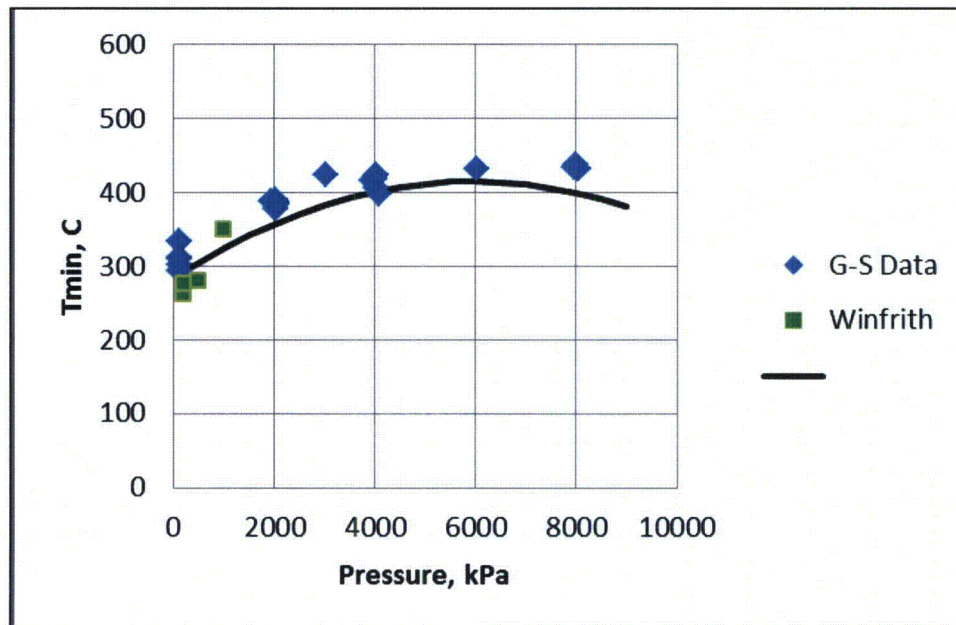


Figure 6-20 Calculated and Measured T_{min}

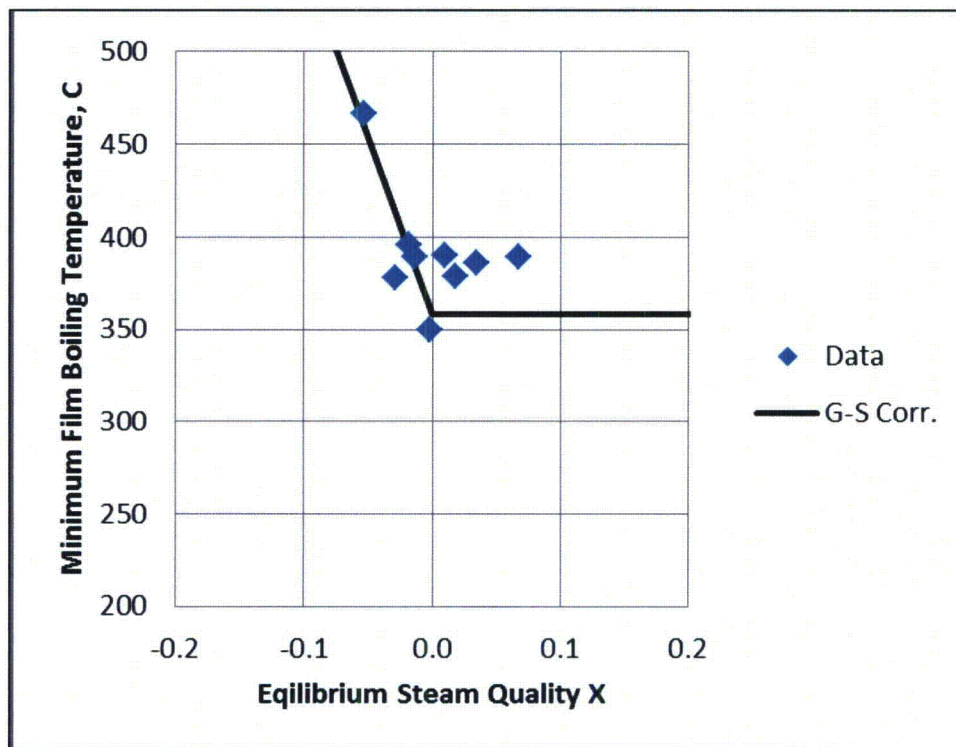


Figure 6-21 T_{min} versus Steam Quality at 2 MPa

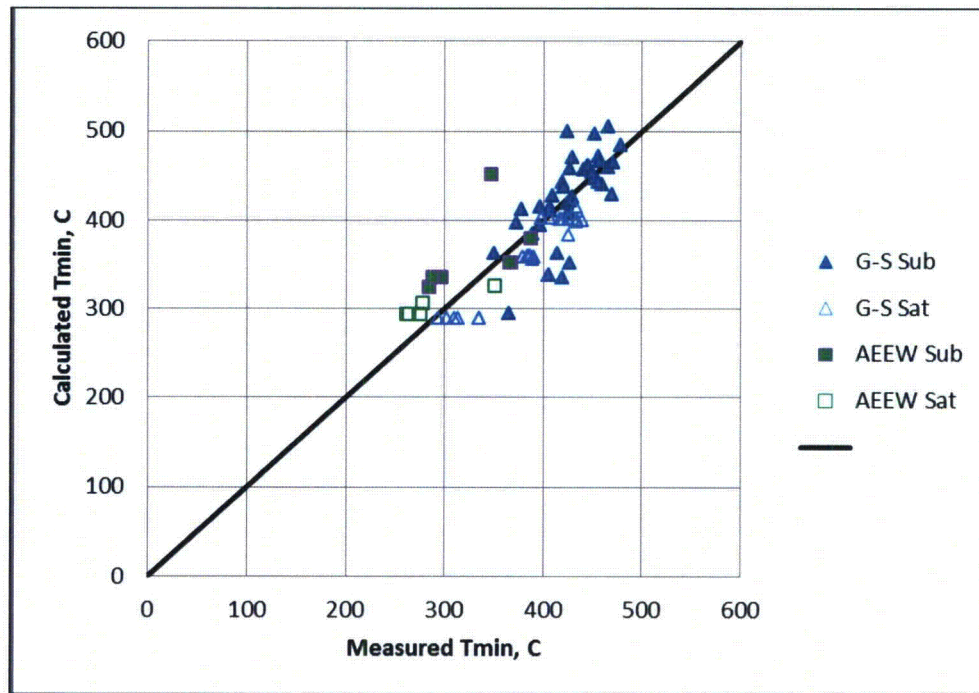


Figure 6-22 Calculated versus Measured T_{min}

6.4.13 Film Boiling Heat Transfer

The heat flux in the film boiling region consists of three parts, boiling heat transfer to liquid, convection heat transfer to vapor and wall-to-fluid radiation. Wall-to-fluid radiation is addressed in Section 6.4.14. Steady or stable film boiling is defined as film boiling below a void fraction of 0.6. Dispersed film boiling is defined as film boiling above a void fraction of 0.9 and less than 1.0. Dispersed film boiling is modeled with no boiling heat transfer to liquid from the wall. The transition between steady film boiling and dispersed flow film boiling [

] The Bromley attenuation is presented in Figure 6-23, and is discussed in Section 4.8 of Reference 6.

6.4.13.1 Boiling Heat Transfer to Liquid

A modified form of the Bromley correlation is used to define film boiling heat transfer to liquid. The Bromley correlation is widely used and it has provided the basis for steady film boiling heat transfer ever since its publication in 1950, Reference 49. The modified Bromley correlation is based on the original Bromley correlation with the characteristic length (D) replaced by the Taylor or Helmholtz characteristic length.

The selection of the characteristic length distinguishes the various applications of the Bromley correlation. The form based on the Taylor characteristic length is consistent with the correlation developed by Berenson in 1961, Reference 50. His correlation was based on considerations of the Taylor-Helmholtz stability of the liquid-vapor interface. Applications of the Bromley correlation have considered either the Taylor or the Helmholtz characteristic lengths for stability of the liquid-vapor interface. Figure 6-24 shows a comparison of the Bromley heat transfer coefficient for both Taylor and Helmholtz characteristic lengths at atmospheric pressure and 292 psia. The shapes of the curves are very similar. "The relatively close agreement obtained for the two criteria indicates that either one could be used for BWR LOCA calculations." as stated in Reference 51 by General Electric, General Electric selected the Helmholtz criteria. The Taylor length is used by S-RELAP5 as originally provided in RELAP5.

Reference 51 presents an extensive validation of the modified Bromley correlation. The modified correlation in that context includes the Bromley film boiling correlation plus the added heat transfer by radiation from the hot wall to the liquid. The data sources and general results include:

Quenching Experiments. Single-tube quench tests were performed by heating an 18-inch tube to high temperature and plunging the tube into saturated and subcooled water. The film boiling heat transfer was inferred from the time history of the temperature and the thermal-mechanical properties of the tube. The results of the test are in good agreement with the modified Bromley correlation. Figure 6-25, shows typical results from a series of quenching experiments.

Reflood Experiments. The modified Bromley correlation provides a conservative lower-bound calculation of the PWR-FLECHT heat transfer data as shown in Figure 6-26. The modified Bromley correlation in combination with the Hsu transition boiling correlation is in excellent agreement with data from KWU reflood experiments as shown in Figure 6-27.

Blowdown Heat Transfer Experiments. Full scale 49-rod bundle data from the Two-Loop Test Apparatus (TLTA) on the cooperative NRC/EPRI/GE BWR Blowdown Heat Transfer (BDHT) program show the conservatism of the recommended (modified Bromley) correlation for non-zero flow conditions. These transient tests are important because they provide information in typical rod bundle geometry under representative flow and heat flux conditions. Numerous plots show that film boiling heat transfer coefficients are generally conservative relative to the experimentally based heat transfer coefficients inferred from an inverse heat conduction solution. Figure 6-28 shows a typical result where the Bromley correlation provides a lower bound on the film boiling heat transfer coefficient.

The above sample results are applicable to the Bromley correlation with either the Helmholtz or the Taylor characteristic lengths as indicated by Figure 6-24. Thus, the above stated results are also applicable to the AREVA form of the modified Bromley correlation used in S-RELAP5. These comparisons demonstrated that the correlation predicted values of the heat transfer coefficient were equal or less than the mean value of the experimental heat transfer data.

Independent validation of the implementation of the AREVA form of the modified Bromley correlation in S-RELAP5 is done by comparison to heater rod wall temperatures reported for the THTF and FLECHT-SEASET reflood experiments shown in subsections of Section 7.3. The results show that the Bromley film boiling correlation together with the McEligot convection correlation and radiation heat transfer to liquid and vapor produce conservative results. The peak temperatures are higher and the quench times are later than indicated by the experimental data.

6.4.13.2 Convection Heat Transfer to Vapor

The AURORA-B LOCA EM utilizes the McEligot forced convection correlation which is similar to the Dittus-Boelter correlation. Specifically, the McEligot correlation (Equation 4.70 of Reference 6) was chosen as a conservative vapor heat transfer correlation, the main differences between the Dittus-Boelter and McEligot correlations is the base term of 0.023 versus 0.021, the exponent on the Prandtl number, and a wall temperature correction term. McEligot is conservative relative to Dittus-Boelter. For laminar flow, heat transfer is calculated from a Nusselt number of 4.36. For natural convection, heat transfer is based on products of Grashof number and Prandtl number (Equation 4.68 of Reference 6). For the fuel bundle heat structures, the overall convection heat transfer to vapor is determined as the maximum of the McEligot, laminar flow and natural circulation correlations. For non-heated structures, the Sleicher-Rouse correlation (Reference 6 Equation 4.66) is used instead of McEligot. As noted earlier, within the dispersed film boiling regime, there is no liquid boiling heat transfer above a void fraction of 0.90; however, vapor-phase heat transfer is enhanced according to the two-phase turbulent heat transfer enhancement for rod bundles by Drucker and Dir. Additional details are provided in Reference 6 Sections 4.8 and 4.9.

[

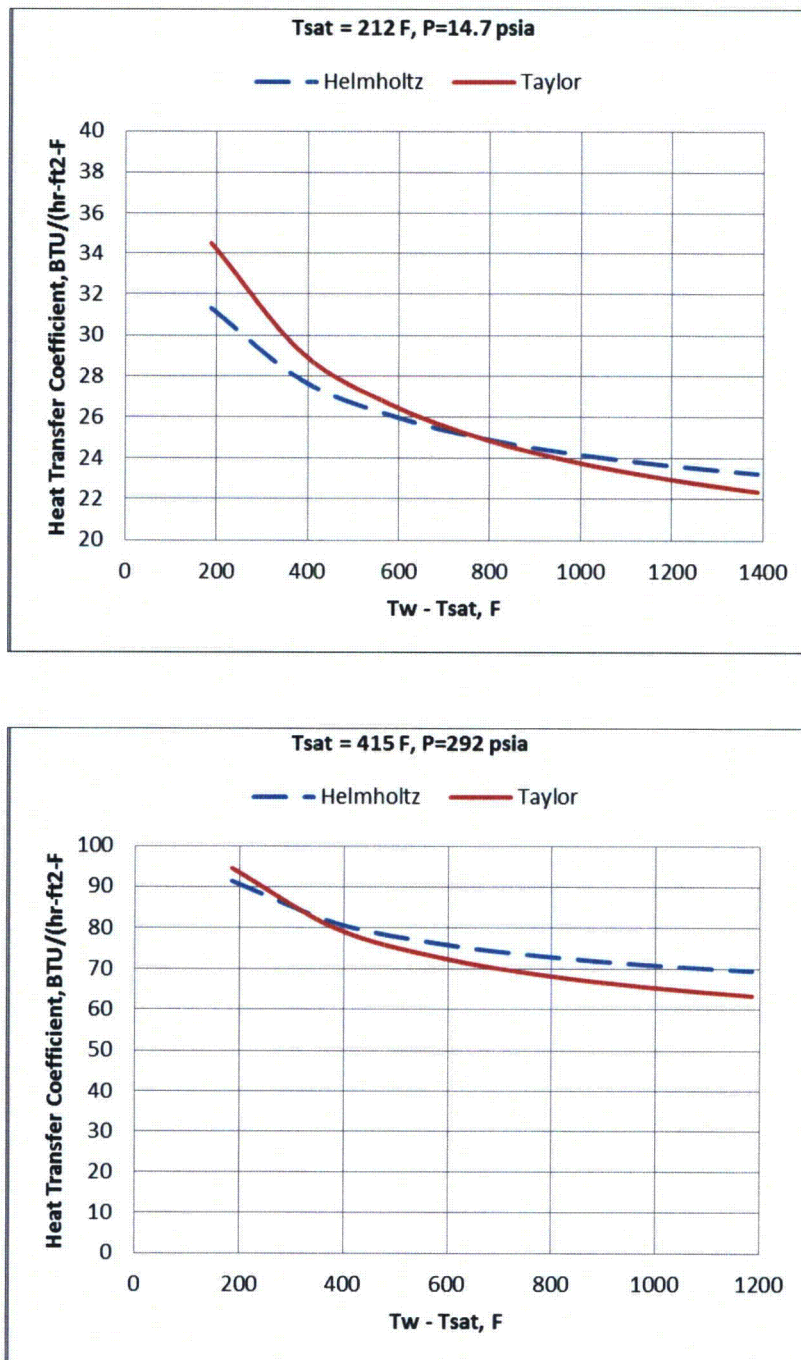
]

[

]



**Figure 6-23 Bromley Correlation Attenuation versus Void
Fraction in S-RELAP5**



**Figure 6-24 Bromley HTC with Helmholtz and Taylor
Characteristic Length, 14.7 and 292 psia**

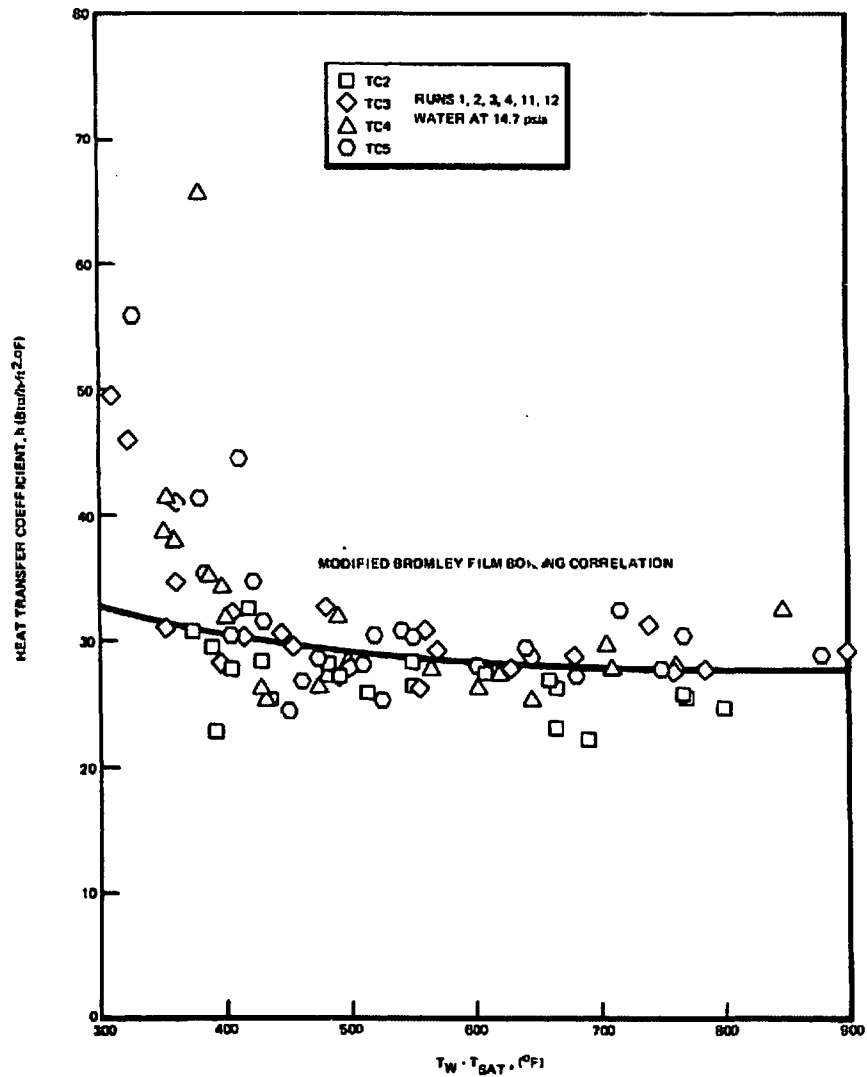


Figure 6-25 Comparison of Saturated Film Boiling Data with Modified Bromley Correlation*

* Reproduced from Reference 51, page 12

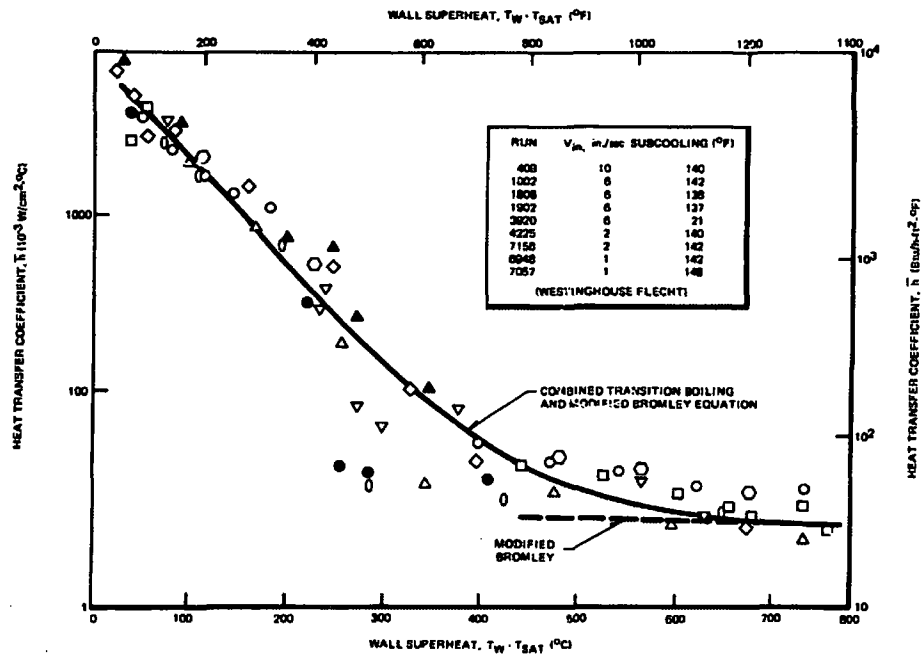


Figure 6-26 Heat Transfer Coefficient for Transition and Film Boiling at 60 psi*

* Reproduced from Reference 51, page 18

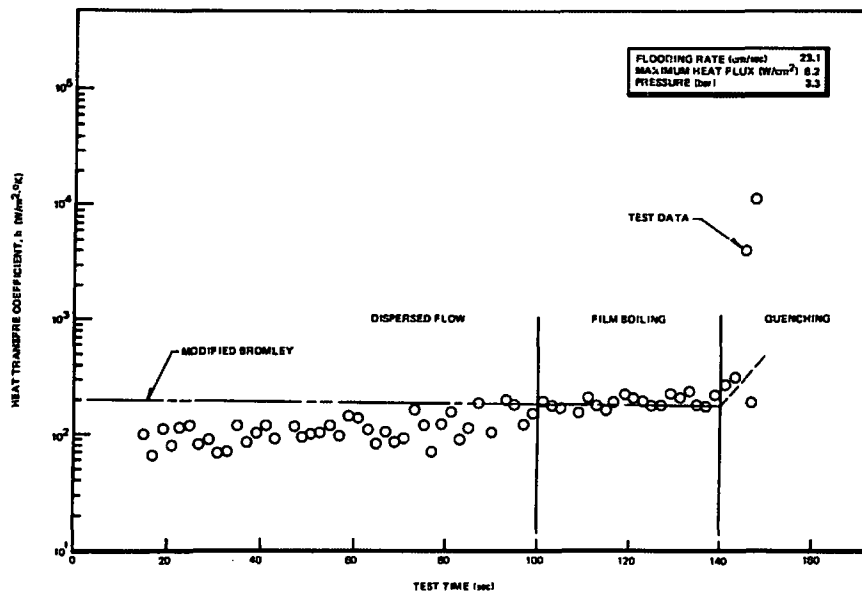


Figure 6-27 KWU Reflood Data Compared to Modified Bromley Correlation*

* Reproduced from Reference 51, page 20

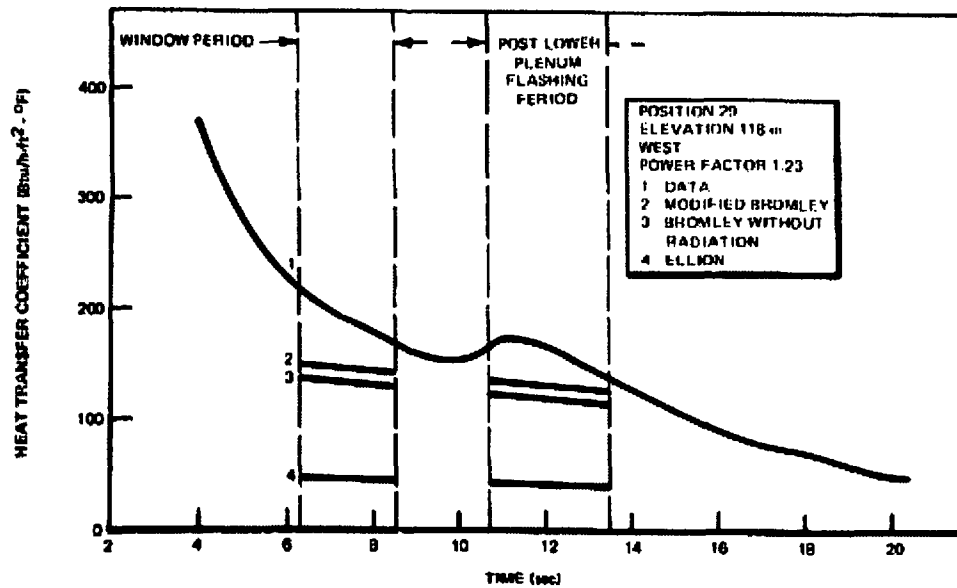


Figure 6-28 Comparison of Measured Heat Transfer Coefficients with Various Correlations for TLTA Test 4914, Run 8*

*

Reproduced from Reference 51, page 40

Figure 6-29 Dispersed Film Boiling Calculated versus Measured HTC for Steady State THTF Tests

6.4.14 Radiation Heat Transfer From Wall to Fluid

[

]

At high wall temperatures, the radiation heat transfer from wall to fluid is treated using a model developed by Sun (Reference 6, Section 4.10). The wall-to-fluid radiation model considers the vapor-droplet mixture as an optically thin medium and uses an electric network analogy to analyze the radiation energy exchange among three nodes: wall, liquid droplets and vapor.

[

]

6.4.15 Surface to Surface Radiation Heat Transfer

The model for wall to wall thermal radiation is unchanged from RELAP5/MOD3.3. It is a simplistic approach that assumes the surfaces have a line of sight or a reflection path through which they can communicate with each other in the same enclosure. The computation method is a lumped-system approximation for gray diffuse surfaces contained in an enclosure. The assumptions are:

The fluid in the enclosure neither emits nor absorbs radiant thermal energy.

Reflectance from a surface is neither a function of incident nor reflected direction nor of radiation frequency.

Temperature, reflectance and radiosity are constant over each surface.

Equations describing the radiation heat transfer are presented in Reference 6 Section 4.10.2. View factors are computed external to S-RELAP5 and are included through input.

6.4.16 Vapor Convection Heat Transfer

For a void fraction of 1.0, the heat transfer correlations are the same as used for dispersed film boiling, [

]

6.4.17 Appendix K BWR Core Spray Heat Transfer

Consistent with Appendix K, the AURORA-B LOCA EM calculates convective heat transfer following blowdown based on appropriate experimental data. Specifically, the convective heat transfer is based on correlations developed from experimental data and validated with test assessments as presented in Section 7.0.

The Appendix K acceptable approach for core spray heat transfer was based on a method and an approach current at the time, but is considered dated now. The approach was based on using specific heat transfer coefficients for 7x7 fuel bundle arrays and lacked correlations or mechanistic solutions. The acceptable values originated from the BWR-FLECHT tests that consisted of a single bundle (References 55 and 56). The references appeared to have little or no insight on CCFL behavior and multidimensional effects with the core and upper plenum (which wasn't fully understood until the BWR refill and reflood test program in the 1980s). The BWR-FLECHT tests could not address spray distribution or upper plenum drainage.

[

]

[

]

Heat transfer correlations in the AURORA-B LOCA EM address the phenomena consisting of steam cooling, dispersed film boiling and steady film boiling. Steam cooling and dispersed film boiling correlations will create small heat transfer coefficients, not unlike the *acceptable* values of Appendix K if the same conditions are applied from the BWR FLECHT tests. The *acceptable* value in Appendix K for a two-phase level representing reflood is 25 (BTU/hr-ft²-°F) at atmospheric pressure, this value is approximately equivalent to the modified Bromley correlation for boiling heat transfer to liquid as shown in Figure 6-24 and Figure 6-23 shows the void range of Bromley. Both figures demonstrate that Bromley gives a good representation of reflood heat transfer.

CCFL characterization is important to the behavior of top-down cooling; so CCFL characterization is performed for each unique BWR fuel design. This is generally needed when a design changes array size, i.e., 9x9 to 10x10. The Mini-Loop discussion in Section 7.6.5 shows examples of measured CCFL performance for the ATRIUM 10 fuel design and the UPTF CCFL assessments in Section 7.3.17 demonstrates the CCFL correlation as used within AURORA-B LOCA EM. Modern day characterizations can consist of either tests or qualified computational fluid dynamics (CFD) analyses.

[

]

6.4.18 3-D Heat Transfer within Fuel Bundle

For film boiling and steam cooling, 3-D effects are included in the radiation wall-to-wall heat transfer via view factors; however, convective heat transfer in the bundle is based on 1-D hydraulics. Differences seen in temperature between rod locations in assessments may in whole or in part be due to differences in radiation heat transfer; for example, rods near colder surfaces (channel and unheated rods) are lower in temperature due to radiation heat transfer to the colder surfaces. However, for film boiling it is hypothesized at a plane in the bundle that larger water droplets are in colder regions and smaller droplets are near the hotter regions. This implies that the hot rod would have a smaller convective heat transfer coefficient than colder rods in the plane; this phenomenon is not captured with 1-D hydraulics. [

]

7.0 Assess Evaluation Model Adequacy (EMDAP Element 4)

Evaluation model adequacy was assessed after the previous elements were established and the EM capability was programmed. The process proceeded on an iterative basis between the various elements and steps, though only the final results were documented and are presented in the LTR.

The EM assessment is divided into two parts. The first part (EMDAP Steps 13–15) pertains to the “bottom-up” evaluation of the closure relations for each component calculational device. In this part, important closure models and correlations are examined by considering their pedigree, applicability, fidelity to appropriate fundamental or SET data, and scalability. The bottom-up evaluation assessments are addressed in Sections 7.3 and 7.6.

The second part (EMDAP Steps 16–19) pertains to the “top-down” evaluations of code-governing equations, numerics, the integrated performance of each code, and the integrated performance of the overall EM. This includes examining the field equations, numerics, applicability, fidelity to integral effects and plant transient data. The top-down evaluation assessments are addressed in Section 7.7.

Assessment Criteria

The assessment results described in the following sections provide statements about the ability of the EM to predict key parameters of each assessment. Reference 4 suggests how this may be done by defining criteria associated with levels of code-data agreement. The four levels of agreement defined in the reference are used within this LTR. These criteria move from the most desirable correlation of data to the code system to the unacceptable prediction of the data by the code system. For PIRT high-ranked phenomena, the minimum standard for acceptability with respect to fidelity is generally “reasonable agreement.” The criteria are:

- **Excellent Agreement:** Applies when the code exhibits no deficiencies in modeling a given behavior. Major and minor phenomena and trends are correctly predicted. The calculated results are judged to agree closely with data.
- **Reasonable Agreement:** Applies when the code exhibits minor deficiencies. Overall, the code provides an acceptable prediction. All major trends and phenomena are predicted correctly. Differences between calculated values and data are greater than are deemed necessary for excellent agreement.

- **Minimal Agreement:** Applies when the code exhibits significant deficiencies. Overall, the code provides a prediction that is not acceptable. Some major trends or phenomena are not predicted correctly, and some calculated values lie considerably outside the specified or inferred uncertainty bands of the data.
- **Insufficient Agreement:** Applies when the code exhibits major deficiencies. The code provides an unacceptable prediction of the test data because major trends are not predicted correctly. Most calculated values lie outside the specified or inferred uncertainty bands of the data.

7.1 *Regulatory Basis*

Based on the application of the first principle, especially the phenomena importance determination, an assessment should be made regarding the inherent capability of the EM to achieve the desired results relative to the figures of merit.

7.2 *Determine Model Pedigree and Applicability to Simulate Physical Processes (EMDAP Step 13)*

The physical basis of closure models, assumptions and limitations attributed to the models, and details of the adequacy characterization at the time the models were developed are captured in the software QA documentation associated with the component calculational devices. Much of the information is also captured in the theoretical descriptions of the devices (References 6, and 9).

7.3 *Prepare Input and Perform Calculations to Assess Model Fidelity or Accuracy (EMDAP Step 14)*

The fidelity and accuracy of the closure relations and process models have been assessed using separate effects test data from numerous facilities. Comparison to separate effects tests demonstrates the capability of the EM to predict the important phenomena and processes. The nodalization and option selections used in the separate effects tests are consistent (as far as achievable) with those used in plant analyses. Table 5-1 lists the assessment matrix which includes the SETs, and the phenomena and processes from the PIRT to be addressed by each SET. It is noted here that the SET assessment cases, whether developed explicitly for BWR or PWR related phenomena, have been used to validate S-RELAP5 performance regardless of the plant type application. In addition, phenomenon dependent on Appendix K input requirements or correlations are also described.

The following sections provide the results from the application of S-RELAP5 to the assessment cases. The assessment discussions are limited to brief facility and analysis descriptions followed by comparisons between S-RELAP5 and the key results. Additional facility and analysis descriptions are presented in References 1 and 67. The results presented in this document demonstrate the accuracy of the EM to predict key parameters of each assessment. The impact of biases and uncertainties in the predictions is quantified via sensitivity analyses provided in Section 7.9.

7.3.1 Appendix K Requirements

In some instances, Appendix K requires specific input assumptions or correlations. These requirements are part of the application of the EM to operating reactors.

- Core: Stored energy (Sections 6.2.2 and 6.4.2)
- Core: Decay heat (Sections 6.2.3, 6.2.4, 6.2.5, and 6.4.3)
- Core: Clad swelling and rupture parameters (Sections 6.2.9 and 6.4.5)
- Core: Metal water reaction parameters (Sections 6.2.6 and 6.4.4)
- JP: Critical flow at jet pump nozzle (Sections 6.2.11 and 6.4.6)
- RL: Critical flow at break (Sections 6.2.11 and 6.4.6)

7.3.2 Summary of Core Simulator Qualification

Assessed phenomena and processes

This section addresses the following highly ranked PIRT phenomena identified in Table 5-1;



Assessment conclusions

[

] Qualification of the MICROBURN-B2 core simulator code

for BWR applications is described in Reference 7. Qualification of the phenomena is achieved in the reference. Qualification of XCOBRA is in Reference 23.

Assessment description

Current core simulators used by AREVA for BWRs are MICROBURN-B2 and XCOBRA (thermal-hydraulics only).

MICROBURN-B2 is a modern nodal method for solving the three-dimensional, two group neutron diffusion equation. A high order spatial method based on polynomial expansion of the nodal flux distribution is used to solve the spatial fast and thermal flux distribution within the BWR core. The MICROBURN-B2 code and underlying lattice physics method which together make up the code system have been qualified versus a very broad range of plant operational data, higher order numerical models, and isotopic inventory measurements. Assessment and qualification of the code system is described in Reference 7. [

]

XCOBRA is a steady-state thermal-hydraulic code used to predict steady-state thermal hydraulic performance of fuel bundles at various operating conditions and power distributions.

[

]

Since the core simulator provides input to the AURORA-B LOCA EM, it is expected that future (new) core simulator methodologies approved by the USNRC would also be applicable for use.

7.3.3 Summary of RODEX4 Qualification

Assessed phenomena and processes

This section addresses the following highly ranked PIRT phenomena identified in Table 5-1;

[

]

Assessment conclusions

Thermal-mechanical fuel rod modeling in the EM is performed by the RODEX4 fuel rod code. This code has been developed to perform best-estimate fuel performance predictions considering normal operation and anticipated operational occurrence scenarios as described in Reference 8. The underlying methodology development was based on CSAU principles as described in Reference 18. As such, a very detailed qualification of the underlying processes and phenomena has been undertaken at a deep level of detail. The overall code performance shows overall excellent agreement with a broad database of fuel rod data, and is capable of accurately modeling heat release rates from the fuel rods to the coolant during target scenarios in this EM.

Assessment description

RODEX4 is a modern realistic thermal-mechanical fuel rod code with the necessary models and correlations to predict fuel rod thermal-mechanical behavior to high burnup. The code has been qualified versus a very broad range of data. Also, the processes and phenomena have been USNRC approved to predict transient strain and pellet temperature in typical AOO applications. With its capability to predict transient conditions, RODEX4 is well qualified for modeling heat release rates from the fuel rods to the coolant during transients. Therefore, RODEX4 is well qualified for use in the AURORA-B LOCA EM with the conservative application described in Section 6.4.2.

7.3.4 Rod Bundle Void Tests

Assessed phenomena and processes

This section addresses the following highly ranked PIRT phenomena identified in Table 5-1;

Assessment conclusions

The assessment data base includes a total of [] from 3 different test facilities. These tests were performed for a wide range of system pressures (725 to 1260 psia) and flow conditions that cover the typical operating BWR conditions. The S-RELAP5 calculation with a prediction uncertainty band of []

[] These assessment results show excellent code-data agreement for these rod bundle void tests. From this, it is inferred that the EM makes excellent predictions of the indicated PIRT phenomena. Specific conclusions are drawn for the result of each test facility below.

Assessment description

This assessment was originally performed for the AURORA-B AOO EM and remains applicable for the LOCA EM.

The S-RELAP5 models [] have been improved and the range of assessment expanded over what was described in the RLBLOCA methodology (Reference 5). The characteristics of the rod bundle void fraction tests used to assess the models are summarized in Table 7-1. The FRIGG2 and FRIGG3 experiments have been included in the database because of the broad industry use of these experiments in benchmarking activities, including TRAC, TRACE, and RETRAN. These experiments include a wide range of system pressures, subcooling, and quality from which to validate the general applicability of the models. The reported instrument uncertainty on the void fraction for these tests is provided in Table 7-1, based on mockup testing. However, the total uncertainty of the measurements (including power and flow uncertainties) is expected to be larger than the indicated values.

The ATRIUM-10A void fraction tests were performed at the KATHY test facility. This experiment used prototypical BWR fuel bundle geometry, part length fuel rods, mixing vane grids, and a prototypic axial/radial power distribution. The range of test conditions for the ATRIUM-10A void data covers the typical reactor operating conditions, including the EPU conditions.

[

] Specific assessment results from the rod bundle void tests are presented in the following subsections.

7.3.4.1 FRIGG2 Void Tests

The FRIGG2 void distribution experiments were performed in the FRIGG Loop Facility in the late 1960s (Reference 66). The test section had 36 heated rods with uniform axial and radial power distribution, and was designed to give a full-scale simulation of a boiling channel for the Marviken reactor. The void distribution was measured for pre-CHF flow regimes at several axial locations by the multi-beam gamma method and the range of tested conditions is indicated in Table 7-1.

Figure 7-1 compares the calculated void fraction against the measured void fraction for all 27 tests with a total of 174 points. [

]

Based on this code-data comparison and the criteria described in Section 7.0, the FRIGG2 void test assessment results show excellent agreement between the predicted and measured void fraction.

7.3.4.2 FRIGG3 Void Tests

The FRIGG3 void distribution experiments were performed as a follow-on test after the FRIGG2 tests (References 68 and 69). The range of tested conditions is indicated in Table 7-1 of notable interest was the increase in tested pressure and slight increase in maximum measured void fraction.

Figure 7-2 compares the calculated void fraction against the measured void fraction for all 39 tests with a total of 157 points. [

]

Based on this code-data comparison and the criteria described in Section 7.0, the FRIGG3 void test assessment results show excellent agreement between the predicted and measured void fraction.

7.3.4.3 ATRIUM-10A Void Tests

The ATRIUM-10A void fraction tests were performed at the KATHY test facility using a prototypical BWR CHF test bundle. The test bundle used part length fuel rods, mixing vane grids, a [] and a radial power peaking typical of CHF tests.

Void measurements were made at one of three different elevations in the bundle for each test point: just before the end of the part length fuel rods, midway between the last two spacers, and just before the last spacer. A scanning gamma apparatus was used to measure the void fraction.

Figure 7-3 compares the calculated void fraction against the measured void fraction for all [

] Based on this code-data comparison and the criteria described in Section 7.0, the ATRIUM-10A void test assessment results show excellent agreement between the predicted and measured void fraction.

Table 7-1 Rod Bundle Void Fraction Test Characteristics

	FRIGG2	FRIGG3	ATRIUM*-10A
Axial Power Shape	uniform	uniform	
Radial Power Peaking	uniform	mild peaking	
Bundle Design	circular array with 36 rods + central thimble	circular array with 36 rods + central thimble	
Pressure (psia)	725	725, 1000, and 1260	
Inlet Subcooling (^o F)	4.3 to 40.3	4.1 to 54.7	
Mass Flow Rate (lbm/s) (calculated from mass flux assuming ATRIUM-10 inlet flow area)	14.3 to 31.0	10.1 to 42.5	
Equilibrium Quality at Measurement Plane (fraction)	-0.036 to 0.203	-0.058 to 0.330	
Max Void at Measurement Plane [fraction]	0.828	0.848	
Reported Instrument Uncertainty (fraction)	±0.025	±0.016	
Number of Data	27 tests, 174 points	39 tests, 157 points	

* ATRIUM is a trademark of AREVA Inc.

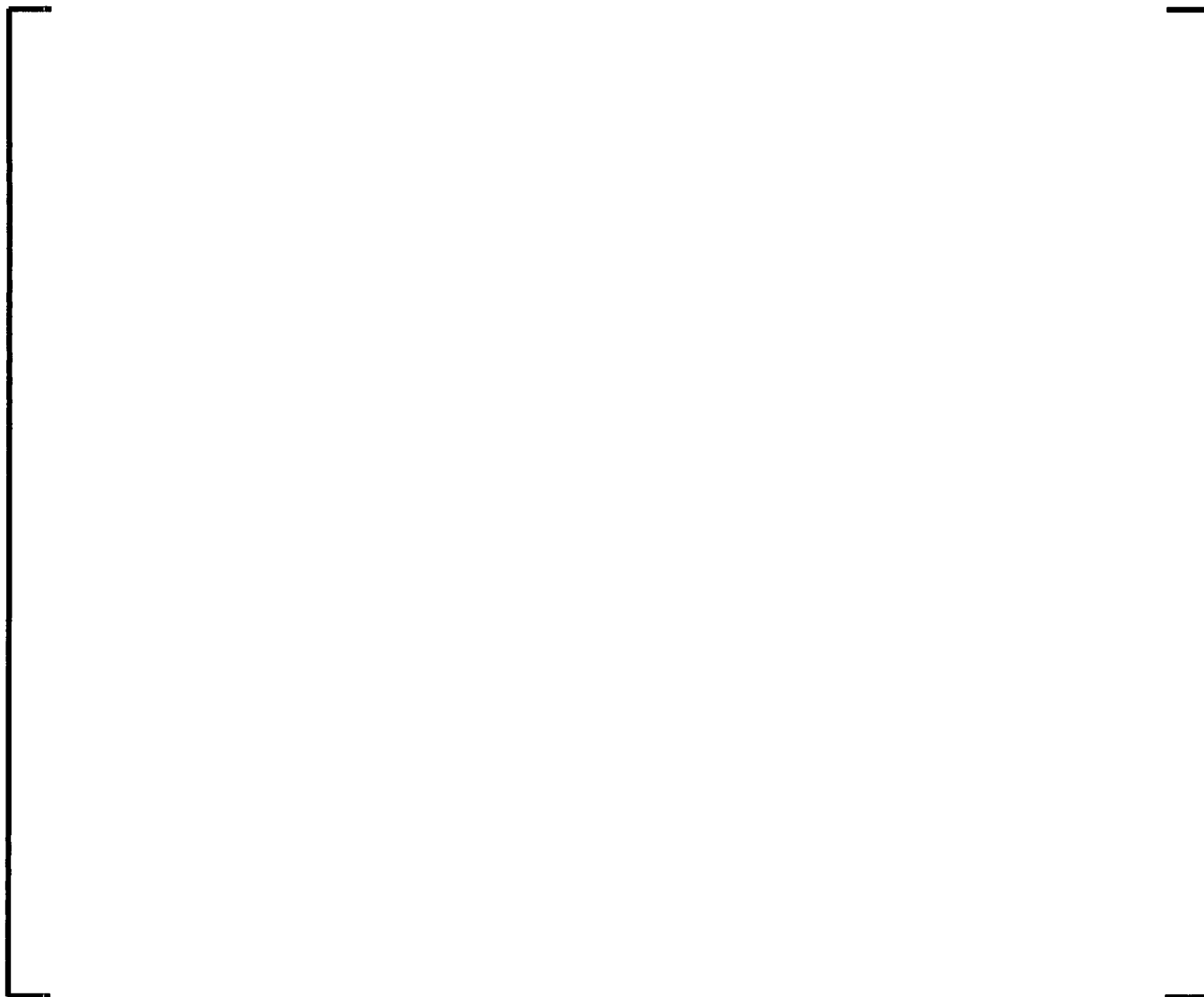


Figure 7-1 Calculated vs. Measured Results for all FRIGG2 Void Fraction Tests



Figure 7-2 Calculated vs. Measured Results for all FRIGG3 Void Fraction Tests



Figure 7-3 Calculated vs. Measured Results for all ATRIUM-10A Void Fraction Tests

7.3.5 Christensen Void Tests

Assessed phenomena and processes

This section addresses the following highly ranked PIRT phenomena identified in Table 5-1;

Assessment conclusions

The assessment data base includes a total of 7 tests (or a total of 112 test points) from the Christensen test facility. These tests were performed for a wide range of system pressures (725 to 1260 psia), inlet subcooling and flow conditions that cover the typical operating BWR conditions. The S-RELAP5 calculated void fraction with a prediction uncertainty [

] The effect of subcooled boiling is also assessed and the result shows excellent agreement between prediction and data.

This assessment results show excellent code-data agreement for the Christensen void fraction tests. From this, it is inferred that the EM makes excellent predictions of the indicated PIRT phenomena.

Assessment description

This assessment was originally performed for the AURORA-B AOO EM and remains applicable for the LOCA EM.

The Christensen void fraction tests were used in the development of the Lahey subcooled models implemented in the RELAP5 family of codes, including S-RELAP5. These tests also provide a good model assessment for [

]

The Christensen void fraction tests were performed in a test apparatus at the Argonne National Laboratory in 1961 (Reference 70). The test section for these experiments was a stainless steel

uniformly heated vertical rectangular tube. The primary purpose of these tests was to study void oscillations and stability in BWR systems, but the experiments also provided data on steady state axial void distributions, particularly for the subcooled boiling region. The void measurements were made using the gamma-ray attenuation technique and the void fraction at 16 axial locations.

Seven tests were reported in Reference 70 with 16 measurement points for each test along the axial length of the heated section. The boundary conditions for the tests are summarized in Table 7-2.

Figure 7-4 compares the calculated void fraction against the measured void fraction for all 7 tests with a total of 112 points. This figure also compares the measurement uncertainty and the [

]

Based on this code-data comparison and the criteria described in Section 7.0, the Christensen void test assessment results show excellent agreement between the predicted and measured void fraction.

Figure 7-5 compares the calculated and measured void fraction as a function of equilibrium quality, for Tests 11, 12 and 13 (a total of 48 points). These three tests used the same pressure, inlet flow rate, and power level – the only variable between them being the inlet subcooling. The inlet subcooling was 27.4 °F, 14.2 °F, and 2.2 °F for Tests 11, 12, and 13 respectively. Figure 7-5 shows excellent code-data agreement and the ability of S-RELAP5 to accurately predict the phenomena associated with subcooled boiling.

Table 7-2 Christensen Test Characteristics

Axial Power Shape	uniform
Radial Power Peaking	uniform
Bundle Design (inch)	0.437x1.748 - duct
Test Section Height (inch)	50
Pressure (psia)	400-1000
Inlet Subcooling (⁰ F)	2.2 to 27.4
Mass Flux (Mlbm/ft ² -hr)	0.472 to 0.693
Equilibrium Quality at Measurement Plane (fraction)	-0.044 to 0.040
Max Void at Measurement Plane (fraction)	0.65
Reported Instrument Uncertainty (fraction)	± 0.025 (tests 9-13) ± 0.050 (tests 15-16)
Number of Data	7 tests, 112 points



Figure 7-4 Calculated vs. Measured Results for all Christensen Tests



Figure 7-5 Christensen Tests at 600 psia with varying Subcooling

7.3.6 Allis-Chalmers Large Diameter Void Tests

Assessed phenomena and processes

This section addresses the following highly ranked PIRT phenomena identified in Table 5-1;



Assessment conclusions

The selected test facilities for this assessment covered 3 different sizes in diameter (2.9, 18 and 36 inches) and length/diameter ratios (16.5, 7.85 and 3.92), for a total of 162 data points. The experiments were performed for a wide range of system pressures (615 to 2015 psia) and flow conditions. The assessment results show reasonable agreement between the predicted and measured void fraction. The experimental uncertainty was not provided with the test data, [

From this, it is inferred that the EM makes reasonable predictions of the indicated PIRT phenomena.

Assessment description

This assessment was originally performed for the AURORA-B AOO EM and remains applicable for the LOCA EM.

The large diameter adiabatic void fraction tests (References 71, 72, and 73) performed by Allis-Chalmers have been included in the S-RELAP5 assessment database. The characteristics of these void fraction tests are summarized in Table 7-3.

Results from these void fraction tests have been widely used in the industry to develop void correlations, such as the Wilson Bubble Rise model (Reference 74) and the Kataoka-Ishii correlation (Reference 75). Instrument uncertainties on these void fraction tests were not reported. [

[

]

The S-RELAP5 assessment results from the Allis-Chalmers large diameter void tests are presented in the following subsections.

7.3.6.1 2.9 Inch Void Tests

A series of experiments (Reference 71), designed to measure steady-state void fractions in the vertical flow of steam-water mixtures in a 2.9 inch inside diameter pipe, was performed over a wide range of flow conditions. The experiments covered a range of superficial liquid velocity from 0.0 to 20.0 ft/s, and the system pressures were set at 615, 1015, and 1515 psia. Table 7-3 summarizes the range of tested conditions. Instrument uncertainties on these void fraction tests were not reported. [

]

The void fractions were determined from measurements by a gamma ray attenuation system. The void fractions taken at the axial location corresponding to a length-to-diameter (L/D) ratio of 16.5 are used in the S-RELAP5 assessment calculations.

Figure 7-6 shows the S-RELAP5 results - the comparison of the calculated versus measured void fraction for all 52 data points. This figure also compares the [

Based on this code-data comparison and the criteria described in Section 7.0, the assessment results show reasonable agreement between the predicted and measured void fraction.

7.3.6.2 18 Inch Void Tests

The measurements of void fraction in a bubbling two-phase mixture in an 18 inch vertical pipe (Reference 72) were conducted in a test loop with a 3 ft diameter by 25 ft high pressure vessel located in an electrical power plant in Oak Creek, Wisconsin. The internals of the 3 ft pressure vessel consisted of an 18 inch diameter channel (test section) running the full length of the vessel. The void fraction was determined by differential pressure cells, which were measured at an axial elevation well below the water level inside the test section. In a typical test run, the vessel pressure and the water level were set at the test conditions. The steam flow was next set to a predetermined rate. When equilibrium conditions were reached, the differential pressure cell readings and the steam flow rate were recorded.

Table 7-3 summarizes the range of tested conditions. Instrument uncertainties on these void fraction tests were not reported. [

]

Figure 7-7 shows S-RELAP5 results - the comparison of the calculated versus measured void fraction for all 56 data points. This figure also compares the [

] Based on this code-data comparison and the criteria described in Section 6.0, the assessment results show reasonable agreement between the predicted and measured void fraction.

7.3.6.3 36 Inch Void Tests

The entire 3 ft diameter vessel discussed in the previous section was used in a follow-up series of void fraction tests. This test series (Reference 73) measured the void fraction in a bubbling two-phase mixture in a 36 inch vertical vessel (test section). The void fraction was determined by differential pressure cells, which were measured at an axial elevation well below the water level inside the test section. In a typical test run, the vessel pressure and the water level were set at the test conditions. The steam flow was next set to a predetermined rate. When

equilibrium conditions were reached, the differential pressure cell readings and the steam flow rate were recorded. Table 7-3 summarizes the range of tested conditions. Instrument uncertainties on these void fraction tests were not reported. [

] Figure 7-8 shows the S-RELAP5 results - the comparison of the calculated versus measured void fraction for all 54 test points. This figure also compares the [

] Based on this code-data comparison and the criteria described in Section 7.0, the assessment results show reasonable agreement between the predicted and measured void fraction.

Table 7-3 Allis-Chalmers Large Diameter Void Test Characteristics

	2.9 inch	18 inch	36 inch
Test Section Design	2.9 inch inner diameter circular pipe (Ref. 71)	18 inch inner diameter circular pipe (Ref. 72)	36 inch inner diameter circular pipe (Ref. 73)
Pressure (psia)	615 – 1515	615 – 2015	615 – 1615
Inlet Subcooling (^o F)	0	0	0
Mass Flux (lbm/ft ² -sec)	0.26 – 956.	0.786 – 9.43	0.393 – 2.36
Max Void at Measurement Plane (fraction)	0.035 – 0.694	0.255 – 0.687	0.107 – 0.463
Percentage of data covered within the prediction uncertainty band of ± 0.10 (by the Kataoka-Ishii Correlation)	83%	89%	100%
Number of Data	52	56	54
Test Section (Length/Diameter) Ratio	16.5	7.85	3.92



**Figure 7-6 Calculated vs. Measured Results for all 2.9 Inch
Diameter Void Fraction Allis-Chalmers Tests**



**Figure 7-7 Calculated vs. Measured Results for all 18 Inch
Diameter Void Fraction Allis-Chalmers Tests**



**Figure 7-8 Calculated vs. Measured Results for all 36 Inch
Diameter Void Fraction Allis-Chalmers Tests**

7.3.7 GE Level Swell Test

Assessed phenomena and processes

This section addresses the following highly ranked PIRT phenomena identified in Table 5-1;

Assessment conclusions

The assessment is performed via measured and predicted void fraction and their evolution during the event. The level swell test produced excellent code-data comparisons for the void fraction distribution. From this, it is inferred that the EM makes excellent predictions of the indicated PIRT phenomena.

Assessment description

The GE Level Swell Test 1004-3 is essentially a small break blowdown of a vertical vessel 14 ft high by 1 ft in diameter (Reference 76). The vessel was initially pressurized to 1011 psi and filled with saturated water up to the 10.4 ft elevation. The test was initiated by blowing down the pressure vessel with the blowdown rate controlled by losses in the blowdown line. The void fraction distribution was measured axially in the test using differential pressure sensors spaced at 1 ft intervals. The test facility is shown in Figure 7-9, the S-RELAP5 model is shown in Figure 7-10.

The purpose of this assessment is to test the two-fluid interfacial models in predicting the flow regimes and void fraction distributions that occur under level swell in depressurization conditions. The assessment validates the interfacial drag and heat transfer submodels that contribute to predicting level swell. The key model affecting these assessments is the interfacial friction for the bubbly and slug flows.

Comparisons of measured versus calculated axial void fraction distributions are made at two transient times, 40 and 100 sec, Figure 7-11 and Figure 7-12 show the S-RELAP5 calculated void fraction results compared to measured data. Results from S-RELAP5 compare well with

the data. The void fractions calculated by S-RELAP5 are within typical experiential expectations for uncertainty, providing excellent agreement. [

] The results indicate that, for this slow transient condition, the two-fluid interfacial friction model implemented in S-RELAP5 makes excellent predictions of the indicated PIRT phenomena.

The jump of void fraction from ~0.4 to ~0.99 within neighboring volumes distinctly defines the location of a two-phase mixture level. The interfacial friction models for slug flow, vertical stratification, and annular-mist flow work in harmony to produce a smooth, but sharp transition from a low void fraction region to a very high void fraction (close to 1.0) region.

In a non-equilibrium code such as S-RELAP5, the phase exchange (vapor generation) process during blowdown is calculated through the use of an interfacial heat transfer model. The calculated liquid and vapor (steam) temperatures are close to the saturation temperature. This shows that the interfacial heat transfer submodels, particularly those for the metastable state conditions, are appropriate and adequate for treating the depressurization phenomena.

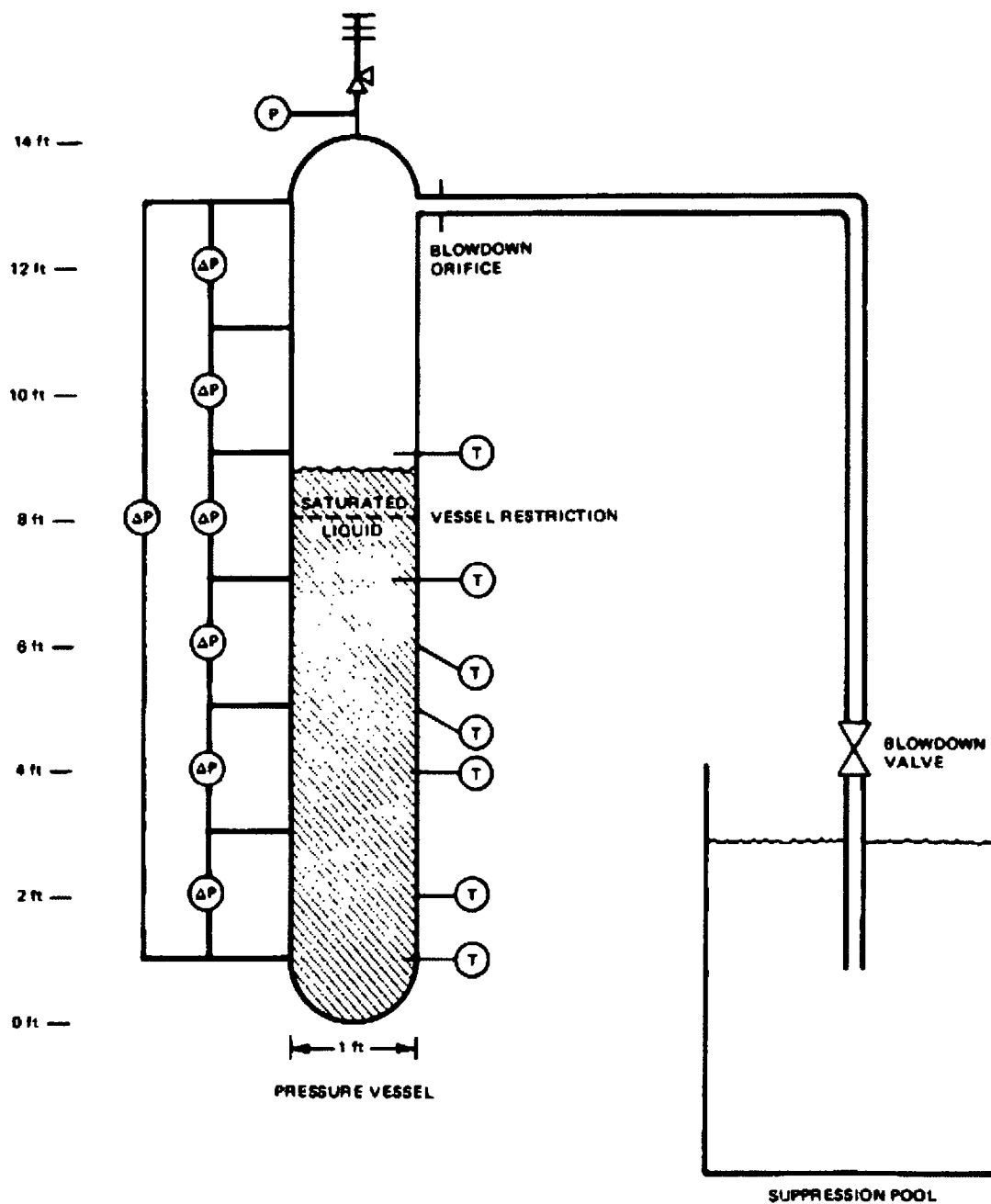


Figure 7-9 GE Small Blowdown Vessel*

* Reproduced from Reference 76, Figure A-2.

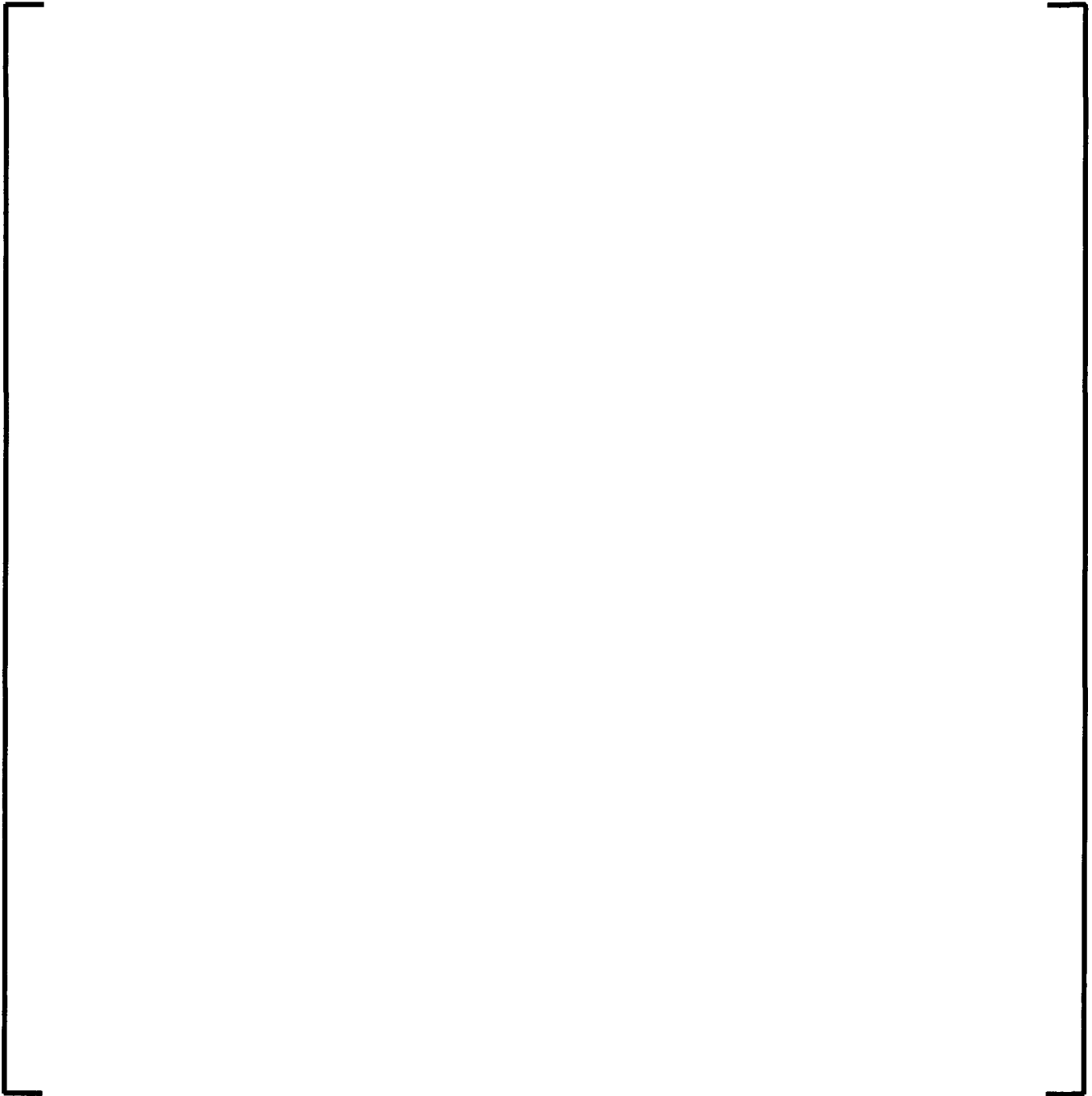


Figure 7-10 Nodalization for 1 ft GE Test 1004-3



Figure 7-11 Predicted Void Fraction for GE 1ft 1004-3 at 40 Seconds



Figure 7-12 Predicted Void Fraction for GE 1ft 1004-3 Test at 100 Seconds

7.3.8 THTF Mixture Level Test

Assessed phenomena and processes

This section addresses the following highly ranked PIRT phenomena identified in Table 5-1.

Assessment conclusions

The EM predicts the general behavior of the THTF mixture level test. That includes the excellent agreement with the prediction of level swell as indicated by void fraction, and reasonable agreement with vapor temperatures and heater-rod wall temperatures. The comparisons contribute to the validation of S-RELAP5 for the computation of fuel rod temperatures under conditions of core uncover with superheated vapor and under very low flow conditions. The assessment results overall show reasonable predictions of the indicated PIRT phenomena.

This conclusion is made within the context of the uncertainties of the ORNL level swell tests presented. The vapor and heated rod wall temperatures are generally predicted within reported uncertainty. The exception is Test K where there are data inconsistencies that tend to invalidate that test. It should be noted that the ORNL reported vapor temperatures within the test section are not actual data. The vapor temperature is measured at the exit and the vapor temperatures at test section exit and within the test section at lower elevations are computed by extrapolation based on a heat balance with the estimated heat loss (last sentence in Section 5.3.2.1 on page 29 from Reference 80). The uniform axial heat flux produces a linear rise in the calculated steam temperature with elevation when the heat loss is small. That is in agreement with the higher flow rate Tests I, J and M. It does not show the curvature reported by the low flow rate Tests K and N. Heat loss to a sink (using a selected heat transfer coefficient) produces the curvature of the vapor temperature versus elevation. Therefore, Test K has inconsistencies and may not be a reliable test.

Assessment description

The THTF facility, operated by ORNL, is a large high pressure thermal-hydraulic loop with non-nuclear (electrically heated) rods simulating a nuclear fuel bundle consisting of 64 rods. While the electrically heated 8x8 rod bundle was intended for PWR fuel designs, the fuel rod diameter and pitch (0.374", 0.501") [

] Furthermore, the facility was designed to simulate the thermal-hydraulic environments expected during LOCA events, thus providing test data applicable to BWR LOCA analysis. References 80 and 82 describe the tests and the test facility. Three THTF experiments were investigated for the EM: (1) mixture-level swell tests; (2) transient boil-off tests; and (3) reflood tests. The THTF facility is shown in Figure 7-13 through Figure 7-18.

This section addresses the level swell test assessments. Figure 7-19 shows the S-RELAP5 nodalization for the level swell model. The level swell test series investigates the steady-state thermal-hydraulic behavior of the rod-bundle when the operating conditions produce a two-phase mixture that extends about 70 to 80% up the test section. Superheated vapor exists above the two-phase mixture level with elevated vapor and heater rod wall temperatures. The flow rates are very low with some Reynolds numbers less than 2000 and in the mixed laminar-turbulent regime. The pressure ranges from 581 to 1173 psia. The assessments consisted of 3.09 Series 10 Tests I, J, K, M, N and DD (note that Test DD had no temperature data).

This is a challenging experimental environment and some of the data have considerable uncertainty. There are two flow rates (inlet, outlet) and there are significant reported uncertainties. The mass and energy balance is not resolved in the test report. Thus, the power, flow rate, heat loss, inlet temperature and outlet temperature are not self-consistent by a simple mass and heat balance. This is important because the heat balance establishes the vapor temperature whether it comes from a simple heat balance, or, from S-RELAP5. A vapor temperature is needed to compute the heater rod wall temperature. Test K has the greatest flow uncertainty and Test I only reports an outlet flow rate. The overall, mass balance is generally poor. A flow rate was selected from the data for each test. [

]

[] Thus, the heater rod surface temperatures are also minimized.

The power has a reported uncertainty ranging from 5.5 to 6.3 percent. That uncertainty is surprisingly high. Power should be measurable to higher accuracy. Power is important because it defines the heat flux on the heater-rods and the enthalpy rise along the test section.

The uncertainty in power and flow are very important because the power/flow ratio defines the enthalpy rise along the test section and in the superheated vapor region above the two-phase mixture level.

The superheated vapor temperature at the outlet is reported to have an uncertainty ranging from 25.2 to 67.5 °F. The largest uncertainty is for the lowest flow Test K.

The reported heater rod wall temperature is an average of the rods at the selected elevation. The reported uncertainty for a single rod is about 3 °F and, for an averaged set of rods, the uncertainty is up to about 30 °F. The larger uncertainty for a set of rods depends on the number of rods in a set, and, it also indicates the rod-to-rod variation over the cross-section of the rod bundle.

The reported outlet vapor temperature is a measured value which accounts for radiation heat transfer to the vapor and to the heater rods. There is uncertainty in both the vapor temperature measurement and the radiation heat transfer. There is no reported variation of vapor temperatures over the cross-section of the rod bundle. Vapor temperature uncertainties range from about 24 to 96 °F.

Heat loss is computed from pairs of thermocouple placed radially in the shroud at ten axial locations. The loss heat flux is computed for each thermocouple pair and integrated along the axial length. Only the total heat loss fraction is reported for each test. Details of the heat loss along the axial length of the test section are not presented.

In conclusion, the THTF level swell tests have considerable uncertainty in the reported flow rates and vapor temperatures. The reported vapor and heater rod wall temperatures of the THTF level swell tests are marginally suitable for a validation of heat transfer. The tests are, however, suitable for comparing the trends of computed versus reported data. The

comparisons presented in this section are presented and interpreted in that context. In spite of those uncertainties, the S-RELAP5 computations produce void fraction, vapor temperature and heater rod wall temperature that are generally consistent with the reported data.

7.3.8.1 Level Swell Results

Figure 7-20 through Figure 7-25 show the computed void fraction versus elevation. There is excellent agreement between the calculated and reported void fraction. The notable exception is Test K where the calculated axial elevation of the void fraction rise is at a higher elevation than indicated by the reported data. This mismatch in void fraction distribution suggests an inconsistency of measured void fraction, vapor temperature and flow rate for Test K.

The specific void fraction response depends on the flow rate. At the higher flow rates (Tests DD, I, J and M), there is a gradual rise to a void fraction of 1.0. At the lower flow rates (Tests K and N) there is a slower rise followed by a sudden rise to a void fraction of 1.0. The elevation of the two-phase mixture level is near the sudden rise of the void fraction to 1.0.

7.3.8.2 Rod Temperature Results

Figure 7-26 through Figure 7-30 present the computed and reported vapor temperature and heater rod wall temperature for Tests I, J, K, M and N. The computations generally follow the trends of the data. There is tendency to over predict the vapor temperature. The heater-rod wall temperatures are both under and over predicted; however, the trend show an overall conservatism.

Test I: There is excellent agreement between the computed vapor and heater rod wall temperatures in Figure 7-26. The drop in wall temperature followed by the rise is caused by the enhanced heat transfer downstream of a grid spacer. [

] This is the highest flow rate test.

Test J: The vapor temperatures are over predicted and the wall temperature agrees reasonably well with the reported data in Figure 7-27. Again, the drop in wall temperature followed by the rise is caused by the enhanced heat transfer downstream of a grid spacer. This is one of the intermediate flow rate tests.

It should be noted that the computed superheated vapor temperature result in S-RELAP5 is equivalent to the solution of the one-dimensional energy equation for vapor temperature. The primary uncertainties are the measured flow rate and exit vapor temperature and the extrapolation to lower elevations. Either the flow rate is too low; or, the reported vapor temperature is too low.

Test K: The vapor temperatures are predicted reasonably well and the wall temperatures are under-predicted in Figure 7-28. Test K has the greatest uncertainty in measured flow rate and vapor temperature. This is the lowest flow rate test.

Based on the reported void fraction data, the superheated vapor region should start at an elevation of about 6.5 ft. The temperature data indicates an elevation at about 7.5 ft. If the void fraction data is correct, the reported vapor temperatures are too low. If the temperature slope with elevation is taken as correct, the vapor temperatures should be translated to the left by about 1 ft. That would increase the temperature in the superheated region by more than 100 °F and the wall temperatures would follow. There is considerable uncertainty in Test K, and, it was considered for rejection. However, the S-RELAP5 computation agrees with the trends of the data; this trend is of value and Test K was retained.

Test M: There is excellent agreement between the computed vapor and heater rod wall temperatures in Figure 7-29. This is one of the intermediate flow rate tests.

Test N: The vapor and wall temperatures are over-predicted. This is one of the lowest flow rate tests, along with Test K.

Based on the reported void fraction data presented in Figure 7-25, the superheated vapor region should start at an elevation of about 7.0 ft. The temperature data indicates an elevation near 7.5 ft. As for Test K, if the void fraction data is correct, the reported vapor temperatures are too low. If the temperature slope with elevation is taken as correct, the vapor temperatures should be translated to the left by about 0.5 ft. That would increase the reported vapor temperature by less than 100 °F and the wall temperatures would follow. The overall agreement would improve.

**Table 7-4 Summary of THTF and BWR
 ATRIUM-10 Rod Bundles**

--	--

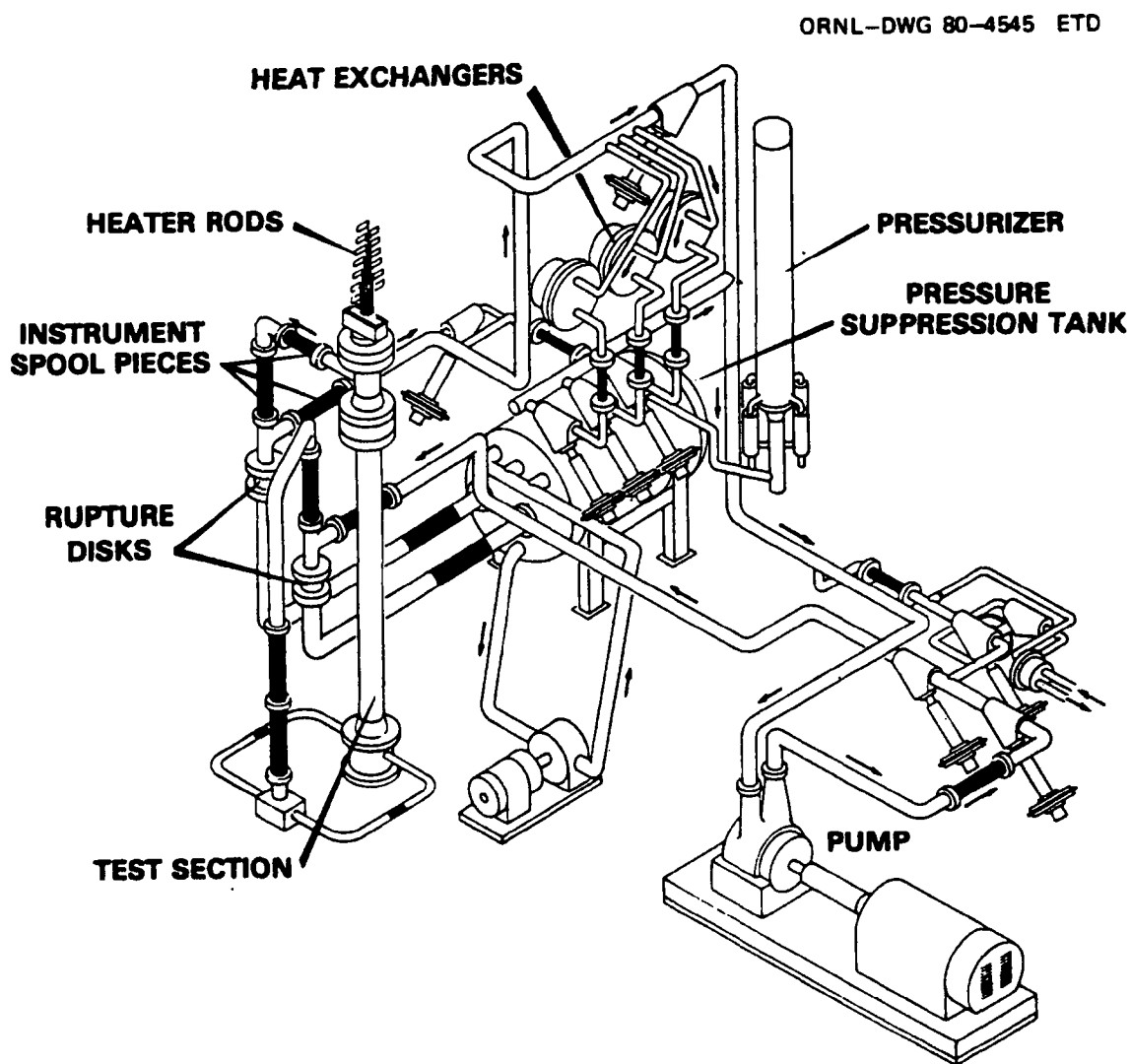


Figure 7-13 Schematic of THTF*

* Reproduced from Reference 81 Figure 2

ORNL-DWG 80-4551R ETD

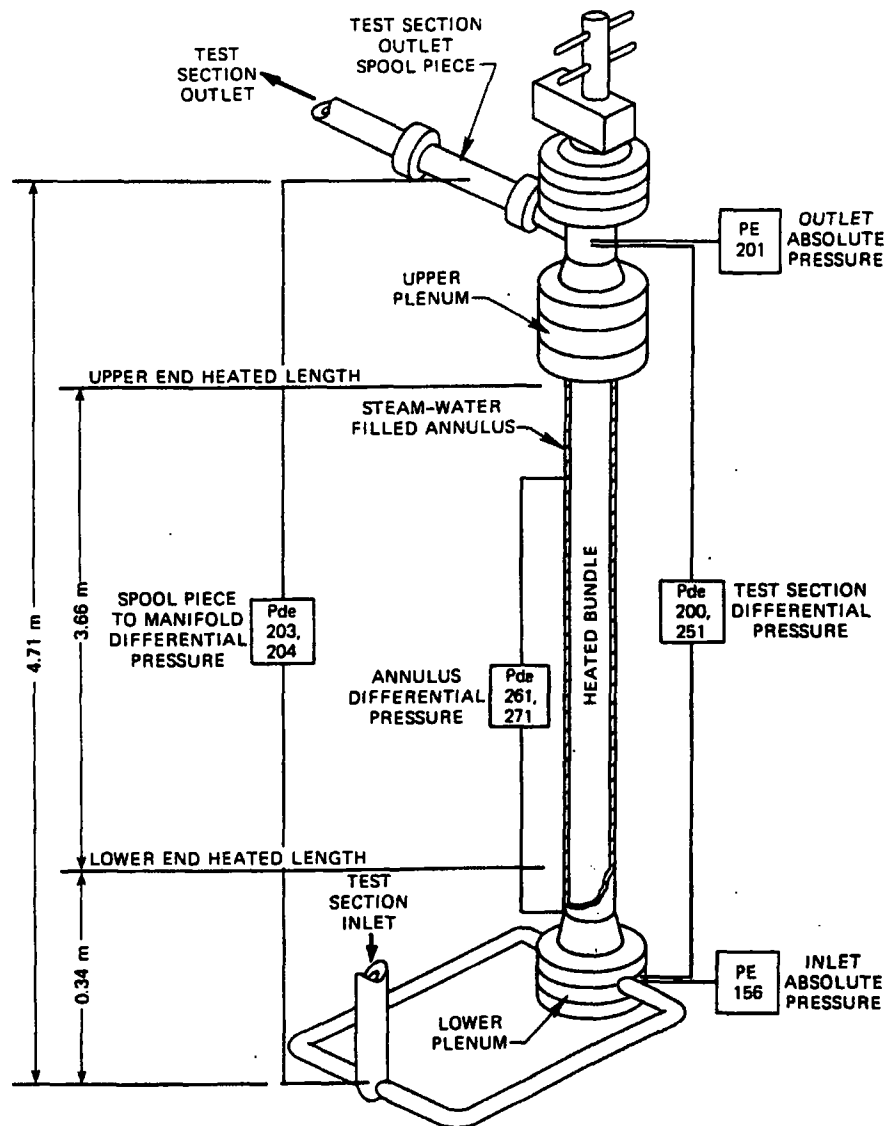


Figure 7-14 Diagram of THTF Test Section*

* Reproduced from Reference 81 Figure 6

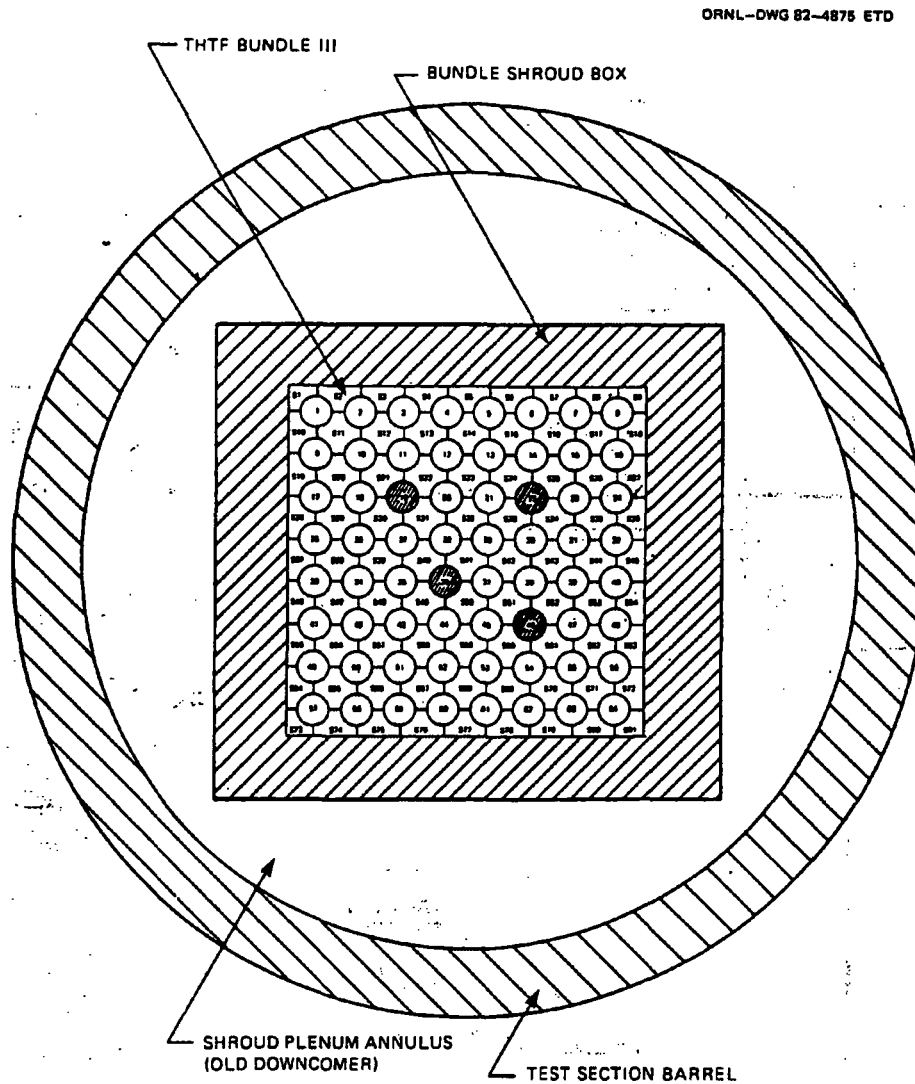


Figure 7-15 Cross-Section View of THTF Test Section*

* Reproduced from Reference 80 Figure 2

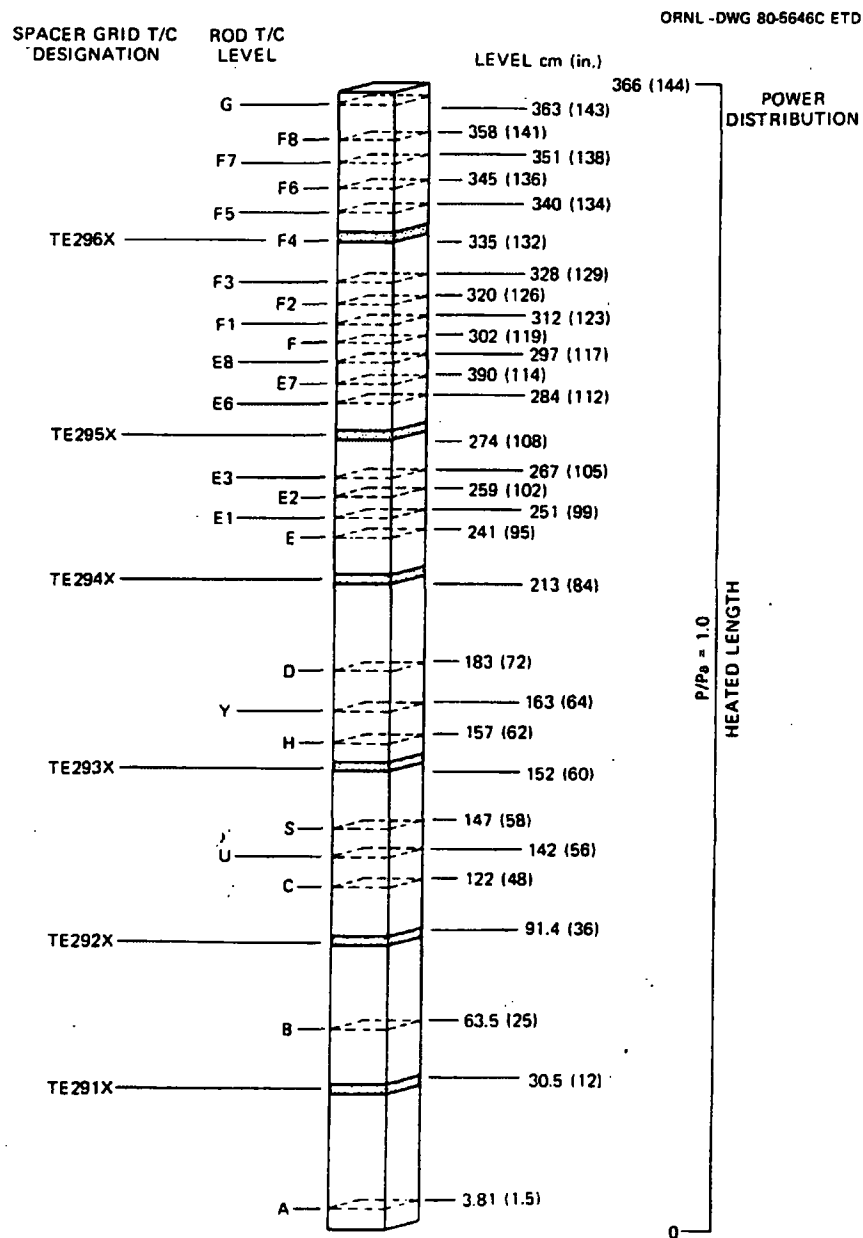


Figure 7-16 Axial Locations of Thermocouples in THTF Test Section*

* Reproduced from Reference 83 Figure 4

ORNL-DWG 77-5718D

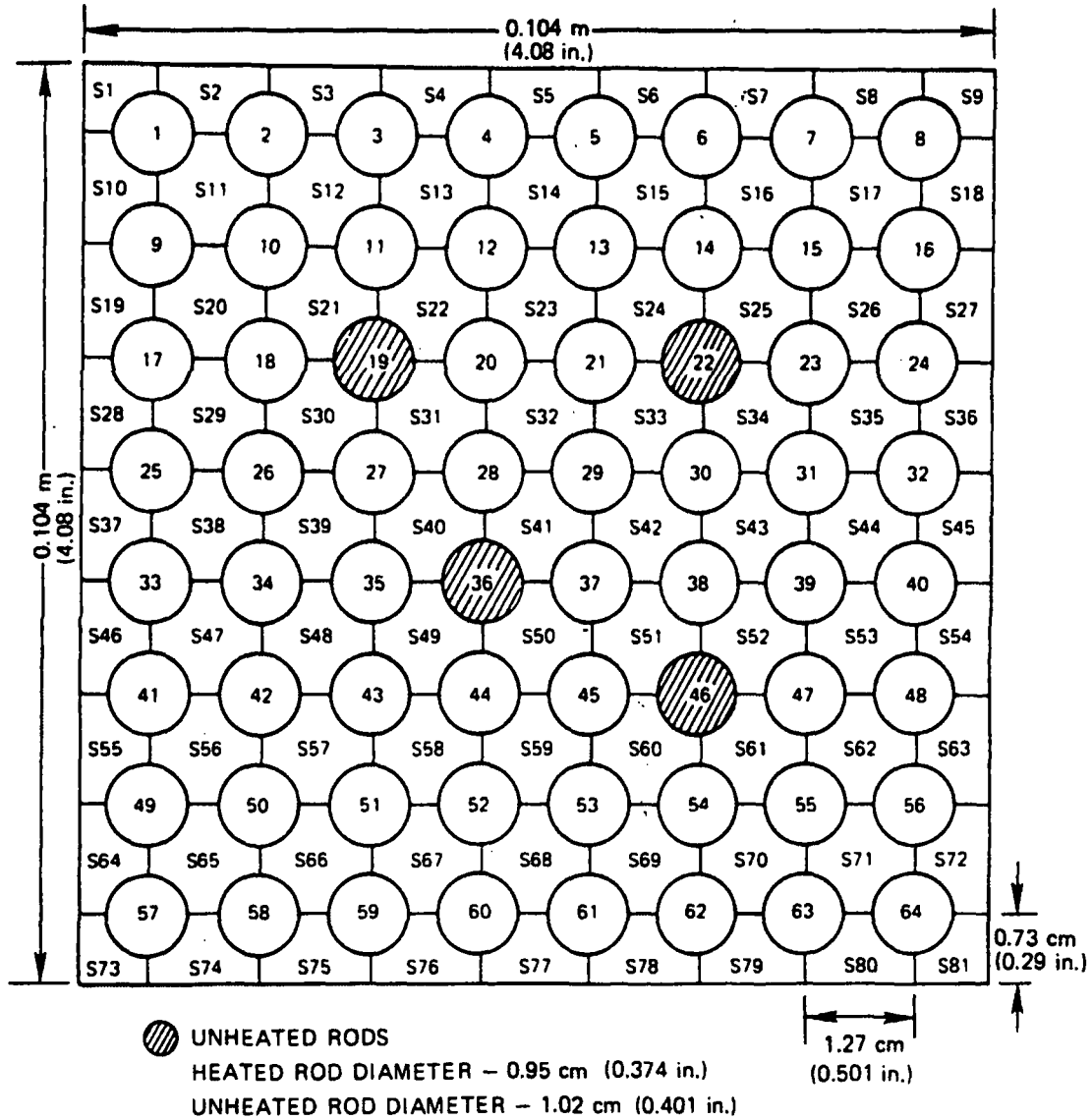


Figure 7-17 Map of Rods in THTF Simulated Fuel Bundle*

* Reproduced from Reference 80 Figure 3

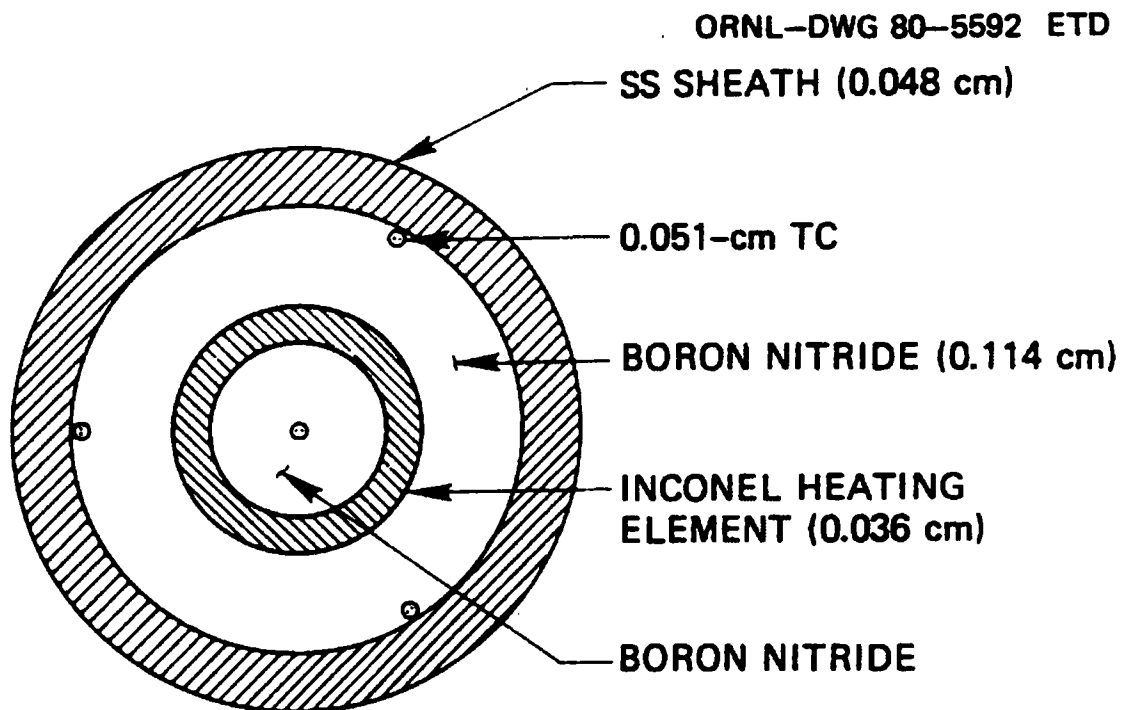


Figure 7-18 Cross-Sectional View of THTF Simulated Fuel Rod*

* Reproduced from Reference 81 Figure 3

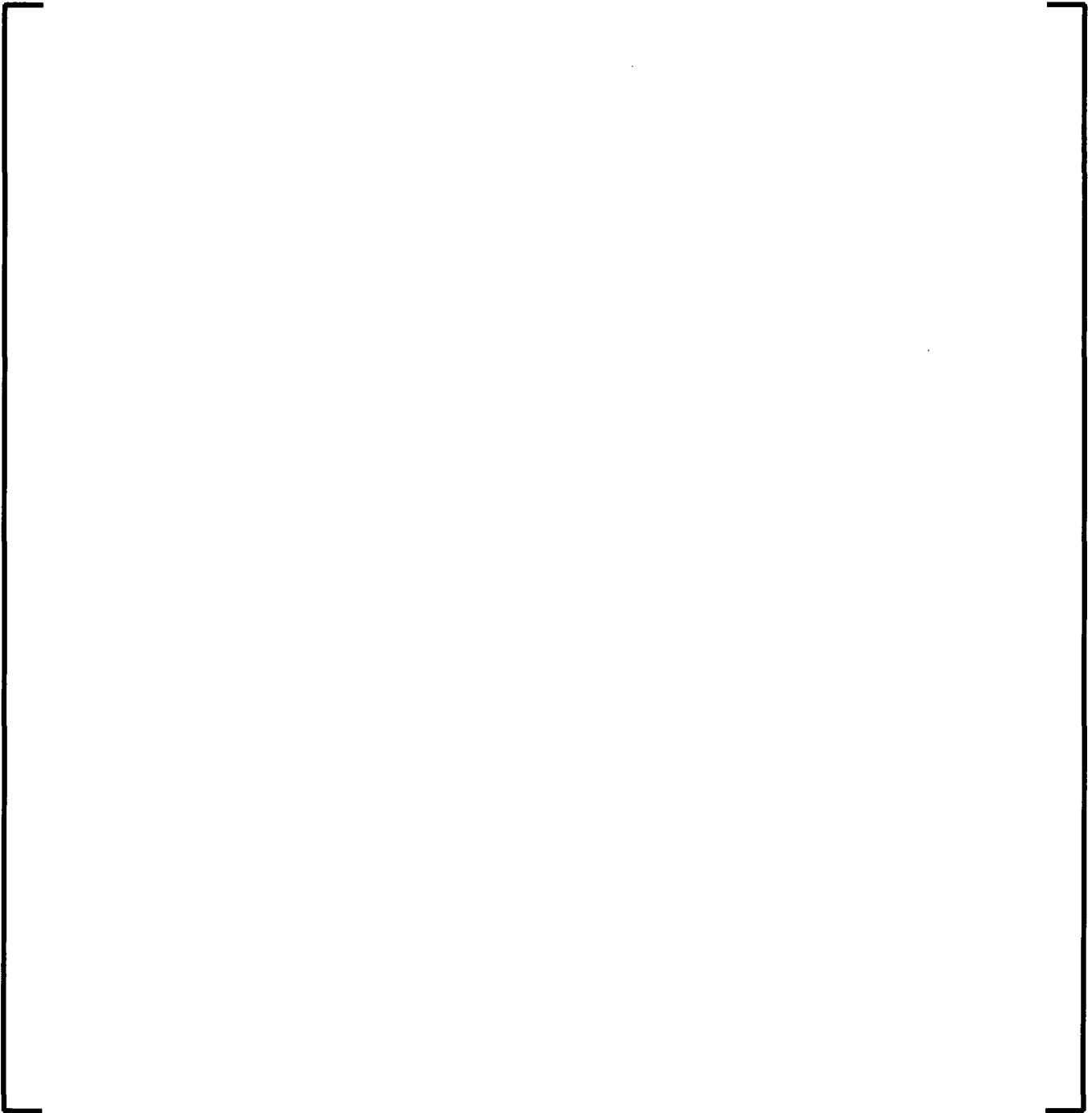


Figure 7-19 S-RELAP5 Nodalization of ORNL THTF for Level Swell Test



Figure 7-20 Calculated and Reported Void Fraction for THTF Test DD



Figure 7-21 Calculated and Reported Void Fraction for THTF Test I



Figure 7-22 Calculated and Reported Void Fraction for THTF Test J



Figure 7-23 Calculated and Reported Void Fraction for THTF Test K



Figure 7-24 Calculated and Reported Void Fraction for THTF Test M



Figure 7-25 Calculated and Reported Void Fraction for THTF Test N



Figure 7-26 **Calculated and Reported Temperature THTF Test I**



Figure 7-27 **Calculated and Reported Temperature THTF Test J**



Figure 7-28 Calculated and Reported Temperature THTF Test K



Figure 7-29 Calculated and Reported Temperature THTF Test M



Figure 7-30 Calculated and Reported Temperature THTF Test N

7.3.9 TLTA Boiloff Test

Assessed phenomena and processes

This section addresses the following highly ranked PIRT phenomena identified in Table 5-1.

Assessment conclusions

The EM predicts the general behavior of the TLTA boiloff test. For the tests which were performed at approximately 400 psia, the downcomer, bypass and bundle void fractions were predicted closely. The calculated fuel bundle temperatures above the two-phase level also matched the data closely. For the TLTA boil-off test which was performed at 800 psi, the predicted void fractions in the bypass and bundle show that the two-phase level rise was delayed compared to data. Consistent with the level predictions, the calculated fuel bundle temperature rise were also delayed, which resulted in lower predicted peak bundle temperatures. Based on the 400 psia assessment and previous assessments, the EM has demonstrated good comparisons for void fractions, the delayed level rise in the 800 psi assessment implies a problem with the reported test data and/or assumptions of the conditions. If the simulation results are time shifted, the trends show good agreement for bundle and bypass void fractions and rod temperatures. The assessment results overall show reasonable predictions of the indicated PIRT phenomena.

Assessment description

The two-loop test apparatus (TLTA) was built to simulate LOCA scenarios in a BWR. It was originally built as a part of the BWR blowdown heat transfer (BDHT) program jointly sponsored by the General Electric Company, the United States nuclear regulatory commission (USNRC) and the Electric Power Research Institute (EPRI). The scope of the original program was to be able to simulate the blowdown period of a BWR LOCA event, which is the time period from the occurrence of the break to the onset of the emergency core cooling system (ECCS).

The original apparatus was subsequently modified for the BWR Blowdown / Emergency Core Cooling (BD/ECC) program under the same joint sponsorship. This extended the simulation period of the LOCA event to include ECC operation. The tests being simulated for EM are from this modified facility.

The TLTA is a scaled version of a BWR/6, with one fuel bundle. The apparatus includes one full-length (150 inches long) fuel bundle simulator. Figure 7-31 shows a schematic diagram, corresponding to Configuration 5. The original TLTA configuration used a 7x7 rod bundle, and later TLTA configurations used an 8x8 rod bundle, and other sequential modifications to arrive at a better representation of the BWR LOCA event being simulated. The bundle uses electrically heated rods (direct heating), with a peak power of 6.5 MW, which is representative of a peak power bundle in a BWR/6. The rest of the TLTA system is scaled down, relative to a BWR/6 with a 218-inch reactor vessel and 624 fuel bundles. There are two recirculation loops, each loop feeding a jet pump located in the downcomer region of the TLTA vessel. Blowdown lines are provided from both legs of one recirculation loop, allowing the simulation of a LOCA from the suction side or the discharge side of the recirculation pump. ECC water can be delivered at several locations in the system.

The facility is primarily volume-scaled. This caused the jet pumps to be relatively short compared to a BWR/6, where the jet pump extends up to about 2/3 of the core height. Figure 7-32 shows an elevation comparison of the TLTA vessel with a BWR/6 vessel. The TLTA was primarily intended for simulation of large break LOCA (LBLOCA) events and hence the short jet pumps do not have a significant effect. In small break LOCA (SBLOCA) events, the height of the jet pumps can affect the event progression. Hence only one SBLOCA test was performed in the TLTA. Although it is not an ideal representation of an SBLOCA event in a BWR, the test still provides useful information for assessment of analysis methods.

Although the TLTA bundle could be operated at full power (about 6.5 MW), steady-state operation of the facility is possible only up to about 2 MW. This is because of limited capacity for cooling the electrical cables of the power supply system and due to the limited heat removal capacity of the system overall. Hence, in the LBLOCA simulations, a steady-state is first achieved at about 2 MW, the power is then ramped up to the desired initial power for the test, and the LOCA event is initiated from a transient state. For the SBLOCA and other simulations, the tests are initiated from a steady-state condition.

Table 7-5 provides a list of all the tests conducted under the BD/ECC 1A program, using Configurations 5, 5A, 5B and 5C.

A series of boil-off tests were conducted with configuration 5A (Series 6441 in Table 7-5). Table 7-6 provides a summary of the initial conditions for the boil-off tests, showing the initial conditions for each test. Figure 7-33 shows configuration 5A.

The boil-off tests were conducted with TLTA configuration 5A by bringing the system to the desired test pressure and power level and turning off recirculation pumps, allowing the two-phase level in the core to drop. System pressure and bundle power are held constant during the test. Natural circulation exists under these conditions between the heated bundle and the downcomer and the bypass. Data recording starts when two-phase level reaches near the top of bundle. The test descriptions and the results are provided in Reference 105.

Two boil-off tests were simulated, test 6 (6441-6) and 7 (6441-7). Both tests were performed at a power level of 250 kW, test 6441-6 was at a pressure of approximately 400 psia and test 6441-7 at a pressure of approximately 800 psia. Test 6441-6 was terminated by turning on feedwater flow when the peak bundle temperature reaches 800 °F. Test 6441-7 was set to terminate when the upper plenum temperature reached 800 °F or the peak bundle temperature reached 1000 °F.

[

]

7.3.9.1 TLTA Test 6441-6 Results

Comparison of the measured and predicted downcomer void fractions is shown in Figure 7-35. As mentioned earlier, the predictions are shifted so the downcomer void fraction at time zero matches the data. Figure 7-35 shows that the downcomer void fraction for the remainder of the transient is closely predicted. Figure 7-36 to Figure 7-41 show that the bypass and bundle void fractions are also closely predicted. The predicted fuel bundle temperatures above the two-phase mixture level at different elevations, Figure 7-42 to Figure 7-47, are consistent with the level predictions and also match the data closely.

7.3.9.2 TLTA Test 6441-7 Results

The calculated downcomer void fraction is compared to the data in Figure 7-48. Comparison of the measured and predicted void fractions in the bypass and the bundle, Figure 7-49 to Figure 7-54, show that the predicted two-phase level rise is slightly delayed compared to data. Consistent with the level predictions, the calculated fuel bundle temperature rise is also delayed, Figure 7-55 to Figure 7-60, which results in a lower predicted peak bundle temperatures. Based on the 400 psia assessment and previous level swell assessments, the EM has demonstrated good comparisons for void fractions, the delay in the simulation of Test 7 implies a problem with the reported test data and/or assumptions of the conditions. If the simulation results are time shifted, the trends show good agreement for bundle and bypass void fractions and rod temperatures.

**Table 7-5 Summary of TLTA Tests under the
BD/ECC 1A Program**

Test	Power (MW)	Spray	ECC Temp	Break Size	TLTA Config	Test Date
6401/4	2.63	High	Nominal	DBA	5	Jun 78
6405/3	5.05	Average	Nominal	DBA	5	Jul 78
6406/1	5.05	Average	Nominal	DBA	5	Aug 78
6406/3	5.05	-	-	DBA	5	Sep 78
6414/3	6.49	Low	High	DBA	5	Sep 78
6421/2	5.05	-	-	DBA	5A	Sep 79
6422/3	5.05	Average	Nominal	DBA	5A	Oct 79
6423/3	6.49	Low	High	DBA	5A	Nov 79
6431/1	2.0*	Average	Nominal	DBA	5B	Dec 79
6431/2	2.0*	Average	Nominal	DBA	5C	Mar 80
6441	Boil-Off†	-	-	-	5A	Jun 80
6424/1	6.49	Average	Nominal	DBA	5A‡	Jul 80
6425/2	5.05	Average	Nominal	DBA	5A‡	Jul 80
6426/1	5.05	-	-	DBA	5A‡	Sep 80

* Bundle power for small break tests was held at 2 MW for 7 seconds, then decayed in accordance with the 5.05 MW initial power decay curve.

† There were five boil-off tests conducted under the test series 6441. The test conditions are shown in Table 7-6.

‡ With turbine meter and drag disc measurements for break flow and new automatic pressure controller.

**Table 7-6 Summary of TLTA Boil-off Tests under the
BD/ECC 1A Program**

No.	Run	Point	Initial Conditions		
			Pressure (psia)	Power (kW)	Initial Level
1	7	5	800	250	Bundle Top
2	3	4	400	150	100 in. above BHL
3	6	1	400	250	Bundle Top
4	3	5	400	400	Bundle Top
5	5	9	200	250	Bundle Top

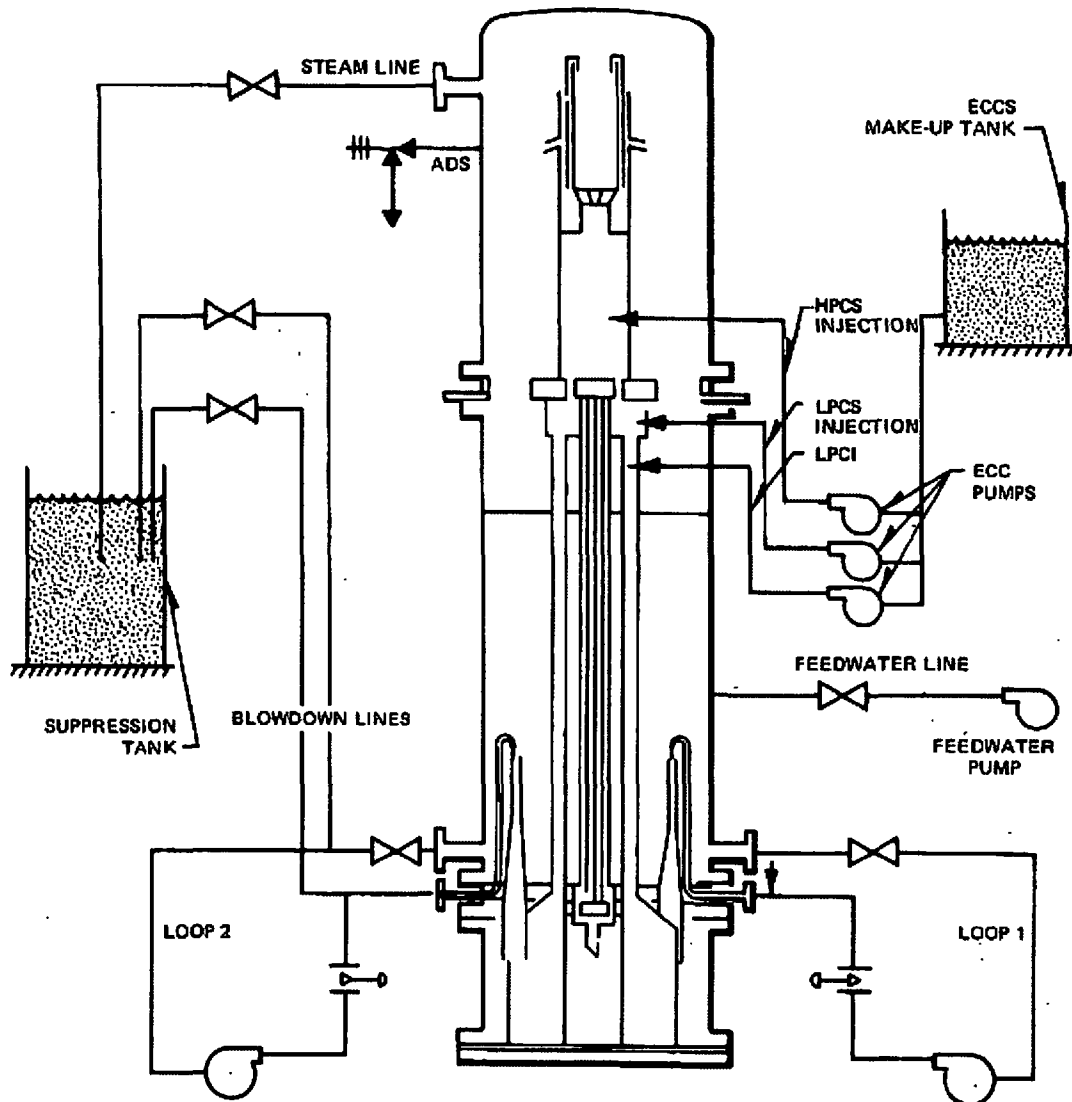


Figure 7-31 TLTA System Configuration 5*

* Reproduced from Reference 105 Figure 2-1

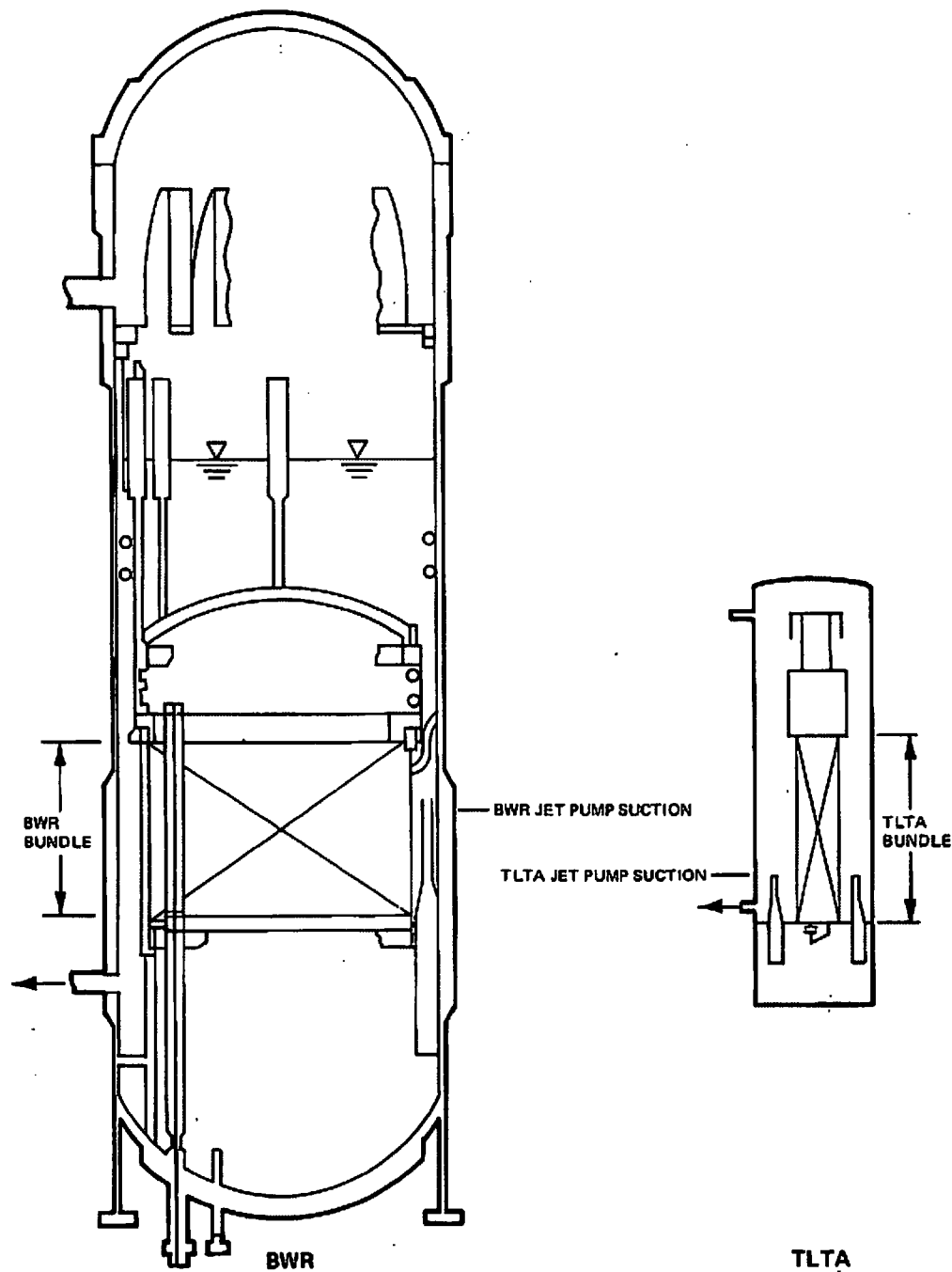


Figure 7-32 Elevation Scaling Comparison BWR/6 vs. TLTA*

* Reproduced from Reference 115 Figure 3-2

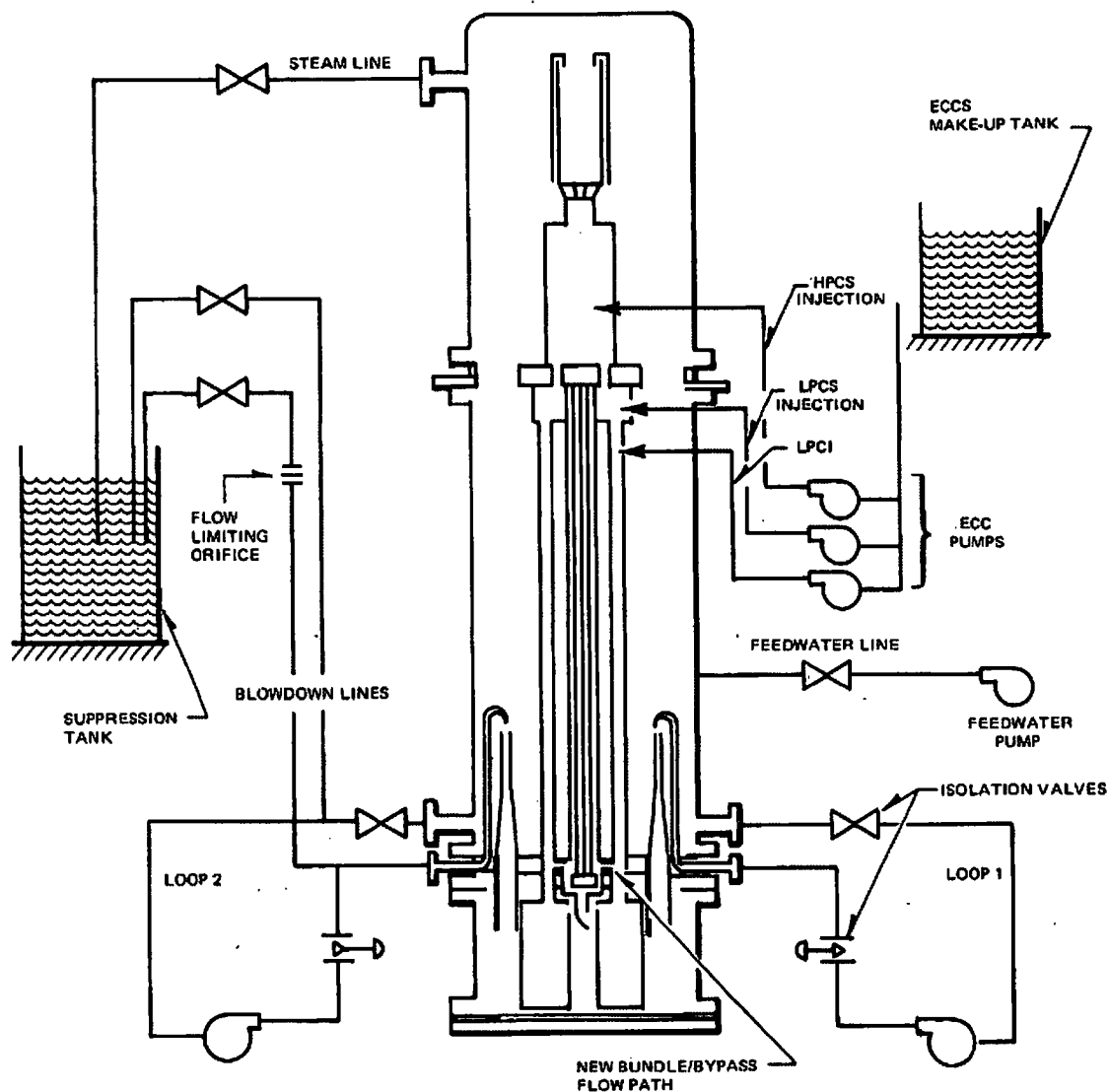


Figure 7-33 TLTA System Configuration 5A*

* Reproduced from Reference 105 Figure 2-1

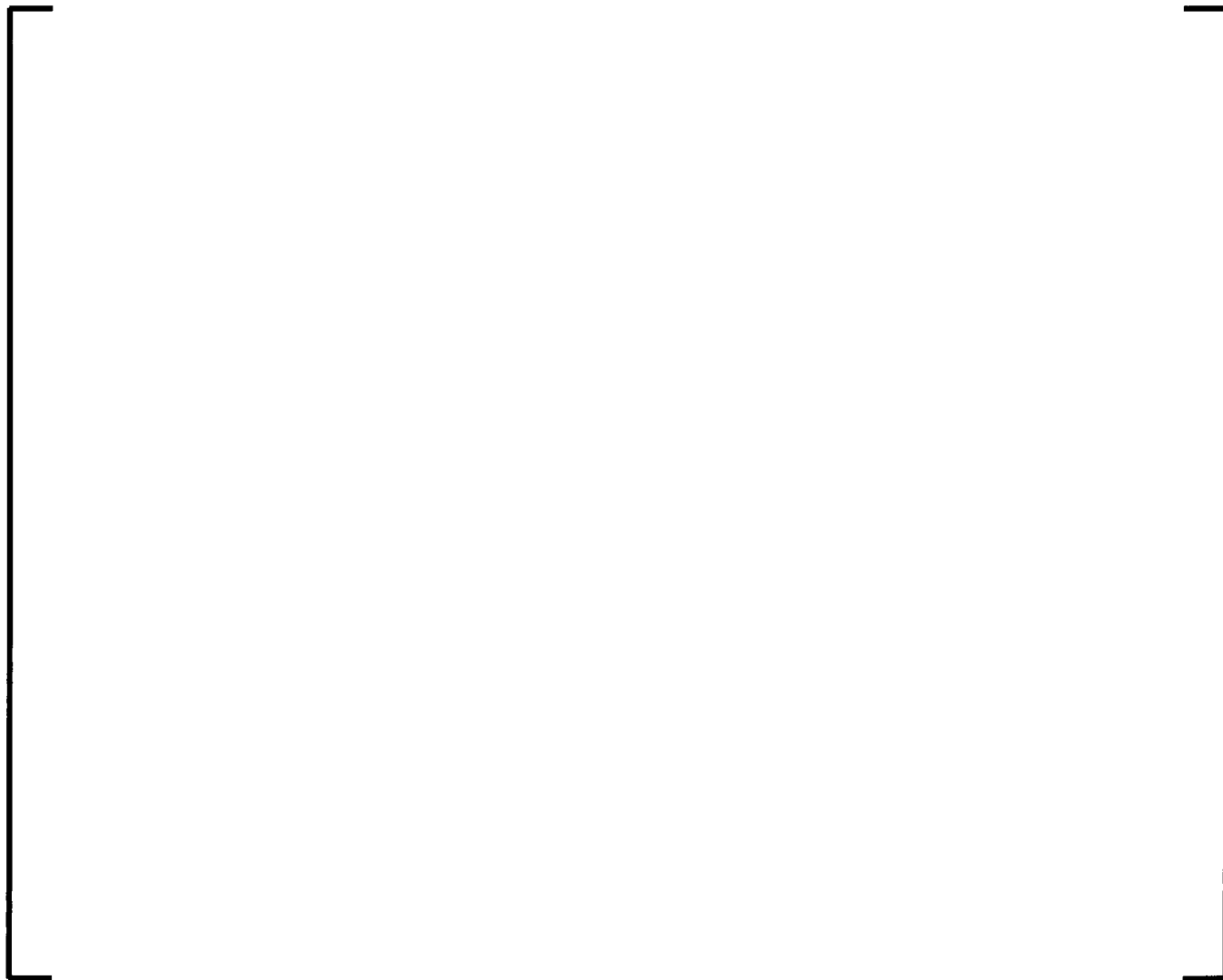


Figure 7-34 Nodalization of TLTA-5A



Figure 7-35 Comparison of the Measured and Predicted Downcomer Void Fractions for TLTA Boil-Off Test 6441-6



Figure 7-36 Comparison of the Measured and Predicted Bypass Void Fractions for TLTA Boil-Off Test 6441-6



Figure 7-37 Comparison of the Measured and Predicted Bundle Void Fractions at DP Cell Location 27 for TLTA Boil-Off Test 6441-6



Figure 7-38 Comparison of the Measured and Predicted Bundle Void Fractions at DP Cell Location 28 for TLTA Boil-Off Test 6441-6



Figure 7-39 Comparison of the Measured and Predicted Bundle Void Fractions at DP Cell Location 29 for TLTA Boil-Off Test 6441-6



Figure 7-40 Comparison of the Measured and Predicted Bundle Void Fractions at DP Cell Location 30 for TLTA Boil-Off Test 6441-6



Figure 7-41 Comparison of the Measured and Predicted Bundle Void Fractions at DP Cell Location 31 for TLTA Boil-Off Test 6441-6



Figure 7-42 Comparison of the Measured and Predicted Cladding Temperatures at 107" Elevation for TLTA Boil-Off Test 6441-6

Figure 7-43 Comparison of the Measured and Predicted Cladding Temperatures at 115" Elevation for TLTA Boil-Off Test 6441-6

Figure 7-44 Comparison of the Measured and Predicted Cladding Temperatures at 120" Elevation for TLTA Boil-Off Test 6441-6



Figure 7-45 Comparison of the Measured and Predicted Cladding Temperatures at 130" Elevation for TLTA Boil-Off Test 6441-6



Figure 7-46 Comparison of the Measured and Predicted Cladding Temperatures at 135" Elevation for TLTA Boil-Off Test 6441-6

Figure 7-47 Comparison of the Measured and Predicted Cladding Temperatures at 140" and 143" Elevation for TLTA Boil-Off Test 6441-6

Figure 7-48 Comparison of the Measured and Predicted Downcomer Void Fractions for TLTA Boil-Off Test 6441-7



Figure 7-49 Comparison of the Measured and Predicted Bypass Void Fractions for TLTA Boil-Off Test 6441-7



Figure 7-50 Comparison of the Measured and Predicted Bundle Void Fractions at DP Cell Location 27 for TLTA Boil-Off Test 6441-7



Figure 7-51 Comparison of the Measured and Predicted Bundle Void Fractions at DP Cell Location 28 for TLTA Boil-Off Test 6441-7



Figure 7-52 Comparison of the Measured and Predicted Bundle Void Fractions at DP Cell Location 29 for TLTA Boil-Off Test 6441-7



Figure 7-53 Comparison of the Measured and Predicted Bundle Void Fractions at DP Cell Location 30 for TLTA Boil-Off Test 6441-7



Figure 7-54 Comparison of the Measured and Predicted Bundle Void Fractions at DP Cell Location 31 for TLTA Boil-Off Test 6441-7

**Figure 7-55 Comparison of the Measured and Predicted Cladding
Temperatures at 107" Elevation for TLTA Boil-Off Test 6441-7**

**Figure 7-56 Comparison of the Measured and Predicted Cladding
Temperatures at 115" Elevation for TLTA Boil-Off Test 6441-7**



**Figure 7-57 Comparison of the Measured and Predicted Cladding
Temperatures at 120" Elevation for TLTA Boil-Off Test 6441-7**



**Figure 7-58 Comparison of the Measured and Predicted Cladding
Temperatures at 130" Elevation for TLTA Boil-Off Test 6441-7**



**Figure 7-59 Comparison of the Measured and Predicted Cladding
Temperatures at 135\" Elevation for TLTA Boil-Off Test 6441-7**



**Figure 7-60 Comparison of the Measured and Predicted Cladding
Temperatures at 140\" Elevation for TLTA Boil-Off Test 6441-7**

7.3.10 Bennett Tube

Assessed phenomena and processes

This section addresses the following highly ranked PIRT phenomena identified in Table 5-1;

Assessment conclusions

Assessment of two Bennett heated tube tests was performed. The tests selected are a low flow test, and a high flow test. The calculated CHF positions agree well for the low flow case and is conservative for the high flow case. For the low flow case, the wall temperatures in the film boiling region are well predicted. For the case of high flow, the calculated wall temperature stays rather flat in the post-CHF region and is conservatively higher than the data, particularly in the top-end region. From this, it is inferred that the EM makes reasonable and conservative predictions of the indicated PIRT phenomena.

Assessment description

The Bennett heated tube experiments (Reference 106) were conducted by the UKAEA Research Group to measure the dryout or critical heat flux (CHF) location and the surface temperature profiles in the region beyond the dryout point. Calculations for Test Case 5358 and Test Case 5379 were performed. The main purpose of the assessment is to validate the applicability of Groeneveld CHF LUT correlation (Section 6.4.10). Post-CHF heat transfer is also examined.

The test tube was a simple heated tube 0.497-inch I.D. and 0.625-inch O.D. with a total length of 19 feet. Figure 7-61 shows the test section along with the construction of the end flanges and current clamps. Twenty-seven thermocouples were attached to the test section (Figure 7-62) to measure wall temperatures along the length of the heated tube. Two series of experiments were carried out; in the first, the current clamps were placed to give a heated length of 219 inches and in the second the lower busbar connection was moved to just above the joining flange to give a heated length of 144 inches.

The water entered the test section bottom at a pressure adjusted to give a nominal pressure at the outlet (top) of the test section of 1000 psia. The power to the test section was raised until the end thermocouple (No. 27) showed a rapid increase indicating CHF condition. Conditions were allowed to steady out and the thermocouple readings were read off on the data logging system together with power input, flow, exit pressure, etc. The power was raised again until the next thermocouple (No. 26) showed a rapid increase in temperature and the readings taken again. This procedure was repeated until the maximum temperature read by any thermocouple along the test section approached 1400 °F. Some 224 temperature profiles were determined during the experiments.

Two of the tests from the series of 219-inch heated length were selected for this assessment. They are Tests 5358 and 5379 and their conditions are shown in Table 7-7. [

]

Shown in Figures 7-64 and 7-65 are the comparison plots of calculated wall temperatures and data for two of the Bennett heated tube tests (Reference 106), Test 5358 with a mass flux of 379.7 kg/m²-s and Test 5379 with a mass flux of 3797.4 kg/m²-s. The CHF positions agree well with low flow case and show a conservative (lower) prediction for the high flow case. For the low flow case, the calculated temperature rise immediately after CHF is not as high as the measured temperature but the temperature continues to rise in the post-CHF region and the wall temperatures in the film boiling region are predicted closely. For the high flow case, the calculated wall temperature stays rather flat in the post-CHF region and is higher than the data, particularly in the top-end region.

The results of this assessment validate the S-RELAP5 correlations for predicting CHF and post-CHF heat transfer.

Table 7-7 Conditions for Bennet Tube Tests 5358 and 5379

Parameter	Test 5358	Test 5379
Pressure (outlet), psia	1000	1000
Power, kW	113	377
Mass flow, lb/ft ² hr (lb/s)	0.28 x 10 ⁶ (0.10478)	2.8 x 10 ⁶ (1.0478)
Inlet subcooling, Btu/lb (°F)	75 (61.9)	25 (19.7)

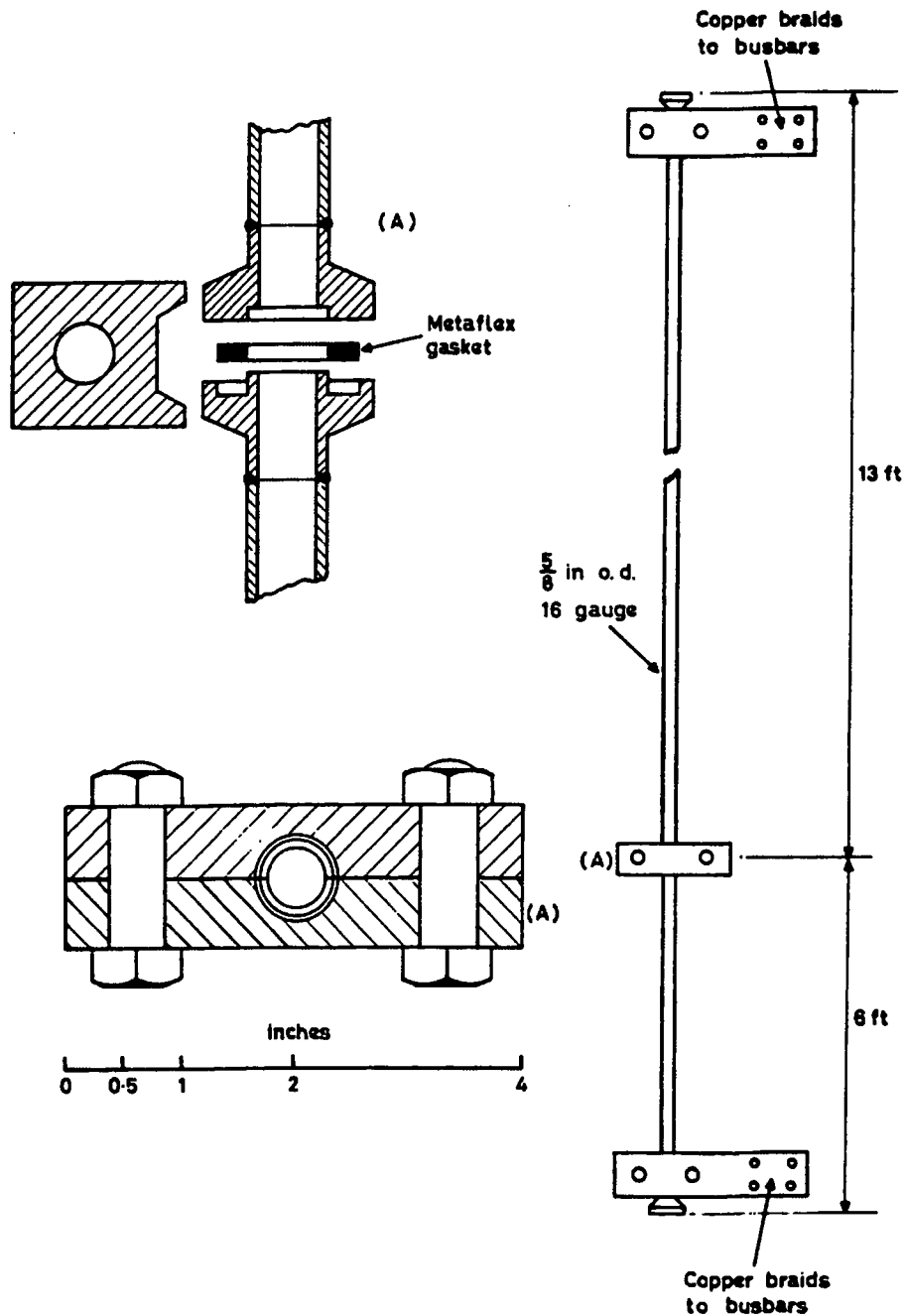


Figure 7-61 Diagram of Test Section and Flange Arrangement for the Bennett Heated Tube Tests*

* Reproduced from Reference, 106 Figure 2.

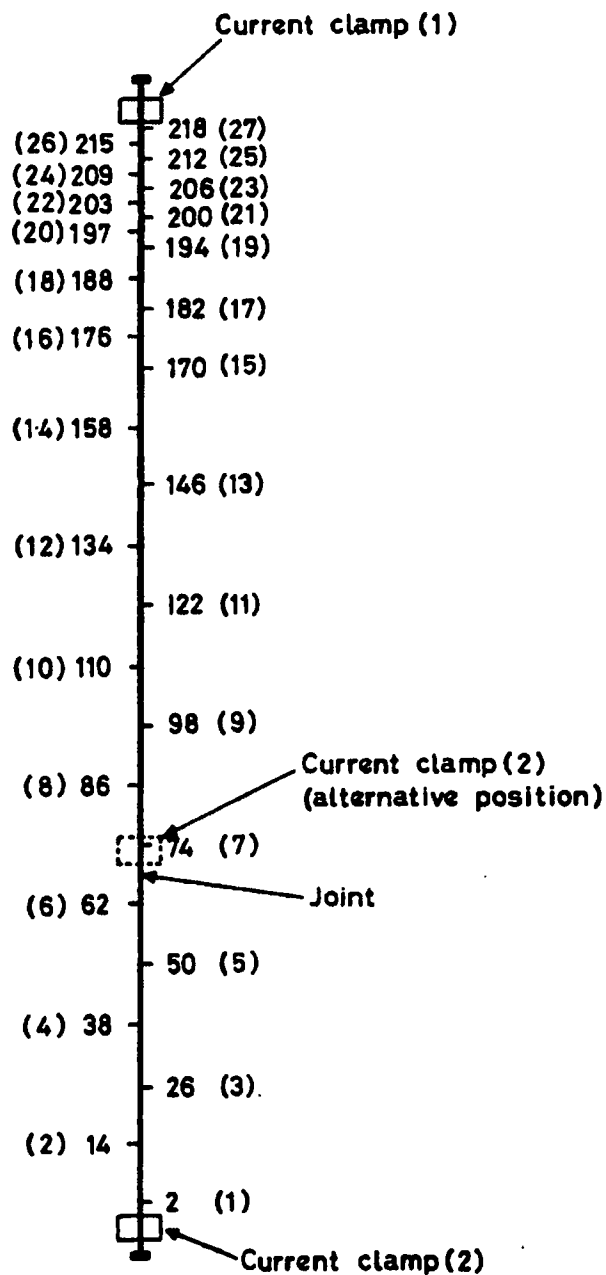


Figure 7-62 Arrangement of Thermocouples for the Bennett Heated Tube Tests*

* Reproduced from Reference 106, Figure 3.

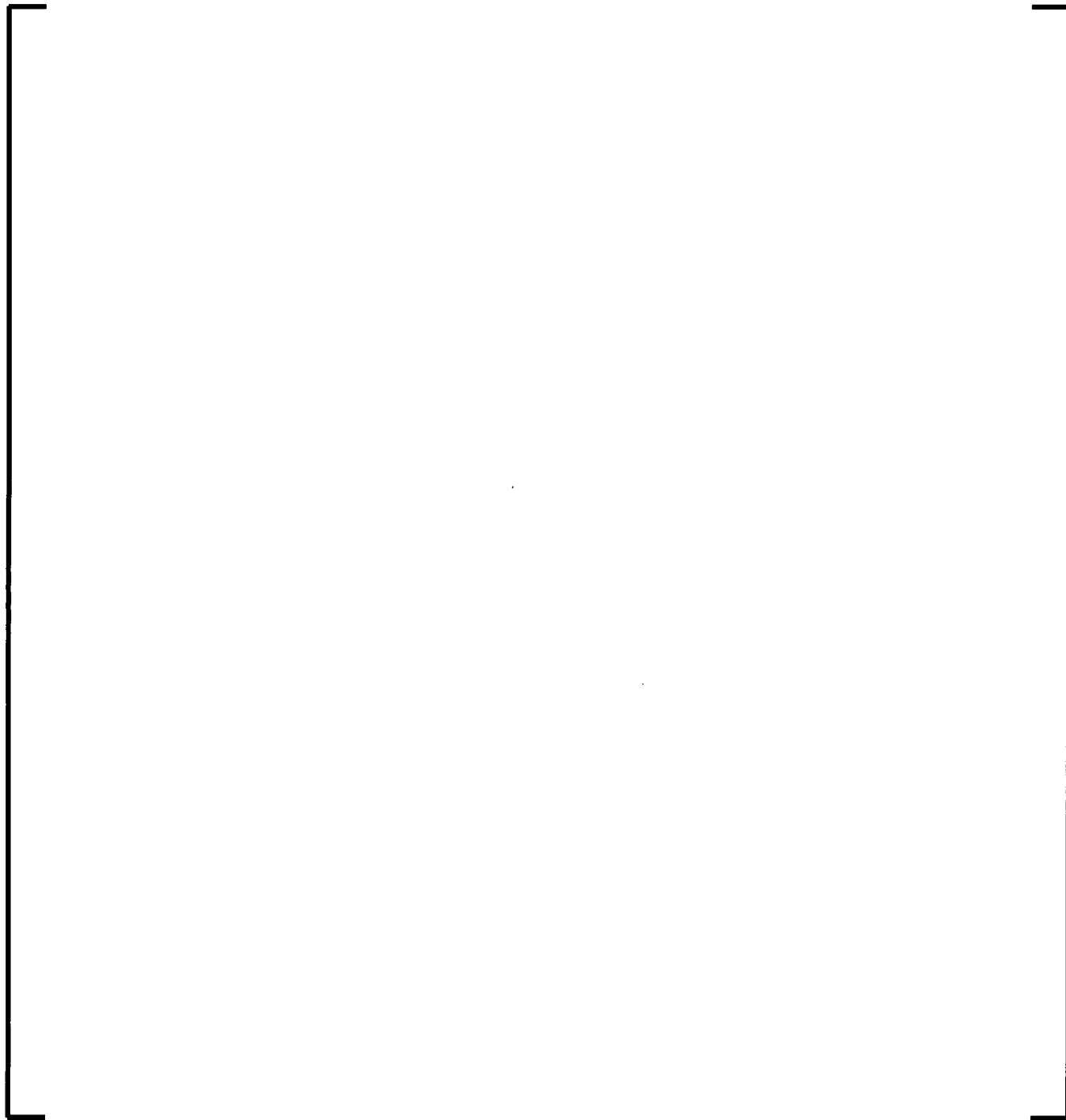


Figure 7-63 Nodalization for the Bennett Heated Tube Tests



Figure 7-64 Wall Temperature Profiles - Bennett Test 5358



Figure 7-65 Wall Temperature Profiles - Bennett Test 5379

7.3.11 THTF Steady State Film Boiling Tests

Assessed phenomena and processes

This section addresses the following highly ranked PIRT phenomena identified in Table 5-1;



Assessment conclusions

The purpose of this assessment is to validate the application of EM heat transfer correlations to the THTF steady-state film-boiling heat transfer tests. [

] This final result is limited to pressures less than 1250 psig, which is within the pressure range of BWR vessels under LOCA conditions.

From this, it is inferred that the EM makes reasonable and conservative predictions of the indicated PIRT phenomena.

Assessment description

The THTF facility is described in Section 7.3.8. [

]

All THTF steady state film boiling heat transfer tests (22) were processed in the assessment.

[

]

[

]

7.3.11.1 Comparison of THTF and CE/Columbia Dispersed Film Boiling Data

The heat transfer performance of THTF was compared to the CE/Columbia steady-state film-boiling tests of Reference 84. [

]



Figure 7-66 THTF Calculated versus Measured HTC



Figure 7-67 THTF Calculated versus Measured HTC for All Data

7.3.12 FCTF Spray and Steam Cooling Tests

Assessed phenomena and processes

This section addresses the following highly ranked PIRT phenomena identified in Table 5-1.

Assessment conclusions

The assessments show single phase vapor heat transfer is well predicted and film boiling heat transfer is conservatively under predicted. Bundle distortions during the test and lack of accurate channel heat transfer data added to the uncertainty. From this, it is inferred that the EM makes reasonable predictions of the indicated PIRT phenomena.

Assessment description

The AREVA Fuel Cooling Test Facility (FCTF) is used to assess bundle heat transfer at pressures near atmospheric. Downdraft, updraft, CCFL and reflood tests were performed to assess the heat transfer prediction for the EM.

A schematic of the facility is shown in Figure 7-68. [

]

[

]

7.3.12.1 FCTF Test 64: No Steam Updraft

[

]

Average Rod Model

Figure 7-69 to Figure 7-71 show the rod surface temperatures from S-RELAP5 compared to FCTF average powered rods at the 65-in, 75-in mid-plane and 85-in elevations. S-RELAP5 shows good agreement at the 85-in elevation. [

] Overall, this test shows good agreement.

All Rod Model Without Radiation

A second calculation was performed for Test 64 with the single average rod replaced by a model with all powered rods. Figure 7-72 shows the mid-plane surface temperature for an average powered rod in the all-rod model compared to the results from the average rod model. The good agreement validates the all-rod model.

All Rod Model With Radiation

Figure 7-73 shows the surface temperature of the peak power rod, at the mid-plane elevation with radiation compared to the same rod without radiation. This case demonstrates the impact of applying the rod-to-rod radiation model.

7.3.12.2 FCTF Test 63: []

[

]

7.3.12.3 FCTF Test 66: []

[

]

[

]

7.3.12.4 FCTF Test 79: [

]

[

]

7.3.12.5 FCTF Test 29: [

]

[

]



Figure 7-68 Diagram of FCTF Test Section



Figure 7-69 FCTF Test 64 Average Rod Model Surface Temperatures at 65-in



Figure 7-70 FCTF Test 64 Average Rod Model Surface Temperatures at 75-in



Figure 7-71 FCTF Test 64 Average Rod Model Surface Temperatures at 85-in



Figure 7-72 FCTF Test 64 Average Power Rod Surface Temperatures for the All Rod Model



Figure 7-73 FCTF Test 64 Peak Power Rod Surface Temperatures at Mid-plane with Radiation



Figure 7-74 FCTF Test 63 Average Rod Surface Temperatures at 65-in



Figure 7-75 FCTF Test 63 Average Rod Surface Temperatures at 75-in



Figure 7-76 FCTF Test 63 Average Rod Surface Temperatures at 85-in



Figure 7-77 FCTF Test 66 Average Rod Surface Temperatures at 65-in



Figure 7-78 FCTF Test 66 Average Rod Surface Temperatures at 75-in



Figure 7-79 FCTF Test 66 Average Rod Surface Temperatures at 85-in



**Figure 7-80 FCTF Test 66 Average Rod Surface Temperatures
for Insulated Channels at 75-in**



Figure 7-81 FCTF Test 79 Average Rod Surface Temperatures at 65-in



Figure 7-82 FCTF Test 79 Average Rod Surface Temperatures at 75-in



Figure 7-83 FCTF Test 79 Average Rod Surface Temperatures at 85-in



Figure 7-84 FCTF Test 29 Average Rod Surface Temperatures at 65-in



Figure 7-85 FCTF Test 29 Average Rod Surface Temperatures at 75-in



Figure 7-86 FCTF Test 29 Average Rod Surface Temperatures at 85-in

7.3.13 THTF Reflood

Assessed phenomena and processes

This section addresses the following highly ranked PIRT phenomena identified in Table 5-1.

Assessment conclusions

The EM computations produce heater-rod wall temperatures that are generally consistent with, or greater, than the THTF reflood data for the test series. The quench times are conservative (later in time) than the reported data. It is concluded that the conservative temperatures produced by these computations contribute to the validation of the heat transfer package in the EM. From this, it is inferred that the EM makes reasonable (or conservative) predictions of the indicated PIRT phenomena.

Assessment description

The THTF facility is described in Section 7.3.8. This assessment addresses the THTF reflood tests. Figure 7-87 shows the S-RELAP5 nodalization for the THTF reflood model. The purpose of this calculation is to compare the results of the EM computations of heater-rod wall temperature to the reported values from the ORNL high pressure reflood tests with the pressures ranging from 303 to 1092 psia. Reflood is simulated by establishing a water level with 25-30 percent of the rod bundle uncovered at steady-state. The transient is initiated by increasing the inlet makeup flow rate to simulate reflood. Table 7-9 shows the key conditions of the two test series. Series I (3.02.10C-H) is reported in Reference 81 and Series II

(3.09.10O-S) is reported in Reference 82. Series II expands the data set over Series I and includes added instrumentation.

While the reflood tests are intended for PWR small break LOCA, the pressures are within the operating range of a BWR. The tests provide an S-RELAP5 validation data set for the AURORA-B LOCA EM.

[

]

Figure 7-88 through Figure 7-98 show plots of the S-RELAP5 computed and the reported heater-rod wall temperatures for two reflood test series. Figure 7-88 to Figure 7-93 represent the first set of tests (designated 3.02.10C-H), and Figure 7-94 to Figure 7-98 the second set (designated 3.09.10O-S).

For the first set of tests (3.02.10C-H), three measured temperatures are plotted, from three different rods at two different azimuthal locations. For the second set of tests (3.09.10O-S), measured temperatures are represented by up to six rod sheath thermocouples and two azimuthal locations. The plotted nominal temperature data are reported at the highest elevation in the bundle (level G). The plots generally show the following:

- The calculated initial temperatures match the test data quite well. The temperatures are through, or above, the steady-state temperature data. [
- The shapes of the calculated and reported temperatures are consistent. In some cases there is a gradual heat-up from the initial condition. All cases have a gradual cool-down followed by a sudden temperature decrease at quench.
- The calculated temperatures are generally at, or above, the reported temperatures.
- The calculated quench times for all tests are at, or beyond, the reported quench times.

Table 7-9 High-Pressure Reflood THTF Test Matrix

Test	Test Series	Initial Pressure, psia	Flooding Velocity, in/s	Linear Heat Rate, kWt/ft
3.02.10C	I	400	6.5	0.36
3.02.10D	I	600	5.6	0.25
3.02.10E	I	605	5.4	0.41
3.02.10F	I	1006	1.1	0.27
3.02.10G	I	989	2.8	0.38
3.02.10H	I	303	2.2	0.42
3.09.10O	II	563	4.8	0.62
3.09.10P	II	621	3.6	0.30
3.09.10Q	II	573	2.3	0.31
3.09.10R	II	1065	4.6	0.66
3.09.10S	II	1092	4.0	0.42

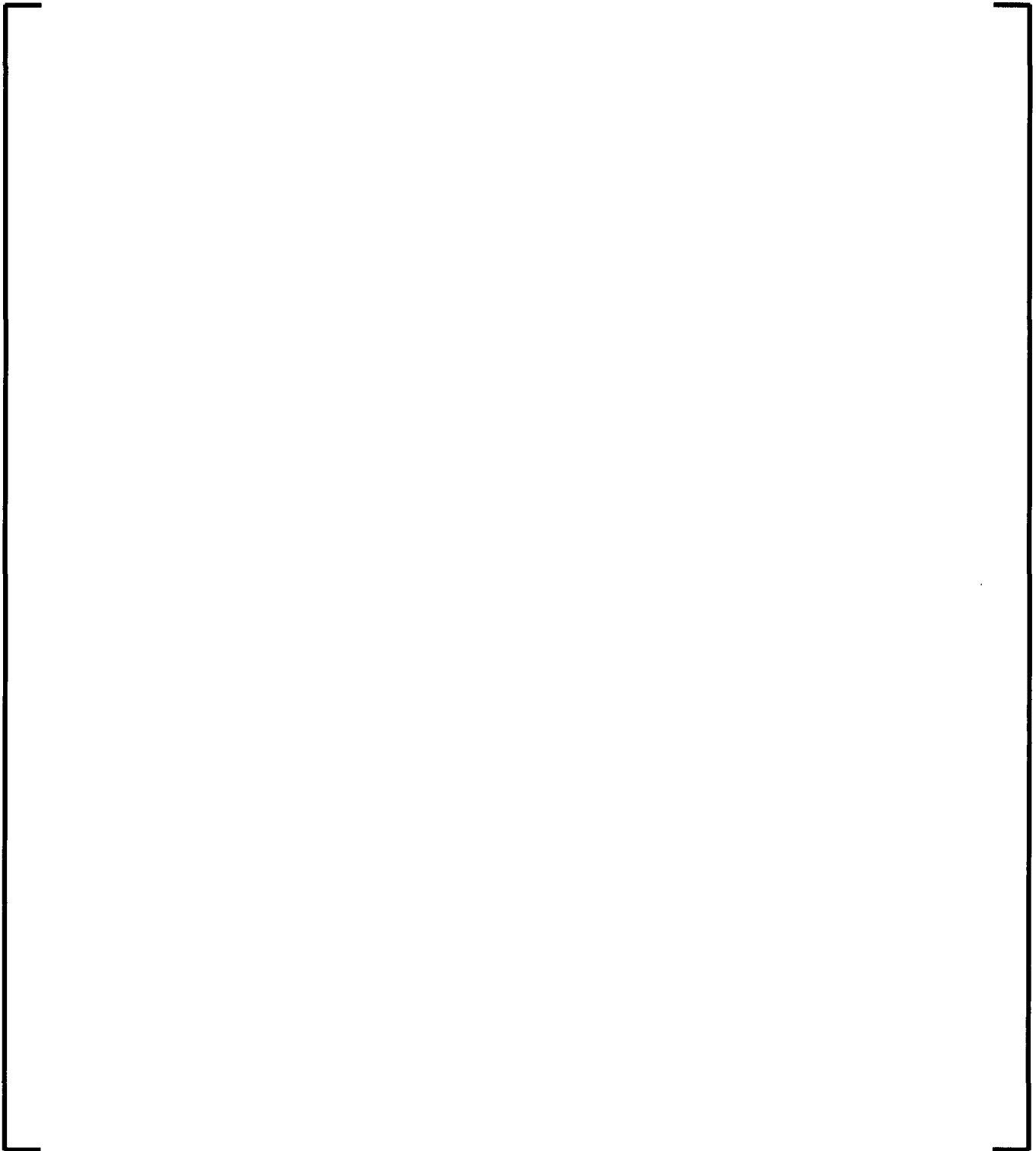


Figure 7-87 S-RELAP5 Nodalization of ORNL THTF for Reflood Tests



Figure 7-88 Temperatures at Level G, THTF Test 3.02.10C, 400 psia, 6.5 in/sec



Figure 7-89 Temperatures at Level G, THTF Test 3.02.10D, 600 psia, 5.6 in/sec

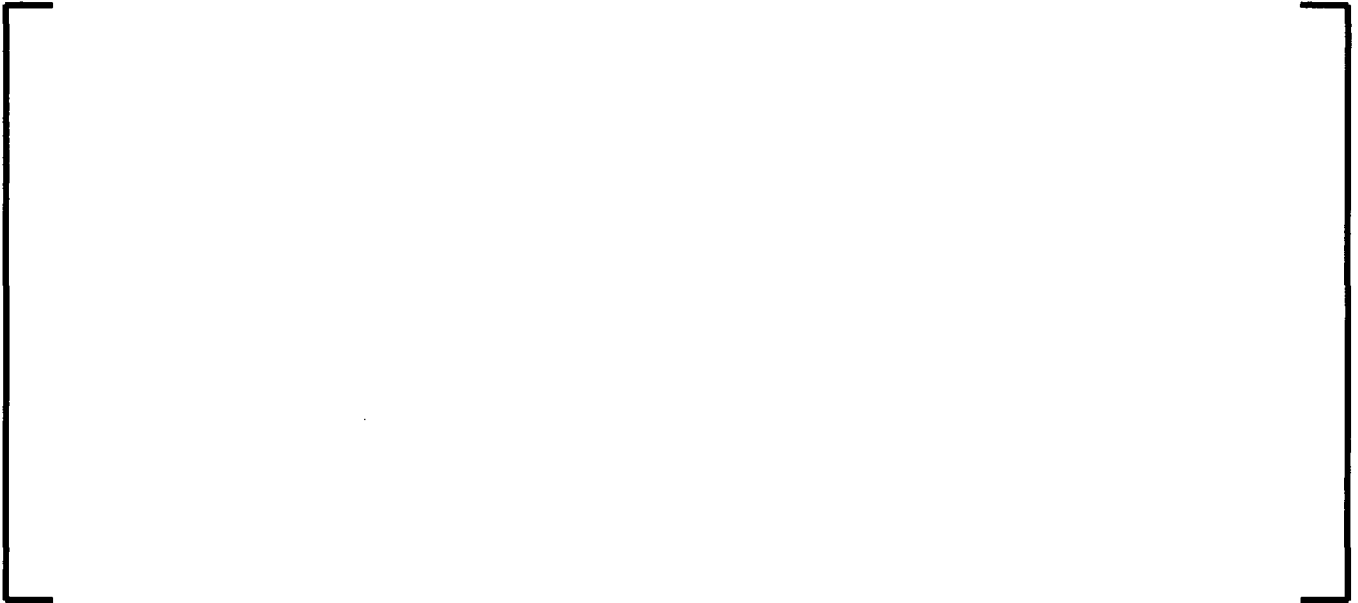


Figure 7-90 **Temperatures at Level G, THTF Test 3.02.10E, 605 psia, 5.4 in/sec**



Figure 7-91 **Temperatures at Level G, THTF Test 3.02.10F, 1006 psia, 1.1 in/sec**



Figure 7-92 Temperatures at Level G, THTF Test 3.02.10G, 989 psia, 2.8 in/sec



Figure 7-93 Temperatures at Level G, THTF Test 3.02.10H, 303 psia, 2.2 in/sec



Figure 7-94 Temperatures at Level G, THTF Test 3.09.10O, 563 psia, 4.8 in/sec



Figure 7-95 Temperatures at Level G, THTF Test 3.09.10P, 621 psia, 3.6 in/sec



Figure 7-96 **Temperatures at Level G, THTF Test 3.09.10Q, 573 psia, 2.3 in/sec**



Figure 7-97 **Temperatures at Level G, THTF Test 3.09.10R, 1065 psia, 4.6 in/sec**



Figure 7-98 Temperatures at Level G, THTF Test 3.09.10S, 1092 psia, 4.0 in/sec

7.3.14 FLECHT Reflood and Steam Cooling Tests

Assessed phenomena and processes

This section addresses the following highly ranked PIRT phenomena identified in Table 5-1;

Assessment conclusions

FLECHT-SEASET Reflood Tests 31203, 31302, 31504, 31701, 31805, 32013, 34209 (Reference 85), FLECHT Reflood Tests 13609 and 13914 (Reference 86) and FLECHT-SEASET Steam Cooling Test 33056 (Reference 85) are assessed with the AURORA-B LOCA EM wall heat transfer package. The EM heat transfer package has produced maximum cladding temperatures that are generally above the reported data. Quench times are generally greater than the reported times, especially at the higher elevations at the location of the maximum temperatures. Other aspects of the test are also adequately predicted. The computation for Steam Cooling Test 33056 has conservative agreement with the reported data. From these results, it is inferred that the EM makes reasonable and conservative predictions of the indicated PIRT phenomena.

Assessment description

The FLECHT SEASET and FLECHT skewed series of tests were performed to provide assessment data for PWR LOCA forced reflood phenomena. Since the data are so well known and are widely used for validation of PWR reflood models, the test series also provides excellent data for the SET PIRT phenomena assessments for BWR LOCA, particularly heat transfer phenomena for peak cladding temperature and rod quench predictions. The main goal

of this assessment is the validation of the wall heat transfer correlations used for the AURORA-B LOCA EM.

The FLECHT-SEASET facility used the Westinghouse 17x17 geometry for the reference fuel design while the FLECHT facility used the Westinghouse 15x15 geometry for the reference fuel design; the tests consisted of a 161-rod bundle for the FLECHT SEASET tests and a 105-rod bundle for the FLECHT Skewed tests. The test bundles utilize stainless steel cladding, boron nitride filled heater rods with coiled Kanthal wire heating elements.

Figure 7-101 shows the axial power profile for FLECHT SEASET tests. The power step size is 7.2 in (182.9 mm) for the elevations between 24 and 120 in (609.6 - 3048.0 mm). The profile is based on a center peaked cosine shape. Figure 7-102 shows the axial power profile for FLECHT skewed tests. The FLECHT skewed profile has a peak power at 10 ft (3.048 m) elevation. The bundle radial power profile for both the FLECHT SEASET and FLECHT skewed tests presented is uniform. [

] The nodalization scheme is shown in Figure 7-103.

The tests consist of FLECHT-SEASET tests 31504, 31701, 31302, 31203, 31805, 32013, and 34209, and FLECHT skewed tests 13609 and 13914. The test matrix is shown in Table 7-10. In addition to these reflood tests an additional assessment was made for the FLECHT-SEASET steam cooling test 33056.

7.3.14.1 Rod Surface Temperatures at 78 in (SEASET) and 60 in (Skew)

Figure 7-104 through Figure 7-111 present plots of the rod surface temperatures as a function of time. The plots are for an elevation of 78 in except for an elevation of 60 in for the two skewed tests. All plots show similar transient behavior. There is a heatup followed by a gradual cooldown and quench. The calculated quench times are both earlier and later than reported. The calculated temperatures also follow above and below the reported temperatures. In general the shape of the transient response agrees quite well with the reported response. There is tendency to over-predict the temperature and quench times.

7.3.14.2 Rod Surface Temperatures at 90 in (SEASET) and 84 in (Skew)

Figure 7-112 through Figure 7-120 present plots of the rod surface temperatures as a function of time. The plots are for an elevation of 90 in except for an elevation of 84 in for the two skewed tests. All plots show similar transient behavior. There is a heatup followed by a gradual cooldown and quench. The calculated quench times are both earlier and later than reported. The calculated temperatures also follow above and below the reported temperatures. In general the shape of the transient response agrees quite well with the reported response. There is tendency to over-predict the temperature and quench times.

7.3.14.3 Rod Surface Temperatures at 111 in (SEASET) and 108 in (Skew)

Figure 7-121 through Figure 7-129 present plots of the rod surface temperatures as a function of time. The plots are for an elevation of 111 in except for an elevation of 108 in for the two skewed tests. All plots show similar transient behavior. There is a heatup followed by a gradual cooldown and quench. The calculated quench times are both earlier and later than reported. The calculated temperatures also follow above and below the reported temperatures. In general the shape of the transient response agrees quite well with the reported response. There is tendency to over-predict the temperature and quench times.

7.3.14.4 Maximum Cladding Temperature

Figure 7-130 through Figure 7-138 present plots of the maximum rod surface temperatures at all elevations. The solid symbols are from the S-RELAP5 calculation and the open symbols are from reported data. The plots show that the calculated maximum values generally bound the observed maximums. This shows the conservatism in the computation using AURORA-B LOCA EM.

7.3.14.5 Steam Cooling Results

Figure 7-139 presents a plot of calculated and reported heater-rod wall temperatures for FLECHT SEASET test 33056. The results show a conservative overprediction of temperature at the 72 in elevation.

**Table 7-10 FLECHT SEASET, FLECHT Skewed
Test Conditions**

Run #	Pressure (psia)	Peak Power (kw/ft)	Flow Rate (in/s)	Coolant Temp. (°F)	Axial Power Profile
FLECHT SEASET Tests					
Reflow Rate					
31805	40	0.70	0.81	124	Cosine, Center Peak
31203	40	0.70	1.51	126	Cosine, Center Peak
31302	40	0.69	3.01	126	Cosine, Center Peak
31701	40	0.70	6.10	127	Cosine, Center Peak
Pressure Variation					
34209	20	0.72	1.07	90	Cosine, Center Peak
31504	40	0.70	0.97	123	Cosine, Center Peak
32013	60	0.70	1.04	150	Cosine, Center Peak
FLECHT Tests					
Subcooling Variation					
13609	21	0.70	1.00	87	Skewed, Top Peak
13914	21	0.70	1.00	223	Skewed, Top Peak

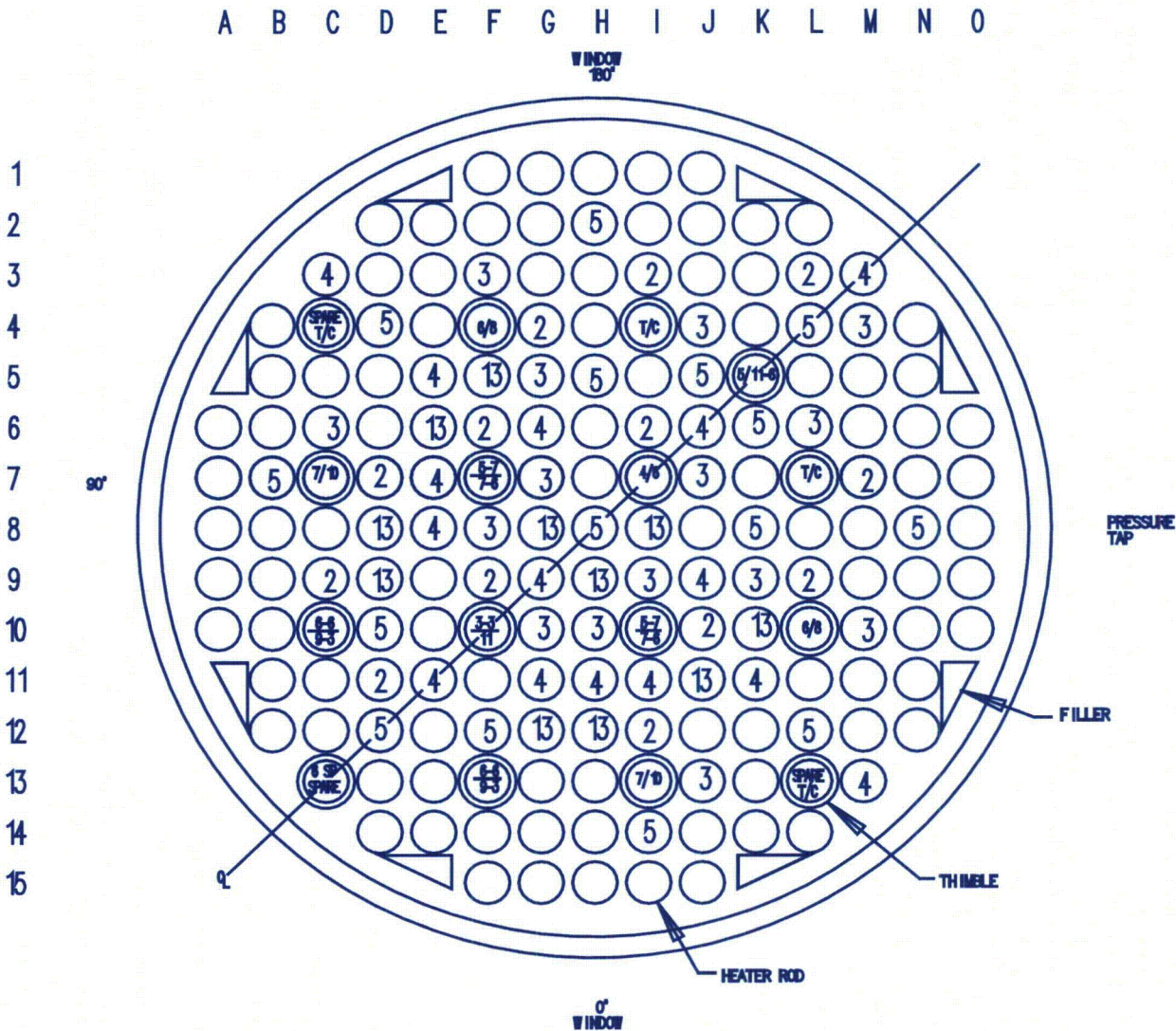


Figure 7-99 FLECHT-SEASET Bundle Cross Section*

* Reproduced from Reference 85, Figure 3-3.

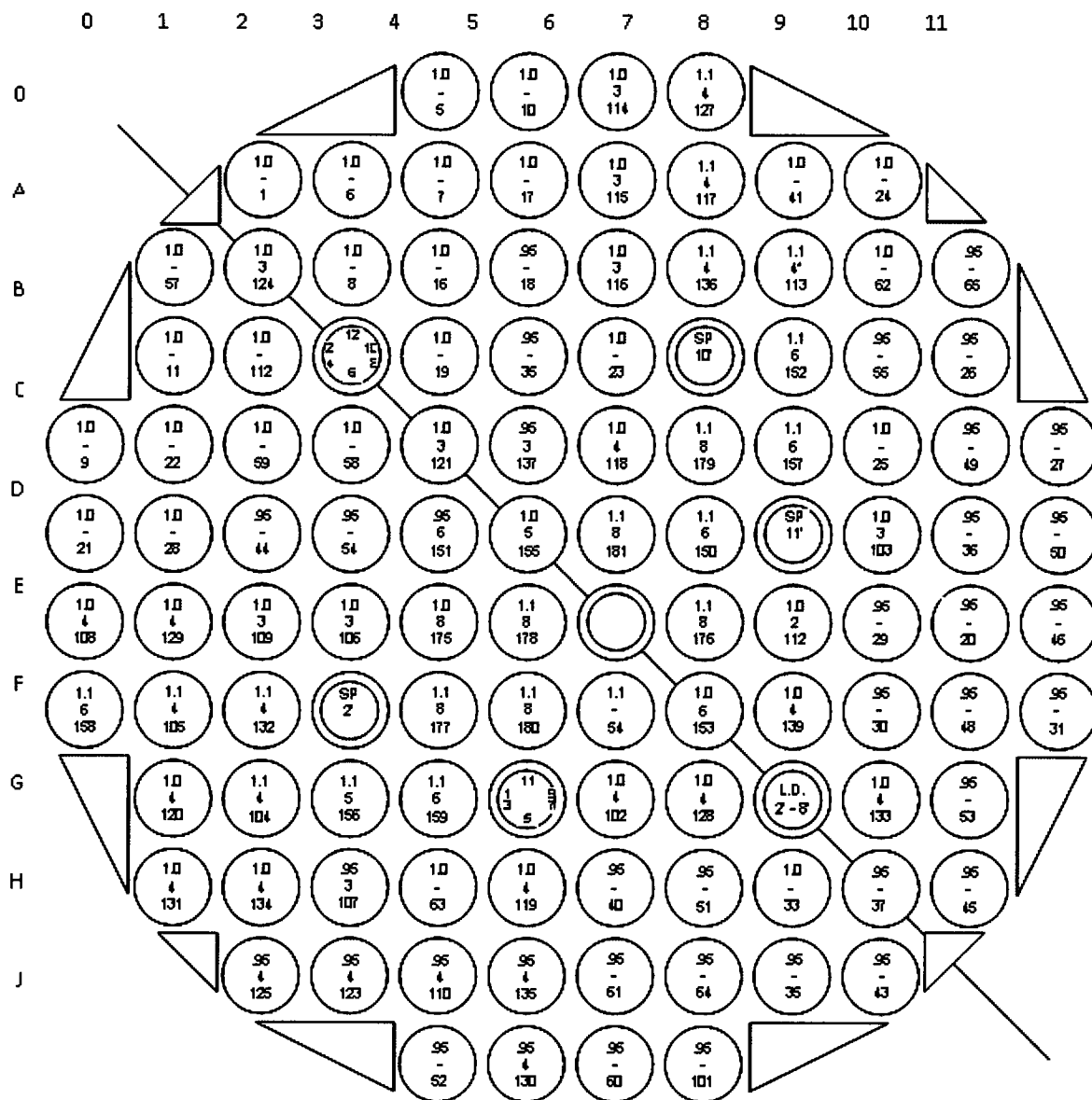


Figure 7-100 FLECHT Skewed Bundle Cross Section*

* Reproduced from Reference 86, Figure 3-3.

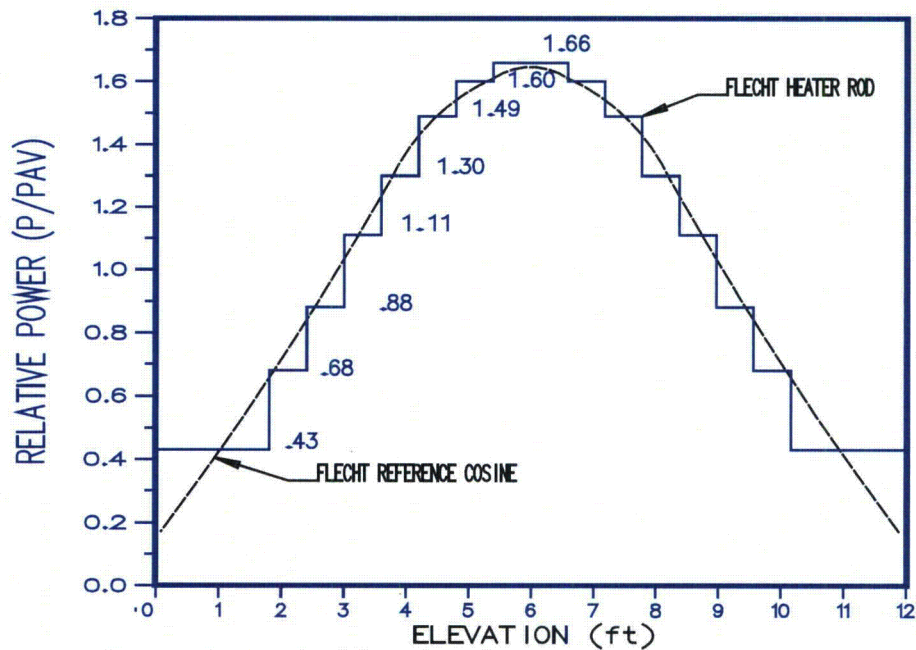


Figure 7-101 FLECHT-SEASET Axial Power Profile*

* Reproduced from Reference 85, Figure 2-2.

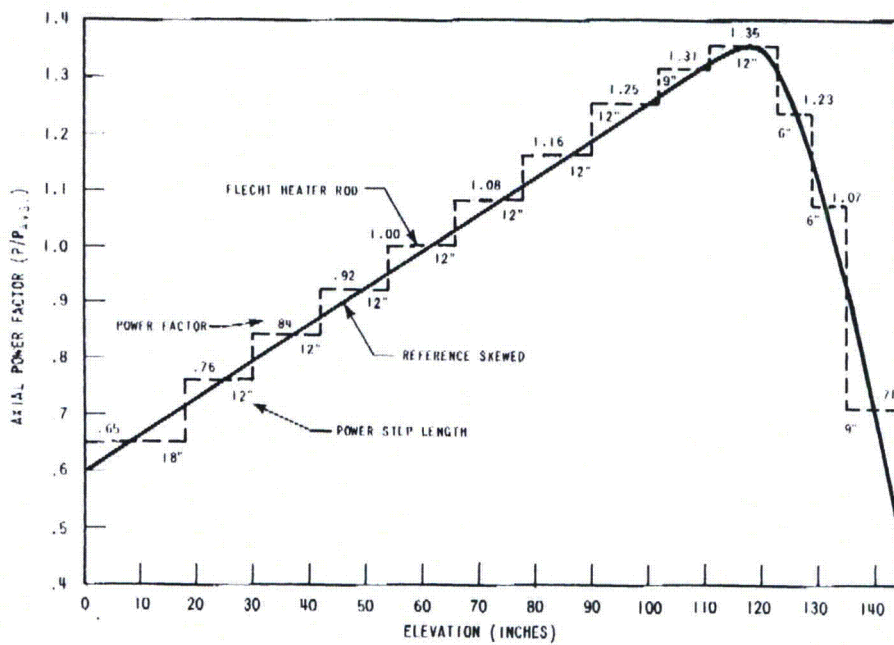


Figure 7-102 FLECHT Skewed Axial Power Profile*

* Reproduced from Reference 86, Figure 2-1.



Figure 7-103 FLECHT-SEASET / Flecht Skewed Bundle Axial Nodalization



Figure 7-104 **Heater - Rod Surface Temperatures at 78 in,
FLECHT-SEASET Test 31302**



Figure 7-105 **Heater - Rod Surface Temperatures at 78 in,
FLECHT-SEASET Test 31504**



Figure 7-106 **Heater - Rod Surface Temperatures at 78 in,
FLECHT-SEASET Test 31701**



Figure 7-107 **Heater - Rod Surface Temperatures at 78 in,
FLECHT-SEASET Test 31805**



Figure 7-108 **Heater - Rod Surface Temperatures at 78 in,
FLECHT-SEASET Test 32013**



Figure 7-109 **Heater - Rod Surface Temperatures at 78 in,
FLECHT-SEASET Test 34209**



**Figure 7-110 Heater - Rod Surface Temperatures at 60 in, FLECHT
Skewed Test 13609**



**Figure 7-111 Heater - Rod Surface Temperatures at 60 in, FLECHT
Skewed Test 13914**



**Figure 7-112 Heater - Rod Surface Temperatures at 90 in,
FLECHT-SEASET Test 31203**



**Figure 7-113 Heater - Rod Surface Temperatures at 90 in,
FLECHT-SEASET Test 31302**



**Figure 7-114 Heater - Rod Surface Temperatures at 90 in,
FLECHT-SEASET Test 31504**



**Figure 7-115 Heater - Rod Surface Temperatures at 90 in,
FLECHT-SEASET Test 31701**



**Figure 7-116 Heater - Rod Surface Temperatures at 90 in,
FLECHT-SEASET Test 31805**



**Figure 7-117 Heater - Rod Surface Temperatures at 90 in,
FLECHT-SEASET Test 32013**



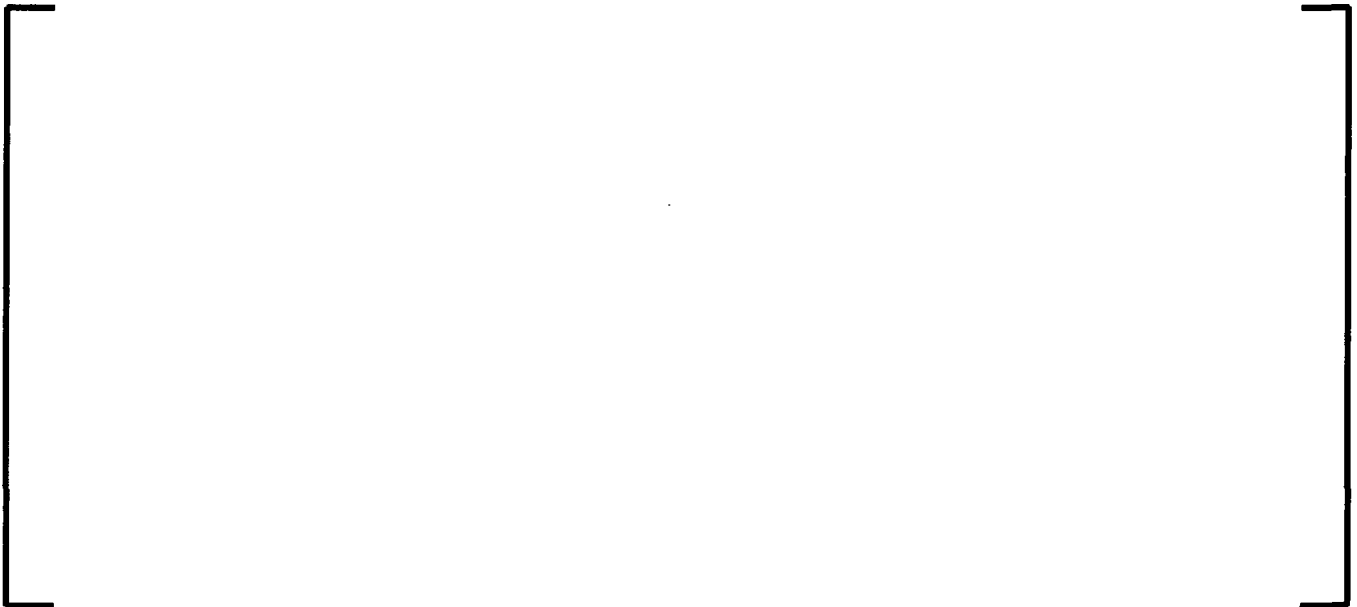
Figure 7-118 **Heater - Rod Surface Temperatures at 90 in,
FLECHT-SEASET Test 34209**



Figure 7-119 **Heater - Rod Surface Temperatures at 84 in, FLECHT
Skewed Test 13609**



**Figure 7-120 Heater - Rod Surface Temperatures at 84 in, FLECHT
Skewed Test 13914**



**Figure 7-121 Heater - Rod Surface Temperatures at 111 in,
FLECHT-SEASET Test 31203**



Figure 7-122 **Heater - Rod Surface Temperatures at 111 in,
FLECHT-SEASET Test 31302**



Figure 7-123 **Heater - Rod Surface Temperatures at 111 in,
FLECHT-SEASET Test 31504**



Figure 7-124 **Heater - Rod Surface Temperatures at 111 in,
FLECHT-SEASET Test 31701**



Figure 7-125 **Heater - Rod Surface Temperatures at 111 in,
FLECHT-SEASET Test 31805**



Figure 7-126 **Heater - Rod Surface Temperatures at 111 in,
FLECHT-SEASET Test 32013**



Figure 7-127 **Heater - Rod Surface Temperatures at 111 in,
FLECHT-SEASET Test 34209**



**Figure 7-128 Heater - Rod Surface Temperatures at 108 in, FLECHT
Skewed Test 13609**



**Figure 7-129 Heater - Rod Surface Temperatures at 108 in, FLECHT
Skewed Test 13914**



**Figure 7-130 Maximum Cladding Temperature at All
Measured Elevations, FLECHT-SEASET Test 31203**



**Figure 7-131 Maximum Cladding Temperature at All
Measured Elevations, FLECHT-SEASET Test 31302**

0

**Figure 7-132 Maximum Cladding Temperature at All
Measured Elevations, FLECHT-SEASET Test 31504**

**Figure 7-133 Maximum Cladding Temperature at All
Measured Elevations, FLECHT-SEASET Test 31701**



**Figure 7-134 Maximum Cladding Temperature at All
Measured Elevations, FLECHT-SEASET Test 31805**



**Figure 7-135 Maximum Cladding Temperature at All
Measured Elevations, FLECHT-SEASET Test 32013**



**Figure 7-136 Maximum Cladding Temperature at All
Measured Elevations, FLECHT-SEASET Test 34209**



**Figure 7-137 Maximum Cladding Temperature at All
Measured Elevations, FLECHT Skewed Test 13609**



**Figure 7-138 Maximum Cladding Temperature at All
Measured Elevations, FLECHT Skewed Test 13914**



**Figure 7-139 Heater-Rod Surface Temperatures Steam Cooling
FLECHT-SEASET Test 33056**

7.3.15 CCTF Test

Assessed phenomena and processes

This section addresses the following highly ranked PIRT phenomena identified in Table 5-1;

Assessment conclusions

The EM heat transfer package has produced maximum cladding temperatures that are generally above the reported data; likewise, quench times are generally greater than the reported times. From these results, it is inferred that the EM makes reasonable predictions of the indicated PIRT phenomena.

Assessment description

The Cylindrical Core Test Facility (CCTF) Core-II Test Series were undertaken to provide a major and useful data base for large-break LOCA reflood behavior in PWRs. CCTF is a full-height, 1/21 scale model of the primary coolant system of a 4-loop PWR plant. The facility was designed to reasonably simulate the flow conditions, including ECC flow behavior in the downcomer, and reactor core responses in the primary system of a PWR during the refill and reflood phases of a LOCA. The reflood phenomena is well captured by this test series which provides assessment data for core heat transfer and rod quenching during the reflood process. The purpose here is to assess the BWR LOCA heat transfer model with measured data. Data from CCTF runs 54, 62, 67 and 68 (References 87, 88, 89 and 90) are used in the assessment.

Table 7-11 shows the comparison of the measured and predicted PCT and the corresponding time of PCT. The range of S-RELAP5 predicted PCT is from 48°K overprediction to 46°K underprediction. The predicted time of PCT was later than measured for all the cases.

Figure 7-140 to Figure 7-142 show the comparison of the hot rod of test run 54. The predicted temperatures flatten out during the film boiling regime and quenching for the hot rod and

medium power rods occur later in the transient. From Figure 7-142, the predicted PCT of 1067°K occurs just above the 2 m in elevation at 146 s. With the chopped-cosine axial power profile, the peak temperature rise is expected to occur just above the mid-plane. The reported measured PCT is 1113 °K recorded by the thermocouple at 1.83 m and occurs at 130 s.

The predicted heater rod temperatures for test runs 62 and 67, shown in Figure 7-143 to Figure 7-145 and Figure 7-146 to Figure 7-148 respectively, are similar. The temperatures are closely predicted during heatup when the rods are in steam cooling mode. After switching to film boiling at around 100s, the heat transfer mode for the heat structures representing the hot rod, alternate between film boiling and steam cooling which results in further temperature increase. The maximum surface temperatures from all measurements in the high-power core region for tests runs 62 and 67 are plotted along with the calculated peak temperatures as a function of elevation in Figure 7-145 and Figure 7-148, respectively. The predicted PCT of 1151°K (at 242 seconds) for test run 62 and 1192°K (at 228 seconds) for test run 67 occur at elevation of 2.235 m (node 11). These temperatures compare to the measured PCT of 1132°K for test 62 and 1144°K for test 67 at 1.83 m.

The comparison of the predicted and measured heater rod temperatures for test run 68 are shown in Figure 7-149 to Figure 7-151. The predicted time of PCT for majority of rod type/elevation combinations are close to the data. Similar to the other test runs, rewetting occurs later for the hot and medium power rods. The predicted PCT of 1095°K occurs at elevation of 2.235 m (node 11) at around 166 s, Figure 7-151. The reported measured PCT is 1122°K at 1.83 m.

These comparisons to data show that S-RELAP5 predictions of the PCT are reasonable, particularly at higher elevations where top-down cooling may be affecting the quenching of the heated rods. Rewetting generally occurs later which is conservative because higher temperatures are maintained for longer period of time.

Table 7-11 Summary of PCT Results for CCTF Tests

--	--



Figure 7-140 Comparison of Rod Surface Temperature for High Power Bundle at 1.830 m Elevation, CCTF Test Run 54



Figure 7-141 Comparison of Rod Surface Temperature for High Power Bundle at 2.035 m Elevation, CCTF Test Run 54



**Figure 7-142 Comparison of Peak Surface Temperature vs.
Elevation for High Power Bundle, CCTF Test Run 54**



**Figure 7-143 Comparison of Rod Surface Temperature for High
Power Bundle at 1.830 m Elevation, CCTF Test Run 62**



Figure 7-144 Comparison of Rod Surface Temperature for High Power Bundle at 2.035 m Elevation, CCTF Test Run 62

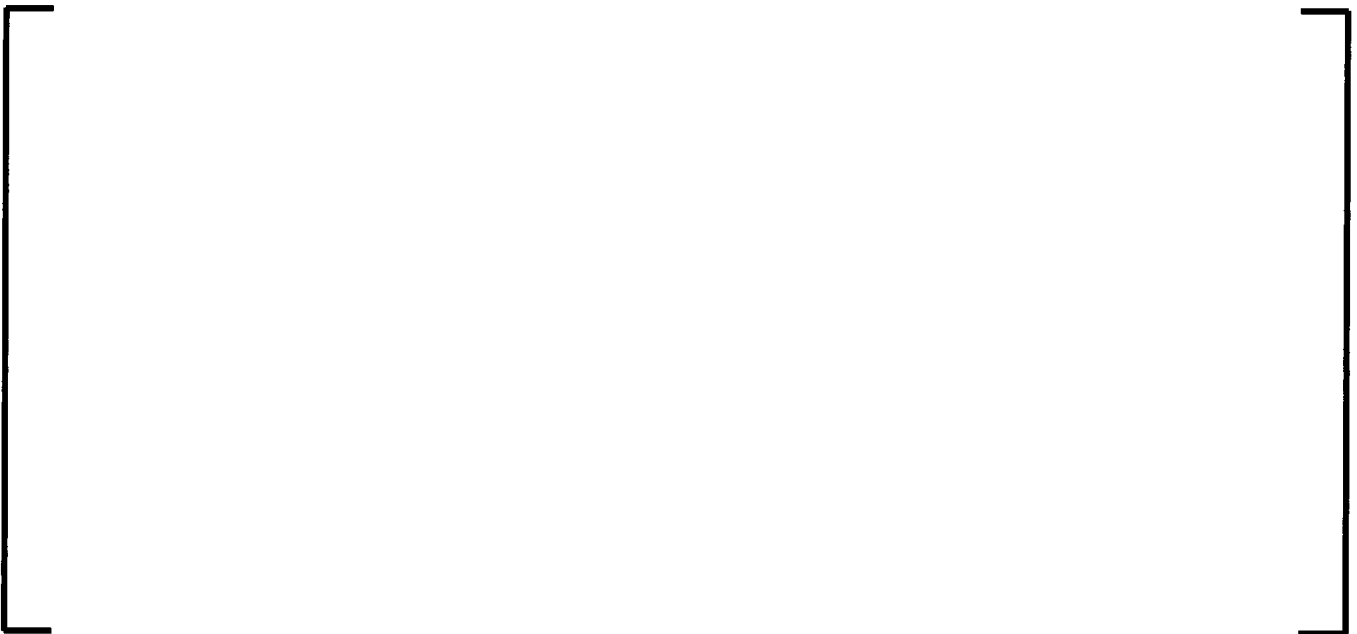


Figure 7-145 Comparison of Peak Surface Temperature vs. Elevation for High Power Bundle, CCTF Test Run 62



**Figure 7-146 Comparison of Rod Surface Temperature for High
Power Bundle at 1.830 m Elevation, CCTF Test Run 67**



**Figure 7-147 Comparison of Rod Surface Temperature for High
Power Bundle at 2.035 m Elevation, CCTF Test Run 67**



**Figure 7-148 Comparison of Peak Surface Temperature vs.
Elevation for High Power Bundle, CCTF Test Run 67**



**Figure 7-149 Comparison of Rod Surface Temperature for High
Power Bundle at 1.830 m Elevation, CCTF Test Run 68**



Figure 7-150 Comparison of Rod Surface Temperature for High Power Bundle at 2.035 m Elevation, CCTF Test Run 68



Figure 7-151 Comparison of Peak Surface Temperature vs. Elevation for High Power Bundle, CCTF Test Run 68

7.3.16 Marviken

Assessed phenomena and processes

This section addresses the following highly ranked PIRT phenomena identified in Table 5-1.

Assessment conclusions

The EM critical flow model for best estimate predictions (homogenous equilibrium model (HEM)) showed excellent agreement with Marviken tests. As expected, the Appendix K Moody model predicts higher (conservative) critical flow. From these results, it is inferred that the EM makes reasonable and conservative predictions of the indicated PIRT phenomena.

Assessment description

The Marviken Full Scale Critical Flow Tests have been conducted as a multi-national project at the Marviken Power Station in Sweden (Reference 91). The test facility (Figure 7-152) consists of four major components: a full scale BWR vessel, a discharge pipe attaching to the bottom of the vessel, a test nozzle connecting to the downstream end of the discharge pipe, and a rupture disk bundle attaching to the downstream end of the nozzle. A detailed description of the test facility, procedures, and results are found in Reference 91. The Marviken test data has been widely used in assessing critical flow models of various system codes.

The pressure vessel was originally a part of the Marviken nuclear power plant. Of the original vessel internals, only the peripheral part of the core superstructure, the cylindrical wall, and the bottom of the moderator tank remain. Gratings are installed at three levels in the lower part of the vessel to prevent the formation of vortices that might enter the discharge pipe. The vessel has an inside diameter of 5.22 m and is 24.55 m high as measured from the vessel bottom to the top of the top cupola. The net available internal volume is 420 m³.

The discharge pipe consists of seven elements, including an axisymmetric inlet section, a connection piece, two pipe stools, two instrumentation rings, and an isolation ball valve. The internal diameters of the connection piece, pipe stools, and instrumentation rings are all 752 mm. The flow path through the ball valve contains a fairly abrupt diameter change of

30 mm. The axial distance from the discharge pipe entrance to the end of the discharge pipe (nozzle entrance) is 6.3 m.

The test nozzle connects to the lower end of the discharge pipe. The nozzle consists of a rounded entrance section followed by a test section of different inside diameters and various length-to-diameter (L/D) ratios for different tests (Figure 7-153). Nozzles of four different diameters are used in the tests: 200 mm, 300 mm, 500 mm, and 509 mm. The range of the L/D ratio is 0.3 to 3.7 for different tests.

The rupture disc bundle attaches to the downstream end of the test nozzle. The bundle contains two identical rupture discs. The test was initiated by over pressurizing the volume between the discs. This over pressurization caused the outer disc to fail, which subsequently resulted in the failure of the inner disc. Failure of the discs was designed to occur along the entire periphery so that they were completely removed from the nozzle exit.

Water initially filled up the system and then drained to a specific level in the vessel. A warm-up process was applied to produce a temperature profile in the vessel. A sketch of typical vessel temperature profile is shown in Figure 7-154. The steam dome was at 5 MPa saturated conditions. The water level was between 16.5 m and 20 m in the vessel. The liquid region consisted of a saturation zone, a transition zone, and a zone of relatively constant subcooling. The initial subcooling in the lower vessel relative to steam dome temperature was varied for different tests. The measurement recording system was started approximately 180 seconds before the initiation of the test. The test was terminated when the ball valve began to close or when the steam entered the discharge pipe.

Nine tests are selected for this assessment, Tests 2, 6, 8, 16, 17, 20, 22, 24, and 25. The nozzle diameters and L/D's for the nine tests are listed in Table 7-12.

[

]

For the Appendix K Moody model, the prediction of the discharge flow rates for tests 2 and 6 are shown in Figure 7-159 and Figure 7-160. It can be seen that break flow is conservatively predicted for two-phase stagnation conditions. The comparison of the predicted and measured mass fluxes for all nine Marviken tests with Moody critical flow model is shown in Figure 7-161. The predicted mass fluxes for two-phase stagnation conditions are under 30,000 kg/m²-s and are generally overpredicted. The predicted flow rates for subcooled and saturated liquid conditions are not affected by application of the Moody model.

Table 7-12 Marviken Critical Flow Test Nozzle Dimensions for the Nine Tests Selected

Test Number	Diameter (D, mm)	L/D
2	300	3.0
6	300	1.0
8	509	3.1
16	500	3.6
17	300	3.7
20	500	1.5
22	500	1.5
24	500	0.3
25	300	1.7

Table 7-13 Summary of Marviken Tests Statistical Results

[illegible]

Table 7-14 Summary of Marviken Tests Statistical Results with Moody Option

The image consists of a single, large rectangle with a thick, solid black border. The interior of the rectangle is completely white and contains no other elements, text, or markings.

- 1 Floor beneath vessel
- 2 Drywell floor
- 3 Transport channel floor
- 4 Transport channel wall
- 5 Front wall
- 6 Cable passages

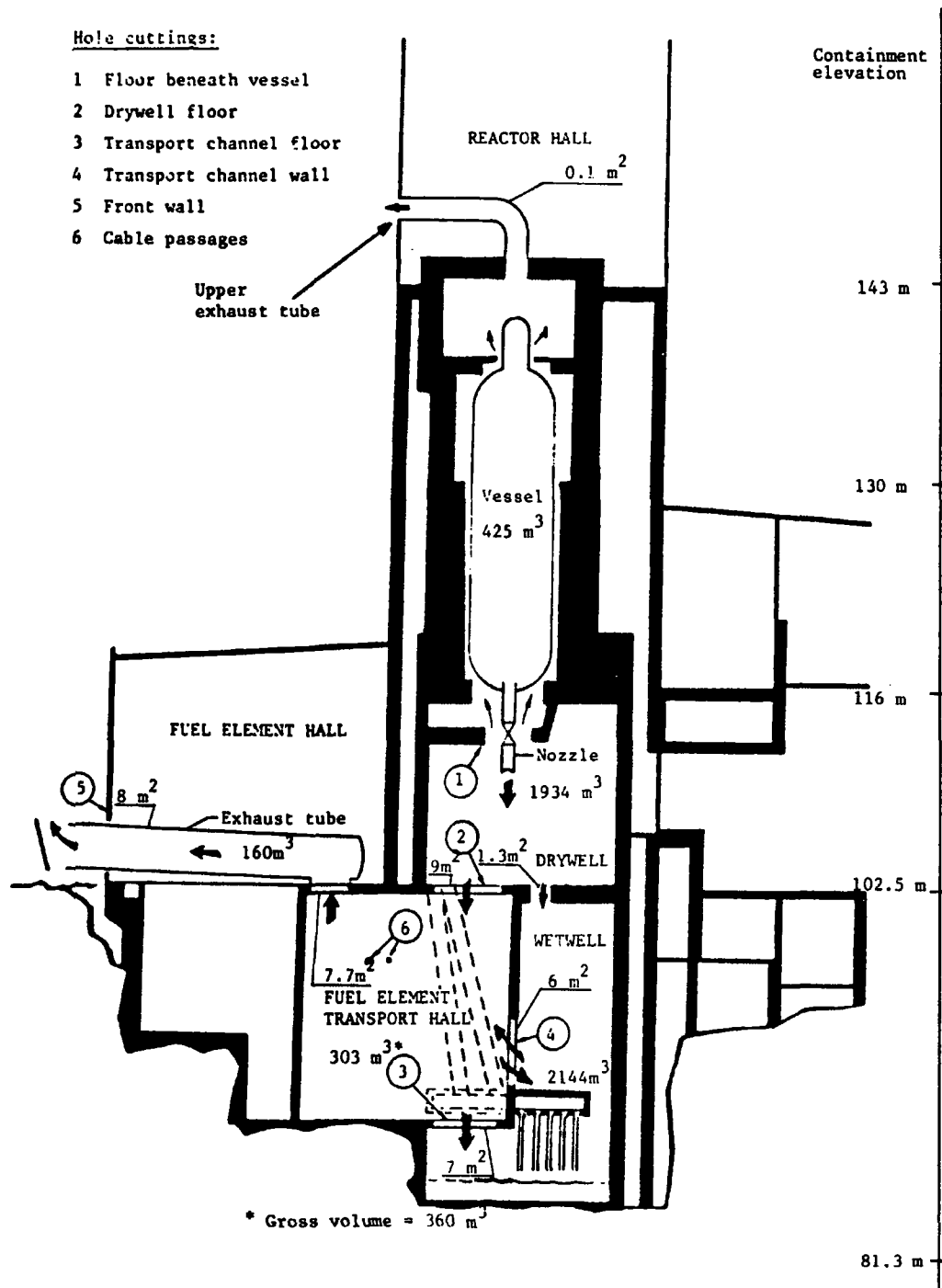


Figure 7-152 Marviken Test Facility Diagram*

* Reproduced from Reference 91, Figure 3:1.

Note: All dimensions are in millimeters
at room temperature.

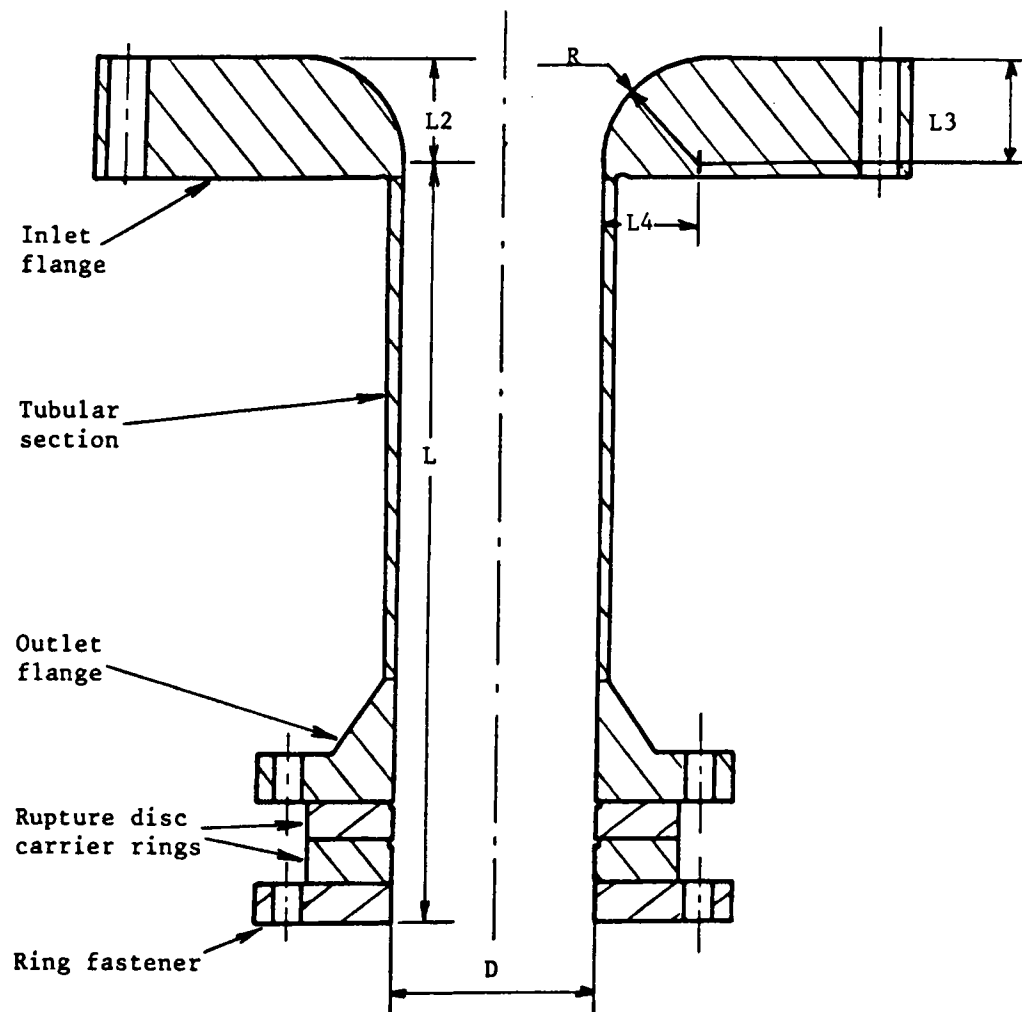


Figure 7-153 Marviken Test Nozzles Dimensions*

* Reproduced from Reference 91, Figure 3:5.

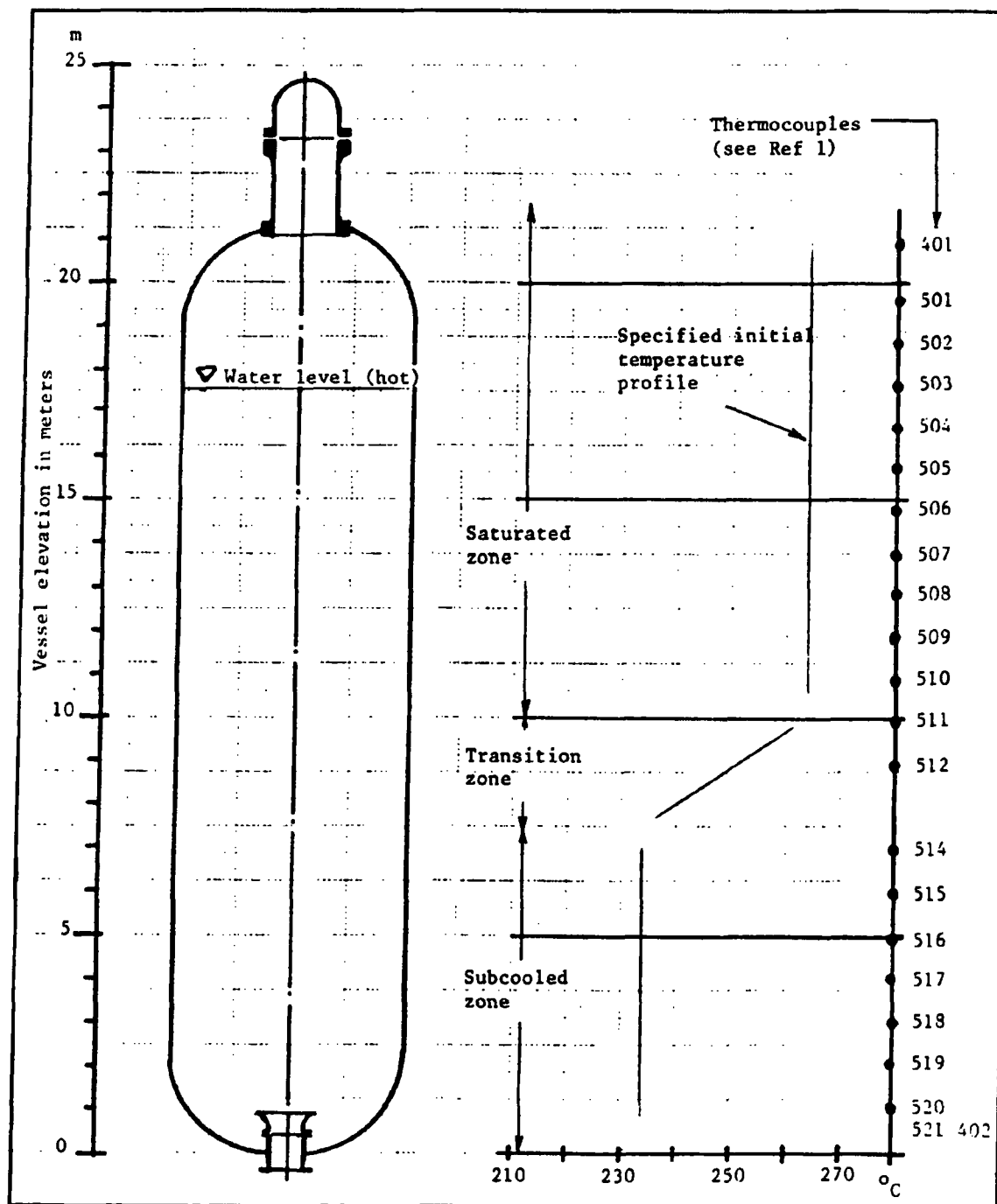


Figure 7-154 Typical Temperature Profile Specification for Marviken Tests*

* Reproduced from Reference 91, Figure 4:1.



Figure 7-155 Nodalization for Marviken Tests



**Figure 7-156 Break Mass Flow at the Nozzle Entrance, Marviken
Test 2 – []**



**Figure 7-157 Break Mass Flow at the Nozzle Entrance, Marviken
Test 6 – []**

7.3.17 UPTF

Assessed phenomena and processes

This section addresses the following highly ranked PIRT phenomena identified in Table 5-1.

Assessment conclusions

The Upper Plenum Test Facility (UPTF) was designed to simulate a German four loop 3,900 MWt pressurized water reactor (PWR) primary system, similar in size and geometry as a Westinghouse four-loop PWR. The facility was intended to provide a full-scale simulation of thermal-hydraulic behavior in the primary system during the end-of-blowdown, refill, and reflood phases of a PWR large break loss-of-coolant accident (LBLOCA). Although this test facility was developed to study PWR LOCA phenomena, several specific SET tests are applicable for BWR LOCA, specifically, tests that assess the capability of predicting countercurrent flow behavior and liquid entrainment.

S-RELAP5 simulations of UPTF Tests 6 and 7 were performed to simulate the downcomer penetration and ECC bypass behaviors displayed by these tests. The results of these simulations indicate that S-RELAP5 conservatively underestimates the rate of lower plenum refill.

S-RELAP5 simulations of UPTF Test 10 Run 080 and Test 12 Run 014 were specifically designed to simulate upper core, upper plenum, and hot-leg fluid flow behavior during the reflood phase of a LBLOCA transient. [

The S-RELAP5 code is demonstrated to conservatively limit the water downflow in the countercurrent flow mode. The code predictions show conservative predictions relative to the data (adequate agreement) in both tests. The calculated UPTF water downflow also was compared with the S-RELAP5 calculated water downflow. The results show that overall (co-current and countercurrent) S-RELAP5 conservatively underpredicts downflow. The results are consistent with the UPTF results, which indicate breakthrough of ECC liquid near the hot-leg

upper plenum junction. The S-RELAP5 results are based on describing the core-to-upper-plenum junction with the fuel bundle UTP area consistent with the BWRLOCA EM method.

S-RELAP5 simulations of UPTF Test 10, Run 081 (Test 10B), and Test 29, Runs 211 and 212 (Test 29B), were analyzed to show the countercurrent flow limit at the UTP during the reflood phase of a postulated LBLOCA and to provide specific S-RELAP5 input modeling guidelines for the hot leg and steam generator inlet plenum regions to ensure adequate prediction of the liquid entrainment to the steam generator tube region. The results of the simulation of Tests 10B and 29B show that S-RELAP5 will conservatively predict the countercurrent flow at the UTP during the LOCA reflood phase and conservatively predicts liquid entrainment to the steam generator tube region.

Assessment description

This section documents the assessment of the EM using the Upper Plenum Test Facility (UPTF). The UPTF was operated by Kraftwerk Union AG (KWU) where several separate effects and integral tests were run in support of the 2D/3D LOCA simulation program. The UPTF was designed to simulate a German four loop 3,900 MWt pressurized water reactor (PWR) primary system, similar in size and geometry as a Westinghouse four-loop PWR. The facility was intended to provide a full-scale simulation of thermal-hydraulic behavior in the primary system during the end-of-blowdown, refill, and reflood phases of a PWR large break loss-of-coolant accident. Although the tests simulated scenarios that are applicable to U.S. PWRs, the thermal hydraulic phenomena that occur in the facility are equally applicable to BWR specific analysis. Tests 6, 7, 10, 12 and 29 were used for the assessment of S-RELAP5 in providing thermal hydraulic behavior, such as self-limiting countercurrent flow in the downcomer, countercurrent flow limiting at the UTP and liquid entrainment in various components.

7.3.17.1 UPTF Tests 6 and 7

UPTF Tests 6 and 7 were separate-effects tests (SET) that investigated the countercurrent flow of steam and ECC water in the downcomer during a postulated large break of a cold-leg pipe in a PWR. These investigations focused on steam-water flow phenomena in the intact cold legs, the downcomer, and the lower plenum during the refill phase of an LBLOCA. The objective of these tests was to obtain test data for a complete flooding curve in a full-scale down-comer.

The area of investigation for these downcomer SETs encompassed the intact-loop cold legs and associated ECC injection system, the cold leg of the broken loop from the vessel to the containment, the downcomer, and the lower plenum. Simulating these UPTF tests demonstrates the ability of the S-RELAP5 code to self-limit countercurrent flow in the downcomer and to predict the refill behavior described by the experimental data, including ECC bypass.

Runs 131, 132, 133, 135, and 136 from Test 6 and from the Phase IV results of Run 203 from Test 7 were selected to be simulated using S-RELAP5 for this analysis (References 92, 93 and 94). Table 7-15 summarizes the steam injection rate, the evaluation period, and the lower plenum fill rate (downcomer penetration rate) for each test run. Note that just the Phase IV results from Test 7, Run 203 were analyzed because this phase was the only part of the test that used the same pattern of ECC injection as that used during the runs of Test 6.

As the lower plenum fills, the slope of the mass inventory curve (Figure 7-162, Figure 7-163, Figure 7-164, Figure 7-165, Figure 7-166 and Figure 7-167) provides a measure of the rate at which ECC water penetrates the downcomer to the lower plenum. To be useful, this slope must be evaluated during an appropriately chosen time interval, referred to here as the evaluation period, which determines the time span over which the region is filled at a roughly constant rate. A separate evaluation period is determined for each run using the following method, which is based on the method described in Reference 92.

- The evaluation period begins when the water level in the lower plenum exceeds 0.6 m (1.97 ft).
- The steam injection rate is required to remain steady until the end of the period. This condition is taken here to mean that the rate of steam injection is required to remain above 90% of its nominal rate during the entire evaluation period. It is applicable only for Runs 131 and 135, when the steam injection steadily decreased during the test.
- The end of the evaluation period is conservatively chosen to maximize the flow rate, provided that the duration of the evaluation period is at least 6 seconds, but not longer than 15.5 seconds.

This method yields the evaluation periods in Table 7-15. For comparison, the evaluation periods used by KWU to analyze their test data are also included in this table, and they are similar to the evaluation periods used for the S-RELAP5 results.

The beginning of the evaluation period is the first of two quantities that are used to assess the results of the S-RELAP5 calculations. The time at which the water level in the lower plenum exceeds 0.6 m (1.97 ft) as calculated by S-RELAP5 and as determined from the test measurements were compared. The difference between these two times – called the relative end of bypass, because it marks the transition from water bypassing the downcomer to ECC penetration of the lower plenum is also provided in Table 7-15 for all five runs of Test 6. The S-RELAP5 result is conservatively delayed relative to the test results of the two cases with the highest rate of steam flow (Runs 135 and 131). For the remaining three runs of Test 6, the time predicted by the S-RELAP5 model either matches or is close to the time reported for the test results (within one second).

The second quantity that is used to assess the results of the calculation is the ECC penetration rate to the lower plenum. Since the lower plenum was not drained during Test 6, this quantity is simply the rate of change of the mass inventory in the lower plenum, which is determined from the increase in liquid mass in the lower plenum over the evaluation period. The values calculated from the S-RELAP5 results are presented in Table 7-15 along with the flow rates reported by KWU (Reference 92) for each test and shown graphically in Figure 7-168.

7.3.17.2 Tests 10 and 12

Figure 7-169 presents a plot of Kutateladze parameters calculated from the S-RELAP5 results compared to the UPTF correlation (Reference 95) from Test 10, Run 80 (Reference 96). The comparison shows that S-RELAP5 is correctly limiting liquid downflow as is shown by the upper limit of the vapor Kutateladze parameter. [

] Figure 7-170 compares the S-RELAP5 prediction to the UPTF experimental downflow.

Figure 7-171 presents a plot of Kutateladze parameters calculated from the S-RELAP5 results compared to the UPTF correlation from Test 12, Run 014 (Reference 97). The comparison shows that S-RELAP5 is correctly limiting liquid downflow as is shown by the upper limit of the vapor Kutateladze parameter. [

] Figure 7-172 compares the S-RELAP5 prediction to the UPTF experimental downflow.

Figure 7-173 and Figure 7-175 show the Kutateladze parameters calculated at the core exit from the S-RELAP5 results for UPTF Test 10 Run 081 (Reference 96) and Test 29 (Reference 98), respectively. Also shown on each figure is the measured CCFL correlation for UPTF. From these figures, as well as the CCFL results from Test 10 Run 80 and Test 12 shown in Figure 7-169 and Figure 7-171, the S-RELAP5 CCFL model strictly limits the counter current flow to the requested input limits.

Figure 7-174 and Figure 7-176 show the liquid carryover to the steam generators for UPTF Tests 10 and 29, respectively. Again, both plots clearly show S-RELAP5 generally overpredicts the carryover of liquid to the steam generators. Figure 7-177 and Figure 7-178 show the calculated liquid fallback from the upper plenum into the core and the upper plenum liquid mass, respectively. Overall, these results show distinct conservatism with respect to the core (bundle) exit into the upper plenum during reflood conditions.

Table 7-15 UPTF Test 6 and 7 Calculated S-RELAP5 Downcomer Penetration Rates and Evaluation Periods

[illegible]

* The evaluation period for Test 7 is not calculated, the same evaluation period as the test is used.



Figure 7-162 Lower Plenum Liquid Mass Inventory for UPTF Test 6 Run 135



Figure 7-163 Lower Plenum Liquid Mass Inventory for UPTF Test 6 Run 131



Figure 7-164 Lower Plenum Liquid Mass Inventory for UPTF Test 6 Run 132



Figure 7-165 Lower Plenum Liquid Mass Inventory for UPTF Test 6 Run 133



Figure 7-166 Lower Plenum Liquid Mass Inventory for UPTF Test 6 Run 136



Figure 7-167 Lower Plenum Liquid Mass Inventory for UPTF Test 7 Run 203



**Figure 7-168 ECC Penetration Rate to Downcomer for All
UPTF Tests 6 and 7**



Figure 7-169 Calculated Kutateladze Parameters UPTF Test 10 Run 080




Figure 7-170 Calculated Downflow Comparison
UPTF Test 10 Run 080 ($m=1.0$, $c=1.8$, $\beta=1.0$)



Figure 7-171 Calculated Kutateladze Parameters UPTF Test 12 Run 014




Figure 7-172 Calculated Downflow Comparison
UPTF Test 12 Run 014 ($m=1.0$, $c=1.8$, $\beta=1.0$)



Figure 7-173 Countercurrent Flow of Steam and Water UPTF Test 10B



Figure 7-174 Water Carryover to Steam Generators UPTF Test 10B



Figure 7-175 Countercurrent Flow of Steam and Water UPTF Test 29B



Figure 7-176 Cumulative Water Carryover to Steam Generators UPTF Test 29B



Figure 7-177 Cumulative Water Fallback to Lower Core UPTF Test 29B



Figure 7-178 Upper Plenum Water Mass UPTF Test 29B

7.4 Assess Scalability of Models (EMDAP Step 15)

The scalability of the models and correlations that are assessed in EMDAP Step 14 to the configuration and conditions of the plants and transients under evaluation has been confirmed. Specifically, the assessments include separate effects tests that are prototypic in geometry and/or tested conditions, or overlapping prototypic tests confirm the scalability of non-prototypic tests. Because the EM is based on Appendix K criteria, a detailed scaling and uncertainty analysis method is not employed.

7.5 Determine Capability of Field Equations to Represent Processes and Phenomena and the Ability of Numeric Solutions to Approximate Equation Set (EMDAP Step 16)

The thermal-hydraulic and thermal conduction field equations have been determined to adequately represent processes and phenomena for the selected scenarios. The numerical solutions have also been determined to adequately solve the field equations, including adequate capabilities for solution convergence, property conservation, and stability of code calculations to solve the original equations when applied to the target applications.

The thermal-hydraulic and thermal conduction field equations and numerical solutions contained in RELAP5 have been extensively demonstrated in numerous assessments reported in the open literature. These numerics have been improved in S-RELAP5 as described in Reference 5 and 6. The adequacy of the S-RELAP5 specific field equations and numerics has been demonstrated in the performance of the assessments reported in Reference 1 and within this LTR.

No field equations are solved within the kernel of RODEX4 installed within S-RELAP5. This is because S-RELAP5 solves the thermal conduction equations using its own equations for heat structures. The numerical solutions for determining the thermal-mechanical properties have been well validated and have been determined to provide stable numerical predictions of fuel thermal-mechanical properties.

7.6 Determine Applicability of Evaluation Model to Simulate System Components (EMDAP Step 17)

Comparison to component effects tests demonstrates the capability of the EM to predict the relevant characteristics of entire components or regions of the BWR plant, examples being the jet-pumps and steam separator. Table 5-1 is the assessment matrix which shows the component effects tests that were selected, and the highly ranked PIRT phenomena addressed by each. The results of the assessments are summarized in the following sections.

7.6.1 Rod Bundle Pressure Drop

Assessed phenomena and processes

This section addresses the following highly ranked PIRT phenomena identified in Table 5-1;

Assessment conclusions

The assessment is performed by comparing the calculated and measured pressure drop across prototypical fuel bundles, which directly addresses the indicated PIRT phenomenon. The broad range of data and reasonable to excellent code-data comparisons for the bundle pressure drop demonstrate that the EM provides excellent predictions of the indicated PIRT phenomena.

Assessment description

The closure relations that define pressure drop within a rod bundle in S-RELAP5 have been assessed to demonstrate their adequacy over a broad experimental database that includes the 7x7, 8x8, 9x9 and 10x10 fuel designs, the egg-crate spacer [

The statistical performance of the assessment is tabulated in Table 7-16 as a function of flow quality and graphically in Figure 7-179 through Figure 7-181 for other informative metrics. These assessments demonstrate the capability of the AURORA-B LOCA EM to accurately predict BWR assembly pressure drop.

**Table 7-16 Pressure Drop Benchmark Statistics by Exit Flow Quality
(Calculated - Measured) / Measured**

[illegible]



Figure 7-179 Histogram of Relative Error for Pressure Drop Benchmark



Figure 7-180 Two-Phase Pressure Drop Benchmark



Figure 7-181 Relative Error vs. Exit Void Fraction for Pressure Drop Benchmark

7.6.2 Jet-pump Performance Tests

Assessed phenomena and processes

This section addresses the following highly ranked PIRT phenomena identified in Table 5-1;

Assessment conclusions

The single phase assessments are performed by comparing the calculated and measured pressure drop across reduced scale (Reference 99) and prototypical jet-pumps bundles over a wide range of flow rates, which directly addresses the indicated PIRT phenomenon. The comparisons are made using non-dimensional pressure ratio (n-ratio) and mass flow ratio (m-ratio). The broad range of data and the excellent code-data comparisons for the jet-pump pressure drop demonstrate that the EM provides excellent predictions of the indicated PIRT phenomena. These tests also demonstrate that the revised jet pump modeling required for two-phase applications, yields acceptable (i.e. the same) results for single phase conditions. [

]

The two blowdown tests (two-phase flow) from the reduced scale facility were used to assess the forward and reverse flow that occurs in BWR LOCA scenarios for recirculation line breaks:

- 1) The first test is for flow in an intact loop. The flows are in the normal forward direction with blowdown through the jet pump discharge.
- 2) The second test is for a broken loop. The suction flow is in the normal forward direction and the drive and discharge (exit) flows are in the reverse direction with blowdown through the drive line.

The performance of the HEM and Moody critical flow models in the jetpump model are shown to have acceptable performance with respect to data.

Assessment description

Jet pump performance tests were analyzed to develop and validate the jet-pump model implemented in S-RELAP5. Test data from 18 jet-pump bundles was used to develop or assess the performance of the jet-pump model. The data was available from a mixture of sources; bench top tests for reduced scale and production jet-pumps, “component tests” performed within integral test facilities, and in-situ measurements within operating reactors.

The dimensional characteristics for the 18 jet-pump bundles are summarized in Table 7-17. The diameters are indicated in centimeters, angles are indicated in degrees, and dimensionless lengths (length divided by throat diameter) are presented in the following tables.

The 18 jet-pump bundles represent the full spectrum of jet-pump designs found in operating jet-pump BWR plants, from BWR/3 through BWR/6 and reduced scale facilities such as the Two Loop Test Apparatus. The results for selected jet-pump designs are presented in the following sections.

The results are presented in these sections using the classical presentation format for jet-pump performance. The format consists of plotting the non-dimensional pressure ratio versus the mass flow ratio. The pressure ratio (alternatively called head ratio or n-ratio) is determined from the pressure differential between the lower plenum and downcomer divided by the pressure differential between the drive line and lower plenum, where elevation head is typically removed from the pressure differences. The mass flow ratio (alternatively called flow ratio or m-ratio) is the flow rate of liquid passing directly from the downcomer into the jet-pump bundle (the suction flow rate) divided by the flow rate entering from the recirculation system.

7.6.2.1 EGG-LTSF 1/6 Scale Tests

The LOFT Test Support Facility (LTSF) operated at Idaho National Laboratory was used to collect data for a 1/6 scale Browns Ferry type jet-pump. This data spanned all six potential operating flow regimes (e.g. permutations of steady flow direction in the legs of a Tee) in a BWR jet-pump, and represents the reference data set for validation of virtually all jet-pump models developed to date. The EGG-LTSF data has been used to develop and assess the performance of the jet-pump model implemented in S-RELAP5.

Assessment of the jet-pump model with best-estimate model coefficients (indicated as “Optimal Params”) versus the measured data is shown in Figure 7-182. The measured 2σ data uncertainties for the pressure ratio and mass flow ratio of each data point are also shown on the figure.

This figure shows the jet-pump model predicts the data with excellent agreement and within the range of experimental uncertainty for the operating flow regimes typically experienced in the events of interest, particularly the normal (1+) regime for which flow is entering the jet-pump volume from the downcomer and from the recirculation system. The capability of the jet-pump model to predict all operating regimes is important in transitory conditions and cases where one recirculation system is not operating. [

] This last figure shows the jet-pump model predicts the data with excellent agreement and within the range of experimental uncertainty for the operating flow regimes not clearly indicated in the earlier figure.

7.6.2.2 Other Jet-pump Tests

Test data from 17 additional jet-pump bundles, Table 7-17, was used to develop and assess the performance of the jet-pump model implemented in S-RELAP5 in addition to the EGG-LTSF data. Use of these data to develop and assess the jet-pump model assures the scalability of the jet-pump model from reduced scales, through a wide variety of full scale jet-pump designs. Results for two jet-pump designs are provided in Figure 7-184 and Figure 7-185 for the normal (1+) operating regime of a jet-pump. These two designs are representative of the “single nozzle” and “five nozzle” designs found in BWR/3-/4 and BWR/5-/6 plants respectively.

These figures indicate the jet-pump model is in excellent agreement with the experimental data for full scale jet-pumps in the normal (1+) operating regime. Also indicated in these figures are upper and lower bound predictions where the model coefficients have been set to their joint 97.5% confidence upper and lower values. The impact of the model parameters uncertainty will be demonstrated later for a plant transient.

7.6.2.3 Two-Phase Tests

The INL 1/6th scale jet pump test series include two blowdown tests that produce two-phase flow conditions. The test design is such that boundary conditions can be defined and applied to existing S-RELAP5 modeling for the 1/6th scale jet pump. Calculations are performed with three choking models (no choking, homogeneous equilibrium (HEM), and Moody) at the jet pump drive nozzle.

Test 1 represents a jet pump in an intact loop during a LOCA. Blowdown is through the jet pump discharge and all flows are in the normal forward direction. The JETPUMP model follows the trends of the data well, while agreement is best with the HEM and Moody choking models.

Test 2 represents a jet pump in a broken loop during a LOCA. Blowdown is reverse flow through the jet pump drive. The suction has positive flow and the discharge has reverse flow. The JETPUMP model follows the trends of the test data. The pressure drop at the drive nozzle is very high with the HEM choking model and details of the pressure drop computed by JETPUMP are of minor importance. The Moody choking model produces a smaller pressure drop and has acceptable agreement with the data of Test 2.

Figure 7-186 presents the calculated drive pressure for the three drive nozzle choking models. Also shown are the discharge pressure boundary condition and the data for the drive (buried in the plot). The calculated drive pressure is not significantly impacted by the choking model choice. The results are consistent with the data.

Figure 7-187 presents the calculated drive pressure drops for the three drive nozzle choking models. Also shown are the data. The calculated drive pressure trends below the data and as shown in Figure 8-8. The agreement is best with the HEM and Moody models at the drive nozzle.

Figure 7-188 presents the calculated suction pressure drops for the three drive nozzle choking models. Also shown are the data. The calculated suction pressure drop trends below the data. There is no significant difference for the three choking models at the drive nozzle.

Figure 7-189 presents the calculated discharge pressures for the three choices of drive nozzle choking model. Also shown are the drive line pressure boundary condition and the data for the

discharge pressure. The calculated discharge pressures are significantly impacted by the choice of drive choking model. The HEM and Moody choking model results bracket the data. The HEM result is closest to the data but above it. The Moody model trends below the data and the no-choking model even lower.

Figure 7-190 presents the calculated drive pressure drops for the three choices of drive nozzle choking model. Also shown are the data for the drive pressure drop. The calculated pressure drops for the HEM and Moody models bracket the data. The Moody model results trend above the data and the no-choking model even higher. The pressure drop with the HEM model trends below the data. As mentioned in the discussion for experimental data in Section 8.2.2, there is an inconsistency in pressure and pressure drop. If the pressures are accepted, the pressure drop is closer to -3000 kPa with better agreement using the HEM choking model.

Figure 7-191 presents the calculated suction pressure drops for the three choices of drive nozzle choking model. Also shown are the data for the suction pressure drop. The calculated pressure drops for all choking models follow the trend of the data with better agreement with the HEM and Moody models. The suction pressure drop is very small compared to the drive pressure drop.

Table 7-17 Jet-Pump Characteristic Information

	EGG-LTSF	TLTA	JP-1QS	JP-2QS	Dresden	Peach Bottom	Browns Ferry
Diameter							
nozzle	1.44	1.15	2.10	2.11	8.41	7.98	7.98
throat	2.90	2.32	5.23	5.23	20.75	20.78	20.78
discharge	7.20	5.76	12.82	12.27	50.80	48.26	48.26
Angle							
Nozzle	16	15	15	15	15	14	14
Discharge	5.6	5.6	8.0	6.0	8.0	7.2	7.4
Length							
throat	12.5	12.5	10.5	12.0	10.9	12.4	12.4
diffuser	15.1	15.1	10.4	12.8	10.4	10.5	10.2
tailpipe	2.0	15.3	2.5	0.0	1.6	1.2	1.3
number of nozzles	1	1	1	1	1	1	1

Table 7-19 Jet-Pump Characteristic Information (cont.)

	Susquehanna	Duane Arnold	Vermont Yankee	Columbia Generating Station	Kuosheng	Grand Gulf
Diameter						
nozzle	7.98	7.49	7.90	3.30	2.87	3.15
throat	20.78	15.54	15.56	16.26	15.24	16.26
discharge	48.26	35.45	36.20	48.26	34.16	37.34
Angle						
Nozzle	14	13	16	20	22	21
Discharge	7.3	5.9	6.0	4.4	3.9	6.3
Length						
throat	12.4	12.0	12.0	3.7	3.6	9.9
diffuser	10.4	12.4	12.7	25.5	18.3	11.7
tailpipe	1.2	6.6	6.6	1.7	7.8	6.6
number of nozzles	1	1	1	5	5	5

Table 7-19 Jet-Pump Characteristic Information (cont.)

	FS69Proto	Monticello	Nuclenor	Zimmer	Lasalle
Diameter					
nozzle	2.99	6.86	7.89	2.87	3.30
throat	17.42	15.49	15.49	15.24	16.26
discharge	43.18	36.00	36.00	34.16	48.26
Angle					
Nozzle	20	25	18	22	20
Discharge	4.1	6.0	6.0	3.9	4.4
Length					
throat	3.6	12.0	12.0	3.6	3.7
diffuser	20.5	12.6	12.6	18.3	25.5
tailpipe	4.1	8.1	8.1	7.8	1.7
number of nozzles	5	1	1	5	5



Figure 7-182 N-M Plot of 1/6 Scale Jet-Pump Results



Figure 7-183 Alternate Plot of 1/6 Scale Jet-Pump Results



Figure 7-184 N-M Plot of Browns Ferry Jet-Pump Results



Figure 7-185 N-M Plot of Columbia Generating Station & LaSalle Jet-Pump Results



Figure 7-186 **INL Test 1, Drive Pressure**



Figure 7-187 **INL Test 1, Drive Pressure Drop**



Figure 7-188 **INL Test 1, Suction Pressure Drop**



Figure 7-189 **INL Test 2, Discharge Pressure**



Figure 7-190 **INL Test2, Drive Pressure Drop**



Figure 7-191 **INL Test 2, Suction Pressure Drop**

7.6.3 Steam Separator Tests

Assessed phenomena and processes

This section addresses the following highly ranked PIRT phenomena identified in Table 5-1;

Assessment conclusions

The assessment is performed by comparing the calculated and measured steam carryover, steam carryunder, and separator pressure drop across prototypical steam separator bundles for prototypical reactor conditions, which directly addresses the indicated PIRT phenomena. The reasonable code-data agreement for the first phenomenon and excellent agreement for the second phenomenon shows the EM makes reasonable and excellent predictions of the indicated PIRT phenomena, respectively. [

]

Experimental data from full scale production steam separators has been used to develop and assess the performance of the steam separator model implemented in S-RELAP5. Two different separator designs are considered in S-RELAP5. The “two stage” design is used in BWRs through the BWR/5 plant. The “three stage” design is used on BWR/6 and advanced boiling water reactor (ABWR) plants. Data and assessment for both designs are presented in the following sections. A description of the steam separator test facility can be found in Reference 100.

7.6.3.1 Two Stage Steam Separator

An extensive series of full-scale test data is available to develop and validate the steady state performance of the two stage BWR steam separator model for carryover, carryunder, and pressure drop (References 100 and 102). Assessment of the separator model for two stage BWR steam separators is shown in Figure 7-192 through Figure 7-196 for representative conditions. The conclusions of the assessment are described in the introduction to the section.

The units associated with Figure 7-196 are selected because they quantify the separator performance in terms of physical parameters experienced within the actual plant applications over a broad range of conditions. The differential pressure is presented as “differential head in terms of feet of inlet fluid” on the ordinate because the elevation difference of the liquid level inside and outside the separator is a key impact of steam separator pressure drop. Inlet volumetric flow is used on the abscissa to simultaneously quantify the flow conditions as a function of both mass flow rate and inlet quality.

7.6.3.2 Three Stage Steam Separator

An extensive series of full-scale test data is available to develop and validate the steady state performance of the three stage BWR steam separator model for carryover, carryunder, and pressure drop (References 101 and 102). Assessment of the separator model for three stage BWR steam separators is shown in Figure 7-197 through Figure 7-201 for representative conditions. The conclusions of the assessment are described in the introduction to the section.



Figure 7-192 **Carryover Comparison for 2-Stage Separator with
Mass Flow Rate of 372,000 lb/hr**



Figure 7-193 **Carryover Comparison for 2-Stage Separator with
Mass Flow Rate of 550,000 lb/hr**



Figure 7-194 **Carryunder Comparison for 2-Stage Separator with
Mass Flow Rate of 372,000 lb/hr**



Figure 7-195 **Carryunder Comparison for 2-Stage Separator with
Mass Flow Rate of 550,000 lb/hr**



Figure 7-196 Differential Pressure Comparison for 2-Stage Separator



**Figure 7-197 Carryover Comparison for 3-Stage Separator with
Mass Flow Rate of 355,000 lb/hr**



Figure 7-198 **Carryover Comparison for 3-Stage Separator with
Mass Flow Rate of 500,000 lb/hr**



Figure 7-199 **Carryunder Comparison for 3-Stage Separator with
Mass Flow Rate of 355,000 lb/hr**



Figure 7-200 **Carryunder Comparison for 3-Stage Separator with
Mass Flow Rate of 500,000 lb/hr**



Figure 7-201 **Differential Pressure Comparison for 3-Stage Separator**

7.6.4 Critical Power Tests

This section addresses the following highly ranked PIRT phenomena identified in Table 5-1;

The critical power tests for fuel specific steady state CPR/CHF correlations are a primary phenomenon for the AURORA-B AOO EM and were assessed in Reference 1 Section 6.5.4. The calculation of critical power based on a fuel specific correlation is retained for the AURORA-B LOCA EM and is used to initialize the Groeneveld CHF LUT as described in Section 6.4.10. The AURORA-B AOO EM assessment concluded that reasonable predictions of phenomena were obtained; these conclusions remain applicable for the LOCA EM.

7.6.5 CCFL Mini Loop Test

Assessed phenomena and processes

This section addresses the following highly ranked PIRT phenomena identified in Table 5-1.

Assessment conclusions

The EM CCFL model for the fuel assembly is shown to be accurate and flexible to characterize CCFL phenomena. From these results, it is inferred that the EM makes reasonable predictions of the indicated PIRT phenomena.

Assessment description



Figure 7-202 ATRIUM-10 Upper Tie Plate CCFL



Figure 7-203 ATRIUM-10 Grid Spacer CCFL

7.7 *Prepare Input and Perform Calculations to Assess System Interactions and Global Capability (EMDAP Step 18)*

The ability of the EM is assessed in this section for predicting system interactions and the global capability of the EM is demonstrated. First, comparisons to three tests performed in an electrically heated integral test facility are made. The facilities are SSTF, TLTA and FIST. Calculations of the thermal-hydraulic response are compared for the three tests to the measured system response. Finally, demonstration LOCA analyses are provided for BWR/4 and BWR/6 distinct plant types to demonstrate the global capability of the EM to predict the relevant event characteristics. Several of these demonstration analyses will be investigated in more detail in Section 7.9 to examine EM biases and uncertainties.

7.7.1 SSTF Integral Tests

Assessed phenomena and processes

This section addresses the following highly ranked PIRT phenomena identified in Table 5-1.

Phenomenon

--

Assessment conclusions

The SSTF direct measurement of the highly ranked PIRT phenomena were compared to the EM calculation. Bundle pressure drop (DP), lower plenum liquid temperature, upper plenum collapsed level, upper plenum liquid temperature, and top of bundle liquid temperatures. Comparisons of the EM calculation with the SSTF measurements are provided in the following figures in this section. From this, it is inferred that the EM makes reasonable predictions of the indicated PIRT phenomena.

Assessment description

The full scale 30-degree sector test facility (SSTF) (Figure 7-204 and Figure 7-205) mocks up 58 individual fuel bundles, the surrounding peripheral and interstitial bypass region, upper plenum (UP) and lower plenum (LP), guide tubes, jet pump flow paths, downcomer, and ECCS injection systems. Tests were performed to investigate BWR system refill/reflood during a LOCA event. The system transients were experimental simulations of the later phase of the LOCA blowdown from 150 psia with core heat simulated by steam injections. Significant phenomena include Upper Tie Plate (UTP) CCFL drainage characteristics, inlet Side Entry Orifice (SEO) CCFL drainage characteristics, top of bypass CCFL drainage characteristics, upper plenum mixing and parallel channel effects.

The facility includes the following main features:

- A full-scale, 30° sector (58 full and partial bundles) representation of a BWR (i.e., 1/12 volume scaling).
- The facility had provisions for steam injection in the lower plenum, bypass and guide tubes to simulate steam generation from vessel stored heat during a blowdown and to simulate flashing when running constant pressure separate effects tests.
- Steam could also be injected into each of the bundles to simulate steam generation from decay heat in a prototypical fuel bundle.

- The bundles had prototype 8x8 BWR production hardware for the upper tie plate and the side entry orifice (SEO) regions.
- For the BWR/4 tests, ECC systems included a third sparger and set of nozzles (at an elevation in the upper plenum typical of a BWR/4) for the low pressure core spray (LPCS). Also, the low pressure coolant injection (LPCI) are directed into the jet pumps.
- For the BWR/6 tests, ECC systems included the spargers and nozzles for the high pressure core spray (HPCS), low pressure core spray (LPCS) to the upper plenum and for the LPCI into the bypass.

The key consideration of the S-RELAP5 nodalization scheme used for SSTF is that it should provide adequate details to capture the multi-dimensional interaction effects observed in the SSTF tests. The current scheme is consistent with the amount of nodalization details in the previous SSTF simulations by other industrial computer codes (TRAC and TRACE). The nodalization scheme developed to model the SSTF simulations was the basis for the AURORA-B LOCA EM and BWR/4 and BWR/6 sample problems in follow on sections.

Figure 7-206 shows the S-RELAP5 nodalization for modeling the SSTF facility. [

]

[

]

Figure 7-210 portrays the core spray injection into the upper plenum volumes. In this case, the two-phase level in the UP is below the sparger elevation. The core spray is injected in the form of droplets. The spray drops reach saturation temperature in a short distance from the sparger nozzle exit, usually a few nozzle diameters. When the two-phase level rises above the sparger elevation and covers the spargers, the core spray is injected in the form of submerged jets. With submerged jet, most of the subcooling in the core spray water is retained when the water reaches the bottom of the UP. The UP mixing model is detailed in Section 6.4.7.

7.7.1.1 Assessment of the SSTF System Test EA3.1 Run 111, BWR/4 LOCA

SSTF Test EA3.1 Run 111 (Reference 112) was the reference test for a BWR/4 LOCA. This test was run to assess the impact of the BWR/4 ECCS configuration on the refill-reflood responses. Test EA3.1 Run 111 simulated a 100% design basis accident (DBA) break transient (full diameter guillotine break). The test simulated the latter portion of the DBA break transient after the reactor vessel had depressurized to 150 psia. The ECCS systems are initiated after this time. The test was performed with one LPCS and two LPCI systems. The LPCI water was injected through the jet pumps into the lower plenum.

Prior to the break initiation (start of the transient test), steam was injected into the lower plenum, guide tubes, and core bundles. In addition, the lower plenum water was re-circulated through the test section. The test section was brought to saturation condition at 150 psia. The test section regional mass distribution was adjusted to the prescribed values by controlling the regional steam injections, and by recirculating and draining the liquid as necessary.

After the break initiation (start of the transient test), the steam injection rates (core, lower plenum, and guide tubes) were controlled to simulate the heat transfer from the core and vessel structures. For this test, one LPCS and two LPCI were initiated to simulate the BWR/4 ECCS configuration. The BWR/4 case injects LPCI water through the jet pumps and into the LP. Test

results show that the lower plenum is refilling quickly and two-phase level reaches the SEO elevation early in the transient.

Event Initialization

Figure 7-211 to Figure 7-213 show the collapsed levels in the UP, BP, LP, and selected fuel bundles []. The first 300 seconds of the calculation uses the quasi-steady boundary conditions to setup the regional mass distribution and hydraulic conditions in the SSTF facility, just prior to the initiation of the ECCS systems. At 300 seconds, the UP is almost empty and the bundle inventories reach the approximate levels at the start of the test transient. The second half (300 to 600 seconds) of the calculation simulates the test transient. The key calculated results are summarized in the following bullets.

- Due to the injection of LPCI water through the jet pumps, the lower plenum is refilling quickly. The collapsed levels in LP reach to the top in about 60 to 100 seconds after the transient.
- The collapsed levels in core and bypass rise before the LP is full. After the LP is full (in the peripheral ring at 60 seconds after the transient), the core collapsed levels rise slightly and maintain at more than 50% filled.
- The peripheral bundles are quickly filled to the top with 2-phase mixture, in about 25 seconds after the ECCS initiation.
- The bypass is filled to the top with two-phase mixture in about 200 seconds after the ECCS initiation. The filling rates are about the same in all three radial rings.
- The inventory in the UP quickly builds up after the LPCS initiation, and covers the LPCS nozzles for the remainder of the transient.
- There is a small radial gradient in the UP collapsed levels, higher in the peripheral ring and lower in the apex ring.

In the following discussions, the time zero used in the figures (Figure 7-214 to Figure 7-227) corresponds to the time after the start of the transient testing.

Comparison of the Pressure Drops in Selected Bundles

Table 7-18, Table 7-19 and Figure 7-208 shows the channel locations with delta pressure (DP) measurement. The following paragraphs and figures compare the calculated and measured DPs in these bundles.

[

]

Comparison of the Liquid Temperatures in the Lower Plenum

[

]

[

]

Comparison of the Collapsed Liquid Levels in the Upper Plenum

In this test, LPCS water at 120 F was injected through the LPCS nozzles into the upper plenum at the peripheral locations. Figure 7-220, Figure 7-221 and Figure 7-222 show the comparisons of the calculated and measured UP collapsed levels in [

] The calculated collapsed levels are higher than the measurements, by about 100%. However, the calculated transient responses, i.e., the timings for peaks and valleys, compare reasonably well with the measurements.

Comparison of the Liquid Temperatures at the Bottom of the Upper Plenum

Figure 7-223, Figure 7-224, and Figure 7-225 show the comparisons of the calculated and measured liquid temperatures in the UP bottom in [

] The calculated saturation temperatures at the corresponding locations are also shown in these figures. The calculated liquid temperatures in [

] lower than the measured values. The measured liquid temperature [

] The trend is in reasonable agreement with the measurement.

Comparison of the Liquid Temperatures at the Top of Selected Bundles

Figure 7-226 shows the comparison of the calculated and measured liquid temperatures at the top of the apex bundle []. The calculated saturation temperatures at the corresponding locations are also shown in these figures (Figure 7-226 and Figure 7-227). The

calculated liquid temperature is about 20 to 40 F lower than the measurement. Figure 7-227 shows the comparison of the calculated and measured liquid temperatures at top of the peripheral bundle []. The calculated liquid temperature is in reasonable good agreement with the measurement.

7.7.1.2 Assessment of the SSTF System Test SRT-3 Run 26, BWR/6 LOCA

SSTF Test SRT-3 Run 26 (Sections 5.2 and 5.3, Reference 64) was the reference test for BWR/6 LOCA. This test simulates the BWR/6 refill-reflood transient during a large break LOCA. The ECCS includes 1 HPCS and 1 LPCS injected into the UP, and 1 LPCI injected into the outer bypass region. The initial system pressure is at 150 psia. The SSTF simulates the LOCA transient starting from the time when the vessel pressure drops to 150 psia.

Event Initialization

Figure 7-228 to Figure 7-230 show the collapsed levels in the UP, BP, LP, and selected fuel bundles in []. The first 400 seconds of the calculation uses the quasi-steady boundary conditions to setup the regional mass distribution and hydraulic conditions in the SSTF facility, just prior to the initiation of core spray systems. At 400 seconds, the UP is almost empty and the bundle inventories reach the approximate levels at the start of the test transient. The second half (400 to 540 seconds) of the calculation simulates the test transient. The key calculated results are summarized in the following bullets.

- Due to the injection of LPCI water into the peripheral bypass, the bypass is refilling quickly.
- The collapsed level in peripheral bypass reaches to the top in about 40 seconds after the transient. The filling rates in the inner bypass regions are lower than that in the peripheral bypass.
- The collapsed levels in the core and the bypass rise before the LP is full.
- The peripheral bundles are quickly filled to the top with 2-phase mixture. The collapsed level in the peripheral bundle follows closely with that in the peripheral bypass.
- The inventory in the UP quickly builds up after the initiations of the LPCS and HPCS. The collapsed levels reach to 5 to 10 inches in about 50 seconds.

In the following discussions, the time zero used in the figures (Figure 7-231 to Figure 7-244) corresponds to the time after the start of the transient testing.

Comparison of the Pressure Drops in Selected Bundles

Table 7-18, Table 7-19 and Figure 7-208 shows the channel locations with delta pressure (DP) measurement. The following paragraphs and figures compare the calculated and measured delta pressures in these bundles.

Comparison of the calculated and measured Collapsed Levels in the Upper Plenum

During the initial 60 seconds of the transient, the calculated collapsed levels in all radial rings agree reasonably well with the measurements. After 60 seconds, the calculated collapsed levels are higher than the measurements, by about 30 inches. However, the calculated transient responses, i.e., the timings for peaks and valleys, compare reasonably well with the measurements.

Comparison of the calculated and measured Liquid Temperatures in the Upper Plenum Bottom

The calculated liquid temperatures generally follow the trend of the measured data, but are lower by about 20 to 40 degree F. The higher subcooling in the liquid, in turn, could cause lower pressure in UP. Lower UP pressure could result in lower drainage rate or higher collapsed levels as shown in Figure 7-237, Figure 7-238 and Figure 7-239.

Comparison of the calculated and measured Liquid Temperatures at the top of Selected
Bundles



[illegible][illegible]

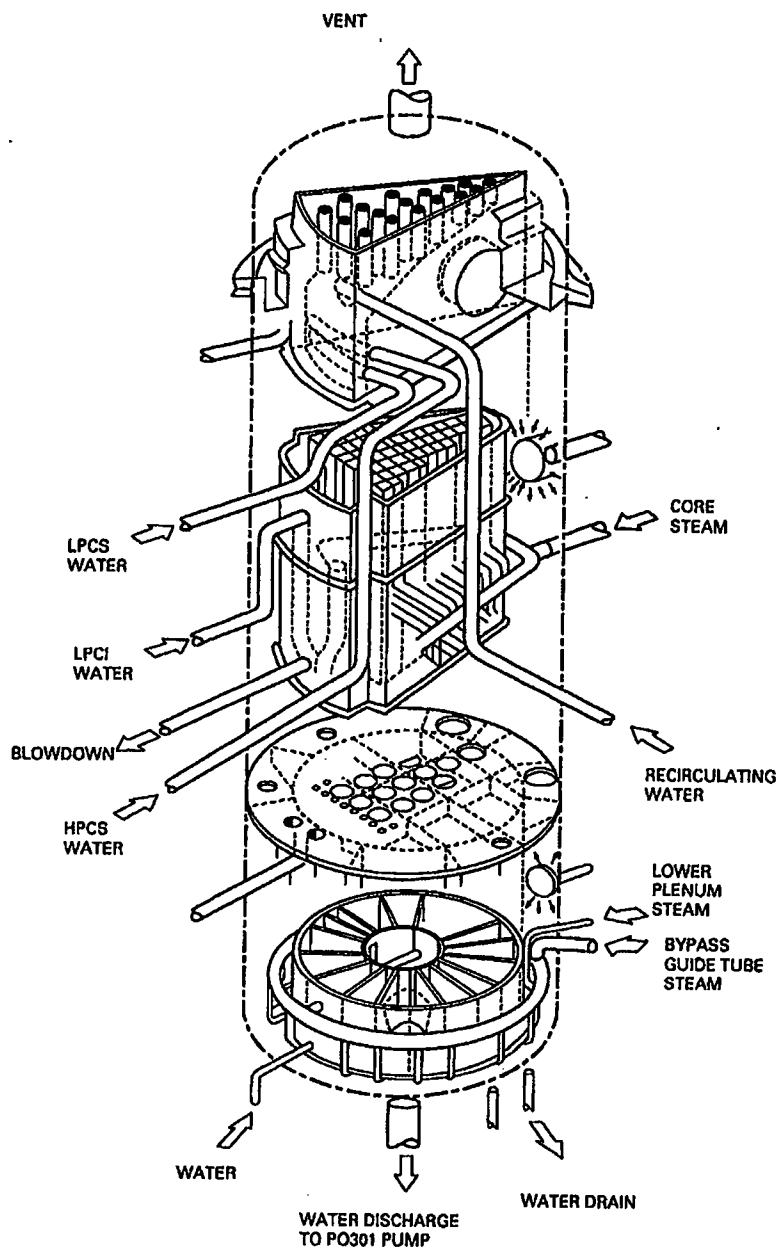


Figure 7-204 **Thirty-degree Steam Section Test Facility***

* Based on Reference 112, Figure 1.

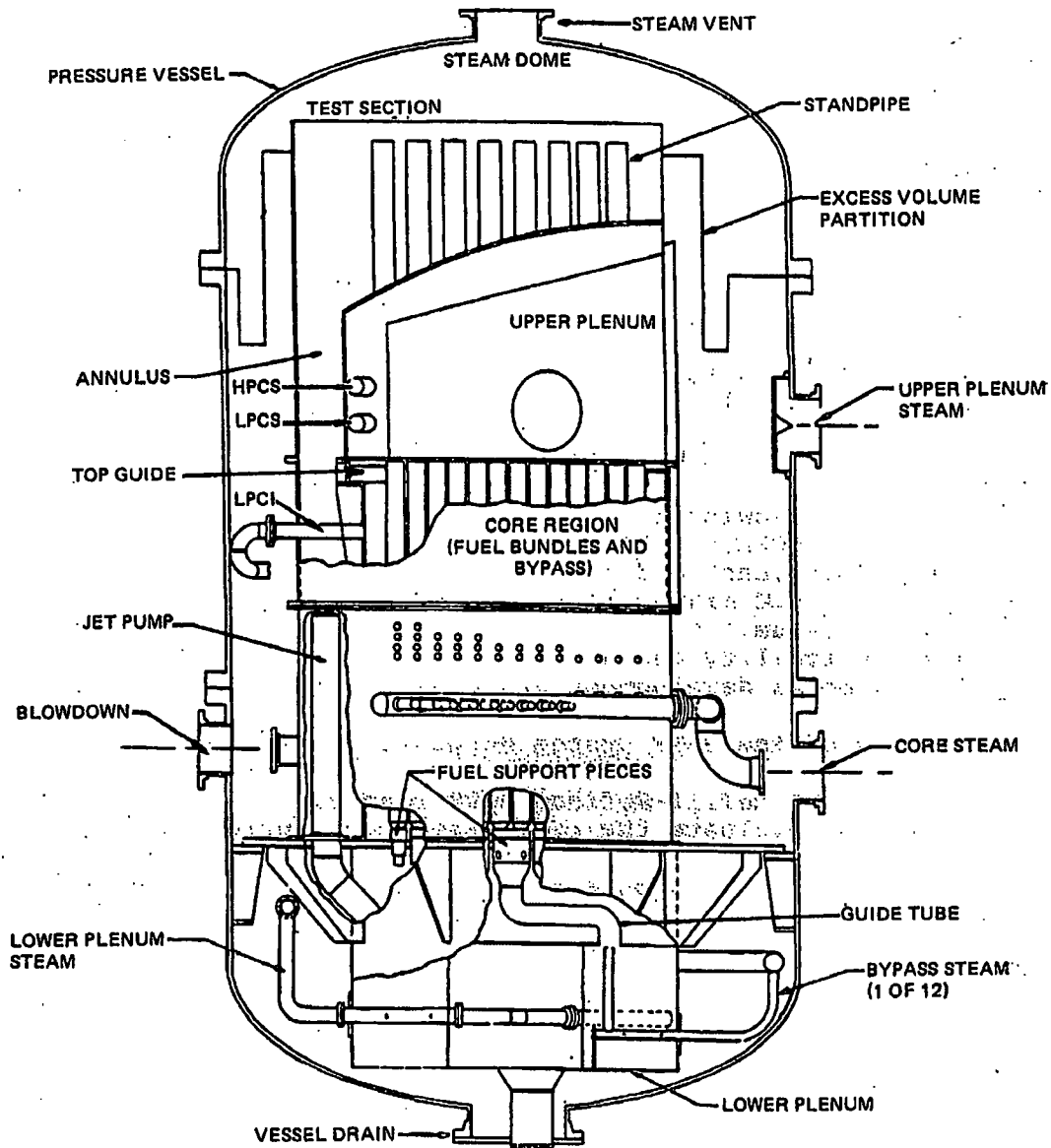


Figure 7-205 SSTF Test Section Schematic*

* Reproduced from Reference 113, Figure 1.

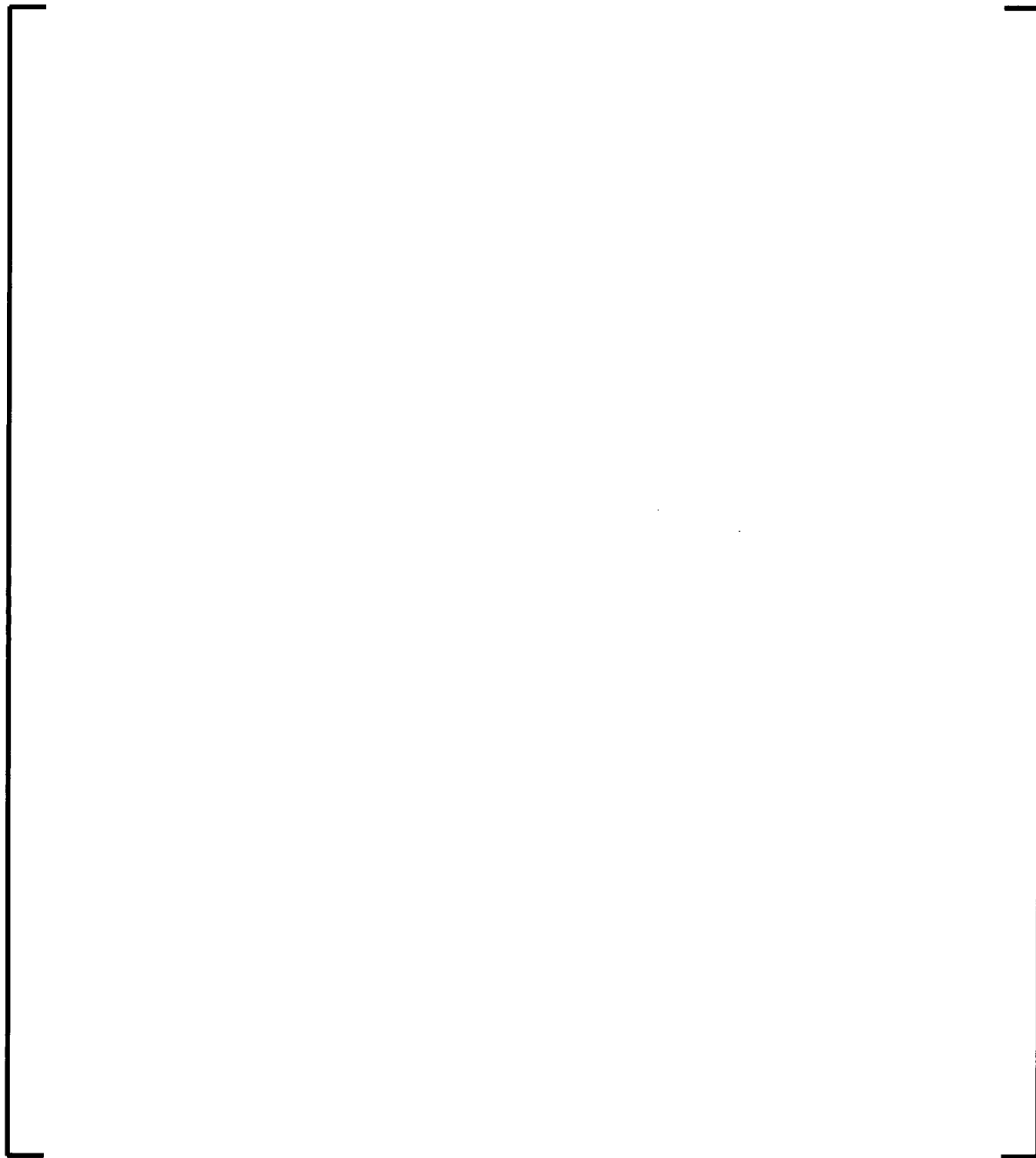


Figure 7-206 SSTF Nodalization

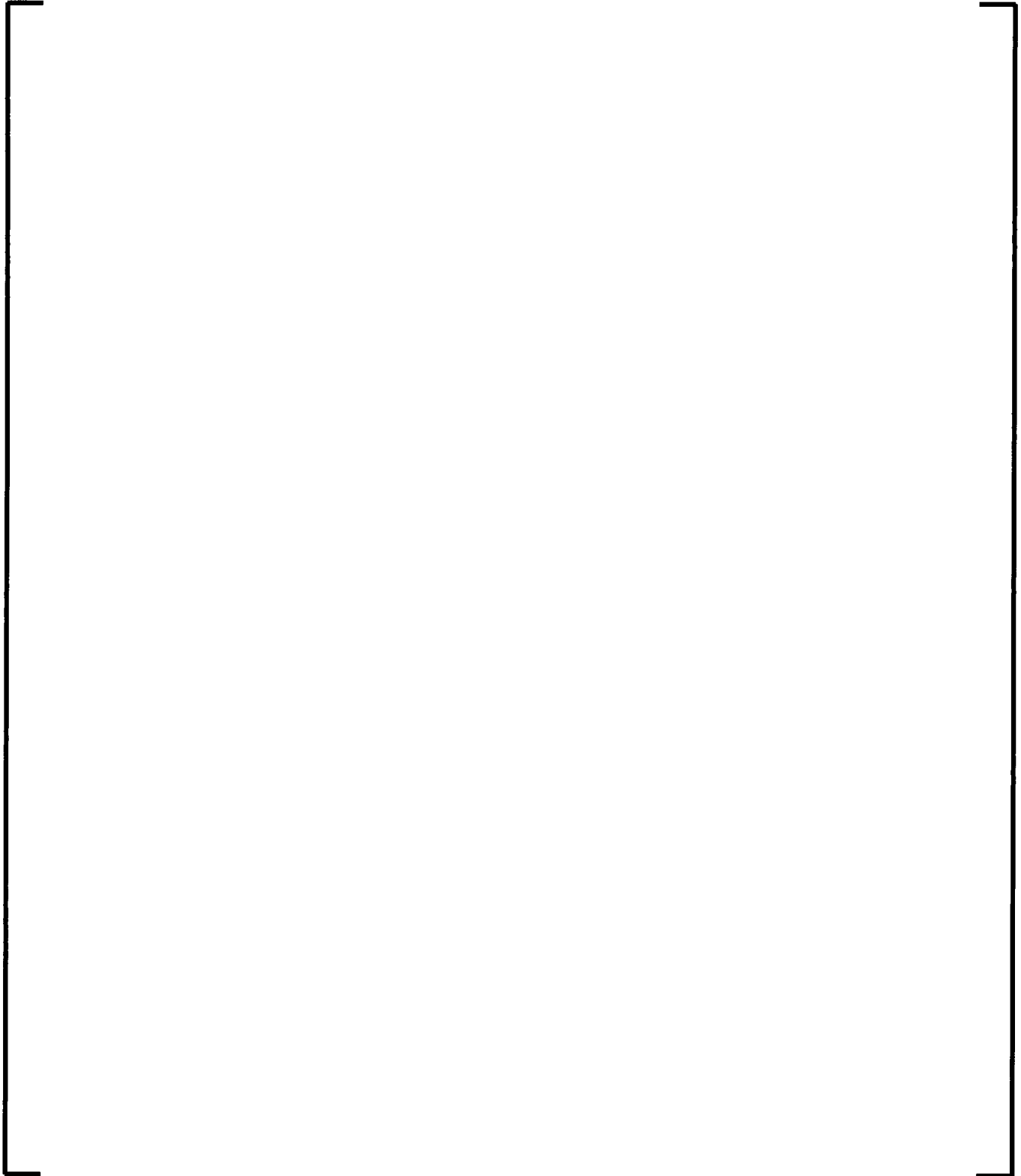


Figure 7-207 SSTF Bundle Nodalization

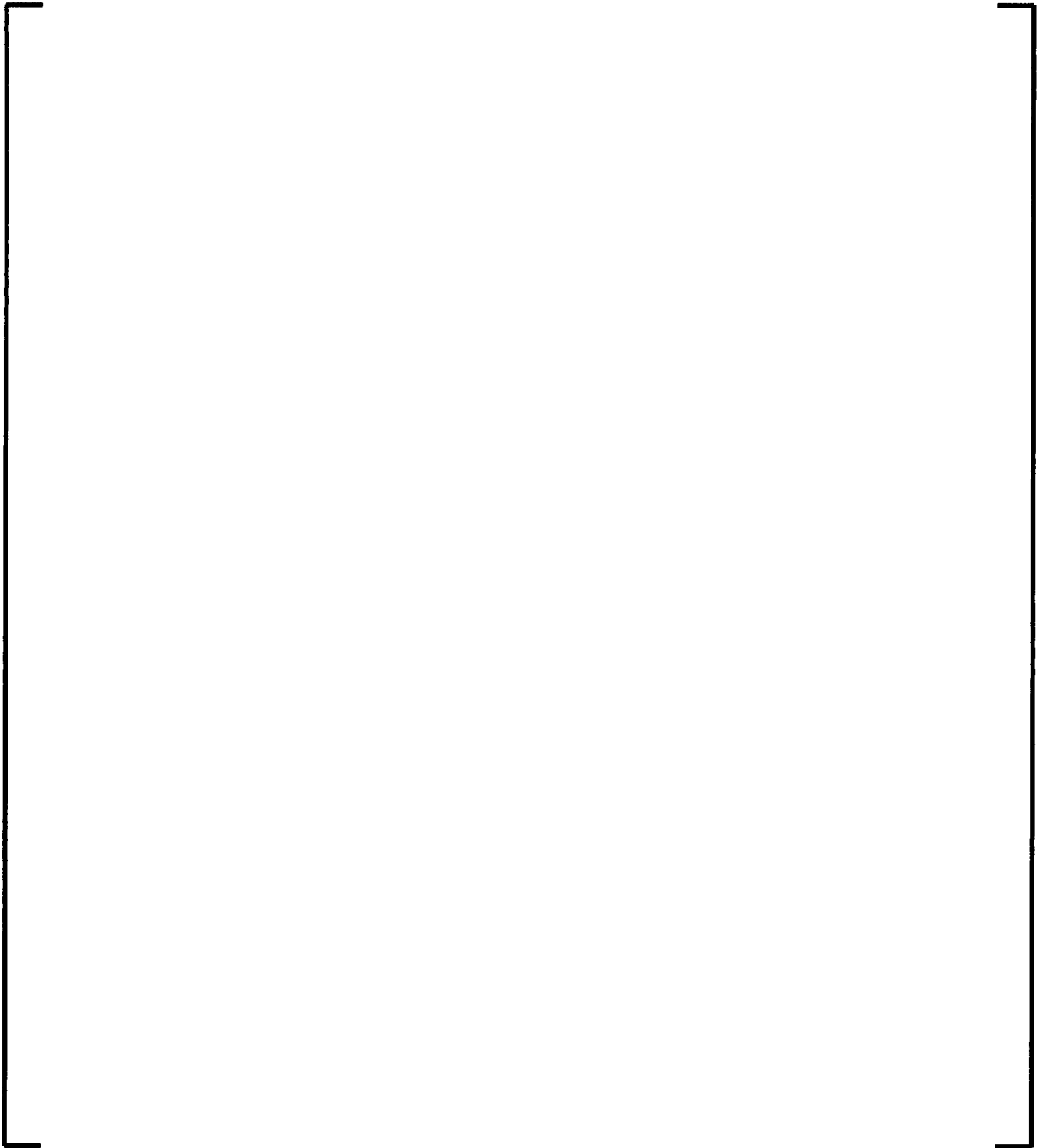


Figure 7-208 SSTF Bundle Grouping

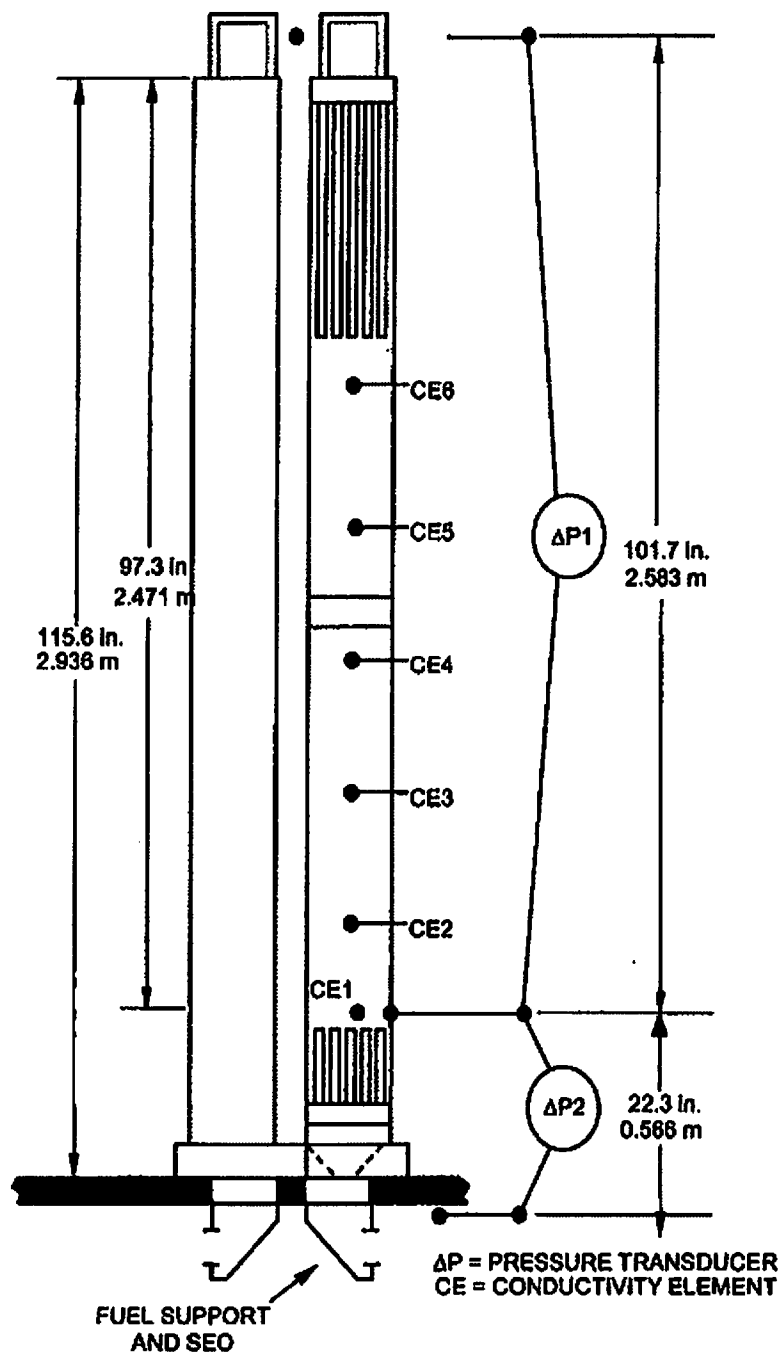


Figure 7-209 SSTF Bundle DP Measurements*

* Based on Reference 113, Figure 5.



**Figure 7-210 SSTF Core Spray injection into the UP Volumes
(2-Phase Level below the Sparger Elevation)**

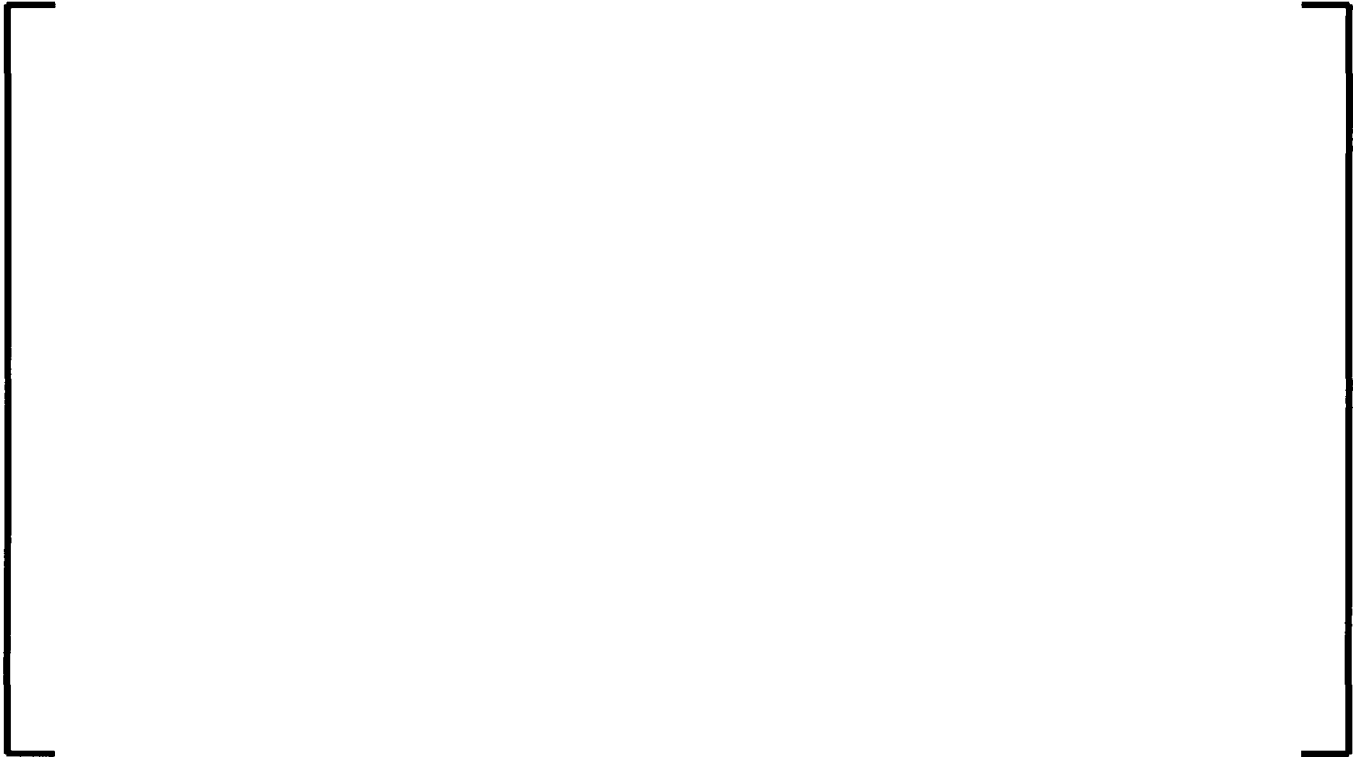


Figure 7-211 SSTF BWR/4: Ring 1 Collapsed Levels



Figure 7-212 SSTF BWR/4: Ring 2 Collapsed Levels



Figure 7-213 SSTF BWR/4: Ring 3 Collapsed Levels



**Figure 7-214 SSTF BWR/4: Calculated and
Measured Ring 3 DPs (F031 vs. B5)**

**Figure 7-215 SSTF BWR/4: Calculated and
Measured Ring 2 DPs (F025 vs. B26)**

**Figure 7-216 SSTF BWR/4: Calculated and
Measured Ring 2 DPs (F026 vs. B40)**

**Figure 7-217 SSTF BWR/4: Calculated and
Measured LP Liquid Temperature in Ring 1**

**Figure 7-218 SSTF BWR/4: Calculated and
Measured LP Liquid Temperature in Ring 2**



**Figure 7-219 SSTF BWR/4: Calculated and
Measured LP Liquid Temperature in Ring 3**



**Figure 7-220 SSTF BWR/4: Calculated and Measured UP
Collapsed Levels in Ring 1**



Figure 7-221 **SSTF BWR/4: Calculated and Measured UP
Collapsed Levels in Ring 2**




Figure 7-222 **SSTF BWR/4: Calculated and Measured UP
Collapsed Levels in Ring 3**



Figure 7-223 SSTF BWR/4: Calculated and Measured Liquid Temperature at UP Bottom in Ring 1




Figure 7-224 SSTF BWR/4: Calculated and Measured Liquid Temperature at UP Bottom in Ring 2



**Figure 7-225 SSTF BWR/4: Calculated and Measured Liquid
Temperature at UP Bottom in Ring 3**



**Figure 7-226 SSTF BWR/4: Calculated and Measured Liquid
Temperature in Apex Bundle (Below UTP)**



**Figure 7-227 SSTF BWR/4: Calculated and Measured Liquid
Temperature in Peripheral Bundle (Below UTP)**



Figure 7-228 SSTF BWR/6: Ring 1 Collapsed Levels



Figure 7-229 SSTF BWR/6: Ring 2 Collapsed Levels



Figure 7-230 SSTF BWR/6: Ring 3 Collapsed Levels




Figure 7-231 **SSTF BWR/6: Calculated and Measured Ring 3
DPs (F031 vs. B5)**




Figure 7-232 **SSTF BWR/6: Calculated and Measured Ring 3
DPs (F031 vs. B4)**




Figure 7-233 **SSTF BWR/6: Calculated and Measured Ring 2
DPs (F025 vs. B26)**




Figure 7-234 **SSTF BWR/6: Calculated and Measured Ring 2
DPs (F022 vs. B12)**

Figure 7-235 **SSTF BWR/6: Calculated and Measured Ring 2
DPs (F026 vs. B40)**

Figure 7-236 **SSTF BWR/6: Calculated and Measured Ring 1
DPs (F013 vs. B54)**



Figure 7-237 **SSTF BWR/6: Calculated and Measured UP
Collapsed Levels in Ring 1**



Figure 7-238 **SSTF BWR/6: Calculated and Measured UP
Collapsed Levels in Ring 2**



Figure 7-239 **SSTF BWR/6: Calculated and Measured UP Collapsed Levels in Ring 3**



Figure 7-240 **SSTF BWR/6: Calculated and Measured Liquid Temperature at UP Bottom in Ring 1**



Figure 7-241 **SSTF BWR/6: Calculated and Measured Liquid Temperature at UP Bottom in Ring 2**




Figure 7-242 **SSTF BWR/6: Calculated and Measured Liquid Temperature at UP Bottom in Ring 3**



**Figure 7-243 SSTF BWR/6: Calculated and
Measured Liquid Temperatures in
Apex Bundle (Below UTP)**



**Figure 7-244 SSTF BWR/6: Calculated and Measured Liquid
Temperatures in Peripheral Bundle (Below UTP)**

7.7.2 TLTA Integral Tests

The TLTA integral tests simulate large and small break BWR LOCA. TLTA test results are used to validate the PIRT phenomena listed below.

Assessed phenomena and processes

This section addresses the following highly ranked PIRT phenomena identified in Table 5-1.

Assessment conclusions

For the TLTA large break test, the major event timings including jet pump suction uncover, lower plenum flashing and ECC initiation time were predicted satisfactorily. The vessel depressurization history was closely predicted and the flow rates in different regions of vessel were predicted reasonably well during the time period that data is available. The annulus and bypass mass are predicted closely but the upper plenum mass was overpredicted by S-RELAP5 particularly after 100 s. The bundle mass history showed that S-RELAP5 predicts less fluid in the bundle due to bundle drainage to the lower plenum. The predicted peak clad temperatures were higher than the measured temperatures at all elevations.

All the thermal hydraulic parameters including the depressurization history, ECC initiation and flow, flow rates in different vessel regions, and the mass inventory variations were predicted well by S-RELAP5 for the TLTA small break test. There was no heat-up during this small break test; therefore the bundle temperatures followed the saturation temperature until late in the transient when the bundle became subcooled due to ECC flow.

The small break test was repeated with the Appendix-K assumptions to demonstrate the conservatism of the Appendix-K assumptions used in the plant models. The results showed that the S-RELAP5 calculation with Appendix-K assumptions predicted considerable heat-up and bounded the measured heater rod temperatures and PCT. This assessment is presented in Section 7.9.2.1.

Assessment description

The TLTA is a scaled version of a BWR/6, with one fuel bundle. The apparatus includes one full-length (150 inches long) fuel bundle simulator. Figure 7-31 shows a schematic diagram,

corresponding to Configuration 5. The original TLTA configuration used a 7x7 rod bundle, and later TLTA configurations used an 8x8 rod bundle, and other sequential modifications to arrive at a better representation of the BWR LOCA event being simulated. The bundle uses electrically heated rods (direct heating), with a peak power of 6.5 MW, which is representative of a peak power bundle in a BWR/6. The rest of the TLTA system is scaled down, relative to a BWR/6 with a 218-inch reactor vessel and 624 fuel bundles. There are two recirculation loops, each loop feeding a jet pump located in the downcomer region of the TLTA vessel. Blowdown lines are provided from both legs of one recirculation loop, allowing the simulation of a LOCA from the suction side or the discharge side of the recirculation pump. ECC water can be delivered at several locations in the system.

The facility is primarily volume-scaled. This caused the jet pumps to be relatively short compared to a BWR/6, where the jet pump extends up to about 2/3 of the core height. Figure 7-32 shows an elevation comparison of the TLTA vessel with a BWR/6 vessel. The TLTA was primarily intended for simulation of large break LOCA (LBLOCA) events and hence the short jet pumps do not have a significant effect. In small break LOCA (SBLOCA) events, the height of the jet pumps can affect the event progression. Hence only one SBLOCA test was performed in the TLTA. Although it is not an ideal representation of a SBLOCA event in a BWR, the test still provides useful information for assessment of analysis methods.

Although the TLTA bundle could be operated at full power (about 6.5 MW), steady-state operation of the facility is possible only up to about 2 MW. This is because of limited capacity for cooling the electrical cables of the power supply system and due to the limited heat removal capacity of the system overall. Hence, in the LBLOCA simulations, a steady-state is first achieved at about 2 MW, the power is then ramped up to the desired initial power for the test, and the LOCA event is initiated from a transient state. For the SBLOCA and other simulations, the tests are initiated from a steady-state condition.

7.7.2.1 TLTA Large Break Test 6425-2 Simulation

The TLTA large break LOCA test 6425-Run 2 simulated a 2.23 ft² double ended guillotine break in one of the recirculation lines. The transient starts with a bundle power of 5.05 MW and a steam dome pressure of 1044 psi, and is simulated by opening the suction and discharge blowdown valves at time zero.

The broken loop recirculation line is isolated, the power decay is initiated, the recirculation pumps are tripped, and the feedwater flow is shut-off with break opening. The intact recirculation loop is isolated 20 s after break initiation. The sequence of events of the test compared to the EM simulation is presented in Table 7-20. The specified measured times in this table are based on the reported values in Reference 114, Table 3-4.

The plots of some of the other major parameters are compared to S-RELAP5 predictions in Figure 7-245 to Figure 7-278.

The break in the suction and discharge lines open at time zero which result in reversal of flow in the broken loop jet pump and sudden drop in core flow, Figure 7-245 and Figure 7-246. Most of the major event timings are predicted closely. However, the ECC injection is delayed due to the predicted pressure history.

The predicted suction and discharge break flows are shown in Figure 7-247 and Figure 7-248. There seems to be some entrainment in the recirculation suction line at around 110 s which results in an increase in measured break flow. This entrainment is not predicted by S-RELAP5. The close prediction of discharge flow rates results in good prediction of the pressure history, as shown in Figure 7-249. Higher predicted pressures prior to 70 s result in later ECC injection initiation times and lower flow rates, Figure 7-250 to Figure 7-253. When the level reaches the break location and uncovers the break the depressurization rate increases due to two-phase discharge. The downcomer void fraction histories show predicted break uncover occurs around 10 s compared to the reported time of 9.4 s. The predicted steam dome depressurization rate between 10 s and 70 s is very close to the measured rate. However, at around 70 s the measured pressure levels off earlier and ends up at higher system pressure. The rapid depressurization results in bulk flashing within the vessel with lower plenum flashing at around 13 s, compared to the reported value of 11 s.

The flow rates in different regions of the vessel are shown in Figure 7-254 to Figure 7-257. The bundle inlet flow, Figure 7-254 and Figure 7-255, and jet pump exit flow, Figure 7-246 and Figure 7-256, are predicted reasonably well during the time period that data is available. Figure 7-254 shows bundle drainage into the lower plenum starts at around 50 s and increases after 150 s. The comparison of measured and predicted mass in different vessel regions are shown in Figure 7-258 to Figure 7-264. The annulus and bypass mass are predicted closely. Figure

7-259 shows that the bypass is filled at approximately 130 s compared to a predicted time of around 150 s. The upper plenum mass is overpredicted particularly after 100 s, Figure 7-260. Neither the measured nor the predicted upper plenum mass shows any accumulation after ECC initiation. The predicted bundle inlet and exit flow rates, Figure 7-254 and Figure 7-265, show that the upper plenum starts draining into the bundle and the bundle starts draining into the lower plenum at around 50 s. Figure 7-266 shows that there is significant drainage from the upper plenum to the bypass after around 100 s. Therefore, the ECC fluid mass added to the upper plenum is being drained to the bundle and bypass, keeping the mass in the upper plenum relatively constant until around 150 s. The bundle mass history, Figure 7-261, shows less fluid in the bundle after 100 s than measured. It is believed that lower mass inventory in the bundle is due to bundle drainage to the lower plenum. Figure 7-262 shows that S-RELAP5 predicts fluid accumulation in the lower plenum after 140 s which completely fills up the lower plenum at around 210 s. The measured lower plenum mass remains relatively constant for most of the transient. The total mass in the vessel is closely predicted during the early part of the accident simulation.

Comparison of the predicted and measured bundle temperature for different elevations and heater rods are shown in Figure 7-267 to Figure 7-276. The S-RELAP5 model contains only an average rod for the bundle while there are several temperature measurements for different rods at the same elevation. These figures show predicted peak clad temperatures (PCT) are higher than the measured temperatures at all elevations. The comparison of the measured and predicted PCT is shown in Figure 7-277. Only the predicted wall temperatures below 20 inch and above 100 inch quench within the test duration. In order to show that predicted wall temperatures quench, and also to predict the PCT for all elevations, the transient calculations were performed for 1000 s. The predicted temperature, Figure 7-278, show all elevations quench before 900 s. S-RELAP5 conservatively overpredicts the PCT during the TLTA large break LOCA transient. The higher predicted PCT and later quench is believed to be due to lower liquid holdup in the bundle.






Figure 7-245 Broken Loop Jet Pump Exit Flow Rate – TLTA Test 6425-2



Figure 7-246 Broken Loop Jet Pump Exit Flow Rate (Expanded) – TLTA Test 6425-2



Figure 7-247 Suction Side Break Flow Rate – TLTA Test 6425-2



Figure 7-248 Discharge Side Break Flow Rate – TLTA Test 6425-2



Figure 7-249 Steam Dome Pressure History – TLTA Test 6425-2



Figure 7-250 HPCS Flow Rate – TLTA Test 6425-2



Figure 7-251 LPCI Flow Rate – TLTA Test 6425-2



Figure 7-252 LPCS Flow Rate – TLTA Test 6425-2



Figure 7-253 Total ECC Flow Rate – TLTA Test 6425-2



Figure 7-254 Bundle SEO Flow Rate – TLTA Test 6425-2



Figure 7-255 Bundle SEO Flow Rate (Expanded) –TLTA Test 6425-2



Figure 7-256 Intact Loop Jet Pump Exit Flow rate – TLTA Test 6425-2



Figure 7-257 Steam Line Flow Rate – TLTA Test 6425-2



Figure 7-258 Annulus Fluid Mass History – TLTA Test 6425-2



Figure 7-259 Bypass Fluid Mass History – TLTA Test 6425-2



Figure 7-260 Upper Plenum Fluid Mass History – TLTA Test 6425-2



Figure 7-261 Bundle Fluid Mass History – TLTA Test 6425-2



Figure 7-262 Lower Plenum Fluid Mass History – TLTA Test 6425-2



Figure 7-263 Guide Tube Fluid Mass History – TLTA Test 6425-2



Figure 7-264 Total Fluid Mass History – TLTA Test 6425-2



Figure 7-265 Bundle Exit Flow Rate – TLTA Test 6425-2



Figure 7-266 Bypass Exit Flow Rate – TLTA Test 6425-2



**Figure 7-267 Comparison of Measured and Predicted Heater
Wall Temperatures, 10 inch Elevation – TLTA Test 6425-2**



**Figure 7-268 Comparison of Measured and Predicted Heater
Wall Temperatures, 35 inch Elevation – TLTA Test 6425-2**



**Figure 7-269 Comparison of Measured and Predicted Heater
Wall Temperatures, 50 inch Elevation – TLTA Test 6425-2**



**Figure 7-270 Comparison of Measured and Predicted Heater
Wall Temperatures, 71 inch Elevation – TLTA Test 6425-2**



**Figure 7-271 Comparison of Measured and Predicted Heater
Wall Temperatures, 90 inch Elevation – TLTA Test 6425-2**



**Figure 7-272 Comparison of Measured and Predicted Heater
Wall Temperatures, 100 inch Elevation – TLTA Test 6425-2**



**Figure 7-273 Comparison of Measured and Predicted Heater
Wall Temperatures, 107 inch Elevation – TLTA Test 6425-2**



**Figure 7-274 Comparison of Measured and Predicted Heater
Wall Temperatures, 120 inch Elevation – TLTA Test 6425-2**



**Figure 7-275 Comparison of Measured and Predicted Heater
Wall Temperatures, 130 inch Elevation – TLTA Test 6425-2**



**Figure 7-276 Comparison of Measured and Predicted Heater
Wall Temperatures, 140 inch Elevation – TLTA Test 6425-2**



Figure 7-277 Comparison of Measured and Predicted Peak Cladding Temperature (PCT) – TLTA Test 6425-2



Figure 7-278 Predicted Heater Wall Temperature Histories at Different Elevations – TLTA Test 6425-2

7.7.2.2 TLTA Small Break Test 6432-1 Simulation

TLTA SBLOCA Test 6432-1 simulates a 0.05 ft² break in the recirculation loop of a BWR-6, with the High Pressure Core Spray (HPCS) disabled. The test was performed with TLTA configuration 5C, Figure 7-279, by placing an orifice, with a scaled diameter of 0.125 inch, in the broken loop recirculation blowdown line. The S-RELAP5 Nodalization diagram is presented in Figure 7-280. The test description and the sequence of events can be found in Reference 115.

It was expected that the water level in this test will drop sufficiently to trip the MSIV and ADS. For this kind of transient, it is important to simulate the water level variation. In order to accomplish this, it was necessary to remove excess mass from the downcomer in order to simulate a representative response of the water level variations. This simulation was achieved by adding a second break of 0.153-inch diameter, Figure 7-279, to the blowdown line. The initial water level was set as high as possible at the exit plane of the separator line. The initial bundle power (2 MW) was the highest power at which the facility could be operated at steady-state conditions. The reference time for beginning the transient is 0.0 seconds. The bundle power decay was started at 7 seconds to compensate for the lower initial power. This compromise in the early period was considered acceptable since the major interest in the test was the long-term system response and the core was expected to be covered for a long period after the event began.

The TLTA vessel is shorter than a BWR-6 vessel. The level in a BWR-6 is substantially higher than the 283-inch water level that could be maintained in the TLTA during steady-state operation. Hence the test could not be started from all the same initial conditions as in a BWR-6. In a BWR-6, the water level is expected to reach the 283-inch elevation at about 138 seconds. During this time, the recirculation pumps (tripped early in the transient) would have coasted down. Also, the reactor power would have reached decay power levels. At 138 seconds, the fluid distribution in a BWR-6 would be governed mainly by natural circulation flows.

To simulate this sequence of events, the initial water level in the test was set at 283 inches, and the break opening was delayed to 138 seconds. One recirculation pump was tripped at 0.0 seconds and the other pump was tripped at 4 seconds because the two pumps in the TLTA have slightly different moment of inertia. With the bundle power decay started at 7 seconds, the system is at natural circulation conditions when the two breaks were opened at 138 seconds.

The main steam control valve was used as a pressure regulator in the test and was set to hold system pressure at 970 psia at the beginning of the transient event at time 0.0. After the breaks were opened at 138 seconds, the steam valve continued to regulate system pressure until it was completely closed at 166 seconds. The closure of the valve caused a slight pressure increase to about 1000 psia.

Activation of the ADS was delayed 120 seconds after steam valve closure as in typical BWR operations. Simultaneous with ADS activation, the break with diameter of 0.153 was closed; better simulate the water level transient. The opening of the ADS valve caused rapid depressurization and level swell inside and outside the shroud. The mixture level inside the shroud remained above the top of the bundle throughout the test and hence no bundle heatup was observed in the test. A mixture level was observed in the lower plenum indicating that flashing in the lower plenum contributed to holding up liquid in the bundle (counter-current flow limit (CCFL) at the side entry orifice (SEO)). Similarly there was CCFL at the bypass outlet indicated by a mixture level in the bypass with substantial liquid above in the mixing and upper plenum regions.

The LPCS and LPCI were activated on low system pressure signals at 435 and 445 seconds respectively. Shortly after injection, the levels started to increase and the liquid in the upper plenum became subcooled. The bypass filled at about 500 seconds and the upper plenum level started to increase steadily. This resulted in a higher hydrostatic head inside the shroud, which began to drive fluid out of the lower plenum through the jet pumps, and into the annulus region. The lower plenum level decreased further, eventually reaching the jet pump discharge elevation in the lower plenum at about 575 seconds. This allowed steam in the lower plenum to vent through the jet pumps. The availability of a new steam release path resulted in less steam flow at the SEO, changing the CCFL condition at the SEO, and allowing liquid drainage from the bundle into the lower plenum.

As the steam flow rate from the bundle decreased, the fluid in the upper plenum drained into the bundle. Fluid in the bundle started to become subcooled around 580 seconds. With continued delivery of subcooled water from the LPCS and LPCI systems, the fluid draining into the lower plenum became subcooled. This led to breakdown of CCFL at the SEO at about 610 seconds causing bulk drainage into the lower plenum and redistribution of fluid inventory in the regions inside the shroud. The system refill continued until the test was ended at 800 seconds.

The plots of some of the major parameters are compared to S-RELAP5 predictions in Figure 7-281 to Figure 7-297.

There is good agreement between the predicted break flow, Figure 7-281, and the measured flow presented in Figure D-8 of Reference 115.

The depressurization history and the small break LOCA scenario are mainly controlled by ADS timing and flow rate. The ADS valve discharge coefficient was set to match the ADS flow, Figure 7-282. Prediction of the measured ADS flow results in good pressure agreement after ADS opening, Figure 7-283, and ECC initiation timing and flow rates, Figure 7-284 and Figure 7-285. The predicted pressure rise following the steam line control valve closure at 165 s is larger than the measured rise.

Comparisons of the predicted and measured mass histories in different regions of the vessel are shown in Figure 7-286 to Figure 7-291. Generally, the trends of variation of mass inventory in all the regions are predicted well.

Comparison of the predicted and measured bundle temperature for different elevations and heater rods are shown in Figure 7-293 to Figure 7-297. There was no heat-up during this test; however, measured and calculated fuel temperatures are in good agreement. The thermal-hydraulic parameters for the TLTA small break test 6432-1 were predicted well.

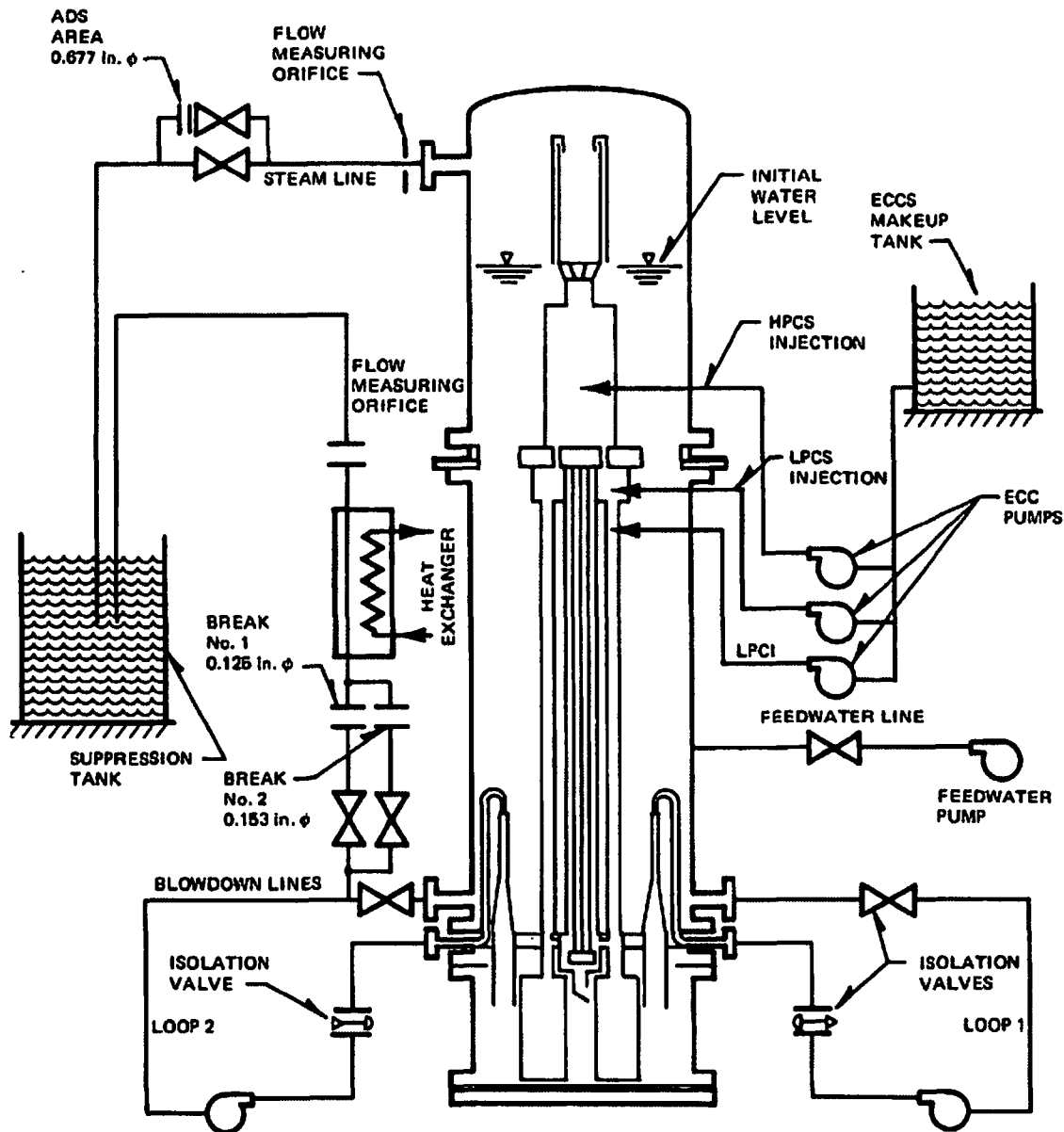


Figure 7-279 Schematic of TLTA Configuration 5C*

* Reproduced from Reference 115, Figure 3-4.



Figure 7-280 S-RELAP5 Nodalization of TLTA Configuration 5C



Figure 7-281 Predicted Total Break Flow Rate – TLTA Test 6432-1



Figure 7-282 Comparison of Predicted and Measured ADS Flow Rate – TLTA Test 6432-1



**Figure 7-283 Comparison of Predicted and Measured Steam
Dome Pressure-TLTA Test 6432-1**



**Figure 7-284 Comparison of Predicted and Measured LPCI
Flow Rate – TLTA Test 6432-1**



**Figure 7-285 Comparison of Predicted and Measured LPCS
Flow Rate – TLTA Test 6432-1**



**Figure 7-286 Comparison of Predicted and Measured Bundle
Mass – TLTA Test 6432-1**



**Figure 7-287 Comparison of Predicted and Measured Bypass
Mass – TLTA Test 6432-1**



**Figure 7-288 Comparison of Predicted and Measured Lower
Plenum Mass – TLTA Test 6432-1**



**Figure 7-289 Comparison of Predicted and Measured Upper
Plenum Mass – TLTA Test 6432-1**



**Figure 7-290 Comparison of Predicted and Measured
Annulus Mass – TLTA Test 6432-1**



**Figure 7-291 Comparison of Predicted and Measured Guide
Tube Mass – TLTA Test 6432-1**



**Figure 7-292 Comparison of Predicted and Measured Total
Vessel Mass – TLTA Test 6432-1**



**Figure 7-293 Comparison of Measured and Predicted Heater
Wall Temperatures, 10 inch Elevation – TLTA Test 6432-1**



**Figure 7-294 Comparison of Measured and Predicted Heater
Wall Temperatures, 63 inch Elevation – TLTA Test 6432-1**



**Figure 7-295 Comparison of Measured and Predicted Heater
Wall Temperatures, 103 inch Elevation – TLTA Test 6432-1**



**Figure 7-296 Comparison of Measured and Predicted Heater
Wall Temperatures, 120 inch Elevation – TLTA Test 6432-1**



**Figure 7-297 Comparison of Measured and Predicted Heater
Wall Temperatures, 143 inch Elevation – TLTA Test 6432-1**

7.7.3 FIST Integral Tests

The test results from the Full Integral Simulation Test (FIST) facility are used to assess the capability of S-RELAP5 to predict:

- System response and thermal hydraulic behavior during BWR LOCA scenarios in a scaled facility with full power capability,
- The important phenomena, sequence of events, inventory distribution, and thermal response of the heated bundle for a range of break sizes.

The FIST tests provide sufficient information for validating the capability of S-RELAP5 to predict several PIRT phenomena during transient conditions. Generally, separate effect tests will provide the data for direct assessment of the specific models in the code. However, integral test data generally can also be used to validate the capability of the code to predict certain phenomena, and more importantly, the interaction between these phenomena (models in the code) during the transient events. FIST test results are used to validate the PIRT phenomena listed below.

Assessed phenomena and processes

This section addresses the following highly ranked PIRT phenomena identified in Table 5-1;

Assessment conclusions

S-RELAP5 predicted the depressurization rate, heat-up initiation, ECC injection time and the heat-up rate fairly closely. The conservative heat transfer package in S-RELAP5 resulted in a later quench time and a higher PCT for the large and intermediate size break tests.

The major LOCA phenomena during the small break transient were predicted by S-RELAP5. The flow rates and mass accumulation in different regions were predicted satisfactorily. The hydraulic conditions predicted in the lower plenum and bundle resulted in larger liquid hold up (due to lower SEO drainage), later heat-up and earlier bundle quench. Therefore, predicted PCT was considerably lower. The small break test was repeated with the conservative Appendix K assumptions which are used for plant model simulation. The predicted PCT with Appendix K assumptions presented in Section 7.9.2.2 bounded the measured test

temperatures. This demonstrated the conservatism of the EM model with Appendix K assumptions.

S-RELAP5 predicted the LOCA scenario for the LPCI line break including the pressure, mass in different regions, and void fractions closely. The quench was predicted to occur later than measured, therefore PCT was predicted conservatively.

The BWR/4 large break LOCA test was simulated by modification of the available ECC systems and the corresponding injection points. The major phenomena and the measured data trends, as well as the event timings were predicted well by S-RELAP5. Bundle quench for the BWR/4 large break test occurs due to bottom flooding and the bundle stayed dry above the quench front. Data showed two-phase conditions with void fractions in the range of 60% to 70% at the quench time and the bundle remained voided even after quench.

Based on the above discussions it is concluded that S-RELAP5 is capable of predicting the system response and major LOCA phenomena. The input model nodalization and control systems are capable of simulating the FIST LOCA scenarios. The S-RELAP5 heat transfer package results in conservative prediction of PCT for large and intermediate size break tests. In addition, this validation demonstrated that the EM can adequately predict the dynamic system response and the interaction between different components during LOCA events.

Assessment description

The Full Integral Simulation Test (FIST) facility was cosponsored by the USNRC and industry. The FIST facility was designed for simulating large and small break LOCAs and operational transients in jet-pump BWRs. The FIST facility was a full height, 1/624 scale of a BWR/6 and contained one full sized electrically heated 8x8 test bundle. Three power levels with the same axial power shape were used to model low power, medium power, and high power rods. The distribution of different power rods in the bundle simulated the radial and azimuthal power profiles expected in a BWR. The test bundle also contained several prototypical BWR components including a fuel support piece and a Zircaloy fuel channel.

The facility had two external recirculation loops, two jet-pumps, and all other major nuclear steam supply system components. The recirculation lines in FIST facility were over-scaled and were isolated early in transient to limit the amount of liquid available for flashing. The large

recirculation line break tests utilized a blowdown line in the suction side (with a nozzle sized to the scaled recirculation line size) and a blowdown line in the discharge side with an orifice sized to represent the scaled jet pump nozzle. The small break tests utilized a different blowdown line connected to the recirculation suction line. The facility was also modified to run a LOCA test simulating a double ended break of a BWR/4 recirculation line.

The FIST facility contained one steam line and the steam discharge equipment consisted of a pressure control valve and five air-operated valves which were used to simulate a variety of steam line functions. The pressure control valve was used to maintain the steam dome pressure and also to simulate a MSIV or turbine stop valve. The FIST MSIV control could not simulate the gradual closing of an actual MSIV and a step closing (over 0.5 s) with a 2 seconds delay after the trip signal was employed.

The FIST feedwater supply system was designed mainly for obtaining the desired steady state conditions; it was not capable of simulating the BWR feedwater control or the gradual flow reduction. However, it was designed to supply the correct feedwater flow to the vessel prior to closure.

An extensive facility description (including scaling discussion) is provided in Reference 107, and test results are reported in References 108 and 109 for Phase 1 and Phase 2 of the program, respectively.

The nodalization and selected options used in S-RELAP5 for modeling FIST is consistent, as much as possible, with nodalization and model options used in plant analyses (summarized in Section 6.3.7). The S-RELAP5 FIST facility vessel nodalization is shown in Figure 7-298 and the broken recirculation loop is shown in Figure 7-299. In addition to the vessel, the recirculation loops, the single steam line, and all major heat structures in the vessel are included in the S-RELAP5 model. [

]

A consequence of the full height but volume scaled FIST facility is a narrow downcomer region that may affect two-phase flow behavior in the downcomer region and result in larger interfacial drag than would be experienced in a BWR.

In order to maintain the elevation and volume scaling, a large U-tube was used in the facility to model the lower plenum. A cross-piece was included in the facility (indicated by component 214 in Figure 7-298) to maintain a representative fluid transport path from the jet-pumps discharge to the core inlet. As described in the facility design documentation, this lower plenum distortion was a necessary approximation to maintain scaling.

The S-RELAP5 nodalization models the FIST facility, including the geometrical distortions discussed above. The comparison between the prediction and measurement demonstrate the capability of S-RELAP5 to predict the specified PIRT phenomena and the system interactions during the transient.

A diverse set of instrumentation was available in the tests, including absolute and differential pressure sensors, rod and fluid temperature measurements, and flow measurements based on differential pressure. In addition, void fraction measurements were made at four different elevations in the bundle using gamma densitometers in the phase II tests. The bundle power and feedwater flow during the transients were obtained from the test results and provided as boundary conditions to S-RELAP5.

Four FIST LOCA tests are simulated with S-RELAP5, the BWR/6 large recirculation line break test (6DBA1B), the BWR/6 small break test without HPCS (6SB2C), the BWR/6 LPCI line break test (6LB1A), and the BWR/4 large recirculation line break (4DBA1). The results from these simulations are summarized in the following subsections.

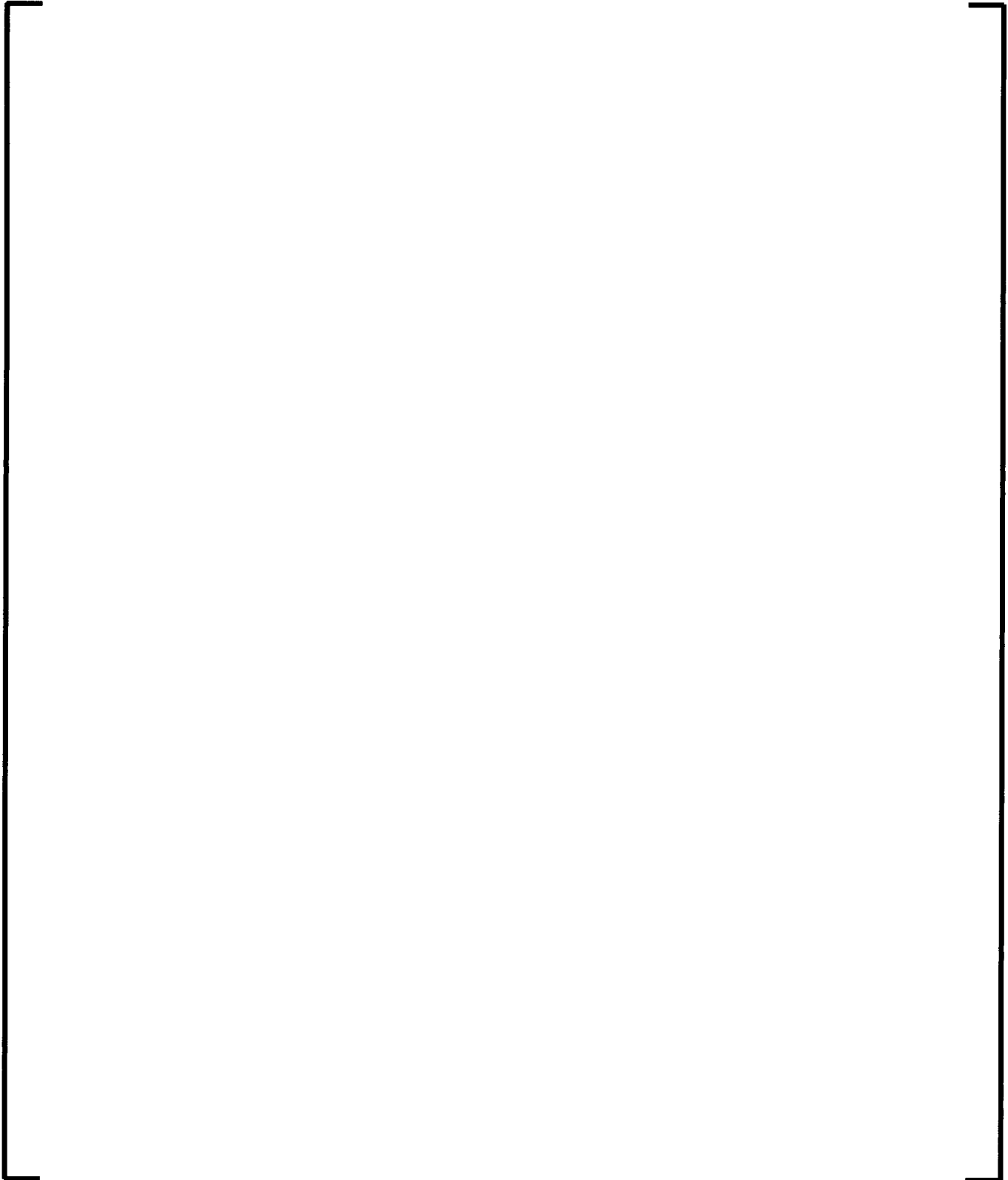


Figure 7-298 FIST Vessel Nodalization

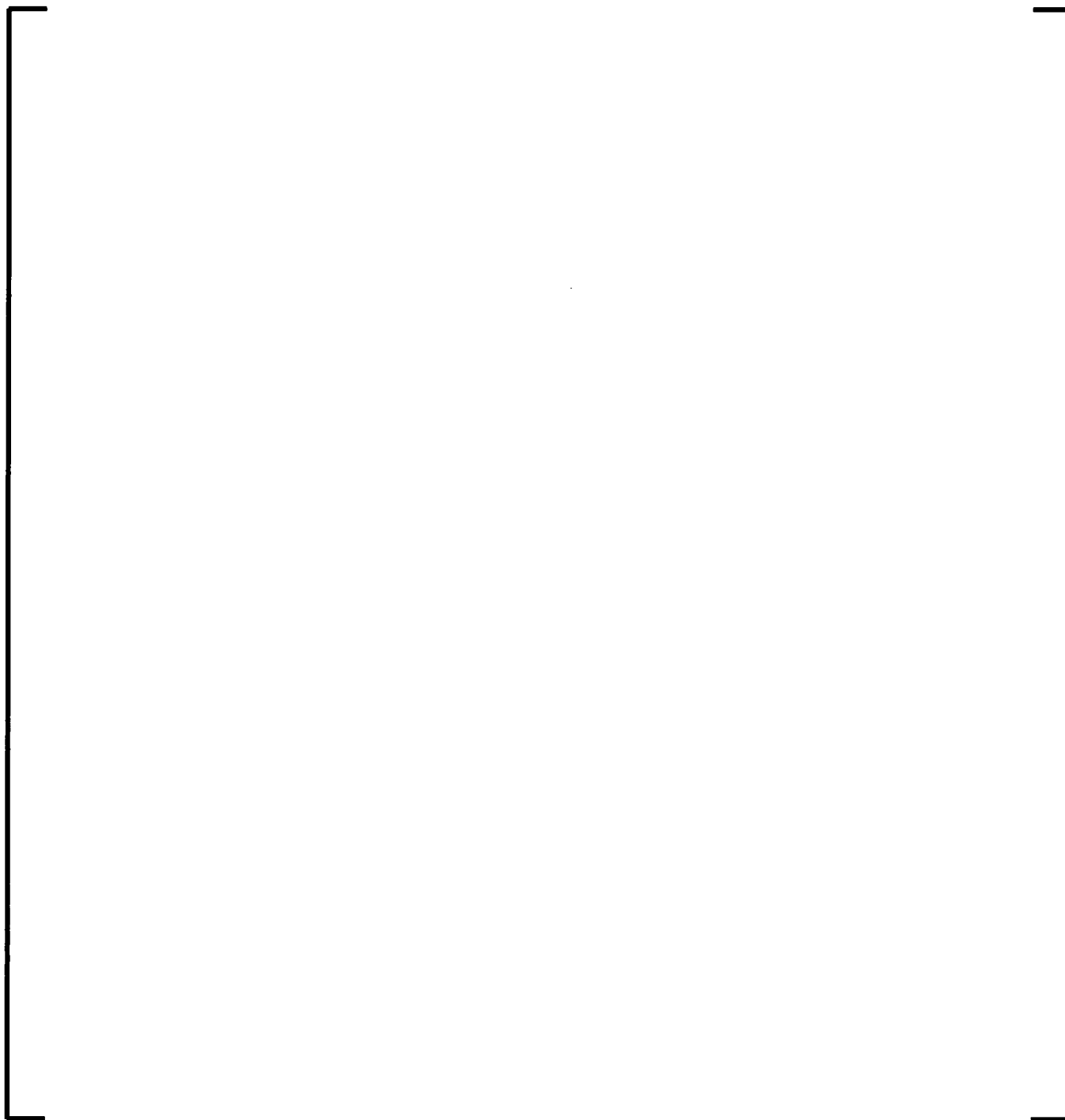


Figure 7-299 FIST Broken Recirculation Loop Nodalization

7.7.3.1 BWR/6 Large Break Test 6DBA1-B

Test description

The BWR/6 large break LOCA test 6DBA1 simulated a 2.23 ft² double ended guillotine break in one of the recirculation lines with a LPCI diesel generator failure. Therefore the available ECC systems were HPCS, LPCS, and one LPCI pump.

The initial conditions of the test are presented in Table 7-21 and are representative of the full power condition. The break is simulated by opening the suction and discharge blowdown valves at time zero. The major event timing is presented in Table 7-22.

The recirculation pumps and feedwater system were tripped at test initiation and the bundle power switched to a programmed decay power. ECC systems were initiated at time zero (on high drywell pressure). LPCI was injected into bypass, and LPCS and HPCS were injected into the upper plenum. The broken loop was isolated following the break and the intact loop was isolated early in the test to minimize the volume available for flashing. The rod temperature measurements show heat-up starting at around 40 s. The test was terminated at around 300 s by shutting the power and ECC flow off.

Comparison objectives

The assessment of test 6DBA1 demonstrates the capability of the EM to predict BWR transient response and phenomena that occur during a large break LOCA. In addition, the assessment demonstrates the conservatism of the heat transfer package by predicting a higher PCT and later quench.

Comparison details

The measured and predicted major event timing is presented in Table 7-22. The break in the suction and discharge lines open at time zero which results in reversal of flow in the broken loop jet pump and a sudden drop in core flow. The level in the downcomer drops due to loss of inventory until it reaches L1 level when the signal to close the MSIV and activate the ADS is given. Since the level drop to L1 is predicted approximately 3 s later than the reported time, MSIV closure and ADS valve opening times are predicted approximately 3 s later than the

reported values. ECC systems are initiated at time zero to simulate high drywell pressure signal. When the level reaches the break location and uncovers the break the depressurization rate increases due to two-phase discharge.

The steam dome pressure predicted by S-RELAP5 is in excellent agreement with the data, as shown in Figure 7-300 and Figure 7-301. The dynamic pressure responses predicted in other regions of the test facility were similar to steam dome response and also in good agreement with data. The depressurization rate is predicted well but delayed by about 3 s due to later break uncover. The rapid depressurization results in flashing within the vessel. Lower plenum flashing is reported to occur at 13.5 s. The predicted void fractions in the lower plenum, Figure 7-302, show lower plenum flashing to occur at around 14 s. Figure 7-303 shows the predicted and measured downcomer void fractions. The predicted break uncover occurs between 12 and 13 s while the measured void fractions show uncover between 8 and 10 s.

The predicted suction and discharge break flows are shown in Figure 7-304 and Figure 7-305. The break flow has not been directly measured for this test but good agreement with the predicted pressure in different regions of the vessel and the ADS flow, shown in Figure 7-306, confirm that the break flow prediction is satisfactory. The ECC injection initiation times are also predicted well due to the good pressure prediction.

The flow rates in different regions of vessel are shown in Figure 7-307 to Figure 7-311. The bundle inlet flow, Figure 7-307 and Figure 7-308, and the jet pump exit flow, Figure 7-309 to Figure 7-311, are predicted reasonably well.

The comparison of measured and predicted mass in different vessel regions are shown in Figure 7-312 to Figure 7-317, total vessel mass is obtained by summing the mass in different regions. Although the mass in different regions and the total mass are predicted reasonably well, the drainage from the upper plenum to the bundle is conservatively delayed. Figure 7-312 shows that following LPCS injection at around 70 s, the measured mass in the upper plenum accumulates until around 130 s when there is CCFL breakdown and intermittent drainage into the bundle and bypass. S-RELAP5 predicts small leakages into the bundle and bypass after ECC initiation but bundle mass accumulation does not start until 150 s with major drainage into the bundle at around 200 s. This is also shown by the measured void fractions at different

elevations in the bundle, Figure 7-318 to Figure 7-320. Generally, the void fractions in the bundle are predicted closely but quench is delayed.

The predicted bundle mid-point temperatures are compared to measured temperatures in Figure 7-321. Heat-up initiation time and the rate of heat-up are predicted very closely. S-RELAP5 predicts later quench and therefore higher PCT as shown in Figure 7-322. The measured PCT is 703°F at around 110 s, compared to a predicted PCT of 752°F at 137 s.

Figure 7-323 to Figure 7-325 show that the void fraction at different elevations in the bypass is predicted well by S-RELAP5. Measured data show that lower elevations stay voided for a longer period of time than predicted by S-RELAP5. This confirms that the upper plenum to bypass leakage phenomena is predicted by S-RELAP5. Figure 7-326 is the measured and predicted void fraction in the upper lower plenum and shows a nearly empty region until after the bundle quenches. This confirms that bundle quench in this transient is due to upper plenum and bypass leakage and not because of bottom flooding.

Result summary

[

]

Table 7-21 FIST Test 6DBA1 Initial Conditions

Bundle power (MW)	5.0
System pressure (psia)	1042.
Water Level (in)	556
Total core flow (lb/s)	42.35
Steam flow rate (lb/s)	5.89

[illegible]



Figure 7-300 Steam Dome Pressure – FIST Test 6DBA1



Figure 7-301 Steam Dome Pressure (to 50 sec) – FIST Test 6DBA1



Figure 7-302 Predicted Lower Plenum Void Fractions – FIST Test 6DBA1



Figure 7-303 Lower Downcomer Void Fraction – FIST Test 6DBA1



Figure 7-304 **Predicted Suction Side Break Flow Rate – FIST Test 6DBA1**



Figure 7-305 **Predicted Discharge Side Break Flow Rate – FIST Test 6DBA1**



Figure 7-306 ADS Flow – FIST Test 6DBA1



Figure 7-307 Core Inlet Flow Rate – FIST Test 6DBA1



Figure 7-308 Core Inlet Flow Rate (Expanded) – FIST Test 6DBA1



Figure 7-309 Jet Pump 1 Exit Flow Rate – FIST Test 6DBA1



Figure 7-310 Jet Pump 1 Exit Flow Rate (Expanded) – FIST Test 6DBA1

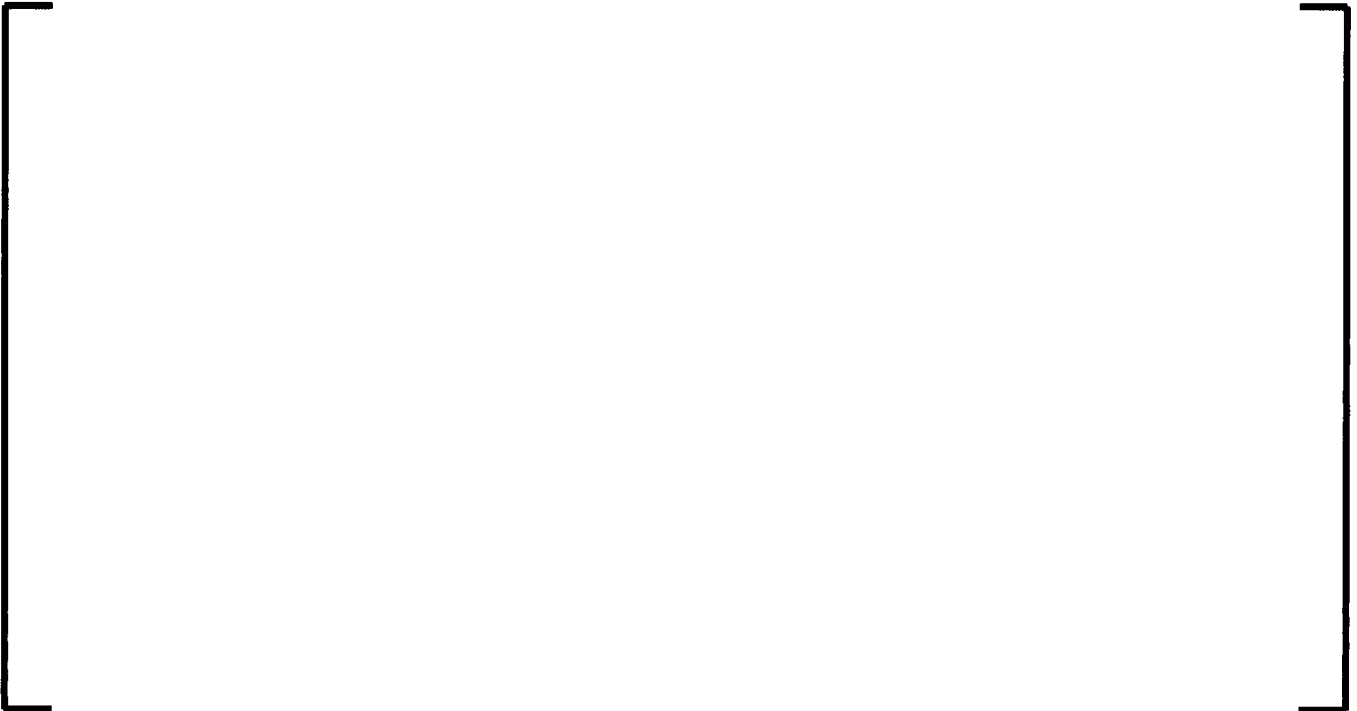


Figure 7-311 Jet Pump 2 Exit Flow Rate (Expanded) – FIST Test 6DBA1



Figure 7-312 Mass of Fluid in Upper Plenum – FIST Test 6DBA1



Figure 7-313 Mass of Fluid in Bypass – FIST Test 6DBA1



Figure 7-314 Mass of Fluid in Bundle – FIST Test 6DBA1



Figure 7-315 Mass of Fluid in Intact Loop Jet Pump – FIST Test 6DBA1



Figure 7-316 Mass of Fluid in Broken Loop Jet Pump – FIST Test 6DBA1



Figure 7-317 Total Mass of Fluid in the Vessel – FIST Test 6DBA1



Figure 7-318 Void Fraction in Bundle Near 37 in. Elevation – FIST Test 6DBA1



Figure 7-319 Void Fraction in Bundle Near 57 in. Elevation – FIST Test 6DBA1



Figure 7-320 Void Fraction in Bundle Near 117 in. Elevation – FIST Test 6DBA1



Figure 7-321 Heater Midpoint Elevation Surface Temperature – FIST Test 6DBA1



Figure 7-322 Peak Temperature Node History – FIST Test 6DBA1



Figure 7-323 Void Fraction in Bypass Near 37 in. Elevation – FIST Test 6DBA1



Figure 7-324 Void Fraction in Bypass Near 71 in. Elevation – FIST Test 6DBA1



Figure 7-325 Void Fraction in Bypass Near 117 in. Elevation – FIST Test 6DBA1



Figure 7-326 Void Fraction in Lower Plenum Upper – FIST Test 6DBA1

7.7.3.2 BWR/6 Small Break Test 6SB2C

Test description

The BWR/6 small break LOCA test 6SB2C simulated a 0.053 ft² break in one of the recirculation lines with an assumed failure of a diesel generator which results in loss of the HPCS pump. Therefore the available ECC systems were LPCS, and three LPCI pumps.

The initial conditions of the test are presented in Table 7-23 and are representative of the full power condition. The break is simulated by opening the small break blowdown valve at time zero. The major event timing is presented in Table 7-24.

The recirculation pumps were tripped and a programmed power and feedwater flow were activated at the initiation of the break. The power decay and feedwater flow were input in the simulation as boundary conditions.

The level initially drops until it reaches L1. The system pressure was maintained at nearly a constant value until MSIV closure. The loops were isolated early in the transient. ADS was activated 120 s after L1.

LPCS and LPCI are initiated on high drywell pressure (assumed to occur at time zero) with 35 s delay but the ECC flow does not start until the pressure falls below the shut off head. LPCI is injected into the bypass, and LPCS is injected into the upper plenum. The rod temperature measurements show heat-up starting at around 250 s.

Comparison objectives

Comparison to test 6SB2C demonstrates the capability of the EM to predict BWR transient response and phenomena that occur during a small break LOCA. It demonstrates the capability of S-RELAP5 in predicting the interaction of important LOCA phenomena, and therefore major parameters, during a small break LOCA scenario. In addition as shown in Section 7.9.2.2, it demonstrates the conservatism of the EM by predicting a higher PCT and later rewetting when Appendix K conservatism is implemented.

Comparison details

Plots of major parameters are compared to S-RELAP5 predictions in Figure 7-327 to Figure 7-357.

The pressure histories in different regions of the vessel are shown in Figure 7-327 to Figure 7-330. As long as the start of depressurization (ADS timing) is correct, S-RELAP5 predicts the pressure very closely. There is small overprediction of pressure between 250 s and 350 s, and a small underprediction between 350 s and 450 s. The predicted depressurization rate depends on the break and ADS flow rates. Close agreement in the depressurization rate confirms that the discharge flows have been predicted by S-RELAP5. Figure 7-331 shows that the ADS flow is accurately predicted by S-RELAP5.

Figure 7-332 to Figure 7-334 show that the pressure drop in different regions of the vessel is predicted closely by S-RELAP5. The mass in different regions are based on pressure drops and are therefore predicted well, Figure 7-335 to Figure 7-342. The difference in the bundle mass shown in Figure 7-335 is believed to be due to different densities used to calculate the masses. Mass measurements are based on pressure drop and estimated region density and as shown in Figure 7-332, the initial pressure drop across the bundle is predicted accurately. The variation of total mass in the system, Figure 7-341, is closely predicted by S-RELAP5.

The upper plenum mass variation shown in Figure 7-342 is predicted well and can be explained by the predicted bundle and bypass flow to the upper plenum, Figure 7-343. Initially fluid flows from the bundle and bypass into the upper plenum. At around 20 s, direction of flow to the bypass changes and the flow is from the upper plenum to the bypass while the bundle flow to the upper plenum decreases. At around 100 s, the flow from the bundle to the upper plenum becomes less than flow from the upper plenum to the bypass and upper plenum mass decreases until the upper plenum is empty at around 170 s. The flow into the bypass from below also goes to zero. The measured mass shows the same trend but levels off at a higher upper plenum mass. This is also believed to be due to errors in upper plenum density used in data reduction because it is unlikely to hold the mass at a constant value (other than empty or zero mass) for such a long period. After ADS opening and flashing in the vessel, there is flow into upper plenum and this process is repeated again between 200 and 350 s.

The predicted bundle void fractions at different elevations are compared to the measured data in Figure 7-344 to Figure 7-346. The measured data shows that the bundle is almost empty at around 250 s, S-RELAP5 predictions show that the bundle dries out later and quenches earlier, therefore it stays dry for a shorter period of time. The predicted void fractions at 37 in. elevation, Figure 7-344, show two-phase conditions except for a short period at around 350 s. As mentioned earlier, the upper plenum is empty during this period, Figure 7-342, and there is no flow into the bundle from above, Figure 7-343. There is minimal leakage flow from the bypass into the bundle, Figure 7-347, therefore the bundle condition should be controlled by the differences in inlet flows, shown in Figure 7-348 and expanded in Figure 7-349. The measured data show that flow from the lower plenum to the bundle stops at around 200 s, there are fluctuating flow conditions between 200 and 300 s, typical of CCFL breakdown and bundle drainage. At around 300 s there is significant drainage which results in an empty bundle at around 320 s, Figure 7-335. S-RELAP5 predictions show flow into the bundle from the lower plenum between 200 and 250 s and no drainage until around 350 s. The comparison of void fractions in the upper section of the lower plenum, Figure 7-350, confirms that a level is formed in the lower plenum and the upper sections are empty after 200s, while S-RELAP5 shows two-phase conditions in the upper lower plenum until around 350 s. It seems that bundle drainage starts when a level is formed in the lower plenum and entrance to the bundle becomes all steam.

The predicted bundle hydraulic conditions impact the temperature as shown in Figure 7-351. Although the initial heat-up rates are comparable, S-RELAP5 predicts later and shorter bundle heat-up, resulting in a much lower PCT. Nearly equal heat-up rate indicates that the S-RELAP5 post-CHF heat transfer coefficients are predicting the correct heat loss but the hydraulic conditions are not matching test data.

The average of measured and predicted midpoint temperatures are shown in Figure 7-352. S-RELAP5 predicts a reduced heat-up rate later in the transient and quench at around 380 s. The measured average temperature rises faster and quenches around 410 s, resulting in a higher peak temperature. S-RELAP5 predictions show the highest temperature at 96" elevation while the measured PCT occurs at 77". The comparison of the highest measured and the highest predicted temperature, Figure 7-353, shows a measured PCT of 925° F compared to a predicted temperature of 655°F.

Bypass void fractions are predicted well at higher elevations but show a shorter dry period at lower elevations, Figure 7-354 to Figure 7-356. Figure 7-357 shows the predicted and measured upper plenum liquid temperature. S-RELAP5 enhanced condensation model prevents subcooling of the liquid until the liquid starts accumulating in the upper plenum after 400 s and covers the LPCS injection point.

Result summary

[

]

Table 7-23 FIST Test 6SB2C Initial Conditions

Bundle power (MW)	5.0
System pressure (psia)	1049.
Water Level (in)	554
Total core flow (lb/s)	42.53*
Steam flow rate (lb/s)	5.76

$$*19.64 \text{ (JP1)} + 22.89 \text{ (JP2)} = 42.53 \text{ lb/s}$$

Table 7-24 Predicted Major Event Timing for FIST 6SB2C with L1 Calculated from ΔP

[illegible]



Figure 7-327 Upper Plenum Pressure – FIST Test 6SB2C



Figure 7-328 Lower Plenum Pressure – FIST Test 6SB2C



Figure 7-329 Bundle Pressure – FIST Test 6SB2C



Figure 7-330 Steam Line Pressure – FIST Test 6SB2C



**Figure 7-331 Measured and Predicted ADS Flow
Rates – FIST Test 6SB2C**



Figure 7-332 Bundle Pressure Drop – FIST Test 6SB2C



Figure 7-333 Bypass Pressure Drop – FIST Test 6SB2C



**Figure 7-334 Total Downcomer Pressure Drop – FIST Test
6SB2C**



Figure 7-335 **Mass of Fluid in Bundle – FIST Test 6SB2C**



Figure 7-336 **Mass of Fluid in Bypass – FIST Test 6SB2C**



**Figure 7-337 Mass of Fluid in Intact Loop Jet
Pump – FIST Test 6SB2C**



**Figure 7-338 Mass of Fluid in Broken Loop Jet
Pump – FIST Test 6SB2C**



**Figure 7-339 Mass of Fluid in Lower Plenum
above Jet Pump Exit – FIST Test 6SB2C**



**Figure 7-340 Mass of Fluid in Lower Plenum
below Jet Pump Exit – FIST Test 6SB2C**



Figure 7-341 Total Fluid Mass in Vessel – FIST Test 6SB2C



Figure 7-342 Mass of Fluid in Upper Plenum – FIST Test 6SB2C



**Figure 7-343 Predicted Bundle and Bypass to Upper Plenum
Flow Rate – FIST Test 6SB2C**



Figure 7-344 Void Fraction in Bundle near 37” Elevation – FIST Test 6SB2C



**Figure 7-345 Void Fraction in Bundle near 57" Elevation –
FIST Test 6SB2C**



Figure 7-346 Void Fraction in Bundle near 117" Elevation – FIST Test 6SB2C



**Figure 7-347 Predicted Bundle to Bypass Leakage
Flow Rate – FIST Test 6SB2C**



Figure 7-348 Bundle Inlet Flow Rate – FIST Test 6SB2C



Figure 7-349 **Bundle Inlet Flow Rate (Expanded) –
FIST Test 6SB2C**



Figure 7-350 **Lower Plenum (Upper Section) Void
Fraction – FIST Test 6SB2C**



Figure 7-351 Heater Midpoint Temperature – FIST Test 6SB2C



**Figure 7-352 Heater Midpoint Average
Temperature – FIST Test 6SB2C**



Figure 7-353 Peak Temperature Node History – FIST Test 6SB2C



Figure 7-354 Void Fraction in Bypass near 37” Elevation – FIST Test 6SB2C



Figure 7-355 Void Fraction in Bypass near 71" Elevation – FIST Test 6SB2C



Figure 7-356 Void Fraction in Bypass near 117" Elevation – FIST Test 6SB2C



**Figure 7-357 Upper Plenum Liquid and Saturation
Temperature – FIST Test 6SB2C**

7.7.3.3 BWR/6 LPCI Line Break Test 6LB1

Test description

The LPCI Line Break LOCA test 6LB1 simulated a full size break of one of the LPCI lines (0.34 ft²) in a BWR/6. HPCS is assumed to be unavailable; therefore, the available ECC systems were LPCS and two LPCI pumps.

The initial conditions of the test are presented in Table 7-25 and are representative of full power operation. The break is simulated by opening a blowdown valve at time zero. The major event timing is presented in Table 7-26.

The recirculation pumps were tripped and a programmed power and feedwater flow were activated at the initiation of the break. The power decay and feedwater flow were input in the simulation as boundary conditions.

The level initially drops until it reaches L1. The system pressure was maintained at nearly a constant value until MSIV closure. The loops were isolated early in the transient. ADS was activated 120 s after L1.

LPCS and LPCI are initiated on high drywell pressure (assumed to occur at time zero) with 35 s delay but the ECC flow does not start until the pressure falls below the shut off head. LPCI is injected into the bypass, and LPCS is injected into the upper plenum. The rod temperature measurements show heat-up starting at around 175 s.

Comparison objectives

Comparison to test 6LB1 demonstrates the capability of the EM to predict BWR transient response and phenomena that occur during a LOCA. It demonstrates the capability of S-RELAP5 in predicting the interaction of important LOCA phenomena, and therefore major parameters, during a LOCA scenario. In addition it demonstrates the conservatism of the EM by predicting a higher PCT and later quench than the test measurements.

Comparison details

Plots of major parameters are compared to S-RELAP5 predictions in Figure 7-358 to Figure 7-391.

The predicted steam dome pressure during this transient and an expanded pressure plot are shown in Figure 7-358 and Figure 7-359. The pressure is kept nearly constant prior to MSIV closure. The predicted bypass void fraction at the elevation of the LPCI line connection, Figure 7-360, shows that the break uncovers at around 35 s and recovers at around 250 s. The measured void fraction shown in Figure 7-360 is at 326" elevation, 25" below the LPCI connection elevation. Figure 7-361 shows the measured and predicted lower plenum void fractions close to jet pump exit elevation. The reported time of 66 s for lower plenum flashing seems to correspond to the time of major void generation on the bundle side at 124" elevation. The predicted void fractions in all the lower plenum nodes, Figure 7-362, show S-RELAP5 lower plenum flashing occurs at around 62 s.

The ECC signal is given on L1 but LPCS and LPCI start when the steam dome pressure drops to the corresponding pressure permissive. Figure 7-363 shows that LPCS and LPCI are initiated at around the same time. The measured pressure is predicted closely around the LPCS and LPCI shut-off head, 200 to 220 s, Figure 7-358. Therefore, the ECC initiation time is predicted closely. However, the pressure is slightly underpredicted after 220 seconds so the predicted ECC flows are larger. Reference 109 has reported a jet pump uncover time of 227 s and a recovery time of 350 s. The measured and predicted void fractions at the jet pump exits, shown in Figure 7-364, agree reasonably well and show an uncover time of 130 s and recovery time of 250 s.

The pressure in different regions of the vessel are shown in Figure 7-365 to Figure 7-368. The trend of the pressure history and the major events are predicted well. There is a pressure rise following MSIV closure at 15 s followed by a depressurization after break uncover at around 35 s. The slope of the depressurization changes at around 62 s when there is major flashing in the vessel followed by a significant depressurization after ADS opening at around 128 s. The predicted depressurization rate in this period is smaller than measured because of larger predicted void fractions in the bypass (Figure 7-365) and therefore smaller break flow. The opposite trend is shown between 220 s and 250 s, when the predicted bypass void is lower and

the depressurization rate is higher. The predicted and measured pressure curves are nearly parallel for the remainder of the transient.

Steam flow and ADS flow rates are predicted well by S-RELAP5, Figure 7-369 and Figure 7-370. The ADS valve opens 6 seconds later than the reported time because of the delay in reaching L1. Good agreement between predicted and measured ADS flow rates confirm the capability of S-RELAP5 critical flow model for two-phase conditions (with the discharge coefficient used).

Figure 7-371 to Figure 7-373 show the predicted and measured void fractions at different elevations in the bundle. The void fractions at all elevations are predicted fairly closely until bundle quench occurs between 250 s and 300 s.

The pressure drop and mass inventory in the bundle, Figure 7-374 and Figure 7-375, show the same trend. Bundle pressure drop and mass inventory are predicted very closely until around 250 s, beyond which S-RELAP5 underpredicts the mass in the bundle. As mentioned earlier, the deviation in predicting the initial mass is believed to be due to densities used to calculate mass from the measured pressure drop, which is predicted well by S-RELAP5.

The void fractions in the bypass, Figure 7-376 to Figure 7-378, show that void is underpredicted early in the transient. The predicted pressure drop in the bypass, Figure 7-379, confirms this trend. The mass histories in the bypass and other regions of the vessel and the total inventory are predicted well, Figure 7-380 to Figure 7-386.

The measured and predicted bundle midpoint temperatures are shown in Figure 7-387. S-RELAP5 predicts the heat-up rate but quench is predicted to occur later and the maximum midpoint temperature is higher. The PCT for this transient is obtained at 269 s for 97" elevation and is 635 °F, Figure 7-388. S-RELAP5 predicted PCT is 674 °F at 293 s and is for 102" elevation. Figure 7-383 and Figure 7-384 show that the upper plenum and lower plenum regions above the jet pump are nearly empty around the time of bundle quench and there is no flow into the bundle from the lower plenum, Figure 7-388. The bundle is draining after 230 s. Therefore, quench for this transient is controlled by bypass to bundle leakage rate. S-RELAP5 predictions show a continuous increase in bypass to bundle leakage rate after 220 s, Figure 7-389.

Figure 7-391 shows the predicted and measured upper plenum liquid temperatures. Since the upper plenum remains nearly empty and the core spray location does not get covered until after 300 s, the S-RELAP5 enhanced condensation model prevents subcooling of the liquid as shown in Figure 7-391.

Result summary

[

]

Table 7-25FIST Test 6LB1 Initial Conditions

Bundle power (MW)	4.65
System pressure (psia)	1042.
Water Level (in)	556.5
Total core flow (lb/s)	39.78
Steam flow rate (lb/s)	5.545

Table 7-26 Measured and Predicted Major Event Timing for FIST 6LB1





Figure 7-358 Steam Dome Pressure History – FIST Test 6LB1



Figure 7-359 Steam Dome Pressure History (Expanded) – FIST Test 6LB1



**Figure 7-360 Bypass Void Fraction at LPCI Line
Elevation – FIST Test 6LB1**



**Figure 7-361 Lower Plenum Void Fraction near Jet
Pump Exit – FIST Test 6LB1**



**Figure 7-360 Bypass Void Fraction at LPCI Line
Elevation – FIST Test 6LB1**



**Figure 7-361 Lower Plenum Void Fraction near Jet
Pump Exit – FIST Test 6LB1**

**Figure 7-362 Predicted Void Fractions in all Lower
Plenum Nodes – FIST Test 6LB1**

Figure 7-363 LPCS and LPCI Flow Rates – FIST Test 6LB1



Figure 7-364 Void Fraction at Jet Pump Exit – FIST Test 6LB1



Figure 7-365 Upper Plenum Pressure History – FIST Test 6LB1



Figure 7-366 Lower Plenum Pressure History – FIST Test 6LB1



Figure 7-367 Bundle Pressure History – FIST Test 6LB1



Figure 7-368 Steam Line Pressure History – FIST Test 6LB1



Figure 7-369 Steam Line Flow Rate – FIST Test 6LB1



Figure 7-370 ADS Flow Rate – FIST Test 6LB1



Figure 7-371 Void in Bundle at 37” Elevation – FIST Test 6LB1



Figure 7-372 Void in Bundle at 57" Elevation – FIST Test 6LB1



Figure 7-373 Void in Bundle at 117" Elevation – FIST Test 6LB1



Figure 7-374 Bundle Pressure Drop – FIST Test 6LB1



Figure 7-375 Mass of Fluid in Bundle – FIST Test 6LB1



Figure 7-376 Void in Bypass at 37" Elevation – FIST Test 6LB1



Figure 7-377 Void in Bypass at 71" Elevation – FIST Test 6LB1

Figure 7-378 Void in Bypass at 117" Elevation – FIST Test 6LB1

Figure 7-379 Bypass Pressure Drop – FIST Test 6LB1



Figure 7-380 Mass of Fluid in Bypass – FIST Test 6LB1



Figure 7-381 Broken Loop Jet Pump Mass – FIST Test 6LB1



Figure 7-382 Intact Loop Jet Pump Mass – FIST Test 6LB1



Figure 7-383 Mass of Lower Plenum Above Jet Pump Exit – FIST Test 6LB1



Figure 7-384 Mass of Lower Plenum Below Jet Pump Exit – FIST Test 6LB1



Figure 7-385 Upper Plenum Mass – FIST Test 6LB1



Figure 7-386 Total Mass in Vessel – FIST Test 6LB1



Figure 7-387 Heater Midpoint Surface Temperature – FIST Test 6LB1



Figure 7-388 Peak Temperature Node History – FIST Test 6LB1



Figure 7-389 Bundle to Bypass Leakage Rate – FIST Test 6LB1



Figure 7-390 Bundle Inlet Flow Rate – FIST Test 6LB1



Figure 7-391 Liquid Temperature in Upper Plenum Node 1 – FIST Test 6LB1

7.7.3.4 BWR/4 Large Break Test 4DBA1

Test description

The BWR/4 large break LOCA test 4DBA1 simulated the conditions in the peak power bundle of a BWR/4 following a 5.33 ft² double ended guillotine break in one of the recirculation lines with a LPCI diesel generator failure. The available ECC systems were one HPCI, one LPCS, and one LPCI pumps.

The initial conditions of the test are presented in Table 7-27 and are representative of the full power condition. The break is simulated by opening the suction and discharge blowdown valves at time zero. The major event timing is presented in Table 7-28.

The recirculation pumps and feedwater system were tripped at test initiation and the bundle power switched to programmed decay power. ECC systems were initiated at time zero (on high drywell pressure). The broken loop was isolated following the break and the intact loop was isolated early in the test to minimize the volume available for flashing. HPCI injected into feedwater line and LPCI injected into the intact loop drive line. The rod temperature measurements show heat-up starting at around 30 s.

Comparison objectives

Comparison to test 4DBA1 demonstrates the capability of the EM to predict BWR transient response and phenomena that occur during a large break LOCA. It demonstrates the capability of S-RELAP5 in predicting the interaction of important LOCA phenomena, and therefore major parameters, during a large break LOCA scenario. In addition, it demonstrates the conservatism of the heat transfer package by predicting a higher PCT and later quench.

Comparison details

Plots of major parameters are compared to S-RELAP5 predictions in Figure 7-392 to Figure 7-421.

The predicted steam dome pressures are shown in Figure 7-392 and Figure 7-393. The pressure is maintained nearly constant during the test until break uncover at 4.0 s. The predicted pressure rises after the MSIV starts to close and then drops at around 3 s when two

phase conditions are predicted at the node containing the recirculation suction line entrance. The comparison of the predicted and measured lower downcomer void fraction in the vicinity of the recirculation suction line is shown in Figure 7-394 and Figure 7-395. There is a gradual increase in void and the pressure starts decreasing as soon as two-phase conditions are generated at around 3 s.

Measured and predicted void fractions in the lower plenum, Figure 7-396 and Figure 7-397, show the predicted lower plenum flashing for most of the nodes occur around 6 s which is nearly the same as the reported flashing time. ECC systems are initiated at 30 s followed by a larger depressurization rate compared to measured pressure. The measured and predicted void fractions at the break, Figure 7-394, show an all steam condition at the time of ECC injection. The reason for a larger predicted depressurization rate at the time of ECC injection could be due to larger void collapse predicted by S-RELAP5. The larger predicted depressurization rate due to void collapse results in lower predicted pressures between 30 s and 100 s.

The predicted and measured void fractions in the upper section of lower plenum region, Figure 7-398, show that the reported time of lower plenum refill corresponds to the time when two-phase conditions are measured near the top of the lower plenum. S-RELAP5 predicts the lower plenum void fraction in the first 100 s very closely but shows complete filling of the lower plenum with liquid at around 140 s. Measured void fractions show that the lower plenum is full of liquid at around 320s. The predicted void fraction at the bundle entrance, Figure 7-399, shows the lower plenum refilling and two-phase flow reaching into the fuel support piece at approximately 80 s.

Figure 7-400 compares the measured and predicted ECC flows. All ECC systems start after 30 s delay, HPCI stops when the system pressure drops to 110 psi.

The pressure in different vessel regions are shown in Figure 7-401 to Figure 7-404. The pressure histories shown are similar to the steam dome pressure, and with the exception of the period between 30 s and 100 s, are predicted well.

Quench for this transient is from the bottom up. S-RELAP5 predicts the lower plenum refills mainly from LPCI injection into the bundle and quenches the bundle as it advances upward.

Data shows a similar trend but the bundle quenches much earlier with two-phase flow prior to the single-phase liquid front advancing up in the bundle.

Figure 7-405 and Figure 7-406 show the fluid mass in the lower plenum below and above the jet pump exit, respectively. S-RELAP5 predictions show that the lower plenum below the jet pump exit starts refilling around 40 s and is completely full at 80 s. The data shows the lower plenum below the jet pump to be full at around 130 s. The lower plenum above the jet pump exit starts filling around 50 s and is completely full at 130 s. Data shows this region to be full at around 190 s. The total mass in the lower plenum regions after filling up is different between measured and predicted. S-RELAP5 shows higher mass after leveling off. This can be explained by the differences in void fraction in the lower plenum. S-RELAP5 predicts single-phase liquid after filling up while data shows a voided region at higher elevations in lower plenum until much later in the transient.

Test data and S-RELAP5 predictions show that the broken loop jet pump is empty at around 30 s. S-RELAP5 predicts the broken loop jet pump fills up around 110 s, Figure 7-407, while test data shows more gradual filling until 170 s. Figure 7-408 shows that the intact loop jet pump is drained at around 35 s and fills up very quickly. Test data shows fluctuating intact loop mass measurements after it starts filling up at around 40 s.

The predicted bundle void fraction at different elevations, Figure 7-409 to Figure 7-412, show the liquid level advancing along the bundle (dropping the void fraction to zero) while the data shows void fractions drop to around 60% to 70% and remain voided for a long period. The bundle mass history shown in Figure 7-413 confirms the trend of void predictions, i.e. smaller predicted mass in the bundle between 50 s and 100 s, and larger predicted mass in the bundle after 100 s.

The comparison of the predicted and measured heater surface temperatures at approximately 36 inch elevation and midpoint of bundle are shown in Figure 7-414 and Figure 7-415.

S-RELAP5 predictions show quench when the liquid level reaches the specific elevation, while data shows quench at 70 s for 33 inch and 90-100 s for 77 inch with highly voided bundle conditions. The midpoint temperature is overpredicted by S-RELAP5 because the bundle stays dry longer. The predicted PCT is conservative for this test compared to the measured PCT.

The measured temperatures show a PCT of 960°F at 128" elevation while the highest predicted

temperature is 1015°F and occurred at 102" bundle elevation. The comparison of the measured and predicted temperature for the highest temperature locations are shown in Figure 7-416.

Comparison of the predicted and measured mass of fluid in the bypass and upper plenum are shown in Figure 7-417 and Figure 7-418. The total mass in the vessel is shown in Figure 7-419. Although the overall trend is satisfactory, the total mass between 100 s and 200s is overpredicted by S-RELAP5. Examination of the mass histories and void fractions in different regions show that S-RELAP5 is predicting a complete void collapse in the lower plenum and a single-phase liquid level rising up the bundle/bypass. Data shows a voided lower plenum following ECC injection with two-phase flow into the jet pump and bundle. Quench during the test occurs due to two-phase flow up into the bundle before it is single-phase liquid. This behavior could be due to the predicted interfacial heat transfer by S-RELAP5. If the LPCI flow injected in the recirculation line stays in non-equilibrium and enters the lower plenum subcooled, then it can contribute to void collapse and formation of a liquid level in lower plenum.

The measured steam line flow rate, Figure 7-420, shows that the flow is nearly zero around 220 s while the ADS valve is open, Figure 7-421. ADS flow is predicted well; therefore, it is believed that the zero measured steam flow is incorrect.

Result summary

[

]

Table 7-27 FIST Test 4DBA1 Initial Conditions

Bundle power (MW)	6.09
System pressure (psia)	1020.
Water Level (in)	563
Total core flow (lb/s)	38.48*
Steam flow rate (lb/s)	7.16

*18.65 (JP1) + 19.83 (JP2) = 38.48 lb/s





Figure 7-392 Steam Dome Pressure History – FIST Test 4DBA1



Figure 7-393 Steam Dome Pressure (Expanded) – FIST Test 4DBA1



Figure 7-394 Lower Downcomer Void Fraction – FIST Test 4DBA1



Figure 7-395 Lower Downcomer Void Fraction (Expanded) – FIST Test 4DBA1



Figure 7-396 Void Fraction in Lower Plenum in Vicinity of Jet Pump Exit – FIST Test 4DBA1



Figure 7-397 Predicted Lower Plenum Void Fractions – FIST Test 4DBA1



**Figure 7-398 Void Fractions in Lower Plenum Above Jet
Pump Exit – FIST Test 4DBA1**



**Figure 7-399 Predicted Void Fractions in Fuel Support and
Bundle Node 1– FIST Test 4DBA1**



Figure 7-400 ECC Flow Rates – FIST Test 4DBA1



Figure 7-401 Upper Plenum Pressure – FIST Test 4DBA1



Figure 7-402 Lower Plenum Pressure – FIST Test 4DBA1



Figure 7-403 Bundle Exit Pressure – FIST Test 4DBA1



Figure 7-404 Steam Line Pressure – FIST Test 4DBA1



**Figure 7-405 Mass of Lower Plenum below Jet
Pump Exit – FIST Test 4DBA1**



**Figure 7-406 Mass of Lower Plenum above Jet
Pump Exit – FIST Test 4DBA1**



Figure 7-407 Broken Loop Jet Pump Mass – FIST Test 4DBA1



Figure 7-408 Intact Loop Jet Pump Mass – FIST Test 4DBA1



Figure 7-409 Void in Bundle near 37 inch Elevation – FIST Test 4DBA1



Figure 7-410 Void in Bundle near 57 inch Elevation – FIST Test 4DBA1



Figure 7-411 Void in Bundle near 77 inch Elevation – FIST Test 4DBA1



Figure 7-412 Void in Bundle near 117 inch Elevation – FIST Test 4DBA1



Figure 7-413 Mass of Fluid in Bundle – FIST Test 4DBA1



Figure 7-414 Heater Surface Temperature near 36 inch Elevation – FIST Test 4DBA1



Figure 7-415 Heater Surface Midpoint Temperature – FIST Test 4DBA1

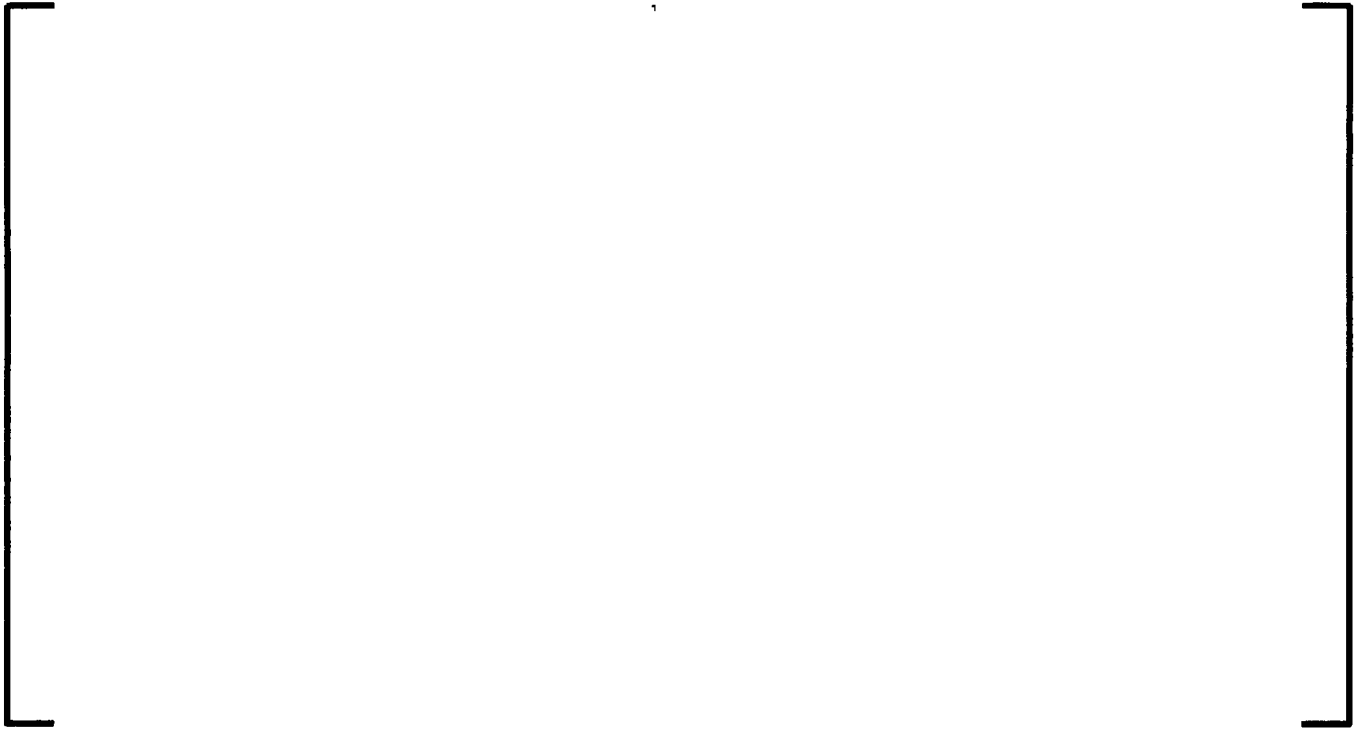


Figure 7-416 Peak Temperature Node History – FIST Test 4DBA1



Figure 7-417 Mass of Fluid in Bypass – FIST Test 4DBA1



Figure 7-418 Mass of Fluid in Upper Plenum – FIST Test 4DBA1



Figure 7-419 Total Mass in Vessel – FIST Test 4DBA1



Figure 7-420 Steam Line Flow Rate – FIST Test 4DBA1



Figure 7-421 ADS Flow Rate – FIST Test 4DBA1

7.7.4 BWR/4 Baseline Analyses

The ability of the AURORA-B LOCA EM to model system interactions is demonstrated in this section for a typical BWR/4 plant. The results are representative of how the EM is applied in licensing calculations, and provides a baseline analysis for subsequent parametric sensitivity evaluations in EMDAP Step 20.

Plant Parameters

Table 7-29 provides a summary of reactor initial conditions used in the BWR/4 sample problem. Table 7-30 lists selected reactor system parameters. The analysis is performed for a full core of ATRIUM-10 fuel. The key ATRIUM-10 fuel parameters used in the analysis are summarized in Table 7-31.

Table 7-32 through Table 7-35 provides the important ECCS characteristics assumed in the analysis. The ECCS is modeled as fill junctions connected to the appropriate reactor locations: LPCS injects into the upper plenum, HPCI injects into the upper downcomer, and LPCI injects into the recirculation lines.

The flow through each ECCS valve is determined based on system pressure and valve position. Flow versus pressure for a fully open valve is obtained by linearly interpolating the pump capacity data provided in Table 7-32 - Table 7-34. No credit for ECCS flow is assumed until ECCS pumps reach rated speed.

The ADS valves are modeled as a junction connecting the reactor steam line to the suppression pool. The flow through the ADS valves is calculated based on pressure and valve flow characteristics. The valve flow characteristics are determined such that the calculated flow is equal to the rated capacity at the reference pressure shown in Table 7-35.

In the AREVA LOCA analysis model, ECCS initiation is assumed to occur when the water level drops to the applicable level setpoint. No credit is assumed for the start of HPCI, LPCS, or LPCI due to high drywell pressure. [

]

Single Failure

The single failures and the available ECCS for each failure assumed in this analysis are summarized in Table 7-36.

Sample Problem Breaks

Recirculation line break analyses are performed for breaks in both the discharge and suction side of the recirculation pump. Two break types (geometries) are considered for the recirculation line break. The two types are the double-ended guillotine (DEG) break and the split break.

Sample Problem Analysis Results



Table 7-29 BWR/4 Initial Conditions

Reactor power (% of rated)	102 EPU
Total core flow (% of rated)	108
Reactor power (MWt)	4031
Total core flow (Mlb/hr)	108
Steam flow rate (Mlb/hr)	16.93
Steam dome pressure (psia)	1054.1
Core inlet enthalpy (Btu/lb)	523.8
[
Axial power shape	Figure 7-422
]	

Table 7-30 BWR/4 Reactor System Parameters

Parameter	Value
Vessel ID (in)	254
Number of fuel assemblies	764
Recirculation suction pipe area (ft ²)	3.503
1.0 DEG suction break area (ft ²)	7.007
Recirculation discharge pipe area (ft ²)	3.503
1.0 DEG discharge break area (ft ²)	7.007

The image consists of a solid white rectangular area enclosed within a thick, black, L-shaped frame. The frame is composed of two perpendicular segments: one running vertically along the left edge and another running horizontally along the top edge, meeting at a right angle in the upper-left corner. The interior of the frame is entirely white and devoid of any markings or text.

Table 7-32 BWR/4 High-Pressure Coolant Injection Parameters

Parameter	Value
Coolant temperature (°F)	100
<i>Initiating Signals and Setpoints</i>	
Water level*	L2 (457.5 in)
<i>Time Delays</i>	
Startup time, sec	1.0
Delay to startup, sec	34.0
<i>Delivered Flow Rate Versus Pressure</i>	
Vessel to Drywell ΔP (psid)	Flow Rate (gpm)
0	0
128	0
165	4500
1120	4500

* Relative to vessel zero.

Table 7-33 BWR/4 Low-Pressure Coolant Core Spray Parameters

Parameter	Value	
Reactor pressure permissive for opening valves (psig)	400	
Coolant temperature (°F)	120	
Initiating Signals and Setpoints		
Water level*	L1 (366.5 in)	
Time Delays		
Diesel generator start time, sec	25.1	
Diesel generator power at pump, sec	11.5	
LPCI pump at rated speed, sec	3.5	
Start opening injection valves, sec	9.0	
LPCI injection valve stroke time, sec	19.0	
Delivered Flow Rate Versus Pressure		
Vessel to Drywell ΔP (psid)	Flow Rate (gpm)	
	2 Loops	1 Loop
0.0	13,770.0	6,885.0
186.0	8,430.0	4,215.0
223.0	6,630.0	3,315.0
283.0	2,290.0	1,145.0
303.0	0.0	0.0

* Relative to vessel zero.

Table 7-34 BWR/4 Low-Pressure Coolant Injection Parameters

Parameter	Value	
Reactor pressure permissive for opening valves (psig)	400	
Coolant temperature (°F)	120	
Initiating Signals and Setpoints		
Water level*	L1 (366.5 in)	
Time Delays		
Diesel generator start time, sec	25.1	
Diesel generator power at pump, sec	40.0	
LPCI pump at rated speed, sec	7.5	
Start opening injection valves, sec	9.0	
LPCI injection valve stroke time, sec	24.0	
Delivered Flow Rate Versus Pressure		
Vessel to Drywell ΔP (psid)	Flow Rate (gpm)	
	2 Pumps Into 1 Loop	1 Pump Into 1 Loop
0.0	19,307.0	11,347.0
152.0	12,422.0	---
177.0	---	6420.0
230.0	6,283.0	---
237.0	---	2971.0
270.0	---	0.0
272.0	0.0	0.0

* Relative to vessel zero.

**Table 7-35 BWR/4 Automatic Depressurization
System Parameters**

Parameter	Value
Number of valves installed	6
Number of valves available	5
Flow capacity of available valves (Mlbm/hr at psig)	4.0 at 1,125
<i>Initiating Signals and Setpoints</i>	
Water level*	L1 (366.5 in)
<i>Time Delays</i>	
ADS timer, sec	120

* Relative to vessel zero.

Table 7-36 BWR/4 ECCS Single Failure

Assumed Failure	Systems Remaining	
	Recirculation Suction Break	Recirculation Discharge Break
Battery (SF-BATT)	ADS, 1 LPCS, 3 LPCI*	ADS, 1 LPCS, 1 LPCI
Opposite unit false LOCA signal (SF-LOCA)	ADS, HPCI, 1 LPCS, 2 LPCI†	ADS, HPCI, 1 LPCS, 1 LPCI
LPCI injection valve (SF-LPCI)	ADS, HPCI, 2 LPCS, 2 LPCI‡	ADS, HPCI, 2 LPCS

* Two LPCI pumps into broken loop. One LPCI pump into intact loop.

† One LPCI pump into broken loop. One LPCI pump into intact loop.

‡ Two LPCI pumps into broken loop.

**Table 7-40 Results for Highest PCT for Example BWR/4
Recirculation Line Break
0.10 ft² Split Pump Discharge SF-BATT
Top-Peaked Axial**

**Table 7-41 Event Times for Example BWR/4
Small Recirculation Line Break
0.1 ft² Split Pump Discharge SF-BATT
Mid-Peaked Axial**

Event	Time (sec)
Initiate break, loss of offsite power	
Initiate MSIV closure	
Initiate scram (MSIV < 85% open)	
MSIV fully closed	
L2 low water level, HPCI signaled	
HPCI flow starts	
L1 low water level, DG signaled	
DG power at ESS bus	
LPCI pumps start	
LPCS pump starts	
ADS valve starts to open	
LPCI valves start to open	
LPCI flow starts	
LPCS valve starts to open	
LPCS flow starts	
RDIV closure starts	
Begin rated spray	
RDIV closure complete	
PCT	
Bypass reflood	

**Table 7-42 Results for Example BWR/4
 Large Recirculation Line Break
 1.0 DEG Pump Suction SF-LOCA
 Mid-Peaked Axial**

--	--

**Table 7-43 Event Times for Example BWR/4
Large Recirculation Line Break
1.0 DEG Pump Suction SF-LOCA
Mid-Peaked Axial**

Event	Time (sec)
Initiate break, loss of offsite power	
Initiate MSIV closure	
Initiate scram (MSIV < 85% open)	
MSIV fully closed	
L2 low water level, HPCI signaled	
L1 low water level, DG signaled	
DG power at ESS bus	
LPCI pumps start	
RDIV closure starts	
HPCI flow starts	
LPCI valves start to open	
LPCI flow starts	
LPCS valve starts to open	
LPCS pump starts	
LPCS flow starts	
Begin rated spray	
RDIV closure complete	
ADS valve starts to open	
PCT	
Bypass reflood	



Figure 7-422 BWR/4 Axial Power Distributions

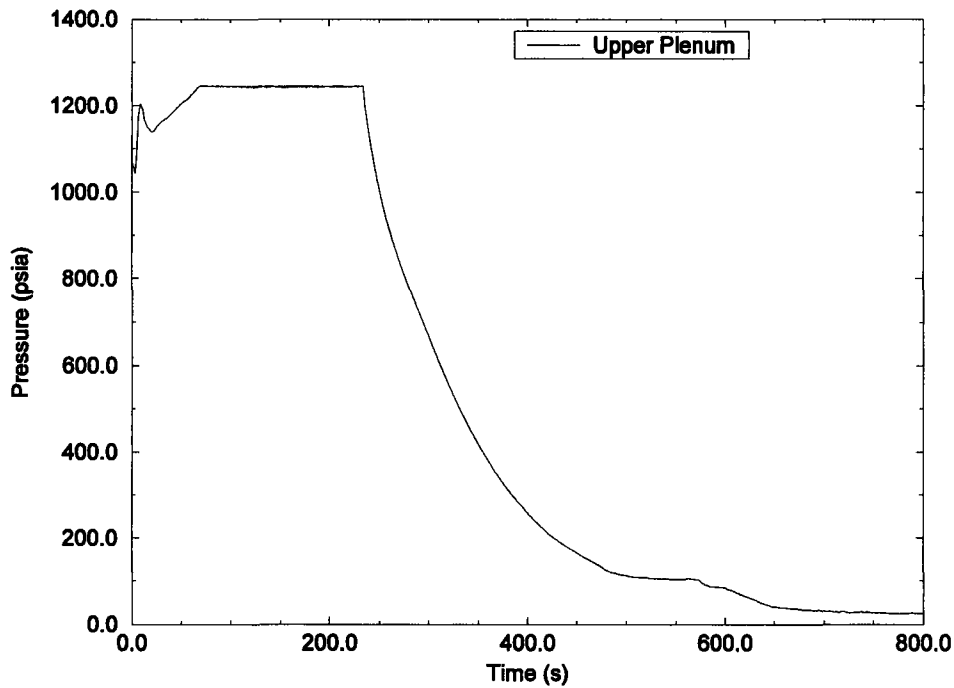


Figure 7-423 BWR/4 SBA Upper Plenum Pressure

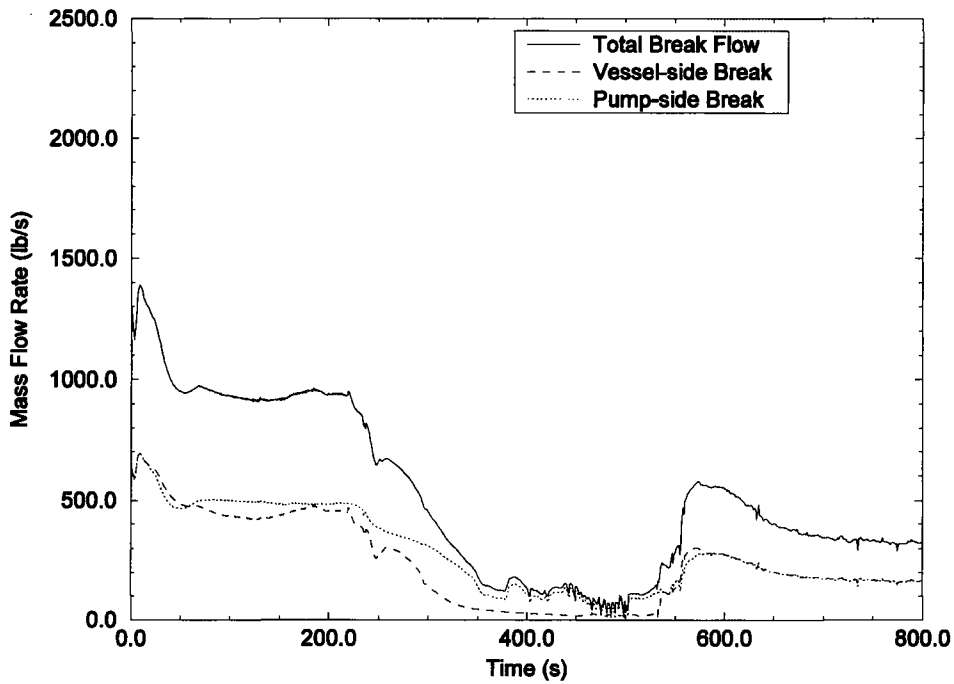


Figure 7-424 BWR/4 SBA Break Flow Rate

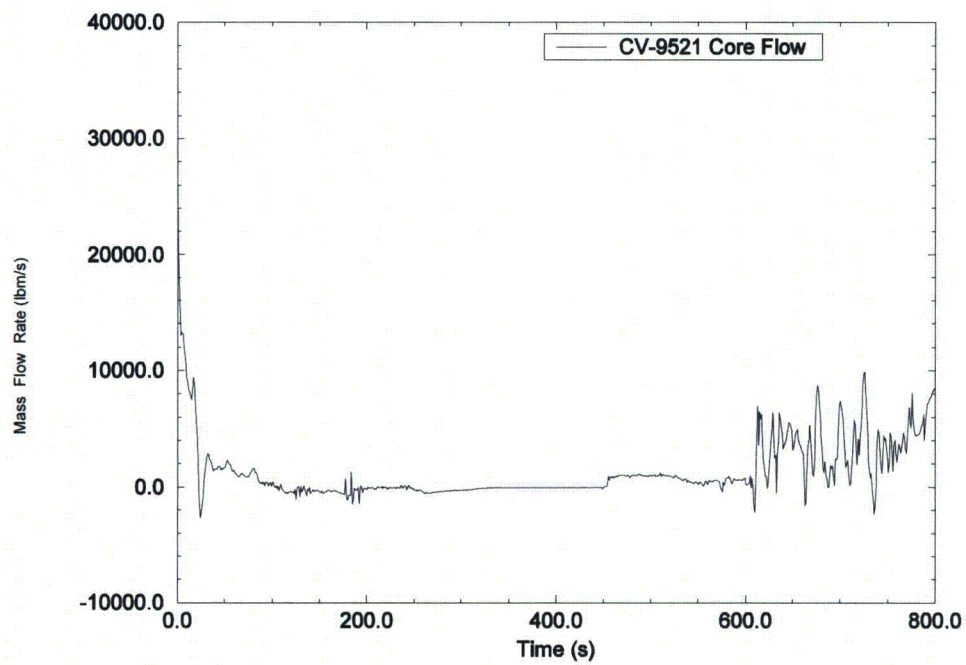


Figure 7-425 BWR/4 SBA Total Jet Pump Flow

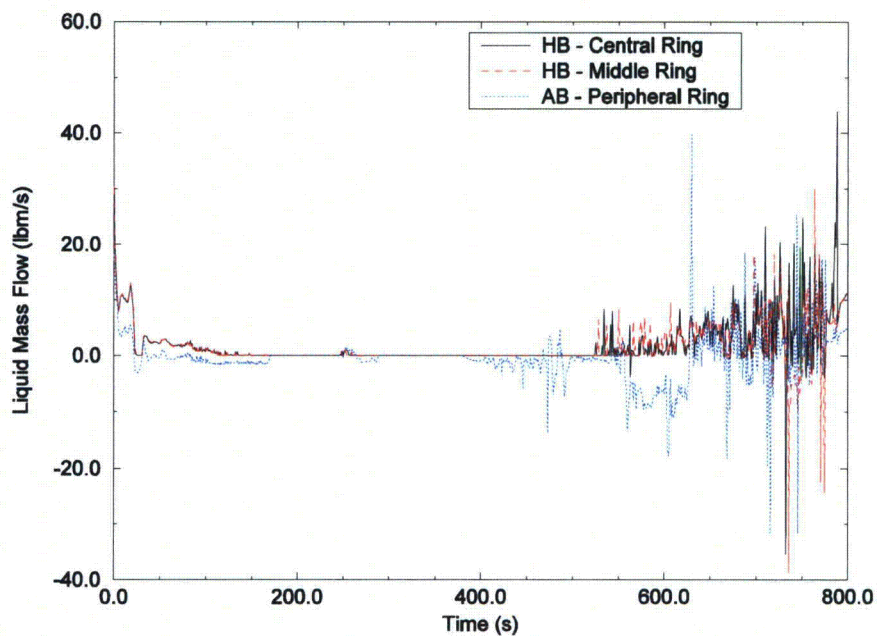


Figure 7-426 BWR/4 SBA Core Outlet Flow

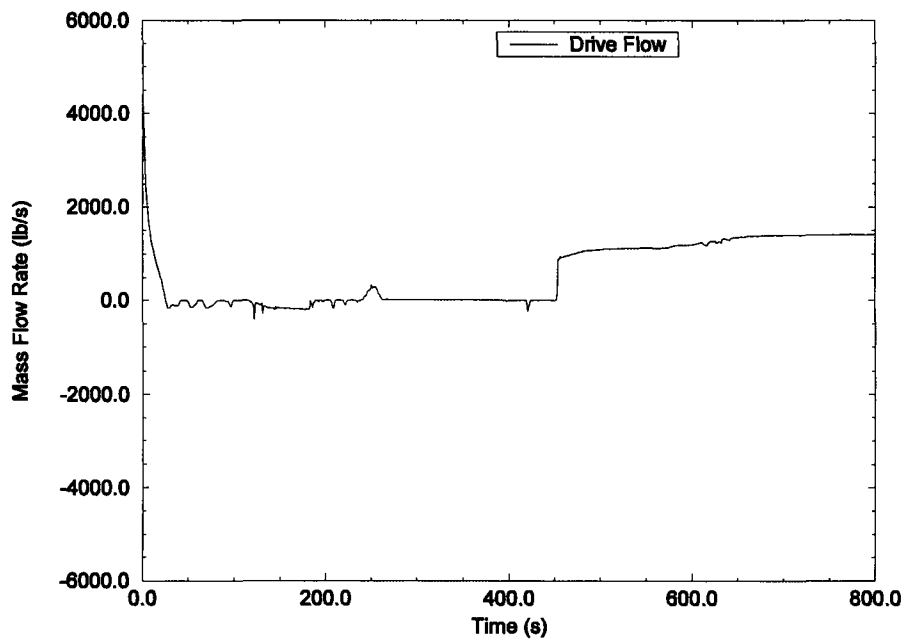


Figure 7-427 BWR/4 SBA Intact Loop Jet Pump Drive Flow

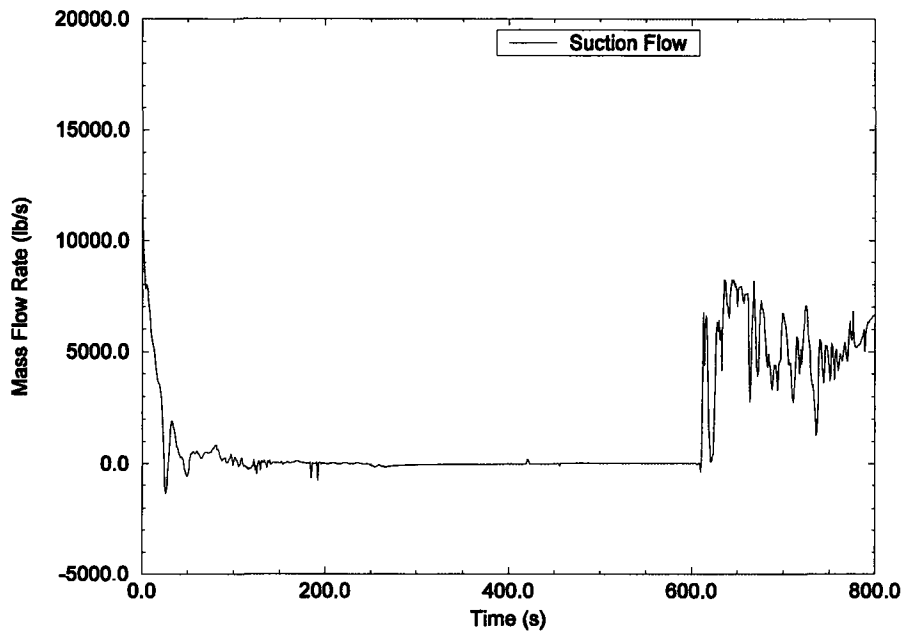


Figure 7-428 BWR/4 SBA Intact Loop Jet Pump Suction Flow

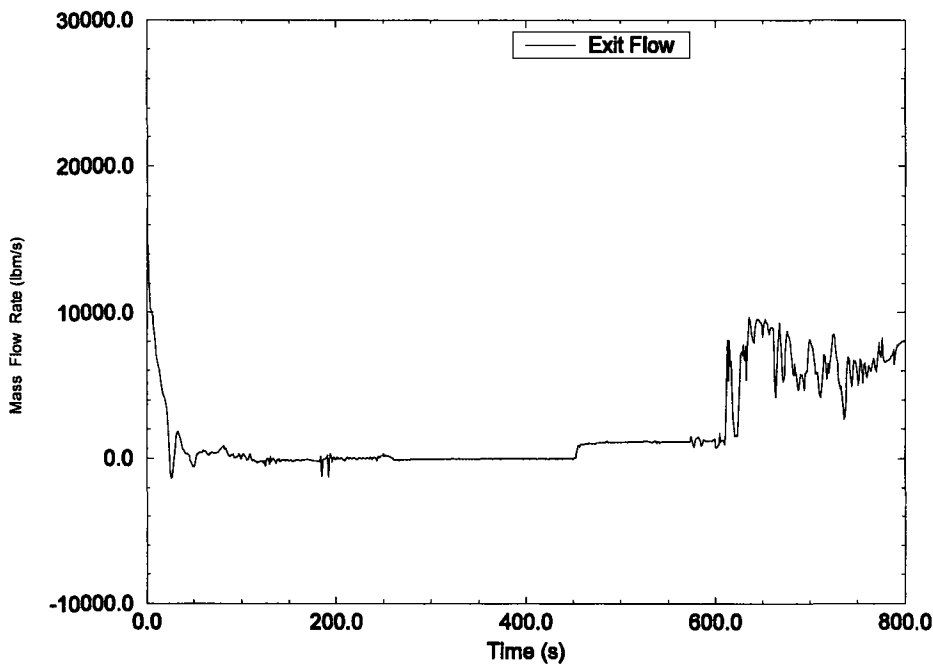


Figure 7-429 BWR/4 SBA Intact Loop Jet Pump Exit Flow

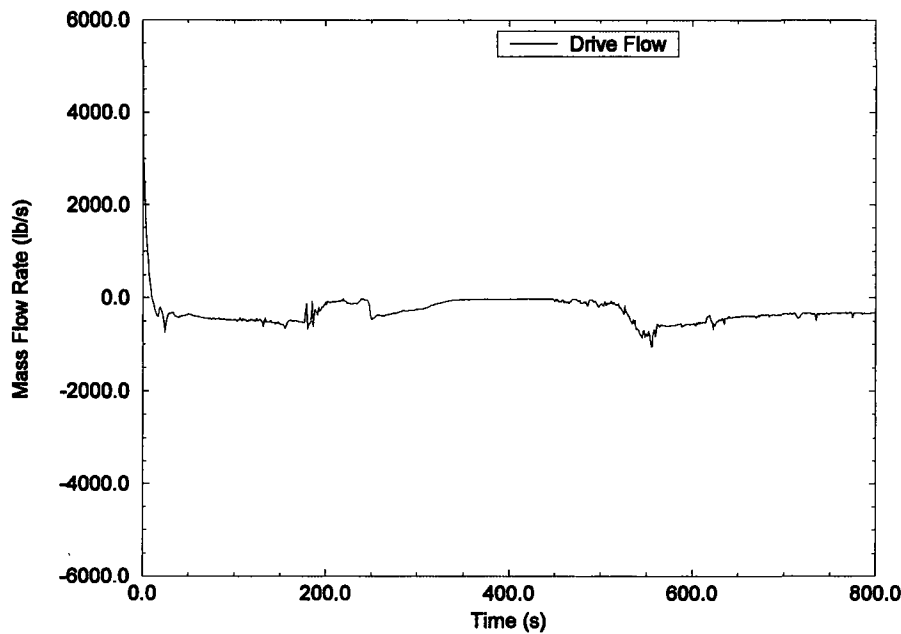


Figure 7-430 BWR/4 SBA Broken Loop Jet Pump Drive Flow

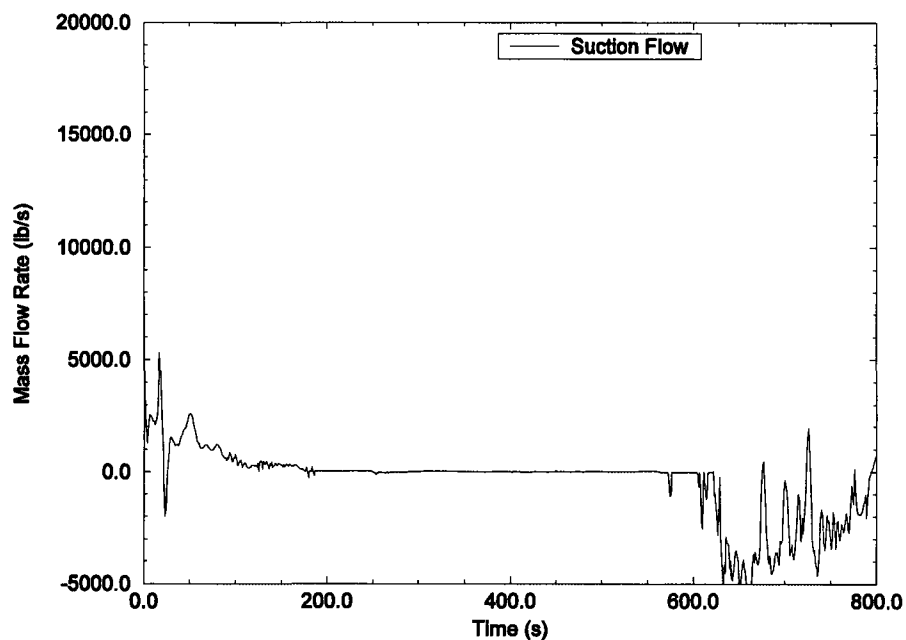


Figure 7-431 BWR/4 SBA Broken Loop Jet Pump Suction Flow

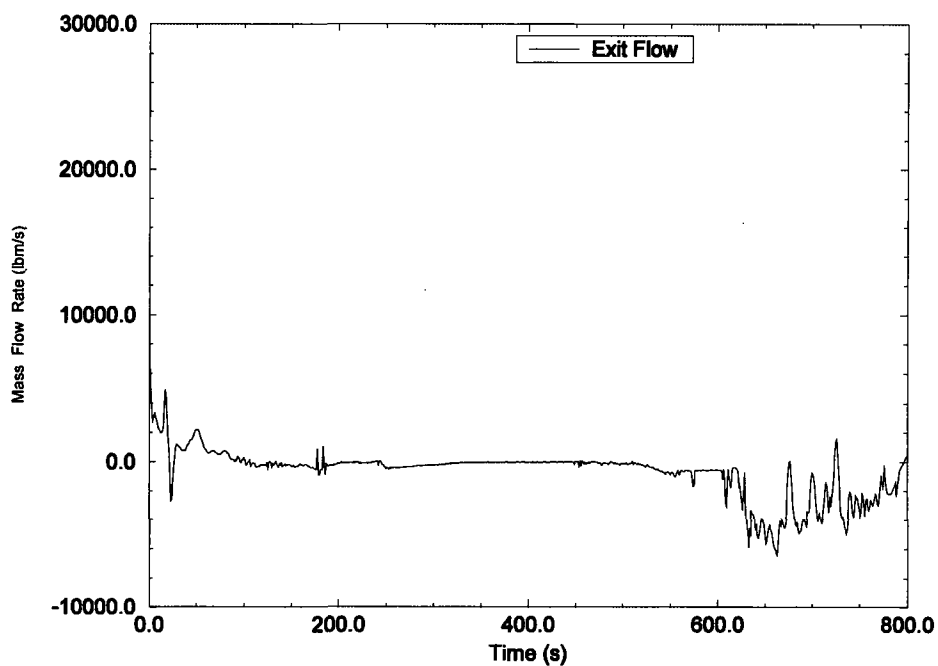


Figure 7-432 BWR/4 SBA Broken Loop Jet Pump Exit Flow

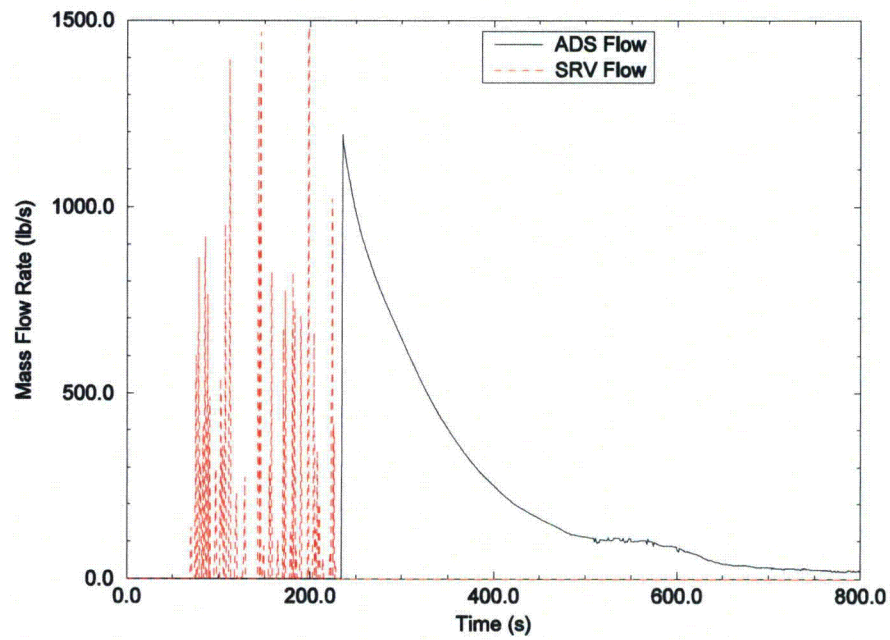


Figure 7-433 BWR/4 SBA ADS/SRV Flows

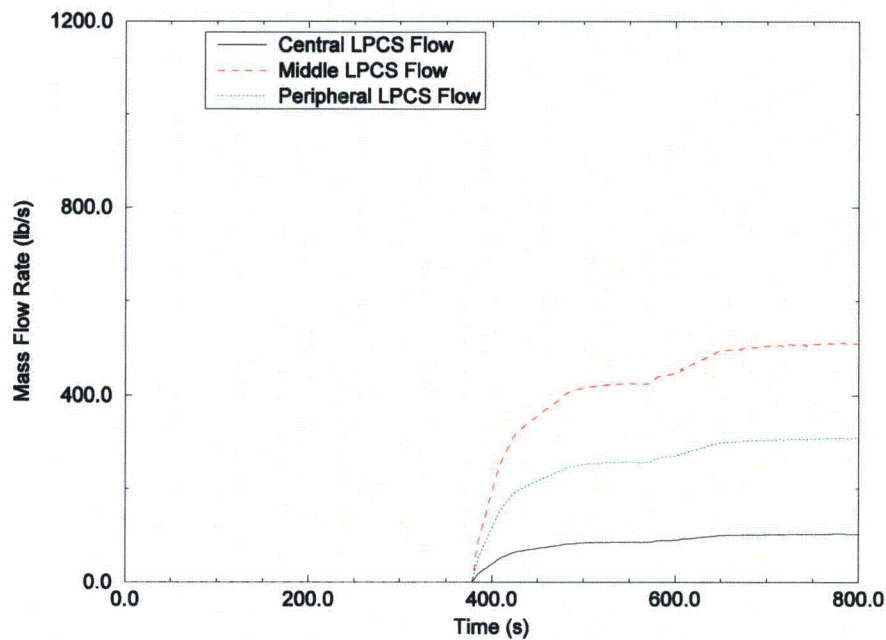


Figure 7-434 BWR/4 SBA LPCS Flow

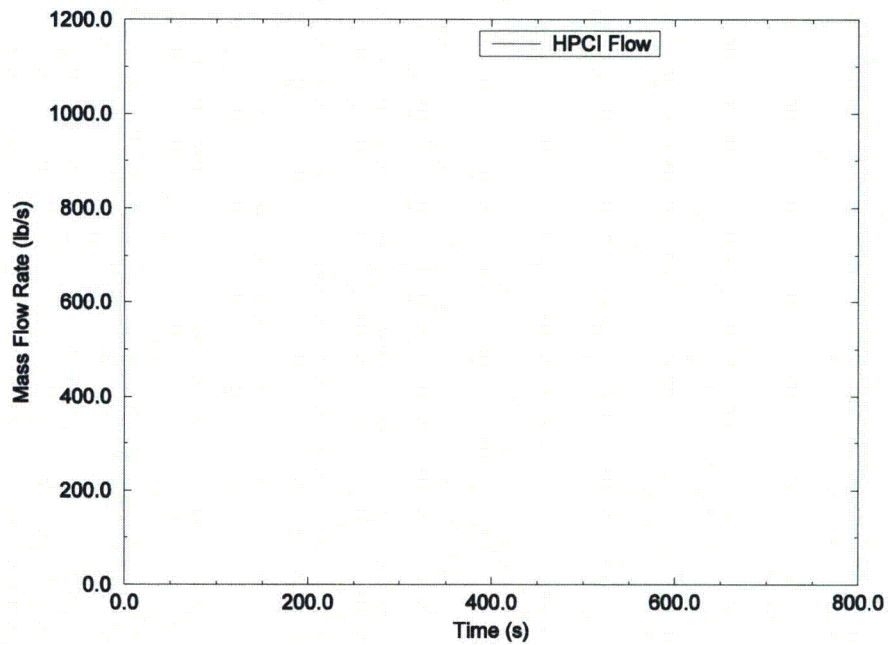


Figure 7-435 BWR/4 SBA HPCI Flow

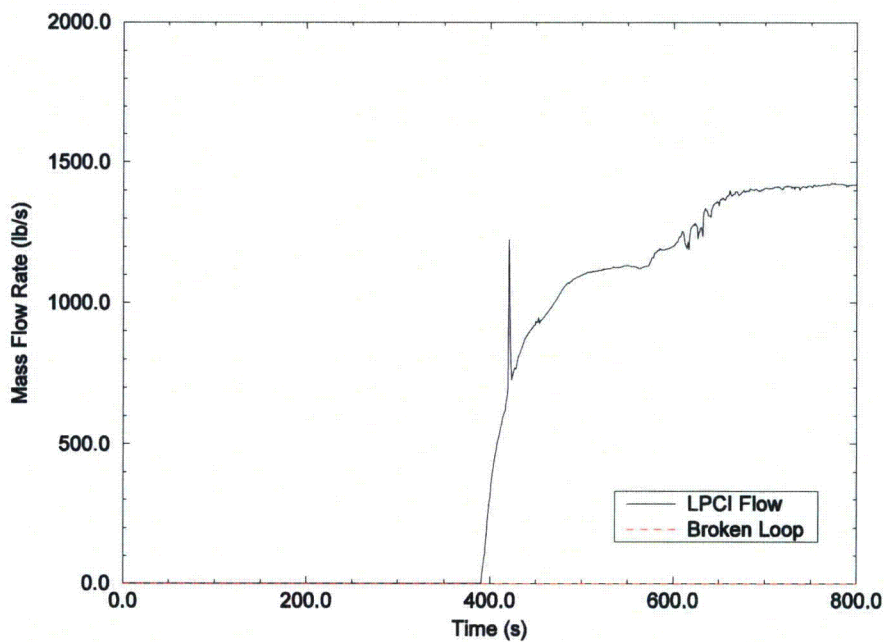


Figure 7-436 BWR/4 SBA LPCI Flow

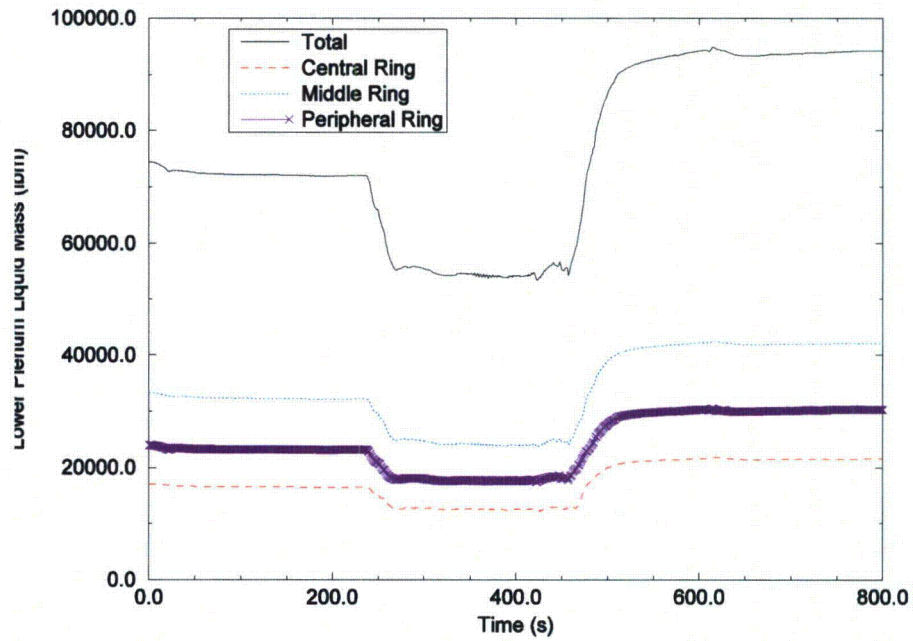


Figure 7-437 BWR/4 SBA Lower Plenum Liquid Mass

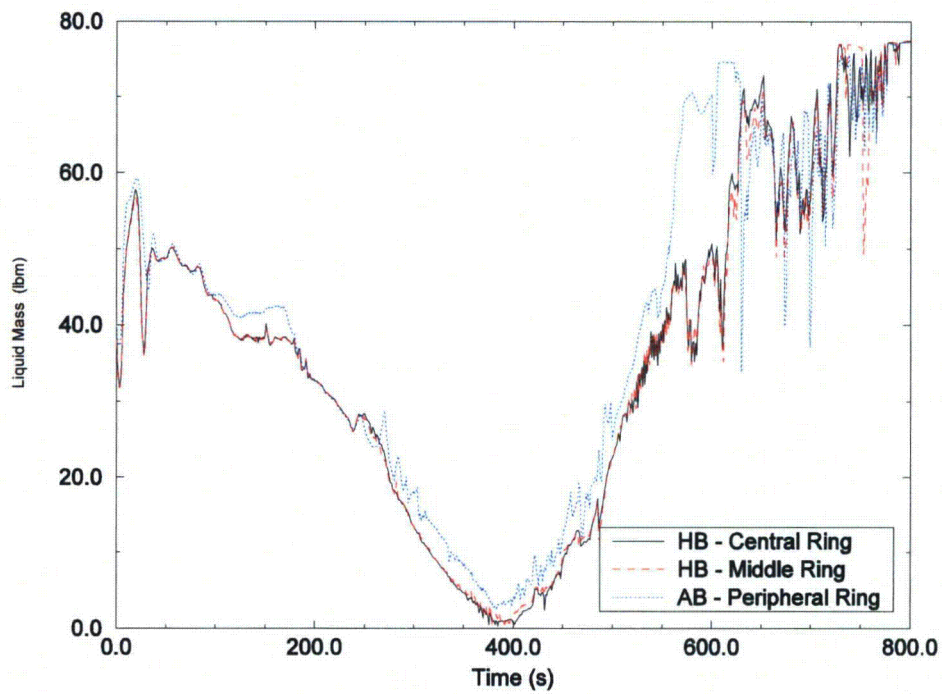


Figure 7-438 BWR/4 SBA Core Channels Liquid Mass

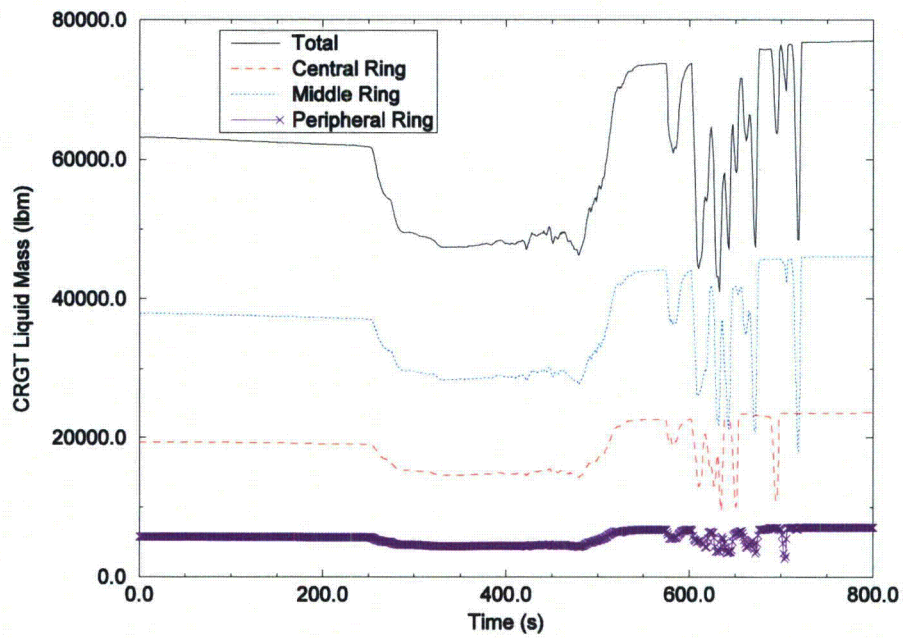


Figure 7-439 BWR/4 SBA Guide Tube Liquid Mass

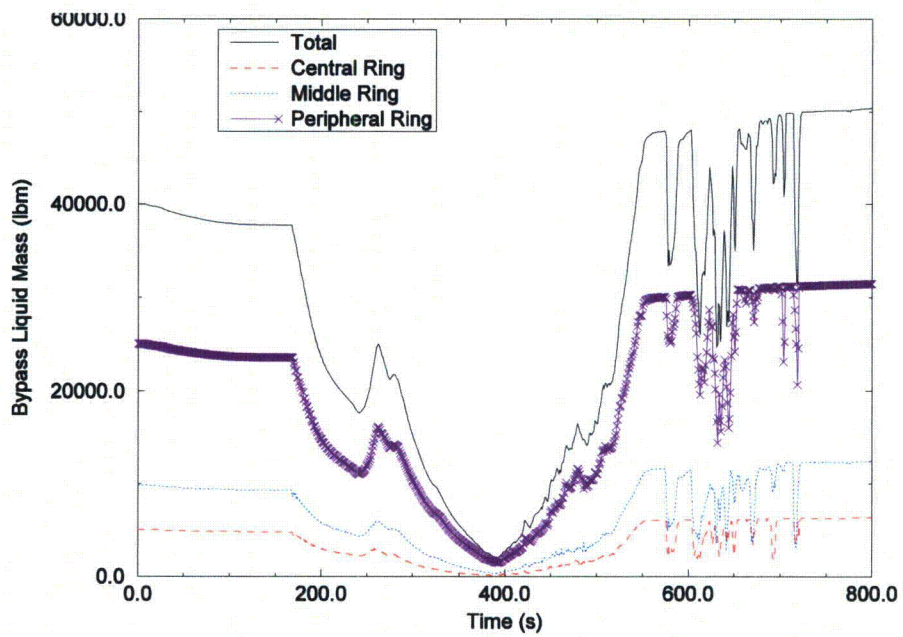


Figure 7-440 BWR/4 SBA Bypass Liquid Mass

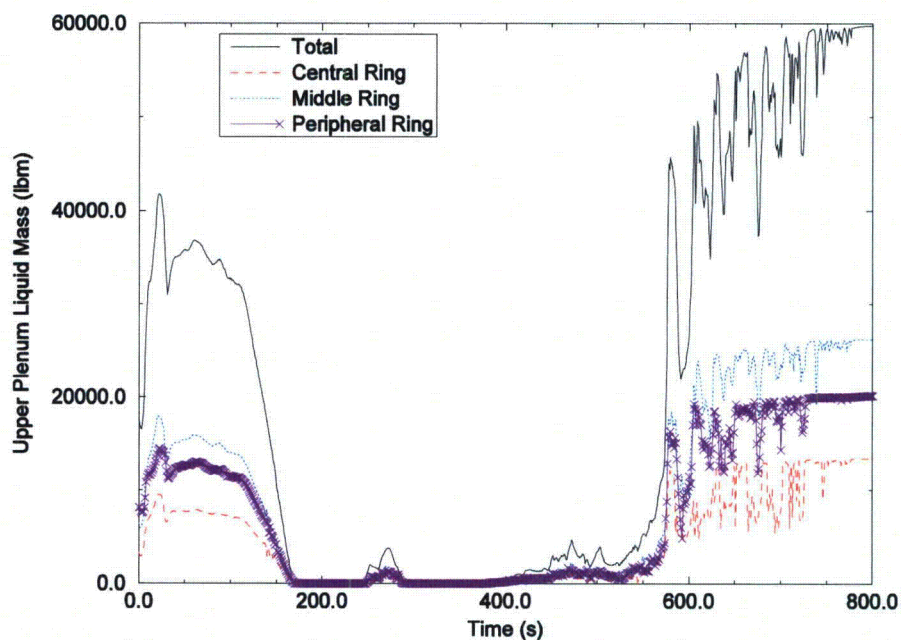


Figure 7-441 BWR/4 SBA Upper Plenum Liquid Mass

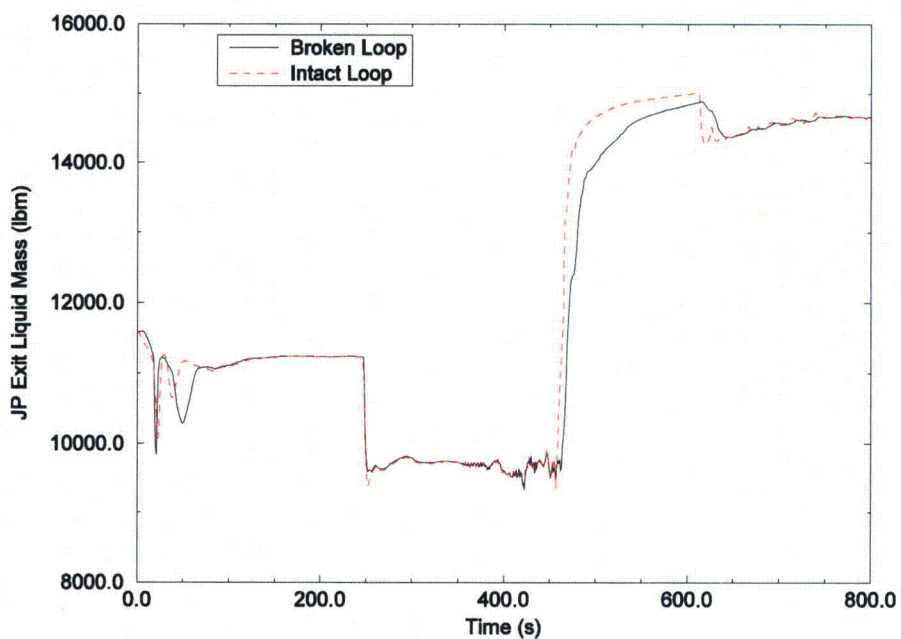


Figure 7-442 BWR/4 SBA Jet Pump Exit Liquid Mass

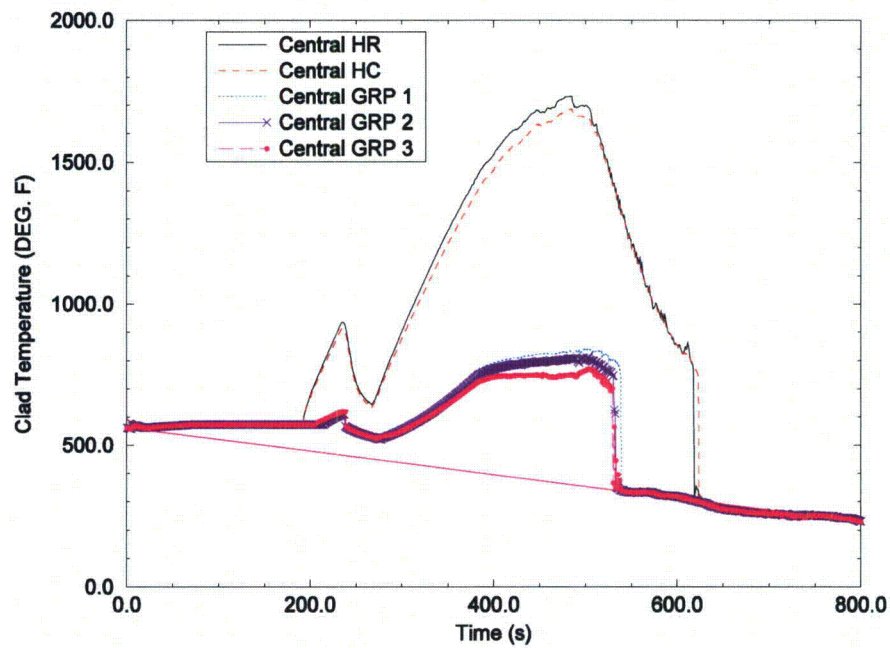


Figure 7-443 BWR/4 SBA Central Region Peak Node Temperature

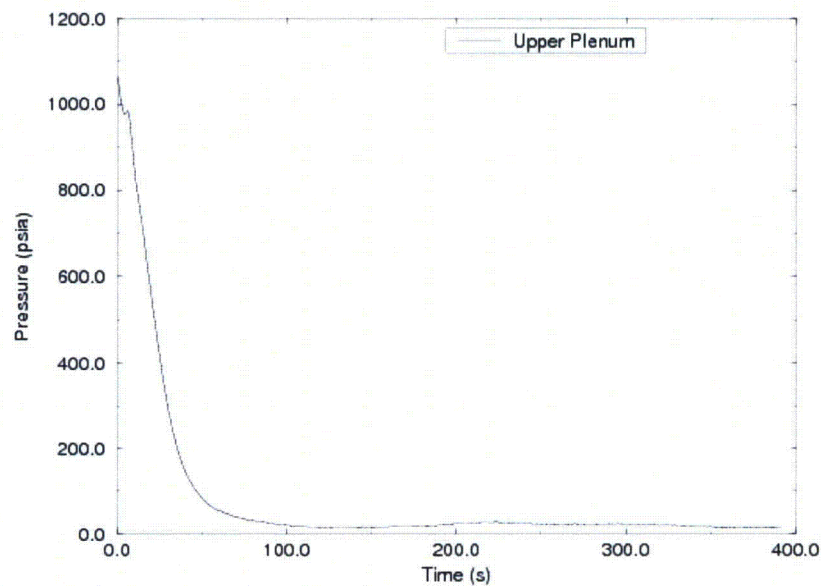


Figure 7-444 BWR/4 LBA Upper Plenum Pressure

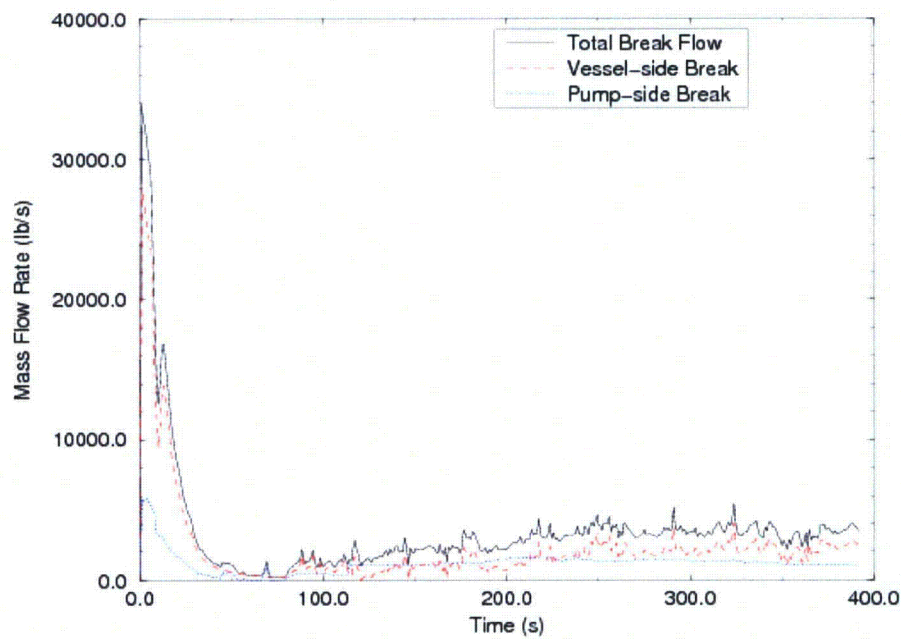


Figure 7-445 BWR/4 LBA Break Flow Rate

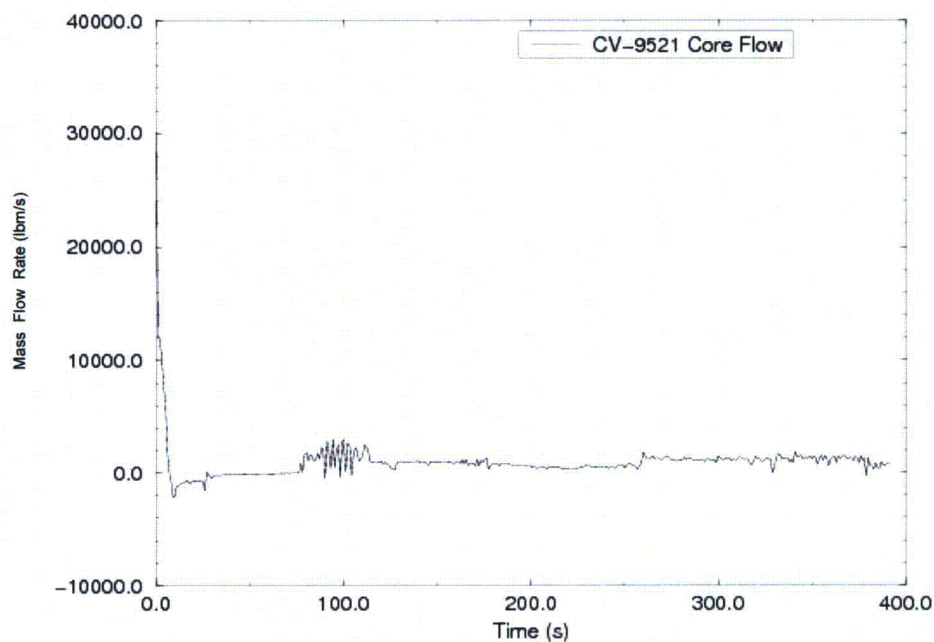


Figure 7-446 BWR/4 LBA Total Jet Pump Flow

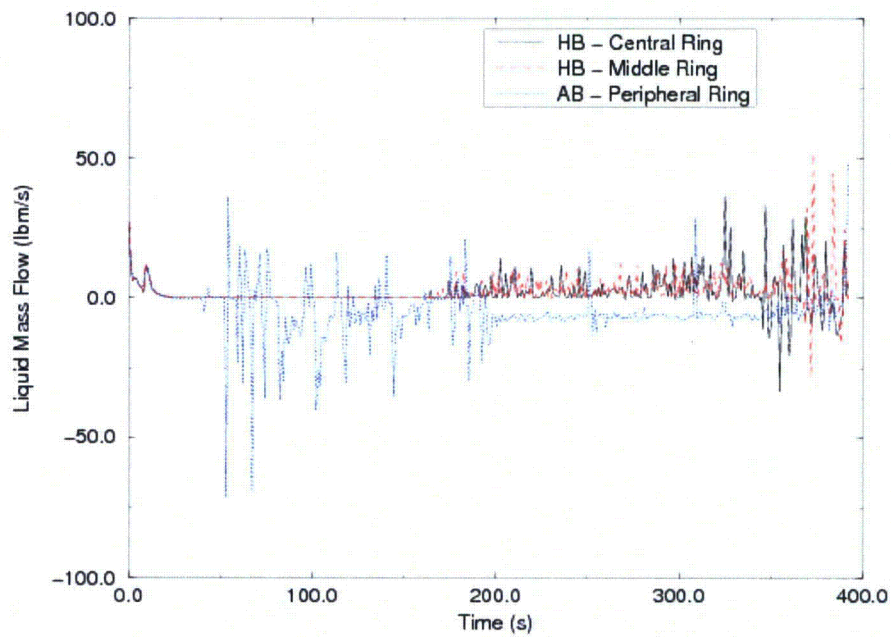


Figure 7-447 BWR/4 LBA Core Outlet Flow

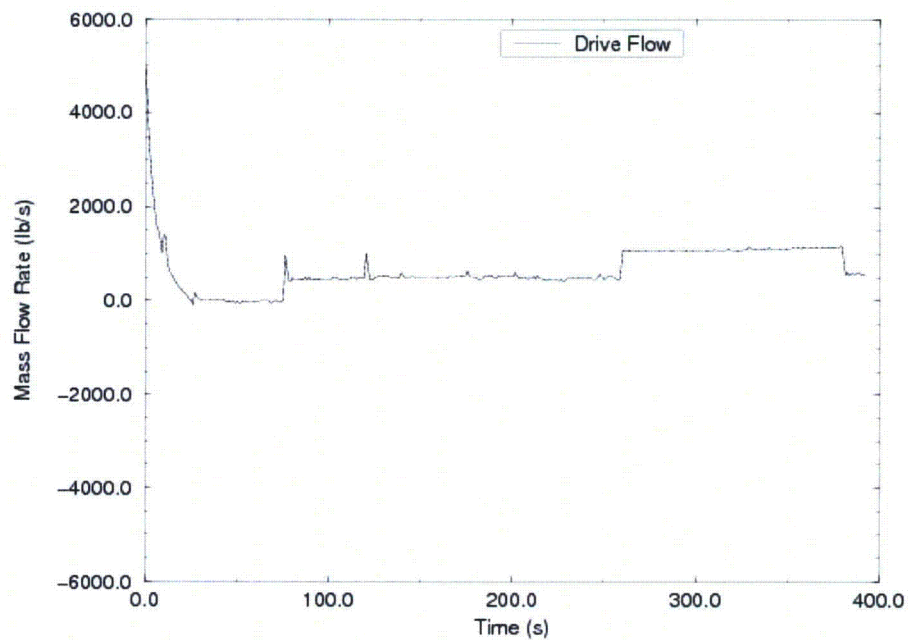


Figure 7-448 BWR/4 LBA Intact Loop Jet Pump Drive Flow

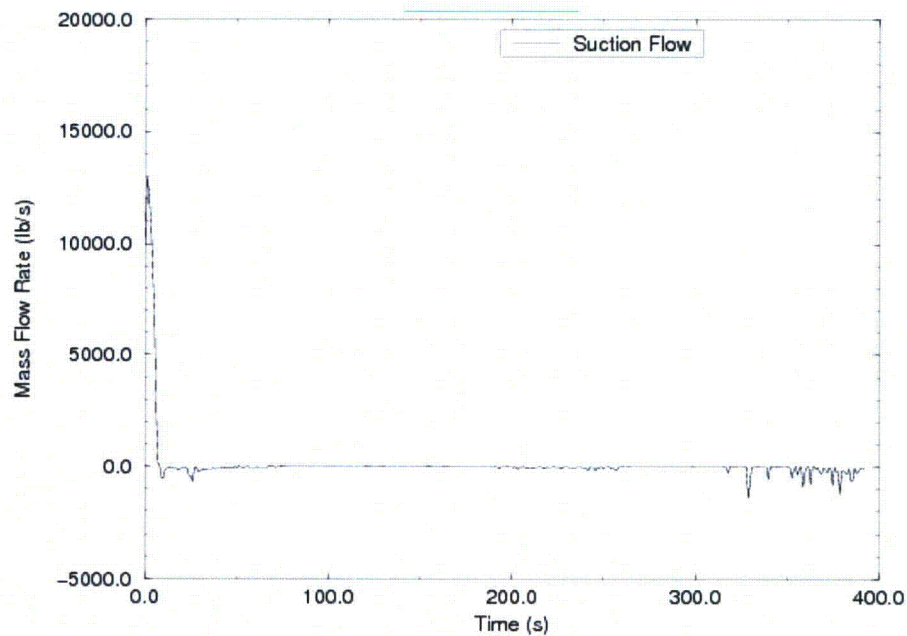


Figure 7-449 BWR/4 LBA Intact Loop Jet Pump Suction Flow

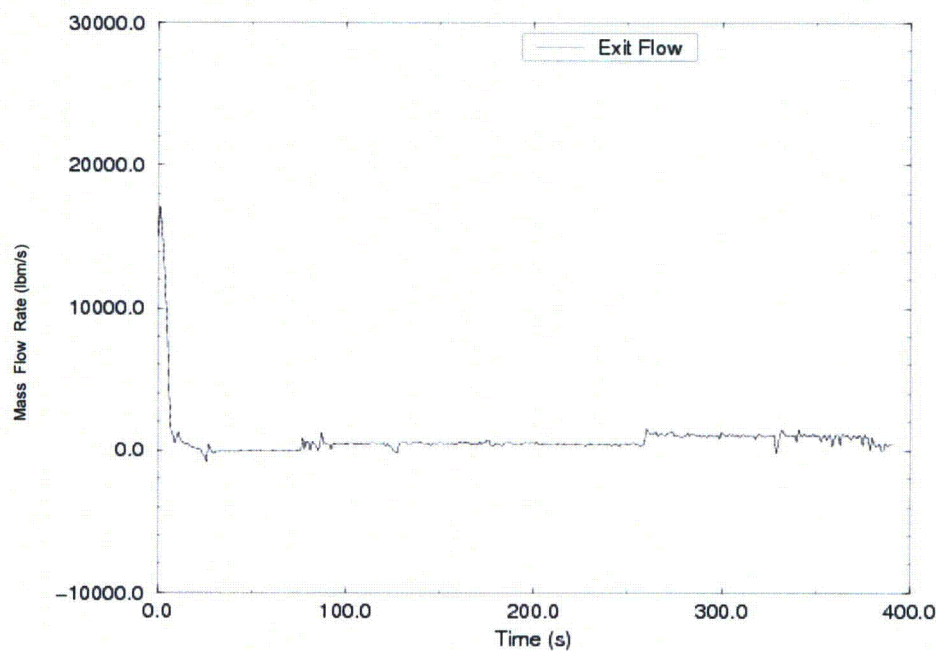


Figure 7-450 BWR/4 LBA Intact Loop Jet Pump Exit Flow

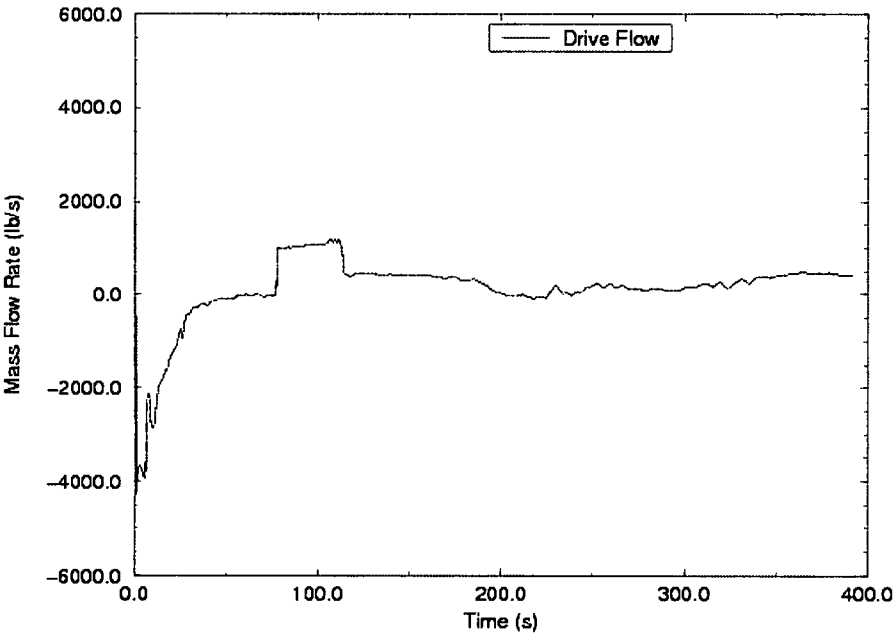


Figure 7-451 BWR/4 LBA Broken Loop Jet Pump Drive Flow

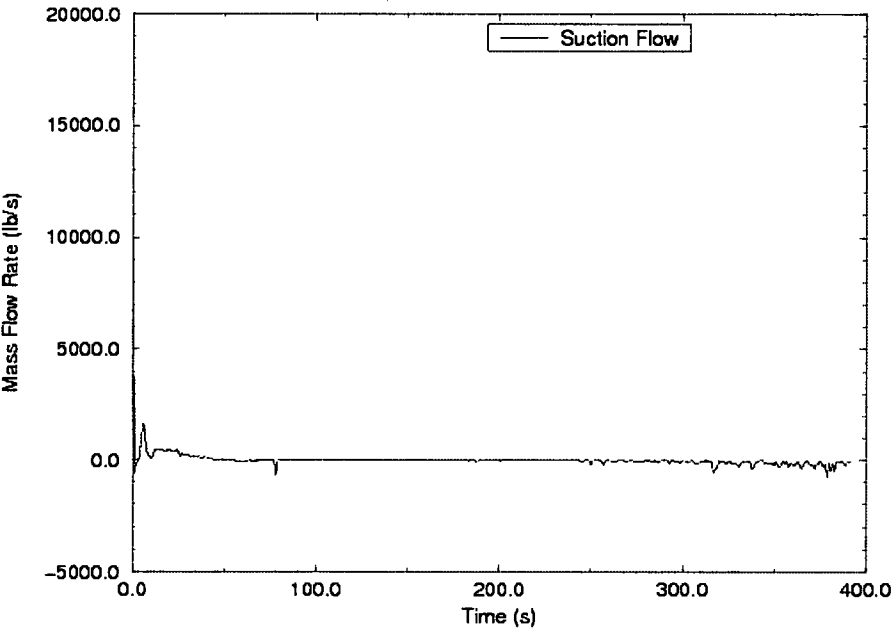


Figure 7-452 BWR/4 LBA Broken Loop Jet Pump Suction Flow

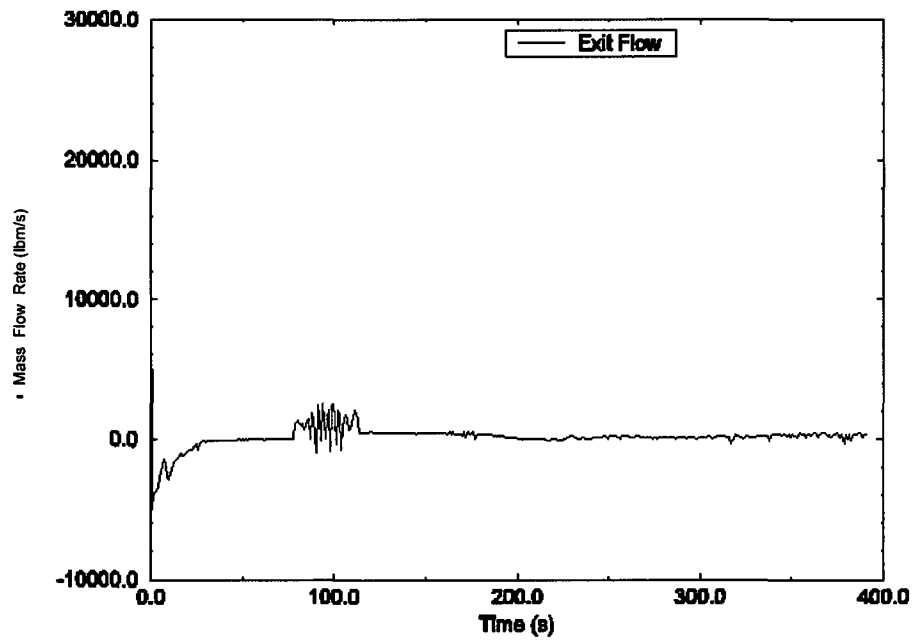


Figure 7-453 BWR/4 LBA Broken Loop Jet Pump Exit Flow

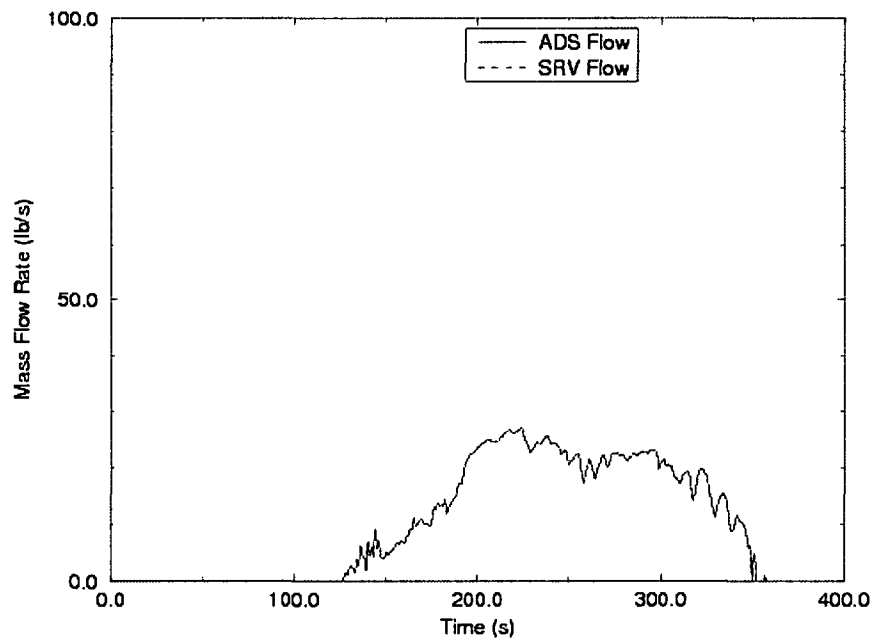


Figure 7-454 BWR/4 LBA ADS/SRV Flows

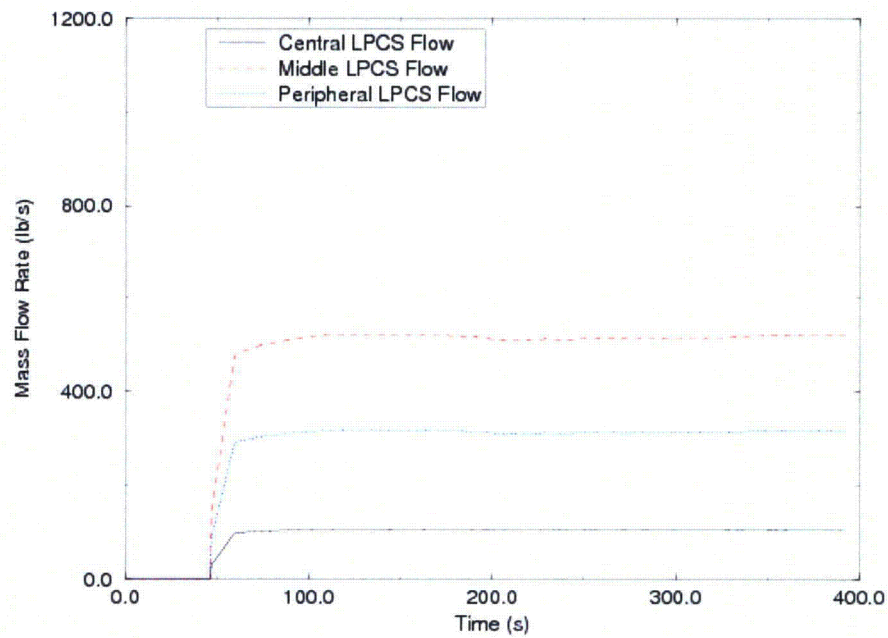


Figure 7-455 BWR/4 LBA LPCS Flow

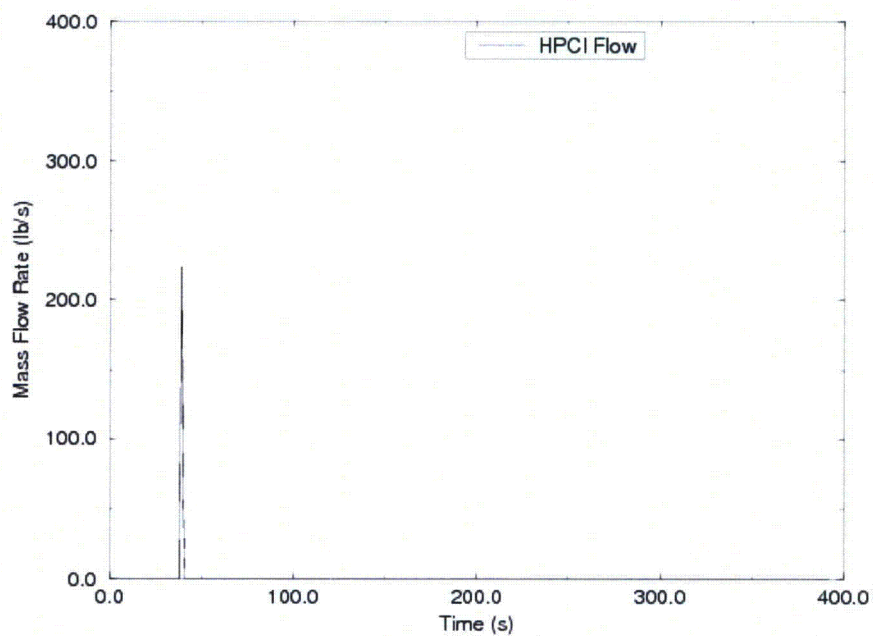


Figure 7-456 BWR/4 LBA HPCI Flow

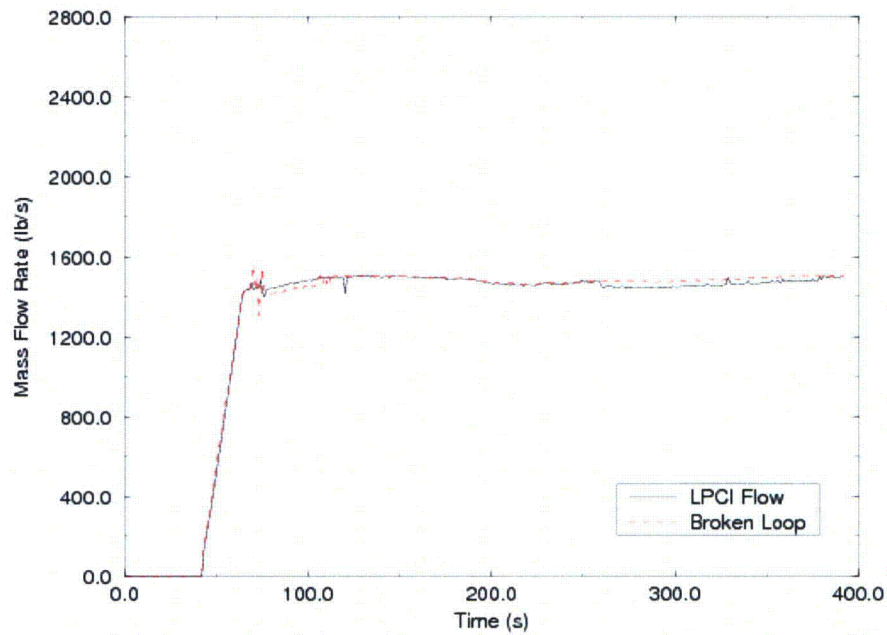


Figure 7-457 BWR/4 LBA LPCI Flow

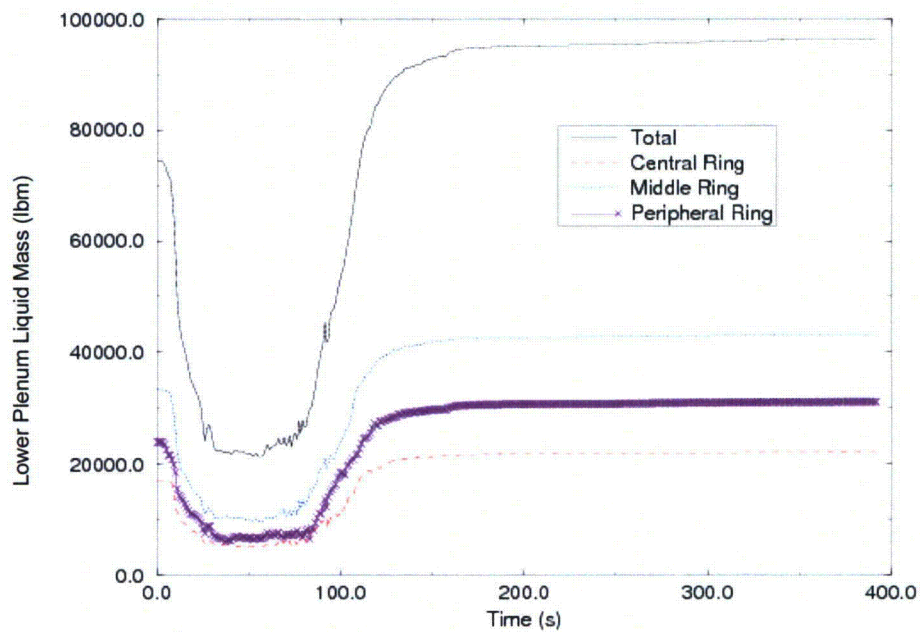


Figure 7-458 BWR/4 LBA Lower Plenum Liquid Mass

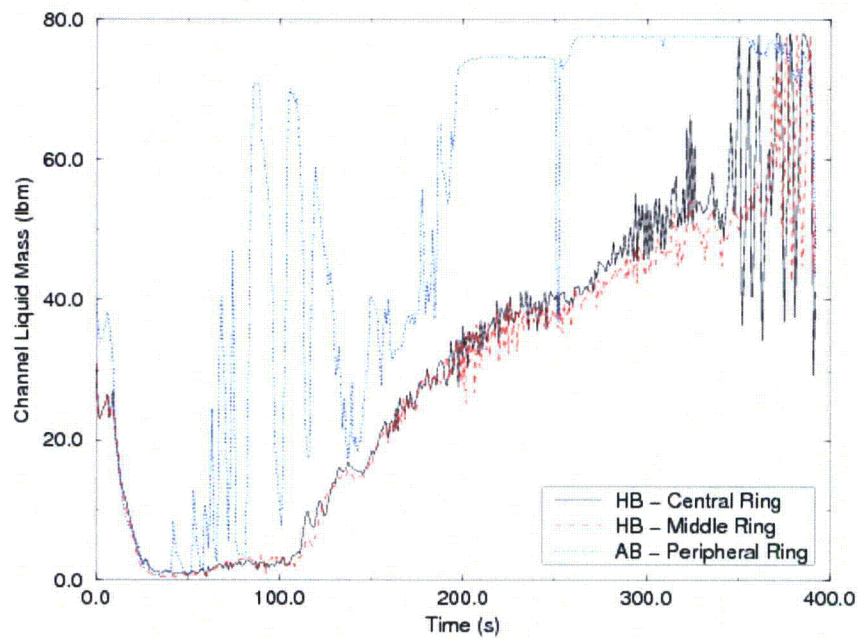


Figure 7-459 BWR/4 LBA Core Channels Liquid Mass

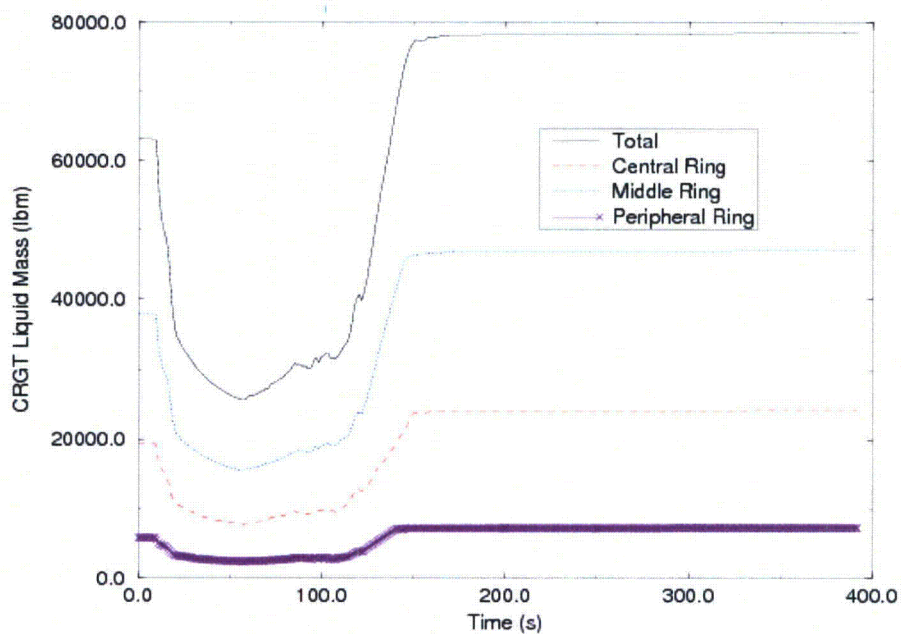


Figure 7-460 BWR/4 LBA Guide Tube Liquid Mass

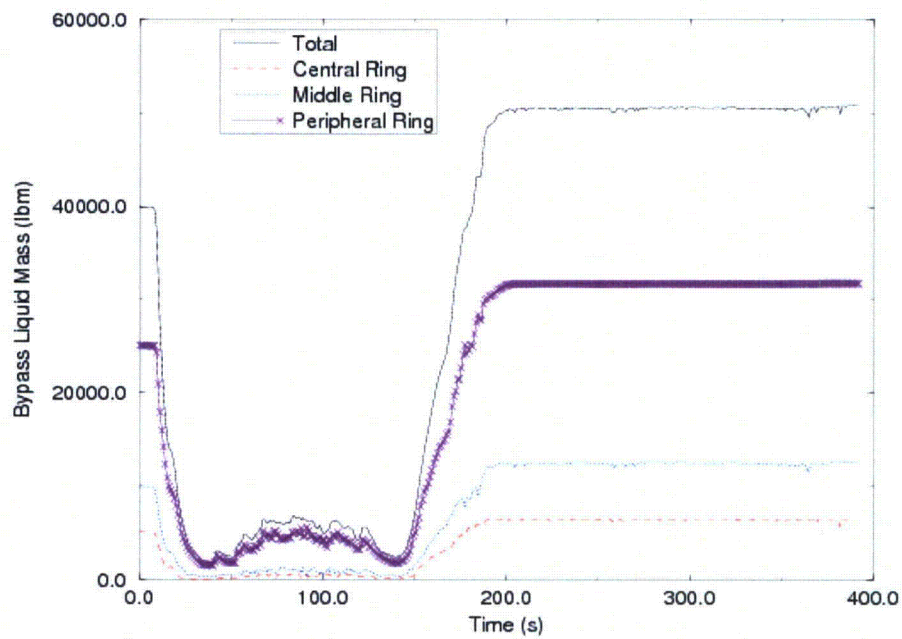


Figure 7-461 BWR/4 LBA Bypass Liquid Mass

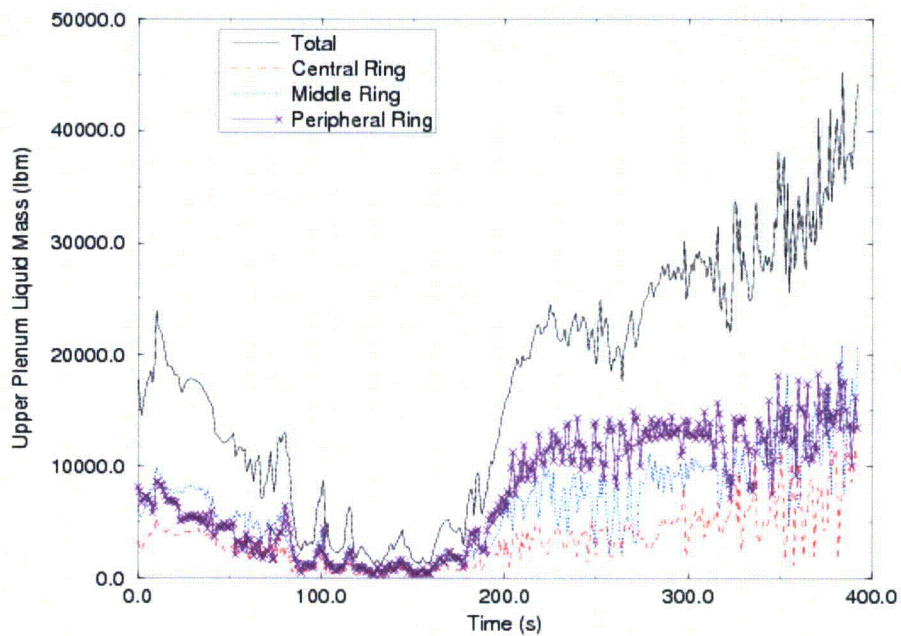


Figure 7-462 BWR/4 LBA Upper Plenum Liquid Mass

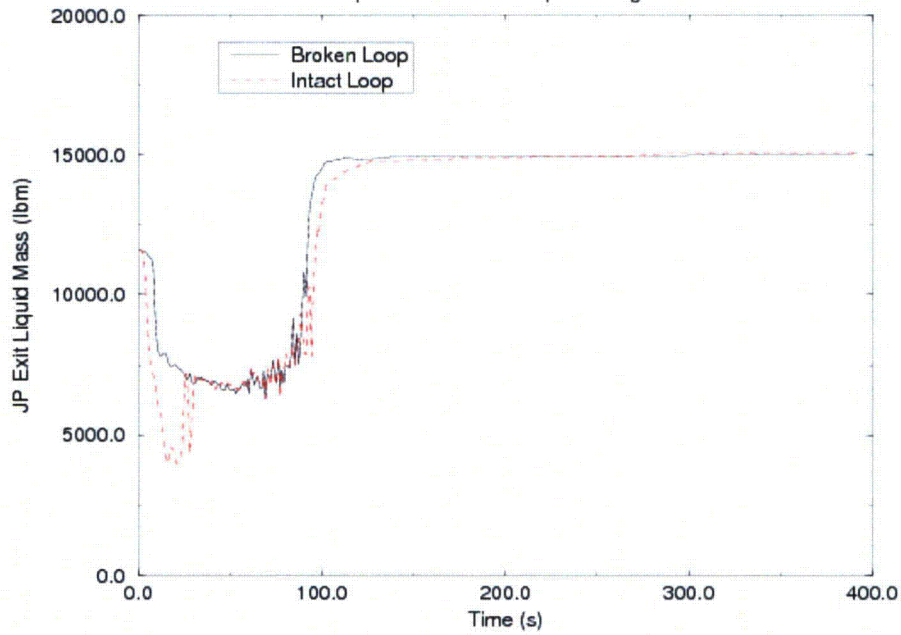


Figure 7-463 BWR/4 LBA Jet Pump Exit Liquid Mass

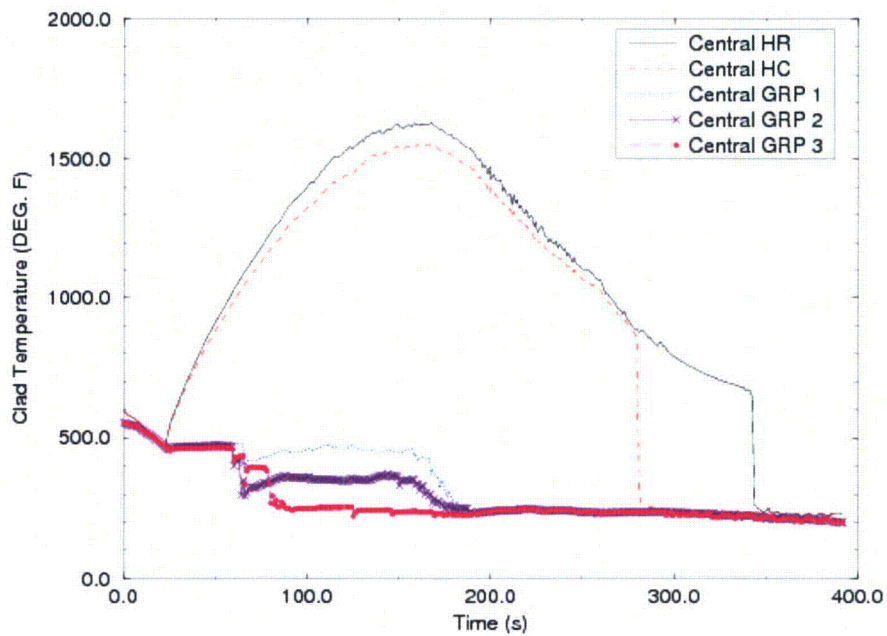


Figure 7-464 BWR/4 LBA Central Region Peak Node Temperature

7.7.5 BWR/4 Reduced ECCS Analyses

A BWR/4 sample problem representing a more challenging ECCS condition is presented. The case exhibited a greater challenge to the LOCA FoM due to reduced ECCS availability compared to the cases presented in Section 7.7.4. The results are representative of how the EM is applied in licensing calculations.

Plant Parameters

The parameters are unchanged from those presented in Section 7.7.4 with exception that only the top-peaked axial power distribution presented in Figure 7-422 was considered.

Single Failure

Only a single LPCS train is assumed available. HPCI and LPCI are not credited. The ADS assumptions presented in Section 7.7.4 are not changed from the previous analysis including 5 of 6 ADS valves available.

Sample Problem Breaks

Recirculation line break analyses were performed for breaks on the discharge side of the recirculation pump which is consistent with the assumption that no LPCI is credited. Two break types (geometries) are considered for the recirculation line break. The two types are the double-ended guillotine (DEG) break and the split break.

Sample Problem Analysis Results

**Table 7-44 Results for Highest PCT
Recirculation Line Break
0.40 ft² Split Pump Discharge Reduced ECCS
Top-Peaked Axial**

**Table 7-45 Events Times for BWR/4 Recirculation
Line Break 0.4 ft² Split Pump Discharge Reduced
ECCS Top-Peaked Axial**

Event	Time (sec)
Initiate break, loss of offsite power	
Initiate MSIV closure	
Initiate scram (MSIV < 85% open)	
MSIV fully closed*	
L2 low water level, HPCI signal	
HPCI flow starts {1700}	
L1 low water level, DG signaled	
DG power at ESS bus	
LPCI pumps start	
LPCS pump starts	
ADS valve starts to open	
LPCI valves start to open	
LPCI flow starts	
LPCS valve starts to open	
LPCS flow starts	
RDIV closure starts	
Begin rated spray (TSPRAY)	
RDIV closure complete	
Hot Node Rupture	
PCT @ 2129. F	
Bypass reflood	

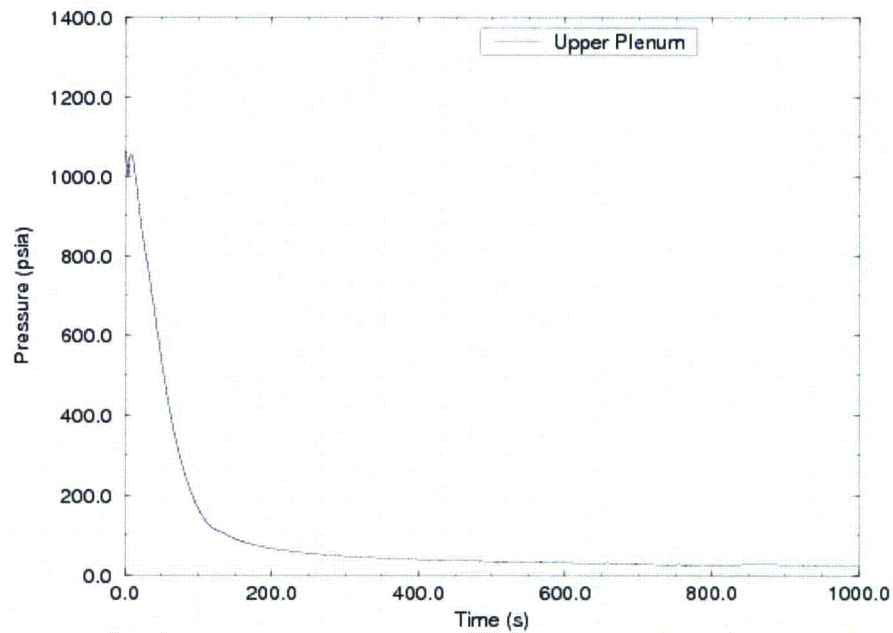


Figure 7-465 BWR/4 Reduced ECCS Upper Plenum Pressure

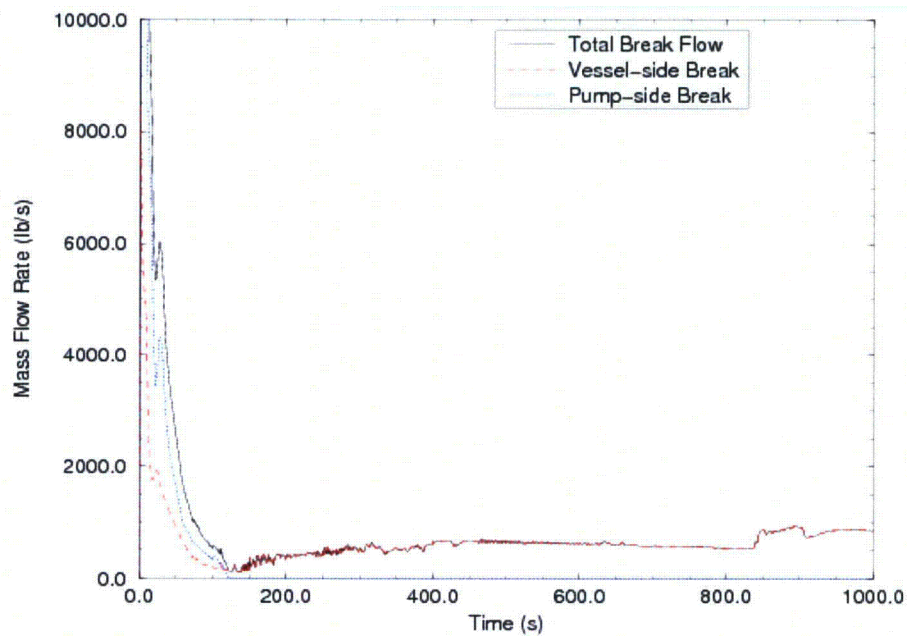


Figure 7-466 BWR/4 Reduced ECCS Break Flow Rate

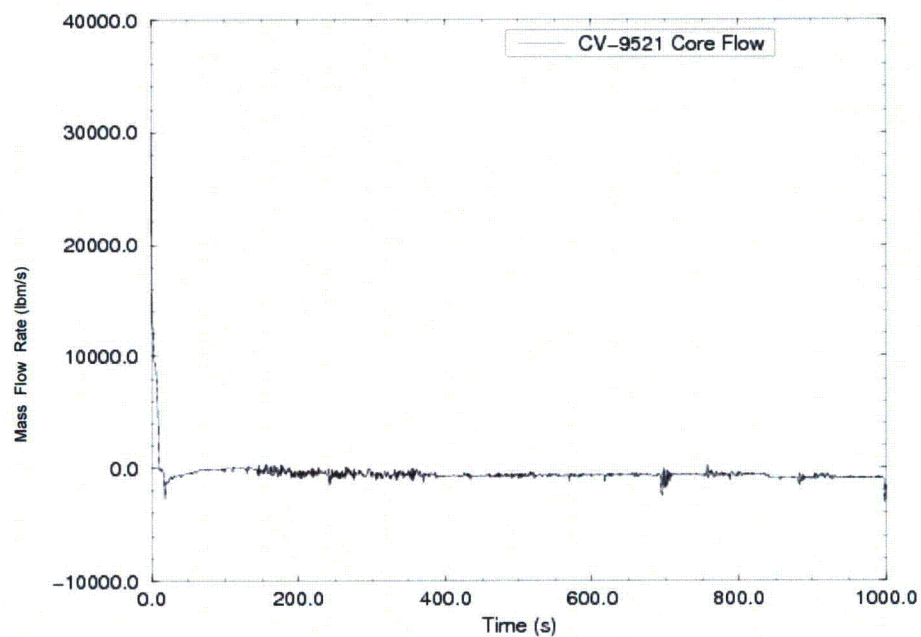


Figure 7-467 BWR/4 Reduced ECCS Total Jet Pump Flow

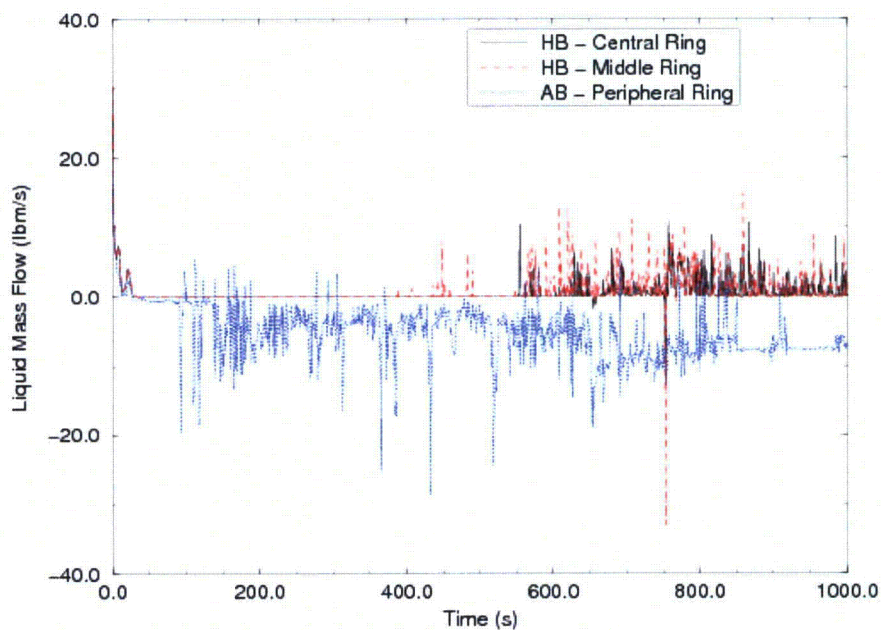


Figure 7-468 BWR/4 Reduced ECCS Core Outlet Flow

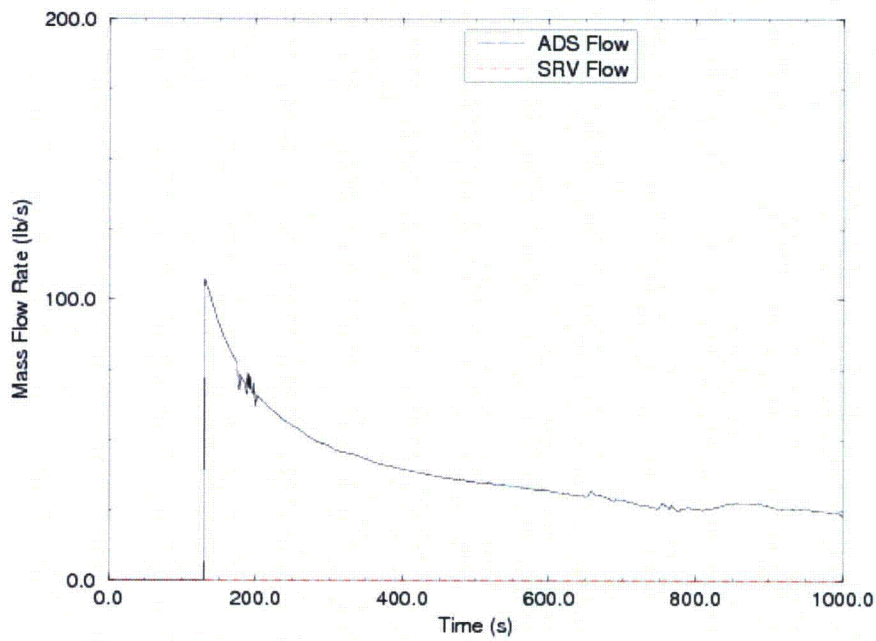


Figure 7-469 BWR/4 Reduced ECCS ADS/SRV Flows

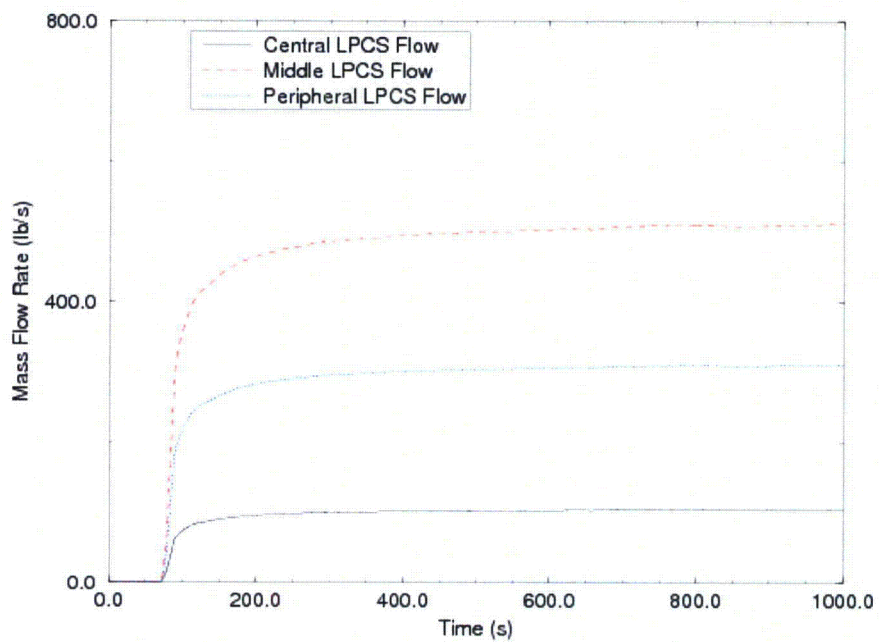


Figure 7-470 BWR/4 Reduced ECCS LPCS Flow

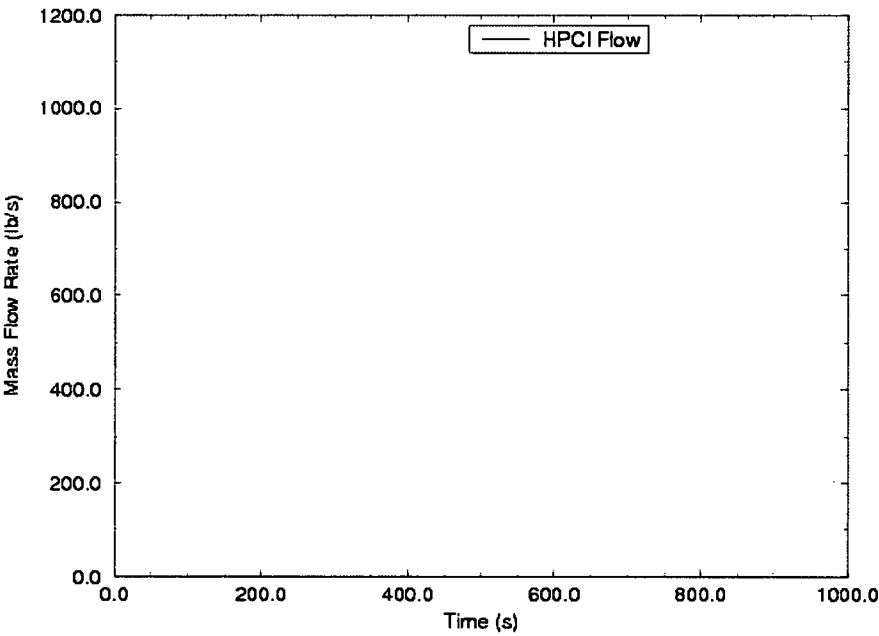


Figure 7-471 BWR/4 Reduced ECCS HPCI Flow

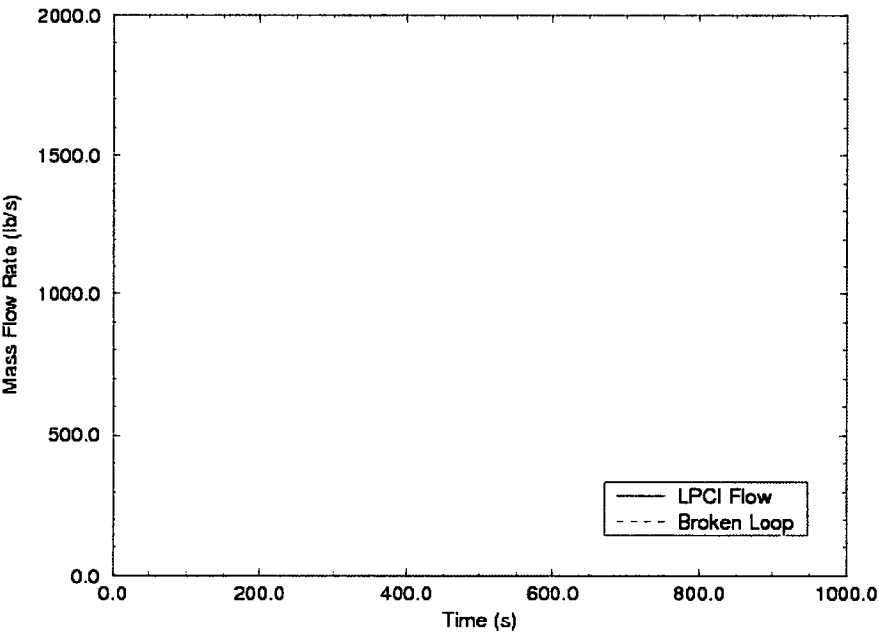


Figure 7-472 BWR/4 Reduced ECCS LPCI Flow

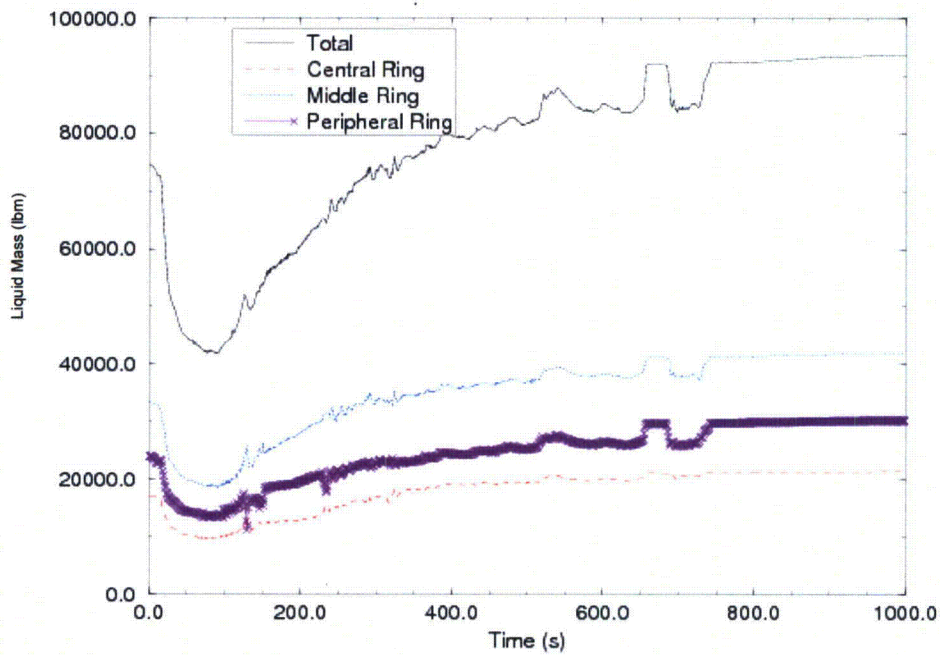


Figure 7-473 BWR/4 Reduced ECCS Lower Plenum Liquid Mass

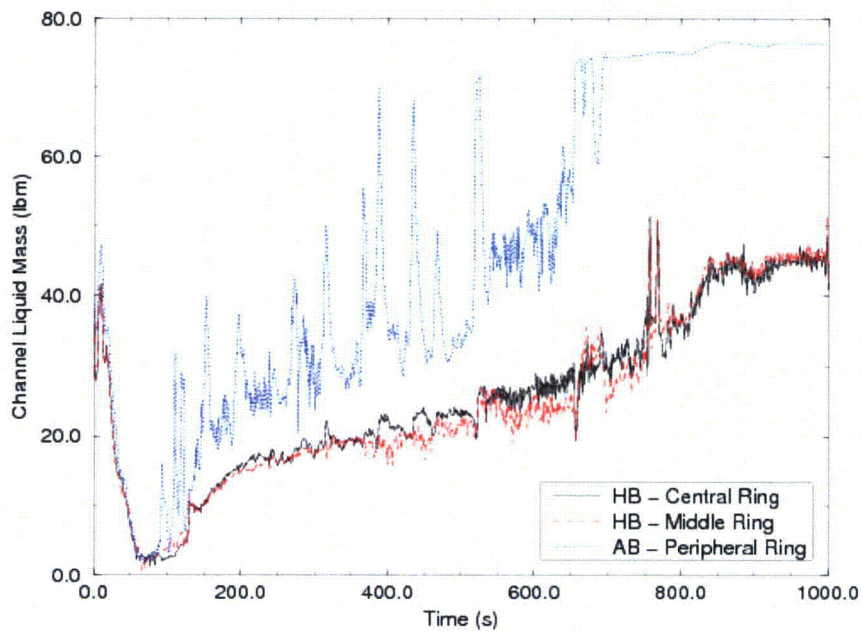


Figure 7-474 BWR/4 Reduced ECCS Core Channels Liquid Mass

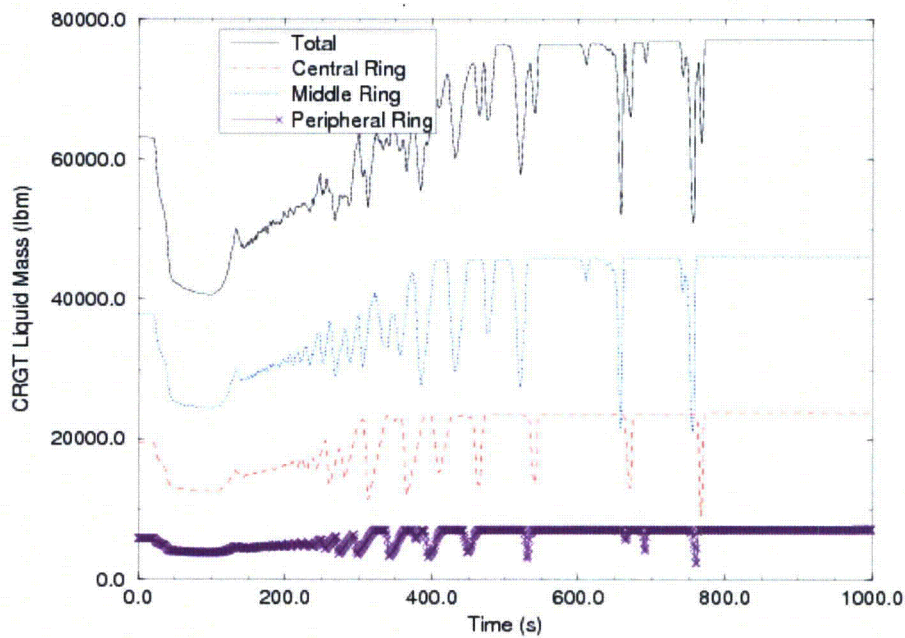


Figure 7-475 BWR/4 Reduced ECCS Guide Tube Liquid Mass

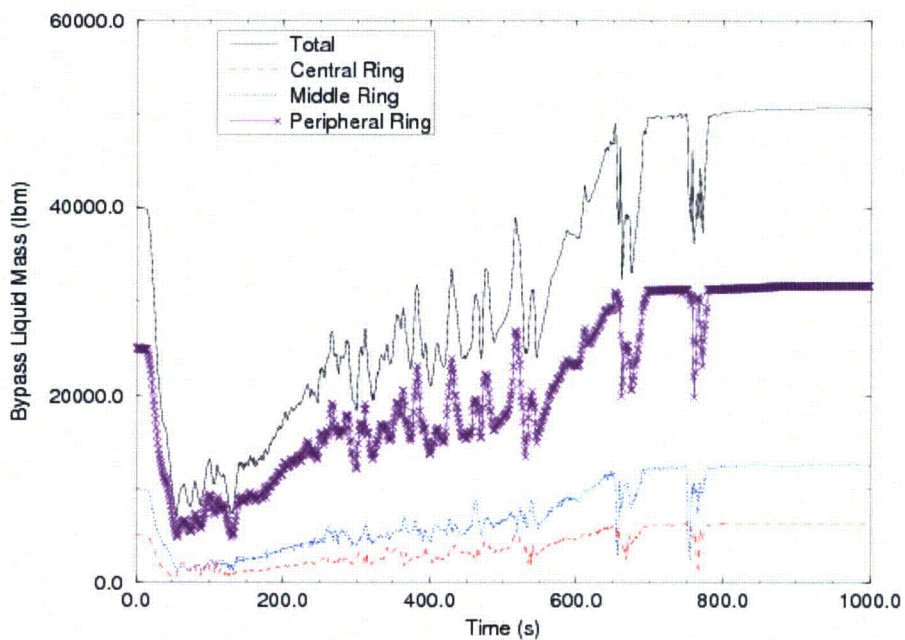


Figure 7-476 BWR/4 Reduced ECCS Bypass Liquid Mass

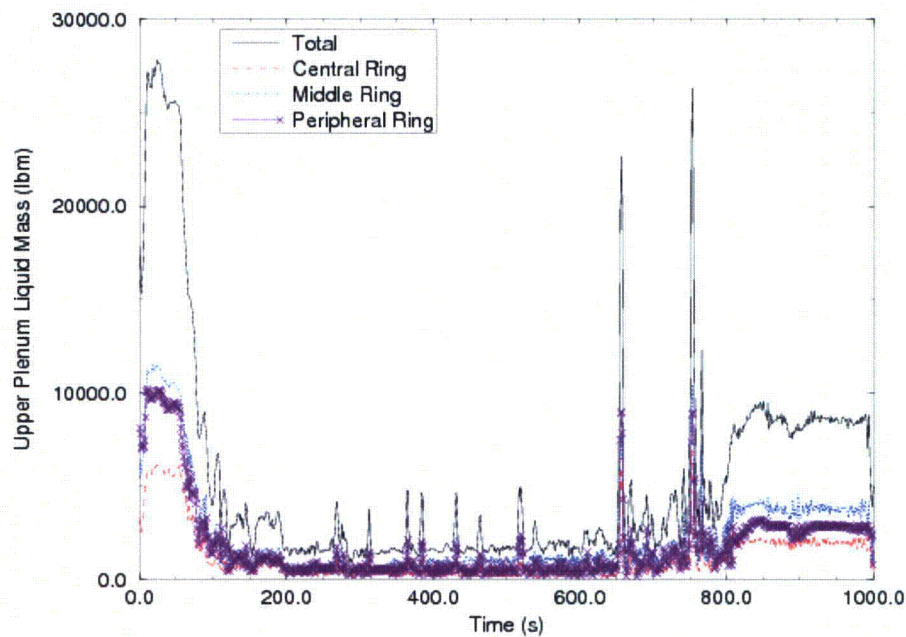


Figure 7-477 BWR/4 Reduced ECCS Upper Plenum Liquid Mass

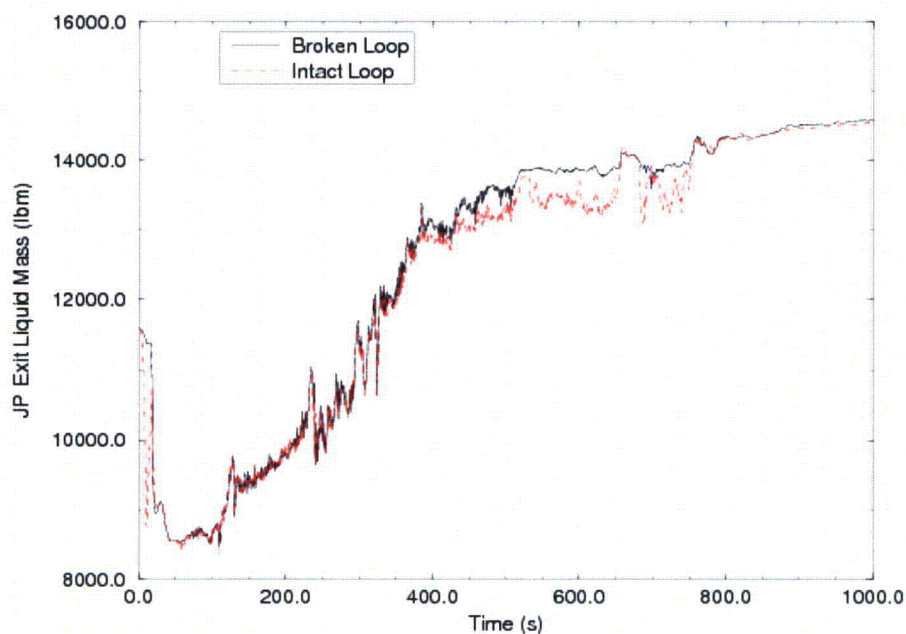


Figure 7-478 BWR/4 Reduced ECCS Jet Pump Exit Liquid Mass

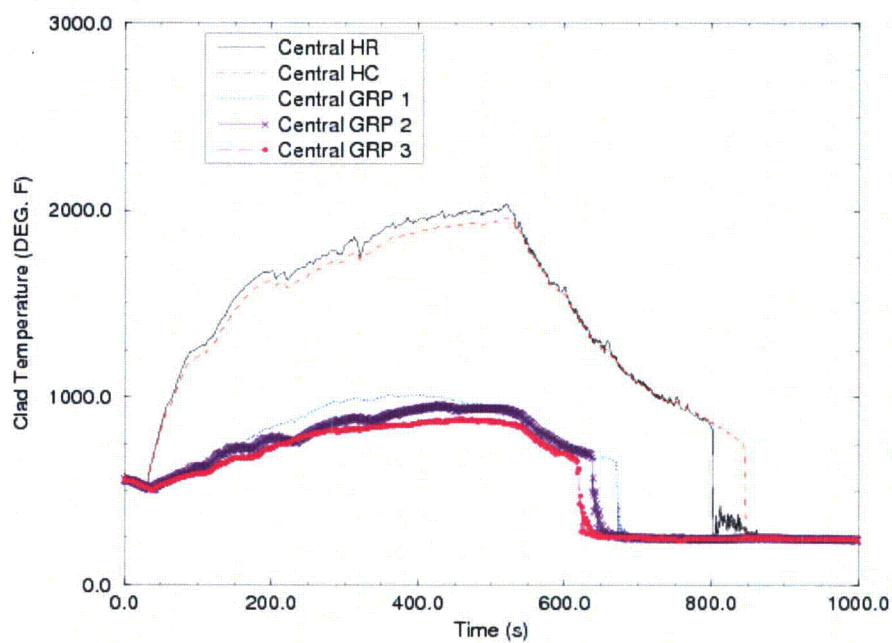


Figure 7-479 BWR/4 Reduced ECCS Central Region Peak Node Temperature

7.7.6 BWR/6 Baseline Analyses

The ability of the AURORA-B LOCA EM to model system interactions is demonstrated in this section for a typical BWR/6 plant. A smaller set of analyses were performed to demonstrate the BWR/6 plant model since many trends shown for the BWR/4 are applicable to other BWR plants. The sample analyses presented in this section utilize just one axial power shape (mid-peaked) and assumes a typical power history prior to the LOCA event.

Plant Parameters

Table 7-46 provides a summary of reactor initial conditions used in the BWR/6 sample problem. Table 7-47 lists selected reactor system parameters. The analysis is performed for a full core of ATRIUM-10 fuel. The key ATRIUM-10 fuel parameters used in the analysis are the same as the BWR/4 sample problem and are summarized in Table 7-31.

The ECCS is modeled as fill junctions connected to the appropriate reactor locations: HPCS and LPCS inject into the upper plenum, and LPCI injects into the peripheral region of the bypass through penetrations in the core shroud wall.

The flow through each ECCS valve is determined based on system pressure and valve position. Flow versus pressure for a fully open valve is obtained by linearly interpolating the pump capacity data provided in Table 7-48 through Table 7-50. No credit for ECCS flow is assumed until ECCS pumps reach rated speed.

The ADS valves are modeled as a junction connecting the reactor steam line to the suppression pool. The flow through the ADS valves is calculated based on pressure and valve flow characteristics. The valve flow characteristics are determined such that the calculated flow is equal to the rated capacity at the reference pressure shown in Table 7-51.

In the AREVA LOCA analysis model, ECCS initiation is assumed to occur when the water level drops to the applicable level setpoint. No credit is assumed for the start of HPCS, LPCS, or LPCI due to high drywell pressure. [

]

Single Failure

The single failures and the available ECCS for each failure assumed in this analysis are summarized in Table 7-52.

Sample Problem Breaks

Recirculation line break analyses are performed for breaks in both the discharge and suction side of the recirculation pump. Two break types (geometries) are considered for the recirculation line break. The two types are the double-ended guillotine (DEG) break and the split break.

Sample Problem Analysis Results

Table 7-53 through Table 7-55 provides results for the sample problem. The sample analyses produced the highest PCT for 1.0 DEG break in the pump suction piping with an SF-LPCS single failure. The PCT is 1612°F. The key results and event times for this break are provided in Table 7-56 and Table 7-57, respectively. Figure 7-481 through Figure 7-501 provides plots of key parameters.

The small break analysis for the 0.05 ft² break in the pump discharge piping with an SF-HPCS single failure is also presented for comparison. The PCT is 1268°F. The key results and event times for this limiting break are provided in Table 7-58 and Table 7-59, respectively. Figure 7-502 through Figure 7-522 provides plots of key parameters.

Table 7-46 BWR/6 Example Problem Initial Conditions

Total core flow (% of rated)	105
Reactor power (MWt)	4105.5
Total core flow (Mlb/hr)	118.1
Steam flow rate (Mlb/hr)	17.9
Steam dome pressure (psia)	1100.
Core inlet enthalpy (Btu/lb)	534.4
[]	
Axial power shape	Figure 7-480

Table 7-47 BWR/6 Example Reactor System Parameters

Parameter	Value
Vessel ID (in)	251
Number of fuel assemblies	800
Recirculation suction pipe area (ft ²)	2.536
1.0 DEG suction break area (ft ²)	5.072
Recirculation discharge pipe area (ft ²)	3.503
1.0 DEG discharge break area (ft ²)	5.072

Table 7-48 BWR/6 High-Pressure Coolant Core Spray Parameters

<i>Parameter Description</i>	<i>Value</i>
Coolant temperature, °F	120
<i>Initiating Signals and Setpoints</i>	
Low water level (L2), in	475
<i>Time Delays</i>	
Startup time, sec	1.0
Delay to startup, sec	34.0
<i>Delivered Flow Rate Versus Pressure</i>	
Vessel to Drywell ΔP (psid)	Flow Rate (gpm)
0	7000
200	6300
1147	1485
1177	495
> 1177	0

Table 7-49 BWR/6 Low-Pressure Coolant Core Spray Parameters

<i>Parameter Description</i>	<i>Value</i>
Reactor pressure permissive for opening LPCS injection valves, psia	450.0
Coolant temperature, °F	120.0
<i>Initiating Signals and Setpoints</i>	
Low water level (L1), in	366.3
<i>Time Delays</i>	
LPCS pump at rated speed, sec	47
LPCS injection valve stroke time, sec	35
<i>Delivered Flow Rate Versus Pressure</i>	
Vessel to Drywell ΔP (psid)	Flow Rate (gpm)
0	7000.0
122	6300.0
289	0.0

Table 7-50 BWR/6 Low-Pressure Coolant Injection Parameters

<i>Parameter Description</i>	<i>Value</i>
Reactor pressure permissive for opening LPCI injection valves, psia	450.0
Coolant temperature, °F	120.0
<i>Initiating Signals and Setpoints</i>	
Low water level (L1), in	366.3
<i>Time Delays</i>	
LPCI pump at rated speed, sec	47
LPCI injection valve stroke time, sec	35
<i>Delivered Flow Rate Versus Pressure</i>	
Vessel to Drywell ΔP (PSID)	Flow Rate Per Loop (gpm)
0	7333.33
20	7333.33
225	0.0

Table 7-51 BWR/6 Automatic Depressurization System Parameters

<i>Parameter Description</i>	<i>Value</i>
Number of valves installed	8*
Flow capacity of 6 valves (Mlbm/hr at psid)	5.550 at 1241
<i>Initiating Signals and Setpoints</i>	
Low water level (L1), in	366.3
<i>Time Delays</i>	
ADS timer, sec	120.0

* Only 6 ADS valves are credited in the break spectrum calculations

Table 7-52 BWR/6 ECCS Single Failure

Assumed Failure	Available ECCS			
SF-LPCS	2 LPCI	--	HPCS	ADS (6 valves)
SF-LPCI	1 LPCI	LPCS	HPCS	ADS (6 valves)
SF-HPCS	3 LPCI	LPCS	--	ADS (6 valves)

Table 7-54 BWR/6 Recirculation Line Break Results for SF-LPCS

[illegible]



**Table 7-56 Results for Highest PCT for Example BWR/6
Recirculation Line Break
1.0 DEG Pump Suction SF-LPCS Mid-Peaked Axial**

[illegible]

**Table 7-57 Event Times for Highest PCT for Example BWR/6
Large Recirculation Line Break
1.0 DEG Pump Suction SF-LPCS
Mid-Peaked Axial**

Event	Time (sec)
Initiate break, loss of offsite power	
Initiate scram (MSIV < 85% open)	
MSIV fully closed	
Low-low water level	
Low-low-low water level	
HPCS diesel at speed	
HPCS pump at speed	
HPCS valve fully open	
HPCS flow starts	
LPCS diesel at speed	
LPCS valve permissive	
LPCS valve starts to open	
LPCS pump at speed	
LPCS valve fully open	
LPCS flow starts	
LPCI diesel at speed	
LPCI valve permissive	
LPCI valve starts to open	
LPCI pump at speed	
LPCI valve fully open	
LPCI flow starts	
End of blow down	
ADS valve starts to open	
PCT @ 1612 F	
Bypass reflood	

Table 7-58 Results for Example BWR/6
Small Recirculation Line Break
0.05 DEG Pump Discharge SF-HPCS Mid-Peaked Axial

--	--

**Table 7-59 Event Times for Example BWR/6
Small Recirculation Line Break
0.05 ft² Split Pump Discharge SF-HPCS
Mid-Peaked Axial 102% Licensing Power 105% Flow**

Event	Time (sec)
Initiate break, loss of offsite power	
Initiate scram (MSIV < 85% open)	
MSIV fully closed	
Low-low water level	
Low-low-low water level	
HPCS diesel at speed	
HPCS pump at speed	
HPCS valve fully open	
HPCS flow starts	
LPCS diesel at speed	
LPCS valve permissive	
LPCS valve starts to open	
LPCS pump at speed	
LPCS valve fully open	
LPCS flow starts	
LPCI diesel at speed	
LPCI valve permissive	
LPCI valve starts to open	
LPCI pump at speed	
LPCI valve fully open	
LPCI flow starts	
End of blow down	
ADS valve starts to open	
PCT @ 1268 F	
Bypass reflood	



Figure 7-480 BWR/6 Mid-Peaked Axial Power Distribution

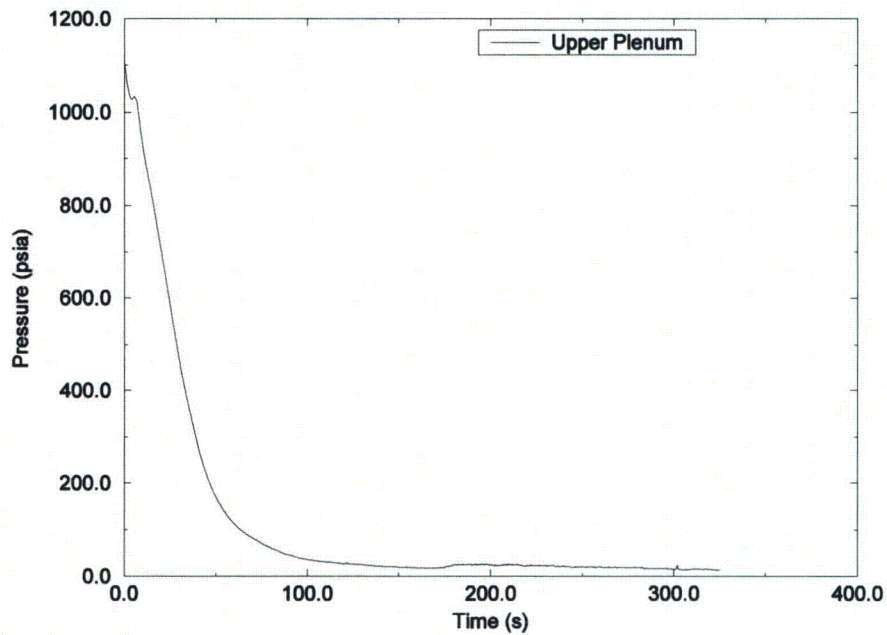


Figure 7-481 BWR/6 LBA Upper Plenum Pressure

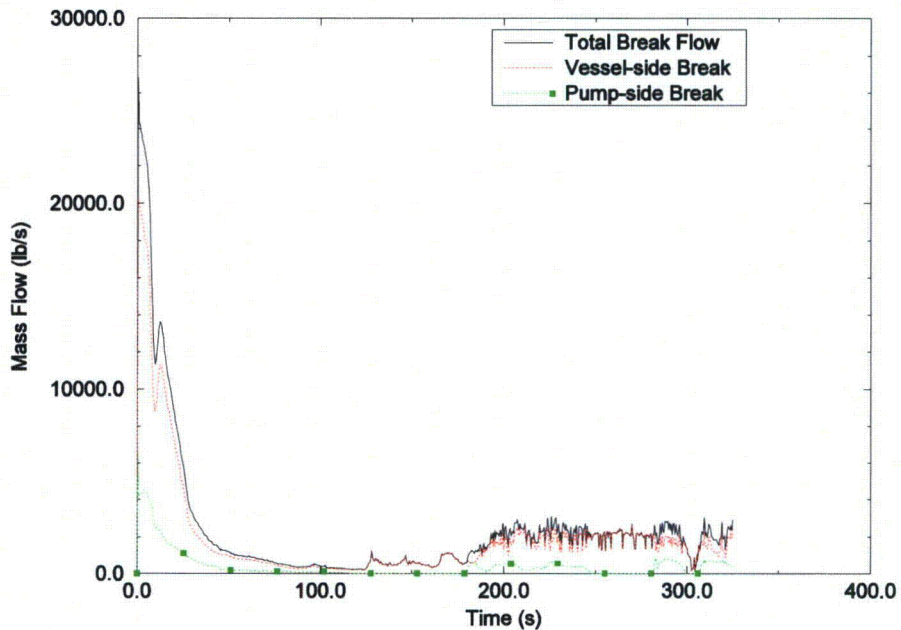


Figure 7-482 BWR/6 LBA Break Flow Rate

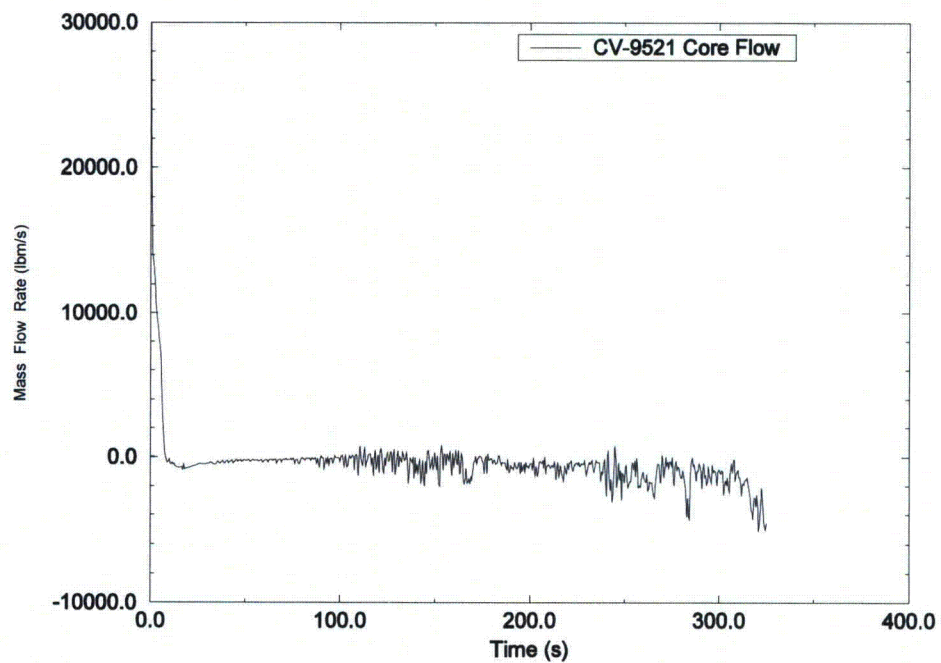


Figure 7-483 BWR/6 LBA Total Jet Pump Flow

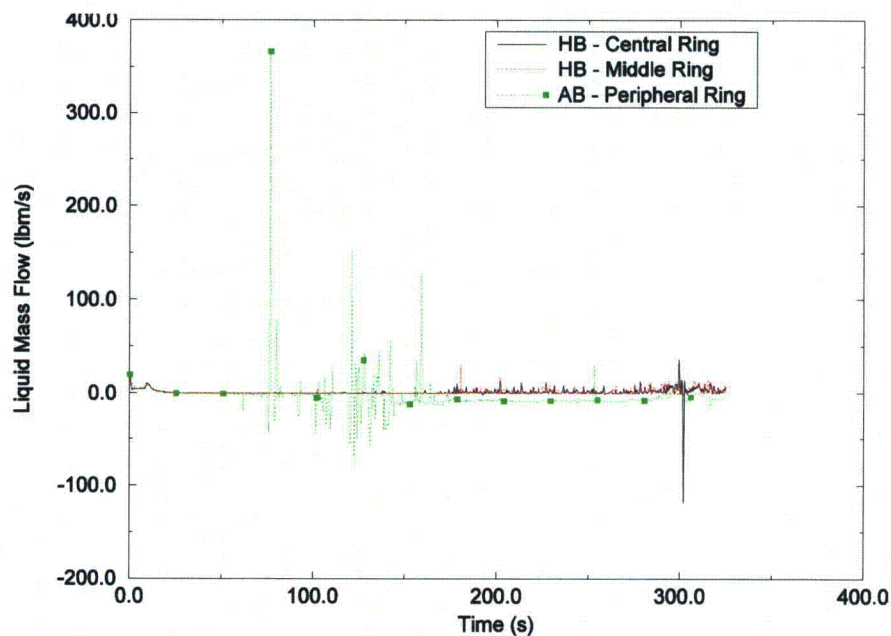


Figure 7-484 BWR/6 LBA Core Outlet Flow

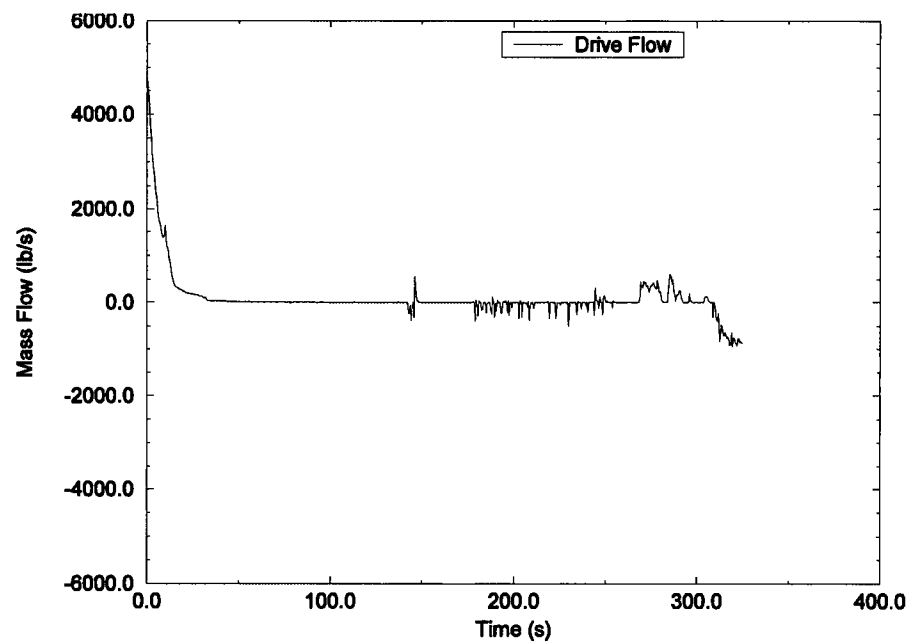


Figure 7-485 BWR/6 LBA Intact Loop Jet Pump Drive Flow

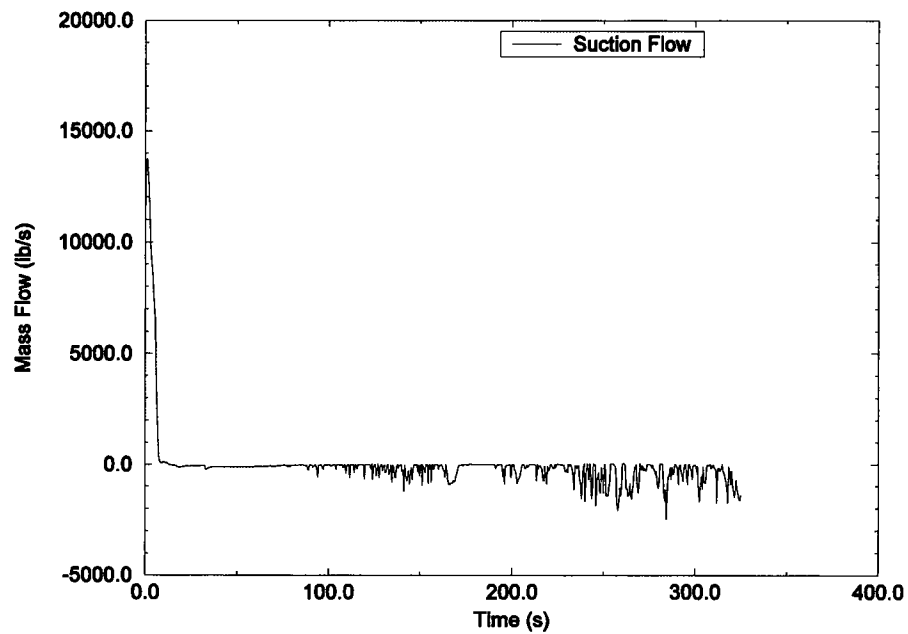


Figure 7-486 BWR/6 LBA Intact Loop Jet Pump Suction Flow

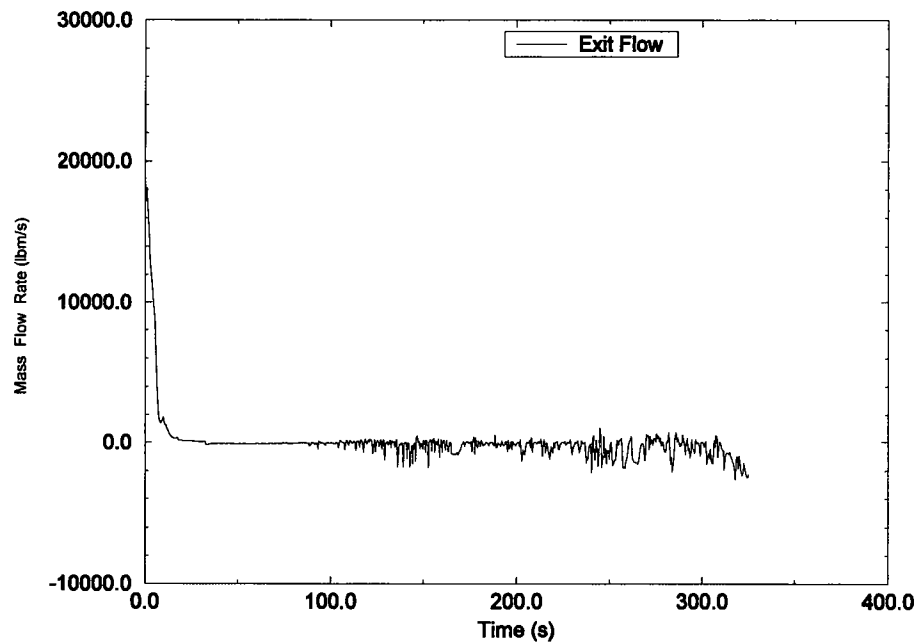


Figure 7-487 BWR/6 LBA Intact Loop Jet Pump Exit Flow

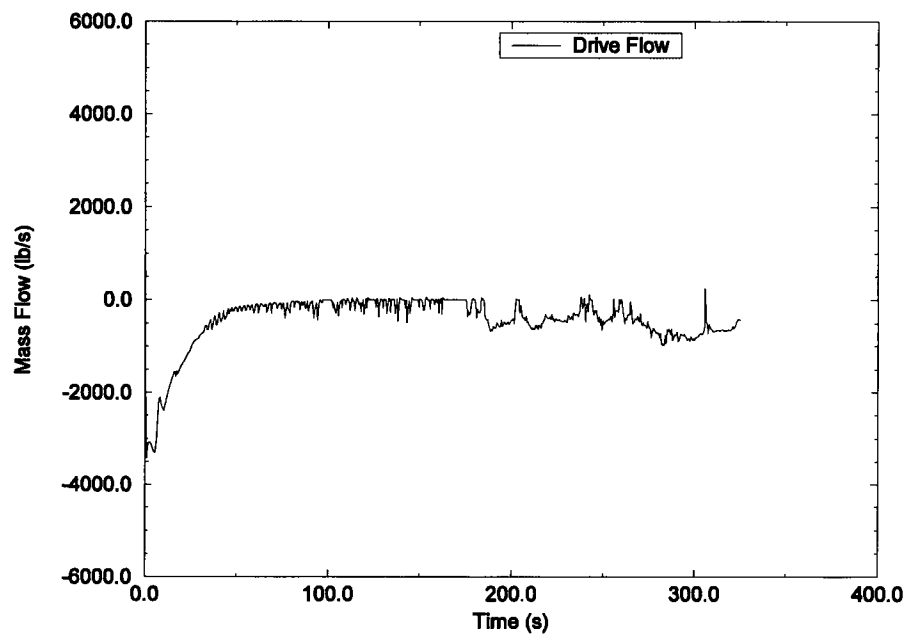


Figure 7-488 BWR/6 LBA Broken Loop Jet Pump Drive Flow

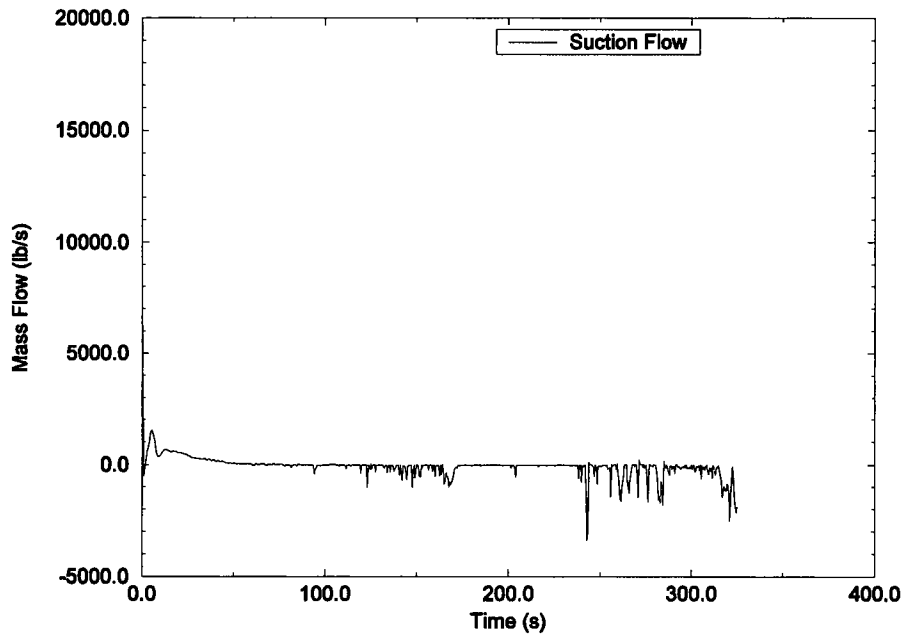


Figure 7-489 BWR/6 LBA Broken Loop Jet Pump Suction Flow

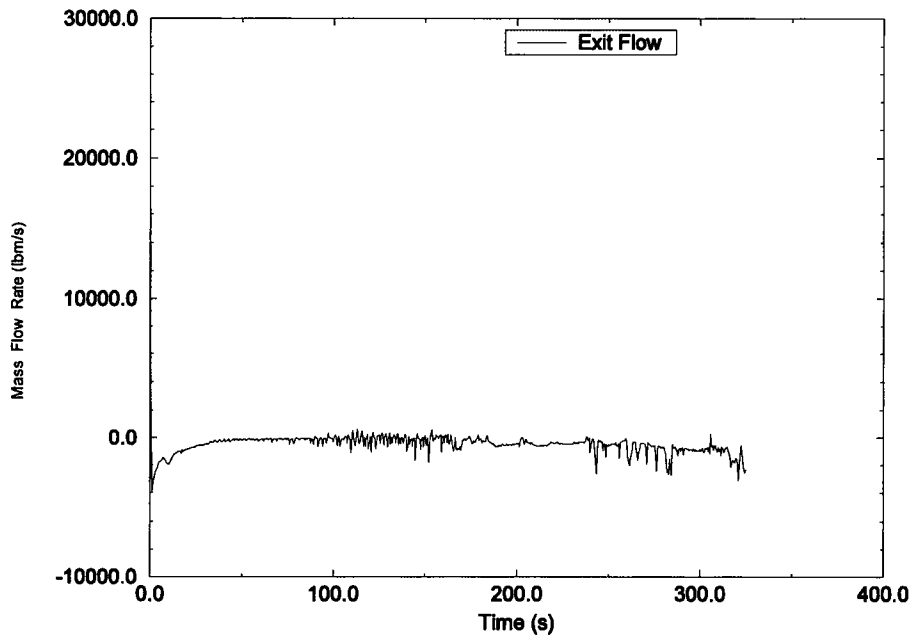


Figure 7-490 BWR/6 LBA Broken Loop Jet Pump Exit Flow

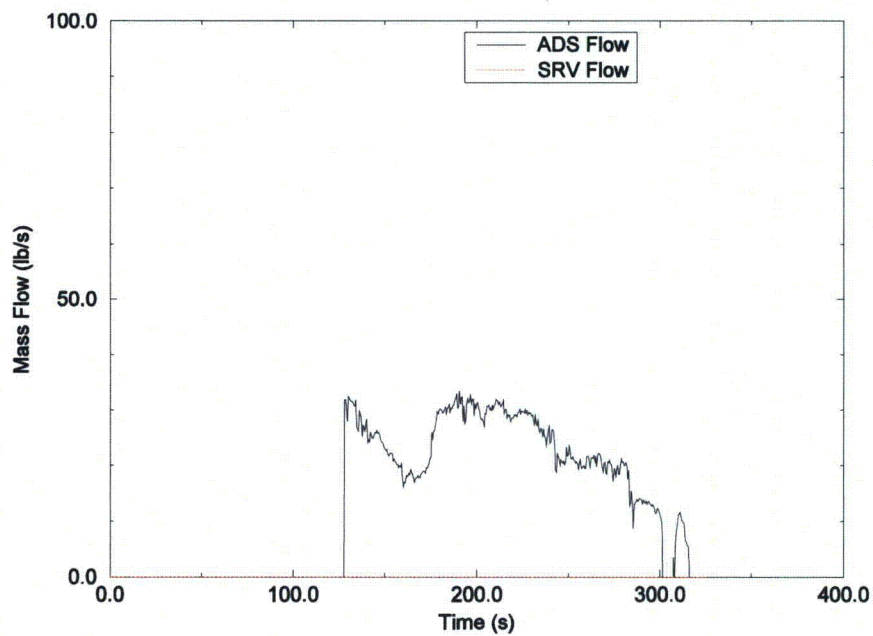


Figure 7-491 BWR/6 LBA ADS/SRV Flows

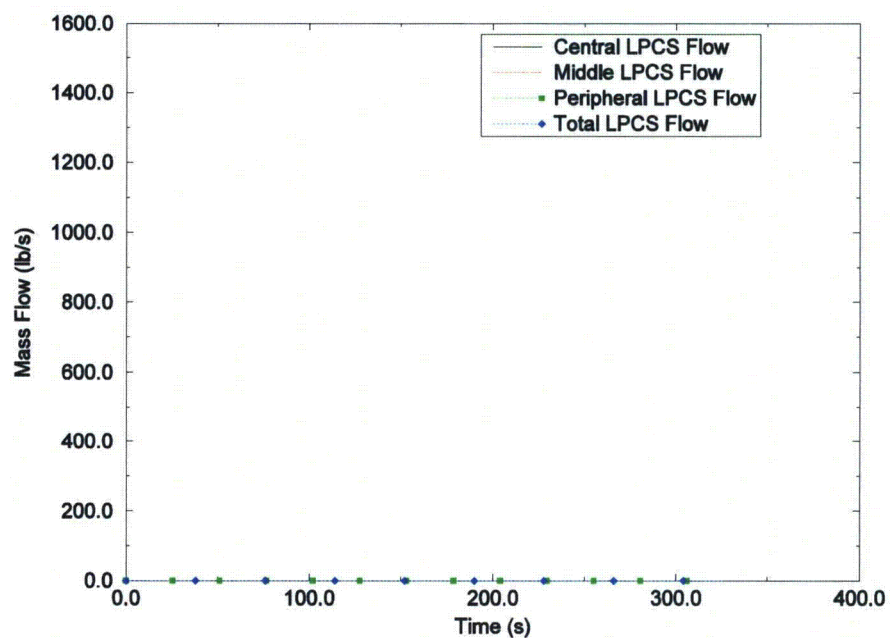


Figure 7-492 BWR/6 LBA LPCS Flow

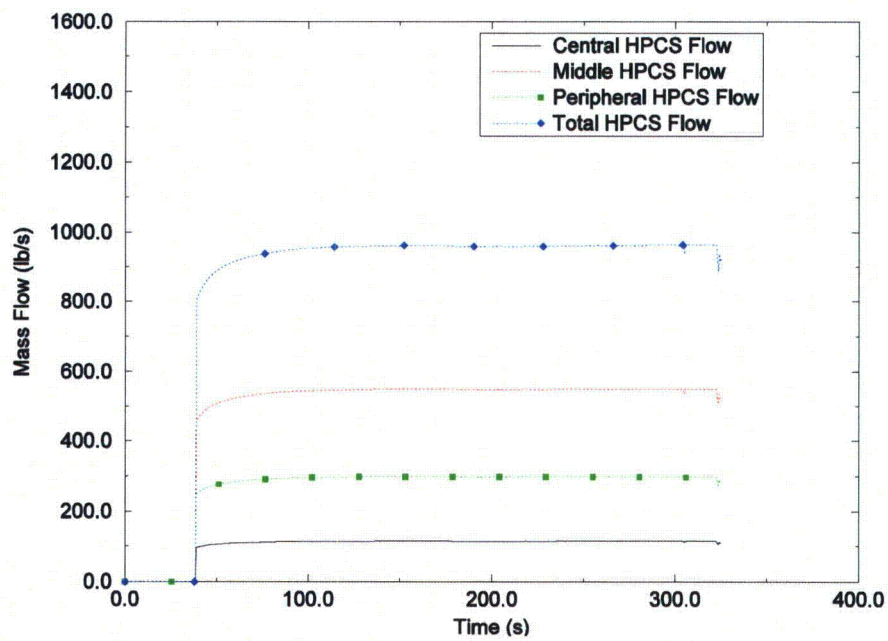


Figure 7-493 BWR/6 LBA HPCS Flow

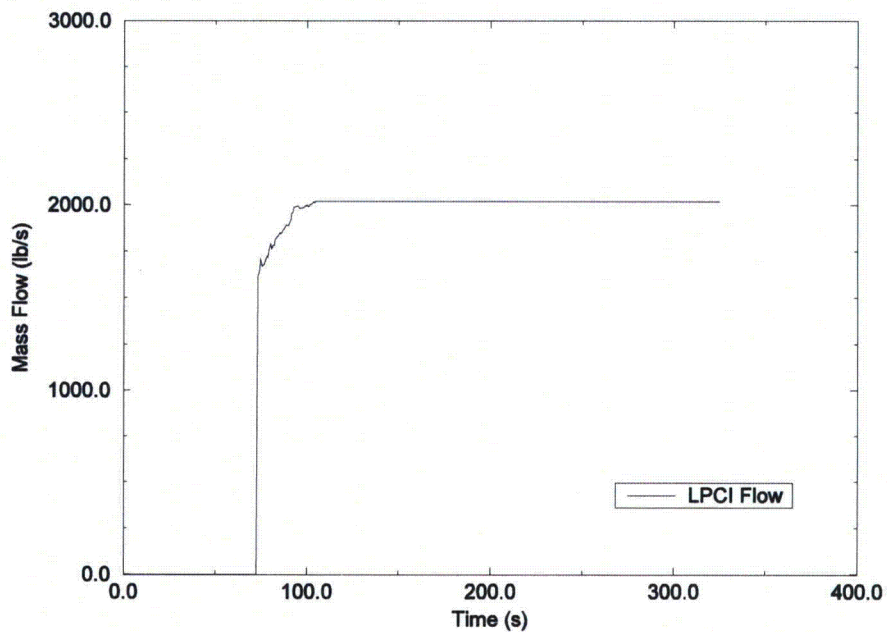


Figure 7-494 BWR/6 LBA LPCI Flow

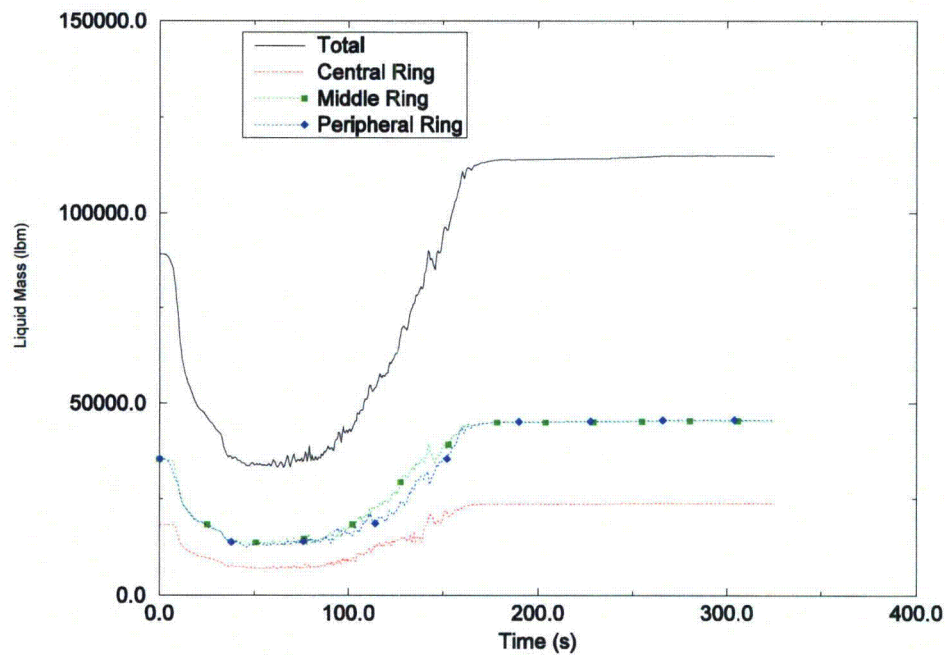


Figure 7-495 BWR/6 LBA Lower Plenum Liquid Mass

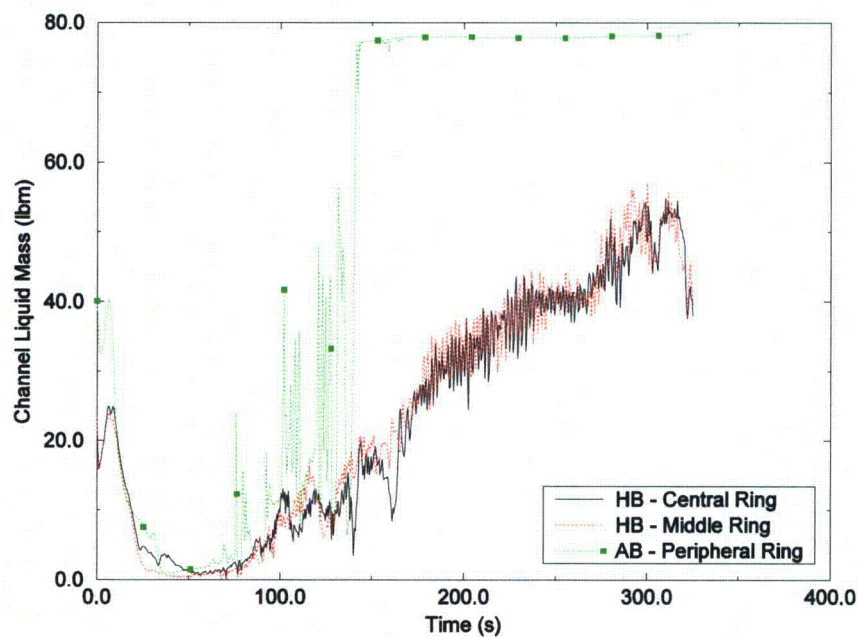


Figure 7-496 BWR/6 LBA Core Channels Liquid Mass

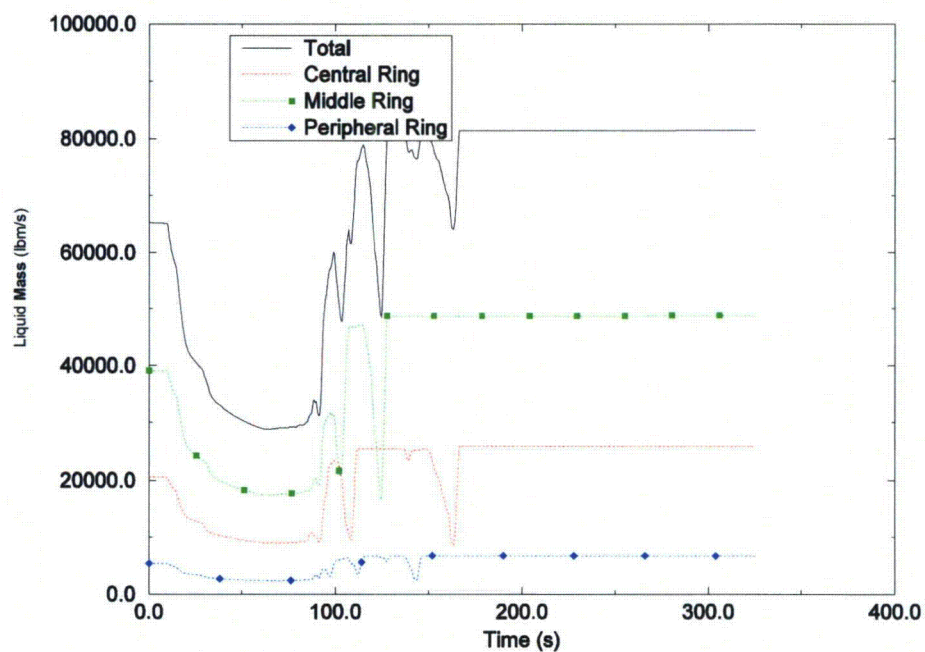


Figure 7-497 BWR/6 LBA Guide Tube Liquid Mass

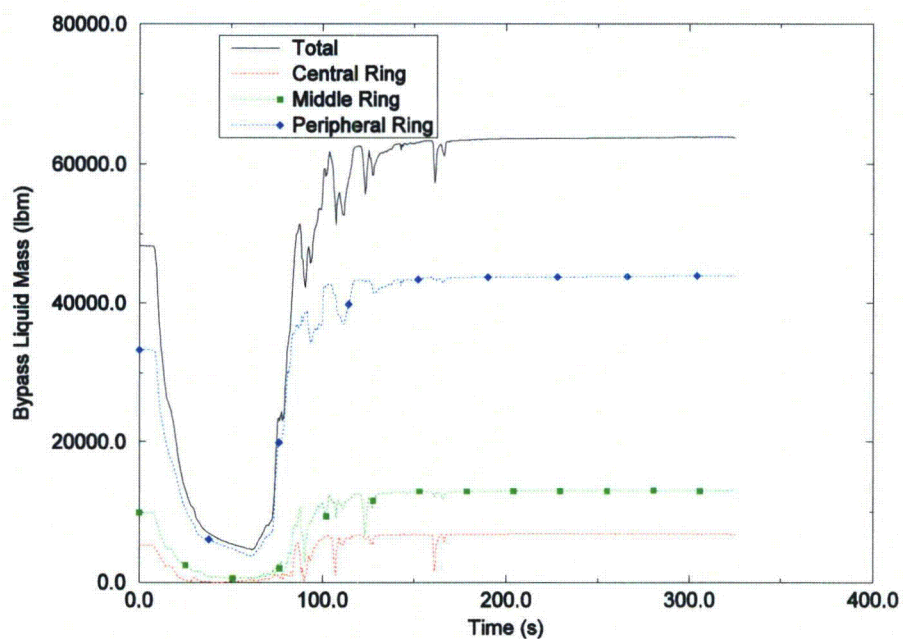


Figure 7-498 BWR/6 LBA Bypass Liquid Mass

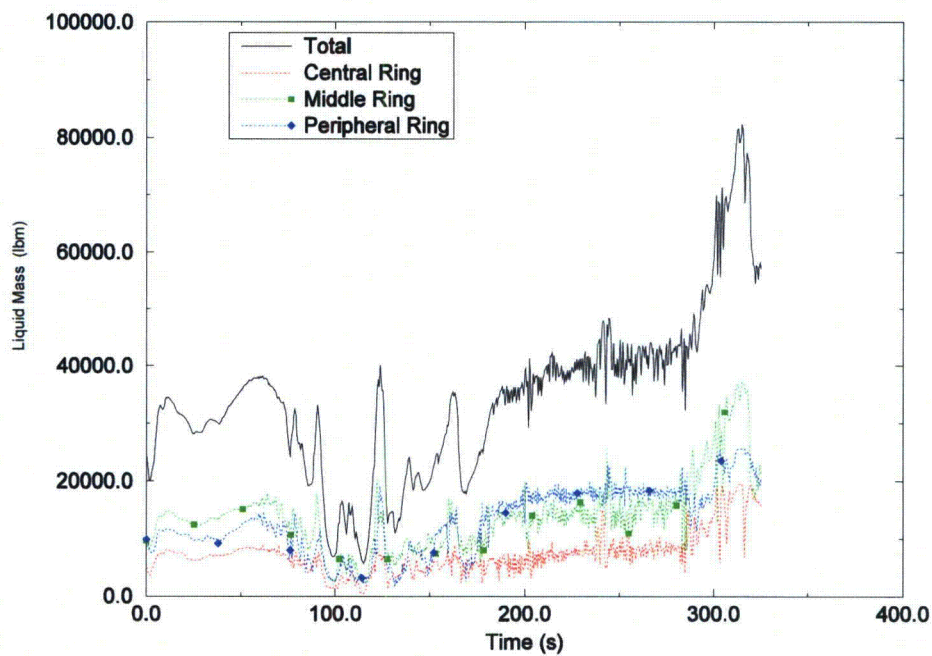


Figure 7-499 BWR/6 LBA Upper Plenum Liquid Mass

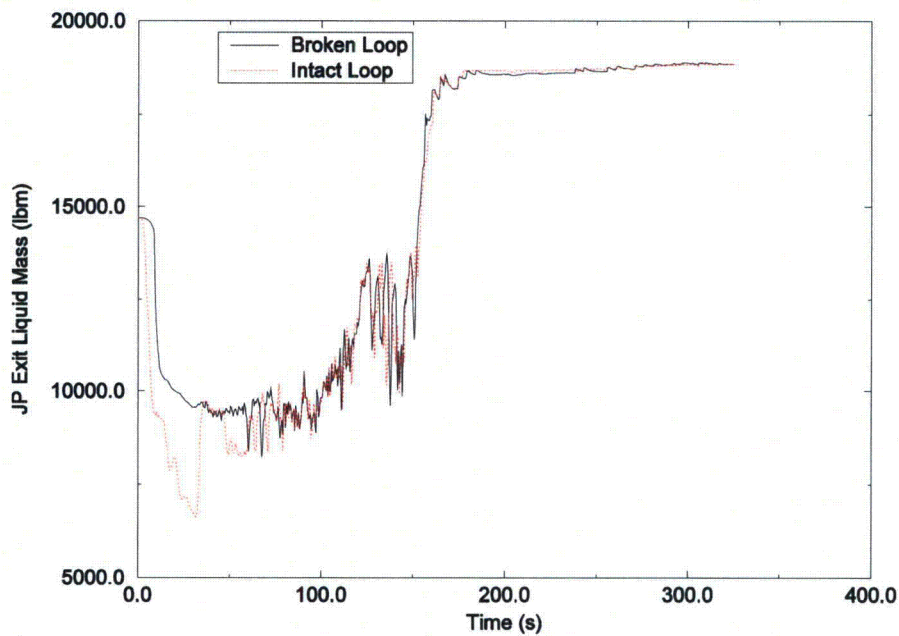


Figure 7-500 BWR/6 LBA Jet Pump Exit Liquid Mass

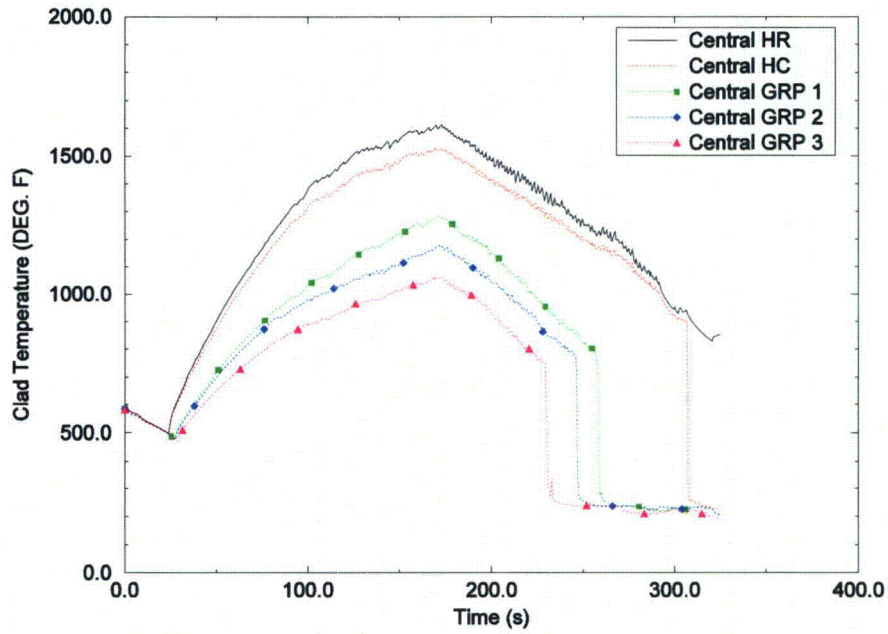


Figure 7-501 BWR/6 LBA Central Region Peak Node Temperature

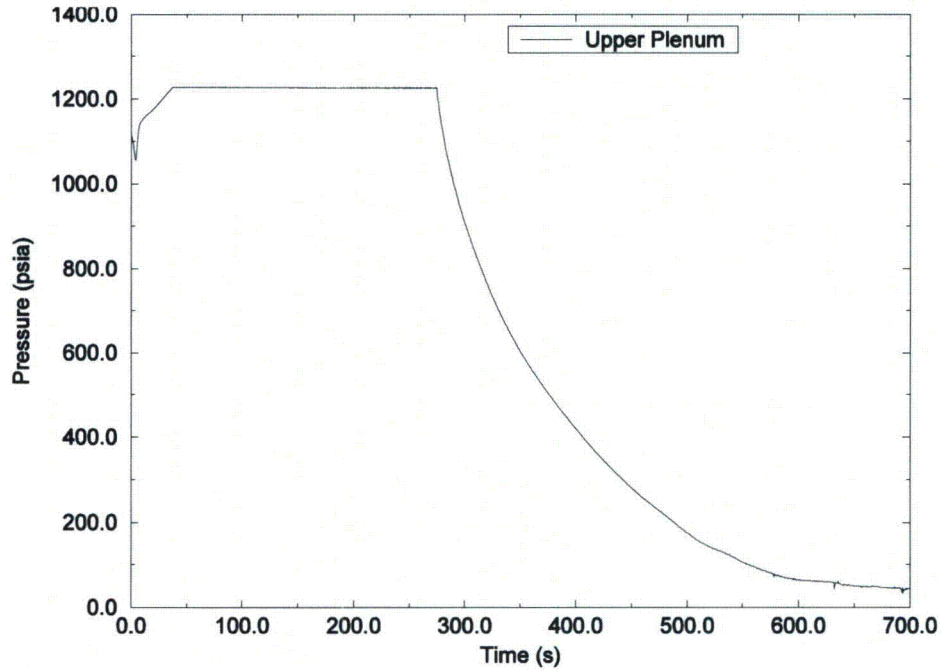


Figure 7-502 BWR/6 SBA Upper Plenum Pressure

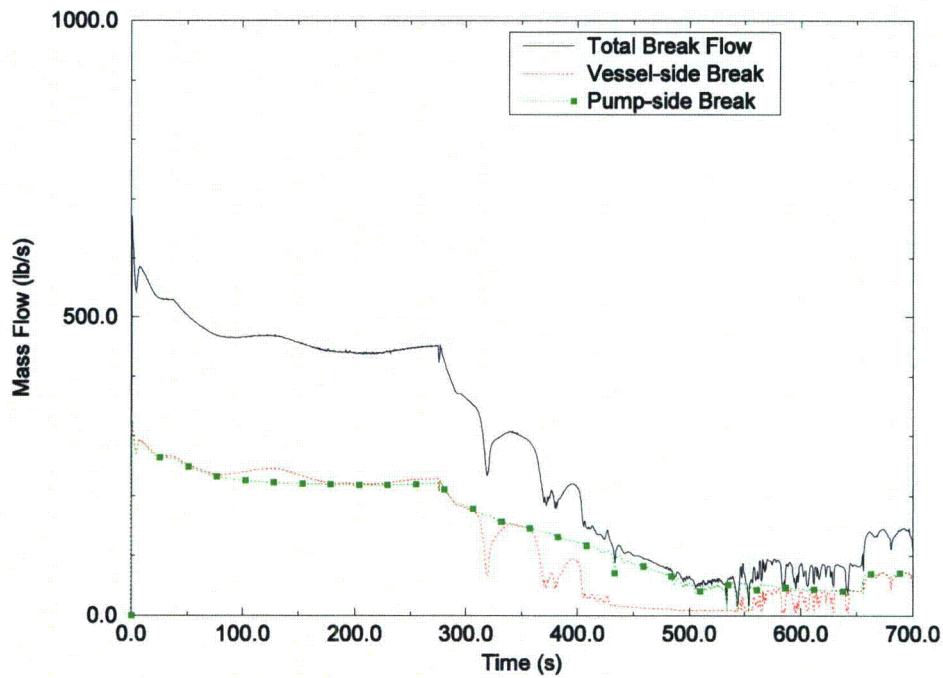


Figure 7-503 BWR/6 SBA Break Flow Rate

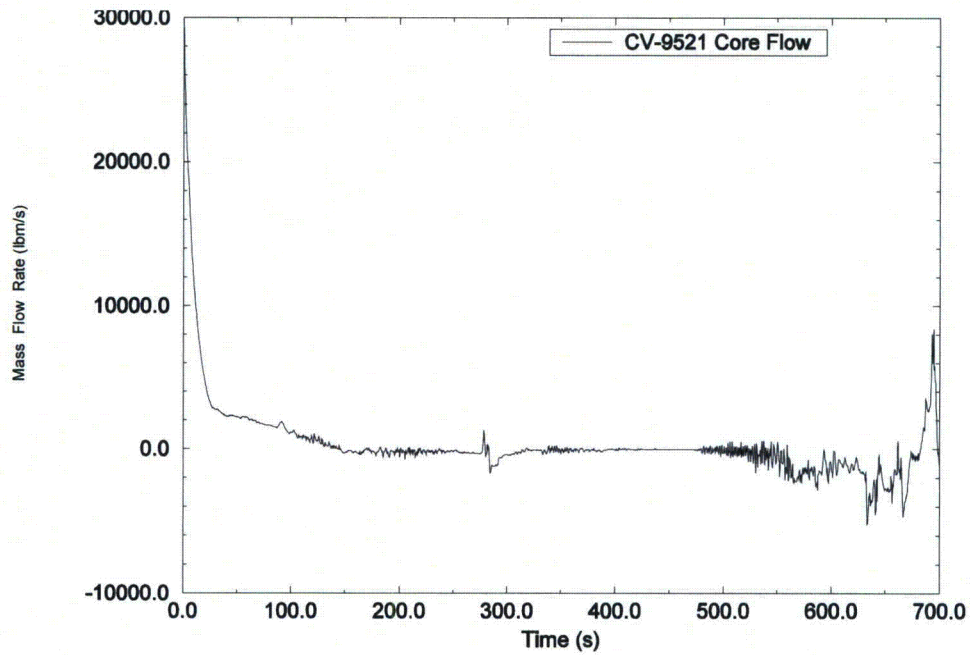


Figure 7-504 BWR/6 SBA Total Jet Pump Flow

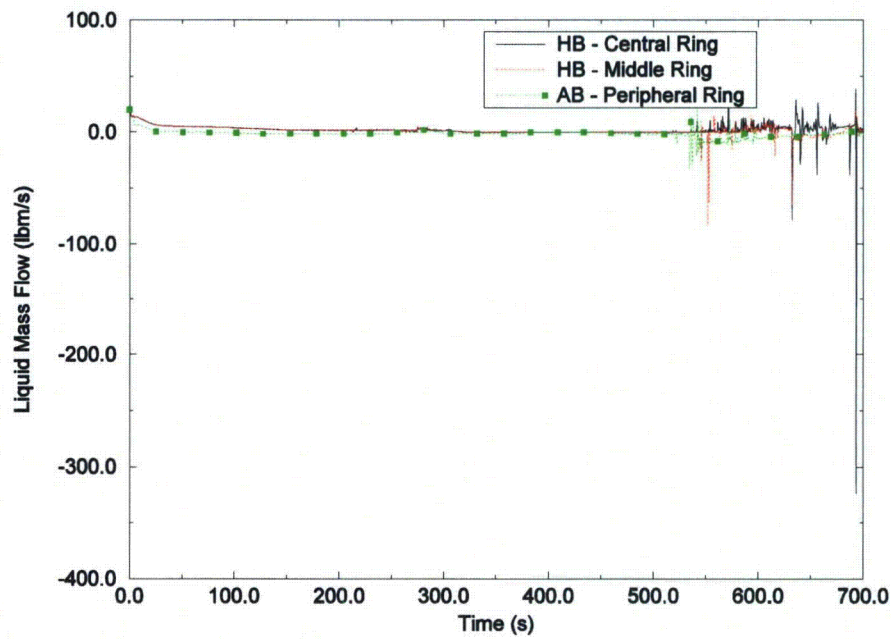


Figure 7-505 BWR/6 SBA Core Outlet Flow

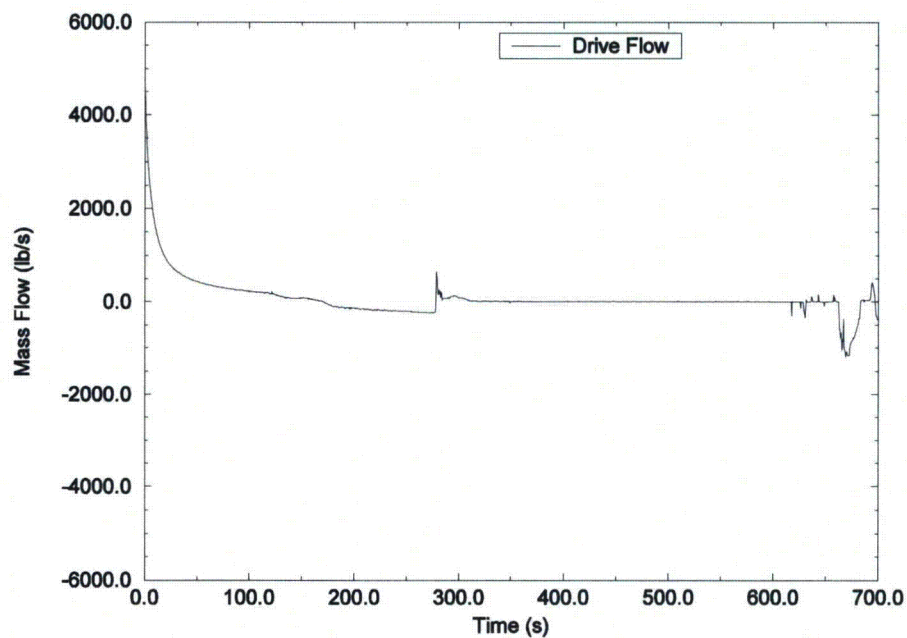


Figure 7-506 BWR/6 SBA Intact Loop Jet Pump Drive Flow

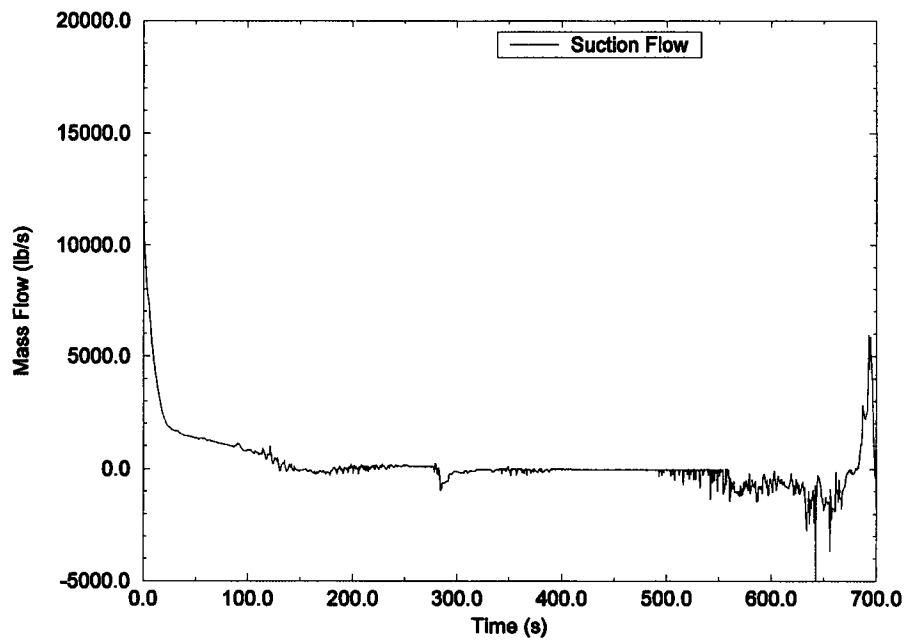


Figure 7-507 BWR/6 SBA Intact Loop Jet Pump Suction Flow

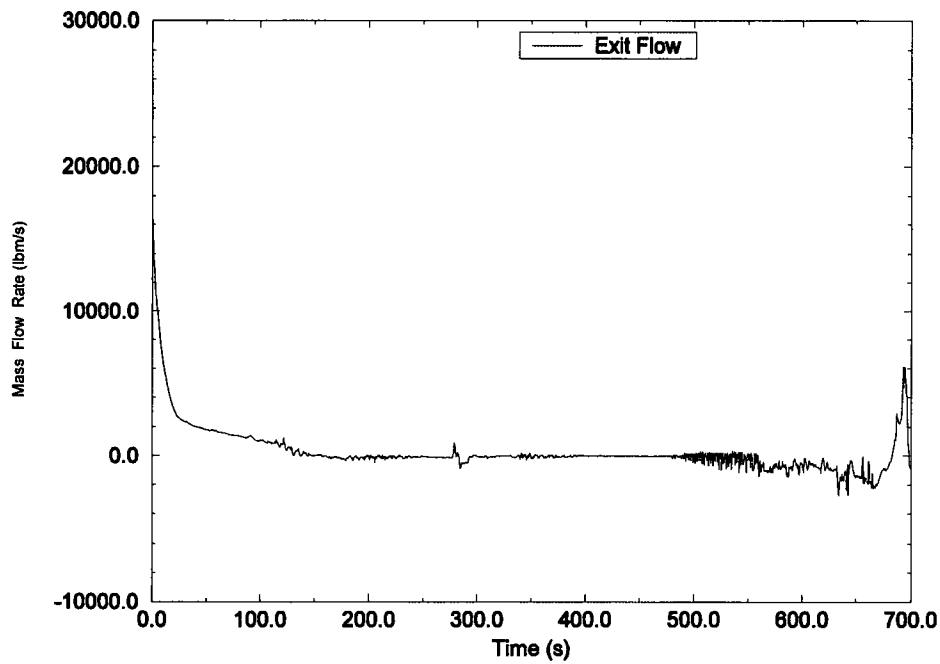


Figure 7-508 BWR/6 SBA Intact Loop Jet Pump Exit Flow

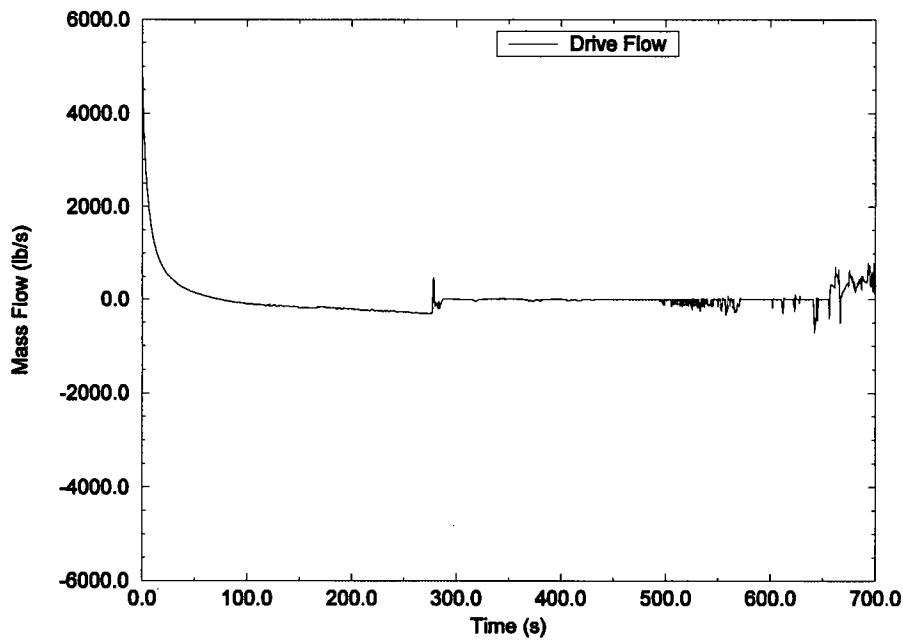


Figure 7-509 BWR/6 SBA Broken Loop Jet Pump Drive Flow

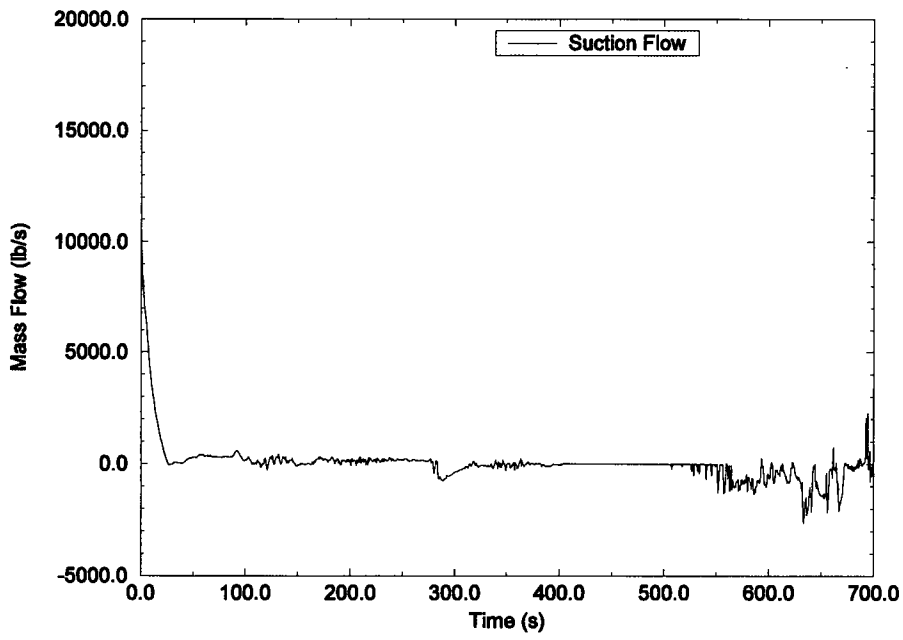


Figure 7-510 BWR/6 SBA Broken Loop Jet Pump Suction Flow

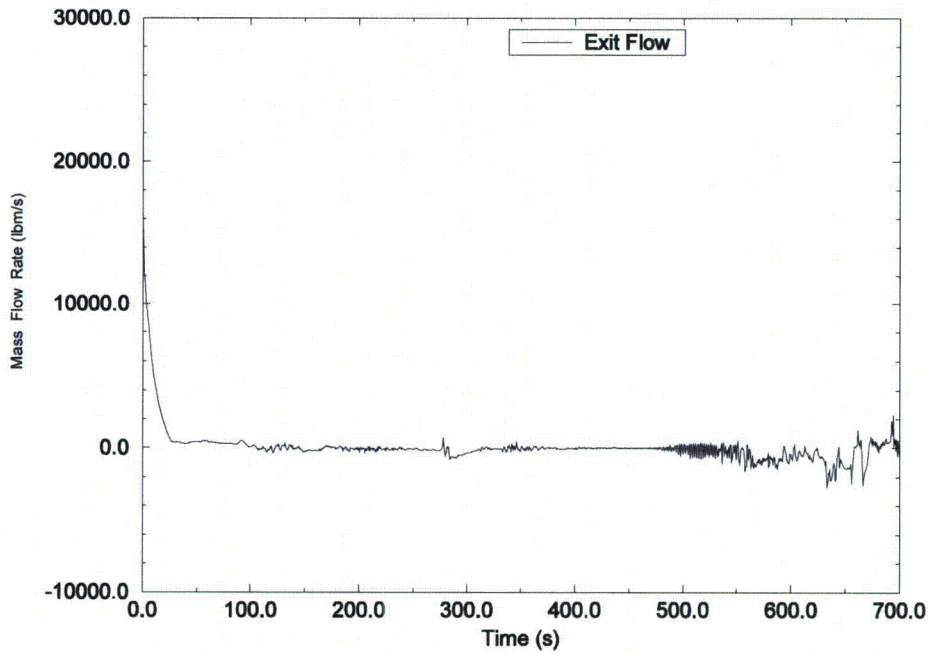


Figure 7-511 BWR/6 SBA Broken Loop Jet Pump Exit Flow

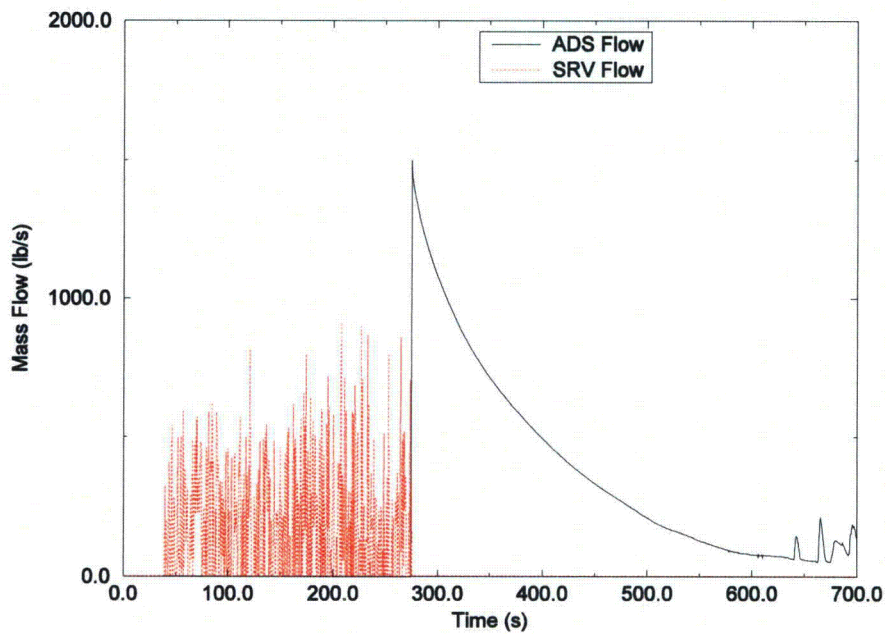


Figure 7-512 BWR/6 SBA ADS/SRV Flows

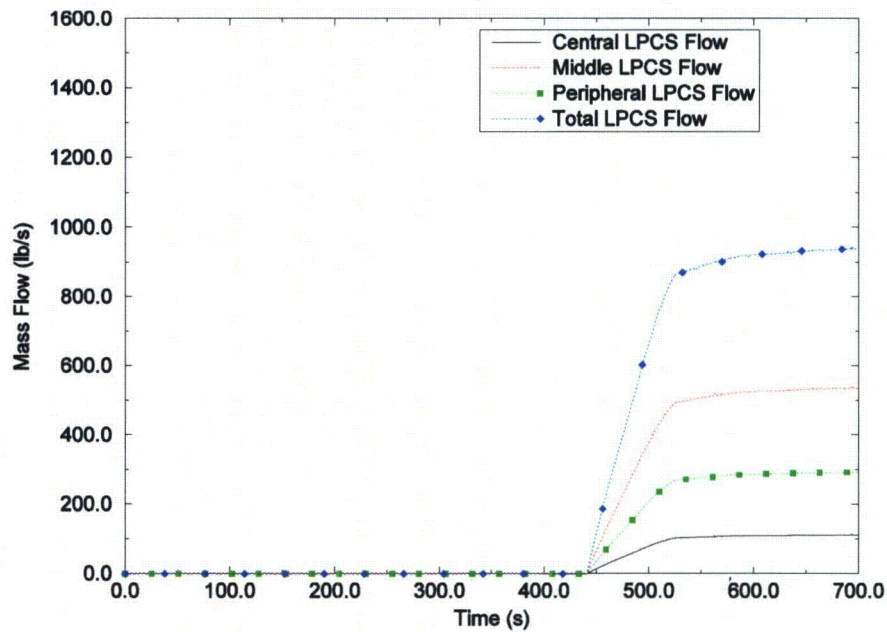


Figure 7-513 BWR/6 SBA LPCS Flow

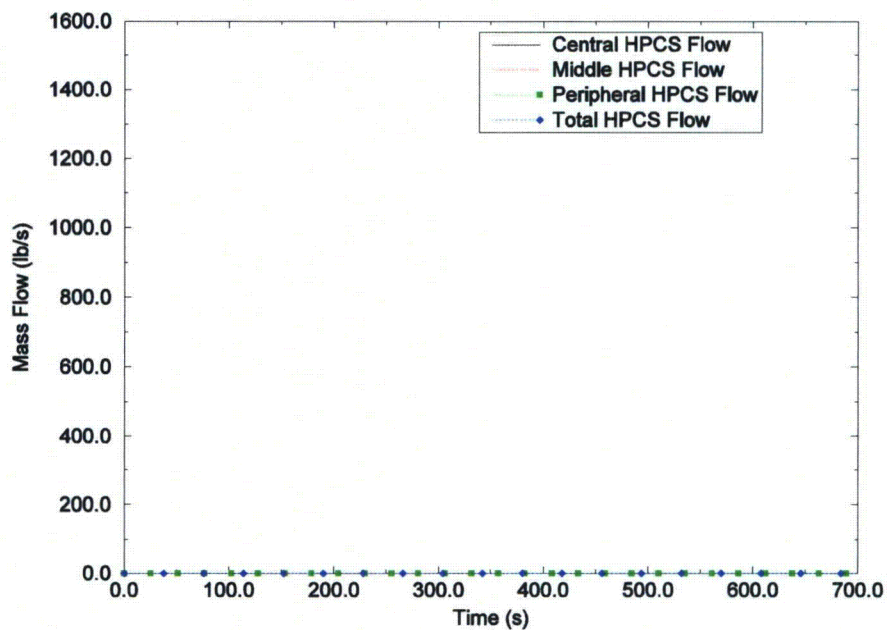


Figure 7-514 BWR/6 SBA HPCS Flow

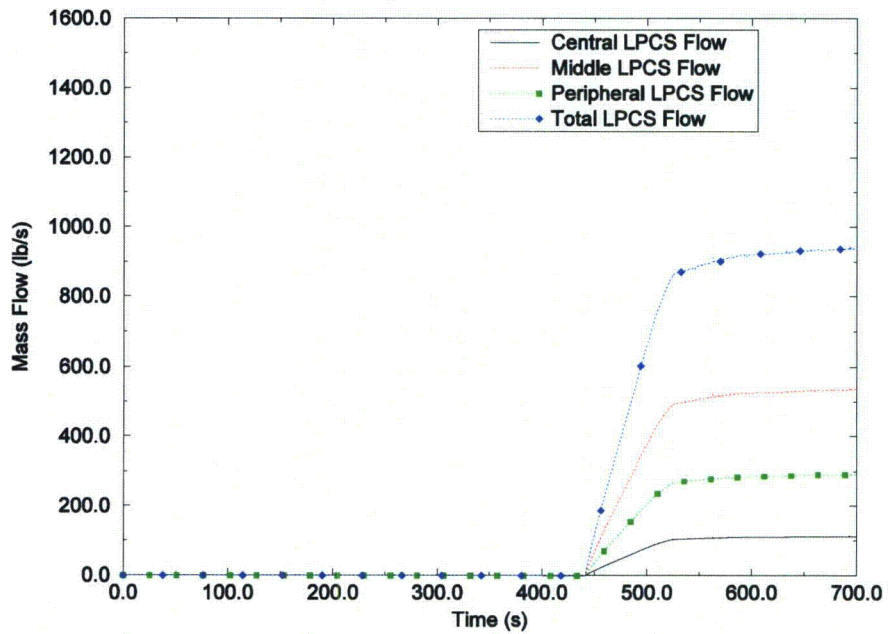


Figure 7-515 BWR/6 SBA LPCI Flow

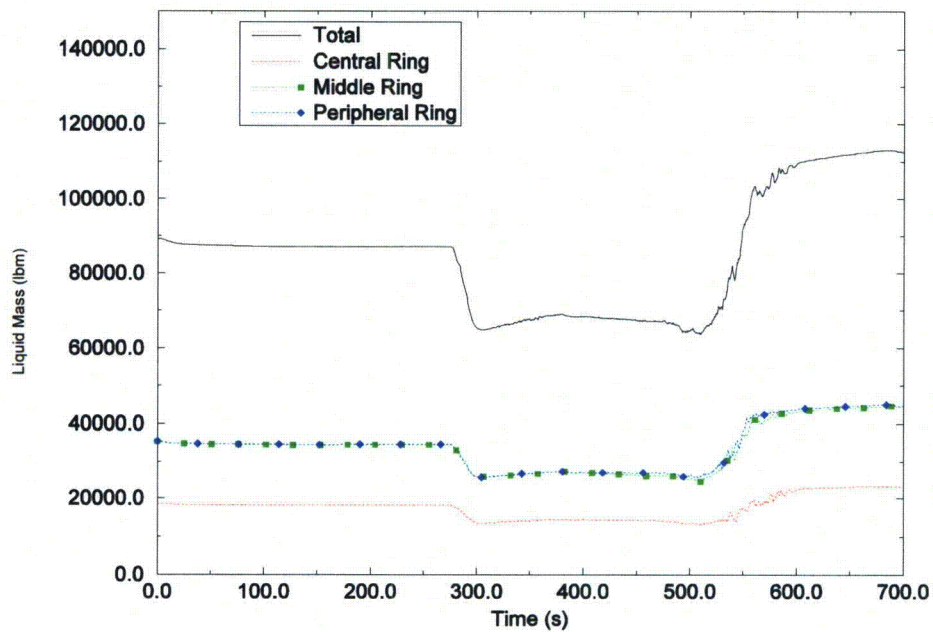


Figure 7-516 BWR/6 SBA Lower Plenum Liquid Mass

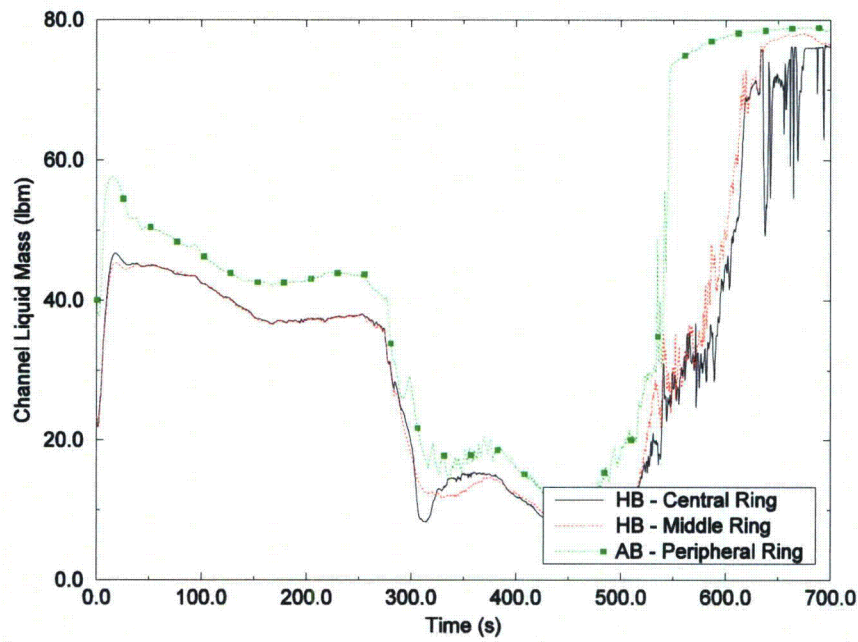


Figure 7-517 BWR/6 SBA Core Channels Liquid Mass

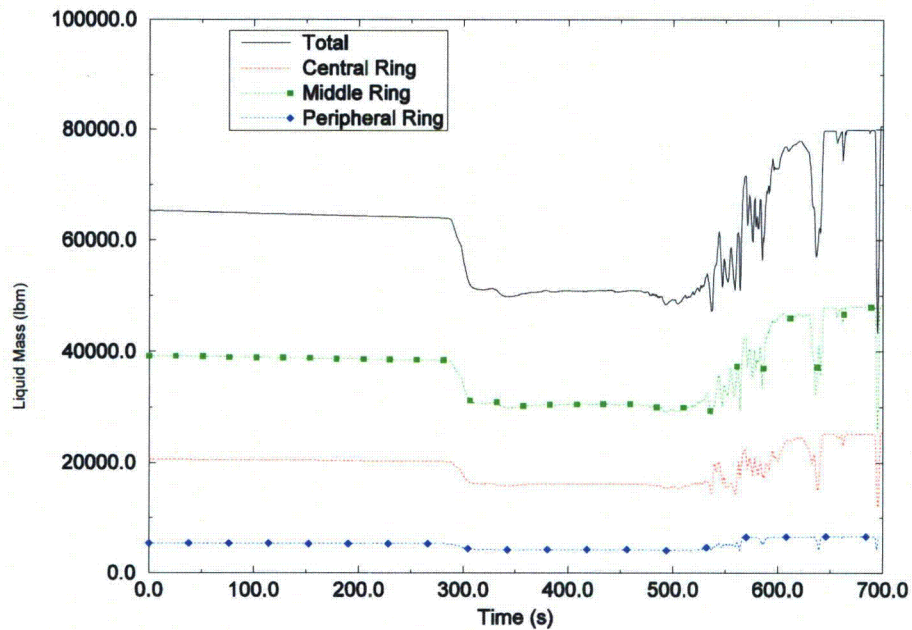


Figure 7-518 BWR/6 SBA Guide Tube Liquid Mass

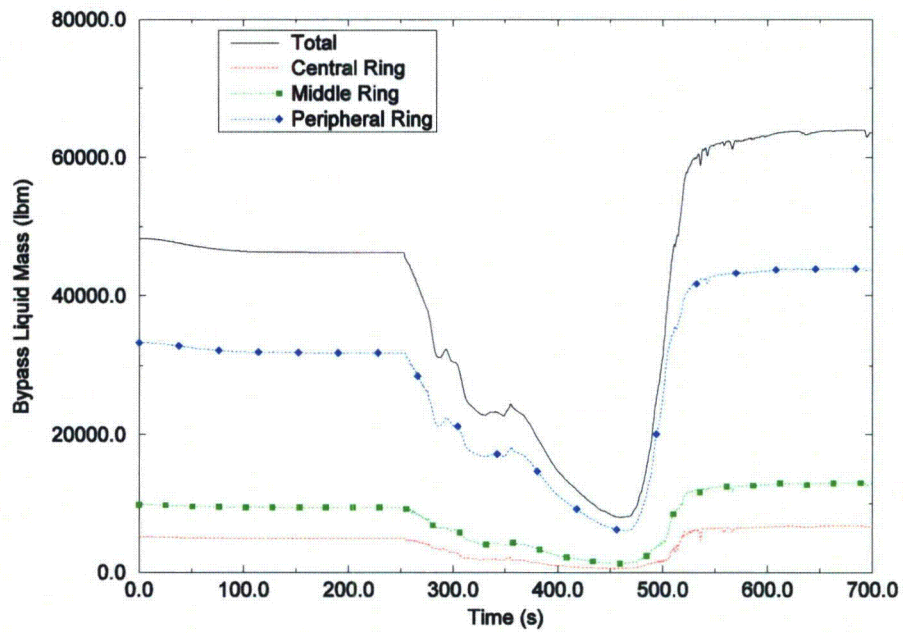


Figure 7-519 BWR/6 SBA Bypass Liquid Mass

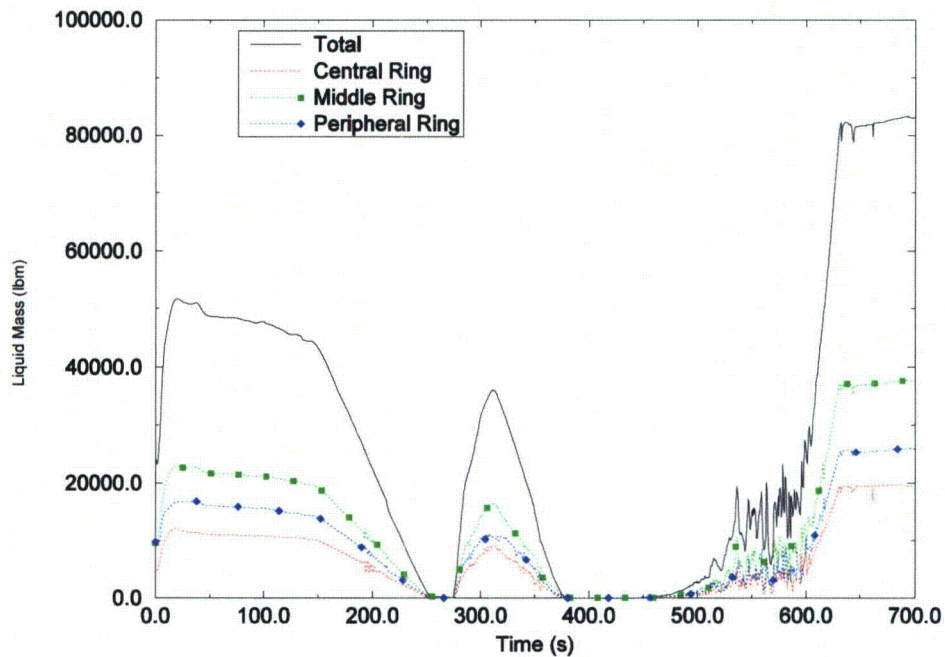


Figure 7-520 BWR/6 SBA Upper Plenum Liquid Mass

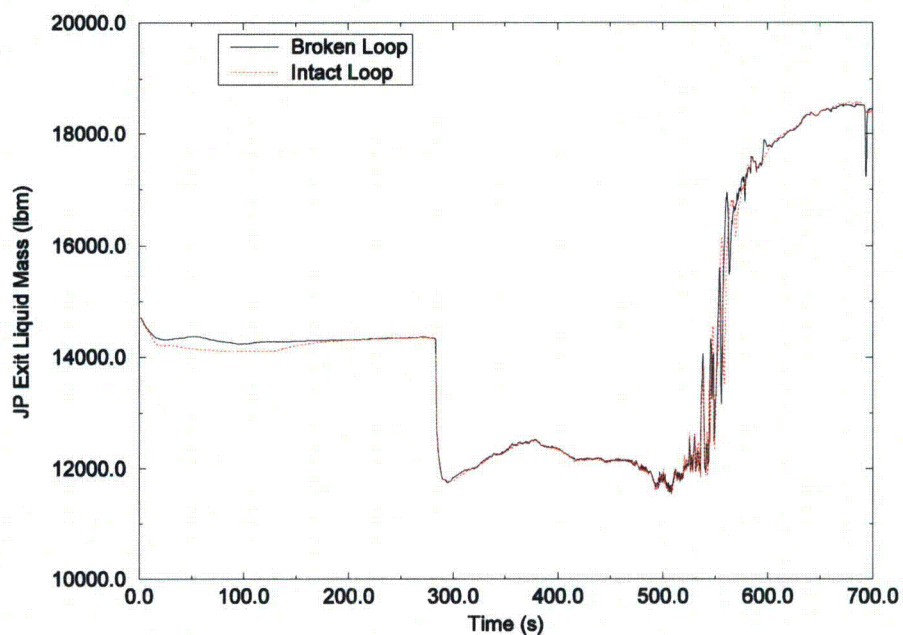


Figure 7-521 BWR/6 SBA Jet Pump Exit Liquid Mass

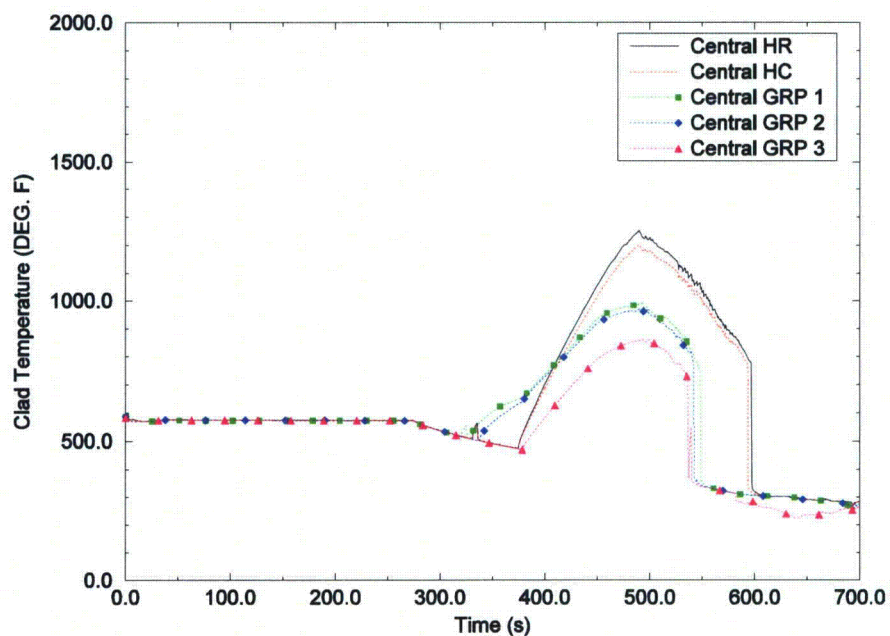


Figure 7-522 BWR/6 SBA Central Region Peak Node Temperature

7.8 Assess Scalability of Integrated Calculations and Data for Distortions (EMDAP Step 19)

The scalability of the integrated calculations and distortions in test facilities and data are addressed in the previous section where they are observed. When observed, their impact and consequences for the noted situation were described.

7.9 Determine Evaluation Model Biases and Uncertainties (EMDAP Step 20)

The AURORA-B LOCA EM is based on Appendix K criteria; therefore, it is a conservative method and does not rely on uncertainty analysis. In summary, Reference 4 best defines the needs in the EMDAP process:

The amendment to 10 CFR Part 50 and Regulatory Guide 1.157 now permit licensees or applicants to use either the conservative analysis methods defined in Appendix K or a realistic EM (commonly referred to as best-estimate plus uncertainty analysis methods). That is, the uncertainty in the best-estimate analysis must be quantified and considered when comparing the results of the calculations with the applicable limits

An uncertainty methodology is not required for the original conservative Appendix K option in 10 CFR 50.46. Rather, the features required by Appendix K provide sufficient conservatism without the need for an uncertainty analysis. It should be noted that Section II.4 of Appendix K requires that "To the extent practicable, predictions of the EM, or portions thereof, shall be compared with applicable experimental information."

Thus, Appendix K requires comparisons to data similar to those required for the best-estimate option, but without the need for an uncertainty analysis. However, poor comparisons with applicable data may prevent NRC acceptance of the Appendix K model.

Consistent with Appendix K requirements, nodalization and time steps studies are presented in later sections.

7.9.1 Regulatory Basis: Appendix K Conservatism in AURORA-B LOCA EM

The following are the general conservatisms of Appendix K.

- Initialization at 102% power (plant specific application may be different based on USNRC approval)
- Decay heat based on the ANS-71 Draft Standard decay heat with a multiplier of 1.2
- Conservative stored energy
- Discharge model based on Moody which results in an overprediction of lost liquid inventory from the break
- Restriction during blowdown for returning to nucleate and transition boiling

Specific to the AURORA-B LOCA EM other conservatisms include:

- Heat transfer correlations, specifically the application of dispersed film boiling and steam cooling
- []

7.9.2 Examples of Appendix K Conservatism for Select Assessments

To demonstrate the conservatisms of the Appendix K EM, the TLTA and FIST small break assessments were re-analyzed with the following changes.

- Power decay increased by a multiplier of 1.2
- Discharge model based on Moody (assessment used best estimate HEM)
- []

7.9.2.1 TLTA Case 6432-1

The Appendix-K assumptions included in the model are:

- a. Moody critical flow model used instead of HEM at break locations.
- b. []

- c. Appendix-K requires increasing the decay heat by 20% over the estimated values from the ANS-71 standard.

The TLTA small break input model discussed in Section 7.7.2.2 was used in this analysis.

The TLTA bundle power decay model was programmed to represent ANS-5 decay plus the stored energy. The plant model with Appendix-K EM assumptions uses a 1.2 multiplier on the representative (ANS-71) decay power.

S-RELAP5 predictions (with Appendix-K EM assumptions) for the heater rod temperatures at several elevations are shown in Figure 7-523 to Figure 7-528 and the PCT history is shown in Figure 7-529. Except for elevations below 20 inch, S-RELAP5 predicts heat-up and higher wall temperatures. The predicted PCT using the Appendix-K assumptions bounds the measured values. The mass inventory in the bundle and upper plenum are shown in Figure 7-530 and Figure 7-531. [

]

The bundle mass is underpredicted due to higher power which results in more steaming and also the downflow restriction from upper plenum.

The results of this simulation confirm that S-RELAP5 calculation with the Appendix-K assumptions used in plant modeling conservatively bounds the measured PCT.



Figure 7-523 Comparison of Measured and Predicted Heater Wall Temperatures, 19 inch Elevation – TLTA Test 6432-1 with Appendix-K Assumptions




Figure 7-524 Comparison of Measured and Predicted Heater Wall Temperatures, 63 inch Elevation – TLTA Test 6432-1 with Appendix-K Assumptions




Figure 7-525 Comparison of Measured and Predicted Heater Wall Temperatures, 83 inch Elevation – TLTA Test 6432-1 with Appendix-K Assumptions



Figure 7-526 Comparison of Measured and Predicted Heater Wall Temperatures, 100 inch Elevation – TLTA Test 6432-1 with Appendix-K Assumptions



**Figure 7-527 Comparison of Measured and Predicted Heater Wall Temperatures,
120 inch Elevation – TLTA Test 6432-1 with Appendix-K Assumptions**



**Figure 7-528 Comparison of Measured and Predicted Heater Wall Temperatures,
143 inch Elevation – TLTA Test 6432-1 with Appendix-K Assumptions**


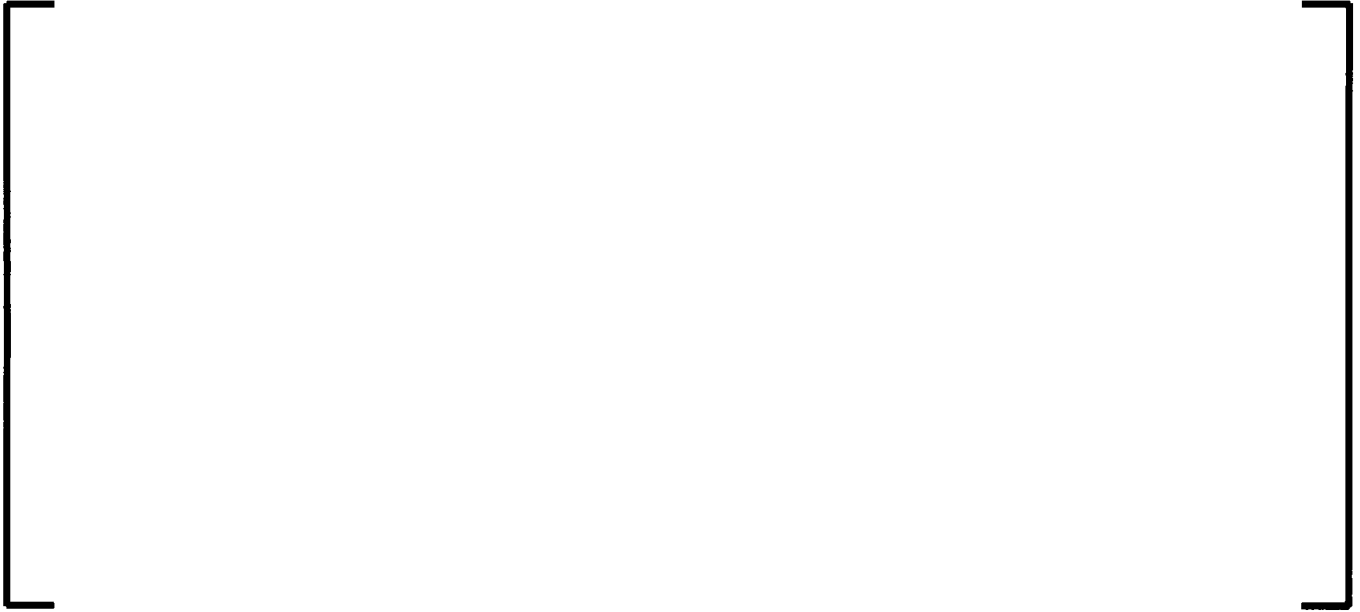


Figure 7-529 Comparison of Measured and Predicted Peak Cladding Temperature – TLTA Test 6432-1 with Appendix-K Assumptions



Figure 7-530 Comparison of Measured and Predicted Bundle Mass – TLTA Test 6432-1 with Appendix-K Assumptions



**Figure 7-531 Comparison of Measured and Predicted Upper
Plenum Mass – TLTA Test 6432-1 with Appendix-K Assumptions**

7.9.2.2 FIST Small Break Case

The BWR/6 small break test 6SB2C presented in Section 7.7.3.2 was repeated with the Appendix-K assumptions to evaluate if the measured temperatures would be bounded with the options used in the plant modeling. The Appendix-K assumptions included in the model are:

- a) Moody critical flow model used instead of HEM at break locations.
- b) []
- c) Appendix-K recommends increasing the decay heat by 20% over the estimated values.

The major event timing and the hydraulic parameters were predicted satisfactorily in Section 7.7.3.2 but the predicted bundle mass and void fractions showed that the bundle was holding more liquid and the predicted PCT was considerably lower than measured values. The objective of the present evaluation is to show the capability of S-RELAP5 with Appendix-K assumptions in predicting the heater rod surface temperatures. The comparison of the measured and predicted heater rod mid-point temperatures is shown in Figure 7-532. S-RELAP5 predicts later heat-up initiation with a comparable heat-up rate. However, the predicted temperature rise continues and the predicted temperature for node 14 bounds the highest measured mid-point temperature. Figure 7-533 compares the predicted and measured PCTs and again the measured values are bounded by the predicted PCT which is at node 16. The measured PCT of 925°F at 390 s compares to a predicted PCT of 945°F at 435s, S-RELAP5 calculated PCT and time of rod quench at all elevations occur later than measured times.

The predicted bundle mass and void fractions at different elevations are shown in Figure 7-534 to Figure 7-537. In comparison to similar figures in Section 7.7.3.2, the case with Appendix-K assumptions results in less liquid in the bundle after heat-up initiation. Bundle void fraction is closer to the measured values and show nearly dry bundle after 300 s.

The results of this prediction confirm that S-RELAP5 with the Appendix-K assumptions used in plant modeling bounds the measured temperatures.



Figure 7-532 Comparison of the Measured and Predicted Mid-Point Heater Rod Temperatures – FIST Test 6SB2C with App-K Assumptions



Figure 7-533 Comparison of the Measured and Predicted PCT – FIST Test 6SB2C with App-K Assumptions



**Figure 7-534 Comparison of the Measured and Predicted Bundle Mass –
FIST Test 6SB2C with App-K Assumptions**



**Figure 7-535 Comparison of the Measured and Predicted Bundle Void
Fraction at 37”– FIST Test 6SB2C with App-K Assumptions**



Figure 7-536 Comparison of the Measured and Predicted Bundle Void Fraction at 57"– FIST Test 6SB2C with App-K Assumptions



Figure 7-537 Comparison of the Measured and Predicted Bundle Void Fraction at 117"– FIST Test 6SB2C with App-K Assumptions

7.9.3 Time Step Sensitivity Analyses

A time step sensitivity is made to demonstrate a converged solution with time. This demonstration was made to cover the range of time steps, power shape and break size. The range of parameters is shown in Table 7-60. The BWR/4 plant design was chosen for the sensitivity as it provides a wide range of response from large to small breaks due to larger recirculation lines and lower ECCS flow.

The following BWR/4 cases are used to demonstrate the sensitivity to the maximum time step request.

1.0 DEG PS SF-LOCA MID (Figure 7-538)

1.0 DEG PD SF-BATT TOP (Figure 7-539)

0.10 DES PD SF-BATT MID (Figure 7-540)

0.10 DES PD SF-BATT TOP (Figure 7-541)

The results of the time step study are presented in Figure 7-538 through Figure 7-541. The results show that the solution is converged in time by the relatively small impact of the PCT FoM from reducing the time step from the nominal time step. The results show that a time step larger than the nominal should not be used since the results can be significantly altered in the SBA.

Table 7-60 LOCA Time Step Study Variables

Variable	Range in this analysis
State point	102%P/108%F
Maximum Time step Request	Large – 0.010 S, Nominal – 0.005 S Small – 0.0025 S, Smallest – 0.001 S
Power Shape	TOP, MID
Single Failure	BATT, LOCA
Break Location	Suction (PS), Discharge (PD)
Break Size/Type	1.0DEG, 0.10DES



Figure 7-538 Time Step Study, LBA, MID Result for 1.0 DEG PS SF-LOCA



Figure 7-539 Time Step Study, LBA, TOP Result for 1.0 DEG PD SF-BATT

Figure 7-540 Time Step Study, SBA, MID Result for 0.10 ft² DES PD SF-BATT

Figure 7-541 Time Step Study, SBA, TOP Result for 0.10 ft² DES PD SF-BATT

7.9.4 Hot Channel Axial Nodalization Sensitivity Analyses

A study was made to demonstrate hot channel nodal convergence. [

]

The comparison was made for a LBA, 1.0 DEG recirculation pump suction line with the single failure SF-BATT, and a SBA, 0.10 ft² split break in the recirculation pump discharge line with the single failure SF-BATT.

[

]



Figure 7-542 Core Node Sensitivity – Large and Small Break Result

7.9.5 Core Axial Power Shape Sensitivity Analyses

The sensitivity to axial power shape is demonstrated in two ways. First, a comparison is made that shows the impact of changing the power shape of the hot channel only (mid-peaked vs. top peaked). Secondly, a comparison is made that shows the impact of changing the power shape in the balance of the core other than the hot channel (mid-peaked vs. top-peaked).

The comparisons are made with the BWR/4 LBA and SBA.

Top-peaked Core Sensitivity – (Top Peaked to Mid Peaked Hot Channel)

[

]

Top-peaked Core Sensitivity – (Top Peaked Core to Top Peaked Hot Channel)

[

]

[

]



Figure 7-543 Mid-peaked Hot Channel Vs. Top-peaked Hot Channel Cases

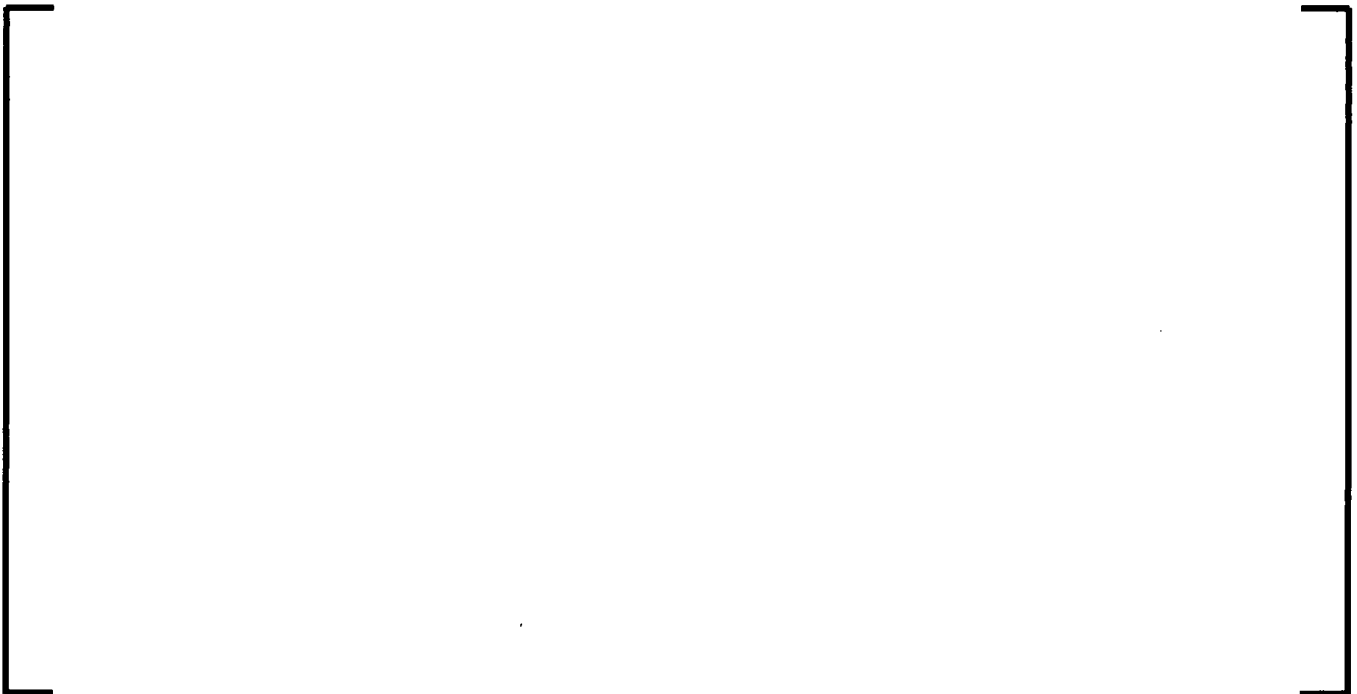


Figure 7-544 Top-peaked Hot Channel Vs. Entire Core Top-peaked Cases

7.9.6 Core Radial Sensitivity Analyses

7.9.6.1 BWR/4 Bundle Radial Power Sensitivity Analysis

A study of the impact of the radial power shape was made. The amount of the power in a region (Central or Middle) was changed as well as the distribution of the power in the region (uniform versus graded from above average to below average power).

[

]



Figure 7-545 Uniform vs. Non-uniform Channels and Radial Power

7.9.6.2 SSTF Bundle Radial Power Sensitivity Analysis

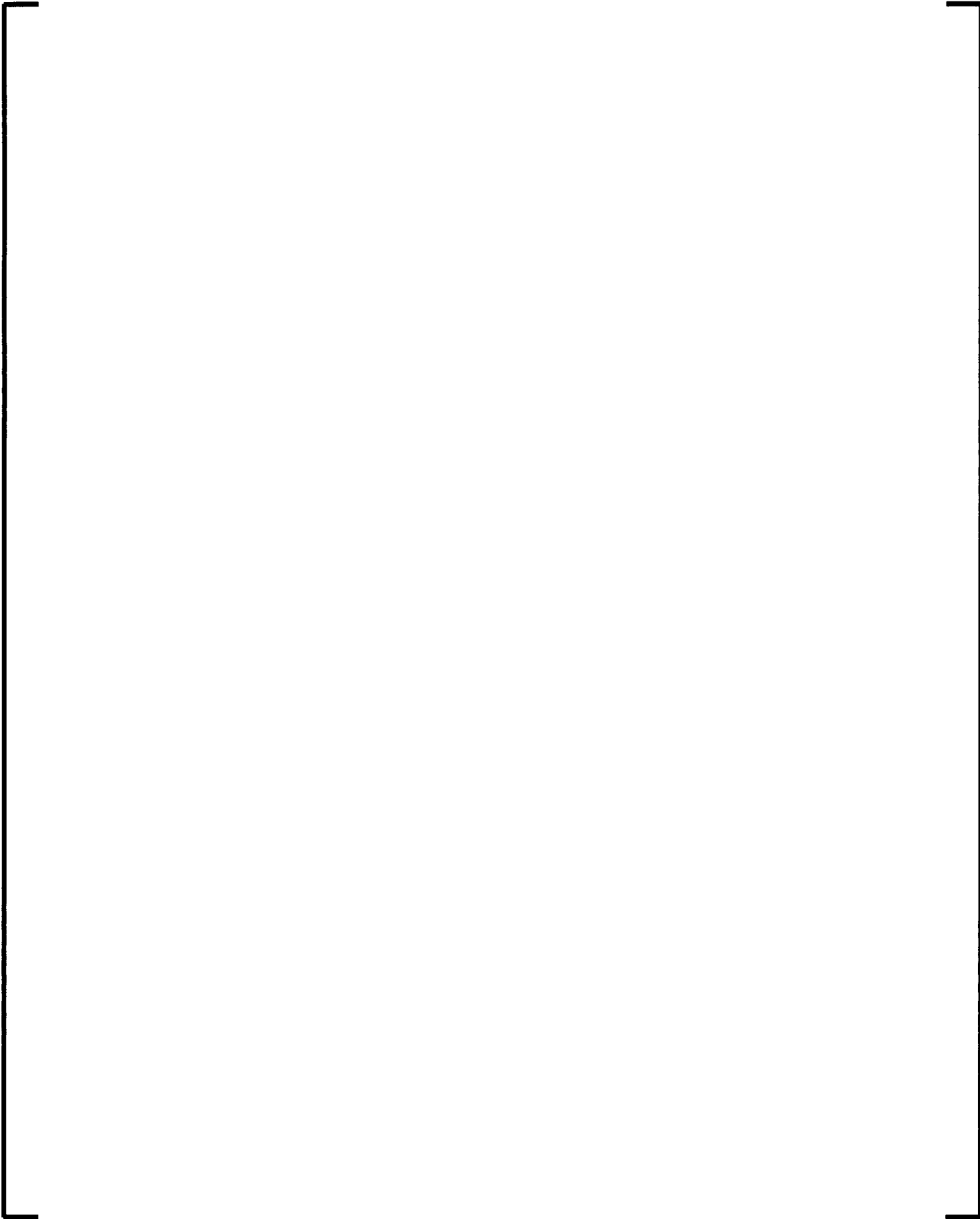


Table 7-61 Summary of Bundle Groups in SSTF Parametric Cases

--

7.9.6.2.1 T026_y52 Base Case (13 Bundle Groups) Results

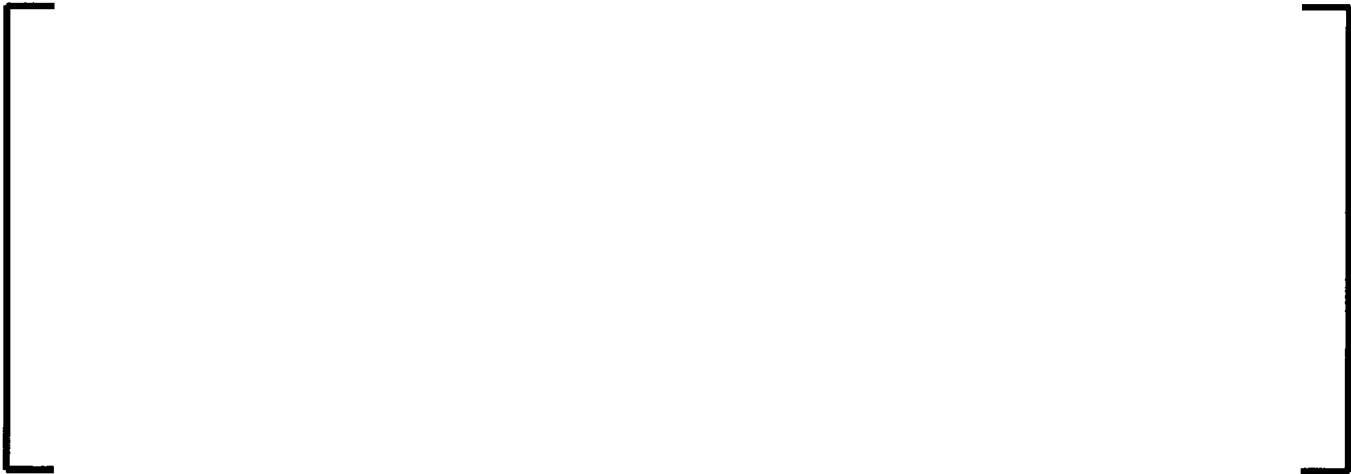


Table 7-62 SSTF Central Bundle Grouping (Base Case, 13 Groups, T026_y52) and Bundles in Counter-Current Flow



Figure 7-546 SSTF Base Case (T026_y52) – Liquid and Vapor Mass Flows at F011 SEO



Figure 7-547 SSTF Base Case (T026_y52) – Liquid and Vapor Mass Flows at F012 SEO

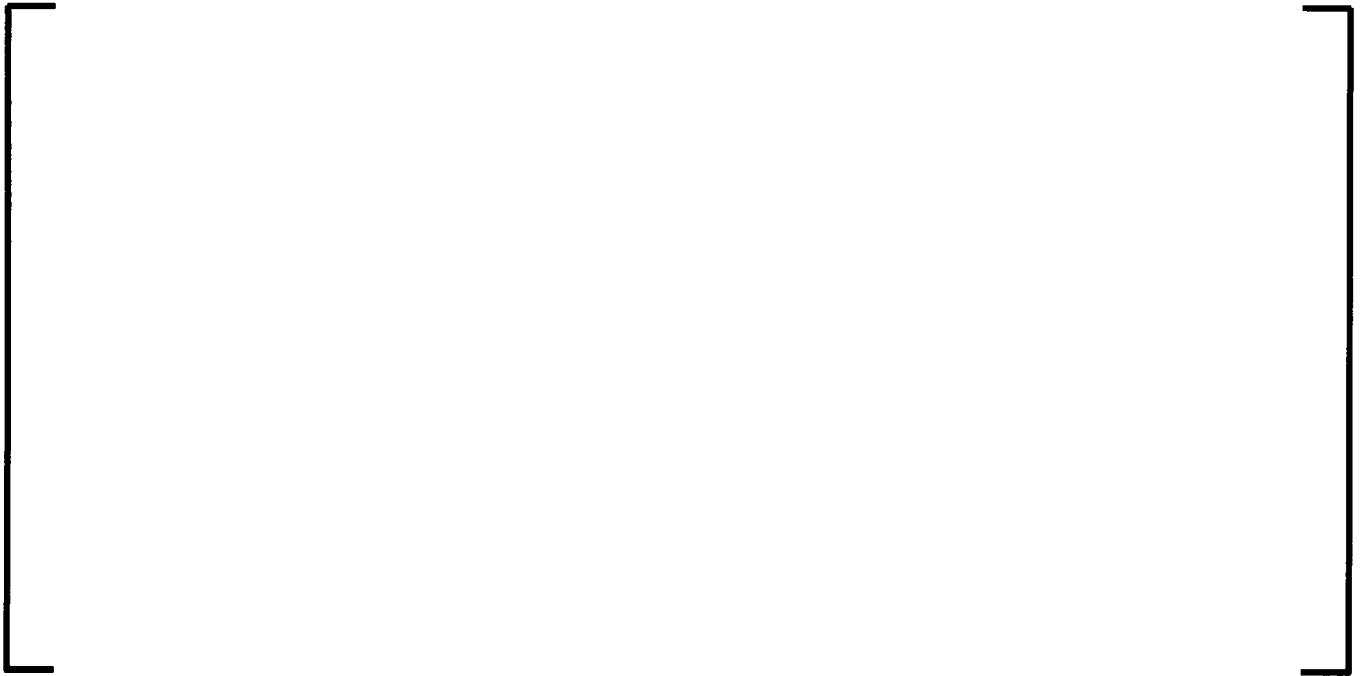


Figure 7-548 SSTF Base Case (T026_y52) – Liquid and Vapor Mass Flows at F013 SEO



Figure 7-549 SSTF Base Case (T026_y52) – Liquid and Vapor Mass Flows at F014 SEO



Figure 7-550 SSTF Base Case (T026_y52) – Liquid and Vapor Mass Flows at F021 SEO



Figure 7-551 SSTF Base Case (T026_y52) – Liquid and Vapor Mass Flows at F022 SEO



Figure 7-552 SSTF Base Case (T026_y52) – Liquid and Vapor Mass Flows at F023 SEO



Figure 7-553 SSTF Base Case (T026_y52) – Liquid and Vapor Mass Flows at F024 SEO



Figure 7-554 SSTF Base Case (T026_y52) – Liquid and Vapor Mass Flows at F025 SEO

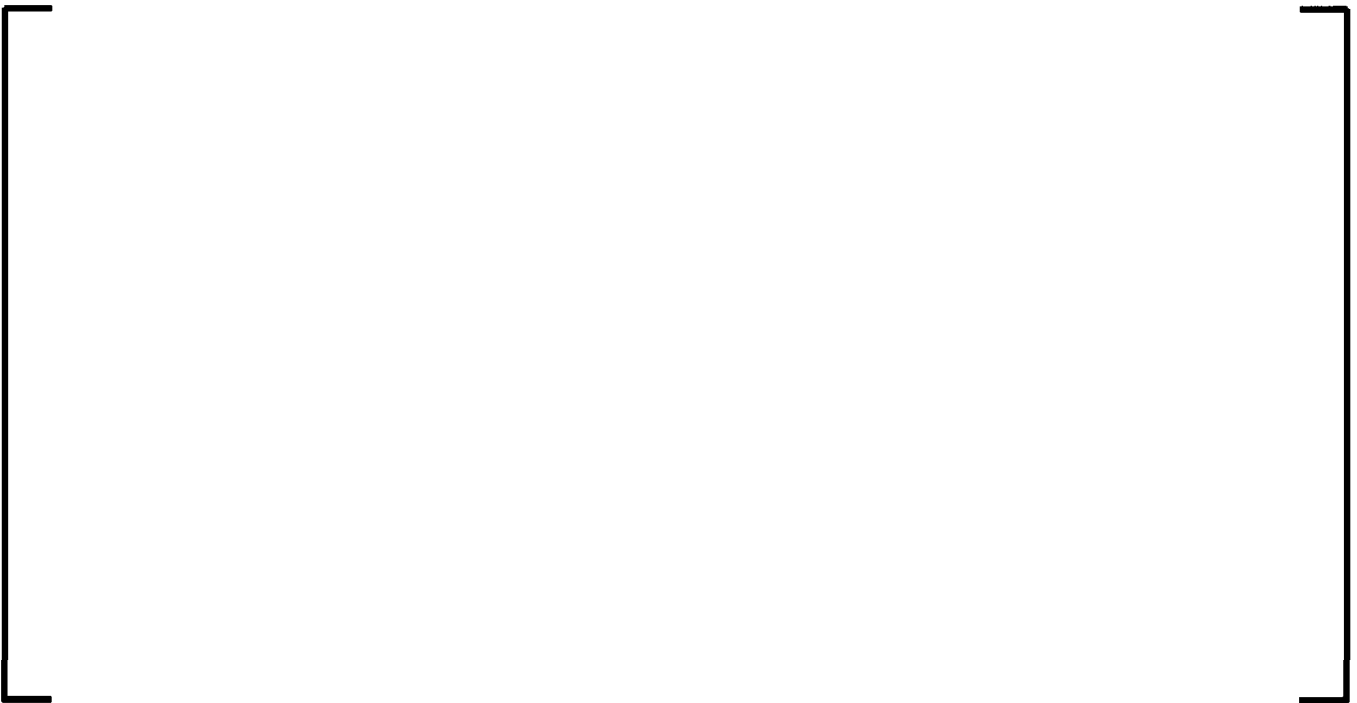


Figure 7-555 SSTF Base Case (T026_y52) – Liquid and Vapor Mass Flows at F026 SEO



Figure 7-556 SSTF Base Case (T026_y52) – Liquid and Vapor Mass Flows at F027 SEO



Figure 7-557 SSTF Base Case (T026_y52) – Liquid and Vapor Mass Flows at F028 SEO



Figure 7-558 SSTF Base Case (T026_y52) – Liquid and Vapor Mass Flows at F031 SEO



Figure 7-559 SSTF Base Case (T026_y52) – Collapsed Level in F011



Figure 7-560 SSTF Base Case (T026_y52) – Collapsed Level in F022



Figure 7-561 SSTF Base Case (T026_y52) – Collapsed Level in F025



Figure 7-562 SSTF Base Case (T026_y52) – Collapsed Level in F026



Figure 7-563 SSTF Base Case (T026_y52) – Collapsed Level in F028



Figure 7-564 SSTF Base Case (T026_y52) – Collapsed Level in F031

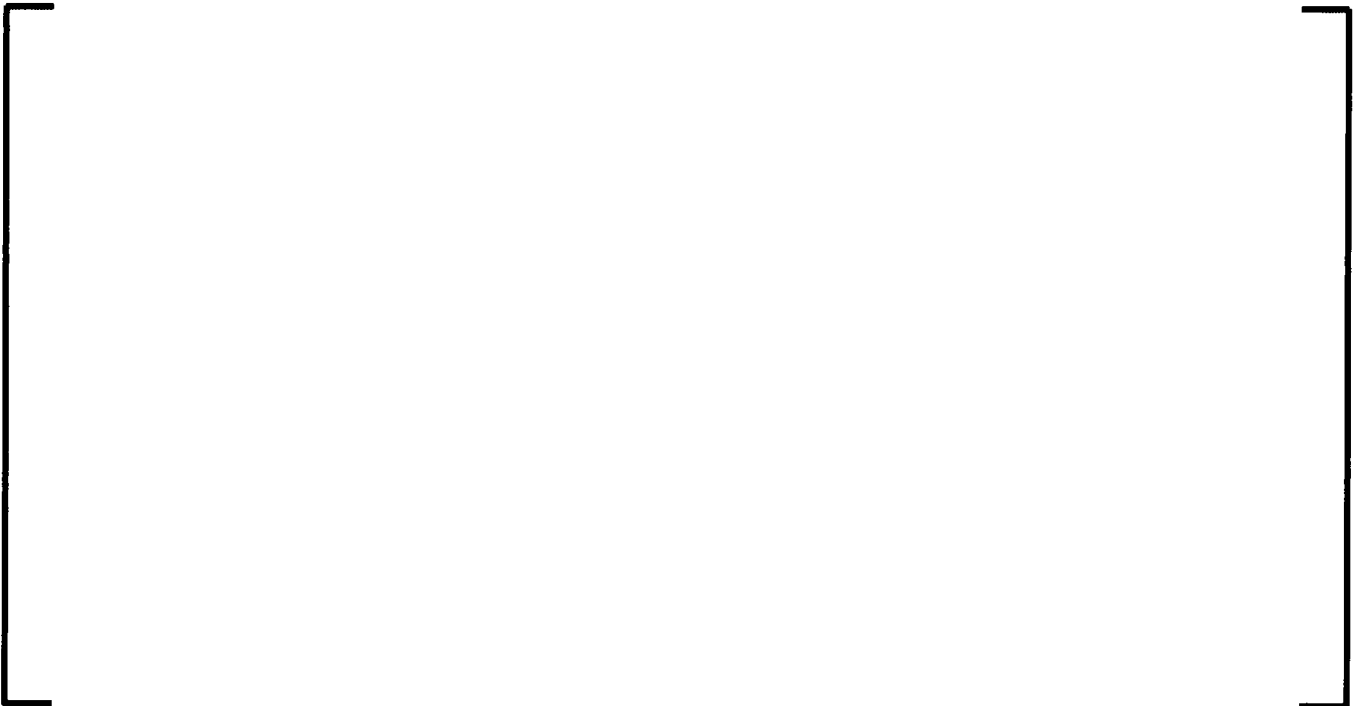


Figure 7-565 SSTF Base Case (T026_y52) – Liquid and Vapor Mass Flows at F012 UTP




Figure 7-566 SSTF Base Case (T026_y52) – Liquid and Vapor Mass Flows at F013 UTP




Figure 7-567 SSTF Base Case (T026_y52) – Liquid and Vapor Mass Flows at F023 UTP



Figure 7-568 SSTF Base Case (T026_y52) – Liquid and Vapor Mass Flows at F025 UTP



Figure 7-569 SSTF Base Case (T026_y52) – Liquid and Vapor Mass Flows at F026 UTP



Figure 7-570 SSTF Base Case (T026_y52) – Liquid and Vapor Mass Flows at F028 UTP



Figure 7-571 SSTF Base Case (T026_y52) – Liquid and Vapor Mass Flows at F031 UTP

7.9.6.2.2 T026_y53 Case (9 Bundle Groups) Results

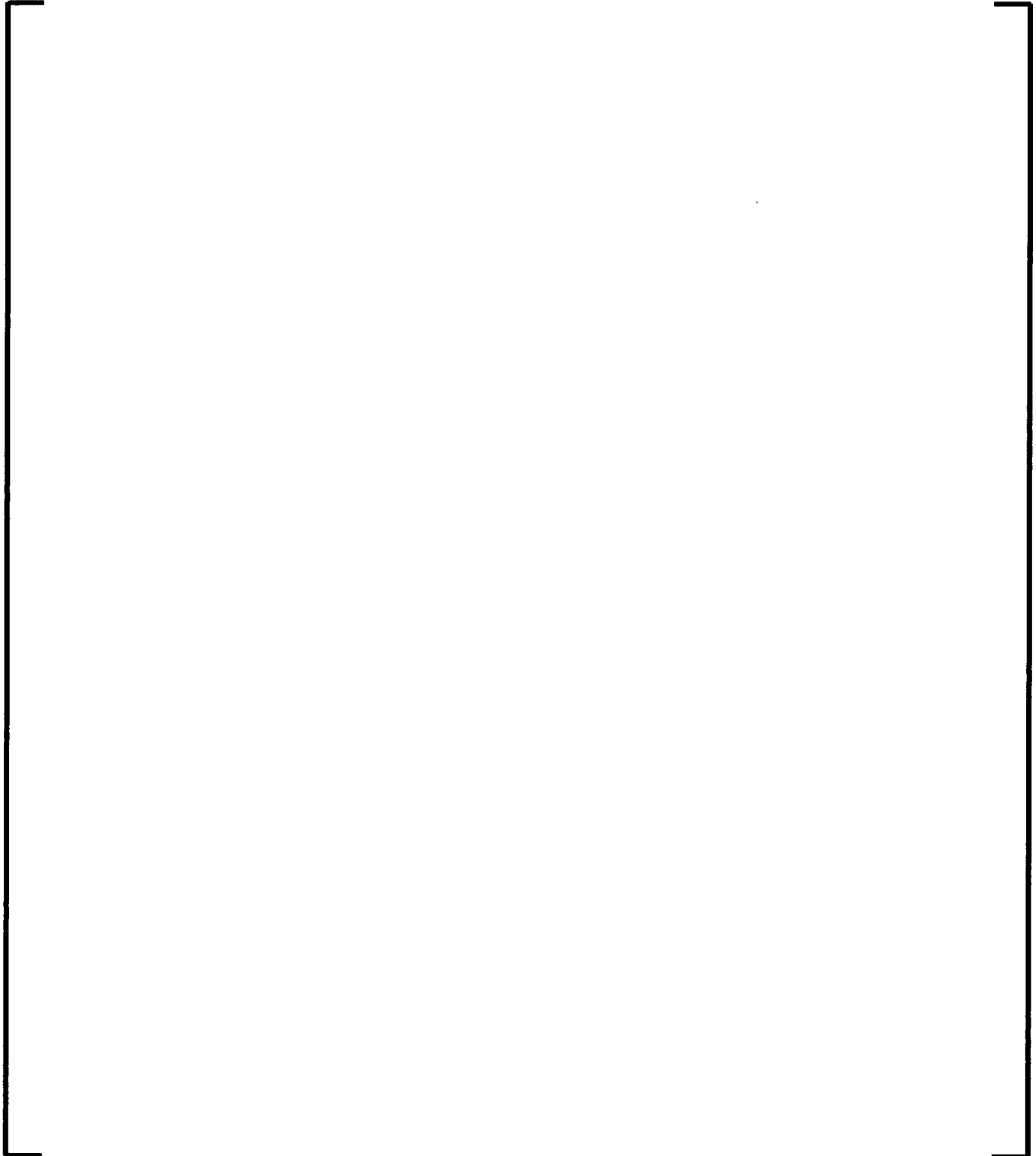




Table 7-63 SSTF Central Bundle Grouping for Case T026_y53 and Bundles in Counter-Current Flow

[illegible]



Figure 7-572 SSTF Case T026_y53 – Liquid and Vapor Mass Flows at F011 SEO



Figure 7-573 SSFT Case T026_y53 – Liquid and Vapor Mass Flows at F013 SEO



Figure 7-574 SSTF Case T026_y53 – Liquid and Vapor Mass Flows at F021 SEO



Figure 7-575 SSTF Case T026_y53 – Liquid and Vapor Mass Flows at F022 SEO



Figure 7-576 SSTF Case T026_y53 – Liquid and Vapor Mass Flows at F023 SEO



Figure 7-577 SSTF Case T026_y53 – Liquid and Vapor Mass Flows at F025 SEO

Figure 7-578 SSTF Case T026_y53 – Liquid and Vapor Mass Flows at F026 SEO

Figure 7-579 SSTF Case T026_y53 – Liquid and Vapor Mass Flows at F028 SEO



Figure 7-580 SSTF Case T026_y53 – Liquid and Vapor Mass Flows at F031 SEO



Figure 7-581 SSTF Case T026_y53 – Collapsed Level in F011



Figure 7-582 SSTF Case T026_y53 – Collapsed Level in F023



Figure 7-583 SSTF Case T026_y53 – Collapsed Level in F025



Figure 7-584 SSTF Case T026_y53 – Collapsed Level in F026




Figure 7-585 SSTF Case T026_y53 – Collapsed Level in F028



Figure 7-586 SSTF Case T026_y53 – Collapsed Level in F031



Figure 7-587 SSTF Case T026_y53 – Liquid and Vapor Mass Flows at F025 UTP



Figure 7-588 SSTF Case T026_y53 – Liquid and Vapor Mass Flows at F026 UTP



Figure 7-589 SSTF Case T026_y53 – Liquid and Vapor Mass Flows at F028 UTP



Figure 7-590 SSTF Case T026_y53 – Liquid and Vapor Mass Flows at F031 UTP

7.9.6.2.3 T026_y54 Case (9 Bundle Groups) Results

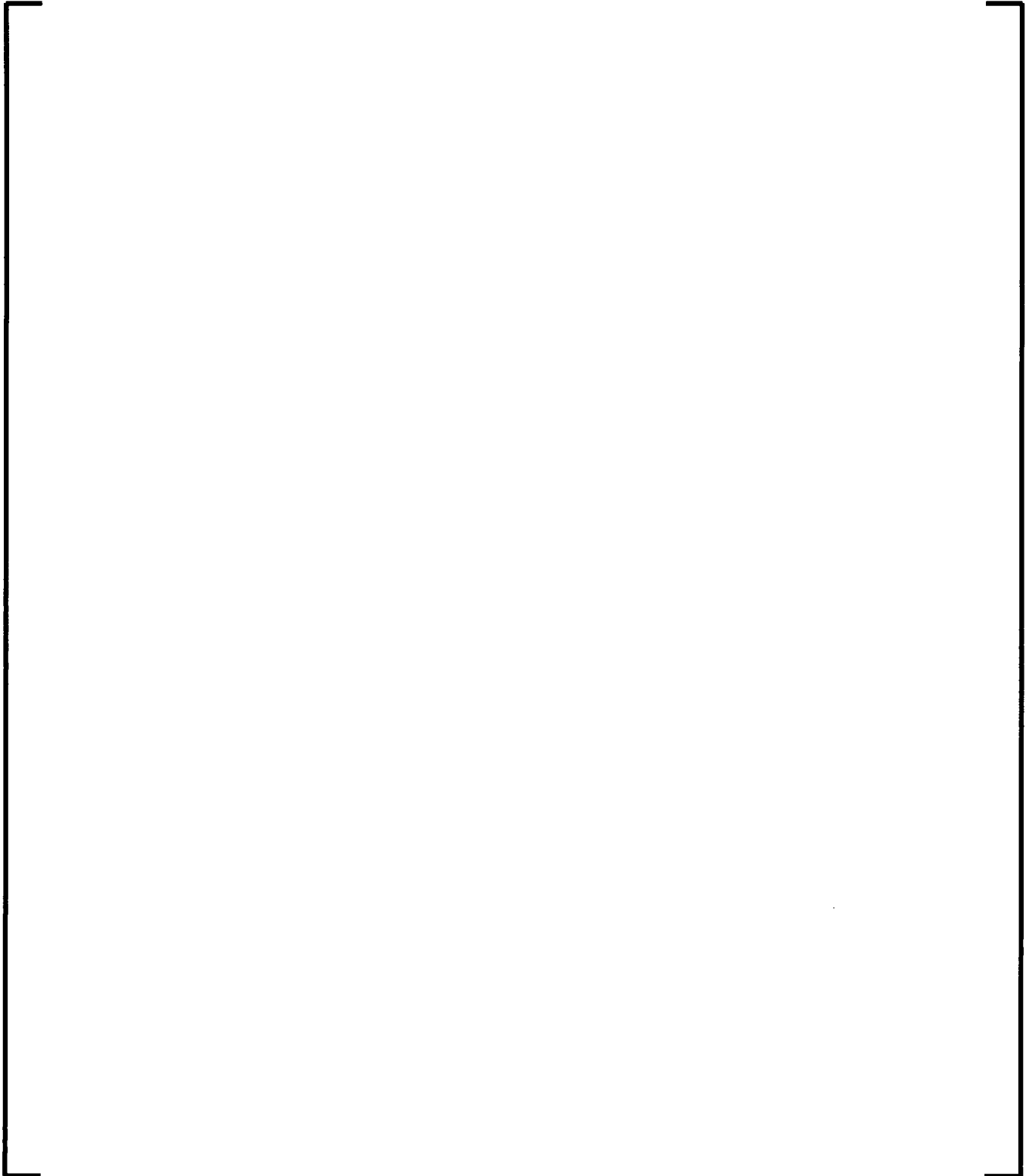


Table 7-64 SSTF Central Bundle Grouping for Case T026_y54 and Bundles in Counter-Current Flow

The image consists of a single, large rectangle with a thick, solid black border. The interior of the rectangle is completely white and contains no other elements, text, or markings.



Figure 7-591 SSTF Case T026_y54 – Liquid and Vapor Mass Flows at F011 SEO



Figure 7-592 SSTF Case T026_y54 – Liquid and Vapor Mass Flows at F013 SEO



Figure 7-593 SSTF Case T026_y54 – Liquid and Vapor Mass Flows at F021 SEO



Figure 7-594 SSTF Case T026_y54 – Liquid and Vapor Mass Flows at F022 SEO



Figure 7-595 SSTF Case T026_y54 – Liquid and Vapor Mass Flows at F023 SEO



Figure 7-596 SSTF Case T026_y54 – Liquid and Vapor Mass Flows at F025 SEO



Figure 7-597 SSTF Case T026_y54 – Liquid and Vapor Mass Flows at F026 SEO



Figure 7-598 SSTF Case T026_y54 – Liquid and Vapor Mass Flows at F028 SEO



Figure 7-599 SSTF Case T026_y54 – Liquid and Vapor Mass Flows at F031 SEO




Figure 7-600 SSTF Case T026_y54 – Collapsed Level in F022




Figure 7-601 SSTF Case T026_y54 – Collapsed Level in F023




Figure 7-602 SSTF Case T026_y54 – Collapsed Level in F025




Figure 7-603 SSTF Case T026_y54 – Collapsed Level in F026




Figure 7-604 SSTF Case T026_y54 – Collapsed Level in F028




Figure 7-605 SSTF Case T026_y54 – Collapsed Level in F031



Figure 7-606 SSTF Case T026_y54 – Liquid and Vapor Mass Flows at F028 UTP



Figure 7-607 SSTF Case T026_y54 – Liquid and Vapor Mass Flows at F031 UTP

7.9.6.2.4 T026_y55 Case (9 Bundle Groups) Results

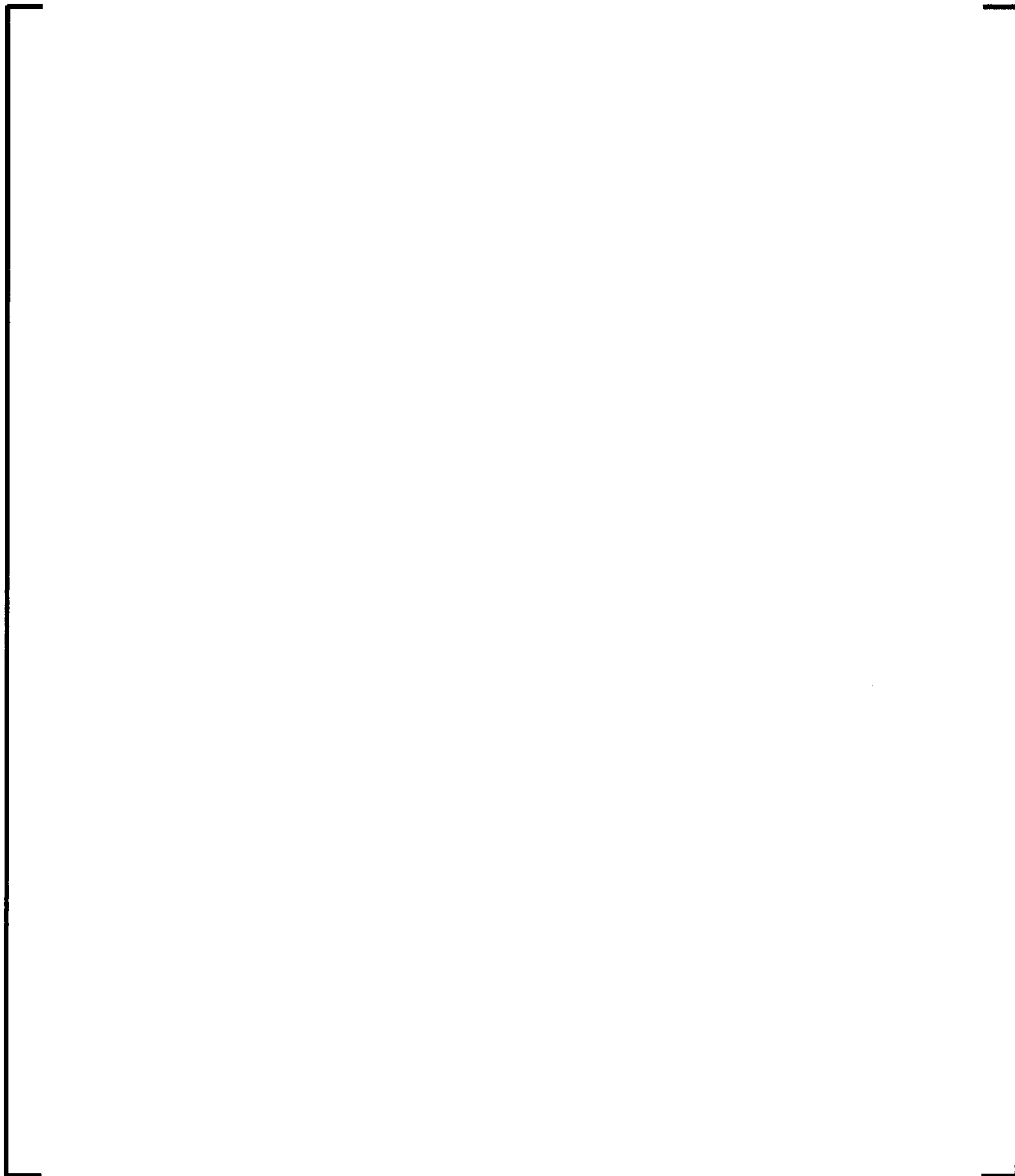




Table 7-65 SSTF Central Bundle Grouping for Case T026_y55 and Bundles in Counter-Current Flow

[illegible]



Figure 7-608 SSTF Case T026_y55 – Liquid and Vapor Mass Flows at F011 SEO



Figure 7-609 SSTF Case T026_y55 – Liquid and Vapor Mass Flows at F022 SEO



Figure 7-610 SSTF Case T026_y55 – Liquid and Vapor Mass Flows at F025 SEO



Figure 7-611 SSTF Case T026_y55 – Liquid and Vapor Mass Flows at F026 SEO



Figure 7-612 SSTF Case T026_y55 – Liquid and Vapor Mass Flows at F028 SEO



Figure 7-613 SSTF Case T026_y55 – Liquid and Vapor Mass Flows at F031 SEO




Figure 7-614 SSTF Case T026_y55 – Collapsed Level in F026




Figure 7-615 SSTF Case T026_y55 – Collapsed Level in F028



Figure 7-616 SSTF Case T026_y55 – Collapsed Level in F031

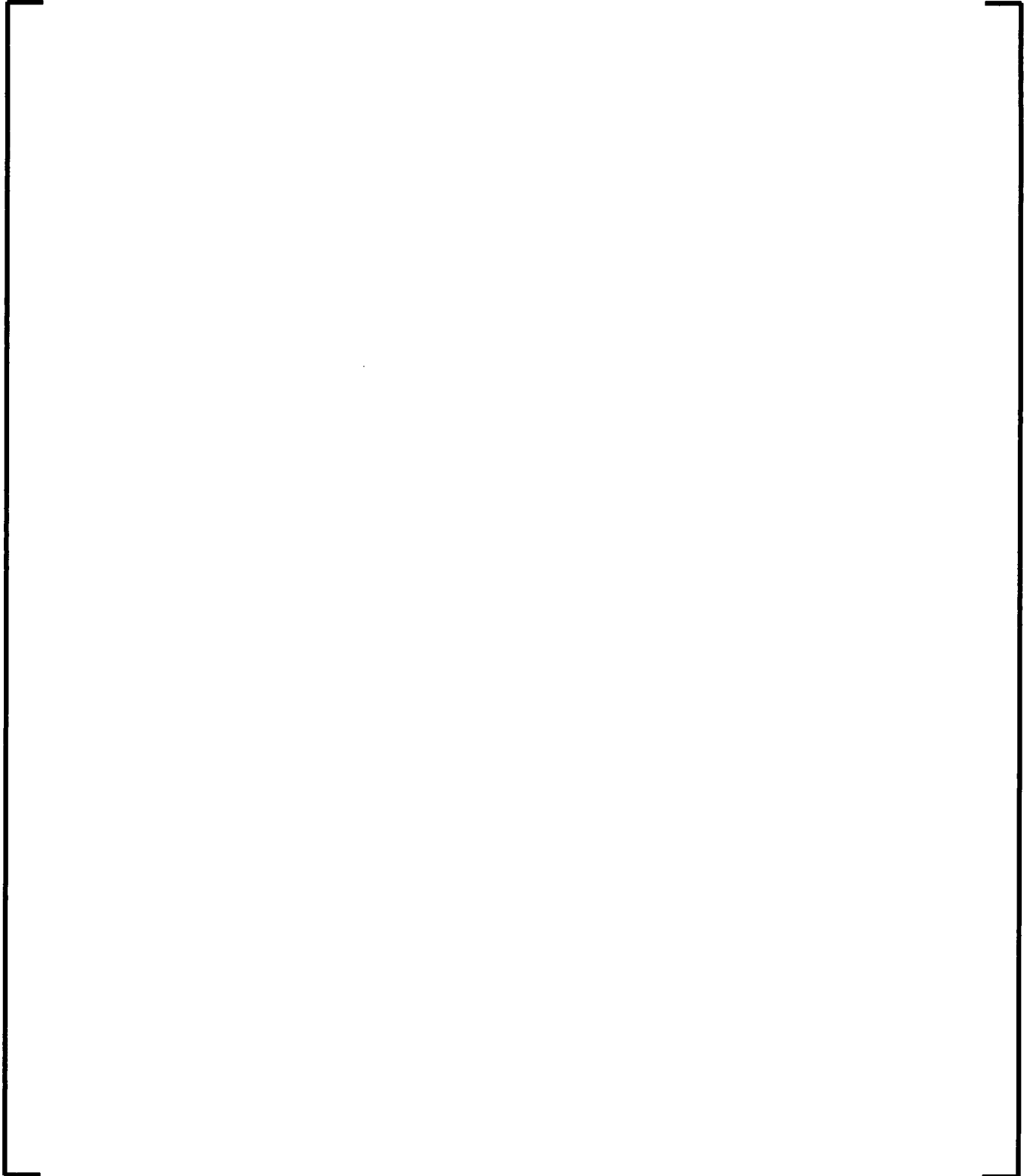


Figure 7-617 SSTF Case T026_y55 – Liquid and Vapor Mass Flows at F028 UTP



Figure 7-618 SSTF Case T026_y55 – Liquid and Vapor Mass Flows at F031 UTP

7.9.6.2.5 T026_y48 Case (3 Bundle Groups) Results





**Table 7-66 SSTF Central Bundle Grouping for Case T026_y48 and
Bundles in Counter-Current Flow**

--	--



Figure 7-619 SSTF Case T026_y48 – Liquid and Vapor Mass Flows at F013 SEO



Figure 7-620 SSTF Case T026_y48 – Liquid and Vapor Mass Flows at F025 SEO



Figure 7-621 SSTF Case T026_y48 – Liquid and Vapor Mass Flows at F031 SEO



Figure 7-622 SSTF Case T026_y48 – Collapsed Level in F013



Figure 7-623 SSTF Case T026_y48 – Collapsed Level in F025




Figure 7-624 SSTF Case T026_y48 – Collapsed Level in F031



Figure 7-625 SSTF Case T026_y48 – Liquid and Vapor Mass Flows at F031 UTP

8.0 Adequacy Decision

The decision regarding the adequacy of the EM is the culmination of the four EMDAP elements. Throughout the development process, questions concerning the adequacy of the model were asked and numerous iterations were made until the EM was determined to be adequate for the target applications. The final product of the development process is documented in this LTR, which includes showing results from fully certified computer codes using consistent nodalization and modeling options.

The AURORA-B LOCA EM has been determined to be adequate for simulating the target applications described in Section 4.0, as demonstrated through completion of the EMDAP documented in this LTR.

8.1 Code Versions Used in the Adequacy Decision

Calculations shown in this LTR were generated using computer codes that satisfy the AREVA software QA program and have a “fully certified” status.

- Most separate effects, component effects, and integral effects assessments for the S-RELAP5 thermal-hydraulic and thermal conduction models were performed using the USEP12 version of S-RELAP5 with the “BWRLOCA” methodology option* or earlier certified code versions that provide equivalent results. As mentioned in the assessments of Section 7, some of the assessments are unchanged from the AURORA-B AOO evaluations are based on a previous version of S-RELAP5 current at that time. Those assessments were confirmed to remain unchanged with the USEP12 version.
- The fuel rod thermal-mechanical calculations to determine the “permanent effects” on the fuel at the desired level of burnup were performed using the UMay10 version of RODEX4. This RODEX4 version is consistent with the USNRC approval of Reference 8. This version is consistent with the RODEX4 “kernel” coupled within S-RELAP5.

Going forward, all error corrections and code modifications will be built upon the above described code versions for the purposes of determining the continuity of assessment within the software QAP.

* Numerous methodologies are based on S-RELAP5. The methodologies use slight variations of the constitutive relations. The methodology option is an input field in S-RELAP5 that selects the specific constitutive relations consistent with the desired methodology.

8.2 Summary of Updates to S-RELAP5 since AURORA-B AOO Submittal

The S-RELAP5 computer code is USNRC approved for pressurized water reactor (PWR) large and small break loss of coolant accident (LOCA) analysis and PWR non-LOCA transient analysis (References 5, 16, and 17). Updates to S-RELAP5 were made for the AURORA-B AOO EM and were reported in Section 1.1 of Reference 6. This section summarizes the updates made to S-RELAP5 since the creation of the AURORA-B AOO EM.

The following additions and changes were made for and utilized in the AURORA-B LOCA EM:

- Groeneveld CHF LUT (Section 6.4.10)
- Rupture, swelling and fuel relocation added to RODEX4 (Section 6.4.5)
- Nucleate and transition boiling Appendix K lockout logic (Section 6.4.9)
- Groeneveld-Stewart minimum film boiling temperature correlation (Section 6.4.12)
- []
- McDonough/Milich/King transition boiling correlation (Section 6.4.11)
- Revised dispersed film boiling and single phase vapor correlations (Section 6.4.13)
- Improve reflood heat transfer scheme
 - []
- []
- Spray droplet condensation model for upper plenum mixing model (Section 6.4.17)
- Moody critical flow model improved numerics
 - []
- []
- Countercurrent flow limiting (CCFL)
 - Added the option to remove Tien's factor in the Kutateladze form (Section 7.6.5)
 - []
- []
- Jet pump modification for LOCA conditions

Other changes consisted of input, output and plotting options. Other changes not utilized for the EM are not discussed here.

The S-RELAP5 code changes have been implemented without affecting the existing capabilities and approvals of the code. Application of the specific models associated with an approved methodology is controlled through the methodology option selected by the user.

9.0 Application Methodology Description

The AURORA-B LOCA EM will be used to analyze the plant response during LOCA events over the range of expected plant operating conditions (Section 4.3). Event analyses are performed to determine the transient response of the key plant and fuel parameters (figures of merit) that are used to assess compliance with the applicable event acceptance criteria (Section 4.4). The results of the event analyses are used to establish or confirm operating limits and constraints that are necessary to ensure that acceptance criteria are not exceeded during the event.

The AURORA-B LOCA EM development and assessment are described in earlier sections of this LTR. The development and assessment demonstrate the applicability of the EM for analysis of the intended scope of events over the range of expected operating conditions. The development and assessment also demonstrate the accuracy of the EM for calculation of the key figures of merit used to confirm compliance with event acceptance criteria.

The application methodology defines the framework for using the EM to perform the event analyses required to establish or confirm plant operating limits and constraints. The application methodology includes the following elements;

- applicability of the EM for event analysis
- use of analysis results
- addressing EM calculation uncertainty
- determining appropriate analysis conditions
- developing plant input parameters

The application methodology elements define a process that ensures conservative predictions of plant transient response over the entire operating domain. The application methodology combined with the assessments of the EM relative to separate effects and plant test data provide a high degree of confidence that AURORA-B LOCA can be used to conservatively demonstrate compliance with event acceptance criteria.

An Appendix K application methodology is defined in this LTR; statistical sampling of code model uncertainties, initial conditions, and plant parameters is not performed.

The sections below describe elements of the application methodology that will be used with the AURORA-B LOCA EM.

9.1 *Application for LOCA Analysis*

9.1.1 EM Applicability for Event Analysis

The EM is intended for LOCA events in support of the requirements of 10 CFR 50.46.

9.1.2 Use of Analysis Results

The primary purpose of the LOCA analyses is to establish and/or confirm the LHGR and MAPLHGR operating limits that ensure that fuel acceptance criteria are not exceeded during the event.

9.1.3 Plant Operating Conditions Envelope

The plant operating conditions envelope consists of all parameters which define the spectrum of possible initial operating conditions that are allowed during normal operation. The plant operating conditions envelope is used to establish input parameters for the LOCA analyses. As long as plant operation is within the assumed envelope, the analysis is valid.

9.1.4 Plant Parameters

The input for the AURORA-B LOCA EM is developed using extensive plant specific data to accurately reflect the characteristics of the plant for which the analyses are being performed. The plant data required to prepare the AURORA-B LOCA EM input is identified and documented in a Plant Parameters Document that is verified by the utility operating the plant. This process is summarized in Section 6.3.7.7.

The plant geometry parameters are used to define physical characteristics of the plant systems. The plant systems represented in the AURORA-B EM include the reactor vessel, the main steam lines, and the recirculation system. Plant geometry parameters used to develop the EM input are based on the best available data for the plant. The data is obtained from sources that are verified by the plant operator.

- Plant geometry data is obtained from plant design drawings and documents and and/or other sources of information that can be verified. Nominal values from the design information are used to develop the model input and no additional conservatism is required.

- If some plant geometry parameters are not directly available from design drawings or documents, data from similar plants, previous experience, or engineering judgment can be used with justification. In these situations, the input parameter will be biased in a conservative direction if the parameter has a significant impact on analysis results.

10.0 Quality Assurance Program (QAP)

Licensees and vendors use a variety of methods to evaluate the transients and accidents that could occur at their nuclear power plant. The NRC staff reviews these methods to ensure that they provide a realistic or conservative result and that they adhere to the requirements of the Code of Federal Regulations (CFR). Regulations, which are applicable to transient and accident analysis methods, are found in 10 CFR 50.34, 10 CFR 50.46, and 10 CFR 50 Appendix K. Additionally, because the results of the transient and accident analysis methods are important to the safety of nuclear power plants, these methods must be maintained under a quality assurance program which meets the criteria set forth in 10 CFR 50 Appendix B. The AREVA QAP is documented in Reference 12 of this LTR.

The AREVA QAP has been implemented to ensure quality and uniformity throughout the analysis process, verification and validation, thus insuring compliance with all elements of the EMDAP as provided in Regulatory Guide 1.203.

The topical report ANP-10332(P), Revision 0, confirm that the evaluation model is maintained under a quality assurance program that meets the Regulatory requirements of 10 CFR Part 50.

The AREVA QAP covers the procedures for design control, document control, software configuration control and testing, and error identification and corrective actions used in the development and maintenance of the evaluation model. The program also ensures adequate training of personnel involved with code development and maintenance, as well as those who perform the analyses.

11.0 Documentation

Typically, technical reports containing the technical contents (in a qualitative and quantitative form), for a licensee or vendor requesting a change to an existing code suite or requesting the approval of a new methodology incorporating a more current code suite. In this case, this TR, ANP-10332(P), Revision 0, contains the documentation of the analysis, verification and validation assessment for a large break LOCA subject to Appendix K regulatory requirements, Section 5.4.1 of this document.

The development of an evaluation model for use in reactor safety licensing calculations requires a substantial amount of documentation, Section 6.2.27 of this document. This documentation includes/covers (a) the evaluation model, (b) the accident scenario identification process, (c) the code assessment, (d) the uncertainty analysis, (e) a theory manual, (f) a user manual, and (g) the quality assurance program.

The AURORA-B, an Evaluation Model for Boiling Water Reactors; Application to Loss of Coolant Accident Scenarios documentation, consists of the topical report, ANP-10332P, Revision 0, a theory manual, (Reference 6), verification and validation assessment basis (Reference 67), and a user's manual, (Reference 13). This set of documentation satisfies items A through F in the above paragraph, of the specific types of documentation described in SRP Chapter 15.0.2. The AREVA Quality Assurance Manual, (Reference 12), satisfies item G of the list of documentation. Reference 12 is the basis for quality assurance program in both the development and application of AURORA-B LOCA in compliance with 10 CFR Part 50 Appendix B. The AREVA QA program includes any performed software development in accordance with associated regulatory requirements.

12.0 Uses, Updates, and Modifications

The AURORA-B LOCA EM and the Appendix K application methodology defined in this LTR are used for the following activities within the bounds of the conditions and limitations of the Safety Evaluation (SE) approving the LTR. The EM is applied to BWRs equipped with forced recirculation systems with a refillable core over the full domain of operating conditions, up to and including operation at EPU conditions with expanded flow windows. EPU conditions are typically defined in the US licensing environment as 120% of original licensed thermal power. Expanded flow windows may go as low as 80% of rated core flow when operating at EPU conditions. This LTR can be referenced in the plant Technical Specifications as defining an acceptable methodology for meeting 10 CFR 50.46 requirements.

12.1 Updates and Changes to Components of the EM

At the base of AURORA-B LOCA are several CCDs which have roles in other licensing activities such as cycle design and fuel rod thermal-mechanical analysis for which they have been NRC approved outside of the AURORA-B LOCA EM. These are the “foundation methodology approvals” on which AURORA-B LOCA is built. [

]

AREVA maintains processes to ensure the application of the approved CCDs and CPR correlations used within AURORA-B LOCA are done in a manner consistent with the NRC approval and within the conditions and limitations identified in the SE of the respective approved document and/or as amended in subsequent SEs.

The following requirements are defined with respect to application and use of new foundation methodologies, new CPR correlations, new or revised fuel designs, and use of unapproved methodologies within the framework of AURORA-B LOCA:

1. Thermal hydraulic and pressure drop methodologies – Initial flow conditions created by core simulators or other thermal hydraulic methods will be applied with the NRC approved CCD.
2. Core simulator and cross section methodologies – Cycle depletions and cross sections input used to generate point kinetics input into AURORA-B LOCA EM will be generated using an NRC approved CCD.

3. Fuel-mechanical models – Transient fuel-mechanical properties will be evaluated consistent with an NRC approved fuel-mechanical CCD. Applicability of a new CCD in this role within AURORA-B LOCA will be demonstrated in an NRC approved document.
4. Critical power correlations – Initial critical power will be evaluated using an approved critical power correlation or critical power correlation derived via an approved co-resident fuel methodology for each unique fuel design. The NRC approved range of applicability of critical power correlations will be assured when applying the correlations within AURORA-B LOCA through software and administrative means.
5. New or revised fuel designs – The licensing of new or revised fuel designs will address the impact of the new or revised design on LOCA behavior. The evaluation and/or disposition shall ensure that the AURORA-B LOCA EM and CCDs continue to be used within their conditions and limitations of NRC approval, and within their verification, validation, and assessment bases.
6. Un-approved methodologies for Lead Assemblies – The use of un-approved CCDs or correlations supporting Lead Assemblies within the framework defined within this LTR will not occur without satisfying the requirements of 10 CFR 50.59, informing the USNRC of their use through a license amendment request (10 CFR 50.92), or other appropriate means as determined to be necessary by AREVA and the plant licensee. In such situations, application on a plant specific basis may be performed to support Lead Assemblies containing new features and materials. Use of CCDs or correlations which do not have NRC approval will not occur within the framework defined within this LTR for reload quantities of fuel bundles without approval as delineated above.

12.2 Plant Modifications and Applications

During the course of age management activities and programs to enhance operational flexibility, modifications may be made to the plants that introduce new features, hardware, and/or enhancements not presently incorporated into the BWR fleet. Examples of features, hardware, and/or enhancements already introduced into the operating fleet since the start of commercial operation include: digital feedwater control systems, new steam dryers, more accurate thermal power measurement devices, variable speed recirculation pump drive motors, longer duration fuel cycles, power uprate strategies, and expanded flow domain strategies.

When incorporated in the analyses (i.e. the inputs, initial conditions, plant parameters, and boundary conditions accurately represent the plant configuration), most modifications and enhancements do not alter the relevant BWR event characteristics predicted by AURORA-B LOCA because they do not alter the performance of the underlying systems, components, geometries, or processes. AREVA will ensure changes in the “as operating” state of the plant are communicated between the plant customer and fuel vendor on a cycle specific basis, and these changes are accounted for in the fuel reload licensing activities.

The following actions are taken with respect to accommodating new features, hardware, and/or enhancements not presently incorporated into the BWR fleet. These actions are in addition to any requirements associated with USNRC approved enhancements or modifications such as EPU or EFW;

1. AREVA will review the impact of introducing new features, components, and/or enhancements into plants for which it performs licensing activities to ensure that the characteristics of said features, hardware, and/or enhancements are;
 - a. adequately simulated by AURORA-B LOCA,
 - b. do not adversely impact the basis of highly ranked phenomena and processes delineated in this LTR,
 - c. bounded by the analysis parameters (which can be determined through plant parameter sensitivity studies
 - d. within the conditions and limitations identified with AURORA-B LOCA and affiliated CCD approvals, and
 - e. can be adequately addressed by making code modifications within the scope delineated in Section 12.4.

AREVA will take action through an LTR submittal, plant specific application submittal, License Amendment Request, or other appropriate means if one of these items is not satisfied.

2. If the above stated review finds the change acceptable, AREVA will maintain input models, physical models, and correlations that adequately represent the "as operating" state of the plant. Reporting of changes is dictated by 10 CFR 50.46.

12.3 Definitions of Significance

For LOCA analyses, definitions of significant follow the requirements of 10 CFR 50.46.

12.4 Code Modifications

Code modifications to improve the analysis models may be made to AURORA-B LOCA, the CCDs, and correlations during the course of the software and methodology lifecycle. AREVA maintains a quality program (including software quality) that is compliant with 10 CFR 50 Appendix B requirements. This quality program assures modifications are made within the bounds of USNRC licensing requirements and SE conditions and limitations.

Modifications are defined as changes in the EM that improve the man/machine interface through better input and output processing and checking, enhance the computational performance, improve numerical robustness, accelerate convergence, etc. AREVA may perform such modifications in order to maintain modern, flexible software that is easy to use and

computationally efficient. Modifications will not be made unless they are reported to the USNRC as described above. Examples of potential modifications include;

- **Source Coding and Structure:** Changes in source coding and code structure that improve the readability and maintainability of the computer codes used within AURORA-B may be made as they are modernized.
- **Numerical Methods and Software Architecture:** Changes in the numerical methods may be made to improve computational efficiency and numerical accuracy. For example, these include improvements to code convergence and numerical algorithms, improvements to the temporal coupling between the CCDs to make the coupling more implicit, and parallelization of the individual CCDs as well as the coupling between the CCDs.
- **Water Properties and Equations of State:** Changes to update the water properties routines and equations of state within S-RELAP5 may be made to modernize the code.
- **Computational Platform and Compilers:** Movement to newer computational platforms and compilers may be made as new platforms and compilers become available.
- **Updating Physical Models and Correlations:** Updates and Improvements in physical models and correlations of the CCDs and EM may be made as new data or expanded assessments become available. These updates and improvements are a necessary element of maintaining modern and accurate CCDs and EM, and are particularly important for ensuring the capabilities of the CCDs and EM are maintained at the state of the art.

USNRC approval may be granted for CCDs used with AURORA-B LOCA (for example MICROBURN-B2) that revises or extends their capabilities. Or, future regulatory commitments may be made related to these CCDs. In such cases the changes affecting the AURORA-B LOCA EM can be incorporated within the EM with adherence to 10 CFR 50.46 reporting of changes.

13.0 References

1. ANP-10300P, Revision 0, "AURORA-B: An Evaluation Model for Boiling Water Reactors; Application to Transient and Accident Scenarios," December 2009.
2. United States Code of Federal Regulations, Part 10 (Energy) Section 50 Appendix K, *ECCS Evaluation Model*.
3. United States Code of Federal Regulations, Part 10 (Energy) Section 50 Appendix A, *General Design Criteria for Nuclear Power Plants*.
4. U. S. Nuclear Regulatory Commission Regulatory Guide 1.203, *Transient and Accident Analysis Methods*, December 2005.
5. EMF-2103(P)(A) Revision 0, *Realistic Large Break LOCA Methodology for Pressurized Water Reactors*, Framatome ANP, April 2003.
6. FS1-0009406 Revision 2, "FSQA-08 S_RELAP5 MODELS and Correlations Code Manual (Theory), AREVA NP, July 2013.
7. EMF-2158(P)(A) Revision 0, *Siemens Power Corporation Methodology for Boiling Water Reactors: Evaluation and Validation of CASMO-4 / MICROBURN-B2* Siemens Power Corporation, October 1999.
8. BAW-10247PA Revision 0, *Realistic Thermal Mechanical Fuel Rod Methodology for Boiling Water Reactors*, AREVA NP Inc., February 2008.
9. EMF-2994 Revision 0, *RODEX4: Thermal-Mechanical Fuel Rod Performance Code Theory Manual*, Framatome ANP, Inc., August 2004.
10. U. S. Nuclear Regulatory Commission Regulatory Guide 1.157, *Best-Estimate Calculations of Emergency Core Cooling System Performance*, May 1989.
11. NUREG-0800, *Standard Review Plan for the Review of Safety Analysis Reports for Nuclear Power Plants*, LWR Edition, applicable revisions.
12. FQM, Revision 3, *AREVA NP Fuel Sector Quality Management Manual*, AREVA NP, June 2008.
13. FS1-0009130, Revision 2.0, *S-RELAP5 Input Data Requirements (User's Manual)*, AREVA NP, July 2013.
14. Pump Two-Phase Performance Program, EPRI NP-1556, Volumes 1-8, September 1980.
15. AREVA NP Inc. Letter to NRC, RAC:052:83, "RODEX2 ECCS COMPARISONS FOR A BWR," September 6, 1983.

16. EMF-2328(P)(A), *PWR Small Break LOCA Evaluation Model, S-RELAP5 Based*, Framatome ANP, March 2001.
17. EMF-2310(P)(A) Revision 1, *SRP Chapter 15 Non-LOCA Methodology for Pressurized Water Reactors*, Framatome ANP, May 2004.
18. NUREG/CR-5249, *Quantifying Reactor Safety Margins*, Nuclear Regulatory Commission, December 1989.
19. ANP-2829P, *General BWR Design and Event Descriptions*, AREVA NP, December 2009.
20. ANP-2830P, *Control System and Reactor Protection System Requirements for Modeling BWR Events*, AREVA NP, December 2009.
21. ANP-2831P, *Identification of Code Capabilities and PIRT Development for BWR Transient Analyses*, December 2009.
22. ICONE10-22288, "Proceedings of ICONE10, 10th International Conference on Nuclear Engineering," Arlington VA., April 14-18, 2002.
23. XN-NF-80-19(P)(A) Volume 3 Revision 2, *Exxon Nuclear Methodology for Boiling Water Reactors, THERMEX: Thermal Limits Methodology Summary Description*, Exxon Nuclear Company, January 1987.
24. D. A. Power and R. O. Meyer, *Cladding Swelling and Rupture Models for LOCA Analysis*, NUREG-0630, USNRC, April 1980.
25. XN-NF-82-07(P)(A) Revision 1, *Exxon Nuclear Company ECCS Cladding Swelling and Rupture Model*, Exxon Nuclear Company Inc., November 1982.
26. Technical Report SEMCA-2005-313, STATE-OF-THE-ART REVIEW OF PAST PROGRAMS DEVOTED TO FUEL BEHAVIOR UNDER LOCA CONDITIONS Part One. Clad Swelling and Rupture-Assembly Flow Blockage, Claude Grandjean, IRSN, Saint-Paul-Lez-Durance, France, December 2005.
27. L. J. Siefken, Axial Fuel Relocation in Ballooning Fuel Rods, Transactions of the 7th International Conference on Structural Mechanics in Reactor Technology, Chicago, Illinois, August 1983.
28. NEA/CSNI/R(2010)6, Benchmark Calculations on Halden IFA-650 LOCA Test Results, Organization for Economic Co-operation and Development (OECD) – Nuclear Energy Agency (NEA), November 2010.
29. B. C. Oberlander, M. Espeland, N. O. Solum, H. K. Jenssen, LOCA IFA650-4: Fuel Relocation Study, LOCA Workshop/HPG Meeting, Prague, September 2007.

30. J. D. Duncan, J. E. Leonard, *Thermal Response and Cladding Performance of an Internally Pressurized Zircaloy-Clad, Simulated BWR Fuel Bundle Cooled by Spray Under Loss-of-Coolant Conditions*, GEAP-13112, General Electric Company, April 1971.
31. J. E. Leonard, J. D. Duncan, A. S. Rao and R. C. Cipolla, *Emergency Core Cooling Tests of an Internally Pressurized Zircaloy-Clad, 8x8 Simulated BWR Fuel Bundle*, NEDO-20231-P-A, December 1973.
32. XN-75-55(A), Revision 2, "The Exxon Nuclear Company WREM-Based NJP-BWR ECCS Evaluation Model and Application to the Oyster Creek Plant, Exxon Nuclear Company, April 1977.
33. "BWR Refill-Reflood Program Task 4.7 – Model Development: TRAC-BWR Component Models", NUREG/CR-2574, September 1983
34. NEDO-32176, Revision 4, "TRACG Model Description", GE Hitachi Nuclear Energy, January 2008.
35. J. G. M. Anderson, Y. K. Cheung, J. R. Fitch, J. M. Healzer, C.L. Heck, L. A. Klebanov, J. C. Shaug, and B. S. Shiralkar, "TRACG Qualification", NEDO-32177, Revision 3, GE Nuclear Energy, August 2007.
36. J. G. Collier, J. R. Thome, *Convective Boiling and Condens*, 3rd Edition, Oxford Science Publications, 1994.
37. "RELAP4/MOD5 A Computer Program for Transient Thermal-Hydraulic Analysis of Nuclear Reactors and Related Systems User's Manual, Volume 1 RELAP4/MOD5 Description," ANCR-NUREG1335, Aerojet Nuclear Company, September 1976.
38. D. C. Groeneveld, S. C. Cheng and T. Doan, "1986 AECL-UO Critical Heat Flux Table," *Heat Transfer Engineering*, 7, pp. 46-62, 1986.
39. D. C. Groeneveld, L. K. H. Leung, P. L. Kirillov, V. P. Bobkov, I. P. Smogalev, V. N. Vinogradov, X. C. Huang, E. Royer, "The 1995 look-up tables for critical heat flux in tubes," *Nuclear Engineering and Design*, 163, pp.1-23, 1996.
40. D. C. Groeneveld, L. K. H. Leung, Y. Guo, A. Vasic, M. El Nakla, S. W. Peng, J. Yang and S. C. Cheng, "Lookup Tables for Predicting CHF and Film Boiling Heat Transfer: Past, Present, and Future," *Nucleat Technology*, 152, pp.87-104, 2005.
41. D. C. Groeneveld, J. Q. Shan, A. Z. Vasic, L. K. H. Leung, A. Durmayz, J. Yang, S. C. Cheng and A. Tanase, "The 2006 CHF look-up table," *Nuclear Engineering and Design*, 237, pp. 1909-1922, 2007.
42. M. Lee, "A critical heat flux approach for square rod bundles using the 1995 Groeneveld CHF table and bundle data of heat transfer research facility," *Nuclear Engineering and Design*, 197, pp. 357-374, 2000.

43. N. I. Kolev, Check of the 2005 look up table for prediction of CHF in bundles, Nuclear Engineering and Design (In Press 2006).
44. J. B. McDonough, W. Milich and E. C. King, "An Experimental Study of Partial Film Boiling Region with Water at Elevated Pressures In a Round Vertical Tube," Fourth National Heat Conference Preprint 29, Buffalo, New York, August 14-17, 1960.
45. D. C. Groeneveld and J. C. Stewart, "The Minimum Film Boiling Temperature for Water during Film Boiling Collapse," *Proceedings of the Seventh International Heat Transfer Conference*, München, Germany, 1982.
46. D. Swinnerton, K. G. Pearson, and M. L. Hood, "Steady State Post Dryout Experiments at Low Quality and Medium Pressure," United Kingdom Atomic Energy Authority, AEEW-R 2192, 1988.
47. V. K. Dhir, R. B. Duffey, and I. Catton, "Quenching Studies on a Zircaloy Rod Bundle," *J. Heat Transfer*, 103, 293-299, 1981.
48. L. J. Peterson and S. M. Bajorek, Experimental Investigation of Minimum Film Boiling Temperature for Vertical Cylinders at Elevated Pressure, ICONE10-22520, Proceedings of ICONE10, 10th International Conference on Nuclear Engineering, Arlington, VA, April 14-18, 2002.
49. L. A. Bromley, "Heat Transfer in Stable Film Boiling," *Chemical Engineering Progress*, Volume 46, pp. 221-227, 1950.
50. P.J. Berenson, "Film Boiling Heat Transfer from a Horizontal Surface," *Journal of Heat Transfer*, pp. 351-358, 1961.
51. General Electric Company Analytical Model for Loss-of-Coolant Analysis in Accordance with 10CFR50 Appendix K – Amendment No. 1, Calculation of Low Flow Film Boiling Heat Transfer for BWR LOCA Analysis, NEDO-20566-1-A, Revision 1, January 1982.
52. XN-NF-80-19(P)(A) Volumes 2, 2A, 2B, and 2C, Exxon Nuclear Methodology for Boiling Water Reactors, EXEM BWR ECCS Evaluation Model, September 1982.
53. XN-NF-80-19(P), Volume 2A, Rev 1, RELAX: A RELAP4 Based Computer Code for Calculating Blowdown Phenomena, June 1981.
54. Robert Siegel and John R. Howel, *Thermal Radiation Heat Transfer*, McGraw-Hill, New York, 1981, pp. 624-625.
55. GEAP-13086, J.D. Duncan, J. E. Leonard, Heat Transfer in a Simulated BWR Fuel Bundle Cooled by Spray Under Loss-of-coolant Conditions, General Electric Company, June 1970.
56. GEAP-13197, J.D. Duncan, J.E. Leonard, Emergency Cooling in Boiling Water Reactors Under Simulated Loss-of-coolant Conditions (BWR-FLECHT Final Report), General Electric Company, June 1971.

57. YAE-1547P-A, Revision 1, Vermont Yankee BWR Loss-of-Coolant Accident Licensing Analysis Method, August 1993.
58. ANF-524(P)(A) Revision 2 and Supplements 1 and 2, *ANF Critical Power Methodology for Boiling Water Reactors*, Advanced Nuclear Fuels Corporation, November 1990.
59. ANP-10307P Revision 0, *AREVA MCPR Safety Limit Methodology for Boiling Water Reactors*, AREVA NP Inc., October 2009.
60. NUREG-1230, *Compendium of ECCS Research for Realistic LOCA Analysis*, US Nuclear Regulatory Commission, August 1988.
61. NEA/CSNI/R(96)16, *Evaluation of the Separate Effects Tests (SET) Validation Matrix*, Nuclear Energy Agency, Organization for Economic Co-Operation And Development, Paris, France, November 1996.
62. NEA/CSNI/R(96)17, *CSNI Integral Test Facility Validation Matrix for The Assessment of Thermal-Hydraulic Codes for LWR LOCA and Transients*, Nuclear Energy Agency, Organization for Economic Co-Operation And Development, Paris, France, July 1996.
63. NUREG/CR-6720, *TRAC-M Validation Test Matrix*, US Nuclear Regulatory Commission, July 2001.
64. J.A. Findlay, "BWR Refill-Reflood Program Task 4.4 – CCFL/Refill System Effects Tests (30° Sector), Evaluation of Parallel Channel Phenomena", NUREG/CR-2566, GEAP-22044, EPRI NP-2373, Nov. 1982.
65. Takashi Hara, et al., *Current Status of the Post Boiling Transition Research in Japan Integrity Evaluation of Nuclear Fuel Bundles after Boiling Transition and Development of Rewetting Correlations*, Journal of Nuclear Science and Technology, Vol. 40 (2003) , No. 10 p.852-861.
66. O. Nylund et al., "Hydrodynamic and heat transfer measurements on a full-scale simulated 36-rod Marviken fuel element with uniform heat flux distribution," FRIGG-2, R-447/RTL-1007, May 1968.
67. EMF-2102(P), *S-RELAP5: Code Verification and Validation*, Framatome ANP, Inc., August 2001.
68. O. Nylund et al., *Hydrodynamic and Heat Transfer Measurements on A Full-Scale Simulated 36-Rod Marviken Fuel Element with Non-Uniform Radial Heat Flux Distribution*, FRIGG-3, R-494/RL-1154, November 1969.
69. J. Skaug et al., *FT-36b, Results of void Measurements*, FRIGG-PM-15, May 1968.
70. H. Christensen, *Power-to-Void Transfer Function, Doctorial Dissertation*, Massachusetts Institute of Technology, September 1961 (and ANL-6385, July 1961).

71. Allis-Chalmers Atomic Energy Division, *Joint US/EURATOM R&D Program AT (11-1)-1272; Investigation of Vapor Volume Fraction and Slip Velocity Under the Euratom Program; Final Report*, ACNP-64029, November, 1964.
72. Allis-Chalmers Atomic Energy Division, *Joint US/EURATOM R&D Program AT (11-1)-1186; Steam Separation Technology Under the Euratom Program; Quarterly Progress Report; April 1, 1964-June 30, 1963*, ACNP-63021, July 10, 1963.
73. Allis-Chalmers Atomic Energy Division, *Joint US/EURATOM R&D Program AT (11-1)-1186; Steam Separation Technology Under the Euratom Program; Quarterly Progress Report; October 1, 1963-December 31, 1963*, ACNP-63035, January 10, 1964.
74. J.F. Wilson, R.J. Grenada, J.F. Patterson, *The Velocity of Rising Steam in a Bubbling Two-Phase Mixture*, ANS Transactions 5, 151, 1962.
75. I. Kataoka, M. Ishii, *Drift Flux Model for Large Diameter Pipe and New Correlation for Pool Void Fraction*, International Journal Heat Mass Transfer, 30, No. 9, pp. 1927-1939, 1987.
76. J. A. Findlay, *BWR Refill-Reflood Program Task 4.8 - Model Qualification Task Plan*, NUREG/CR-1899, EPRI NP-1527, GEAP-24898, August 1981.
77. EMF-2209(P)(A) Revision 3, *SPCB Critical Power Correlation*, AREVA NP, September 2009.
78. ANP-10249PA Revision 1, *ACE/ATRIUM-10 Critical Power Correlation*, AREVA NP Inc., September 2009.
79. ANP-10298(P) Revision 0, *ACE/ATRIUM 10XM Critical Power Correlation*, AREVA NP, March 2010.
80. NUREG/CR-2456, ORNL-5848, "Experimental Investigations of Uncovered-Bundle Heat Transfer and Two-Phase Mixture-Level Swell Under High-Pressure Low Heat-Flux Conditions," Oak Ridge National Laboratory, March 1982.
81. NUREG/CR-2114, ORNL-446, "ORNL Small-Break LOCA Heat Transfer Test Series I: High-Pressure Reflood Analysis," September 1981.
82. NUREG/CR-2455, ORNL-5846, "Experimental Investigations of Bundle Boiloff and Reflood Under High Pressure Low Heat Flux Conditions," April 1982.
83. NUREG/CR-2435, ORNL-5822, "Dispersed Flow Film Boiling in Rod Bundle Geometry-Steady State Heat Transfer Data and Correlation Comparisons," April 1982.
84. CENPD-152-P, Blowdown Heat Transfer Program, "Film Boiling Heat Transfer Coefficients," CE/Columbia Tests, May 1975.

85. FLECHT SEASET Program, "PWR FLECHT SEASET Unblocked Bundle, Forced and Gravity Reflood Task Data Report, Volumes 1 and 2," NUREG/CR-1532, EPRI NP-1459, WCAP-9699, June 1980.
86. "FLECHT Low Flooding Rate Skewed Test Series Data Report," WCAP-9108, May 1977.
87. Japan Atomic Energy Research Institute (JAERI), JAERI-memo 58-155. Data Report on Large Scale Reflood Test-43 - CCTF Core II Shakedown Test C2-SH2 (Run 54). May 1983.
88. Japan Atomic Energy Research Institute (JAERI), JAERI-memo 85-026. Evaluation Report on CCTF Core-II Reflood Test C2-4 (Run 62) - Investigation of Reproducibility. March 1985.
89. Japan Atomic Energy Research Institute (JAERI), JAERI-memo 87-001. Evaluation Report on CCTF Core-II Reflood Test C2-8 (Run 67) - Effect of System Pressure. January 1987.
90. Japan Atomic Energy Research Institute (JAERI), JAERI-memo 87-002. Evaluation Report on CCTF Core-II Reflood Test C2-9 (Run 68) - Effect of LPCI Flow Rate. February 1987.
91. Studsvik Eco & Safety AB, MXC-301, NUREG/CR-2671, *The Marviken Full-Scale Critical Flow Tests, Summary Report*, May 1982.
92. Siemens AG UB KWU, U9 316/89/2 *Quick Look Report - UPTF - Test No. 6, Downcomer Countercurrent Flow Test*, March 1989.
93. Siemens AG UB KWU, U9 316/88/18, *Experimental Data Report - UPTF - Test No. 6, Downcomer Countercurrent Flow Test*, March 1989.
94. Siemens AG KWU, E314/90/003, *Quick Look Report - UPTF - Test No. 7, Downcomer Countercurrent Flow Test*, March 1990.
95. Siemens AG KWU, NT31/99/06, *Quick Look Report - UPTF - Test No. 10, Phase C, Run 082, Tie Plate Countercurrent Flow Test*, March 1999.
96. Siemens AG KWU, U9 316/88/1, *Experimental Data Report - UPTF - Test No. 10, Tie Plate Countercurrent Flow Test*, February 1988.
97. Siemens AG KWU, E314/90/05, *Experimental Data Report - UPTF - Test No. 29, Entrainment/Deentrainment*, June 1990.
98. Siemens AG KWU, NT31/99/06, *Quick Look Report - UPTF - Test No. 10, Phase C, Run 082, Tie Plate Countercurrent Flow Test*, March 1999.
99. H. S. Crapo, LOFT Test Support Branch Data Abstract Report, One-Sixth Scale Model BWR Jet Pump Test, EGG-LOFT-5063, LTR 20-105, November 29, 1979.

100. G. W. Fitzsimmons, *Test Performance of Developmental Steam Separators for the 1967 Product Line B.W.R.*, APED-5695, November 1968.
101. S. Wolf, *Performance of AS-2B Development Steam Separators on a 12-Inch Pitch*, NEDM-13252, December 1971.
102. Y. K. Cheung, V. Parameswaran and J.C. Shaug, *BWR Refill-Reflood Program: Model Development – TRAC-BWR Component Models*, NP-2376, NUREG/CR-2574, GEAP-22052, Interim Report, February 1984.
103. S. G. Bankoff, R. S. Tankin, M. C. Yuen, and C. L. Hsieh, "Countercurrent Flow of Air/Water and Steam/Water Through a Horizontal Perforated Plate," *International Journal of Heat and Mass Transfer*, Volume 24, pp. 1381-1395, 1981.
104. C. L. Tien, K. S. Chung, and C. P. Liu, "Flooding in Two-Phase Countercurrent Flows," EPRI NP-1283, December 1979.
105. NUREG/CR-2231, "BWR Low-Flow Bundle Uncovery Test and Analysis." U.S. Nuclear Regulatory Commission, June 1982, (Also issued as EPRI NP-1781 and GEAP- 24964).
106. UKAEA Research Group, AERE-R 5373, "Heat Transfer to Steam-Water Mixtures Flowing in Uniformly Heated Tubes in Which the Critical Heat Flux has been Exceeded," October 1967.
107. NUREG/CR-2576, *BWR Full Integral Simulation Test (FIST) Program Facility Description Report*, U.S. Nuclear Regulatory Commission, December 1982 (Also issued as EPRI NP-2314 and GEAP-22054).
108. NUREG/CR-3711. *BWR Full Integral Simulation Test (FIST) Phase I Test Results*, U.S. Nuclear Regulatory Commission, November 1983 (Also issued as EPRI NP-3602 and GEAP-30496).
109. NUREG/CR-4128, *BWR Full Integral Simulation Test: Phase 2 Test Results and TRAC-BWR Model Qualification*, U.S. Nuclear Regulatory Commission, June 1985. (Also issued as EPRI NP-3988 and GEAP-30876).
110. Electric Power Research Institute, *Core Design and Operating Data for Cycles 1 and 2 of Peach Bottom 2*, Technical Report EPRI NP-563, EPRI, June 1978.
111. ANF-913(P)(A) Volume 1 Revision 1 and Volume 1 Supplements 2, 3 and 4, COTRANSA2: A Computer Program for Boiling Water Reactor Transient Analyses, Advanced Nuclear Fuels Corporation, August 1990.
112. D.G. Schumacher, et al, "BWR Refill-Reflood Program Task 4.4 – CCFL/Refill System Effects Tests (30° Sector), SSTF System Response Test Results", NUREG/CR-2568, GEAP-22046, EPRI NP-2374, April 1983.

113. NUREG/CR-2566, "BWR Refill-Reflood Program Task 4.4 – CCFL/Refill System Effects Tests (30°Sector) Evaluation of Parallel Channel Phenomena," November 1982, (Also issued as EPRI NP-2373 and GEAP-22044).
114. NUREG/CR-2229, "BWR Large-Break Simulation Tests," U.S. Nuclear Regulatory Commission, July 1982, (Also issued as EPRI NP-1783 and GEAP-24962).
115. NUREG/CR-2230, "BWR Small Break Simulation Tests with and without Degraded ECC Systems – BWR Blowdown/Emergency Core Cooling Program," U.S. Nuclear Regulatory Commission, January 1982, (Also issued as EPRI NP-1782 and GEAP- 24963).

Appendix A BWR ECCS

The BWR emergency core cooling system (ECCS) is meant to maintain adequate cooling from a loss of coolant accident (LOCA). The systems are divided in three main groups, high pressure systems, depressurization systems, and low pressure systems.

During the early stage of the LOCA, the reactor system is at high pressure. Coolant delivered to the core during this phase is from the high pressure systems (low pressure is unable to deliver coolant at this stage). Older BWRs have the High-Pressure Coolant Injection System (HPCI – commonly found in BWR/4 plants). HPCI is powered by steam from the reactor, coolant is delivered to the core through the feedwater line. For later BWRs (BWR/5 and BWR/6), the HPCI is replaced with a high pressure core spray (HPCS) which delivers coolant spray above the core for top down cooling and suppression of steam generated. Advanced designs use a high-pressure core flooders (HPCF). The high pressure systems may be able to mitigate small leaks or breaks. If the high pressure systems are unable to mitigate the event, depressurization systems and low pressure systems are activated.

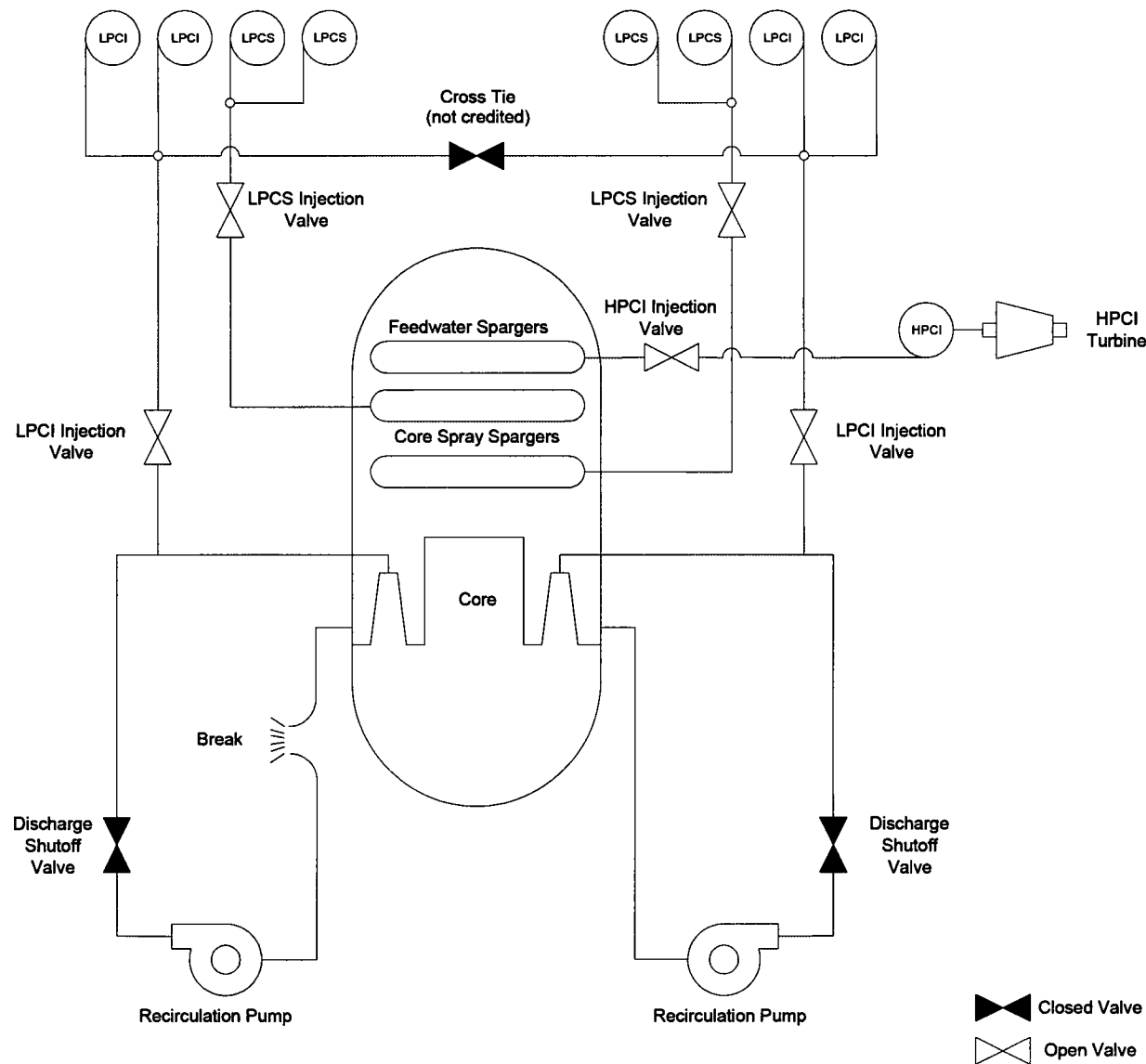
The depressurization system is designed to lower pressure of the reactor such that the low pressure system are able to deliver coolant to the reactor. The system is referred to as the Automatic Depressurization System (ADS). As the name implies, ADS is activated automatically, typically from a timer linked with low water level; however, the ADS can also be activated manually. The system releases reactor steam from the steam lines to depressurize the system with minimal loss of liquid inventory. For very large breaks, the reactor will depressurize to low pressure before ADS is activated.

As the name implies, the low pressure systems are designed to operate at low pressure. These systems have large capacities and are meant to recover the reactor to a maintainable water level and maintain long term cooling. There are multiple low pressure systems. The Low-Pressure Core Spray (LPCS) system delivers coolant spray above the top of the core which provides top down cooling and suppression of steam generated which also aids in reducing pressure. LPCS provides long term cooling by removing decay heat. The Low-pressure coolant injection (LPCI) system is an emergency function of the Residual Heat Removal (RHR)

system. The LPCI consists of several pumps that provides a large amount of coolant capable of quickly reflooding the core (bottom-up). The LPCI systems in older BWRs (typically found in BWR/4s) injects the coolant into the discharge side of the recirculation line and refill the reactor by filling the lower plenum via the jet pumps. In later BWRs (typical BWR/6), the LPCI is injected to the bypass region of the core. Advanced designs use a low-pressure core flooders (LPCF).

There are other systems that are typically not credited in LOCA analyses. Some early BWRs (BWR/2 and BWR/3) have Isolation Condensers (IC). The IC condenses decay heat steam above containment to provide coolant to the reactor. The reactor core isolation cooling (RCIC) is an auxiliary feedwater pump meant for emergency use, like HPCI it operates on steam from the reactor and can function at high pressure. RCIC can make up loss liquid inventory from residual decay heat and very small leaks.

Figure A-1 provides a diagram of the typical ECCS for BWR/3/4 plants. Figure A-2 provides a diagram of the typical ECCS for BWR/5/6 plants.



**Figure A-1 Diagram of the Typical ECCS for
BWR/3/4 Plants**

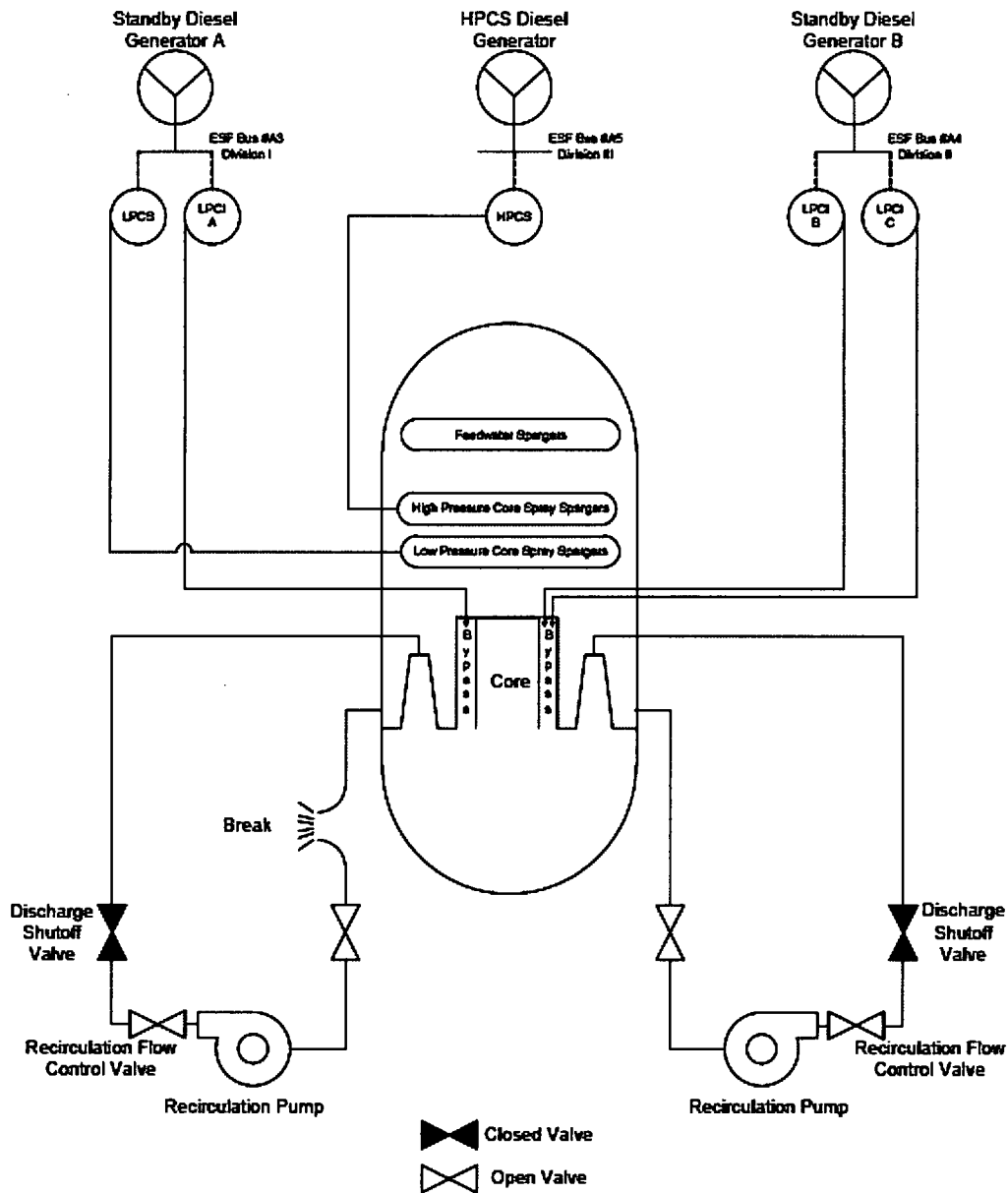


Figure A-2 Diagram of the Typical ECCS for BWR/5/6 plants